DOKUZ EYLÜL UNIVERSITY
GRADUATE SCHOOL OF NATURAL AND APPLIED SCIENCES

PERFORMING FLOOD AND DROUGHT SIMULATIONS BY USING COUPLED LAND SURFACE AND HYDROLOGIC MODELS FOR CLIMATE AND DISASTER RESILIENT SMART CITIES

by

Ayşegül KUZUCU

February, 2024

İZMİR

PERFORMING FLOOD AND DROUGHT SIMULATIONS BY USING COUPLED LAND SURFACE AND HYDROLOGIC MODELS FOR CLIMATE AND DISASTER RESILIENT SMART CITIES

A Thesis Submitted to the
Graduate School of Natural and Applied Sciences of Dokuz Eylül University
In Partial Fulfillment of the Requirements for the Degree of Doctor of Philosophy in Department of Civil Engineering, Hydraulic and Water Resources Program

by

Ayşegül KUZUCU

February, 2024

İZMİR

Ph.D. THESIS EXAMINATION RESULT FORM

We have read the thesis entitled **"PERFORMING FLOOD AND DROUGHT SIMULATIONS BY USING COUPLED LAND SURFACE AND HYDROLOGIC MODELS FOR CLIMATE AND DISASTER RESILIENT SMART CITIES"** completed by AYŞEGÜL KUZUCU under supervision of **PROF.DR. GÜLAY ONUŞLUEL GÜL** and we certify that in our opinion it is fully adequate, in scope and in quality, as a thesis for the degree of Doctor of Philosophy.

Prof.Dr. Gülay ONUŞLUEL GÜL

Supervisor

Prof. Dr. Türkay BARAN

Thesis Committee Member

Assoc. Prof. Dr. Cem Polat ÇETİNKAYA

Thesis Committee Member

Prof. Dr. Şebnem ELÇİ

Examining Committee Member

Prof. Dr. Ülker GÜNER BACANLI

Examining Committee Member

Prof. Dr. Okan FISTIKOĞLU

Director

Graduate School of Natural and Applied Sciences

ACKNOWLEDGMENT

I would like to express my deepest gratitude to my supervisor Prof. Dr. Gülay ONUŞLUEL GÜL for her unwavering support, guidance and invaluable teachings throughout the entire journey of my PhD research. I am appreciative of my supervisor for providing advice and knowledge that has guided my journey and had a significant impact on my professional growth.

I am profoundly grateful to the members of my thesis committee, Prof. Dr. Türkay BARAN and Prof. Dr. Hülya BOYACIOLU for their constructive feedback, thoughtful suggestions, and commitment to excellence. I would like to thank my professors Prof. Dr. Ali GÜL and Assoc. Prof. Dr. Filiz BARBAROS for their contributions and support to my education and life.

I would like to thank my friend Dr. Mohamed NAJAR, with whom I worked on the project during my PhD and who passed away in recent months, for all his help. I would like to thank my dear friends Dr. Semire OĞUZHAN GÜVEN, Görkem TANIR, Mert Can GÜNAÇTI and Sefa Nur YEŞİLYURT, with whom I carried out my doctoral studies in the same period, spent good times and always supported me. I am grateful to my dear friend Esra BAYOĞLU for her support, fun and guidance in every aspect of my life. I would like to thank my dear friends Yasemin ÇAKTU and Dilge VARLI and all my colleagues for their valuable support and helps. I am thankful to F. Sema KANDIR who has always supported me in my life. I am grateful to Oğuz AKAR, who contributed greatly to my personal development and progress with his help.

I would like to express my special thanks to my dear family, my mother Hatice KUZUCU, my father Yalçın KUZUCU and my brother Salih KUZUCU, who have always been with me and provided me with all their support.

I am grateful to the Scientific and Technological Research Council of Turkey (TÜBİTAK) for their support of my research project İKLİM RİSK (116Y423), and to the Council of Higher Education (YÖK) for their support of my PhD studies through the 100/2000 Doctoral Project.

Ayşegül KUZUCU

PERFORMING FLOOD AND DROUGHT SIMULATIONS BY USING COUPLED LAND SURFACE AND HYDROLOGIC MODELS FOR CLIMATE AND DISASTER RESILIENT SMART CITIES

ABSTRACT

This study presents a combined approach that integrates a Land Surface Model (LSM) and hydrological models to perform river basin simulations for future periods in the Küçük Menderes Basin example and subsequently derive drought and flood maps in order to increase the capacity and performance of climate and disaster resilient smart cities. A coupled approach integrating the Variable Infiltration Capacity (VIC) model and the Soil and Water Assessment Tool (SWAT) Model are run for river basin. Calibration and validation of the models were rigorously conducted, followed by an in-depth examination of drought scenarios for the period 2025-2099 using future climate model outputs. Drought maps, delineating intensity, duration, and magnitude on a micro-basin scale, were generated. Parallel drought analyses utilizing observed and grid-based climate data were performed. Additionally, flood modeling, utilizing the VIC model and Hydrologic Engineering Center's Hydrologic Modeling System (HEC-HMS), provided basin parameters and facilitated the computation of flood hydrographs. Employing the HEC-RAS hydraulic model, future flood propagation maps, depth, and velocity maps were created, spatially revealing the impact of flooding. The outcomes of these flood and drought studies establish a comprehensive database for use in risk assessments and the formulation of resilient action plans to address climate-related challenges and disasters.

Keywords: Land surface models, Variable Infiltration Capacity (VIC), hydrological models, Soil and Water Assessment Tool (SWAT), HEC-HMS, hydraulic models, HEC-RAS, drought indices, drought mapping, flood mapping.

İKLİM VE AFETE DİRENÇLİ AKILLI ŞEHİRLER İÇİN ARAZİ MODELİ VE HIDROLOJIK MODELLERİN BİR ARADA KULLANIMI İLE TAŞKIN VE KURAKLIK BENZEŞİMLERİNİN GERÇEKLEŞTİRİLMESİ

ÖZ

Bu çalışma, iklim ve afete dirençli akıllı şehirlerin kapasitesinin ve performansını arttırmak amacıyla Küçük Menderes Havzası örneğinde gelecek dönemler için nehir havzası simülasyonları gerçekleştirmek ve ardından kuraklık ve taşkın haritaları türetmek için bir Arazi Yüzey Modeli (LSM) ve hidrolojik modelleri entegre eden birleşik bir yaklaşım sunmaktadır. Nehir havzası için Değişken Sızma Kapasitesi (VIC) modeli ile Toprak ve Su Değerlendirme Aracı (SWAT) Modelini entegre eden birleşik bir yaklaşım çalıştırılmıştır. Modellerin kalibrasyonu ve validasyonu titizlikle gerçekleştirilmiş, ardından gelecekteki iklim modeli çıktıları kullanılarak 2025-2099 dönemi için kuraklık senaryoları derinlemesine incelenmiştir. Mikro havza ölçeğinde şiddet, süre ve büyüklüğü tanımlayan kuraklık haritaları oluşturulmuştur. Gözlenmiş veri ve grid tabanlı iklim verileri kullanılarak paralel kuraklık analizleri gerçekleştirilmiştir. Ayrıca, VIC modeli ve Hidrolojik Mühendislik Merkezi'nin Hidrolojik Modelleme Sistemi (HEC-HMS) kullanılarak yapılan taşkın modellemesi, havza parametrelerini sağlamış ve taşkın hidrograflarının hesaplanmasını kolaylaştırmıştır. HEC-RAS hidrolik modeli kullanılarak gelecekteki taşkın yayılım haritaları, derinlik ve hız haritaları oluşturulmuş ve taşkının etkisi mekânsal olarak ortaya konmuştur. Bu taşkın ve kuraklık çalışmalarının sonuçları, risk değerlendirmelerinde ve iklimle ilgili zorlukları ve felaketleri ele almak için dirençli eylem planlarının formülasyonunda kullanılmak üzere kapsamlı bir veri tabanı oluşturmaktadır.

Anahtar kelimeler: Arazi yüzey modelleri, Değişken Sızma Kapasitesi (VIC), hidrolojik modeller, Toprak ve Su Değerlendirme Aracı (SWAT), HEC-HMS, hidrolik modeller, HEC-RAS, kuraklık indisleri, kuraklık haritalama, taşkın haritalama.

CONTENTS

Page

Ph.D. THESIS EXAMINATION RESULT FORM ii
ACKNOWLEDGMENT iii
ABSTRACT iv
ÖZ v
CONTENTS vi
LIST OF FIGURES viii
LIST OF TABLES xxxiii
LIST OF SYMBOLS xxxix
ABBREVIATIONS xliv

CHAPTER ONE INTRODUCTION 1

1.1 Study Area 6
1.2 Purpose & Scope 10

CHAPTER TWO - PREVIOUS STUDIES 11

2.1 Reports on Küçük Menderes Basin 11
2.2 Research Involving Land Surface and Hydrological Models 14
2.3 Drought Analyses 21
2.4 Hydraulic Modeling and Flood Analyses 22

CHAPTER THREE - METHODOLOGY AND DATA ANALYSES 25

3.1 Methodology 25
3.1.1 Land Surface Modeling 27
3.1.2 Hydrological Modeling 35
3.1.3 Hydraulic Modeling 50
3.1.4 Drought Analyses 54
3.1.5 Flood Analyses 74
3.2 Data Analyses 80
3.2.1 Data for VIC Modeling 81

3.2.2 Data for SWAT Modeling 85
3.2.3 Data for HEC-HMS Modeling 91
3.2.4 Data for HEC-RAS Modeling 98
3.2.5 Data Preprocessing 98

CHAPTER FOUR - RESULTS AND CONCLUSIONS 117

4.1 VIC Modeling 117
4.2 SWAT Modeling 118
4.2.1 Basin Modeling 119
4.2.2 The SWAT-CUP Processing 126
4.2.3 SWAT Modeling for Future Period 135
4.3 Drought Analyses 135
4.3.1 Drought Analysis by Using Observed Data 135
4.3.2 Drought Analysis by Using Climate Data 144
4.3.3 Drought Analysis by Using SWAT Model Outputs 174
4.4 Flood Analyses 240
4.4.1 Obtaining IDF Curves 240
4.4.2 Obtaining Hyetographs 242
4.4.3 HEC-HMS modeling 243
4.5 HEC-RAS Modeling 251
4.6 Conclusion 270

REFERENCES 272

APPENDICES 297

LIST OF FIGURES

Page

Figure 1.1 Küçük Menderes Basin location map. 7

Figure 1.2 The meteorological and streamflow observation stations, and dams in Küçük Menderes River Basin. 8

Figure 3.1 Flowchart for performing drought simulations by using coupled land surface and hydrologic models. 26

Figure 3.2 Flowchart for performing flood simulations by using coupled land surface and hydrologic models. 27

Figure 3.3 First, second, and third generation LSMs (Pitman, 2003). 28

Figure 3.4 Schema of energy, water, and carbon balance (Bonan, 2008). 29

Figure 3.5 VIC land cover tiles and soil column, with major water and energy fluxes (University of Washington Computational Hydrology Group, 2021) 35

Figure 3.6 Hydrological cycle (Neitsch et al., 2009) 38

Figure 3.7 ArcSWAT extension in ARCGIS. 43

Figure 3.8 Watershed Delineation part of ArcSWAT 43

Figure 3.9 ArcSWAT process 43

Figure 3.10 The linkage between SWAT and SWAT-CUP (Abbaspour, 2015). 44

Figure 3.11 SWAT-CUP process 45

Figure 3.12 Runoff process (Ward, 1975; U.S. Army Corps of Engineers, Hydrologic Engineering Center, 2000) 47

Figure 3.13 The methods in HEC-HMS 48

Figure 3.14 HEC-GeoHMS extension in ARCGIS. 49

Figure 3.15 HEC-GeoHMS process. 49

Figure 3.16 HEC-HMS model interface. 50

Figure 3.17 HEC-HMS process. 50

Figure 3.18 HEC-HMS model interface. 54

Figure 3.19 HEC-HMS model process. 54

Figure 3.20 Drought analyses. 55

Figure 3.21 Relationship between drought indices. 56

Figure 3.22 Representative time series of SPI/SPEI and annual maximum drought severities (Smax), drought duration (D_{Smax}) and the average maximum drought magnitude (M_{Smax}) (Kuzucu and Onuşluel Gül, 2023)..... 62

Figure 3.23 The process of drought analysis by using gridded climate data. 69

Figure 3.24 Küçük Menderes River Basin and micro catchments. 71

Figure 3.25 The flowchart of SWAT Modeling for the study 73

Figure 3.26 The location map of Ergenli Basin. 75

Figure 3.27 Study area for flood analysis (Ergenli Dam Basin and the subbasin). ... 75

Figure 3.28 The structures and settlements at downstream of Ergenli Basin. 76

Figure 3.29 Field studies (Personal archive, 2021). 76

Figure 3.30 Instantaneous Intensity method curve (Te Chow et al.,1988). 77

Figure 3.31 HEC-HMS model, a) Existing situation, b) Operational status of Ergenli Dam 79

Figure 3.32 DEM of Küçük Menderes River Basin..... 81

Figure 3.33 1/16^{o} resolution grids and daily total precipitation (mm). 82

Figure 3.34 1/16^{o} resolution grids and IGBP land use class. 83

Figure 3.35 Streamflow stations in Küçük Menderes River Basin 86

Figure 3.36 Meteorological stations in and around the Küçük Menderes River Basin 88

Figure 3.37 Hydrologic soil groups in Küçük Menderes Basin (İKLİM RİSK, 2021). 89

Figure 3.38 The hourly limnigraph records for D06A027 for the calibration period. 92

Figure 3.39 The flow rating curve for both calibration and validation period. 93

Figure 3.40 The graph to obtain the parameters of the flow rating equation. 93

Figure 3.41 Daily discharge of D06A027 a) for calibration period, b) for validation period. 94

Figure 3.42 Hourly discharge of D06A027 a) for calibration period, b) for validation period. 94

Figure 3.43 The process in order to obtain distributed data. 95

Figure 3.44 Distribution of daily precipitation measured at Ödemiş Meteorological Station (17822) to the grids according to the relevant distribution coefficients. 95

Figure 3.45 a) Zero grid, b) “One” value grid, c) Distribution factor grid for January, d) Distribution factor grid for February. 96

Figure 3.46 Long term average of a) total annual precipitation (mm), b) mean annual temperature (^{o}C). 99

Figure 3.47 Long term average of a) total monthly precipitation (mm), b) mean monthly temperature (^{o}C). 99

Figure 3.48 Daily, monthly, annual total precipitation graphs of Ödemiş Meteorological Station. 103

Figure 3.49 The monthly total precipitation matrix of Ödemiş Meteorological Station. 103

Figure 3.50 Daily, monthly, annual total precipitation graphs of Selçuk Meteorological Station..... 104

Figure 3.51 The monthly total precipitation matrix of Selçuk Meteorological Station. 104

Figure 3.52 Daily, monthly, annual mean temperature graphs of Ödemiş Meteorological Station. 105

Figure 3.53 The monthly mean temperature matrix of Ödemiş Meteorological Station. 105

Figure 3.54 Daily, monthly, annual mean temperature graphs of Selçuk Meteorological Station..... 106

Figure 3.55 The monthly mean temperature matrix of Selçuk Meteorological Station. 106

Figure 3.56 Trend maps of a) total monthly precipitation (mm), b) mean monthly temperature (^{o}C)..... 113

Figure 3.57 Trend maps of a) monthly minimum temperature, b) monthly maximum temperature (^{o}C)..... 113

Figure 3.58 Decomposition of total monthly precipitation (mm) series for Ödemiş station..... 114

Figure 3.59 Decomposition of mean monthly temperature (^{o}C) series for Ödemiş station..... 115

Figure 3.60 Decomposition of total monthly precipitation (mm) series for Selçuk station..... 115

Figure 3.61 Decomposition of mean monthly temperature (^{o}C) series for Selçuk station. 116

Figure 4.1 Model calibration of VIC Model. 117

Figure 4.2 Model validation of VIC Model. 117

Figure 4.3 The process of SWAT and SWAT-CUP modeling. 118

Figure 4.4 Selected periods for modelling. 118

Figure 4.5 The maps of a) DEM, b) flow direction, c) basin characteristics. 119

Figure 4.6 a) The look-up table for land use. a) Identifying the land use data. 120

Figure 4.7 a) The look-up table for soil b) Identifying the soil database. 121

Figure 4.8 Identifying the slope (%) classification. 122

Figure 4.9 The maps of a) land use, b) soil database, c) land slope. 122

Figure 4.10 Selecting Weather Generator Data for Küçük Menderes. 123

Figure 4.11 Meteorological input files for SWAT model, a) Station locations, b) Input data. 123

Figure 4.12 Introducing the application principles to SWAT model in HRUs to be irrigated. 125

Figure 4.13 Agricultural operation. 125

Figure 4.14 SWAT model running. 126

Figure 4.15 SWAT model outputs. 126

Figure 4.16 One-at-a-time sensitivity analysis the parameters. 127

Figure 4.17 One-at-a-time sensitivity analysis the parameters. 128

Figure 4.18 For Subbasin 3: SWAT Model a) calibration and b) validation. 133

Figure 4.19 For Subbasin 9: SWAT Model a) calibration and b) validation. 133

Figure 4.20 For Subbasin 14: SWAT Model a) calibration and b) validation. 134

Figure 4.21 For Subbasin 50: SWAT Model a) calibration and b) validation. 134

Figure 4.22 SPI-12 month and SPEI-12 month series for Ödemiş Station. 136

Figure 4.23 SPI – 12 month and SPEI – 12 month series for Selçuk Station. 136

Figure 4.24 Trend in drought indices series for a) SPI-1 month, b) SPI-3 month, c) SPI-6 month, d) SPI-12 month, e)SPEI for 1-month to12-month. 139

Figure 4.25 The relationship between L-skewness and L-CV for a) annual drought severity, b) annual drought duration. 141

Figure 4.26 Average annual maximum drought severity for the observed period a) SPI-1 month, b) SPI-3 month, c) SPEI-1 month, d) SPEI-3 month. 142

Figure 4.27 Average annual maximum drought duration for the observed period a) SPI-1 month, b) SPI-3 month, c) SPEI-1 month, d) SPEI-3 month. .. 142

Figure 4.28 Trend in average annual maximum drought severity for the observed period a) SPI-1 month, b) SPI-3-month, c) SPEI-1 month, d) SPEI-3 month. 143

Figure 4.29 Trend in average annual maximum drought duration for the observed period a) SPI-1 month, b) SPI-3-month, c) SPEI-1 month, d) SPEI-3 month. 143

Figure 4.30 Average annual maximum drought severity of SPI-1 month for the period a)1971-2004, b)2025-2049, c)2050-2074, d)2075-2099..... 146

Figure 4.31 Average annual maximum drought severity of SPI-3 month for the period a)1971-2004, b)2025-2049, c)2050-2074, d)2075-2099..... 146

Figure 4.32 Average annual maximum drought duration of SPI-1 month for the period a)1971-2004, b)2025-2049, c)2050-2074, d)2075-2099..... 147

Figure 4.33 Average annual maximum drought duration of SPI-3 month for the period a)1971-2004, b)2025-2049, c)2050-2074, d)2075-2099..... 147

Figure 4.34 Average annual maximum drought magnitude of SPI-1 month for the period a)1971-2004, b)2025-2049, c)2050-2074, d)2075-2099. 148

Figure 4.35 Average annual maximum drought magnitude of SPI-3 month for the period a)1971-2004, b)2025-2049, c)2050-2074, d)2075-2099. 148

Figure 4.36 Median month of annual drought start of SPI-1 month for the period a)1971-2004, b)2025-2049, c)2050-2074, d)2075-2099. 149

Figure 4.37 Median month of annual drought start of SPI-3 month for the period a)1971-2004, b)2025-2049, c)2050-2074, d)2075-2099. 149

Figure 4.38 Average annual maximum drought severity of SPEI-1 month for the period a)1971-2004, b)2025-2049, c)2050-2074, d)2075-2099..... 152

Figure 4.39 Average annual maximum drought severity of SPEI-3 month for the period a)1971-2004, b)2025-2049, c)2050-2074, d)2075-2099..... 152

Figure 4.40 Average annual maximum drought duration of SPEI-1 month for the period a)1971-2004, b)2025-2049, c)2050-2074, d)2075-2099. 153

Figure 4.41 Average annual maximum drought duration of SPEI-3 month for the period a)1971-2004, b)2025-2049, c)2050-2074, d)2075-2099. 153

Figure 4.42 Average annual maximum drought magnitude of SPEI-1 month for the period a)1971-2004, b)2025-2049, c)2050-2074, d)2075-2099. 154

Figure 4.43 Average annual maximum drought magnitude of SPEI-3 month for the period a)1971-2004, b)2025-2049, c)2050-2074, d)2075-2099. 154

Figure 4.44 Median month of annual maximum drought start of SPEI-1 month for the period a)1971-2004, b)2025-2049, c)2050-2074, d)2075-2099. 155

Figure 4.45 Median month of annual maximum drought start of SPEI-3 month for the period a)1971-2004, b)2025-2049, c)2050-2074, d)2075-2099. 155

Figure 4.46 Trend in average annual maximum drought severity of SPI-1 month for the period a)1971-2004, b)2025-2049, c)2050-2074, d)2075-2099. 156

Figure 4.47 Trend in average annual maximum drought severity of SPI-3 month for the period a)1971-2004, b)2025-2049, c)2050-2074, d)2075-2099. 157

Figure 4.48 Trend in average annual maximum drought duration of SPI-1 month for the period a)1971-2004, b)2025-2049, c)2050-2074, d)2075-2099. 157

Figure 4.49 Trend in average annual maximum drought duration of SPI-3 month for the period a)1971-2004, b)2025-2049, c)2050-2074, d)2075-2099. 158

Figure 4.50 Trend in average annual maximum drought magnitude of SPI-1 month for the period a)1971-2004, b)2025-2049, c)2050-2074, d)2075-2099. 158

Figure 4.51 Trend in average annual maximum drought magnitude of SPI-3 month for the period a)1971-2004, b)2025-2049, c)2050-2074, d)2075-2099. 159

Figure 4.52 Trend in annual maximum drought start month of SPI-1 month for the period a)1971-2004, b)2025-2049, c)2050-2074, d)2075-2099. 159

Figure 4.53 Trend in annual maximum drought start month of SPI-3 month for the period a)1971-2004, b)2025-2049, c)2050-2074, d)2075-2099. 160

Figure 4.54 Trend in average annual maximum drought severity of SPEI-1 month for the period a)1971-2004, b)2025-2049, c)2050-2074, d)2075-2099. 160

Figure 4.55 Trend in average annual maximum drought severity of SPEI-3 month for the period a)1971-2004, b)2025-2049, c)2050-2074, d)2075-2099. 161

Figure 4.56 Trend in average annual maximum drought duration of SPEI-1 month for the period a)1971-2004, b)2025-2049, c)2050-2074, d)2075-2099. 161

Figure 4.57 Trend in average annual maximum drought duration of SPEI-3 month for the period a)1971-2004, b)2025-2049, c)2050-2074, d)2075-2099. 162

Figure 4.58 Trend in average annual maximum drought magnitude of SPEI-1 month for the period a)1971-2004, b)2025-2049, c)2050-2074, d)2075-2099.162

Figure 4.59 Trend in average annual maximum drought magnitude of SPEI-3 month for the period a)1971-2004, b)2025-2049, c)2050-2074, d)2075-2099.163

Figure 4.60 Trend in annual maximum drought start months of SPEI-1 month for the period a)1971-2004, b)2025-2049, c)2050-2074, d)2075-2099. 163

Figure 4.61 Trend in annual maximum drought start months of SPEI-3 month for the period a)1971-2004, b)2025-2049, c)2050-2074, d)2075-2099. 164

Figure 4.62 Average annual maximum drought severity of SPI-30 day for the period a)1971-2004, b)2025-2049, c)2050-2074, d)2075-2099..... 166

Figure 4.63 Average annual maximum drought severity of SPI-90 day for the period a)1971-2004, b)2025-2049, c)2050-2074, d)2075-2099..... 167

Figure 4.64 Average annual maximum drought duration of SPI-30 day for the period a)1971-2004, b)2025-2049, c)2050-2074, d)2075-2099..... 167

Figure 4.65 Average annual maximum drought duration of SPI-90 day for the period a)1971-2004, b)2025-2049, c)2050-2074, d)2075-2099..... 168

Figure 4.66 Average annual maximum drought magnitude of SPI-30 day for the period a)1971-2004, b)2025-2049, c)2050-2074, d)2075-2099..... 168

Figure 4.67 Average annual maximum drought magnitude of SPI-90 day for the period a)1971-2004, b)2025-2049, c)2050-2074, d)2075-2099..... 169

Figure 4.68 Median day of annual drought start of SPI-30 day for the period a)1971-2004, b)2025-2049, c)2050-2074, d)2075-2099. 169

Figure 4.69 Median day of annual drought start of SPI-90 day for the period a)1971-2004, b)2025-2049, c)2050-2074, d)2075-2099. 170

Figure 4.70 Trend in average annual maximum drought severity of SPI-30 day for the period a)1971-2004, b)2025-2049, c)2050-2074, d)2075-2099. 170

Figure 4.71 Trend in average annual maximum drought severity of SPI-90 day for the period a)1971-2004, b)2025-2049, c)2050-2074, d)2075-2099. 171

Figure 4.72 Trend in average annual maximum drought duration of SPI-30 day for the period a)1971-2004, b)2025-2049, c)2050-2074, d)2075-2099. 171

Figure 4.73 Trend in average annual maximum drought duration of SPI-90 day for the period a)1971-2004, b)2025-2049, c)2050-2074, d)2075-2099. 172

Figure 4.74 Trend in average annual maximum drought magnitude of SPI-30 day for the period a)1971-2004, b)2025-2049, c)2050-2074, d)2075-2099. 172

Figure 4.75 Trend in average annual maximum drought magnitude of SPI-90 day for the period a)1971-2004, b)2025-2049, c)2050-2074, d)2075-2099. 173

Figure 4.76 Trend in annual maximum drought start days of SPI-30 day for the period a)1971-2004, b)2025-2049, c)2050-2074, d)2075-2099..... 173

Figure 4.77 Trend in annual maximum drought start days of SPI-90 day for the period a)1971-2004, b)2025-2049, c)2050-2074, d)2075-2099..... 174

Figure 4.78 Maps obtained using SPI-1 month series for the reference period: a) average annual maximum drought severity, b) duration and c) magnitude. 176

Figure 4.79 Maps obtained using SPI-1 month series for the near future period: a) average annual maximum drought severity, b) duration and c) magnitude. 177

Figure 4.80 Maps obtained using SPI-1 month series for the middle future period: a) average annual maximum drought severity, b) duration and c) magnitude. 178

Figure 4.81 Maps obtained using SPI-1 month series for the far future period: a) average annual maximum drought severity, b) duration and c) magnitude. 179

Figure 4.82 Maps obtained using SPI-3 month series for the reference period: a) average annual maximum drought severity, b) duration and c) magnitude. 180

Figure 4.83 Maps obtained using SPI-3 month series for the near future period: a) average annual maximum drought severity, b) duration and c) magnitude. 181

Figure 4.84 Maps obtained using SPI-3 month series for the middle future period: a) average annual maximum drought severity, b) duration and c) magnitude. 182

Figure 4.85 Maps obtained using SPI-3 month series for the far future period: a) average annual maximum drought severity, b) duration and c) magnitude. 183

Figure 4.86 Maps obtained using SPI-6 month series for the reference period: a) average annual maximum drought severity, b) duration and c) magnitude. 184

Figure 4.87 Maps obtained using SPI-6 month series for the near future period: a) average annual maximum drought severity, b) duration and c) magnitude. 185

Figure 4.88 Maps obtained using SPI-6 month series for the middle future period: a) average annual maximum drought severity, b) duration and c) magnitude. 186

Figure 4.89 Maps obtained using SPI-6 month series for the far future period: a) average annual maximum drought severity, b) duration and c) magnitude. 187

Figure 4.90 Maps obtained using SPI-12 month series for the reference period: a) average annual maximum drought severity, b) duration and c) magnitude. 188

Figure 4.91 Maps obtained using SPI-12 month series for the near future period: a) average annual maximum drought severity, b) duration and c) magnitude. 189

Figure 4.92 Maps obtained using SPI-12 month series for the middle future period: a) average annual maximum drought severity, b) duration and c) magnitude. 190

Figure 4.93 Maps obtained using SPI-12 month series for the far future period: a) average annual maximum drought severity, b) duration and c) magnitude. 191

Figure 4.94 Maps obtained using SPEI-1 month series (with ET_a) for the reference period: a) average annual maximum drought severity, b) duration and c) magnitude..... 192

Figure 4.95 Maps obtained using SPEI-1 month series (with ET_a) for the near future period: a) average annual maximum drought severity, b) duration and c) magnitude..... 193

Figure 4.96 Maps obtained using SPEI-1 month series (with ET_a) for the middle future period: a) average annual maximum drought severity, b) duration and c) magnitude..... 194

Figure 4.97 Maps obtained using SPEI-1 month series (with ET_a) for the far future period: a) average annual maximum drought severity, b) duration and c) magnitude..... 195

Figure 4.98 Maps obtained using SPEI-3 month series (with ET_a) for the reference period: a) average annual maximum drought severity, b) duration and c) magnitude..... 196

Figure 4.99 Maps obtained using SPEI-3 month series (with ET_a) for the near future period: a) average annual maximum drought severity, b) duration and c) magnitude..... 197

Figure 4.100 Maps obtained using SPEI-3 month series (with ET_a) for the middle future period: a) average annual maximum drought severity, b) duration and c) magnitude..... 198

Figure 4.101 Maps obtained using SPEI-3 month series (with ET_a) for the far future period: a) average annual maximum drought severity, b) duration and c) magnitude..... 199

Figure 4.102 Maps obtained using SPEI-6 month series (with ET_a) for the reference period: a) average annual maximum drought severity, b) duration and c) magnitude..... 200

Figure 4.103 Maps obtained using SPEI-6 month series (with ET_a) for the near future period: a) average annual maximum drought severity, b) duration and c) magnitude..... 201

Figure 4.104 Maps obtained using SPEI-6 month series (with ET_a) for the middle future period: a) average annual maximum drought severity, b) duration and c) magnitude..... 202

Figure 4.105 Maps obtained using SPEI-6 month series (with ET_a) for the far future period: a) average annual maximum drought severity, b) duration and c) magnitude..... 203

Figure 4.106 Maps obtained using SPEI-12 month series (with ET_a) for the reference period: a) average annual maximum drought severity, b) duration and c) magnitude..... 204

Figure 4.107 Maps obtained using SPEI-12 month series (with ET_a) for the near future period: a) average annual maximum drought severity, b) duration and c) magnitude..... 205

Figure 4.108 Maps obtained using SPEI-12 month series (with ET_a) for the middle future period: a) average annual maximum drought severity, b) duration and c) magnitude..... 206

Figure 4.109 Maps obtained using SPEI-12 month series (with ET_a) for the far future period: a) average annual maximum drought severity, b) duration and c) magnitude..... 207

Figure 4.110 Maps obtained using SPEI-1 month series (with PET) for the far future period: a) average annual maximum drought severity, b) duration and c) magnitude..... 208

Figure 4.111 Maps obtained using SPEI-1 month series (with PET) for the near future period: a) average annual maximum drought severity, b) duration and c) magnitude..... 209

Figure 4.112 Maps obtained using SPEI-1 month series (with PET) for the middle future period: a) average annual maximum drought severity, b) duration and c) magnitude. 210

Figure 4.113 Maps obtained using SPEI-1 month series (with PET) for the far future period: a) average annual maximum drought severity, b) duration and c) magnitude. 211

Figure 4.114 Maps obtained using SPEI-3 month series (with PET) for the reference period: a) average annual maximum drought severity, b) duration and c) magnitude. 212

Figure 4.115 Maps obtained using SPEI-3 month series (with PET) for the near future period: a) average annual maximum drought severity, b) duration and c) magnitude. 213

Figure 4.116 Maps obtained using SPEI-3 month series (with PET) for the middle future period: a) average annual maximum drought severity, b) duration and c) magnitude. 214

Figure 4.117 Maps obtained using SPEI-3 month series (with PET) for the far future period: a) average annual maximum drought severity, b) duration and c) magnitude. 215

Figure 4.118 Maps obtained using SPEI-6 month series (with PET) for the reference period: a) average annual maximum drought severity, b) duration and c) magnitude. 216

Figure 4.119 Maps obtained using SPEI-6 month series (with PET) for the near future period: a) average annual maximum drought severity, b) duration and c) magnitude. 217

Figure 4.120 Maps obtained using SPEI-6 month series (with PET) for the middle future period: a) average annual maximum drought severity, b) duration and c) magnitude. 218

Figure 4.121 Maps obtained using SPEI-6 month series (with PET) for the far future period: a) average annual maximum drought severity, b) duration and c) magnitude..... 219

Figure 4.122 Maps obtained using SPEI-12 month series (with PET) for the reference period: a) average annual maximum drought severity, b) duration and c) magnitude..... 220

Figure 4.123 Maps obtained using SPEI-12 month series (with PET) for the near future period: a) average annual maximum drought severity, b) duration and c) magnitude..... 221

Figure 4.124 Maps obtained using SPEI-12 month series (with PET) for the middle future period: a) average annual maximum drought severity, b) duration and c) magnitude..... 222

Figure 4.125 Maps obtained using SPEI-12 month series (with PET) for the far future period: a) average annual maximum drought severity, b) duration and c) magnitude..... 223

Figure 4.126 Maps obtained using SSFI-1 month series for the reference period: a) average annual maximum drought severity, b) duration and c) magnitude. 224

Figure 4.127 Maps obtained using SSFI-1 month series for the near future period: a) average annual maximum drought severity, b) duration and c) magnitude. 225

Figure 4.128 Maps obtained using SSFI-1 month series for the middle future period: a) average annual maximum drought severity, b) duration and c) magnitude..... 226

Figure 4.129 Maps obtained using SSFI-1 month series for the far future period: a) average annual maximum drought severity, b) duration and c) magnitude. 227

Figure 4.130 Maps obtained using SSFI-3 month series for the reference period: a) average annual maximum drought severity, b) duration and c) magnitude. 228

Figure 4.131 Maps obtained using SSFI-3 month series for the near future period: a) average annual maximum drought severity, b) duration and c) magnitude. 229

Figure 4.132 Maps obtained using SSFI-3 month series for the middle future period: a) average annual maximum drought severity, b) duration and c) magnitude. 230

Figure 4.133 Maps obtained using SSFI-3 month series for the far future period: a) average annual maximum drought severity, b) duration and c) magnitude. 231

Figure 4.134 Maps obtained using SSFI-6 month series for the reference period: a) average annual maximum drought severity, b) duration and c) magnitude. 232

Figure 4.135 Maps obtained using SSFI-6 month series for the near future period: a) average annual maximum drought severity, b) duration and c) magnitude. 233

Figure 4.136 Maps obtained using SSFI-6 month series for the middle future period: a) average annual maximum drought severity, b) duration and c) magnitude. 234

Figure 4.137 Maps obtained using SSFI-6 month series for the far future period: a) average annual maximum drought severity, b) duration and c) magnitude. 235

Figure 4.138 Maps obtained using SSFI-12 month series for the reference period: a) average annual maximum drought severity, b) duration and c) magnitude. 236

Figure 4.139 Maps obtained using SSFI-12 month series for the near future period: a) average annual maximum drought severity, b) duration and c) magnitude. 237

Figure 4.140 Maps obtained using SSFI-12 month series for the middle future period: a) average annual maximum drought severity, b) duration and c) magnitude..... 238

Figure 4.141 Maps obtained using SSFI-12 month series for the far future period: a) average annual maximum drought severity, b) duration and c) magnitude. 239

Figure 4.142 Rainfall IDF curves for Ödemiş Station 241

Figure 4.143 24-hour hyetographs of Ödemiş Station. 243

Figure 4.144 Project area of Ilıca (Ergenli) Basin for HEC-HMS model..... 244

Figure 4.145 HEC-GeoHMS model schematic representation of Ilıca (Ergenli) Basin. 245

Figure 4.146 HECHMS model schematic representation of Ilıca (Ergenli) Basin. . 245

Figure 4.147 Model results for calibration period. 246

Figure 4.148 Rainfall depth (mm) and flood hydrograph (m^3/s) for calibration period. 247

Figure 4.149 Model results for validation period. 247

Figure 4.150 Rainfall depth (mm) and flood hydrograph (m^3/s) for validation period. 248

Figure 4.151 Rainfall depth (mm) and flood hydrograph (m^3/s) for validation period. 249

Figure 4.152 Elevation – Volume Curve for Ergenli Basin..... 250

Figure 4.153 Ergenli Dam flood routing for observed flows of Jan-2011..... 250

Figure 4.154 Flood hydrographs obtained by flow routing. 251

Figure 4.155 HEC-RAS Modeling interface for Ergenli Basin. 251

Figure 4.156 2D Flow Area 252

Figure 4.157 2D Flow area parameters. 252

Figure 4.158 Defining the bridges. 253

Figure 4.159 Unsteady flow data. 253

Figure 4.160 The hydrograph of Q_{1000} - Ergenli Dam in operation. 254

Figure 4.161 RAS Mapper and the flow depth for Q_{1000} - Ergenli Dam in operation. 254

Figure 4.162 The flow depth map for 2-year flood. 256

Figure 4.163 The flow depth map for 5-year flood. 256

Figure 4.164 The flow depth map for 10-year flood. 257

Figure 4.165 The flow depth map for 25-year flood. 257

Figure 4.166 The flow depth map for 50-year flood. 258

Figure 4.167 The flow depth map for 100-year flood. 258

Figure 4.168 The flow depth map for 250-year flood. 259

Figure 4.169 The flow depth map for 500-year flood. 259

Figure 4.170 The flow depth map for 1000-year flood. 260

Figure 4.171 The flow velocity map for 2-year flood. 260

Figure 4.172 The flow velocity map for 5-year flood. 261

Figure 4.173 The flow velocity map for 10-year flood. 261

Figure 4.174 The flow velocity map for 25-year flood. 262

Figure 4.175 The flow velocity map for 50-year flood. 262

Figure 4.176 The flow velocity map for 100-year flood. 263

Figure 4.177 The flow velocity map for 250-year flood. 263

Figure 4.178 The flow velocity map for 500-year flood. 264

Figure 4.179 The flow velocity map for 1000-year flood. 264

Figure 4.180 The flood inundation map. 265

Figure 4.181 The flood inundation map for Furunlu region. 265

Figure 4.182 The flood inundation map for Bayındır region. 266

Figure 4.183 The flood inundation map for Ergenli region. 266

Figure 4.184 The flow depth map for 100-year flood in case the dam in operation. 267

Figure 4.185 The flow depth map for 500-year flood in case the dam in operation. 267

Figure 4.186 The flow depth map for 1000-year flood in case the dam in operation. 268

Figure 4.187 The flow velocity map for 100-year flood in case the dam in operation. 268

Figure 4.188 The flow velocity map for 500-year flood in case the dam in operation. 269

Figure 4.189 The flow velocity map for 1000-year flood in case the dam in operation. 269

Figure 4.190 The flood inundation map in case the dam in operation. 270

Figure Ap.1 Daily, monthly, annual total precipitation graphs of Aydın Station (mm). 297

Figure Ap.2 Daily, monthly, annual total precipitation graphs of Çeşme Station (mm). 297

Figure Ap.3 Daily, monthly, annual total precipitation graphs of İzmir Station (mm). 298

Figure Ap.4 Daily, monthly, annual total precipitation graphs of Kuşadası Station (mm)..... 298

Figure Ap.5 Daily, monthly, annual total precipitation graphs of Manisa Station (mm). 299

Figure Ap.6 Daily, monthly, annual total precipitation graphs of Nazilli Station (mm). 299

Figure Ap.7 Daily, monthly, annual total precipitation graphs of Salihli Station (mm). 300

Figure Ap.8 Daily, monthly, annual total precipitation graphs of Seferihisar Station (mm)..... 300

Figure Ap.9 Daily, monthly, annual total precipitation graphs of Sultanhisar Station (mm)..... 301

Figure Ap.10 The monthly total precipitation matrix of Aydın Station (mm)..... 301

Figure Ap.11 The monthly total precipitation matrix of Çeşme Station (mm)..... 301

Figure Ap.12 The monthly total precipitation matrix of İzmir Station (mm)..... 302

Figure Ap.13 The monthly total precipitation matrix of Kuşadası Station (mm).... 302

Figure Ap.14 The monthly total precipitation matrix of Manisa Station (mm)..... 302

Figure Ap.15 The monthly total precipitation matrix of Nazilli Station (mm)..... 303

Figure Ap.16 The monthly total precipitation matrix of Salihli Station (mm)..... 303

Figure Ap 17 The monthly total precipitation matrix of Seferihisar Station (mm). 303

Figure Ap.18 The monthly total precipitation matrix of Sultanhisar Station (mm). 304

Figure Ap.19 Daily, monthly, annual mean temperature graphs of Aydın Station (ºC). 304

Figure Ap.20 Daily, monthly, annual mean temperature graphs of Çeşme Station (ºC). 305

Figure Ap.21 Daily, monthly, annual mean temperature graphs of İzmir Station (ºC). 305

Figure Ap.22 Daily, monthly, annual mean temperature graphs of Kuşadası Station (ºC). 306

Figure Ap.23 Daily, monthly, annual mean temperature graphs of Manisa Station (ºC). 306

Figure Ap.24 Daily, monthly, annual mean temperature graphs of Nazilli Station (ºC). 307

Figure Ap.25 Daily, monthly, annual mean temperature graphs of Salihli Station (ºC). 307

Figure Ap.26 Daily, monthly, annual mean temperature graphs of Seferihisar Station (ºC). 308

Figure Ap.27 Daily, monthly, annual mean temperature graphs of Sultanhisar Station (ºC). 308

Figure Ap.28 The monthly mean temperature matrix of Aydın Station (ºC). 309

Figure Ap.29 The monthly mean temperature matrix of Çeşme Station (ºC). 309

Figure Ap.30 The monthly mean temperature matrix of İzmir Station (ºC)..... 309

Figure Ap.31 The monthly mean temperature matrix of Kuşadası Station (ºC)..... 310

Figure Ap.32 The monthly mean temperature matrix of Manisa Station (ºC)..... 310

Figure Ap.33 The monthly mean temperature matrix of Nazilli Station (ºC).. 310

Figure Ap.34 The monthly mean temperature matrix of Salihli Station (ºC)..... 311

Figure Ap.35 The monthly mean temperature matrix of Seferihisar Station (°C). . . 311

Figure Ap.36 The monthly mean temperature matrix of Sultanhisar Station (°C). . 311

Figure Ap.37 Decomposition of total monthly precipitation (mm) series for Aydın Station. 312

Figure Ap.38 Decomposition of total monthly precipitation (mm) series for Çeşme Station. 312

Figure Ap.39 Decomposition of total monthly precipitation (mm) series for İzmir Station. 313

Figure Ap.40 Decomposition of total monthly precipitation (mm) series for Kuşadası Station. 313

Figure Ap.41 Decomposition of total monthly precipitation (mm) series for Manisa Station. 314

Figure Ap.42 Decomposition of total monthly precipitation (mm) series for Nazilli Station. 314

Figure Ap.43 Decomposition of total monthly precipitation (mm) series for Salihli Station. 315

Figure Ap.44 Decomposition of total monthly precipitation (mm) series for Seferihisar Station. 315

Figure Ap.45 Decomposition of total monthly precipitation (mm) series for Sultanhisar Station. 316

Figure Ap.46 Decomposition of mean monthly temperature (oC) series for Aydın Station. 316

Figure Ap.47 Decomposition of mean monthly temperature (°C) series for Çeşme Station. 317

Figure Ap.48 Decomposition of mean monthly temperature (°C) series for İzmir Station. 317

Figure Ap.49 Decomposition of mean monthly temperature (°C) series for Kuşadası Station. 318

Figure Ap.50 Decomposition of mean monthly temperature (°C) series for Manisa Station. 318

Figure Ap.51 Decomposition of mean monthly temperature (°C) series for Nazilli Station. 319

Figure Ap.52 Decomposition of mean monthly temperature (°C) series for Salihli Station. 319

Figure Ap.53 Decomposition of mean monthly temperature (°C) series for Seferihisar Station. 320

Figure Ap.54 Decomposition of mean monthly temperature (°C) series for Sultanhisar Station. 320

Figure Ap.55 Average number of months with moderate drought of SPI-1 month for the period a)1971-2004, b) 2025-2049, c) 2050-2074, d) 2075-2099. 345

Figure Ap.56 Average number of months with moderate drought of SPI-3 month for the period a)1971-2004, b) 2025-2049, c) 2050-2074, d) 2075-2099. 345

Figure Ap.57 Average number of months with severe drought of SPI-1 month for the period a)1971-2004, b) 2025-2049, c) 2050-2074, d) 2075-2099. 346

Figure Ap.58 Average number of months with severe drought of SPI-3 month for the period a)1971-2004, b) 2025-2049, c) 2050-2074, d) 2075-2099. 346

Figure Ap.59 Average number of months with extreme drought of SPI-1 month for the period a)1971-2004, b) 2025-2049, c) 2050-2074, d) 2075-2099. 347

Figure Ap.60 Average number of months with extreme drought of SPI-3 month for the period a)1971-2004, b) 2025-2049, c) 2050-2074, d) 2075-2099. 347

Figure Ap.61 Average number of months with drought pattern of SPI-1 month for the period a)1971-2004, b) 2025-2049, c) 2050-2074, d) 2075-2099.... 348

Figure Ap.62 Average number of months with drought pattern of SPI-3 month for the period a)1971-2004, b) 2025-2049, c) 2050-2074, d) 2075-2099.... 348

Figure Ap.63 Average number of months with moderate drought of SPEI-1 month for the period a)1971-2004, b) 2025-2049, c) 2050-2074, d) 2075-2099. 349

Figure Ap.64 Average number of months with moderate drought of SPEI-3 month for the period a)1971-2004, b) 2025-2049, c) 2050-2074, d) 2075-2099. 349

Figure Ap.65 Average number of months with severe drought of SPEI-1 month for the period a)1971-2004, b) 2025-2049, c) 2050-2074, d) 2075-2099.... 350

Figure Ap.66 Average number of months with severe drought of SPEI-3 month for the period a)1971-2004, b) 2025-2049, c) 2050-2074, d) 2075-2099.... 350

Figure Ap.67 Average number of months with extreme drought of SPEI-1 month for the period a)1971-2004, b) 2025-2049, c) 2050-2074, d) 2075-2099. 351

Figure Ap.68 Average number of months with extreme drought of SPEI-3 month for the period a)1971-2004, b) 2025-2049, c) 2050-2074, d) 2075-2099. 351

Figure Ap.69 Average number of months with drought pattern of SPEI-1 month for the period a)1971-2004, b) 2025-2049, c) 2050-2074, d) 2075-2099. 352

Figure Ap.70 Average number of months with drought pattern of SPEI-3 month for the period a)1971-2004, b) 2025-2049, c) 2050-2074, d) 2075-2099. 352

Figure Ap.71 Average number of months with moderate drought of SPI-30 day for the period a)1971-2004, b) 2025-2049, c) 2050-2074, d) 2075-2099. 353

Figure Ap.72 Average number of months with moderate drought of SPI-90 day for the period a)1971-2004, b) 2025-2049, c) 2050-2074, d) 2075-2099. 353

Figure Ap.73 Average number of months with severe drought of SPI-30 day for the period a)1971-2004, b) 2025-2049, c) 2050-2074, d) 2075-2099. 354

Figure Ap.74 Average number of months with severe drought of SPI-90 day for the period a)1971-2004, b) 2025-2049, c) 2050-2074, d) 2075-2099. 354

Figure Ap.75 Average number of months with extreme drought of SPI-30 day for the period a)1971-2004, b) 2025-2049, c) 2050-2074, d) 2075-2099. 355

Figure Ap.76 Average number of months with extreme drought of SPI-90 day for the period a)1971-2004, b) 2025-2049, c) 2050-2074, d) 2075-2099. 355

Figure Ap.77 Average number of months with drought pattern of SPI-30 day for the period a)1971-2004, b) 2025-2049, c) 2050-2074, d) 2075-2099. 356

Figure Ap.78 Average number of months with drought pattern of SPI-90 day for the period a)1971-2004, b) 2025-2049, c) 2050-2074, d) 2075-2099. 356

LIST OF TABLES

Page

Table 1.1 The information of dams and ponds in Küçük Menderes River Basin. 8

Table 1.2 The historical flood events in Küçük Menderes River Basin 9

Table 3.1 Models applied in the study. 25

Table 3.2 Program languages/tools used in the study. 26

Table 3.3 Model performance (Moriasi et al., 2007). 42

Table 3.4 Available drought indices for the study area according to the required data (WMO and GWP, 2016). 57

Table 3.5 Drought classification 58

Table 3.6 The calibration and validation periods of HEC-HMS modeling 79

Table 3.7 Types of data and their respective sources for VIC modeling. 82

Table 3.8 Look-up table for CORINE and IGBP landuse. 84

Table 3.9 Types of data and their respective sources for SWAT modeling 85

Table 3.10 Streamflow stations and observation periods in Küçük Menderes Basin. 87

Table 3.11 Meteorological stations and their observation periods in Küçük Menderes Basin. 88

Table 3.12 Matching land use codes of CORINE and SWAT model 90

Table 3.13 The data and their respective sources for HEC-HMS modeling 91

Table 3.14 Maximum rainfall (mm) with standard duration of Ödemiş Station (17822). 97

Table 3.15. Statistics of daily, monthly, annual precipitation series (mm). 100

Table 3.16 Statistics of daily, monthly, annual mean temperature series (°C). 100

Table 3.17 Statistics of daily, monthly, annual minimum temperature series (°C). 101

Table 3.18 Statistics of daily, monthly, annual maximum temperature series (°C). 102

Table 3.19 Statistics of seasonally precipitation series (mm). 107

Table 3.20 Statistics of seasonally mean temperature series (°C)..... 108

Table 3.21 Statistics of seasonally minimum temperature series (°C)..... 109

Table 3.22 Statistics of seasonally maximum temperature series (°C). 110

Table 3.23 Statistics of observed total monthly precipitation series (mm). 111

Table 3.24 Statistics of observed mean monthly temperature series (°C)..... 112

Table 3.25 Homogeneity test results of total monthly precipitation (mm) and mean monthly temperature (°C) series. 112

Table 3.26 Best fit distributions of total monthly precipitation and mean monthly mean temperature. 116

Table 4.1 Determination of slope classes (%)..... 121

Table 4.2 The sensitive parameters. 129

Table 4.3 The calibration results. 131

Table 4.4 Relevant best parameter values according to calibration and validation. 132

Table 4.5 Homogeneity test results of SPI series. 137

Table 4.6 Homogeneity test results of SPEI series. 138

Table 4.7 The L-moment statistics of regional frequency analysis for annual drought severities derived from SPI-6 month series. 140

Table 4.8 The L-moment statistics of regional frequency analysis for annual drought durations derived from SPI-6 month series. 140

Table 4.9 The correlations between SPI, SPEI and SSFI drought indices. 175

Table 4.10 Maximum rainfall values (mm) observed at standard times. 240

Table 4.11 Maximum rainfall intensity values (mm/hr) observed at standard times. 240

Table 4.12 Parameters of GEV distribution for each duration. 241

Table 4.13 Obtaining instantaneous hyetograph of 24-hour precipitation with 100-year recurrence for Ödemiş Station. 242

Table 4.14 Calibration and validation periods for HEC-HMS modeling. 246

Table 4.15 HEC-HMS model calibration results. 248

Table 4.16 Flood inundation area and rate for Ergenli Basin. 255

Table 4.17 Flood inundation area and rate for Ergenli Basin. 255

Table Ap.1 Annual maximum drought durations and severities for moderate drought conditions for Manisa, İzmir, Kuşadası, Aydın and Salihli Stations (for SPI-1 and SPI-3 month). 321

Table Ap.2 Annual maximum drought durations and severities for moderate drought conditions for Seferihisar, Ödemiş, Sultanhisar, Selçuk and Nazilli Stations (for SPI-1 and SPI-3 month). 322

Table Ap.3 Annual maximum drought durations and severities for moderate drought conditions for Manisa, İzmir, Kuşadası, Aydın and Salihli Stations (for SPI-6 and SPI-12 month). 323

Table Ap.4 Annual maximum drought durations and severities for moderate drought conditions for Seferihisar, Ödemiş, Sultanhisar, Selçuk and Nazilli Stations (for SPI-6 and SPI-12 month). 324

Table Ap.5 Annual maximum drought durations and severities for moderate drought conditions for Manisa, İzmir, Kuşadası, Aydın and Salihli Stations (for SPEI-1 and SPEI-3 month). 325

Table Ap.6 Annual maximum drought durations and severities for moderate drought conditions for Seferihisar, Ödemiş, Sultanhisar, Selçuk and Nazilli Stations (for SPEI-1 and SPEI-3 month). 326

Table Ap.7 Annual maximum drought durations and severities for moderate drought conditions for Manisa, İzmir, Kuşadası, Aydın and Salihli Stations (for SPI-6 and SPI-12 month). 327

Table Ap.8 Annual maximum drought durations and severities for moderate drought conditions for Seferihisar, Ödemiş, Sultanhisar, Selçuk and Nazilli Stations (for SPEI-6 and SPEI-12 month). 328

Table Ap.9 Annual maximum drought durations and severities for severe drought conditions for Manisa, İzmir, Kuşadası, Aydın and Salihli Stations (for SPI-1 and SPI-3 month). 329

Table Ap.10 Annual maximum drought durations and severities for severe drought conditions for Seferihisar, Ödemiş, Sultanhisar, Selçuk and Nazilli Stations (for SPI-1 and SPI-3 month). 330

Table Ap.11 Annual maximum drought durations and severities for severe drought conditions for Manisa, İzmir, Kuşadası, Aydın and Salihli Stations (for SPI-6 and SPI-12 month). 331

Table Ap.12 Annual maximum drought durations and severities for severe drought conditions for Seferihisar, Ödemiş, Sultanhisar, Selçuk and Nazilli Stations (for SPI-6 and SPI-12 month). 332

Table Ap.13 Annual maximum drought durations and severities for severe drought conditions for Manisa, İzmir, Kuşadası, Aydın and Salihli Stations (for SPEI-1 and SPEI-3 month). 333

Table Ap.14 Annual maximum drought durations and severities for severe drought conditions for Seferihisar, Ödemiş, Sultanhisar, Selçuk and Nazilli Stations (for SPEI-1 and SPEI-3 month). 334

Table Ap.15 Annual maximum drought durations and severities for severe drought conditions for Manisa, İzmir, Kuşadası, Aydın and Salihli Stations (for SPEI-6 and SPEI-12 month). 335

Table Ap.16 Annual maximum drought durations and severities for severe drought conditions for Seferihisar, Ödemiş, Sultanhisar, Selçuk and Nazilli Stations (for SPEI-6 and SPEI-12 month). 336

Table Ap.17 Annual maximum drought durations and severities for extreme drought conditions for Manisa, İzmir, Kuşadası, Aydın and Salihli Stations (for SPI-1 and SPI-3 month). 337

Table Ap.18 Annual maximum drought durations and severities for extreme drought conditions for Seferihisar, Ödemiş, Sultanhisar, Selçuk and Nazilli Stations (for SPI-1 and SPI-3 month). 338

Table Ap.19 Annual maximum drought durations and severities for extreme drought conditions for Manisa, İzmir, Kuşadası, Aydın and Salihli Stations (for SPI-6 and SPI-12 month). 339

Table Ap.20 Annual maximum drought durations and severities for extreme drought conditions for Seferihisar, Ödemiş, Sultanhisar, Selçuk and Nazilli Stations (for SPI-6 and SPI-12 month). 340

Table Ap.21 Annual maximum drought durations and severities for extreme drought conditions for Manisa, İzmir, Kuşadası, Aydın and Salihli Stations (for SPEI-1 and SPEI-3 month). 341

Table Ap.22 Annual maximum drought durations and severities for extreme drought conditions for Seferihisar, Ödemiş, Sultanhisar, Selçuk and Nazilli Stations (for SPEI-1 and SPEI-3 month). 342

Table Ap.23 Annual maximum drought durations and severities for extreme drought conditions for Manisa, İzmir, Kuşadası, Aydın and Salihli Stations (for SPEI-6 and SPEI-12 month). 343

Table Ap.24 Annual maximum drought durations and severities for extreme drought conditions for Seferihisar, Ödemiş, Sultanhisar, Selçuk and Nazilli Stations (for SPEI-6 and SPEI-12 month). 344

LIST OF SYMBOLS

Cv	: Coefficient of variation
ET	: Evapotranspiration
ET_a	: Actual evapotranspiration
PET	: Potential Evapotranspiration
CO_2	: Carbon Dioxide
H	: Homogeneous
NH	: Non-homogeneous
L-cv	: L-moment coefficient of variation
L-kurtosis	: L-moment kurtosis
L-skew	: L-moment skewness
Max	: Maximum
Min	: Minimum
Sd	: Standard deviation
Var	: Variance
95PPU	: 95 percentile performance uncertainty
H	: The rate of exchange for the surface energy fluxes
T_s	: Surface temperature
T_r	: Temperature above the surface
ρ	: The air density
c_p	: Specific heat of air
λE	: The latent heat fluxes
e^* (T_s)	: Saturated vapor pressure at Ts
e_r	: Vapor pressure
γ	: Psychrometric constant
r_s	: Surface resistance
P	: Precipitation
E	: Evaporation
R_{surf}	: Surface runoff
$R_{drain:}$	: Subsurface runoff and ground flow

NEE : Net Ecosystem Exchange

Re : Ecosystem respiration

GPP : Gross Primary Productivity

PAR : Photosynthetically active radiation

LAI : Leaf area index

NPP : Net Primary Productivity

SW_t : Final soil water content (mm)

$SW_{0:}$: Initial soil water content (mm)

R_{day} : The amount of precipitation (mm)

Q_{surf} : Surface runoff (mm)

E_a : Evapotranspiration (mm)

w_{seep} : Water entering the vadose zone from the soil profile (mm)

Q_{gw} : Ground flow (mm)

Q : Discharge (m^3/s)

$\sigma_m^{\ 2}$: Variance of the measured data

Qm : Measured discharge (m^3/s)

Qs : Simulated discharge (m^3/s)

PBIAS : Percent BIAS (%)

NSE : Nash-Sutcliffe Efficiency

R^2 : Coefficient of determination

SAE : Absolute errors

SSR : Sum of squared residuals

PE : Percent error in peak

PW-RMSE : Peak-weighted root mean square error objective function

NQ : Number of computed hydrograph ordinates

$q_{o(i)}$: Observed flows (m^3/s)

$q_{s(i)}$: Calculated flows (m^3/s)

$q_{o(peak)}$: Observed peak (m^3/s)

$q_{o(mean)}$: Mean of observed flows (m^3/s)

$q_{s(peak)}$: Calculated peak (m^3/s)

g(x) : Probability density function of gamma distribution

F(x) : Probability distribution function of gamma distribution

$H(x)$	: Cumulative probability of gamma distribution
q	: The probability of zero
z	: Standard random variable
Γ	: Gamma function
α, β	: Shape and scale parameters for gamma distribution.
D_i	: The difference between precipitation and PET at i month
P_i	: Precipitation at i month (mm)
PET_i	: PET at i month (mm)
$f(x)$	: Probability density function of three-parameter log-logistic distribution
α, β, γ	: Scale, shape and origin parameters of log-logistic distribution
$F(x)$	: The probability distribution function of three-parameter log-logistic distribution
w_s	: The probability weighted moments (PWM) of orders
N	: The number of data points
F_i	: The flow rate in time interval (m^3/s)
$\bar{F}$	: The mean of flow series (m^3/s)
σ	: The standard deviation for series
$S_{t,i}$	: Drought severity value
D_i	: Drought duration
α	: Significance level of the test statistic for The Standard Normal Homogeneity Test (SNHT)
n	: The sample size of the test statistic for SNHT
$T(k)$	: The maximum value of the test statistic for SNHT
k	: The first year of the record for SNHT
n	: The last year of the record for SNHT
T_0	: The test statistic for SNHT
S_k^*	: The test statistic for Buishand's test
R	: Rescaled adjusted range for Buishand's test
Q	: The critical value for Buishand's test
Y_i	: Total precipitation value at time i for Buishand's test
$\bar{Y}$	: The mean value for the series for Buishand's test

r_i : The corresponding rank for Pettitt Test

X_k : Pettitt Test statistic

X_E : The maximum of the absolute values of the X_k statistic for Pettitt Test

S : Mann-Kendall test statistic

P : The number of the yi > yj type of pairs for Mann-Kendall test.

M : The number of the yi < yj type of pairs Mann-Kendall test.

z : The standardized test statistic Mann-Kendall test.

p : Z corresponding P-value (p) for the one-tailed test for Mann-Kendall test

σ_s : The standard deviation

x_j and x_i : The values at time j and i (j > i) for Sen's Slope Test

N : The number of slope estimates for Sen's Slope Test

D : Discordancy statistic for Regional Frequency Analysis (RFA)

Ns : The number of measurement stations in the region for RFA

S_{cm} : The sample covariance matrix for RFA

u_l : A vector containing the L-coefficient of variation (t), L-skewness (t_3), and L-kurtosis (t_4) for RFA

u : A vector (3×1) representing the arithmetic average of u_l for the N_s stations for RFA

T_m r : The transposed matrix for RFA

H_k : The heterogeneity measure for RFA

Ns : The variables in consideration measure for RFA

Nj : The record length at station j measure for RFA

ZDIST : Goodness-of-Fit Statistic

Z : The statistical distribution with the smallest absolute value

t_4^{-R} : The regional average L-kurtosis

σ_{t_4} : The standard deviation of t_4^{-R}

t_4^{dist} : The L-kurtosis of a fitted distribution

F(x) : The cumulative distribution function

μ and σ : Scale and location parameters for Generalized Logistic distribution

ξ, μ and σ	: Shape, location, and scale parameters for Generalized Extreme Value
μ and σ	: The mean of logarithmic values and Standard deviation for Lognormal
Γ and γ	: The upper and lower incomplete gamma function for Pearson Type III
μ, σ and ξ	: Shape, location, and scale parameters for Generalized Pareto
Q	: Discharge (m^3/s) for obtaining flow rating curve equation
h	: Flow depth (m) for flow rating curve equation
h_0	: Flow depth (m) at zero flow for flow rating curve equation
K and n	: The constants for flow rating curve equation
i_{ave}	: The average rainfall intensity (mm/hour)
T	: The recurrence interval (year)
a, b and c	: The coefficients that vary with location and return for IDF curve
d	: The duration of rainfall (hour) for IDF curve

ABBREVIATIONS

1D	: One-dimensional
2D	: Two-dimensional
3D	: Three-dimensional
AED	: Atmospheric Evaporative Demand
AEP	: Annual Exceedence Probability
AFAD	: Disaster and Emergency Management Presidency
AI	: Aridity Index
AR6	: The Sixth Assessment Report of the United Nations (UN) Intergovernmental Panel on Climate Change (IPCC)
ARI	: Average recurrence interval
ASCE	: American Society of Civil Engineers
CESM	: Community Earths System Model
CFD	: Computational Fluid Dynamics
CLHMS	: Coupled Land Surface and Hydrology Model System
CLM	: Community Land Model
CMI	: Crop Moisture Index
CMIP5	: Coupled Model Intercomparison Project Phase 5
CNRM-CM	: Centre National de Recherches Météorologiques - Climate Model
CORINE	: Coordination of Information on the Environment
DEM	: Digital Elevation Model
DHI	: Danish Hydraulic Institute
DRI	: Drought Reconnaissance Index
DRTR	: Dominant River Tracing based Routing
DSİ	: General Directorate of State Hydraulic Works
DSS	: Data Storage System
ECMWF	: European Centre for Medium-Range Weather Forecasts
EDI	: Effective Drought Index
EEA	: European Environment Agency
EFA	: European Flood Awareness System

Et_a–bucket	: Eta model with a bucket-type land surface scheme
Et_a–SSiB	: Eta coupled SSiB model
FHI	: Flooding Hazard Index
FLO-2D	: Two-Dimensional Flood Routing Model
GCM	: Global Circulation Model
GEV	: Generalized Extreme Value
GFDDR	: Global Facility for Disaster Reduction and Recovery
GHG	: Greenhouse Gas
GIS	: Geographical Information System
GLUE	: Generalized Likelihood Uncertainty Technique
GUI	: Graphical User Interface
GWP	: Global Water Partnership
HADGEM2-ES	: Hadley Centre Global Environment Model 2 - Earth System
HBV	: Hydrologiska Byråns Vattenbalansavdelning
HEC-DSS	: Hydrologic Engineering Center - Data Storage System
HEC-GeoHMS	: Hydrologic Engineering Center - Geospatial Hydrologic Modeling System.
HEC-HMS	: Hydrologic Engineering Center - Hydrologic Modeling System
HEC-RAS	: Hydrologic Engineering Center's River Analysis System
HRU	: Hydrological Response Unit
HTESSEL	: Hydrology Tiled ECMWF Scheme for Surface Exchanges over Land
HyMAP	: Hydrological Modeling and Analysis Platform
HWSD	: Harmonized World Soil Database
ICLEI	: International Council for Local Environmental Initiatives
IDF	: Intensity-Duration-Frequency
IDNDR	: International Decade for Natural Disaster Reduction
IDW	: Inverse Distance Method
IGBP	: International Geosphere–Biosphere Programme
IPCC	: International Panel on Climate Change
ISRIC	: International Soil Reference and Information Centre
İKLİM RİSK	: İKLİM değişikliği etkisinde sürdürülebilir su yönetimi için

hidrolojik RİSKler ve su kalitesi değişimi

JULES : The Joint UK Land Environment Simulator

LAI : Leaf Area Index

LDAS : Land Data Assimilation System

LSM : Land Surface Model

MCMC : Monte Carlo Markov Chain

MGM : Turkish State Meteorological Service

MIKE SHE : MIKE Système Hydrologique Européen

MK : Mann Kendall Test

MNS : The Modified Nasch-Sutcliffe Efficiency

MOSART : Model for Scale Adaptive River Transport

MPI-ESM-MR : Max Planck Institute for Meteorology Earth System Model with Middle Resolution

NASA : National Aeronautics and Space Administration

NCAR : National Center for Atmospheric Research

NCEI : National Centers for Environmental Information

NCEP : National Centers for Environmental Prediction/

NDI : NOAA Drought Index

NDVI : Normalized Difference Vegetation Index

NetCDF : Network Common Data Form

NNRP : NCEP/NCAR 40-year Reanalysis Project

Noah-MP LSM : Noah Multi-Physics Land Surface Model

NSE : Nash-Sutcliffe Model Efficiency Coefficient

NSW : New South Wales

ORCHIDEE : Regulating Carbon and Hydrology in Dynamic Ecosystems

ParaSol : Parameter Solution

PBIAS : Percent Bias

PDSI : Palmer Drought Severity Index

PHDI : Palmer Hydrological Drought Severity Index

PRECIS : Providing REgional Climate Information for Impact and Studies.

PSO : Particle Swarm Optimization

PWM : Probability Weighted Moment

PW-RMSE : Peak-Weighted Root Mean Square Error
RAI : Rainfall Anomaly Index
RCM : Regional Climate Model
RCP : Representative Concentration Pathway
RegCM4.3 : Regional Climate Model version 4.3
SAE : Sum of Absolute Errors
SAI : Standardized Anomaly Index
Sc-PDSI : Self-Calibrated Palmer Drought Severity Index
SCS : Soil Conservation Service
SCS-CN : Soil Conservation Service Curve Number
SCS-UH : Soil Conservation Service Unit Hydrograph
SDGs : Sustainable Development Goals
SDI : Streamflow Drought Index
SSiB : Simple Biosphere Model
SMA : Soil Moisture Anomaly
SMI : Soil Moisture Index
SNHT : Standard Normal Homogeneity Test
SPEI : Standardized Precipitation-Evapotranspiration Index
SRI : Standardized Runoff Index
SSFI : Standardized Streamflow Index
SSR : Sum of Squared Residuals
SUFI2 : Sequential Uncertainty Fitting Algorithm
SWAT : Soil and Water Assessment Tool
SWAT-CUP : SWAT Calibration and Uncertainty Programs
SWIM : Soil and Water Integrated Model
SWMM : Storm Water Management Model
SYGM : General Directorate of Water Management
TABB : Türkiye Disaster Data Bank
TARAP : Türkiye Disaster Risk Reduction Plan
TOPMODEL : Topographic Kinematic Wave Model
TUBITAK : Scientific and Technological Research Council of Turkey
TUFLOW : Two-Dimensional Unsteady Flow

UNDRR	: United Nations Office for Disaster Risk Reduction
U.S	: United States
VIC	: Variable Infiltration Capacity
WGEN	: Weather Generator
WET	: Water Ecosystems Tool
WMO	: World Meteorological Organization
WRF	: Weather Research and Forecasting

CHAPTER ONE
INTRODUCTION

Over half of the world's population lives in cities, serving as economic powerhouses and a tangible representation of their heritage. Insufficient infrastructural services, environmental degradation, and climate change can give rise to new risks in urban areas. Cities are significant for the overall welfare and security of humans, particularly in consideration of the growing occurrence of extreme weather phenomena, natural disasters, etc. Therefore, resilience is of greatest significance and smart city programs include technology elements into the process of urban development (Xiong et al.,2022).

Based to the AR6 Synthesis Report: Climate Change 2023 (International Panel on Climate Change [IPCC], 2023), climate change is expected to rapidly increase by around 1.5°C in the near future (2021-2040), which would pose substantial dangers to ecosystems and the well-being of humans. Although short-term measures might mitigate anticipated losses, total eradication remains unattainable. From 2041 to 2100, the anticipated consequences of climate change are poised to present numerous threats to both natural ecosystems and human societies, with the intensity of adverse effects projected to escalate alongside the acceleration of global warming (Türkeş, 2022).

Human-induced climate change refers to a substantial modification in Earth's climate system caused by human activities that disrupt the planet's energy balance, impact natural geography, and involve deforestation (Türkeş, 2022).

Based on the IPCC (2022) report, adaptation in human systems refers to the act of adjusting to the present or anticipated climate conditions and their effects, with the aim of minimizing harm or capitalizing on advantageous circumstances. Adaptation is a crucial consideration that should be taken into account from the outset and throughout every phase of a sustainable development process (Türkeş, 2022). In relation to the IPCC (2012), disaster risk refers to the possibility of significant disruptions in the regular functioning of a community or society over a prolonged period of time. These

disruptions are caused by catastrophic physical events, resulting in widespread negative consequences such as loss of life, damage to property and the economy, and environmental impacts.

Both developed and developing nations have seen the impact of water-related disasters, with quickly expanding middle-income countries being particularly vulnerable to these risks. International Council for Local Environmental Initiatives (ICLEI) (2023) reported that 2023 was the hottest year on record worldwide. As a result of these unusually high global temperatures, India experienced heatwaves in April that resulted in the loss of 300 lives. Additionally, in June, catastrophic floods along the Yangtze River in China caused the death of over 280 individuals. Developing nations are increasingly experiencing significant damages from extreme floods, droughts, and storms as a result of the ongoing global climate change. By 2030, the number of individuals living in poverty and susceptible to weather-related incidents in sub-Saharan Africa and South Asia might reach 325 million (The World Bank and Global Facility for Disaster Reduction and Recovery [GFDDR], 2013).

The potential disasters in Türkiye mostly encompass earthquakes, droughts, torrential rain and floods, landslides, rockfalls, forest fires, industrial explosions and fires, severe temperatures, wind and snowstorms, avalanches, heatwaves, and fog (World Meteorological Organization [WMO], 2012). Urbanization and climate change increase water-related hazards, including shortage or excessive (droughts or floods).

Climate conditions and land-use patterns can be considered as two major drivers contributing to variations of the hydrological cycle. Therefore, knowledge on how the hydrological regime and water resources will be affected by climate variability and change, and by changes in land-use composition, is important for creating reliable adaptation strategies in water management (Krysanova & White, 2015).

Droughts and floods are hydrological disasters that pose a significant risk to several environmental elements, including agriculture, vegetation, animals, and local economies. Increases in vulnerability to these disasters is a result of expanding

exposure. Recent climate variability, and change seems to have adversely affected flood and drought hazard in several areas and this tendency is likely to continue (Kundzewicz et al., 2001).

The IPCC's Sixth Assessment Report provides a precise definition of drought as a transient period characterized by insufficient water supply due to causes such as reduced precipitation, increased temperatures, and wind, and causes water scarcity and aridity (Rossi et al., 2023; United Nations Office for Disaster Risk Reduction [UNDRR], 2021; Van Loon et al., 2016). Human activities like increased abstractions can exacerbate shortages. The consequences of drought on social-ecological systems can be both direct and indirect. The direct consequences encompass reductions in crop yields and increases in unemployment, whilst the indirect consequences arise from the effects on economic sectors and societal difficulties. Agriculture, namely the cultivation of crops and rearing of animals, is extremely vulnerable, resulting in substantial decreases in agricultural productivity. In 2022, European crops experienced up to a 21% yield reduction compared to the 5-year average due to drought. Agriculture losses contribute over 50% of total drought losses in Europe, with the Mediterranean region facing the highest share (Rossi et al., 2023).

Floods are natural occurrences in which water covers area that is typically arid, typically caused by weather patterns that produce a substantial quantity of precipitation. The chance of a flood occurring is determined by its relative severity, which is measured in terms of the annual exceedance probability (AEP) or the average recurrence interval (ARI) of the flood. These phrases quantify the probability of a flood of a specific size being attained or exceeded in a particular year (New South Wales (NSW) Department of Planning and Environment, 2023). Primary effects of floods include loss of life, property destruction, and environmental harm. They affect towns, industrial centers, and agricultural areas. Indirect effects include economic losses, social divisions, decreased production capacity, and increased unemployment. From 1986 to 2006, Europe experienced €100 billion in flood damage (General Directorate of Water Management [SYGM], 2017).

The concept of smart cities, which evolved in 1990, involves the integration of information and communication technologies with existing infrastructure to monitor urban resources in real-time (Xiong et al.,2022). This integration aims to improve competitiveness and promote urban safety. Resilience, as defined by the IPCC (2012), refers to the capacity of a system and its components to anticipate, absorb, adapt to, or recover from the impacts of a hazardous event in a timely and efficient manner. This includes ensuring the protection, restoration, or enhancement of its fundamental structures and functions. A 'Resilient City' is capable of withstanding and recovering from any shocking or prolonged disturbance, while preserving its fundamental operations, structures, and character, and also adjusting and prospering in the midst of ongoing transformation (ICLEI, 2015).

According to the World Bank and GFDDR (2013), climate and disaster resilient development refers to a collection of organizational structures, procedures, and tools that aid in recognizing the hazards posed by disasters, extreme climate events, gradual and long-term climate changes, as well as their resulting effects. It also involves devising strategies to minimize, transfer, and prepare for these risks. By employing a comprehensive strategy that involves several sectors and stakeholders, climate and disaster resilient development effectively decreases vulnerability both in the short and long term. Disaster risk reduction, in essence, has four primary objectives: hazard identification, risk assessment, risk control, and risk control evaluation (Tatar, 2020).

The concept of disaster resilience has become increasingly important in recent years, with global endeavors concentrated on reducing disaster risks. The significance of disaster prevention, risk reduction, and preparedness, especially for vulnerable groups, was underscored by initiatives such as the International Decade for Natural Disaster Reduction (IDNDR) and the Yokohama Strategy. The Millennium Development Goals, the Hyogo Framework, and the Sendai Framework have enhanced the incorporation of disaster risk reduction into sustainable development, poverty reduction, and good governance programs. The Sustainable Development Goals (SDGs) and the Paris Agreement emphasize the interdependence of catastrophe risk reduction, resilience, and climate change adaptation. The New Urban Agenda

outlined by HABITAT III (United Nations, 2017) envisions cities that possess resilience against catastrophes, inclusivity, and compatibility with climate change. The primary objective of these international frameworks is to establish societies that are capable of withstanding disasters and to advance sustainable development (Şen, 2021).

The integration of smart and resilient city concepts attempts to overcome challenges and reduce disaster-related problems. Smart cities prioritize the optimization of resources and processes, whereas resilient cities strengthen their ability to forecast and make decisions regarding disasters (Xiong et al.,2022).

Türkiye focuses significance on several agreements and research pertaining to disaster resilience. Türkiye, committed to the Sendai Framework, prioritizes disaster risk reduction. The 2017 readiness report underscores hazard monitoring, categorization, and data collection, covering geophysical, meteorological, hydrological, climatological, technological, environmental, and man-made hazards. Türkiye actively manages a comprehensive disaster database known as the Türkiye Disaster Data Bank (TABB) created by Disaster and Emergency Management Presidency (AFAD) (Erkan & Hasgül, 2015) and is engaged in urban transformation initiatives. Additionally, there is an upcoming "Spatial Strategy Plan" aimed at effectively addressing settlements in light of natural hazards. (Tatar, 2020).

Türkiye Disaster Risk Reduction Plan (TARAP) (AFAD, 2022) is a sustainable plan and covering the years 2022 and 2030, defining the activities to be carried out before disasters in order to minimize disaster risks within a process together with the responsible parties and responsibilities.

The risk assessments and disaster action plans are included in the Küçük Menderes Basin Drought Management Plan (SYGM, 2018a) and Küçük Menderes River Basin Flood Management Plan (SYGM, 2019).

1.1 Study Area

The Küçük Menderes Basin is situated in western Türkiye, positioned between the Büyük Menderes and Gediz Basins (see Figure 1.1). The administrative boundary of the basin is defined by the General Directorate of State Hydraulic Works. The primary river within this basin is the Küçük Menderes River, accompanied by several individual creeks that directly flow into the Aegean Sea, including Tahtalı and Ilıca Creeks, among others. The wetlands in the basin are the Çakal and Gebekirse Lakes, which are the alluvial-set lakes at the downstream, and Belevi and Gölcük Lakes. The drainage area of Küçük Menderes Basin is about 6907 km^2. The basin contains the lands, from İzmir as 95.35%, from Aydın as 3.88% and from Manisa 0.77%. The study area was selected as Küçük Menderes River Basin which is subbasin of Küçük Menderes Basin (Figure 1.1). Küçük Menderes River Basin is located between the geographical coordinates of 38°14'31.90"N-28°29'18.26"E and 37°57'44.50"N - 27°16'12.67"E. Spanning a flowpath of approximately 129 km, the river covers a drainage area of around 3450 km^2.

Küçük Menderes River Basin is within the borders of Izmir province and a very small part of it is included in Manisa borders. The river basin includes Kiraz, Beydağ, Ödemiş, Tire, Bayındır, and Torbalı; and Kiraz and Beydağ are upstream and Selçuk is downstream. There are many tributary creeks which flow to Küçük Menderes River, such as Fetrek, Uladı, Ilıca, Falaka, Aktaş, Rahmanlar, Kiraz and Pirinççi, etc. According to the 2018 data of CORINE (Coordination of Information on the Environment) database developed by the European Environment Agency (EEA), 58.6% of the basin consists of agricultural areas, 20.3% of pastures and 16% of forest areas (Figure 1.1).

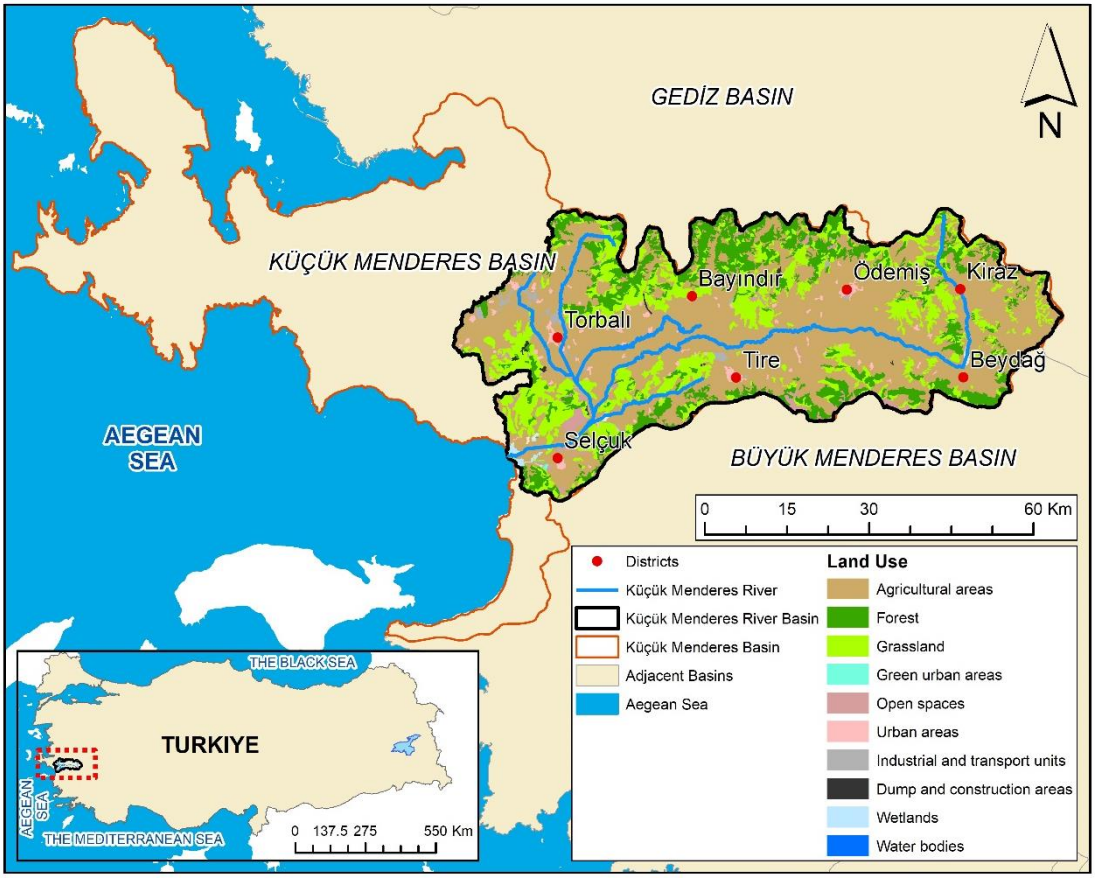


Figure 1.1 Küçük Menderes Basin location map.

As outlined in the Küçük Menderes River Basin Management Plan (SYGM, 2018b), the basin is predominantly characterized by intensive agricultural and animal husbandry activities. In 2016, the crop production value revealed a distribution with 29.4% attributed to fruit products, 13.1% to field products, 10.7% to vegetable products, and 1.5% to ornamental plants. Figure 1.2 illustrates the dams and ponds within the Küçük Menderes Basin, and Table 1.1 provides a summary of these water bodies. Additionally, Figure 1.2 highlights the meteorological and streamflow stations that have sufficient observational data.

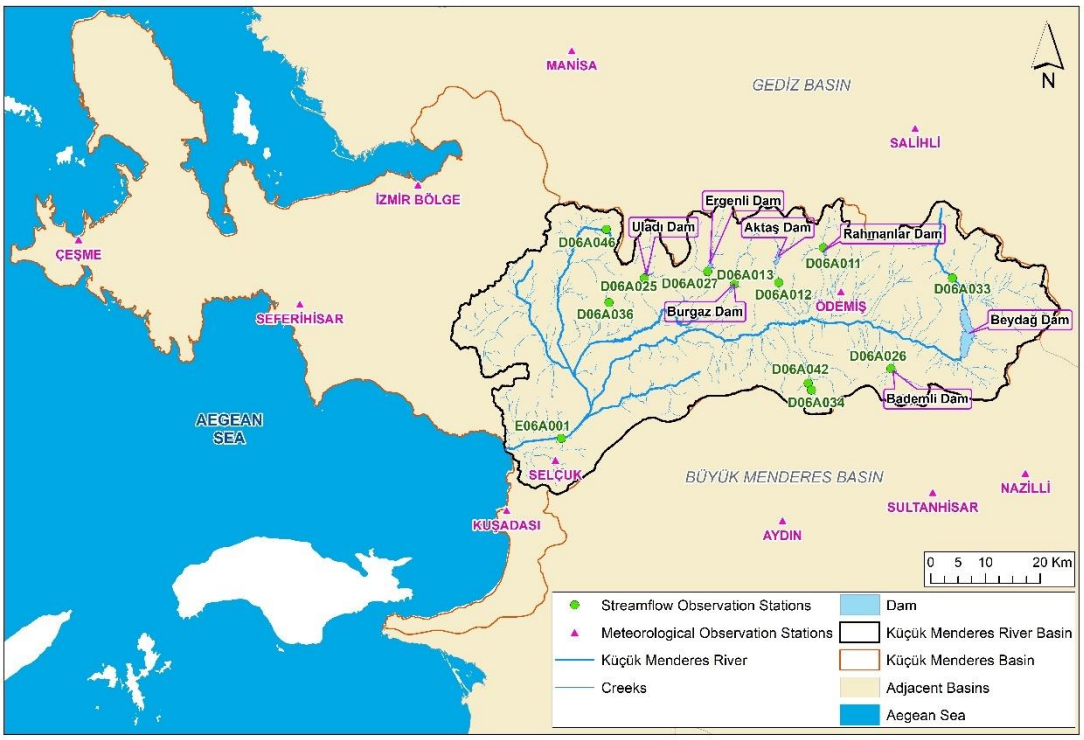


Figure 1.2 The meteorological and streamflow observation stations, and dams in Küçük Menderes River Basin.

Table 1.1 The information of dams and ponds in Küçük Menderes River Basin.

District	***Dam/Pond***	***Purpose of Construction***	***Status***	***Construction Start***	***Construction End***
Bayındır	Burgaz (Zeytinova) Dam	Irrigation	In operation	23.03.2011	21.09.2015
Kiraz	Çatak Pond	Irrigation	In operation	09.03.2012	05.12.2014
Kiraz	Haliller Pond	Irrigation	In operation	17.04.2013	23.10.2014
Ödemiş	Aktaş Dam	Irrigation	In operation	30.12.2011	30.06.2017
Ödemiş	Bademli Dam	Irrigation	In operation	15.04.2011	31.12.2015
Ödemiş	Beydağ Dam	Irrigation	In operation	01.01.1993	05.04.2009
Tire	Eskioba Pond	Irrigation	In operation	29.08.2013	04.05.2015
Tire	Yenişehir Pond	Irrigation	In operation	01.01.2011	24.04.2014
Torbalı	Karakızlar Pond	Irrigation	In operation	21.03.2013	19.10.2014
Bayındır	Ergenli Dam	Irrigation	Under construction	15.07.2014	-
Beydağ	Ovacık Pond	Irrigation	Under construction	06.10.2017	-
Kemalpaşa	Akalan Pond	Irrigation	Under construction	30.10.2017	-
Ödemiş	Rahmanlar Dam	Irrigation, drinking and potable water	Under construction	20.11.2013	-
Tire	Dereli Pond	Irrigation	Under construction	13.10.2017	-

The General Directorate of Water Management (SYGM, 2018) identified historical dry years in the Küçük Menderes Basin as 1985, 1989-1993, 1999-2001, 2004-2005, and 2007-2008, utilizing various drought indices for the period 1981-2016. Table 1.2 presents historical flood events obtained from the State Hydraulic Works (DSİ). According to the Küçük Menderes Basin Flood Management Plan Report (SYGM, 2019), the Bayındır district center is identified as a high-risk area for floods.

Table 1.2 The historical flood events in Küçük Menderes River Basin

Date	Location	Stream	Life Loss
8/24/1956	Ödemiş Kaymakçı	Çınarlı Creek	0
12/28/1960	Ödemiş, Bayındır, Selçuk	Tombaklı, Ergenli, Uladı, Ağzıaçık Creeks	0
5/30/1963	Ödemiş Çaylı	Gavuröldü Creek	0
2/8/1974	Selçuk, Ödemiş, Beydağ	Küçük Menderes River	7
6/4/1974	Ödemiş	Ödemiş Zeytinlik Creek	4
5/12/1976	Ödemiş	Gelinboz Creek	4
1/31/1978	İzmir	Küçük Menderes River	0
1/8/1981	İzmir	Küçük Menderes River	0
12/14/1981	İzmir	Küçük Menderes River	0
1/21/1998	İzmir	Küçük Menderes River	0
5/30/2005	Kiraz	Kiraz Stream	0
6/1/2005	Tire	Eğridere Stream	0
2/6/2006	Kiraz	Haliller Stream	0
12/5/2007	Ödemiş, Kiraz, Sarıkaya	Genev (Zeytinlik) Creek, Birgi Creek and Uluçay Creek	0
10/3/2008	Kiraz	Kısık, Karaburç and Uluçay Creeks	0
1/26/2012	Tire, Ödemiş	Küçük Menderes River, Taş Creek	0
1/26/2013	Ödemiş	Bakırçay River, K.Menderes River	0
12/31/2014	Ödemiş	Gönen Stream, Birgi Creek	0
9/21/2016	Ödemiş, İlkkurşun	Dry stream	0
5/22/2017	Kiraz, Çayağzı	Uluçay Creek	0
1/5/2018	Ödemiş, Karadoğan	Village stream	0
11/1/2019	Tire-Büyükkale and Halkapınar, Torbalı-Yeniköy, Çaybaşı and Sağlık, Bayındır- Hasköy	Village Streams, Vişneli Stream, Küçük Menderes old riverbed	0

1.2 Purpose & Scope

The objective of this study is to assess prospective flood and drought scenarios within the Küçük Menderes River Basin by employing a combination of land surface models and hydrological models. The aim is to leverage the findings from these analyses to develop cities that are resilient to climate change and better equipped to withstand disasters. The significance of this study lies in the semi-arid climate of the Küçük Menderes River Basin, where agriculture plays a predominant role. Given the region's vulnerability to climate change, particularly concerning agricultural irrigation, it becomes crucial to implement measures and basin-wide strategies for effective flood and drought management. Modeling studies play a pivotal role in identifying disaster hazards, assessing impact areas based on future projections, and conducting more detailed risk assessments, leading to the development of comprehensive action plans. Within the scope of the study, Küçük Menderes Basin was analyzed using a coupled land surface model (the Variable Infiltration Capacity (VIC) model) and a hydrological model (the Soil and Water Assessment Tool (SWAT) Model). The models were calibrated and validated in selected periods and drought analyses for the period 2025-2099 were made using indices using future climate model outputs. Drought maps were derived and drought intensity, duration and magnitude for the future period were given on micro-basin basis. Drought analyses were also performed using observed data and grid-based climate data around the basin. By using coupled the VIC model and Hydrologic Engineering Center's Hydrologic Modeling System (HEC- HMS), flood modelling was performed for the calibration and validation periods, basin parameters were obtained, and future flood hydrographs were calculated. With the use of the Hydrologic Engineering Center's River Analysis System (HEC-RAS) hydraulic model, future flood propagation maps, depth and velocity maps were created, and the effect of flooding was revealed spatially. The results obtained as a result of flood and drought studies will form a ready database to be used as a basis for risk assessments and action plans to build resilience against climate and disasters. This study contributes to climate and disaster resilience by coupling land surface modeling with hydrological models to simulate droughts and floods under various scenarios. In addition, SPI values were calculated as daily and grid using climate data. There is no comparable study conducted in Turkey, making this study distinct and unique.

CHAPTER TWO
PREVIOUS STUDIES

2.1 Reports on Küçük Menderes Basin

In the "Impact of Climate Change on Water Resources Project" report (SYGM, 2016), climate models including HADGEM2-ES, MPI-ESM-MR, and CNRM-CM5.1, along with scenarios RCP4.5 and RCP8.5, were employed to analyze changes for the period 2015-2100 at a 10x10 km scale (refer to Figure 9). Hydrological variables were projected until the year 2100 on the scale of the drainage areas determined in the basin by using temperature and precipitation projections. The SWAT hydrological model was employed to generate key values such as surface runoff, soil moisture, and evapotranspiration. The runoff values produced by the hydrological model were converted to runoff and water level values along the deterministic river system with hydraulic modeling studies (Figure 10). According to the results of all three global climate models in the Küçük Menderes Basin, the average temperature values were projected to increase. Considering all models and scenarios, it is expected that temperatures will rise above 2°C after 2050 and the highest temperature increase will be seen in 2091-2100 period with the results up to 5.2° C. Considering the overall rainfall projections for the Küçük Menderes Basin, it is noteworthy that the projected reductions in the second half of the projection period have intensified and a reduction of 25%.

In the Küçük Menderes River Basin Management Plan (SYGM, 2018), within the scope of the "Impact of Climate Change on Water Resources" project, simulations suitable for today's conditions were carried out by integrating the RegCM4.3 regional climate model with HadGEM2-ES, MPI-ESM-MR and CNRM-CM5.1 ground system models. These simulations were carried out to cover the period 2015-2100 based on the 1971-2000 reference period and RCP4.5 and RCP8.5 scenarios. Temperature values throughout the basin are above the average of Türkiye, and especially the number of consecutive dry days is significantly above the average of Türkiye (between 99 days and 75 days). Modelling in the Küçük Menderes Basin predicts an increase in

temperatures above 2°C after 2050 and indicates that the highest temperature increase can reach up to 5.3°C in the period 2091-2100. According to precipitation projections, when all scenario results are brought together, it is observed that the precipitation decreases predicted in the second half of the projection period are intensified and a decrease of up to 25% is expected in general. Precipitation deficiency values in the basin tend to increase from the coast to inland.

In the "Küçük Menderes Basin Drought Management Plan (SYGM, 2018), dry periods were determined as 1985, 1989, 1990, 1991, 1992, 1993, 1999, 2000, 2001, 2004, 2005, 2007 and 2008 using various drought indices for 1981 - 2016. Drought severity and drought risk maps were created. The outputs of three global models selected from the CMIP5 archive (HadGEM2-ES, MPI-ESM-MR and CNRM-CM5.1) and 2 current climate scenarios (RCP4.5 and RCP8.5 emission scenarios), which are the most widely applied and accepted in the literature, and RegCM4.3 regional climate model were run at 10x10 km resolution. The differences of the analyzed parameters until 2100 according to the reference period, which is accepted as the simulations of 1971-2000, were calculated monthly. In the "Water Budget Studies" report, the basin was modelled using the Hydrologiska Byråns Vattenbalansavdelning (HBV) model (Bergström, 1976). According to RCP 4.5 and RCP 8.5 scenarios for the future period, a decreasing trend is observed in river flows for the period 2018-2100. According to the "Sectoral Vulnerability Analyses, Measures and Action Plan", drought vulnerability of the sectors was explained, and an emergency action plan was prepared.

The Flood Management Plan for the Küçük Menderes River Basin (SYGM, 2019) included hydrological and hydraulic modeling of the basin. Three distinct scenarios were utilized to develop flood hazard maps and risk maps for the basin. The hydrographs generated for return periods of 50, 100, and 500 years are used as boundary values for flood modeling in these situations. The outcomes of these research ascertain the peril and vulnerability scenarios in various sections of the basin, predicated on flood levels. The "Flood Hazard Maps and Flood Risk Maps" developed offer valuable insights into the vulnerable locations. By evaluating these maps, specific regions with a high risk of flooding may be identified, allowing for the determination

of objectives aimed at lowering flood risk in such areas. Consequently, steps are established to be executed prior to, during, and after floods, comprising thorough preparatory endeavors.

The İKLİM RİSK Project (2021), funded by TÜBİTAK (The Scientific and Technological Research Council of Türkiye), aims to evaluate hydrological and water quality variations in the context of sustainable water management, considering the influences of both land-use modifications and climate change. As per the project findings, the MPI-ESM-MR model anticipates an escalation in temperatures within the Küçük Menderes Basin under the RCP8.5 scenario. Throughout the period spanning from 2020 to 2049, there is a notable upsurge in average temperatures across all seasons, with the most pronounced elevation observed during the summer months. Projections extend beyond 2050, indicating a substantial continuation of temperature increases.

Specifically, the project outlines projections indicating an average summer temperature increase of approximately 1.6ºC (2020-2049), 3.4ºC (2050-2079), and 5.1ºC (2080-2100) within the Küçük Menderes Basin under the RCP8.5 scenario. In terms of precipitation, the model forecasts an increase in autumn rainfall (around 0.6 mm/day as the regional average) from 2020 to 2049, coupled with a decrease in summer precipitation (approximately 1 mm/day). Moving into the period 2080-2100, a further decline (up to 3 mm/day) in summer precipitation is anticipated, alongside an average increase of 1.2 mm/day in autumn precipitation across the region.

The hydrological and water quality modeling studies in the project employed the SWAT (Soil and Water Assessment Tools) model. The outcome of model runs, conducted under various scenarios for reference and future periods (short term: 2025-2050, medium term: 2050-2075, and long term: 2075-2100), were meticulously evaluated. Combining the effects of land use and climate scenarios revealed a decrease in monthly average flows during the scenario periods compared to the reference period. Flows at the basin outlet are projected to decrease by 2 percent in the near term and more than 80 percent in the long term.

2.2 Research Involving Land Surface and Hydrological Models

Xue et al. (2001) conducted a comparison between two models, Eta–SSiB and Eta–bucket, in their ability to simulate soil moisture. Eta–SSiB utilized soil moisture data from the NCEP/NCAR 40-year Reanalysis Project (NNRP), whereas Eta–bucket depended on a calibrated fixed field of starting soil moisture with an annual average. Further simulations were carried out using the Eta-bucket model started with NNRP soil wetness. The findings demonstrated that, although the starting soil moisture levels were identical, there were still discernible disparities between Eta–SSiB and Eta–bucket. This implied that the enhanced vegetation representation in SSiB had a role in improving the overall simulation.

Gosain et al. (2006) assessed water availability in 12 river basins using SWAT, considering natural conditions. They simulated present (1981-2000) and future (2041-2060) periods with a GHG climate scenario, predicting heightened droughts in Krishna and increased floods in Mahanadi. The basins were divided into 21 sub-basins, and annual precipitation, evapotranspiration, and water yield were simulated. Soil Moisture Index (SMI) was used for drought analysis in Krishna, indicating increased soil moisture deficit in the GHG scenario. Mahanadi is projected to receive more rainfall, leading to higher evapotranspiration and water yield. Flood analysis for a severely affected sub-basin revealed an expected increase in flood peaks, posing a risk to structures.

Bakir & Xingnan (2008) critically examined the application of HEC-GeoHMS, an extension of ArcView in HEC-HMS, designed for rainfall-runoff simulation. They compared its performance with the Xinanjiang conceptual model using historical flood data from the Wanjiabu catchment in China. The study simulated runoff hydrographs with both models, and the results indicated that HEC-HMS was more convenient for flood simulation. It offered advantages in optimizing parameters, provided precipitation specification options, loss models, direct runoff and hydrologic routing models, and included a calibration optimization package.

Pappenberger et al. (2012) The study utilizes the Hydrology Tiled ECMWF Scheme of Surface Exchanges over Land (HTESSEL) and the river routing CaMa-Flood approach. The flow technique automatically adjusts parameters such as channel length, surface altitude, distance to downstream cell, catchment area, and elevation profile to appropriate scales. In addition, the calculation of river water storage and related characteristics such as riverbed slope necessitates the inclusion of channel width and bank height.

Narsimlu et al. (2013) employed the SWAT model to simulate water resources in the Upper Sind River basin. Using the SUFI-2 program for calibration and uncertainty analysis, they utilized the PRECIS Regional Climate Model for IPCC A1B scenarios. The basin was divided into 15 subbasins and 168 Hydrological Response Units. Evaluation metrics included correlation coefficients and efficiency measures. The study identified surface runoff, groundwater, and soil properties as sensitive parameters. Projections indicated a potential increase in average annual stream flow during the midcentury and end century periods, suggesting possible extreme flood and drought events due to climate change.

Trambauer et al. (2013) conducted a comparison of various models to identify an effective combination for studying drought in semi-arid sub-Saharan Africa. They established a framework for selecting models for hydrological drought prediction, organizing them into a vein diagram. Among the models considered, SWAT model as the most suitable for drought studies in the region.

Xu et al. (2013) explored the potential impact of climate change on the hydrology of the Qiantang River Basin for the period 2011–2100 using the Soil Water Assessment Tool (SWAT). They employed the Inverse Distance Method (IDW) to predict data for ungauged locations and then they downscaled monthly data to daily data. Sensitivity analysis, including Latin Hypercube Sampling and One-Factor-At-A-Time were conducted. Calibration was performed assessing model performance with Nash-Sutcliffe efficiency coefficient and Relative BIAS. Calibration and validation were performed for specific periods, and subbasins were calibrated using three

hydrological stations. The SWAT model was run with future projections under different scenarios. A2 scenario showed the highest temperature change, particularly for the period 2071-2100.

Min et al. (2014) evaluated the efficacy of two hydrological models, CLHMS and LSX-HMS, in replicating flood phenomena in the Huaihe River Basin during periods of intense water flow in 2003 and 2007. The CLHMS model provided correct predictions of both the maximum intensity and time of the peak, but the LSX-HMS model exhibited a delayed flood peak. The CLHMS model utilized a two-way coupling approach, which considered the exchange of water between groundwater and soil layers. Additionally, it was enhanced by incorporating spatial variations in important parameters and a sub-grid direct surface runoff scheme. Both models employed characteristics such as soil texture, plant type, and hydrologic and hydrogeological parameters. The CLHMS simulations exhibited a strong correlation with observed hydrographs, surpassing the performance of LSX-HMS.

Chaney et al. (2015) provides a thorough assessment of land surface modeling for monitoring global flood and drought events. The study also proposes strategies to address the difficulties caused by unclear parameters.

Huang et al. (2015) assessed climate scenarios for flood and drought projections in five river basins (upper Danube, Elbe, Ems, Rhine, and Weser) using the SWIM model. They successfully reproduced daily discharge data and evaluated SWIM's performance for 10 and 50-year flood discharge. Flood and low-flow frequency curves were obtained, and RCM simulations were used to calculate 50-year deficit volumes and floods. Results indicated an escalating trend of floods in the Elbe basin, a heightened occurrence of droughts in the Rhine basin for the period 2061–2100, and the Inn basin facing more intense floods and less frequent drought events.

Kauffeldt et al. (2015) conducted a technical review of 24 large-scale models to aid in selecting a suitable model for the European Flood Awareness System (EFAS) at a continental scale. The assessment considered factors such as model code availability,

existing user community, grid structure flexibility, calibration possibilities, resolution flexibility, input data requirements, data assimilation, and existing large domain model set-up. The review compared various models. The goal was to initiate the model selection process for flood forecasting, recognizing that the criteria for selection are inherently subjective.

Khoi (2016) assessed the effectiveness of HEC-HMS and SWAT models in simulating streamflow in Vietnam, undertaking calibration and validation from 1982 to 2009. Both models successfully simulated streamflow, but the comparison favored the SWAT model as the more suitable choice for hydrological modeling.

Krysanova & White (2015) presented a review of 10 research papers that explored diverse applications of the SWAT and SWIM models across various catchment scales. The studies covered topics such as surface runoff, sediments, nonpoint-source pollution, surface water, groundwater, and the impacts of climate and land-use changes. The review specifically delved into investigations of combined climate and land-use change impacts using the SWAT model. Additionally, it highlighted that post-revision, SWAT simulations would be on the order of 3 km² per Hydrological Response Unit (HRU), comparable to the current scale.

Li et al. (2015) introduced CLM4–MOSART, a coupled model that combines MOSART with CLM4 to accurately simulate both surface runoff and base flow. The majority of CLM4's structure remained intact, but MOSART assumed control of the routing procedures. The gridded runoff data obtained from CLM4 was passed to MOSART, a model that simulated both the spatial and temporal variations in flow velocity. Hillslope and channel routing employed distinct time phases. The geographic resolution of runoff routing might be modified, and a resolution of 0.5 degrees was used. The time step for CLM4 was 30 minutes, whereas for MOSART it was 1 hour. Results were stored at each hourly step.

Li et al. (2016) used SWAT modeling to assess the impacts of precipitation variability, land use change, and the construction of check dams on annual runoff. The

study focused on four sub-watersheds, calibrating and validating the SWAT model. Simulations were conducted for both 1970 and 2000 land use data, and the contributions of precipitation variability and land surface change were analyzed. Results indicated that precipitation variability was the primary factor responsible for runoff decrease in all watersheds. The study also evaluated climate conditions using mean annual rainfall and performed four scenarios, revealing that precipitation variability played a key role in runoff decrease in Luanhe and Wuliehe sub-watersheds, while land surface change caused runoff decrease in Yixunhe and Liuhe sub-watersheds.

Boithias et al. (2017) simulated discharge with SWAT and MARINE models, adjusting aperiodic records to hourly data for precipitation input. SUFI-2 facilitated SWAT calibration, validation, sensitivity, and uncertainty analysis. MARINE excelled in peak discharge and timing during flash floods, while SWAT outperformed in recession discharge and exported water volume. Calibration and validation included both low and high flow periods for SWAT.

Brouziyne et al. (2017) calibrated the SWAT model for a semi-arid region dominated by agro-forestry activities using both daily and monthly time scales. Their approach involved a local sensitivity analysis, employing manual calibration and validation methods. The study focused on 12 SWAT input parameters for sensitivity analysis, ultimately selecting four parameters for flow components. The model exhibited satisfactory performance, with NSE and R2 values above 0.5 and 0.7, respectively, and PBIAS lower than 25%.

Cheng et al. (2017) investigated the prolonged effects of detention in mitigating climate change-induced flooding in the Charles River watershed using the SWAT model. They simulated 36 climate change scenarios, comparing outcomes with IPCC projections. Calibration and validation of the SWAT model were performed for the periods 1992–2005 and 2006–2011, using observed daily stream flow data. The flooding hazard index (FHI) was calculated based on SWAT model results, indicating

that FHI rises with increased precipitation mean and variability, and decreases with higher mean temperatures.

Tobin & Bennett (2017) used Global Land Evaporation which uses Amsterdam Model data to physically constrain the ET-related SWAT parameter values to obtain a more realistic range. They reported Nash-Sutcliffe coefficients did not increase after the application of this method but, there is a dramatic increase in the number of days before flow where the simulations match the observed flow.

Yu et al. (2017) employed the SWAT-EVENT model for sub-daily event-based flood simulation in China's Huaihe River. Daily rainfall data from 1991-2010 were used for the SWAT model, while sub-daily data from May and September were used for SWAT-EVENT. The SWAT-EVENT model, adjusting antecedent conditions at the start of a flood event, outperformed the daily SWAT model in simulating flood hydrographs and peak flows. As a result, comparing the performances of two models, in terms of the flood hydrographs simulation, the sub-daily SWAT-EVENT model are better than the daily SWAT model.

Zhu et al. (2017) used the Coupled Land Surface and Hydrology Model System (CLHMS), which is a fusion of the LSX-HMS model. LSX computed the balance of energy at the Earth's surface, whereas HMS incorporates a module for terrestrial hydrology, a module for groundwater hydrology, and a module for the interaction between channels and groundwater. CLHMS modeled the processes of surface runoff, river discharge, and groundwater movement. The integration procedure had three distinct phases: a "cold start" phase lasting 50 years to establish surface water balance, a "spin-up" phase lasting 5000 years to establish groundwater balance, and a final run from 1998 to 2006 consisting of two cycles. The findings from the second cycle were utilized for water cycle analysis in order to minimize model bias. factors encompass surface elevation, soil texture, plant type, hydrogeological factors, and other pertinent components.

Tassew et al. (2019) utilized HEC-HMS to simulate surface runoff in the Gilgel Abay Catchment, located in the Upper Blue Nile Basin, Ethiopia. They used the Soil Conservation Service Curve Number (SCS-CN), Soil Conservation Service Unit Hydrograph (SCS-UH), and Muskingum methods for runoff estimation and flow routing in HEC-HMS. The model underwent calibration, optimization, and sensitivity analysis, demonstrating strong performance compared to observed hydrographs. The study confirmed the model's suitability for hydrological simulations in the Gilgel Abay Catchment, with sensitivity analysis identifying the curve number as the most critical parameter, followed by lag time.

Getirana et al. (2021) applied the prescribed vegetation scheme, based on monthly leaf area index climatology. The TOPMODEL simulated groundwater scheme was selected, and the Noah-based lower boundary of soil temperature option was applied. Other climatology-based vegetation and albedo parameter maps included monthly greenness fraction and global albedo. In the one-way coupling mode, at the end of the LSM run in timestep t-1, surface runoff and baseflow flux fields were transferred from the LSM to HyMAP. The LSM packages these flux fields as an ESMF object and "exports" them to HyMAP. Once these "import" flux states were received, HyMAP converted them into incremental water volume as a function of dth and grid cell size. The incremental water volume was then summed to the surface water storage SWS (mm) at the end of each dth and propagated through the river reach on the following sub timestep. There was no feedback from HyMAP to the LSMs. The same process was repeated at timestep t, and so on.

Chen et al. (2022) introduced the DRIVE model, which combines the Variable Infiltration Capacity (VIC) land surface model with the Dominant River Tracing based Routing (DRTR) model, to conduct extensive hydrological simulations on a broad scale. The study utilized the Storm Water Management Model (SWMM) to mimic the process of urban rainfall-runoff and pipe drainage within the DRIVE model. The SWMM software utilized the Soil Conservation Service-Curve Number (SCS-CN) technique for infiltration, and its routing module incorporated many methods such as steady flow, kinematic wave, and dynamic wave. The integration of DRIVE and

SWMM was designed to tackle the interplay between natural river networks and urban drainage systems. DRIVE is a simulation tool that models river channels, pipe networks, and urban overflow by integrating 1D and 2D processes. The DRIVE model supplied river channel water levels to SWMM, while SWMM computed flooding volumes for manholes and outfalls. The connection enabled a thorough simulation of urban floods, taking into consideration the interplay between river and urban hydrological systems.

Modi et al. (2022) introduced a new hydrological modeling framework integrating climate projections with a coupled Noah-MP land surface model and a two-dimensional HEC-RAS hydrodynamic model. Precipitation indices serve as inputs to a 4-km resolution Noah-MP LSM for the entire Chesapeake Bay watershed. The model estimated water balance components (evapotranspiration, surface runoff, baseflow, soil moisture) and energy fluxes (latent heat flux, ground heat flux, sensible heat flux). Surface runoff and baseflow components were used in a convolution-based routing model to predict river discharges at specific locations in the watershed.

2.3 Drought Analyses

Recently, agricultural drought events are investigated using drought indices combined with remote sensing. Drought impacts on vegetation activity are assessed by using SPEI with Normalized Difference Vegetation Index (NDVI) (Gouveia et al., 2017; Vicente-Serrano et al., 2015). Palmer Hydrological Drought Index (PHDI) (Shin et al.,2018) and Standardized Runoff Index (SRI) (Jehanzaib et al., 2020; Lee et al., 2019) are very commonly used to detect hydrological drought events.

Günaçtı et. al. (2018) analyzed drought patterns in the Küçük Menderes Basin in Western Türkiye. Utilizing observed monthly precipitation data from 1972 to 2016 at a chosen meteorological station, the research employs stochastic techniques to model precipitation. Synthetic precipitation series are then generated based on this model. These synthetic series are used to calculate 6-month Standardized Precipitation Index (SPI) values, providing a quantitative assessment of drought conditions. The

constructed model aims to identify potential drought events and guide the development of drought management plans for the Küçük Menderes Basin.

Jehanzaib et al. (2020) compared the SPI and the SPEI with the SRI on 4-month time scale to determine the meteorologic effects on the hydrologic droughts in South Korea. They indicate that, because of the average drought propagation probability of the extreme state of SPI and SPEI, the severe conditions of SRI are increased by 55% and 78%, respectively, under the RCP 4.5 scenario. However, they are increased by 55% and 123%, respectively under the RCP 8.5 scenario.

Onuşluel Gül et al. (2022) examined the drought patterns in the Thracian, Aegean, and Mediterranean regions of Türkiye's main river basins, with a specific focus on the severe weather conditions caused by climate change. The study utilized yearly maximum drought severity data derived from Standardized Precipitation Index (SPI) derived from daily precipitation data to investigate different elements of drought occurrence using geographic analysis. Trends, shifts in the onset of severe drought episodes, and alterations in geographical coverage were analyzed. The study examined data from two time periods, 1958-1980 and 1981-2004, and identified clear disparities in the intensity, duration, and timing of droughts in the river basin systems of western and southern Türkiye.

2.4 Hydraulic Modeling and Flood Analyses

Berger & Van De Langemheen (2005) examined hydrological processes in the Rhine catchment in the Netherlands, with a focus on floods and low flows. They discussed the impact of the 1993 and 1995 floods on water management, assessed the probability of extreme discharges, and studied the effects of land use change. The study used a rainfall-runoff generator with three modules and the Sobek hydraulic program for retention. The findings indicated a need for preparedness for lower flows than those observed in 2003.

Onuşluel Gül et al. (2010) performed a flood modeling in the Bostanlı river basin, evaluating the possible consequences of the proposed BostanlI Dam by employing

HEC-HMS and HEC-RAS coupled with GIS. The findings indicated a little but favorable effect, resulting in a decrease in possible flood peaks from 68.9 and 158.7 m3/s to 65.5 and 150.7 m3/s for 100- and 500-year storm events, respectively.

Yu et al. (2016) detailed the utilization of FloodMap-HydroInundation2D, a hydro-inundation model, for simulating urban-scale surface water flooding arising from extreme precipitation events. This model, incorporating Flood Map and surface flow routing processes, considers surface runoff, infiltration, evapotranspiration, and drainage capacity. The study applied the model to analyze a significant storm event in Shanghai, China, on August 12, 2011, utilizing 15-minute precipitation data and various topographic inputs. Calibration and sensitivity analysis involved different DEMs and roughness values, with results assessed through fit statistics and root-mean-square error. The model exhibited sensitivity to mesh sizes, resolution, and roughness specifications but effectively simulated inundated areas, highlighting its advantage in requiring minimal information about storm sewer systems.

Patel et al. (2017) assessed the occurrence of flooding in Surat, India, following the release of water from the Ukai Dam in 2006, utilizing hydrodynamic modeling techniques that incorporate both one-dimensional and two-dimensional aspects. Based on simulations using 299 cross-sections and grid data, it was determined that August 9th is the most severe day, with about 75-77% of the region being flooded. The western zone had the most severe floods, with water levels reaching depths of 4 to 5 meters. Simulations that considered flood protection measures implemented after 2006 show that most areas were safe, saved for the western zone, when specific releases were made from the Ukai Dam.

Namara et al. (2022) examined the process of mapping flood inundation in the Awash Bello floodplain, located in the Upper Awash River basin in Ethiopia by the using HEC-RAS model. The research involved the extraction of river cross-sections and the performance of yearly peak flood frequency analysis for different recurrence intervals. The calibrated HEC-HMS model as utilized to calculate exceptional flood values, and its results were compared with functions representing extreme value

distributions. Upon verification, the HEC-RAS model incorporated the peak flood data to generate inundation maps, which depict the areas impacted by floods at various recurrence intervals. The analysis highlighted the susceptibility of the whole Awash Bello floodplain to being flooded due to heavy rainfall occurrences.

CHAPTER THREE
METHODOLOGY AND DATA ANALYSES

3.1 Methodology

Considering the climatic characteristics of Küçük Menderes River Basin, flood and drought simulations for future periods were carried out by utilization of diverse models (Table 3.1) and tools (Table 3.2) in a combined approach. The methodological framework of the study consists of modelling the basin by using hydrological models together with the land surface model, revealing the effects of drought and flood for future periods by using climate data and modelled data and showing their spatial distributions.

Table 3.1 Models applied in the study.

Models	**Used for**
Variable Infiltration Capacity (VIC) Model	Land Surface Modeling
Soil and Water Assessment Tool (SWAT) Model SWAT Calibration and Uncertainty Programs (SWAT - CUP)	Hydrological Modeling
Hydrologic Engineering Center's Hydrologic Modeling System (HEC - HMS) Geospatial Hydrologic Modeling Extension (HEC-GeoHMS)	Hydrological Modeling
Hydrologic Engineering Center's River Analysis System (HEC-RAS)	Hydraulic Modeling

The concept of coupled models refers to the use of two or more models together to simulate interactions between different components or various processes of a system. A land surface model (LSM) and a hydrological model can be coupled to provide a more comprehensive understanding of how changes in land surface conditions affect hydrological processes and vice versa. There are two types of matching in model matching: one-way matching and two-way matching. In one-way coupling modelling, information flows between models in one direction. In two-way coupling modelling, information flows between models in both directions and feedback occurs between models (Benra et al., 2011).

In this study, a land surface model and a hydrological model are employed in a one-way coupled configuration. Figure 3.1 illustrates the combined use of the LSM and hydrological model for generating inputs in the context of drought studies while Figure 3.2 demonstrates their application in flood studies.

Table 3.2 Program languages/tools used in the study.

Program Language / Tool	***Package Name***	***Package Description***	***Purpose***
Python	"climate_indices 1.0.10"	Climate Indices in Phyton	Calculation of drought indices on daily and monthly basis
R/R-Studio	"VIC5"	The Variable Infiltration Capacity (VIC) Hydrological Model	The Variable Infiltration Capacity (VIC) model is a macroscale hydrologic model that solves full water and energy balances,
	"trend"	Non-Parametric Trend Tests and Change-Point Detection	Performing trend and homogeneity tests
	"lmomRFA"	Regional Frequency Analysis using L-Moments	Performing regional frequency analysis of drought indices
	"hydroTSM"	Time Series Management, Analysis, and Interpolation for Hydrological Modelling	Calculation of statistics of observed meteorological data
	"stR"	A Seasonal-Trend decomposition procedure based on Regression	Seasonal-trend decomposition procedure for observed meteorological data
	"SPEI"	Calculation of the Standardized Precipitation-Evapotranspiration Index	Calculation of drought indices on monthly basis
	"hydroGOF"	Goodness-of-Fit Functions for Comparison of Simulated and Observed Hydrological Time Series	Evaluating model performances

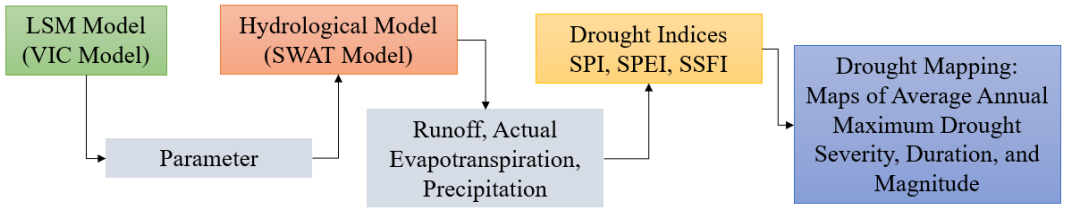


Figure 3.1 Flowchart for performing drought simulations by using coupled land surface and hydrologic models.

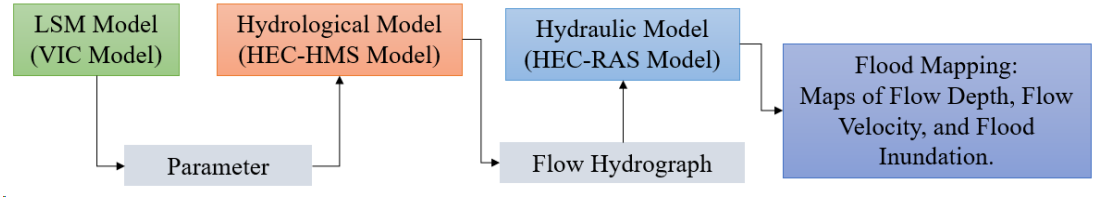


Figure 3.2 Flowchart for performing flood simulations by using coupled land surface and hydrologic models.

3.1.1 Land Surface Modeling

Land surface models (LSMs) play an important role in various scientific disciplines, simulating processes occurring on Earth's land surface to understand and predict interactions between the atmosphere, land surface and subsurface.

According to Pitman (2003), the 'land surface' is defined as the composition of vegetation, soil and snow and influences the exchange of water, energy, and carbon within the Earth system. LSM is often used in climate, hydrology, ecology, and environmental sciences as it is a vital tool for understanding the Earth's carbon cycle.

Land surface models are divided into three generations according to their development over time (Figure 3.3). The first generation, pioneered by Manabe (1969), involved a simple representation of the oceans and continents without accounting for seasonal or diurnal cycles. The 'Manabe bucket model' employed a fundamental energy balance equation and assumed of a uniform soil depth and water-holding capacity across the globe.

The second generation, led by Deardorff (1978), marked a significant advance by introducing a two-layer simulation for soil temperature and moisture as well as a single bulk layer for vegetation. Sellers et al. (1997) categorized Deardorff's model as 'second generation' and influenced subsequent models that explored the sensitivity of the climate model to surface properties, in particular distinguishing between surface soil and vegetation.

In terms of hydrology, second-generation models used diffusion equations for vertical water transfer and adopted a variety of surface runoff parameterization methods ranging from simple to complex. These models acknowledged the limitations of existing land surface models, particularly regarding snow modelling.

The third generation brought notable improvements by introducing open canopy conductivity to enhance evapotranspiration simulation and address carbon uptake by plants. This generation is characterized as the 'greening' of land surface models and focuses on predicting canopy photosynthesis and respiration by developing methods to scale leaf-level models to canopy-scale models. The third generation of models, aligned with ecological or climate models, emphasize responses from the continental biosphere to the atmosphere.

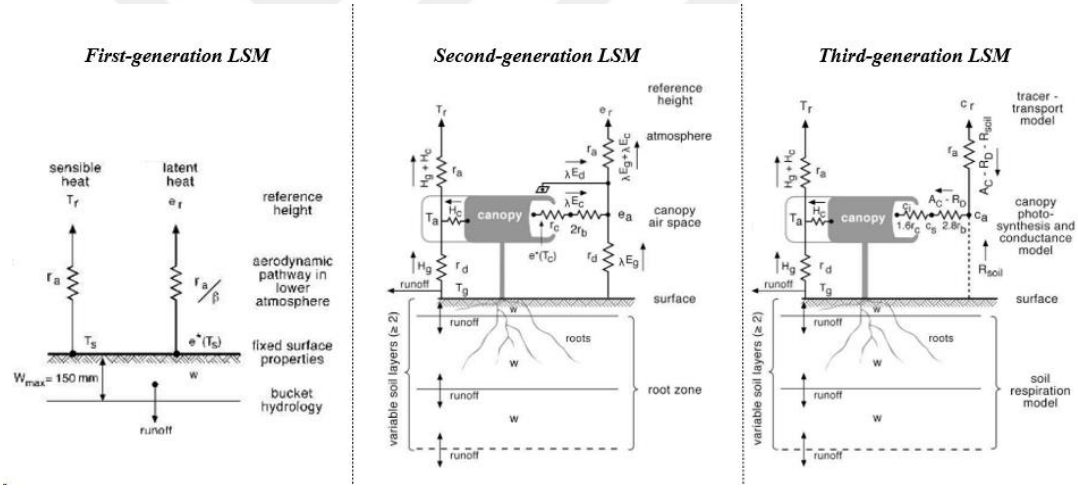


Figure 3.3 First, second, and third generation LSMs (Pitman, 2003).

One of the main functions of LSMs is to control the partitioning of available energy at the surface, managing the balance between sensible and latent heat. They also manage the distribution of available water between evaporation and surface runoff, as outlined by Pitman (2003). The complex relationships modelled by LSMs are expressed in equations representing the surface energy balance, surface water balance and carbon balance (Figure 3.4).

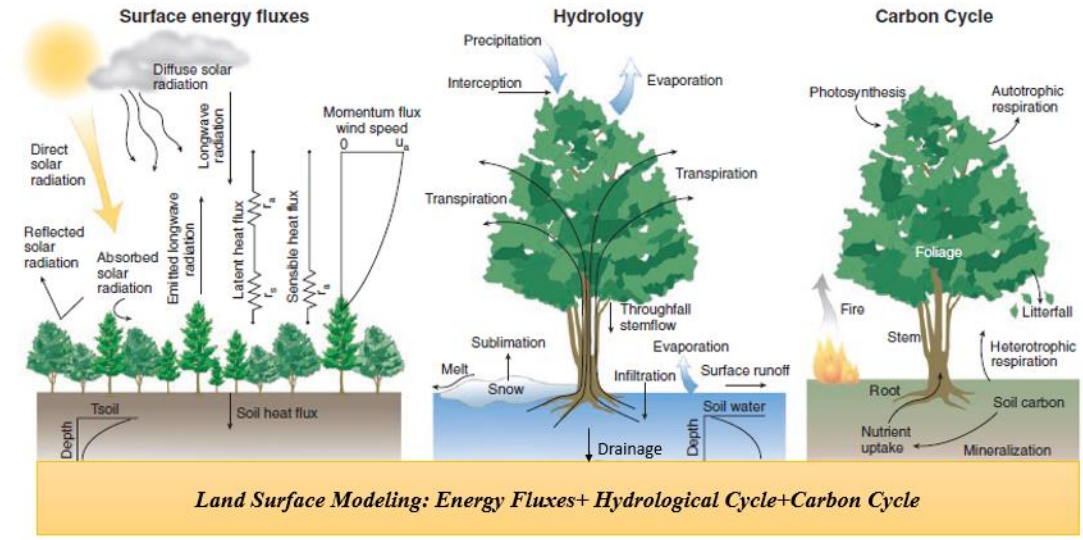


Figure 3.4 Schema of energy, water, and carbon balance (Bonan, 2008).

The surface energy fluxes: A common approach used in land surface modelling is to depict the land surface as an electrical analogue. This methodology is based on the approach that the rate of change of a quantity between two points, such as the land surface and the surrounding atmosphere, is determined by a difference in the potential of the quantity. According to Overgaard et al. (2006), this change is also regulated by various resistances. The land surface significantly influences the timescale of surface-atmosphere exchanges. The characteristics of the land surface influence the extremes, especially in scenarios where evaporation and transpiration and humidity are considered. Consequently, alterations in the nature of the land surface are expected to impact not only the average surface–atmospheric exchanges but also the extremes and the time scale of the land surface's response to different external conditions, as emphasized by Pitman (2003). The rate of exchange (H) can be represented by Equation 3.1.

$$H = \frac{T_s - T_r}{r_a} \rho c_p \tag{3.1}$$

Here, H is the function of the surface temperature (T_s), a reference temperature above the surface (T_r), the air density (ρ) and the specific heat of air (c_p). The latent heat fluxes (λE) can be represented by Equation 3.2.

$$\lambda E = \left(\frac{e^*(T_s) - e_r}{r_s + r_a}\right)\frac{\rho c_p}{\gamma} \quad (3.2)$$

Here, e^* (T_s) is the saturated vapor pressure at T_s and e_r is the vapor pressure at a reference height. γ is the psychrometric constant and r_s is the surface resistance to the transfer of water from the surface to the air.

The surface water fluxes: Precipitation is either retained by vegetation or reaches the soil surface directly. Rainfall that is retained either evaporates or drips to the surface, and the drip, combined with rainfall that reaches directly to the surface, either infiltrates or runs off the land surface (Pitman, 2003).

The main role of the land surface is to divide precipitation (P) between evaporation (E) and runoff, which is combined into a fast component (R_{surf}) and a slow component (R_{drain}). Here, ΔS represents the change in soil moisture storage. The balance between incoming and outgoing fluxes of water is entitled as the surface water balance which is given by Equation 3.3. The two runoff terms (R_{drain} and $R_{surface}$) are affected by the characteristics and wetness of the soil.

$$P = E - R_{drain} - R_{surface} - \Delta S \quad (3.3)$$

The carbon fluxes: The concept of carbon fluxes involves the calculation of the movement of carbon between various components of the ecosystem in land surface models, including the atmosphere, vegetation, soil and, in some cases, water bodies. Photosynthesis, respiration, decomposition and carbon storage and various other processes are considered in the carbon balance of land surface models.

Net Ecosystem Exchange (NEE) which is given by Equation 3.4 is the overall carbon flux between the land surface and the atmosphere and represents the difference between Gross Primary Productivity (GPP) given by Equation 3.5 and ecosystem respiration (Re). GPP is the uptake of carbon through photosynthesis and Re (Equation 3.6) is the release of carbon through respiration.

$$NEE = GPP - Re \quad (3.4)$$

$$GPP = f\ (PAR, LAI, Temperature, CO_2) \quad (3.5)$$

$$Re = f\ (Temperature, Soil\ Moisture, CO_2) \quad (3.6)$$

Here, PAR is photosynthetically active radiation, LAI is leaf area index, CO_2 is atmospheric carbon dioxide concentration. Net Primary Productivity (NPP) given by Equation 3.7 represents the net carbon uptake by plants after subtracting autotrophic respiration from Gross Primary Productivity.

$$NPP = GPP - Autotrophic\ Respiration \quad (3.7)$$

3.1.1.1 Samples of Land Surface Models

All land surface models aim to capture the dynamics of energy, water, and carbon fluxes within terrestrial ecosystems. When choosing a model, it is essential to evaluate its strengths and weaknesses in representing various processes and fluxes (Trambauer et al., 2013). Below are examples of commonly employed land surface models. The Community Land Model (CLM) was developed by the National Center for Atmospheric Research (NCAR) and is part of the Community Earth System Model (CESM). It simulates land surface processes, including vegetation, biogeochemical cycles and hydrological processes (Lawrence and Chase, 2007; Lawrence et al., 2019).

The Noah LSM is part of the Weather Research and Forecasting (WRF) model. It is widely used in atmospheric modeling in general and simulates soil moisture, temperature, snow cover and vegetation characteristics (Mitchell, 2005; Niu et al., 2011; Yang et al., 2011).

The Mosaic LSM was developed at NASA's Goddard Space Flight Center. It is often used in atmospheric modeling studies and aims to represent the spatial variability of land surface properties (Koster & Suarez, 1996; Yang et al., 2003).

The Simple Biosphere Model (SiB) is a simpler and widely used land surface model that simulates land-atmosphere interactions. (Sato et al.,1989; Sellers & Dorman,

1987). The Joint UK Land Environment Simulator (JULES) Model was developed by the UK Met Office and is often used in climate and weather prediction models. The model simulates land surface processes, vegetation dynamics and carbon and nitrogen cycles (Best et al., 2011; Clark et al., 2011).

The Variable Infiltration Capacity (VIC) Model is a widely used hydrological model that simulates land surface processes including snowmelt, soil moisture and surface runoff (Hamman et al, 2018; Liang et al., 1994). Since it also includes energy and carbon cycle processes, it is used as a land surface model in studies (Trambauer et al., 2013). It has applications in water resources and climate studies.

Regulating Carbon and Hydrology in Dynamic Ecosystems (ORCHIDEE) is designed to simulate both energy and hydrological balance in ecosystems. It requires meteorological data such as precipitation, temperature, radiation, humidity, pressure and wind speed. It considers vegetation dynamics and includes a routing module for river flows (Goll et al., 2017; Guimberteau et al., 2018).

Hydrology Tiled ECMWF Scheme for Surface Exchanges over Land (HTESSEL) was developed by the European Center for Medium-Range Weather Forecasts (ECMWF). The model represents various land surface processes, including energy and water fluxes. It provides outputs for variables such as soil moisture, temperature, and surface runoff. It is used in numerical weather prediction models and climate models (Orth et al., 2017; Wipfler et al., 2011).

3.1.1.2 Variable Infiltration Capacity (VIC) Model

The VIC model was developed by Liang et al. (1994). Its basic characteristics are similar to those of other land surface models (LSMs) that are frequently coupled to global circulation models (GCMs). The land surface is depicted using a grid of large cells, each measuring more than one kilometer. Statistical distributions are used to address sub-grid heterogeneity, which includes features like elevation and land cover diversity. The model utilizes sub-daily meteorological inputs such as radiation, wind speed, precipitation, and air temperature, relying on time series data. The model

performs simulations to analyze water and energy balances, as well as the land-atmosphere fluxes.

There is no consideration for non-channel movement between grid cells; water enters a grid cell only through atmospheric mechanisms. It is considered that a grid cell's local channel network receives a substantially greater amount of surface and subsurface runoff than does runoff that crosses grid cell boundaries and enters adjacent cells. The model assumes that water cannot flow back into the soil once it enters the channel network and stays there.

Grid cells function autonomously without inter-cell communication. Stream flow routing is typically executed through a separate model, as suggested by Lohmann et al. (1996, 1998), and is conducted independently of the land surface simulation.

Elevation bands: VIC considers topography heterogeneity as well as storm fronts and local convection when analyzing spatial variation in precipitation using elevation bands. Meteorologic forcings are lapsed from the average elevation of the grid cell to the elevation of each band. For writing to output files, the bands' averaged fluxes and storages are combined to provide a grid-cell average.

Land cover: Each grid cell is divided by the model into "tiles," which group patches of the same kind together. Grid-cell output is computed by averaging fluxes and storages. The computation of transpiration incorporates a Jarvis-style response, independently considering the canopy energy balance. The model takes wind, radiation in the gaps between plants, and soil evaporation into account. The vegetated area fraction determines which fractions are vegetated or non-vegetated. Support is provided for optional daily timeseries input for vegetated area, albedo, and Leaf Area Index (LAI). Taking into account current vegetation and resistance, potential evapotranspiration is calculated as the area-weighted sum of potential transpiration and potential soil evaporation.

Soil: Three soil layers are usually used in the model, and infiltration is determined using the variable infiltration capacity (VIC) parameterization (Liang et al., 1994). The outermost layers lose moisture by soil evaporation utilizing the ARNO formulation (Todini, 1996), while the root area loses moisture through evaporation (Franchini & Pacciani, 1991). Franchini & Pacciani (1991) state that the ARNO base flow formulation is utilized for drainage from the lower layer. According to Cherkauer & Lettenmaier (2003), every type of land cover has a unique profile of soil temperature, which simulates geographic variation in soil temperature across land cover. The method outlined in Bohn et al. (2013) is used by the model to determine the depth of the water table based on soil moisture and texture.

Meteorology: The model is supplied with specific meteorological variables, encompassing precipitation, air temperature, wind speed, long wave radiation, short wave radiation, atmospheric pressure and vapor pressure.

Carbon cycle: Photosynthesis, autotrophic respiration, and heterotrophic respiration are all included in the VIC simulation. When the carbon cycle is closed, vegetation features such as LAI are expected to occur. Soil carbon reservoirs can be classified as litter (with a residence time of 2.86 years), medium (with a residence time of 33.3 years), or slow (with a residence period of 1000 years). In the current year, the total Net Primary Productivity (NPP) from the prior year is continuously added to the litter pool. Each pool contributes a defined percentage of respiration to ambient CO_2, with waste, medium, and slow pools contributing different amounts.

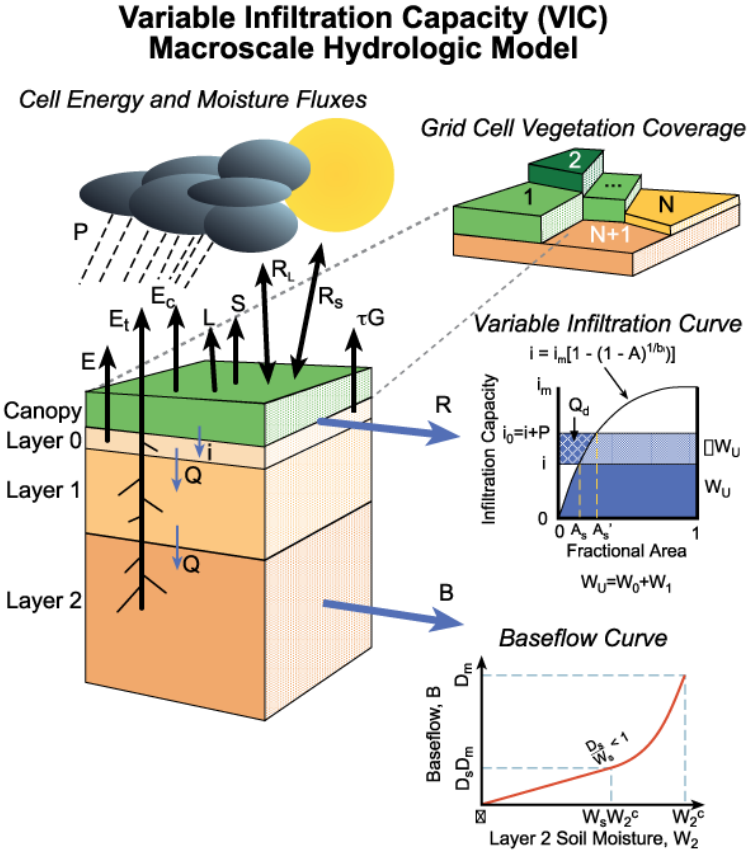


Figure 3.5 VIC land cover tiles and soil column, with major water and energy fluxes (University of Washington Computational Hydrology Group, 2021)

3.1.2 Hydrological Modeling

Hydrological modeling essentially refers to the mathematical representation of the hydrological cycle. Hydrological models predict system behavior in a watershed and serve to understand various hydrological processes (Devia et al., 2015). In general, the components of hydrological models are precipitation, evapotranspiration, evaporation, infiltration, surface runoff, subsurface runoff, and groundwater flow in the hydrological cycle. The model uses various parameters describing the watershed and estimates runoff as a function of these parameters. Model inputs are usually meteorological data (especially precipitation), topographic data, soil data, land use, groundwater data and vegetation cover. Hydrological models used to produce outputs such as runoff, pollution levels and soil moisture in watersheds play an important role in water resources management, flood forecasting, climate studies and environmental impact assessments.

Rainfall-runoff models are hydrological models that simulate the conversion of rainfall to runoff, i.e., the relationship between rainfall input and the resulting runoff output. These models, aiding in the comprehension of the impact of precipitation events on surface runoff formation of in the basin, can be classified according to various factors.

While models that ignore spatial variability and treat the basin as a single unit are called lumped models, models that operate by dividing the basin into sub-basins or grids are called distributed models.

Models that do not explicitly consider time and provide results within a certain period of time are called static models. Models that take the time factor into account and simulate time-dependent hydrological processes are called dynamic models.

A deterministic model enables precise calculation of future events without relying on randomness. Models that derive different outputs for the same set of inputs and consider the uncertainties and randomness in the system are called stochastic models.

3.1.2.1 Samples of Hydrological Models

Hydrological models, some examples of which are given below, are among the models frequently used in studies such as basin modelling, flood studies and groundwater modelling.

The Soil and Water Assessment Tool (SWAT), which simulates sediment transport, water quality, and agricultural management techniques, is particularly useful in agricultural watersheds (Arabi et al., 2008; Arnold et al., 2012; Douglas-Mankin et al., 2010).

The US Army Corps of Engineers created the Hydrological Modelling System (HEC-HMS), which is extensively used for general hydrological modelling (Chu & Steinman, 2009; Halwatura & Najim, 2013).

The Hydrologiska Byråns Vattenbalansavdelning (HBV) model is utilized in rainfall-runoff simulations and general basin modeling. The hydrological cycle, which includes soil moisture, runoff creation, and snow accumulation and melting, is conceptualized by the HBV model (Bergström & Lindström, 2015; Samuel, 2011).

MIKE Système Hydrologique Européen (MIKE SHE) model is an integrated hydrological model, that is used in comprehensive hydrological modeling, including surface water and groundwater interactions. MIKE SHE is developed by Danish Hydraulic Institute (DHI) suite. Multiple hydrological processes can be simulated with Mike SHE, which makes it appropriate for integrated water management research (Graham & Butts, 2005; Thompson et al., 2004).

TOPMODEL stands for "Topographic Kinematic Wave Model", that emphasizes runoff generation and subsurface saturation. Particularly in regions with hilly or mountainous terrain, generic basin modeling is frequently done with it (Beven et al., 1995; Beven, 1997).

Within the scope of this study, SWAT model was used for basin modeling for Küçük Menderes Basin and HEC-HMS model was used for basin Ergenli Basin for flood modeling.

3.1.2.2 Soil and Water Assessment Tool (SWAT) Model

SWAT is a commonly utilized model for evaluating soil erosion prevention and control, non-point source pollution control, and regional management in watersheds. SWAT is a physically based basin scale model that is known as computationally efficient and capable of continuous simulations. Using a daily or monthly time step, the original SWAT model was intended for continuous simulations. According to Jeong et al.,2011; Yu et al., 2018), the SWAT model performs best when long-term hydrological responses to changes in land cover or soil management techniques are predicted using a daily time step. A finer timescale is necessary to accurately capture the instantaneous changes indicative of flood processes when dealing with flood simulation problems (Yu et al., 2018).

SWAT needs specific information about the watershed rather than using regression equations to explain the relationship between input and output variables. SWAT necessitates precise data regarding meteorological conditions, soil characteristics, topographical features, vegetation types, and land management techniques. The model comprises various components like weather, hydrology, soil temperature and characteristics, plant development, nutrients, pesticides, bacteria and diseases, and land management. The hydrological cycle in SWAT (see Figure 3.6) is based on the water balance given by Equation 3.8 (Neitsch et al., 2009).

$$SW_t = SW_0 + \sum_{i-1}^{t}\left(R_{day} - Q_{surf} - E_a - w_{seep} - Q_{gw}\right) \quad (3.8)$$

The variables in the equation are as follows: "SW_t" represents the final soil water content, "SW_0" represents the initial soil water content on day i in millimeters of water t represents the time in days, "R_{day}" represents the amount of precipitation on day i, "Q_{surf} "represents the amount of surface runoff on day i. "E_a" represents the amount of evapotranspiration on day i. w_{seep} represents the amount of water entering the vadose zone from the soil profile on day i, and Q_{gw} represents the amount of return flow on day i. The units for all measurements are in millimeters (mm).

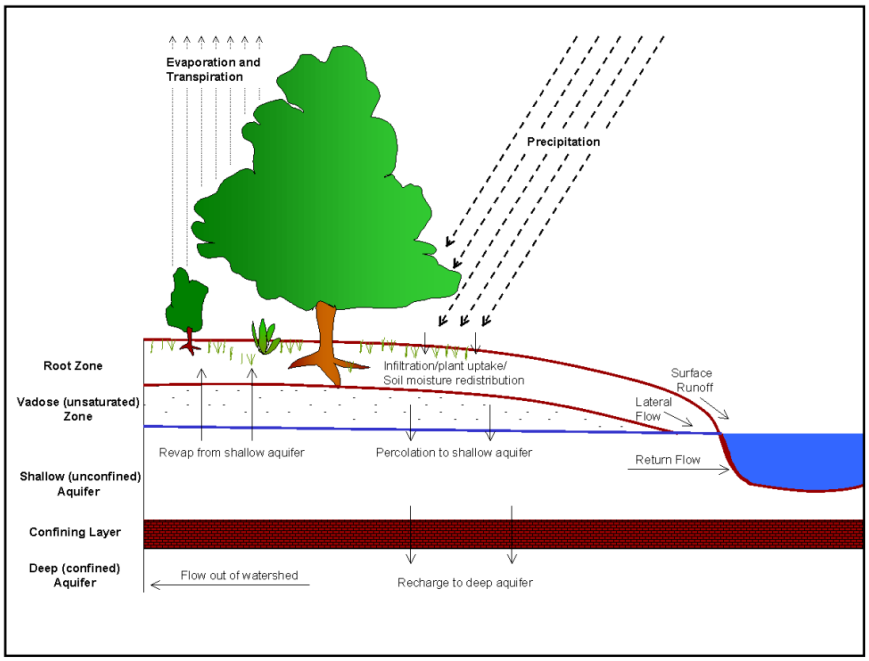


Figure 3.6 Hydrological cycle (Neitsch et al., 2009)

The initial level of division is referred to as the subbasin. Subbasins are located within the watershed and have a spatial relationship with each other. The process of subbasin delineation involves identifying the boundaries of subbasins based on the surface topography. This ensures that all the water within a subbasin flows towards the subbasin outlet. A subbasin is comprised of a minimum of one Hydrologic Response Unit (HRU), a tributary channel, and a main channel or reach. Within a subbasin, two distinct types of impoundments, namely a pond and/or wetland, can be delineated.

HRU is used to partition the land area within a subbasin. HRUs refer to specific sections of a subbasin that possess unique land use/management/soil attributes.

They streamline SWAT simulations by consolidating comparable soil and land use regions into a unified response unit. The loadings from each HRU are computed separately and then combined to determine the overall loadings for the subbasin. HRUs improve the accuracy of predicting the loadings in subbasins.

Each subbasin in a watershed is linked to a single primary channel. The subbasin's loadings are introduced into the channel network of the watershed through the corresponding reach segment.

The term of tributary channel is used to differentiate inputs associated with the channeled movement of surface runoff within a smaller drainage area. The inputs provided are essential for computing the time it takes for the channelized runoff to reach its peak and for assessing the amount of water lost as the runoff flows towards the main channel.

Water bodies along the stream network in the watershed are represented as reservoirs in the model. Each subbasin can define two water bodies (ponds/wetlands), and the water entering these impoundments originates solely within the subbasin; they do not receive water from other subbasins. In contrast, reservoirs collect water contributed by all upstream subbasins in the channel network.

The SWAT model simulates the movement of water, sediment, and nutrients from land areas within a watershed. Users can enter daily loading data for point sources such as sewage treatment plants. The data is incorporated into the primary channel network, and the model subsequently directs these loadings in conjunction with those originating from land areas.

Meteorology: The daily precipitation, maximum and minimum temperatures, solar radiation data, relative humidity, and wind speed data are the climatic inputs used in SWAT. Relative humidity is necessary if the Penman-Monteith or Priestly-Taylor evapotranspiration (ET) routines are applied. Weather Generator (WGEN) is used in case of lack of data. For WGEN certain statistics are generated using daily values. SWAT uses the generated values for simulations when there is no recorded data.

Hydrology: The curve number method considers canopy storage in surface runoff calculations. When using Green & Ampt for infiltration and runoff modeling, canopy storage needs a separate treatment. The evaporation from plants and soils is calculated independently in the model.

The leaf area index (LAI) and potential evapotranspiration are used to calculate the potential amount of soil water evaporation. Penman-Monteith, Priestley-Taylor, and Hargreaves are the options that the model offers for estimating potential evapotranspiration. Exponential functions of soil depth and water content are used to estimate actual soil water evaporation. Potential evapotranspiration and the LAI are used to simulate plant transpiration as a linear function.

The lateral flow in every soil layer is estimated by using a kinematic storage model. A variation of the SCS curve number method or the Green & Ampt infiltration method is used to calculate surface runoff. Using the Manning formula, both channel and overland flow are taken into account when calculating the sub-basin concentration time. Lane's method is used by SWAT to calculate transmission losses in the tributary channels. Groundwater is divided by SWAT into two aquifer systems: a deep, confined

aquifer that supplies return flow to streams outside of the watershed and a shallow, unconfined aquifer that supplies return flow to streams inside the watershed.

Routing phase of hydrological cycle: The main channel routing involves four components: water, sediment, nutrients, and organic chemicals. Williams or the Muskingum routing technique is used to control flow using a variable storage coefficient method. Water balance in reservoirs considers surface rainfall, inflow, outflow, evaporation, seepage, and diversions. There are three ways to estimate outflow: user-input measured outflow, water release rate specification for small, uncontrolled reservoirs, and monthly target volumes for larger, managed reservoirs.

Calibration and validation: The extensive array of input variables in SWAT, a model based on physical principles, poses challenges in the practical implementation of calibration and validation (Arnold et al., 2012). Model calibration is performed to improve the match between simulated and observed values over a specified period. Prior to this, sensitivity analysis is performed to determine which parameters have a high impact on the model. Once the sensitive parameters are identified, these parameters are changed or adjusted so that the model output approaches the observed values.

Manual calibration is done by changing the parameters individually, while for automatic calibration all parameters are changed together. SWAT-CUP program has been developed for automatic calibration. For validation, another period similar to the calibration period is selected and the calibrated parameter values are used for this period.

The performance of the model is evaluated using the observed and simulated values as a result of calibration and validation. Model performance is measured using relations such as coefficient of determination (R^2) (Equation 3.9), Nash-Sutcliffe Efficiency (NSE) (Equation 3.10) and percent BIAS (PBIAS) (Equation 3.11).

$$R^2 = \frac{[\sum_i (Q_{m,i} - \bar{Q}_m)(Q_{s,i} - \bar{Q}_s)]^2}{\sum_i (Q_{m,i} - \bar{Q}_m)^2 \sum_i (Q_{s,i} - \bar{Q}_s)^2} \quad (3.9)$$

$$NSE = 1 - \frac{\sum_i (Q_m - Q_s)_i^2}{\sum_i (Q_{m,i} - \bar{Q}_m)^2} \quad (3.10)$$

$$PBIAS = 100 \frac{\sum_i (Q_m - Q_s)_i}{\sum_i Q_{m,i}} \quad (3.11)$$

Where, Q is a variable (e.g., discharge), m and s are measured and simulated, respectively, i is i^{th} data. $\sigma_m{}^2$ is the variance of the measured data. The bar stands for average. For NSE calculation, if p=2 is, it is called as simply NSE. The Modified Nasch-Sutcliffe Efficiency factor (MNS), with a value of 2 or higher, reduces overestimation of peaks and is more sensitive to over- or underestimation than the square form. It is particularly useful for flood forecasting when high flows are involved, such as when p=1 (Abbaspour, 2015). The evaluation of the model performance is given in Table 3.3.

Table 3.3 Model performance (Moriasi et al., 2007).

Performance Rating	**NSE**	**PBIAS**
Very Good	0.75<NS≤1.00	PBIAS <±10
Good	0.65<NS≤0.75	±10≤PBIAS≤±15
Satisfactory	0.50<NS≤0.65	±15≤PBIAS±25≤
Unsatisfactory	NS≤0.50	PBIAS≥±25

Model interface: There are many interfaces developed for the SWAT model. These are: SWAT+, ArcSWAT, SWAT Calibration and Uncertainty Programs (SWAT-CUP), QSWAT3, SWAT-MODFLOW. Apart from these, auxiliary equipment has also been developed for SWAT. These are Global Weather Data for SWAT, WGN Parameters Estimation Tool and Water Ecosystems Tool (WET). ArcSWAT and SWAT-CUP were used in this study.

ArcSWAT, which was developed by Winchell et al. (2007), is ArcGIS extension that is a graphical user interface for SWAT model (Figure 3.7). ArcSWAT is a tool that utilizes the spatial analytic capabilities of ArcGIS. It allows users to effectively handle, visualize, and analyze spatial data for the purpose of watershed modeling (Figure 3.8).

This tool enhances users' comprehension of the distribution of variables and the outcomes of their models.

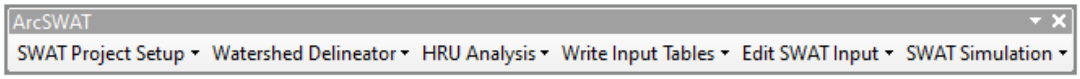


Figure 3.7 ArcSWAT extension in ARCGIS.

As shown in Figure 3.9, inputs are added to ArcSWAT and the model is run.

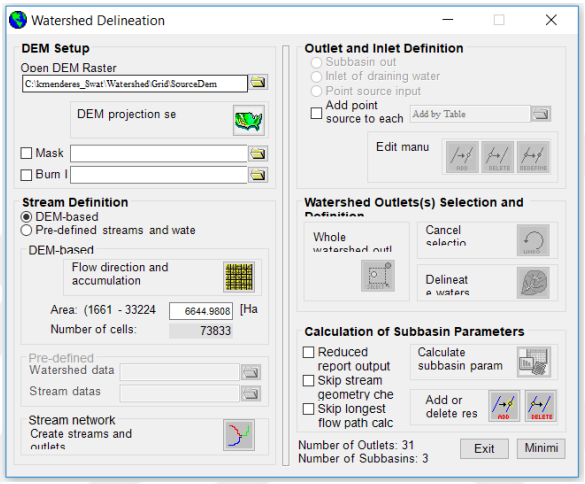


Figure 3.8 Watershed Delineation part of ArcSWAT

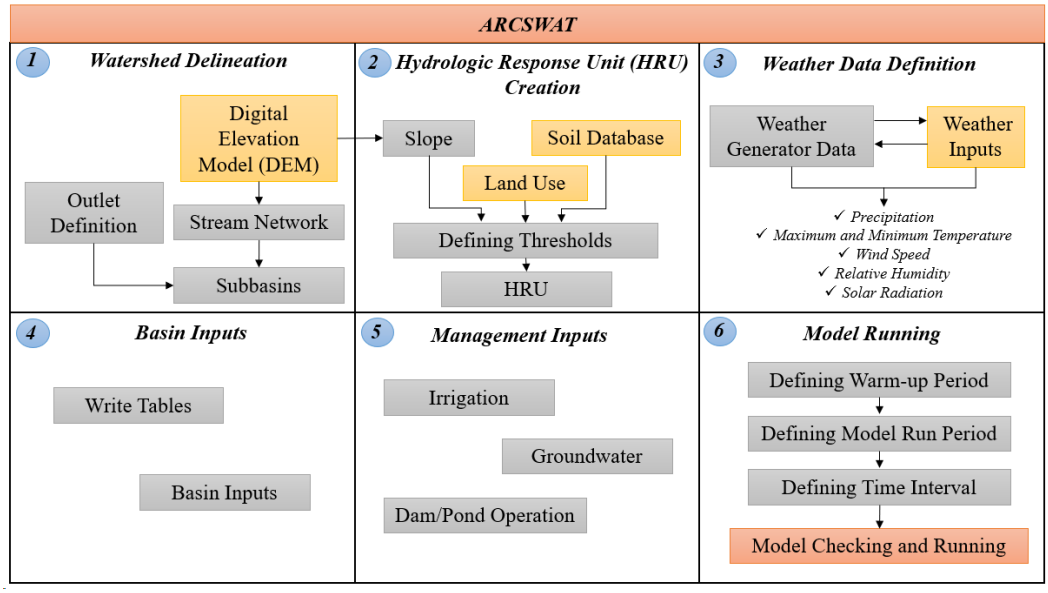


Figure 3.9 ArcSWAT process

SWAT-CUP is a software interface created by Abbaspour (2015) to facilitate the calibration, verification, and sensitivity assessments of SWAT. It aids in the

optimization process and offers automated calibration and uncertainty evaluations. SWAT-CUP enables the refinement and adjustment of model parameters through both automated and manual calibration procedures. SWAT-CUP is appropriate for hydrological model users of all levels, including beginners and experts (Arnold et al., 2012). Optimization can be performed according to Particle Swarm Optimization (PSO), Sequential Uncertainty Fitting Algorithm (SUFI-2), Monte Carlo Markov Chain (MCMC), Generalized Likelihood Uncertainty Technique (GLUE) and Parameter Solution (ParaSol) methods (Figure 3.10).

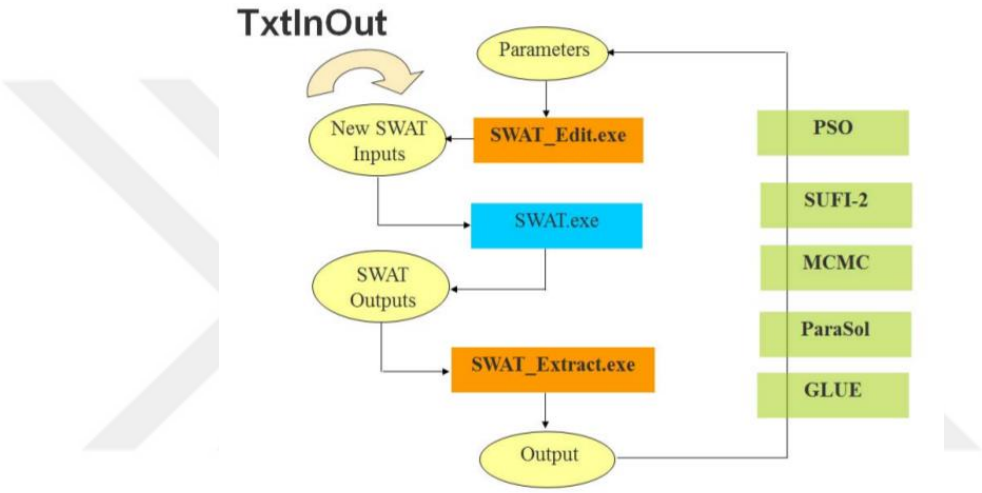


Figure 3.10 The linkage between SWAT and SWAT-CUP (Abbaspour, 2015).

The SUFI-2 model, which is widely used, accounts for uncertainties from input variables and measured parameters, with 95% prediction uncertainty (95PPU) describing the degree of uncertainty. Evaluation of uncertainty analysis uses the percentage of forecast uncertainty, calculated at 2.5 and 97.5 percent of output variable cumulative distribution.

Performing sensitivity analysis is crucial before calibration to evaluate the model's responsiveness to specific inputs. This procedure process involves running simulations to determine the precision of the model. Global sensitivity analysis involves the examination of model results for all parameters, whereas One at a time sensitivity analysis only investigates a particular parameter. Parameter assessments are determined using statistical methods: t-tests and p-values. A parameter is deemed to

make a significant contribution to the model if its p-value is less than 0.05. Following the sensitivity analysis, calibration process involves conducting a varying number of simulations, ranging from 300 to 1000. (Abbaspour, 2015). SWAT-CUP's post-processing capability includes calculating the objective function and 95PPU (percentile performance uncertainty) for all variables, thereby proposing updated parameter ranges for the next iteration. To achieve satisfactory results, the calibration method necessitates completing a maximum of five recommended iterations. (Abbaspour et al., 2015). Following calibration, the model's performance is assessed using objective functions such as R^2, Nash Sutcliffe Efficiency, PBIAS etc. Subsequently, the model is rerun during the validation period, employing the parameter ranges derived from the calibration. The performance of the model is then evaluated for this period as well. The process of SWAT-CUP is given by Figure 3.11.

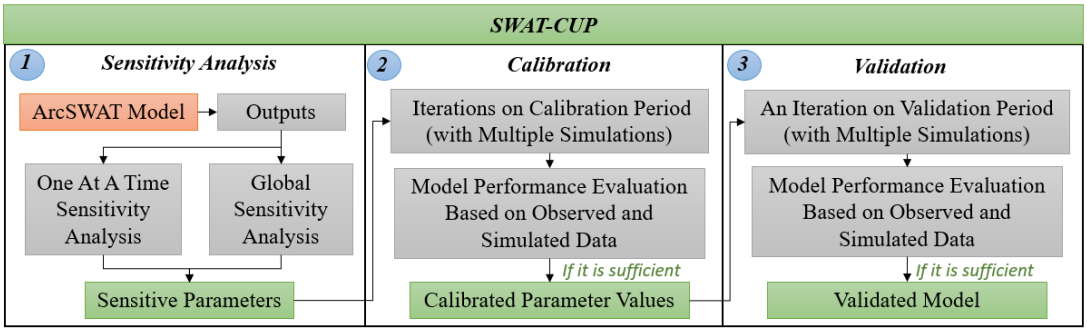


Figure 3.11 SWAT-CUP process

3.1.2.3 Hydrologic Engineering Center's Hydrologic Modeling System (HEC-HMS)

The Hydrological Modelling System (HMS) was developed by the US Army Corps' Hydrologic Engineering Center (HEC). The model was designed to simulate the comprehensive hydrological processes within dendritic watershed systems. This software encompasses conventional hydrologic analysis methods like event infiltration, unit hydrographs, and hydrologic routing. Moreover, HEC-HMS incorporates procedures essential for continuous simulation, encompassing evapotranspiration, snowmelt, and soil moisture accounting. Complementary analysis tools are available for tasks such as model optimization, streamflow forecasting, depth-

area reduction, uncertainty assessment, erosion and sediment transport, and water quality evaluation.

The software offers a fully integrated working environment that includes a database, data input tools, computation engine, and reporting utilities. A user-friendly graphical interface enables smooth navigation between different sections of the software. Results of simulations are stored in HEC-DSS (Data Storage System) and can be utilized alongside other software for investigations related to water availability, urban drainage, flow prediction, anticipated urbanization effects, reservoir spillway design, flood damage mitigation, floodplain regulation, and system operation.

Meteorology: Watershed hydrology involves the response of a watershed to precipitation and evapotranspiration. Precipitation can be historical event-based, frequency-based, or represent the upper limit of possible precipitation at a specific location and time. Meteorological data include precipitation, shortwave and longwave radiation, temperature, wind speed, humidity, pressure, dew point and evapotranspiration.

Hydrology: The hydrologic system facilitates the transfer of water back into the atmosphere via processes such as evaporation, transpiration, and through-fall and flow. During storms, these processes are constrained by meteorological conditions, reduced solar radiation, and decreased temperature. Evaporation and transpiration play a vital role in the overall water balance over extended periods, frequently causing most precipitation to be returned to the atmosphere. Vegetation experiences through-fall and flow when rainwater drips between leaves or cascades down stems, branches, and trunks. Upon reaching the land, water has the potential to accumulate and permeate, becoming stored in saturated layers of soil. This water exhibits both vertical and horizontal movement, eventually reaching its field capacity and subsequently flowing into a stream channel. Overland flow refers to the movement of water that does not accumulate or seep into the soil, ultimately contributing to the overall outflow of a watershed. The hydrological cycle is shown in Figure 3.12.

Evapotranspiration, infiltration, baseflow and transformation methods used in the model are summarized in Figure 3.13.

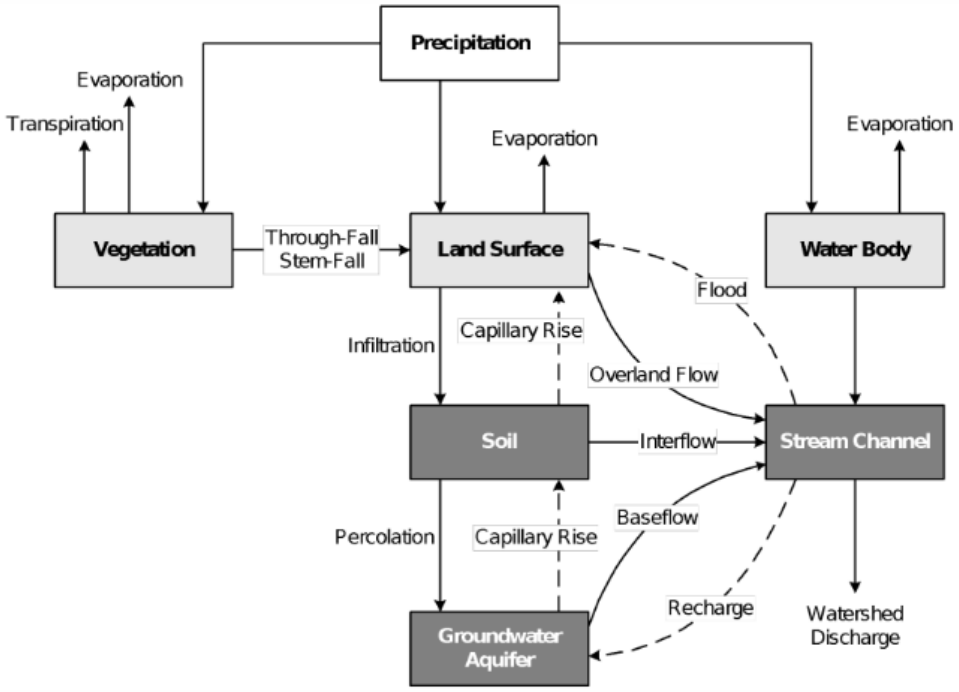


Figure 3.12 Runoff process (Ward, 1975; U.S. Army Corps of Engineers, Hydrologic Engineering Center, 2000)

Routing phase of hydrological cycle: When water from smaller areas flows into designated channels, the depth of the water increases, and it changes into open channel flow. Open channel flow approximations model the movement of flood waves as they travel downstream, considering both the routing and attenuation effects. The program incorporates routing models that utilize continuity and momentum equations to calculate a downstream hydrograph. These models are appropriate for a wide range of flood runoff studies. The methods used for channel routing are summarized in Figure 3.13.

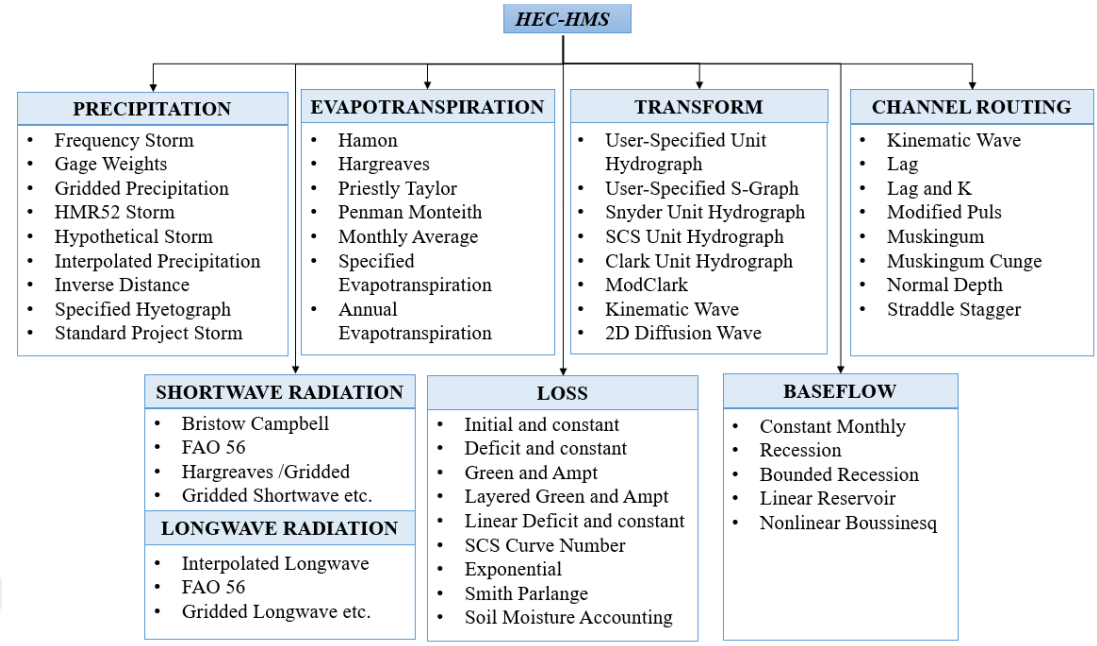


Figure 3.13 The methods in HEC-HMS

Calibration and validation: The application utilizes initial parameter estimates to calculate hydrographs for watershed runoff and channel discharge. The computed hydrograph is compared to the observed hydrograph to evaluate its level of conformity. If the results are not satisfactory, it will modify the settings and repeat the process. Objective functions are used to evaluate model performance. Objective functions for calibration are sum of absolute errors (SAE) (Equation 3.12), sum of squared residuals (SSR) (Equation 3.13), percent error in peak (PE) (Equation 3.14), and peak-weighted root mean square error objective function (PW-RMSE) (Equation 3.15).

$$SAE = \sum_{i=1}^{NQ} |q_o(i) - q_s(i)| \tag{3.12}$$

$$SSR = \sum_{i=1}^{NQ} [q_o(i) - q_s(i)]^2 \tag{3.13}$$

$$PE = 100 \frac{q_s(peak) - q_o(peak)}{q_o(peak)} \tag{3.14}$$

$$PWRMSE = \left\{ \frac{1}{NQ} \left[\sum_{i=1}^{NQ} (q_o(i) - q_s(i))^2 \left(\frac{q_o(i) + q_o(mean)}{2q_o(mean)} \right) \right] \right\}^{1/2} \tag{3.15}$$

Where NQ is number of computed hydrograph ordinates, $q_o(i)$ is observed flows; $q_s(i)$ is calculated flows, computed with a selected set of model parameters; $q_o(peak)$ is observed peak, $q_o(mean)$ is mean of observed flows, and $q_s(peak)$ is calculated peak. After achieving a successful fit, the program provides the optimal parameter values, which can be utilized for flood runoff studies.

Model interface: HEC-GeoHMS (Figure 3.14) is a Geographic Information System (GIS) toolset designed specifically for engineers and hydrologists. It is used to convert drainage pathways and watershed boundaries into hydrologic data formats. It enables the representation, recording, examination, and outlining of smaller drainage areas and watercourses, making it a highly effective approach for producing hydrological data.

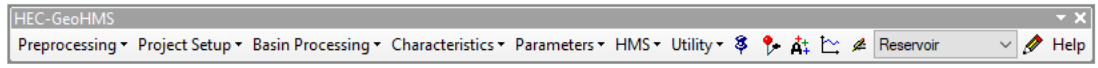


Figure 3.14 HEC-GeoHMS extension in ARCGIS.

The HEC-GeoHMS model is constructed following the sequence depicted in Figure 3.15 to establish the bases for the HEC-HMS model (as illustrated in Figure 3.16). Similarly, the HMS model is developed in the sequence outlined in Figure 3.17.

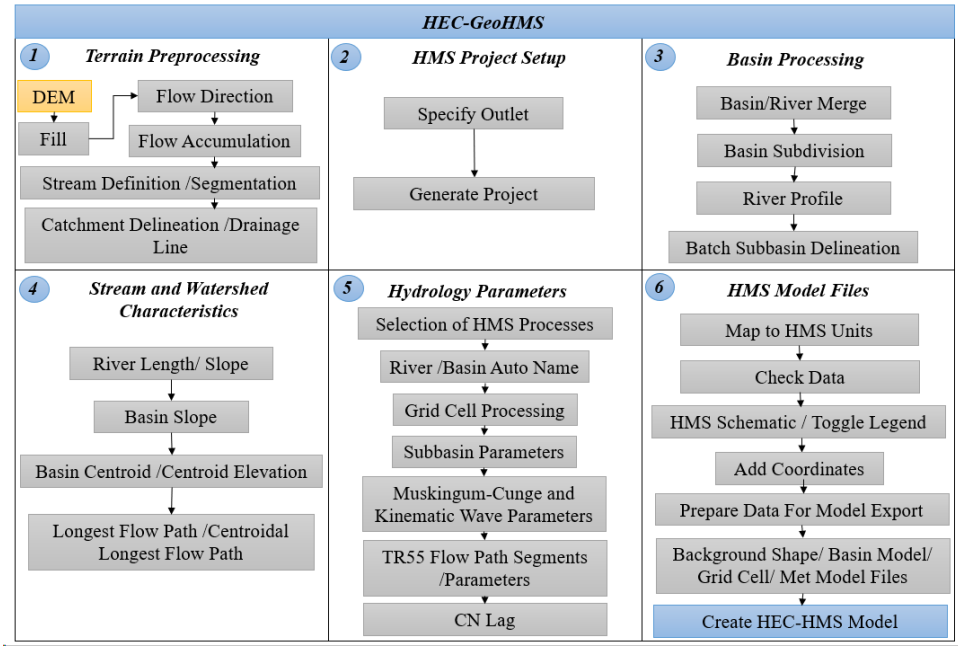


Figure 3.15 HEC-GeoHMS process.

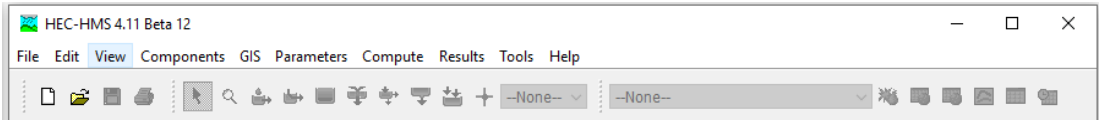


Figure 3.16 HEC-HMS model interface.

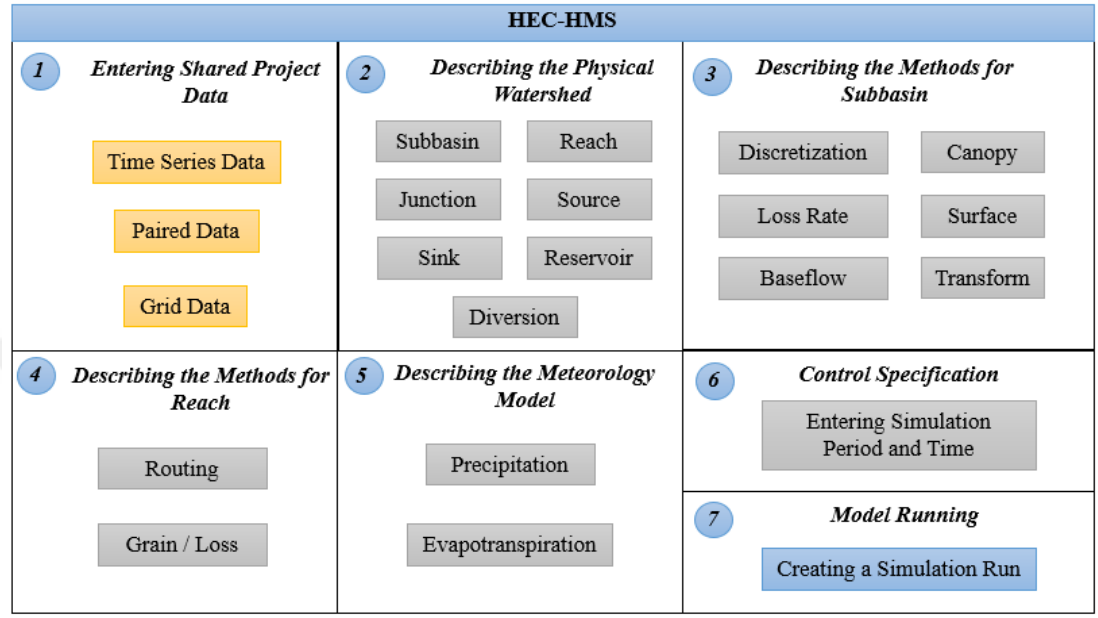


Figure 3.17 HEC-HMS process.

3.1.3 Hydraulic Modeling

Hydraulic modeling is a frequently used technique in hydraulic engineering to analyze design and operational issues. This method entails constructing a scaled replica that imitates the flow and transportation of fluids in different natural flow systems. The level of complexity of the model is contingent upon the objectives of the investigation. It is employed to evaluate the efficiency of hydraulic structures and machines. Typical modeling topics encompass the study of water flow and the movement of sediment in rivers and coastal regions. Additionally, the hydraulic efficiency of water intakes, spillways, outlets, and similar elements is also examined (ASCE, 2000).

Hydraulic models are utilized for the purpose of simulating the movement of water through various conduits such as pipes, channels, rivers, or other hydraulic structures. The primary goal is to comprehend the behavior of water within a hydraulic system

and anticipate its response to different conditions. Hydraulic models are extensively utilized in the design of water distribution systems, stormwater management, floodplain mapping, and river channel analysis. Hydraulic models are categorized as 1-D (one-dimensional) models, 2-D (two dimensional) models, 3-D (three dimensional) models and computational fluid dynamics (CFD) models. Below are examples of frequently used hydraulic models.

3.1.3.1 Samples of Hydrological Models

The River Analysis System (HEC-RAS) is a hydraulic model developed by the US Army Corps of Engineers. It is specifically designed for analyzing river and floodplain hydraulics and is commonly used for flood mapping purposes (Brunner, 1994; Brunner, 2016).

FLO-2D specializes in the modeling of floods in two dimensions. Simulates the movement of water in channels and on land, making it well-suited for mapping floodplains (Erena et al., 2018; Kim et al.,2013).

MIKE Flood is utilized within the MIKE by DHI package to conduct comprehensive flood modeling, considering the intricate interplay among rivers, urban areas, and other elements (Kadam & Sen, 2012; Patro et al., 2009).

TUFLOW (Two-dimensional unsteady flow) was developed by international engineering and environmental consultancy BMT WBM. It is a numerical model that simulates river, coastal, and urban water flow, levels, and hydraulic processes. The model is used for flood modeling, coastal simulations, sediment transport, and urban drainage assessments (Phillips et al., 2005; Syme, 2001).

SOBEK is a hydraulic modeling software, was developed by Deltares, a Dutch research institute specializing in water and subsurface management. The model is used for simulating water flow, quality, and sediment transport in rivers, estuaries, and urban drainage systems (Dhondia & Stelling, 2004, Vanderkimpen et al., 2009).

3.1.3.2 Hydrologic Engineering Center's River Analysis System (HEC-RAS)

HEC-RAS is a comprehensive software system designed for interactive use in a multitasking environment. The main objective of this tool is to assist in the analysis of rivers and the performance of hydraulic calculations. This system is composed of a graphical user interface (GUI), separate analysis modules, data storage and management features, graphics, mapping abilities, and reporting tools. The modeling system includes various components for analyzing rivers, such as calculations for one-dimensional steady flow water surface profiles, simulations for one-dimensional and/or two-dimensional unsteady flow, computations for sediment transport, and analysis of water quality in one dimension. In addition, HEC-RAS provides hydraulic design features and includes a spatial data integration and mapping system called HEC-RAS Mapper.

HEC-RAS provides a variety of features for analyzing rivers and performing hydraulic calculations. It provides users with tools to input and modify geometric data, perform hydraulic analyses, analyze graphical and tabular output, and conduct analyses on bridge scour, and channel modifications. In addition, the system can facilitate complex applications involving the simulation of unsteady flow, such as dam break analysis and the modeling of pump stations. A significant advantage of HEC-RAS is its utilization of a standardized geometric data representation and computation routines for all river analysis components.

Innovations introduced in HEC-RAS version 6.0 and upper versions have significantly enhanced its popularity and applicability across various hydraulic domains. This versatile software is now extensively utilized for flood inundation mapping, urban flood risk analysis, 1D simulations, flash flood modeling, dam failure prediction, and various other applications (Akiyanova et al., 2023).

HEC-RAS's capabilities extend to advancing dam safety management by predicting breach outflow hydrographs and generating downstream flood inundation maps for flood-prone areas. The software's effectiveness is demonstrated in comparative analyses of flood return periods, emphasizing its utility in informing emergency

preparedness plans and floodplain management strategies, particularly through detailed outcomes from 2D simulations (Phyo et al., 2023).

Furthermore, HEC-RAS proves instrumental in quantifying environmental flow targets in hydro ecologically altered streamflow regimes through an integrated modeling approach, as evidenced by a study conducted by Zeiger & Hubbart (2021). This research showcases the effectiveness of coupling HEC-RAS with The Soil and Water Assessment Tool (SWAT) for realistic 2D rain-on-grid simulations. (Zeiger & Hubbart, 2021).

HEC-RAS calculates water surface elevations at all locations of interest using steady flow simulation or hydrograph routing. These computations require geometric, steady, unsteady, sediment, and water quality data. Geometric data is needed for HEC-RAS. Data types like steady flow data for water surface profile computation are only needed for that analysis.

Creating a terrain model is necessary in HEC-RAS Mapper to perform calculations involving two-dimensional (2D) flow areas or to visualize mapping results. Users can link one or multiple terrain models with geometry or results files.

HEC-RAS has a wide range of boundary and initial conditions that can be applied to a model. Boundary conditions consist of external boundary conditions along the perimeter of the 2D area, internal boundary conditions, and global boundary conditions (Meteorological Data) that are applied to the entire model. There are four types of external boundary conditions that are flow hydrograph, stage hydrograph, normal depth, and rating curve. The interface and the process of the model are given by Figure 3.18 and 3.19, respectively. The model interface is given by Figure 3.18.

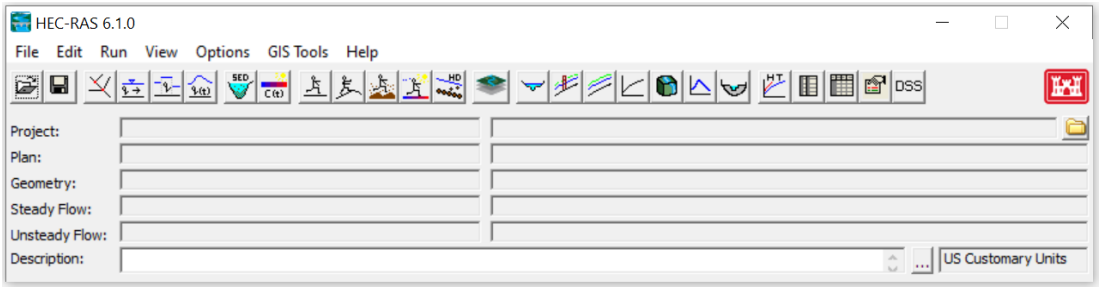


Figure 3.18 HEC-HMS model interface.

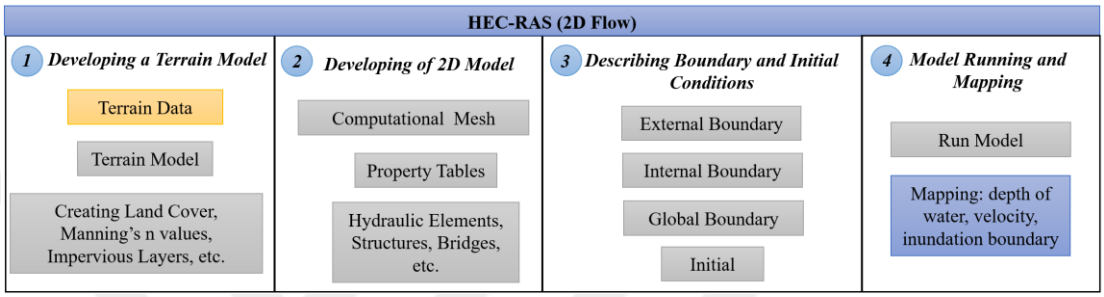


Figure 3.19 HEC-HMS model process.

3.1.4 Drought Analyses

Drought can occur over a wide range of durations, from multi-year or decadal rainfall deficits, also known as "megadroughts," to "flash droughts," which occur over a period of weeks and are characterized by an abrupt onset and quick escalation of drought conditions. Due to close relationship between drought and climatological events, variables such as precipitation, air temperature, and streamflow can be utilized to determine the presence of drought (Ndayiragije & Li, 2022). Indices, which are measurements of the intensity, duration, and frequency of droughts, are frequently used to analyze drought events utilizing drought indicators. The scientific literature has produced many drought indices. These can be anomalies in a single variable (such as runoff, evapotranspiration, precipitation, soil moisture, etc.) or indices that combine many meteorological/hydrometeorological variables.

The focus of the drought assessment is based on the changes of the physical conditions and metrics that directly have impact on drought events such as, precipitation deficits, excess atmospheric evaporative demand (AED), soil moisture deficits, hydrological deficits and atmospheric-based indices that combine

precipitation and AED (IPCC, 2023). In order to determine drought characteristics based on meteorological data in detail, both in terms of spatial extent and time periods, a new framework is applied in the presented study. The drought study utilized outputs from the coupled SWAT and VIC model. The drought analyses were conducted by also using observed meteorological data and grid-based climate data and the relationship between them was investigated. The methodology involved:

1. Using historically observed monthly records from point monitoring station locations, the drought indices were calculated on monthly based.
2. Using gridded data, which are dynamically downscaled on a 1 km resolution over a largely scale river basin, for the reference (1971–2004) and future conditions (2025-2099), the drought indices were calculated on monthly and daily based.
3. Using coupled LSM (VIC model) with hydrological model (SWAT model) outputs as data for the reference (1971–2004) and future conditions (2025-2099), the drought indices were calculated on monthly based.

As illustrated in Figure 3.20 and discussed earlier, a comparison was made in the calculation of drought indices using three types of data namely observed meteorological data, bias corrected climate data and SWAT model outputs.

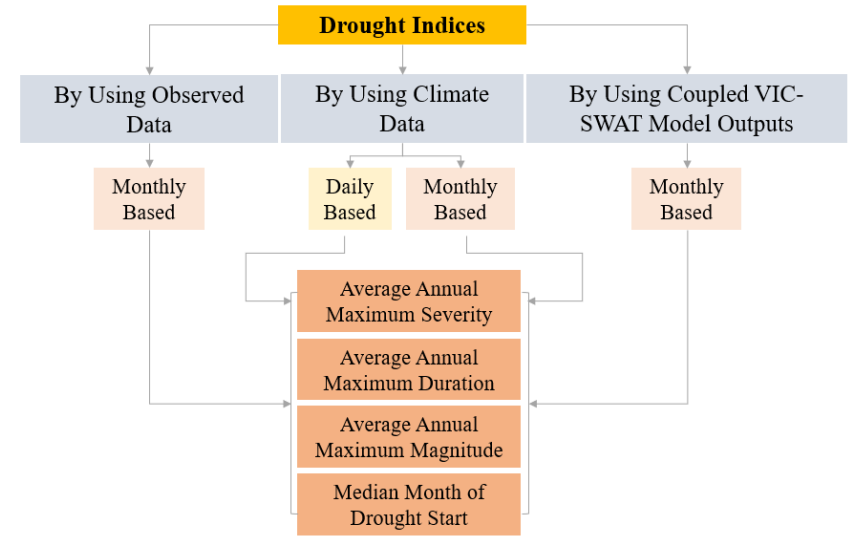


Figure 3.20 Drought analyses.

3.1.4.1 Drought Indices

A list of most widely used drought indicators and indices that are utilized in drought-prone areas can be found in the Handbook of Drought Indicators by World Meteorological Organizations (WMO & Global Water Partnership [GWP], 2016). Every index is thoroughly explained, including its history, traits, input parameters, use, advantages, disadvantages, sources, and references. In Table 3.4, a summary of commonly used drought indices is presented with the type of drought they address, required input parameters and some additional information that contribute the use of that specific index (WMO & GWP, 2016). The selection of indicators/indices is predicated on the unique traits of droughts that are most strongly linked to the consequences that the stakeholders find concerning. The optimal fit for any given location, area, basin, or region must be determined over time using a system of trial and error (GWP & WMO, 2016).

In the study, Standardized Precipitation Index (SPI), Standardized Precipitation Evapotranspiration Index (SPEI) and Standardized Streamflow Index (SSFI) were applied to investigate drought events in Küçük Menderes Basin. “The SPEI” package of the R statistical software developed by Beguería et al. (2014) was used for drought indices calculations on monthly based calculations. Daily based drought index calculations were performed only for SPI and "climate_indices 1.0.10" package (Adams, 2017) written in phyton programme language was used for calculation. The correlations between SPI, SPEI and SSFI drought indices were analysed and the compatibility of the indices with each other was investigated as Figure 3.21.

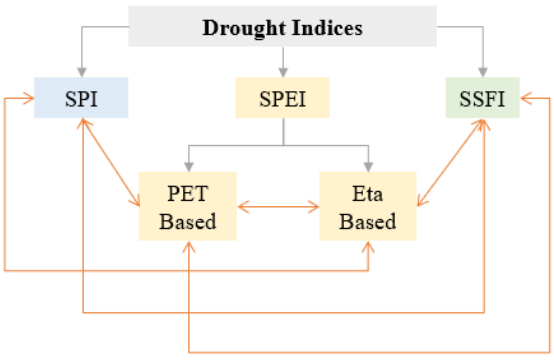


Figure 3.21 Relationship between drought indices.

Table 3.4 Available drought indices for the study area according to the required data (WMO and GWP, 2016).

Droughts	**Drought Indices**	**Input Parameters**	**Additional Information**
Meteorology	Standardized Precipitation Index (SPI)	P	Highlighted by the World Meteorological Organization as a starting point for meteorological drought monitoring
	Aridity Index (AI)	P, T	Can also be used in climate classifications
	Crop Moisture Index (CMI)	P, T	Weekly values are required
	Drought Reconnaissance Index (DRI)	P, T	Monthly temperature and precipitation are required
	Effective Drought Index (EDI)	P	Program available through direct contact with originator
	NOAA Drought Index (NDI)	P	Best used in agricultural applications
	Palmer Drought Severity Index (PDSI)	P, T, AWC	Complexity of calculations and the need for serially complete data
	Palmer Z Index	P, T, AWC	One of the many outputs of PDSI calculations
	Rainfall Anomaly Index (RAI)	P	Serially complete data required
	Self-Calibrated Palmer Drought Severity Index (sc-PDSI)	P, T, AWC	Complexity of calculations and serially complete data required
	Standardized Anomaly Index (SAI)	P	Point data used to describe regional conditions
	Standardized Precipitation Evapotranspiration Index (SPEI)	P, T	Serially complete data required; output similar to SPI but with a temperature component
Soil moisture	Soil Moisture Anomaly (SMA)	P, T, AWC	Intended to improve upon the water balance of PDSI
Hydrology	Palmer Hydrological Drought Severity Index (PHDI)	P, T, AWC	Serially complete data required
	Standardized Streamflow Index (SSFI)	SF	Uses the SPI program along with streamflow data
	Streamflow Drought Index (SDI)	SF	Similar calculations to SPI, but using streamflow data instead of precipitation
Remote Sensing	Normalized Difference Vegetation Index (NDVI)	Sat	Calculated for most locations

3.1.4.1.1 Standardized Precipitation Index (SPI)

The SPI, developed by McKee et al. (1993), is a widely used index globally for measuring normalized anomalies in precipitation and characterizing drought events across different timescales. The long-term precipitation record is fitted to a probability distribution, converted to the normal distribution with mean zero for the location and desired period (Tsakiris & Vangelis, 2004). Standardization involves calculating the difference of precipitation from the mean for a specified period divided by the standard deviation, based on past records (McKee et al., 1993). The gamma distribution given by Equation 3.16 and 3.17 is recommended to fit precipitation series by Thom (1966), but the gamma function is undefined for x=0. Also, a precipitation series may have zero value. Hence the cumulative probability (H(x)) is given by Equation 3.18. Here, q is the probability of zero. H(x) (Equation 3.18) is transformed to the standard random variable Z, or defined as SPI value, with mean zero and variance of one.

$$g(x) = \frac{1}{\beta^{\alpha}\Gamma(\alpha)} x^{\alpha-1} e^{-x/\beta} \tag{3.16}$$

$$G(x) = \int_0^x g(x)dx = \frac{1}{\widehat{\beta}^{\widehat{\alpha}}\Gamma(\widehat{\alpha})} \int_0^x x^{\widehat{\alpha}-1} e^{-x/\widehat{\beta}} dx \tag{3.17}$$

$$H(x) = q + (1-q)G(x) \tag{3.18}$$

Mckee et al. (1993) found that positive SPI values indicate above-median precipitation and negative values indicate below-median. Drought events occur when the SPI is continuously negative and end when it turns positive. In this study, SPI calculations are based on 30 and 90-day index values for daily calculations and 1, 3, 6 and 12-month index values for monthly calculations. Mckee et al. (1993) classified droughts as given by Table 3.5.

Table 3.5 Drought classification

Drought Class	**SPI Values**
Near Normal	-1.0≤SPI<1.0
Moderate	-1.5≤SPI<-1.0
Severe	-2.0≤SPI<-1.5
Extreme	SPI≤-2.0

3.1.4.1.2 Standardized Precipitation Evapotranspiration Index (SPEI)

The SPEI, which was developed by Vicente-Serrano et al. (2010), is a multiscale drought index. The index needs monthly (or daily, weekly) precipitation and temperature data. SPEI, like SPI, can measure drought severity and duration, identify the start and end of drought events, and be compared over time and space, making it useful for many climates ranges. It's beneficial because temperature variability affects drought assessment (Vicente-Serrano et al., 2010).

PET inclusion in SPEI provides accurate drought severity estimates in humid and dry climates (Beguería et al., 2014). The difference (Di) between precipitation and PET (Equation 3.19), calculated for the month (i) at different time scales, is used to calculate SPEI series. In contrast, Di times series are used instead of precipitation time series.

$$D_i = P_i - PET_i \tag{3.19}$$

The log-logistic distribution is selected as best fitted distribution to the D series at all timescales using regional frequency analysis based on L-moment ratios (Vicente-Serrano et al., 2010). The probability density function f(x) of a three-parameter log-logistic distribution is given by Equation 3.20, where α, β, and γ are scale, shape, and origin parameters, respectively. The log-logistic distribution can take into account negative values, and it is capable of adopting different shapes to model the frequencies of the D series at different time scales (Vicente-Serrano et al., 2010). The probability distribution function F(x) of the D series, according to the log-logistic distribution is given by Equation 3.21.

$$f(x) = \frac{\beta}{\alpha}\left(\frac{x-\gamma}{\alpha}\right)^{\beta-1}\left[1+\left(\frac{x-\gamma}{\alpha}\right)^{\beta}\right]^{-2} \tag{3.20}$$

$$F(x) = \left[1+\left(\frac{\alpha}{x-\gamma}\right)^{\beta}\right]^{-1} \tag{3.21}$$

To estimate the parameters of log logistic distribution, It is recommended the use of unbiased probability weighted moments (PWMs) (Equation 3.22), which provides

SPEI series with equal variance throughout the world at different time scales, since it has more excellent results from the use of PWMs based on the plotting position formula (Equation 3.23) (Beguería et al., 2014).

$$w_s = \frac{1}{N}\sum_{i=1}^{N} \frac{\binom{N-i}{s} D_i}{\binom{N-i}{s}} \tag{3.22}$$

$$w_s = \frac{1}{N}\sum_{i=1}^{N} (1 - F_i)^s \, D_i \tag{3.23}$$

Here, w_s is the PWM of order s, N is the number of data points and F_i is a frequency estimator. The following procedure is to obtain the standardized values of F(x) as SPEI values, like SPI.

The methodology of SPEI was improved in terms of the selection of probability distribution (log-logistic or Pearson III), computation method of the distribution function parameters (plotting position PWMs, unbiased PWMs, and maximum likelihood), and PET equation (Thornthwaite, Hargreaves and Penman – Monteith) and given all options were implemented SPEI package of R statistical program (Beguería et al., 2014). The log-logistic and the gamma distribution are selected as default for SPEI and SPI calculations, respectively. The unbiased PWMs is recommended by so it is selected as default. In terms of PET calculation, Penman – Monteith is recommended since it is more robust, but in case the data is not available other methods can be used (Beguería et al., 2014).

The only factor affecting PET is climatic parameters. Therefore, it can be completely compared in different locations or in different seasons (Beguería, et al. 2014). Dai (2011), Homdee et al. (2016) and Joetzjer et. al (2012) compared to PET and ET_a, emphasized that ET_a allow for a better estimation of the soil water balance, so it is better in drought analysis. SPEI calculations can be performed from 1 month to 48 months for monthly calculations.

3.1.4.1.3 The Standardized Streamflow Index (SSFI)

The Standardized Streamflow Index (SSFI) was introduced by Modarres (2007). SSFI addresses hydrological drought and utilizes SPI program along with streamflow data as previously given in Table 3.4. According to Modarres, SSFI and SPI were comparable in that SSFI was defined as the streamflow difference between the mean and standard deviation for a given period. The index can be used for monitoring hydrological conditions of multiple timescales and advantageous as it is easy to use with the SPI program.

The SSFI for a given period is calculated as the streamflow difference divided by the mean and standard deviation (Equation 3.24).

$$SSFI = \frac{F_i - \bar{F}}{\sigma_\tau} \tag{3.24}$$

Where, F_i is the flow rate in time interval, $\bar{F}$ the series mean and σ is the standard deviation for series (Modarres, 2007). SSFI calculations can be performed from 1 month to 48 months for monthly calculations.

3.1.4.2 Drought Characteristics

Drought parameters in a series are drought severity, drought duration and drought magnitude (Figure 3.22). Drought duration (D) refers to the period starting from the beginning of a drought until its end, encompassing the entire duration in which the area experiences drought conditions. Drought severity (S) is obtained by summing the block time series of negative SPI values without gaps as given by Equation 3.25 (Kuzucu and Onuşluel Gül, 2023).

$$S_{t,i} = \sum_{j=1}^{D_i} \left| SPI_{ij} \right| \tag{3.25}$$

The SPI_{ij} represents the negative SPI drought index Di during the drought period j. The drought severity value "$S_{t,i}$" is calculated as the absolute value of the sum of negative SPI values over a specific time period, denoted as “t”. The variable “t” represents the designated time interval, such as 30 days, 90 days, or 1 month, 3 months

for the SPI as the approach that was previously suggested by firstly Onuşluel Gül et al. (2022), then Kuzucu & Onuşluel Gül (2023) and Kuzucu et. al (2023). Drought magnitude (M) is the ratio of drought severity to drought duration.

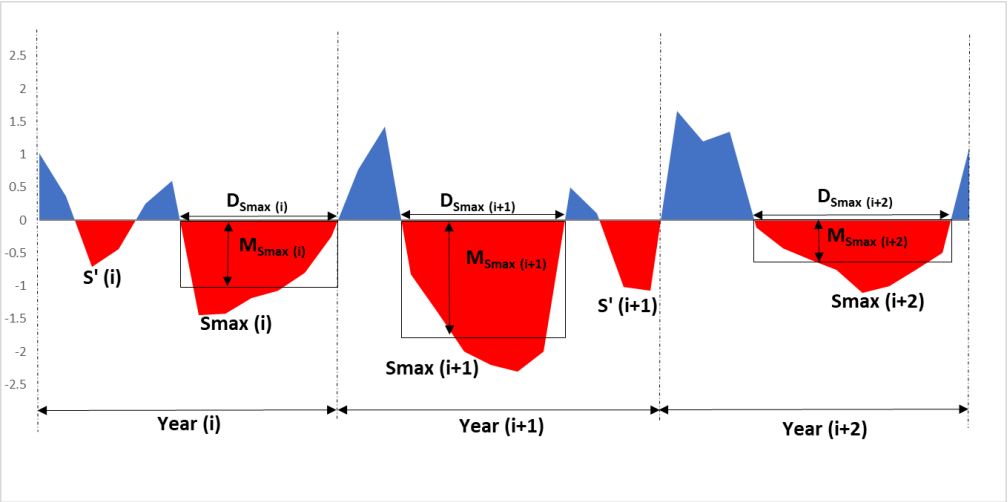


Figure 3.22 Representative time series of SPI/SPEI and annual maximum drought severities (Smax), drought duration (D_{Smax}) and the average maximum drought magnitude (M_{Smax}) (Kuzucu and Onuşluel Gül, 2023).

3.1.4.3 Drought Analysis Using Observed Data

Drought indices were calculated from 1 to 12 months using data observed at selected meteorological and flow stations. The various drought maps were created using drought indices from 1 month to 12 months obtained for 11 meteorological stations.

Homogeneity Tests: To ensure that the resulting drought indices sets used in the study had sufficient quality, homogeneity studies were carried out. For this purpose, standard normal homogeneity test, Buishand range test and Pettitt test were performed to detect a change point on both the SPI and SPEI series. The R package called "trend" developed by Pohlert et al. (2016), was used to perform the homogeneity tests in this study.

The Standard Normal Homogeneity Test (SNHT) is based on comparing the critical value for the selected significance level (α) and the sample size (n) with the maximum

value of the the test statistic (*T(k)*) (Equation 3.26) which is used to compare the mean of the first k years of the record with that of the last $n-k$ years (Equation 3.27) (Wijngaard et al., 2003):

$$T(k) = k\bar{z}_1^2 + (n-k)\bar{z}_2^2 \quad k = 1, \dots, n \tag{3.26}$$

$$\overline{z_1} = \frac{1}{k}\sum_{i=1}^{k}(Y_i - \bar{Y})/s \text{ and } \overline{z_2} = \frac{1}{n-k}\sum_{i=k+1}^{n}(Y_i - \bar{Y})/s \tag{3.27}$$

$$T_0 = \max_{1 \le k < n} T(k) \tag{3.28}$$

When a break is located at a year, then *T(k)* gives a maximum value at the year. The test statistic T_0 is defined by Equation 3.28. The null hypothesis which is defined as "no trend" will be rejected, in case T_0 is above the critical value.

The Buishand range test is based on the adjusted partial sums given by Equation 3.29.

$$S_k^* = \sum_{i=1}^{k}(Y_i - \bar{Y}) \qquad k = 1, \dots, n \tag{3.29}$$

The value of S_k^* will fluctuate around zero, in case series is homogeneous but S_k^* has reached a maximum or minimum in case a year has break (Kang & Yusof, 2012). Rescaled adjusted range (R) is obtained by Equation 3.30.

$$R = \left(\max_{0 \le k \le n} S_k^* - \min_{0 \le k \le n} S_k^*\right)/s \tag{3.30}$$

The critical values given by Buishand (1982) are compared with Q values given by the Equation 3.31. In case Q value is greater than the critical value, the series is not homogeneous.

$$Q = R/\sqrt{n} \tag{3.31}$$

The Pettitt Test calculates the corresponding rank indicated by r_i and test statistics instead of the monthly total precipitation values indicated by Y_i. X_k statistic is obtained by Equation 3.32.

$$X_k = 2\sum_{i=1}^{k} r_i - k(n+1) \quad k = 1, .., n \tag{3.32}$$

The X_k is depicted in the graphs representing the results of this test. When a break occurs in year E, the test statistic will be maximal or minimal near the year k=E (Wijngaard et al., 2003). It is concluded that the homogeneity in the series deteriorates if the X_E statistic (Equation 3.33), which is the maximum of the absolute values of the X_k statistic, exceeds a critical value depending on the sample size and the significance level.

$$X_E = \max_{1 \le k < n} |X_k| \tag{3.33}$$

Trend Test*:* The R package called "trend" developed by Pohlert et al. (2016), was used to perform the trend tests in this study. Drought indices were checked for monotonic trend by using Mann-Kendal nonparametric test (Mann, 1945; Kendall, 1948) and Sen's Slope test. The Mann-Kendall (MK) non parametric test is based on the statistic S (Equation 3.34) that is obtained by the difference of the number of the yi > yj type of pairs (P), and the number of the yi < yj type of pairs (M), for each pair of observed values yi, yj (i > j) of the random variable (Önöz & Bayazıt, 2003).

$$S = P - M \tag{3.34}$$

The statistic S is approximately normally distributed when number of sample (n) is greater than 8 (Yue & Wang, 2004). The standard deviation, the standardized test statistic (z) of the MK test and the corresponding P-value (p) for the one-tailed test are respectively given by Equation 3.35, Equation 3.36 and Equation 3.37.

$$\sigma_s = \sqrt{\frac{n\,(n-1)(2n+5)}{18}} \tag{3.35}$$

$$Z = \begin{cases} (S-1)/\sigma_S & S > 0 \\ 0 & S = 0 \\ (S+1)/\sigma_S & S < 0 \end{cases} \tag{3.36}$$

$$p = 0.5 - \frac{1}{\sqrt{2\pi}} \int_0^{|Z|} e^{-\frac{t^2}{2}}\, dt \tag{3.37}$$

When the calculated Z value is less than $z_{\alpha/2}$ in the absolute value, the null hypothesis that there is no trend is accepted, otherwise it is rejected. By comparing the p with the significance level (α) (Equation 37), in case of p≤α, the trend is considered

as statistically significant. Positive and negative Z values represent an increasing and decreasing trend, respectively. As the sample size increases, the power of the test increases so that the presence of a trend can be more easily distinguished and the test is expected to be less affected by outliers because its statistics are not based directly on the values of the random variable, but on the sign of differences (Önöz & Bayazıt, 2003). Identifying the trend in recorded hydrological time series provides information about the possibility of future trends to change which is useful for effective water resource planning, design, and management (Yue & Wang, 2004).

The Sen's slope test (Sen, 1968), the non-parametric test, is employed to identify the presence of a linear trend and quantify the rate of change over time. Sen's Slope offers a distinct benefit over linear regression in that it is not influenced by the presence of outliers or data errors in the test (Aditya et al., 2021). Equation 3.38 represents the Sen's Slope equation for i=1, 2.., N pairs of data samples.

$$Q_i = \frac{(x_j - x_i)}{j - i} \tag{3.38}$$

Where, xj and xi represent the values at time j and i (j > i). The number of slope estimates, N, in the time series is equal to n(n-1)/2, where n represents the number of values of xj. The N value of Qi is arranged in ascending order, and then Sen's Slope is calculated using the median Qi (Q_{med}). The value of Q_{med} (Equation 3.39) was computed using a two-tailed test at confidence intervals of 90% and 95%.

$$Q_{med} = \begin{cases} Q_{\left[\frac{N+1}{2}\right]} & if\ N = odd \\ \frac{Q_{\left[\frac{N}{2}\right]} + Q_{\left[\frac{N+1}{2}\right]}}{2} & if\ N = even \end{cases} \tag{3.39}$$

Regional Frequency Analysis: The regional frequency analysis has utilized the L-moments procedure, following the four steps outlined by Hosking and Wallis (1997): Data screening, identification of homogeneous regions, selection of a frequency distribution, and estimation of the frequency distribution. The discordancy statistic (D_i) (Equation 3.40), proposed by Hosking & Wallis (1997), utilizes L-moment ratios (L-CV, L-skewness, and L-kurtosis) to characterize the site in a three-dimensional space. When the site number is 11 (for Küçük Menderes Basin, 11 meteorological

stations were used), the critical discordancy statistics (D) is 2.632. However, according to Hosking and Wallis (1997), any site with a D_i value greater than 3 is considered discordant.

$$Di = \frac{N_s}{3(N_s-1)}(u_1 - \bar{u})^{T_m} S_{cm}^{-1}(u_1 - \bar{u}) \quad (3.40)$$

The variables in the equation are defined as follows: Ns represents the number of measurement stations in the region, S_{cm} is the sample covariance matrix, u_l is a vector containing the L-coefficient of variation (t), L-skewness (t_3), and L-kurtosis (t_4), u is a vector (3×1) representing the arithmetic average of u_l for the N_s stations, and T_m represents the transposed matrix and −1 represents the inverse matrix (Santos et al.,2011).

The heterogeneity measure (H_k) (Equation 3.41) quantifies the differences in sample L-moments between different sites and compares them to what would be expected in a region with uniform characteristics.

$$H_k = \frac{V_k - \mu_{vk}}{\vartheta_{vk}} \quad (3.41)$$

The test statistic is located at the L-coefficient of variation (t) for k=1, L-skewness (t_3) for k=2, and L-kurtosis (t_4) for k=3. In case k=1 the test statistic V_1 is given by Equation 3.42.

$$V_1 = \left[\frac{\sum_{j=1}^{N_S} N_j(t^j - t^R)}{\sum_{j=1}^{N_S} N_j}\right]^{1/2} \quad (3.42)$$

The variables in consideration are Ns, which represents the number of stations, Nj, which represents the record length at station j, and tj, which represents the L-coefficient.

Hosking and Wallis (1997) suggested that if H_1 is less than 2, the region should be considered homogeneous. If H_1 is between 2 and 3, the region may be heterogeneous. If H_1 is greater than 3, the region should be considered heterogeneous. The goodness-of-fit statistic (Z_{DIST}) (Equation 3.43) is calculated to assess the degree of agreement

between the theoretical L-kurtosis of the fitted distribution and the regional average L-kurtosis of the observed data (Santos et al., 2011). The statistical distribution with the smallest absolute value of Z is regarded as the optimal selection among the available probability distribution functions (Santos et al., 2011).

$$Z = \frac{(t_4^{-R} - t_4^{dist})}{\sigma_{t_4}} \tag{3.43}$$

Where t_4^{-R} represents the regional average L-kurtosis, σ_{t_4} represents the standard deviation of t_4^{-R}, and t_4^{dist} is the L-kurtosis of a fitted distribution.

This calculation is performed separately for the homogeneous region using the Generalized Logistic, Generalized Extreme-Value (GEV), Lognormal, Pearson Type III, and Generalized Pareto distributions.

The cumulative distribution function of the Generalized Logistic distribution is given by Equation 3.44. Where μ is location parameter and σ is the scale parameter (σ > 0)

$$F(x) = \frac{1}{1+e^{-\frac{x-\mu}{\sigma}}} \tag{3.44}$$

The cumulative distribution function of the Generalized Extreme Value (GEV) distribution is given by Equation 3.45.

$$F(x) = exp\left\{-\left[1 + \xi\left(\frac{z-\mu}{\sigma}\right)\right]^{1/\xi}\right\} \tag{3.45}$$

Where, shape, location, and scale parameters are denoted by ξ, ɱ and σ, respectively. The shape parameter ξ is used to define the type of distribution. ξ < 0 corresponds to Weibull, ξ > 0 to Fréchet, ξ = 0 to Gumbel distribution.

The cumulative distribution function of the Lognormal distribution is given by Equation 3.46. Where, μ represents mean of logarithmic values and σ represents Standard deviation of logarithmic values.

$$F(x) = \frac{1}{\sigma\sqrt{2\pi}} \int_0^x \frac{1}{t} exp\left\{\frac{-(logt-\mu)^2}{2\sigma^2}\right\} dt\,, \quad for\ x > 0 \qquad (3.46)$$

The cumulative distribution function of the Pearson Type III distribution is given by Equation 3.47. Where Γ and γ are the upper and lower incomplete gamma function, respectively.

$$F(x) = \begin{cases} \frac{1}{\Gamma(a)} \Gamma\big(a, b(x-m)\big), & b < 0 \\ \frac{1}{\Gamma(a)} \gamma\big(a, b(x-m)\big), & b > 0 \end{cases} \qquad (3.47)$$

The cumulative distribution function of the Generalized Pareto distribution is given by Equation 3.48. Where, shape, location, and scale parameters are denoted by μ, σ and ξ, respectively.

$$F(x) = \begin{cases} 1 - \left[1 + \xi\left(\frac{x-\mu}{\sigma}\right)\right]^{-1/\xi}, & \xi \neq 0 \\ 1 - exp\left(-\frac{x-\mu}{\sigma}\right), & \xi = 0 \end{cases} \qquad (3.48)$$

If the value of $|Z_{DIST}|$ is below 1.64, then the distribution is considered acceptable. The regional L-moment algorithm is utilized to calculate the quantiles of the regional frequency distribution. Simulation is used to obtain error bounds for the estimated regional growth curves.

The regional frequency analysis was performed to detect the spatial homogeneity for drought severities calculated from SPI-6 monthly series. The R package called "lmomRFA" developed by Hosking (2009), was used to perform the regional frequency analysis in this study.

Drought mapping: The annual maximum severity and duration of drought were determined as shown in Figure 3.22. The trend in the average annual maximum drought severity and duration was investigated from these values. Drought maps were prepared using these station-based indicators and trend values for each drought index and duration. Using the drought classification given in Table 3.5 for SPI and SPEI,

maps were derived by obtaining the number of moderate, severe, and extreme drought events from the series obtained.

3.1.4.4 Drought Analysis Using Gridded Climate Data

The methodology is given by Figure 3.23. The computational algorithm with the potential to extend to other types of drought indices was used for two common drought indices. The study focuses on the computation of SPI and SPEI indices, particularly for individual cell locations in spatial grid-formatted data, in two different time steps, daily and monthly. Adams (2017) developed a Python package for computing drought indices distributed in time and space. This package is a modified version of the original code by the National Centers for Environmental Information (NCEI). Unlike Python algorithms for SPI and SPEI, the developed, by Adams (2017), algorithm can only compute SPI on a daily scale, unlike previous methods.

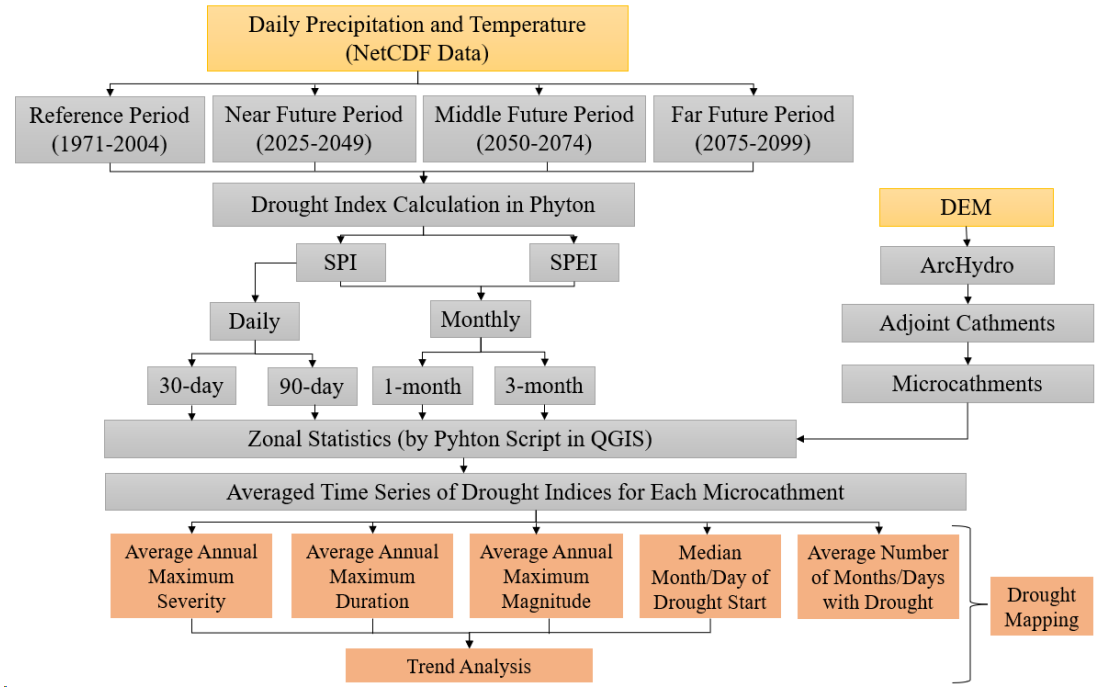


Figure 3.23 The process of drought analysis by using gridded climate data.

Drought indices were calculated at a distributed grid level, utilizing meteorological data provided at each grid. The study involved the calculation of drought indices using the "climate indices" package in Phyton (Table 3.2). Additionally, raster data

containing daily precipitation was converted into a NetCDF file to serve as input for this package. Python codes were utilized to adjust variables, such as size and order, to ensure proper reading of NetCDFs during these transformations.

Calculations were conducted for the 30-day and 90-day SPIs during distinct time intervals: 1971-2004 (reference), 2025-2049 (near future), 2050-2074 (middle future), and 2075-2099 (far future). Given that SPI is the sole index that operates daily within this package, these studies are accorded priority. Over extended periods of time, certain indices demonstrate improved accuracy when utilizing input data that goes beyond just precipitation (Fung et al., 2020). For instance, the SPEI considers the impact of temperature caused by evapotranspiration (Onuşluel Gül et al., 2017). The monthly calculations for SPI and SPEI were also carried out.

In SPI calculation, the Gamma distribution is not defined for zero values, and precipitation data may include zero values when there are no rainy days. This issue was resolved by incorporating adjustments to account for instances of zero probabilities in various SPI calculation methods. However, within the "climate indices" package, when zero values are encountered, they result in zero SPI values. Consequently, the Pearson Type III distribution (Equation 3.47) in the package was utilized to correct zero probabilities.

In order to convert indications of drought into river hydrologic basins, index values were averaged within catchment areas of each micro-basin. This procedure needed the use of bulk processing to calculate the average index values for each month and day inside certain micro-basins (Kuzucu and Onuşluel Gül, 2023; Onuşluel Gül et al., 2022). The time series of gridded SPI values were calculated by averaging over zone with adjoint catchments.

Adjoint catchments and micro catchments were created in ArcHydro package by catchment processing tool using DEM (Figure 3.24). Adjoint catchments are created by progressively merging micro catchments in the direction of surface flow, starting from the most upstream micro catchment, and moving downstream (Onuşluel Gül,

2022). Consequently, the intersecting areas were formed. The number of micro-basins obtained by this method for Küçük Menderes Basin is 213.The full polygons were designated as zones, and zonal averages of indices values for each day during the investigated periods were computed using a specific Python script by Onuşluel Gül et al. (2022) in the QGIS software.

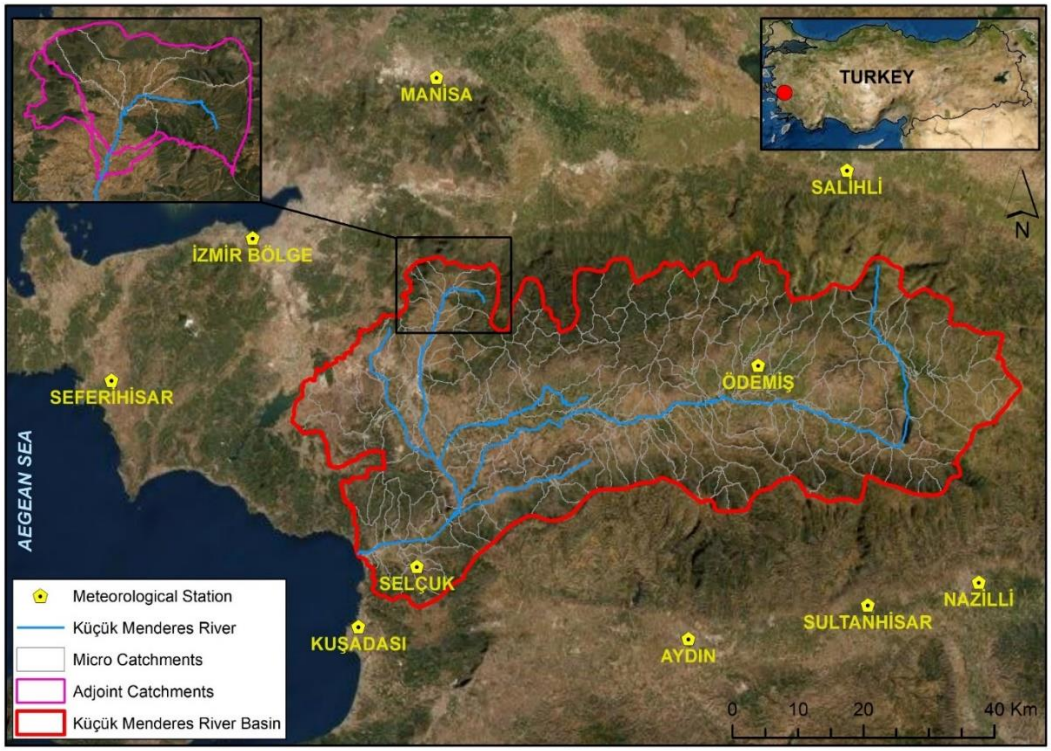


Figure 3.24 Küçük Menderes River Basin and micro catchments.

The following statistical variables were derived in Excel calculations for each period separately from the average index data obtained for each micro catchment, providing comparisons both temporally and spatially: annual maximum drought severity (measured by the accumulated index values during uninterrupted periods of negative index values representing drought cases), annual maximum drought duration (part of the drought pulse with the highest severity), annual maximum drought magnitude (calculated by averaging the annual maximum severity within the corresponding duration) (Dikici, 2020; Onuşluel Gül et al., 2022), and the timing of the start of the annual maximum drought (expressed in days or months, depending on the temporal resolution) and their Sen's Slope trends (Kuzucu & Onuşluel Gül, 2023).

Drought mapping: The droughts were illustrated by mapping average annual maximum drought severity, average annual maximum drought duration, average annual maximum drought magnitude, median day/month of drought start, average number of drought months/days (for moderate, severe, and extreme conditions) and the trends of all these.

3.1.4.5 Drought Analysis Using by Coupled VIC and SWAT Model Outputs

3.1.4.5.1 VIC Modeling

VIC model version 5 (VIC5), developed Hamman et al. (2018), is a macroscale hydrological model that simulates various land surface processes related to water and energy balance, based on originally developed by Liang et al. (1994) at the University of Washington. The R package called as "VIC5" developed by Zhong et al. (2023) was used for modeling in the study.

The study area for the VIC model was created on a grid basis with $1/16^{o}$ resolution as given by Schaperow et al. (2021). Model inputs were prepared using the same grid areas. Runoff was obtained by routing method introduced by Lohmann et al. (1996, 1998), Model calibration was performed for the period 2000-2003 and validation for the period 2004-2005. Flow, evapotranspiration, baseflow and LAI values were calculated as a result of the model.

3.1.4.5.2 SWAT Modeling

The flowchart of SWAT modeling for this study is given by Figure 3.25. The SWAT model was firstly run for the period observed period (2000-2012). Certain simulations necessitate a preliminary phase of adjustment to achieve a state of equilibrium which is named by warm-up period. A one-year warm-up period is typically adequate for complete operationalization of the hydrological cycle (Arnold et al., 2011, Vu et al., 2012, Uniyal et al., 2015). The output files provide averages for the full simulation period, excluding data from the omitted years. The warm-up period was selected as the year 2000 (1 year).

The sensitivity analyses, the calibration (2001-2007) and the validation (2008-2012) processes were carried out in SWAT-CUP. After running the SWAT model, the obtained the output files were imported into SWAT-CUP to analyze the parameters that can be utilized for calibration in hydrological modeling. Given the significance of groundwater in basin models, specific parameters were chosen for calibration purposes. Furthermore, the parameters that influence the proposed flow, as mentioned in the literature by Abbaspour (2015) and Abbaspour et al. (2015), were also chosen.

Both "One-at-a-time" and "Global" sensitivity analysis approaches were used to analyze all parameters. In the Global sensitivity analysis, parameters that have a p-value of less than 0.05, as determined by a t-test, are deemed to be sensitive (Abbaspour, 2015). A few simulations were undertaken for each parameter in the One-at-a-time sensitivity analysis. A graphically comparison was performed of the simulation results obtained for different values of a parameter. If any deviation in the simulation results of the model was detected, it signified that the parameter is sensitive.

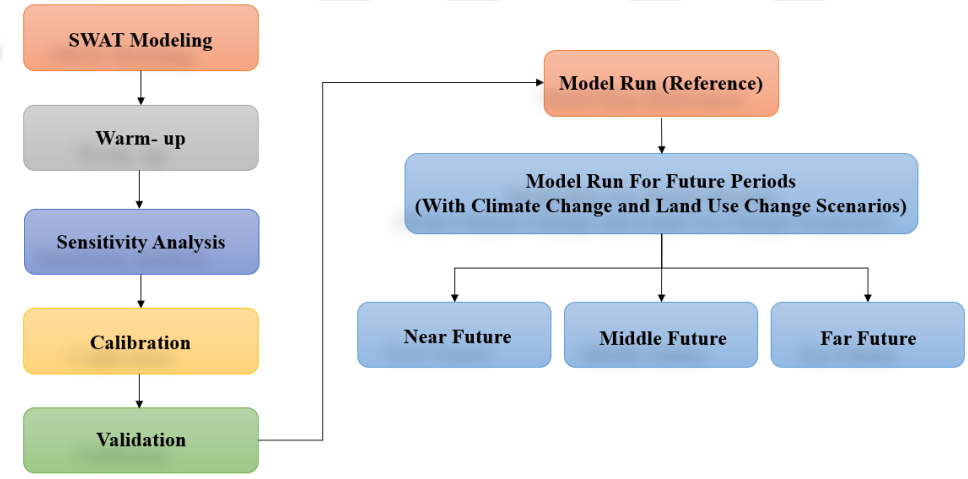


Figure 3.25 The flowchart of SWAT Modeling for the study

After obtaining the sensitive parameters, calibration was carried out. Abbaspour (2015) recommended the calibration method requires performing the maximum five iterations to achieve good results. In the study, 5 iterations and 500 simulations were run for each iteration. After calibration and validation, the best parameter values were obtained, the SWAT model was run separately for the future periods.

SWAT Modeling for Future Period: The future period (2025-2099) was divided into three distinct periods: near future (2025-2049), middle future (2050-2074), and far future (2075-2099). Modeling studies were conducted to account for the impact of climate and land use change. Projections were conducted for runoff and actual evapotranspiration under various scenarios, considering changes in climate and land use. Averaged rainfall data for each subbasin was also obtained for these periods. These variables were used as data SPI, SPEI (for PET and ET_a) and SSFI calculations for each subbasins. The drought indices series were calculated from 1 month to 12 months as time interval.

Drought Mapping: Average annual maximum drought severity, average annual maximum drought duration, average annual maximum drought magnitude, median day/month of drought start, average number of months/days with drought (for moderate, severe, and extreme conditions), the trends of all these parameters were mapping to demonstrate the droughts with modelled series.

3.1.5 Flood Analyses

To perform flood modeling in the Küçük Menderes Basin, the Ilıca (Ergenli) sub-basin (refer to Figure 3.26) was selected as the appropriate study area. This sub-basin, which includes Ilıca Creek-Ergenli (D06A027) flow observation station downstream, was selected due to its favorable conditions in terms of both flood risk and the availability of simultaneous precipitation and flow records.

The construction of Ergenli Dam, which is located downstream of station D06A027, started in 2014 and is still ongoing. Since the dam was not available during the study period, modelling studies were presented separately with and without dam.

Ergenli Dam basin is approximately 55.41 km^2. Ilıca Creek-Ergenli Station D06A027 is located downstream of the dam and the drainage area is calculated as 57.05 km^2 (Figure 3.27).

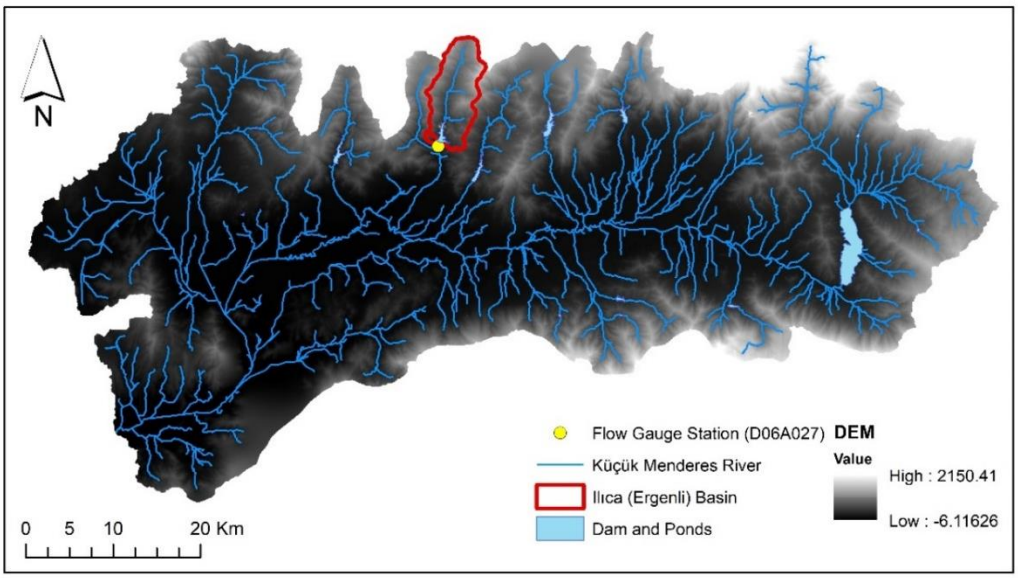


Figure 3.26 The location map of Ergenli Basin.

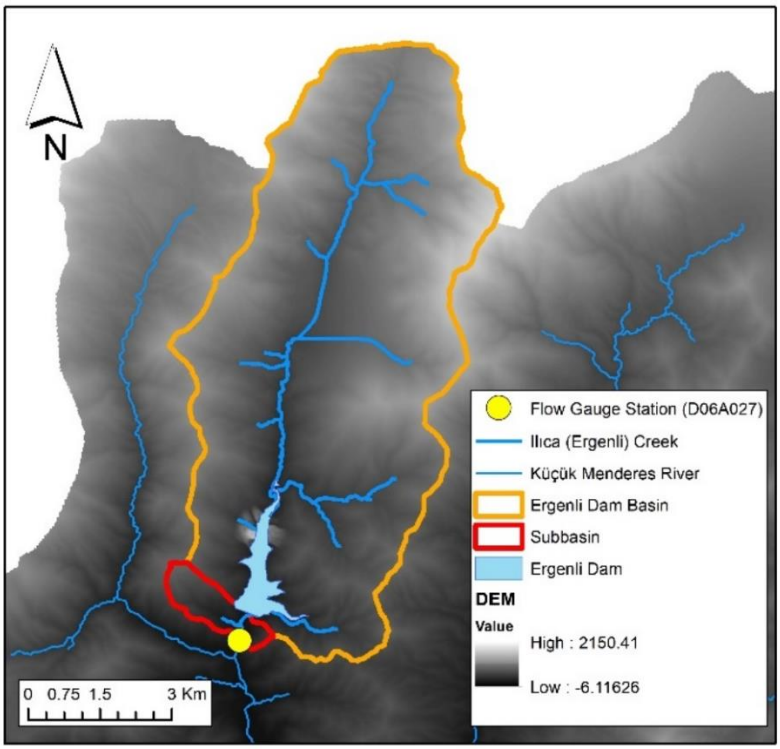


Figure 3.27 Study area for flood analysis (Ergenli Dam Basin and the subbasin).

Field studies were conducted downstream of flow monitoring station D06A027 on Ilıca Creek. The structures depicted in Figure 3.28 were analyzed and their dimensions were measured for the purpose of incorporating them into modeling studies (Figure 3.29). During the summer months, it was discovered that Ilıca Creek was devoid of

water (Figure 3.29). Officials from the State Hydraulic Works (DSİ) have reported that the river channel has expanded as a result of the extraction of material from the original riverbed, and the construction of the Ergenli Dam downstream has been stopped.

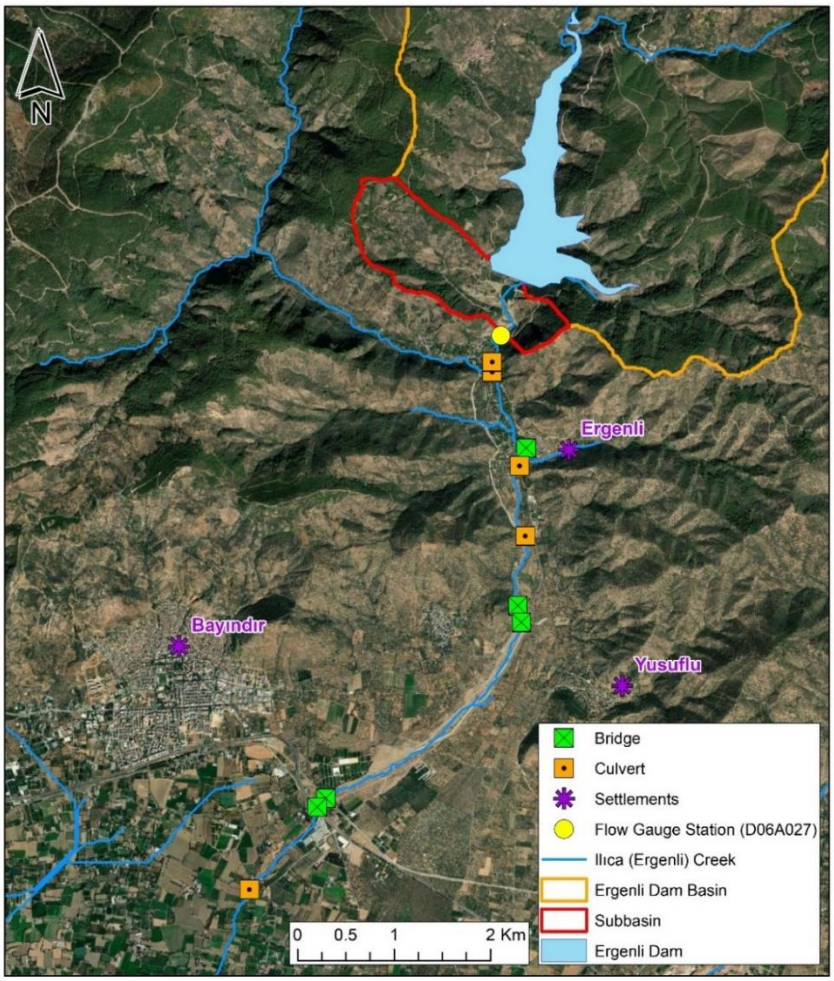


Figure 3.28 The structures and settlements at downstream of Ergenli Basin.



Figure 3.29 Field studies (Personal archive, 2021).

3.1.5.1 Intensity – Duration -Frequency (IDF) Curves and Hyetographs

A design hyetograph is the temporal representation of rainfall in relation to duration (D) and recurrence interval (T). The best distribution of maximum rainfall series (mm) with duration from 5 minutes to 24 hours was investigated. In this study, after determining the best fit probability distribution of rainfall depths (mm) at standard times (from 5 minutes to 24 hours), the intensity-duration-frequency (IDF) values were obtained. Utilizing these values, rainfall intensities were calculated. Subsequently, the IDF parameters were derived, and hyetographs were generated employing the Instantaneous Intensity method (Te Chow et al., 1988).

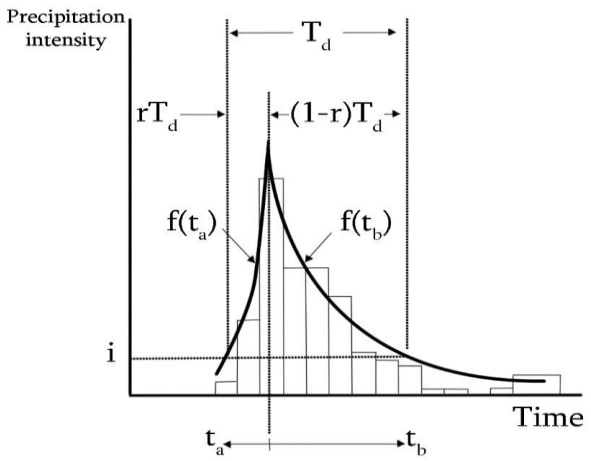


Figure 3.30 Instantaneous Intensity method curve (Te Chow et al.,1988).

The method considers a continuous rainfall intensity over the duration of the storm. Instantaneous intensity functions (Figure 3.30) are characterized using f(ta) and f(tb), both of which represent instantaneous peak rainfall intensities. In this method, the depth of precipitation extracted from the IDF curve is equal to the value at a given period 'Td' of the storm event when the peak is reached.

The cumulative rainfall in the same period 'D' is calculated as the area under the paired curves f(ta) and f(tb) (Najar, 2021). By obtaining the parameters of the IDF equation, the curve equation was obtained and the hyetograph of the design rainfall describing the change in rainfall intensity with time was derived. In order to increase the accuracy of the hyetograph, the smallest possible calculation interval was selected (Chow et al., 1988; Onuşluel Gül et al., 2010).

The IDF equation (Equation 3.49) developed by Bernard (1932) is used. The rainfall intensity in the middle of the storm period is calculated by Equation 3.49.

$$i_{ave} = \frac{aT^b}{{T_d}^c} \tag{3.49}$$

Where, i_{ave} is the average rainfall intensity, T_d is the duration of the storm, T is the return period and a, b and c are coefficients that vary with location and return period (Equation 3.50).

$$i = \frac{aT^b}{{T_d}^c} - \frac{acT^b}{{T_d}^c} = \frac{aT^b(1-c)}{{T_d}^c} \tag{3.50}$$

Within the scope of the present study, a 24-hour storm duration with a peak (r=0.5) at the 12th hour after the onset of the storm was selected. To improve the accuracy of the model, a smaller time interval is defined around the peak, while 1-hour time intervals are considered to represent the hyetograph in general (Najar, 2021).

3.1.5.2 HEC-HMS Modeling

The research aimed to employ the HEC (Hydrologic Engineering Center) model series for flood modeling. Consequently, the hydrological model HEC-HMS and the hydraulic model HEC-RAS have been jointly applied.

In order to prepare a digital base for the HEC-HMS model, HEC-GeoHMS developed as an ArcGIS interface was used. The program allows users to visualize spatial information, identify watershed characteristics, perform spatial analysis, and identify sub-basins and flows. Thus, hydrological inputs for HEC-HMS were created properly.

For the purpose of Ilıca Ergenli Basin (Figure 3.27) flood modeling, the location of the Ergenli gauge station numbered D06A027 in the HEC-GeoHMS model was determined as the basin outlet. In the HEC-HMS model, basin characteristics were obtained by using the digital elevation model of the basin. The construction of Ergenli Dam, which is located at the upstream of station D06A027, was started in 2014. Sub-

basins were combined as two types: there is no control point at the basin upstream and there is a control point at the basin upstream (Figure 3.31).

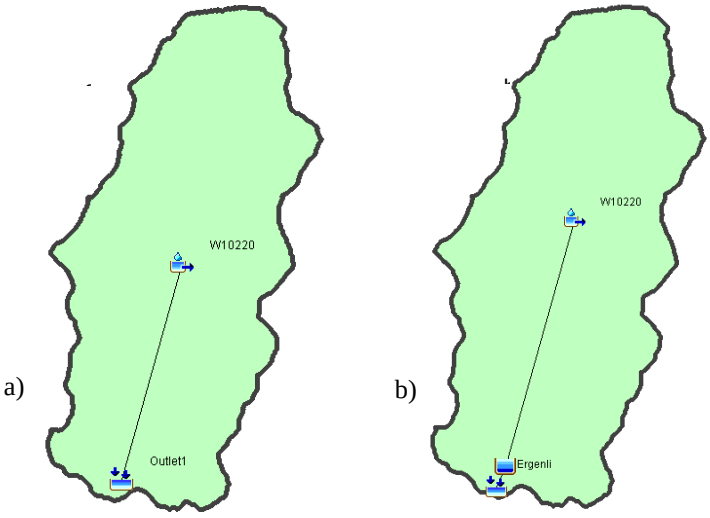


Figure 3.31 HEC-HMS model, a) Existing situation, b) Operational status of Ergenli Dam

Within the scope of the project, the HEC-HMS model was created using geographical, meteorological and flow data. Flood modeling have been conducted by using 1 km^2 grids and hourly meteorological data. Simultaneous hourly precipitation (mm) and runoff (m^3/s) data were used for modelling. All inputs to the model were included as grid based. Distribution factors were used to convert point precipitation to grid-based precipitation. The ModClark method, the Loss rate method, the Recession method, and the Muskingum Cunge method were selected for HMS modeling of Ergenli Basin. The calibration and the validation procedures were carried out using observed flow in the HEC-HMS model for the period given by Table 3.6.

Table 3.6 The calibration and validation periods of HEC-HMS modeling

Modeling Period	**Beginning**		**End**	
	Date	**Time**	**Date**	**Time**
Calibration	1/28/2011	10:00	1/30/2011	10:00
Validation	2/22/2011	02:00	2/24/2011	16:00

Flood hydrographs were obtained for different recurrences (2-, 5-, 10-, 25-, 50-, 100-, 250-, 500- and 1000-year flood) using the design hyetographs in the calibrated model.

3.1.5.3 HEC-RAS Modeling

Calculations were executed to simulate unsteady flow in two dimensions. Hydraulic modeling was conducted by integrating flood hydrographs derived from HEC-HMS, stream sections, and stream structures. The study area was divided into mesh cells measuring 10 meters, with a finer mesh size of 0.5 meters around the hydraulic structures. Consequently, maps were generated to illustrate the depth and velocity water, and the areas to be affected by flood were presented. Additionally, an assessment of the present condition and operational status of Ergenli Dam was conducted through the utilization of the HEC-RAS model.

The maximum depth maps, velocity and inundation maps were derived for recurrent floods of 2, 5, 10, 25, 50, 100, 250, 500 and 1000 years.

3.2 Data Analyses

Within the framework of the study, data pertaining to DEM, meteorological conditions, flow, irrigation, characteristics of dam, climate, land use, and soil were acquired. The data required for modeling in the study are presented separately below.

The Digital Elevation Model (DEM) of the Küçük Menderes Basin (Figure 3.32) was obtained at a resolution of 5 km x 5 km and 10 m. elevation range. The flow tributaries were subsequently generated based on the DEM.

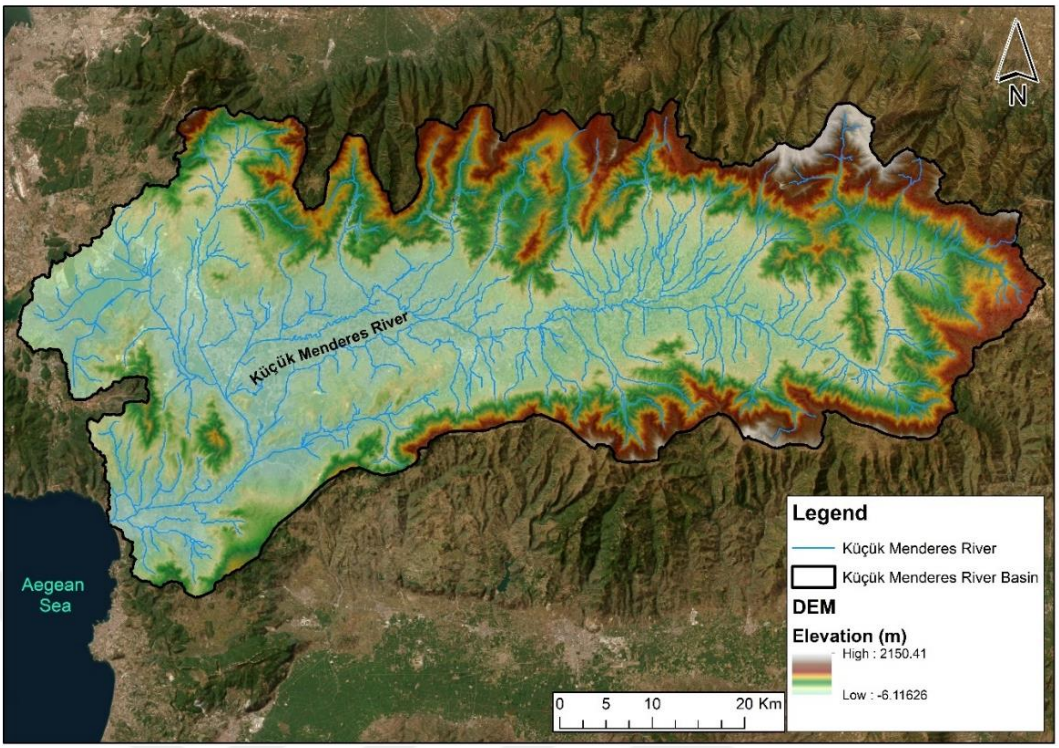


Figure 3.32 DEM of Küçük Menderes River Basin

3.2.1 Data for VIC Modeling

The VIC model requires basically forcing (meteorological), soil and vegetation data for classic driver. Table 3.7 provides details on the sources of the data utilized for VIC modeling. The forcing data are precipitation (mm), temperature (^{o}C), wind (m/s), vapor pressure (kPA) and downward shortwave radiation flux (W/m^2). The model can run daily, but the VIC5 R package requires this data on an hourly basis. The hourly meteorological data were derived from the İKLİM RİSK project data by time interpolation method. Only downward shortwave radiation flux was obtained hourly (Table 3.7). The vapor pressure was derived from humidity and temperature data. Vegetation data include vegetation class, fraction of grid cell covered by vegetation tile, root zone thickness, fraction of root in the current root zone, LAI per month, albedo per month, etc. Vegetation library also includes minimum stomatal resistance of vegetation type, LAI of vegetation type, shortwave albedo for vegetation type, vegetation roughness length, etc. Soil data included the parameters which are variable infiltration curve parameter, maximum velocity of baseflow, fraction of maximum soil moisture where non-linear baseflow occurs, saturated hydrologic conductivity, soil

moisture diffusion parameter, thickness of each soil moisture layer, bulk density of soil layer, etc.

Table 3.7 Types of data and their respective sources for VIC modeling.

Data	Source	Data Type	Description
Digital Elevation Model (DEM)	Local maps in 1/5000 scale	Raster (gridded)	5 km x 5 km resolution
Forcing Data	İKLİM RİSK project	Netcdf (gridded)	Precipitation (mm), Temperature (°C), Wind (m/s), Relative Humidity (%)
	ERA5 by Copernicus Land Monitoring Service	Netcdf (gridded), hourly	Downward shortwave radiation flux (W/m^2): ERA5
Soil Data	VICGlobal: soil and vegetation parameters for the Variable Infiltration Capacity hydrological model	Netcdf (gridded)	For 3 layer (10 cm, 20 cm, 70 cm).
Land Use	CORINE Land Cover by Copernicus Land Monitoring Service	Vector	CORINE land cover was matched to IGBP land cover
Vegetation	VICGlobal: soil and vegetation parameters for the Variable Infiltration Capacity hydrological model	Netcdf (gridded)	with IGBP land use class
Streamflow Gauges	General Directorate of State Hydraulic Works (DSİ)	Point-based, daily time series	Observed streamflow of flow stations

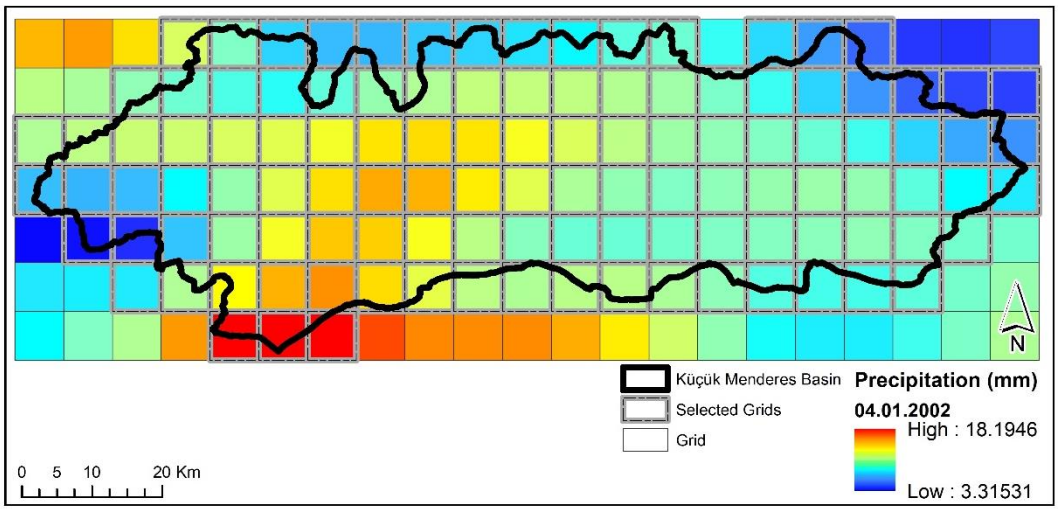


Figure 3.33 1/16° resolution grids and daily total precipitation (mm).

Schaperow et al. (2021) developed “VICGlobal, a near-global dataset of soil and vegetation parameters for the VIC model at 1/16° resolution. The dataset covers almost the entire globe and has a resolution of 1/16°. The soil characteristics were evaluated using the 30 arc-second FAO Harmonized World Soil Database (HWSD). In the dataset, the vegetation characteristics were derived from MODIS data with a precision of 500 meters. The VICGlobal soil parameter file utilizes the Multi-Error-Removed Improved-Terrain (MERIT20) digital elevation model (DEM) to establish the elevations, latitudes, and longitudes of each land grid cells. They employed a set of 17 land cover classifications established by the International Geosphere–Biosphere Programme (IGBP). The Land Data Assimilation System (LDAS) vegetation library36 was modified to include the 17 IGBP land cover classes. They calculated monthly mean LAI, fractional canopy cover (fcanopy) and albedo values derived from the available classes of MODIS data products. In this study, the database with 1/16^{o} resolution gridded given by Figure 3.33 and Figure 3.34 developed by Schaperow and Li (2021) was used for the soil and vegetation data preparing (Table 3.7). However, CORINE land cover used in other models was used for land classification and CORINE classes were matched with IGBP classes and given by Table 3.8. The land use map by IGBP classification is given by Figure 3.34. Streamflow data was used for model calibration and validation. For routing, flow direction grids were derived from DEM given by Figure 3.32 by resampling the given data resolution (Figure 3.34).

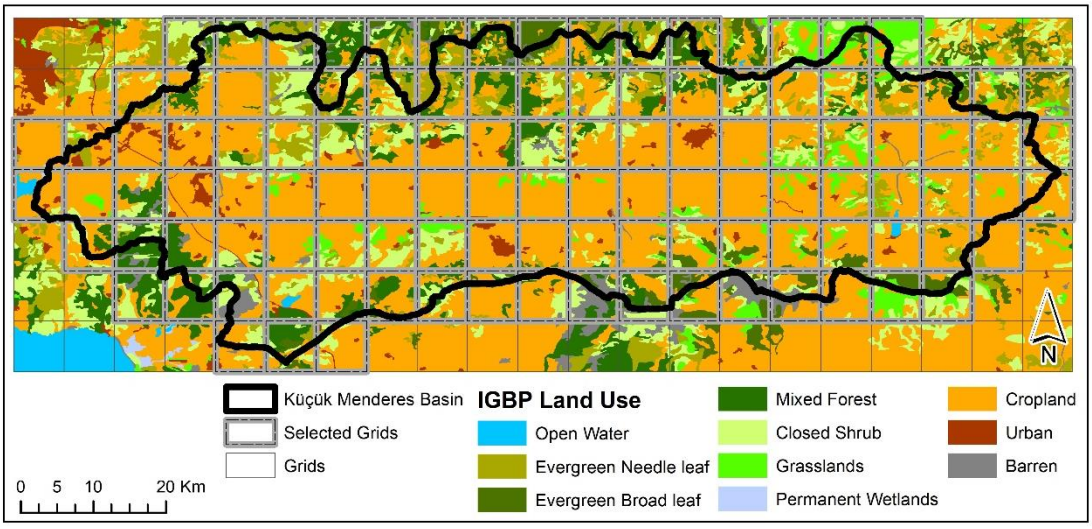


Figure 3.34 1/16^{o} resolution grids and IGBP land use class.

Table 3.8 Look-up table for CORINE and IGBP landuse.

CODE	CORINE	CODE	IGBP
111	Continuous urban fabric	**14**	Urban
112	Discontinuous urban fabric	**14**	Urban
121	Industrial or commercial units	**14**	Urban
122	Road and rail networks and associated land	**14**	Urban
124	Airports	**14**	Urban
131	Mineral extraction sites	**17**	Barren
132	Dump sites	**17**	Barren
133	Construction sites	**17**	Barren
142	Sport and leisure facilities	**11**	Grasslands
211	Non-irrigated arable land	**13**	Cropland
212	Permanently irrigated land	**13**	Cropland
221	Vineyards	**13**	Cropland
222	Fruit trees and berry plantations	**13**	Cropland
223	Olive groves	**13**	Cropland
231	Pastures	**11**	Grasslands
242	Complex cultivation patterns	**13**	Cropland
243	Land principally occupied by agriculture, with significant areas of natural vegetation	**13**	Cropland
311	Broad-leaved forest	**3**	Evergreen Broad leaf
312	Coniferous forest	**2**	Evergreen Needle leaf
313	Mixed forest	**6**	Mixed Forest
321	Natural grassland	**11**	Grasslands
323	Sclerophyllous vegetation	**6**	Mixed Forest
324	Transitional woodland/shrub	**7**	Closed Shrub
331	Beaches, dunes, sands	**17**	Barren
332	Bare rock	**17**	Barren
333	Sparsely vegetated areas	**17**	Barren
411	Inland wetlands	**12**	Permanent Wetlands
512	Water bodies	**1**	Open Water
523	Sea and ocean	**1**	Open Water

3.2.2 Data for SWAT Modeling

The SWAT model requires topographic, meteorological, flow, soil, land use, crop, and irrigation data. Table 3.9 provides details on the sources of the data utilized for SWAT modeling.

Table 3.9 Types of data and their respective sources for SWAT modeling

Data	Source	Data Type	Description
Digital Elevation Model (DEM)	Local maps in 1/5000 scale	Raster (gridded)	5 km x 5 km resolution
Streamflow Gauges	General Directorate of State Hydraulic Works (DSİ)	Point-based, daily time series	Observed streamflow data of 12 flow stations
Meteorological Data	Turkish State Meteorological Service (MGM)	Point-based, daily time series	Observed meteorological data of 11 meteorological stations
Climate Data	İKLİM RİSK project	Netcdf, From grid to point-based, daily time series	MPI-ESM-MR model (RCP 8.5 scenario) Climate data for the reference (1985-2009) and the future periods (2025-2099)
Soil Data	İKLİM RİSK project based on ISRIC World Soil Information's Purpose and Strategy and USGS Earth Explorer Landsat Satellite Imagery	Raster (gridded)	250 m grided data for 7 layers (0-5, 5-15, 15-30, 30-60, 60-100 and 100-200 cm)
Land Use	CORINE Land Cover by Copernicus Land Monitoring Service.	Vector (polygon)	For the years 2000 and 2006 (used for reference (1985-2009) and calibration-validation periods (2000-2012), respectively)
Future Land Use Data	İKLİM RİSK project	Vector (polygon)	For the years 2035, 2065, 2085
Crop pattern	General Directorate of State Hydraulic Works (DSİ)	List	General irrigation information (Crop pattern and irrigation period, irrigation system and water source (groundwater or surface flow))

Figure 3.35 illustrates the long-term monitored flow observation stations within the basin. Comprehensive details about these stations can be referenced in Table 3.10.

General information and data regarding the streamflow observation stations were sourced from the General Directorate of State Hydraulic Works (DSİ) streamflow observation tables. The daily average flow values (m^3/s) recorded at these stations were retrieved, and monthly average flow values (m^3/s) were subsequently computed.

As the Küçük Menderes River - Selçuk station, denoted as E06A001, is situated near the outlet of the basin, it is regarded as a representative of the entire basin for the purposes of this study. This station has the longest observation duration in the basin, spanning from 1953 to 2012. However, it ceased operations in 2012, lacking flow data for subsequent years. No other station on the main streamflow has maintained continuous operations for an extended period.

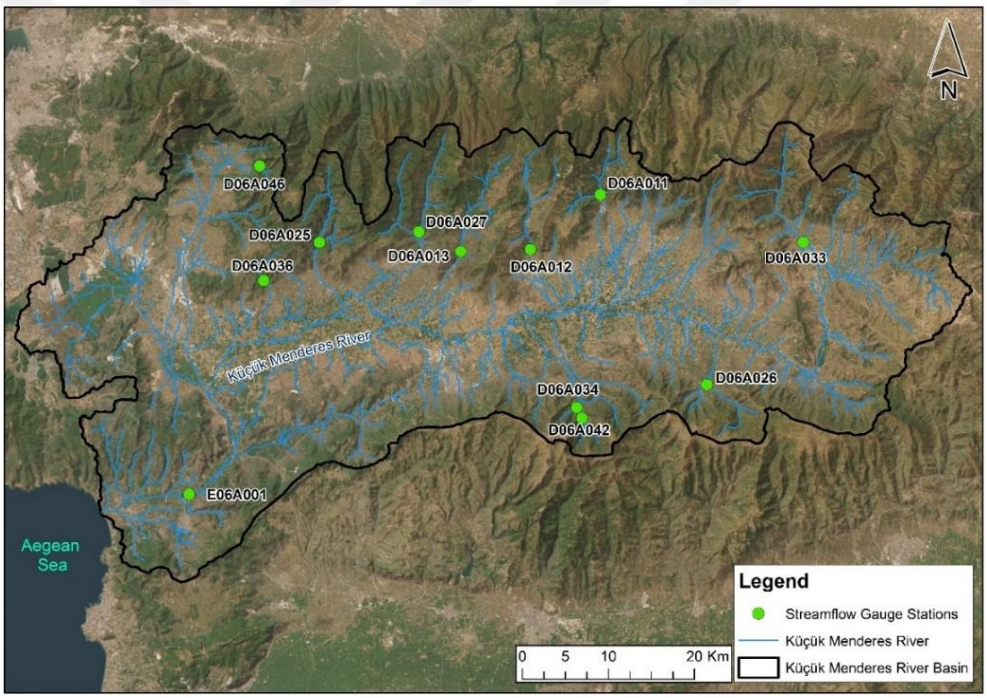


Figure 3.35 Streamflow stations in Küçük Menderes River Basin

Figure 3.36 displays the meteorological stations with extensive long-term observations in and around the Küçük Menderes River Basin, and Table 3.11 provides detailed information about these stations. The basin is exclusively represented by the Ödemiş and Selçuk stations. Meteorological data, encompassing total precipitation, maximum and minimum temperature, solar radiation, relative humidity, and wind on

a daily basis for these locations, were sourced from the Turkish State Meteorological Service (MGM).

Furthermore, the daily and monthly average temperature data collected from these stations were also acquired for the purpose of data analysis and drought analysis using observed data. The studies were conducted by considering the common period of 1972-2018 for all stations.

Table 3.10 Streamflow stations and observation periods in Küçük Menderes Basin.

No	Station No	Station Name	Period	Observed Years	Drainage Area (km^2)	Elevation (m)	Latitude	Longitude
1	E06A001	Küçük Menderes River - Selçuk	1953-2012	57	3255.2	4	37.9781	27.3794
2	D06A011	Rahmanlar Stream - Bebekler	1980-2014	34	37	220	38.2883	27.9282
3	D06A012	Aktaş Stream- Bülbüller	1982-2002	19	73.4	130	38.2317	27.8344
4	D06A013	Falaka Stream - Falaka	1980-2011	23	83	130	38.2302	27.7419
5	D06A025	Uladı Stream - Yakapınar	2001-2017	14	69.1	120	38.2407	27.5542
6	D06A026	Pirinçci Stream - Bademli	2000-2012	10	38.4	250	38.0885	28.0667
7	D06A027	Ilıca Creek - Ergenli	2001-2012	10	57	140	38.2510	27.6863
8	D06A033	Kiraz Stream - Kiraz	2005-2017	11	114.4	351	38.2361	28.1972
9	D06A034	Kızılkaya Creek - Yenişehir	2005-2012	6	15.4	312	38.0661	27.8938
10	D06A036	Künk Creek - Arıkbaşı	2007-2011	5	16.6	93	38.2011	27.4799
11	D06A042	Vakıflar Creek - Eğridere	2011-2017	7	21.2	380	38.0547	27.9006
12	D06A046	Cevizli Creek - Cumalı	2012-2018	7	10.4	326	38.3211	27.4752

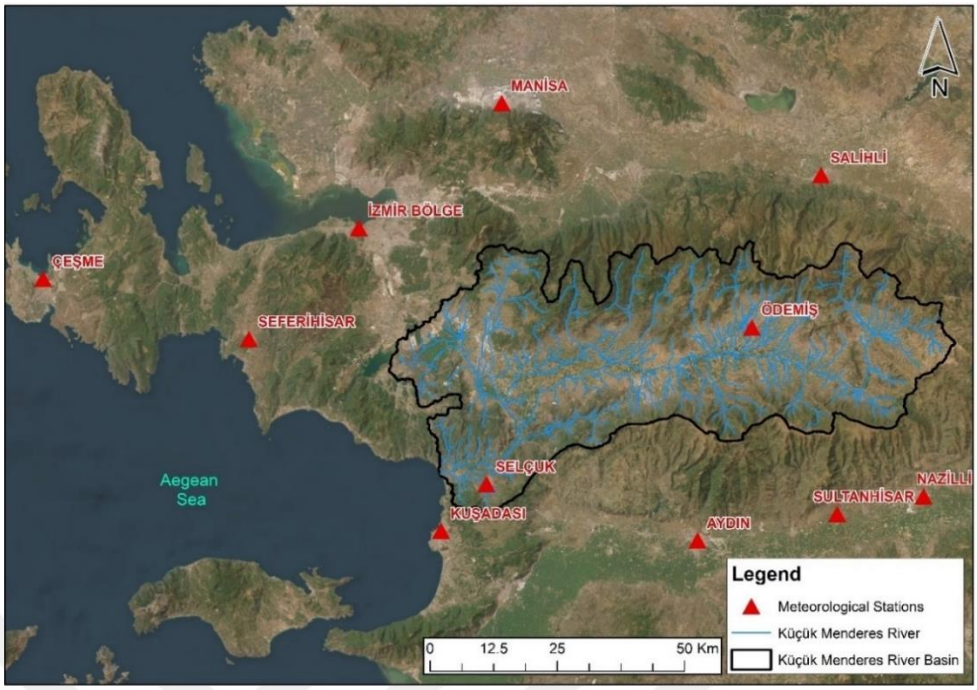


Figure 3.36 Meteorological stations in and around the Küçük Menderes River Basin

Table 3.11 Meteorological stations and their observation periods in Küçük Menderes Basin.

No	Station No	Station Name	Period	Observed Years	Elevation	Latitude	Longitude
1	17186	Manisa	1960-2018	59	71	38.6153	27.4049
2	17220	İzmir Bölge	1960-2018	59	29	38.3949	27.0819
3	17221	Çeşme	1964-2018	55	5	38.3036	26.3724
4	17232	Kuşadası	1964-2018	55	25	37.8597	27.2652
5	17234	Aydın	1960-2018	59	56	37.8402	27.8379
6	17492	Salihli	1965-2018	54	111	38.4831	28.1234
7	17820	Seferihisar	1972-2018	47	22	38.199	26.835
8	17822	Ödemiş	1960-2018	59	111	38.2157	27.9642
9	17850	Sultanhisar	1972-2018	47	73	37.8843	28.1504
10	17854	Selçuk	1964-2018	55	18	37.9423	27.3669
11	17860	Nazilli	1960-2018	59	84	37.9135	28.3437

The gridded climate data were provided by İKLİM RİSK (2021). MPI-ESM-MR dataset from the Max Planck Institute for Meteorology downscaled 1- km resolution and bias corrected data were used for modeling for both reference and future period. After model calibration and validation, the climate data, which contains total precipitation, maximum and minimum temperature, solar radiation, relative humidity, and wind on daily basis, were used instead of the observed meteorological data for

both reference and future periods. The weighted averages of the grid data according to the station locations given in Figure 3.36 were found and converted into point-based data.

SWAT soil database contain hydrological soil groups, soil texture, moist bulk density, available water capacity, saturated hydraulic conductivity, organic carbon content, clay content, silt content, sand content, rock fragment content, moist soil albedo, USLE equation soil erodibility (K) factor) for each soil layer. In the study, the soil database derived within the scope of the İKLİM RİSK (2021) (based on the ISRIC (International Soil Reference and Information Centre) World Soil Information, 2020) Objective and Strategy and USGS Earth Explorer Landsat Satellite Imagery data) was employed. The soil database provides information on the aforementioned parameters for 7 layers of 0-5, 5-15, 15-30, 30-60, 60-100 and 100-200 cm, which are identical to the SoilGrids (ISRIC World Soil Information, 2020) database with a 250 m grid resolution. Hydrologic soil groups (Figure 3.37) were determined using the soil texture triangle with various fractions of sand, clay, silt contents. Group B, characterized by silt loam or loam (Figure 3.37), prevails in the basin. When fully saturated, it exhibits a moderate infiltration rate and is primarily characterized as deep, well-drained, and fine to coarse.

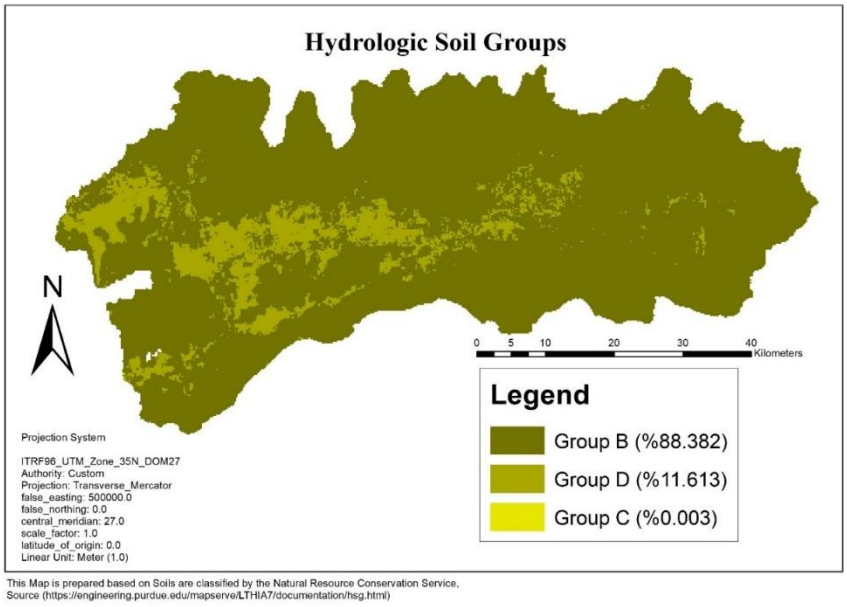


Figure 3.37 Hydrologic soil groups in Küçük Menderes Basin (İKLİM RİSK, 2021).

CORINE Land Cover (LC) map derived by Copernicus Land Monitoring Service was used for land use data. For modelling purposes, CORINE LC 2006 map was used for the period spanning 2000-2012, while CORINE LC 2000 map served as the reference period. CORINE classification was aligned with the SWAT model as shown in Table 3.12. Groundwater information, plant pattern, irrigation water information, dam and pond information were obtained from the DSİ.

Table 3.12 Matching land use codes of CORINE and SWAT model

CORINE Classification	**CORINE Description**	**SWAT Classification**	**SWAT Description**
111	Continuous urban fabric	URML	Residential-Med/Low Density
112	Discontinuous urban fabric		
121	Industrial or commercial units		
133	Construction sites		
142	Sport and leisure facilities		
122	Road and rail networks and associated land	UTRN	Transportation
124	Airports		
211	Non-irrigated arable land	AGRR	Agricultural Land-Row Crops
212	Permanently irrigated arable land	WWHT	Winter Wheat
242	Complex cultivation patterns		
243	Land principally occupied by agriculture, with significant areas of natural vegetation		
221	Vineyards	OLIV	Olives
222	Fruit trees and berry plantations		
223	Olive groves		
311	Broad-leaved forest	FRST	Forest-Mixed
312	Coniferous forest		
313	Mixed forest		
231	Pastures	PAST	Pasture
321	Natural grassland		
323	Sclerophyllous vegetation		
324	Transitional woodland/shrub		
331	Beaches, dunes, sands	BARR	Barren
332	Bare rock		
333	Sparsely vegetated areas		
334	Burnt areas		
131	Mineral extraction sites		
132	Dump sites		
411	Inland wetlands	WATR	Water
512	Water bodies		
523	Sea and ocean		

3.2.3 Data for HEC-HMS Modeling

The HEC-HMS model was exclusively applied to the Ergenli Basin. The data required for the model, along with their respective sources, are outlined in Table 3.13. Streamflow data for the model were sourced from the observation station at the outlet of the basin, specifically the Ilıca Creek Ergenli station with the identification number D06A027.

In the HEC-HMS model, inputs such as meteorological data (hourly precipitation, temperature, solar radiation), SCS curve number were prepared as 1000m*1000m grid based. For model calibration and validation, meteorological data in the same date range as the observed flow values are needed.

Table 3.13 The data and their respective sources for HEC-HMS modeling

Data	Source	Data Type	Description
Digital Elevation Model (DEM)	Local maps in 1/5000 scale	Raster (gridded)	5 km x 5 km resolution
Streamflow Gauges	General Directorate of State Hydraulic Works	Point-based, hourly time series	Limnigraph records for D06A027 flow station
Meteorological Data	Turkish State Meteorological Service (MGM)	Originally point-based, converted grid- based hourly time series. Point-based, from 5-min to 24 -hour	Observed hourly precipitation and temperature data for Ödemiş station. Annual maximum rainfall with standard durations for Ödemiş station
Curve Number	CORINE Land Cover by Copernicus Land Monitoring Service and Hydrologic Soil Groups	Raster (gridded) (1000m*1000m)	CORINE map for the year 2012

Hourly limnigraph records of station D06A027 for January and February 2011 were obtained from DSİ and given by Figure 3.38.

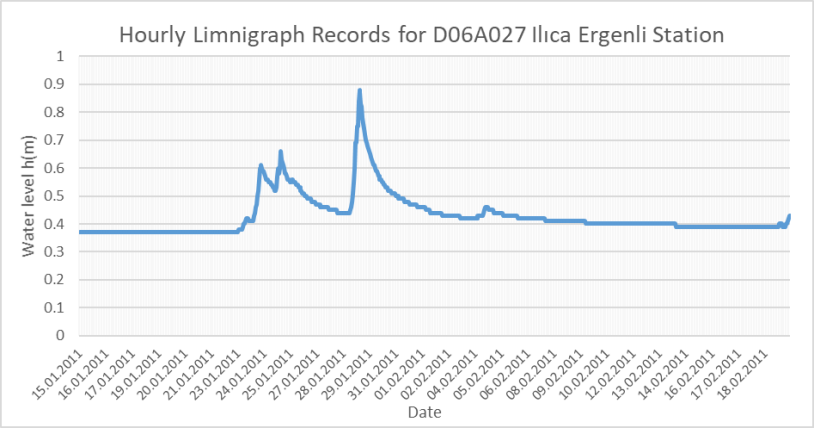


Figure 3.38 The hourly limnigraph records for D06A027 for the calibration period.

To derive the flow rating curve (Equation 3.51), the relationship between flow rate (Q in m^3/s) and flow depth (h in meters) at the relevant cross-section was also established.

$$Q(m^3/s) = K(h - h_0)^n \tag{3.51}$$

The variables in the equation are as follows: "Q" represents the discharge, "h" represents the stage, "h_0" represents the stage at zero flow, and "K" and "n" are constants. The parameters "n" and "K" in the equation were determined through the utilization of flow rating curves (depicted in Figure 3.39) provided by DSİ. Hourly flow values (m^3/s) were derived from hourly limnigraph records (Figure 3.38). Subsequently, the flow rating curve was constructed (Figure 3.39) and the constants in the equation (Equation 3.51) were obtained by graphical method, as illustrated in Figure 3.40. Daily flows were then calculated and compared with the observed flows as shown in Figure 3.41. For the year 2011, hourly flow values for January and February were determined using values K=19.50 and n=4.68 for h_0=0.

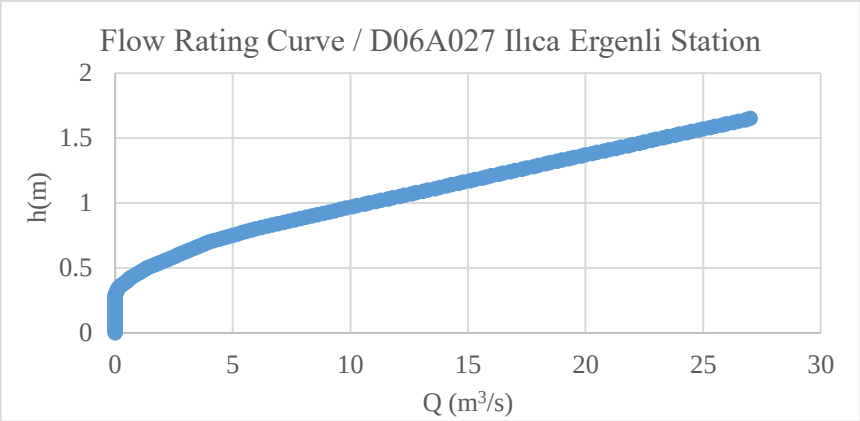


Figure 3.39 The flow rating curve for both calibration and validation period.

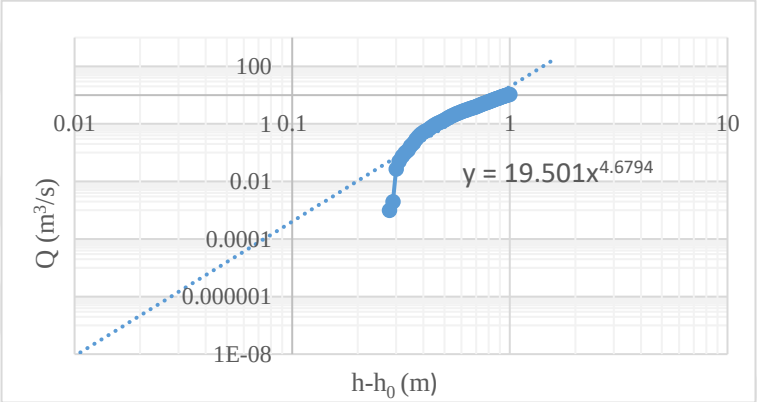
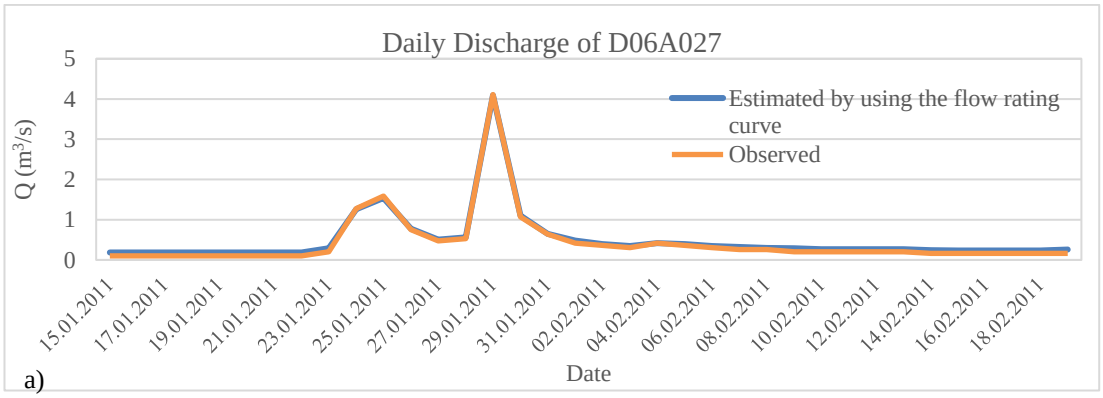


Figure 3.40 The graph to obtain the parameters of the flow rating equation.

Daily and hourly discharge for estimated and observed series the of calibration period were shown by Figure 3.41 and Figure 3.42, respectively.



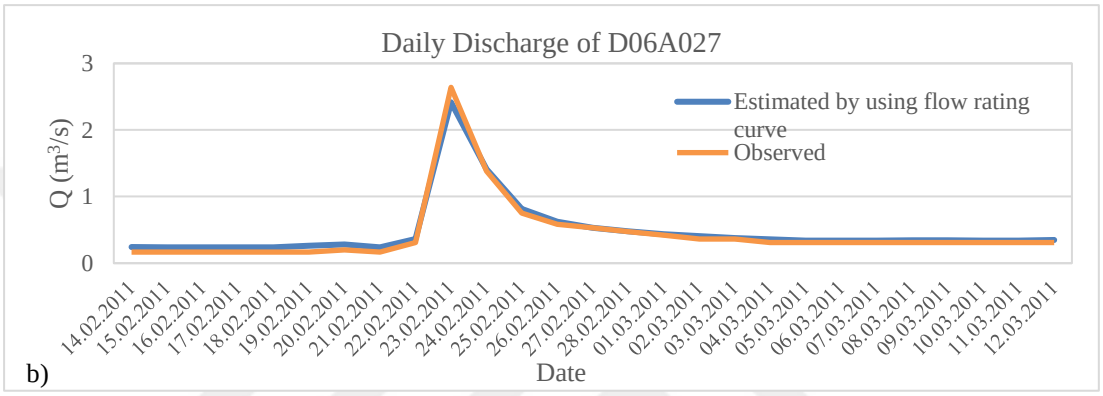
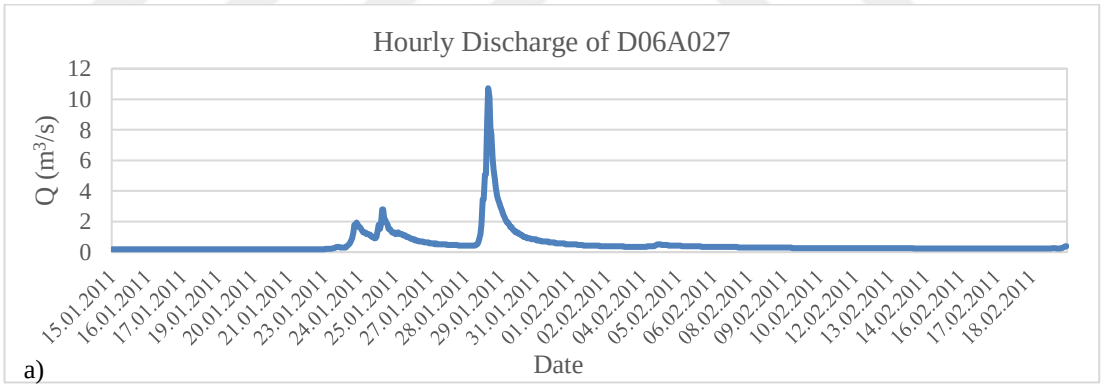


Figure 3.41 Daily discharge of D06A027 a) for calibration period, b) for validation period.



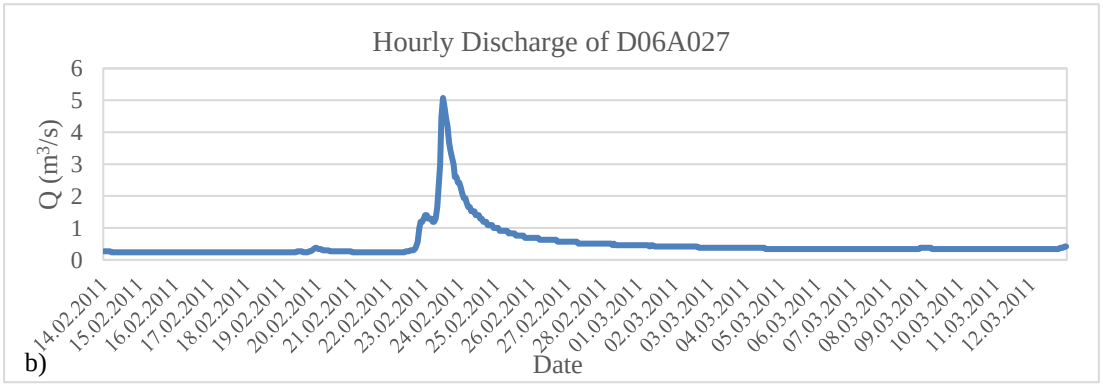


Figure 3.42 Hourly discharge of D06A027 a) for calibration period, b) for validation period.

Hourly meteorological data from Ödemiş station (17822) were used, and the point data recorded at the station were spatially distributed to 1000m*1000m grid cells. Distribution coefficients were calculated by averaging the daily precipitation within the corresponding month and grid, and the point hourly precipitation data were multiplied by these distribution coefficients and distributed across the basin (Figures 3.43 and Figure 3.44 and Figure 3.45). Hourly average temperature and solar radiation values measured at the station were uniformly distributed over the basin.

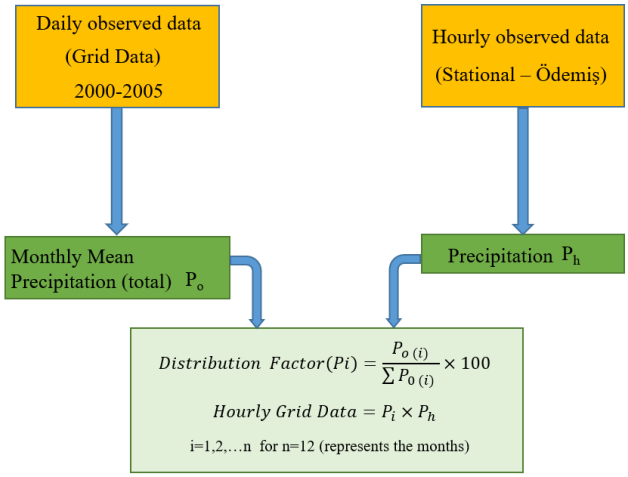


Figure 3.43 The process in order to obtain distributed data.

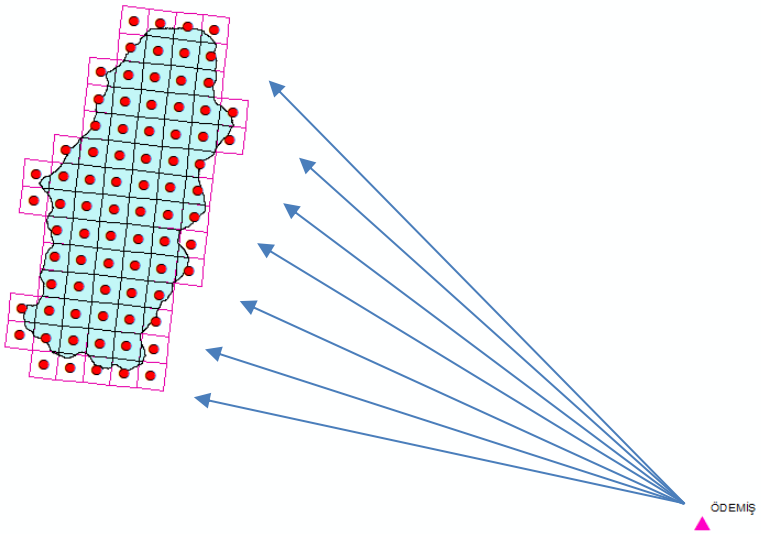


Figure 3.44 Distribution of daily precipitation measured at Ödemiş Meteorological Station (17822) to the grids according to the relevant distribution coefficients.

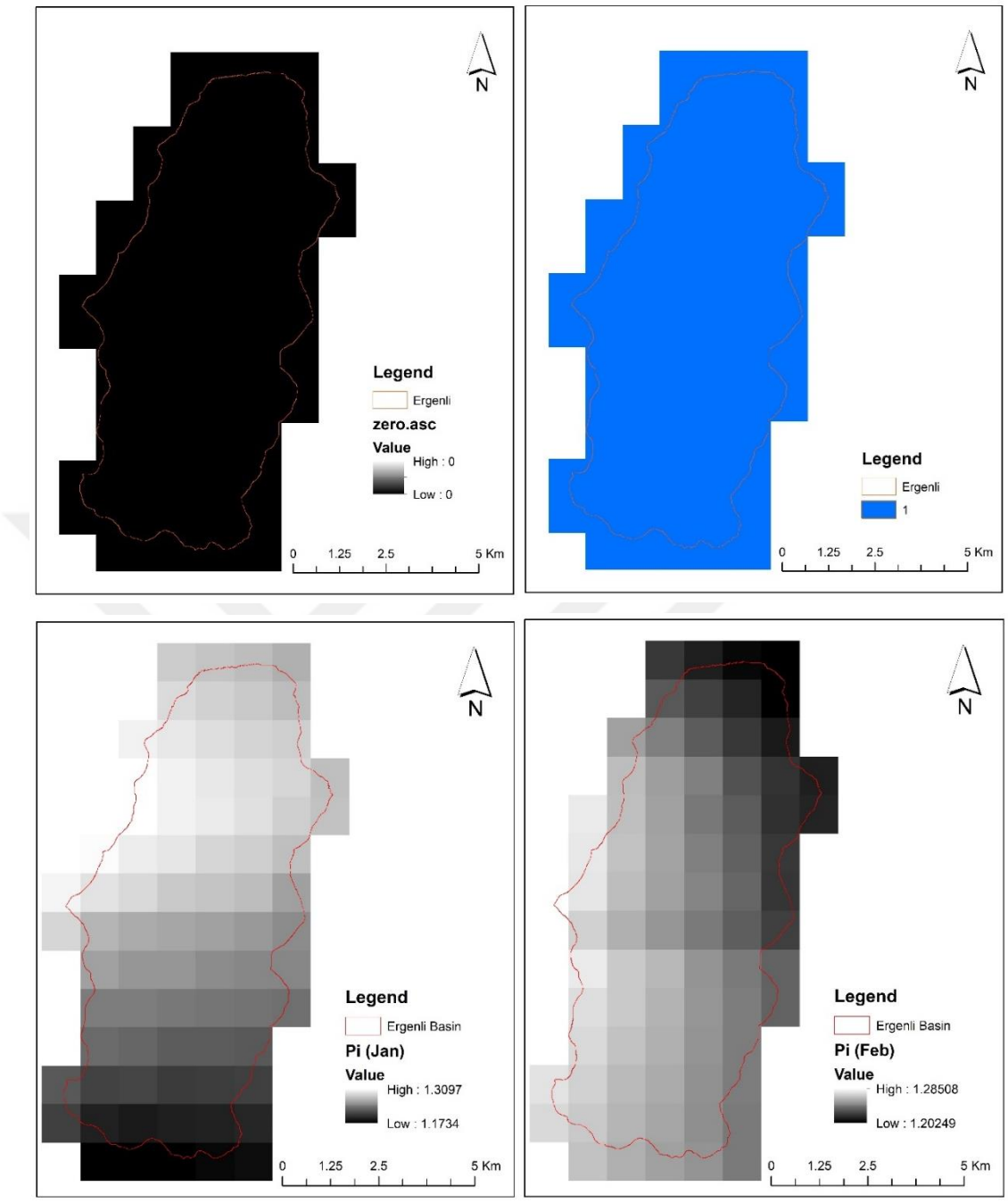


Figure 3.45 a) Zero grid, b) "One" value grid, c) Distribution factor grid for January, d) Distribution factor grid for February.

For Ödemiş station, the annual maximum rainfall with standard durations (from 5 minutes to 24 hours) was obtained and given in Table 3.14. Using these data, rainfall intensity duration frequency (IDF) curves were created.

Table 3.14 Maximum rainfall (mm) with standard duration of Ödemiş Station (17822).

PERIOD	MINUTE				HOUR									
YEAR	5	10	15	30	1	2	3	4	5	6	8	12	18	24
2010	6.1	11.3	14.2	18.2	28	44.5	44.5	44.5	44.5	44.5	47.9	47.9	48	48
2009	2.6	4.2	6	10.4	15.6	16.3	20.2	20.3	20.6	21	21.1	23.7	28.6	47
2008	5.3	8.1	9.3	11	11	11.9	15.2	16.5	17.6	20.7	23.2	23.3	32.4	38.3
2007	4.3	7.2	10.1	10.6	14.7	21.2	26.3	27.6	27.8	28	31.1	38	42.9	44.2
2006	6.9	8.9	9.8	12.6	20.6	20.9	29.5	35.2	35.9	36.1	36.1	36.1	37.8	37.8
2005	2.4	4.9	6.9	9.7	12.5	17.1	20.9	23.9	26.8	32.1	37.9	42.1	49	56.4
2004	2.8	4.8	6.5	10.2	13.1	15.3	19.2	19.9	20.2	20.4	20.4	21.4	31	32.1
2003	5.6	9.1	12.4	15.3	16.7	17.4	17.4	19.7	21.9	24.7	32.6	43.6	57.9	74.5
2002	6	8.3	10.6	14.2	24.6	43	56.1	60.7	60.8	60.8	60.9	65.9	66.2	66.2
2001	4.6	6.8	8.8	11.2	15.5	23.4	28.3	31.4	31.5	31.5	31.6	43.3	44.8	47.3
2000	4.3	6.6	9.5	17.1	18.7	18.8	18.8	19	19.1	19.1	19.1	24.1	24.3	27.8
1999	1.7	2.2	2.8	4.4	4.9	6.5	6.8	6.8	6.8	6.8	6.9	6.9	6.9	6.9
1998	5.9	6.8	7	7.2	10.8	16.9	18.7	19.5	21.1	22.4	23.2	24.9	30.6	42.4
1997	6.1	8.7	9.2	10.2	10.6	11.4	12.2	14.1	15.2	18	23.5	26.3	36	40.1
1996	10.1	17.8	21.6	23.2	23.5	23.7	23.7	27.3	27.7	27.8	27.9	28.4	29.2	50.3
1995	3.3	6.1	7.7	12.2	12.9	12.9	12.9	12.9	12.9	13.1	13.6	13.8	15.6	51.6
1994	8.6	11.2	16.4	24.3	32.5	32.5	32.5	32.6	32.6	32.6	32.6	32.6	32.7	39.3
1993	4.1	6.9	8.9	13.4	17	17.7	21.3	21.8	21.9	21.9	22	23.7	26.6	36.3
1992	5.2	10	12.4	18.8	25.4	26	26	26	26	26	26	26	26	35.9
1991	2.6	4.3	6.2	8.1	9.8	15	18.1	21	21.5	21.6	21.6	22.8	22.8	25.5
1990	3.4	5.5	7	8.5	10.8	13.9	14.9	15.7	21.5	24.6	27.2	30.2	36.3	48.8
1989	1.7	2.9	4.3	5.7	10.9	20.7	28.2	36.4	37.9	39.2	39.3	41.8	53.6	59.2
1988	8.7	10	10.7	10.9	12	12.8	12.8	12.8	12.8	12.8	12.8	15.1	18.1	27.2
1987	6	9.1	8.3	10.8	12.4	13.5	13.5	13.5	13.5	13.5	13.5	13.5	13.5	29.5
1986	5	9	12.8	19	21	21	21	21	21	21	21	21	21	30.6
1985	2.5	4	4	7.3	10.5	17.7	19.4	20.2	21.5	26.9	28.8	33.5	33.6	49.1
1984	3.5	4.7	6	6.5	7.1	9.1	10.7	11	11.2	11.3	11.3	11.3	11.3	61.3
1983	10.3	11.8	14.2	17.5	19.6	26.3	28.9	28.9	28.9	28.9	28.9	28.9	28.9	52.9
1982	5.6	8.8	10.8	14	17.7	20.6	20.6	21.5	22.7	23	23.9	30.7	36.7	36.7
1981	1.6	2.8	3	3.2	4.5	7	7.1	7.1	7.6	8.3	8.5	8.5	8.5	78.1
1980	5.7	7.7	8.1	12.4	20.5	25.2	29.7	33.7	36.9	38.3	43.6	48.2	48.2	58.7
1979	5.2	7.5	9.4	9.9	11.4	13.2	14.6	21	22.7	24.2	25.6	25.6	25.6	41.8
1978	3.5	4.9	5.3	10.6	13.4	20.4	21.1	21.1	21.1	21.1	23.1	25.2	26	47.5
1977	10	13.2	13.4	16.4	20.8	23.8	23.8	23.8	23.8	23.8	23.8	23.8	23.8	32.3
1976	8.7	11.5	14.8	17.6	17.6	22	28.7	32.9	42.4	50.3	53.8	62.3	62.5	62.5
1975	5.5	7.2	7.3	9.7	10	10.1	10.1	10.1	10.1	10.1	10.1	13	14.6	64.4
1974	3	4.2	5.3	8.7	8.7	8.7	8.7	8.7	8.7	8.7	8.7	8.7	8.7	59.7
1973	4.2	7.6	7.9	8.6	9	9	10.7	12.5	13.4	14	14	14	14	42.4
1972	5.2	6.5	7.3	9.7	13.2	18.5	18.5	18.5	18.5	18.5	18.5	18.5	28.9	41.9
1971	4.5	6.5	7.8	10.8	10.8	12	12.5	12.8	12.8	12.8	12.8	12.8	12.8	45.5
1970	5.7	8.6	12.9	16.8	21.6	22.1	22.2	22.2	22.2	22.2	24.7	27.8	27.9	37.3
1969	4.8	6	6.8	9.8	10.6	19.1	24	27.5	27.8	27.8	27.8	27.8	27.8	41.3

CN values were computed as gridded data based on hydrological soil groups in the basin and the CORINE land cover map 2012. According to the hydrological soil groups map (Figure 3.35), which was prepared as a basis for the SWAT hydrological model under the İKLİM RİSK (2021) project, the hydrological soil group in Ergenli Basin was identified as B. The resulting curve numbers were then calculated as 1000m*1000 m grids, following the same grid resolution as other input parameters.

3.2.4 Data for HEC-RAS Modeling

The HEC-RAS model utilized hydrographs derived from the HEC-HMS model. The river cross sections were delineated, and the precise position and measurements of the structures (as shown in Figure 3.28 and Figure 3.29) were added into the model.

3.2.5 Data Preprocessing

The data from 11 meteorological stations situated in and around the Küçük Menderes River Basin were evaluated, considering the common period from 1972 to 2018. Long-term averages of annual total precipitation and annual average temperatures are shown in Figure 3.46. Analysis of the observed precipitation, as shown in Figure 3.46a reveals that Manisa consistently experiences the highest average annual precipitation. Typically, there is a declining trend in precipitation from coastal to inland regions. Regarding average temperatures, Figure 3.46b highlights Izmir station with the highest recorded mean temperature values (17.95 ^{o}C). The long-term averages of monthly total precipitation and monthly mean temperatures are shown in Figure 3.47.

Prior to calculating the drought indices, preliminary data analyses were carried out to identify any missing data, evaluate consistency, and conduct trend analysis to guarantee the data is suitable, dependable, and accurate. Missing data analysis was conducted by linear regression analyses, utilizing corresponding reference series, to fill in the gaps in the precipitation and temperature time series. Homogeneity analysis was conducted to ensure that the data sets used in the study possess sufficient quality.

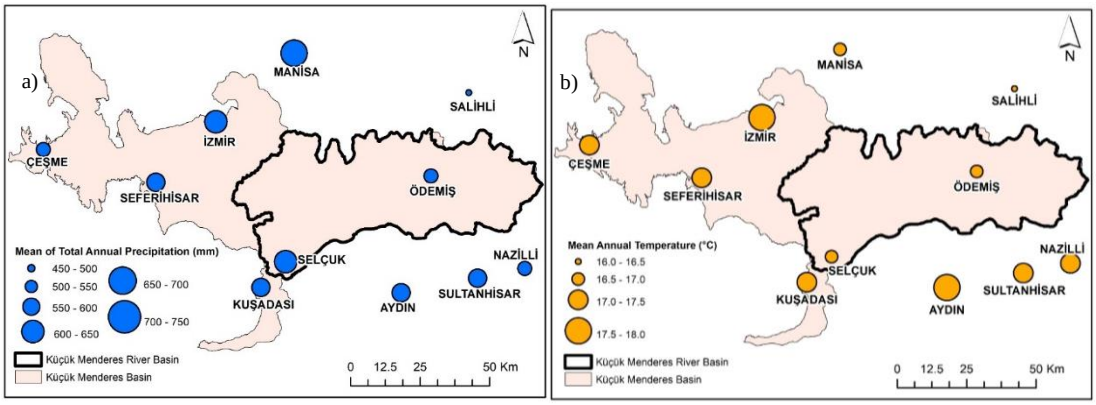


Figure 3.46 Long term average of a) total annual precipitation (mm), b) mean annual temperature (°C).

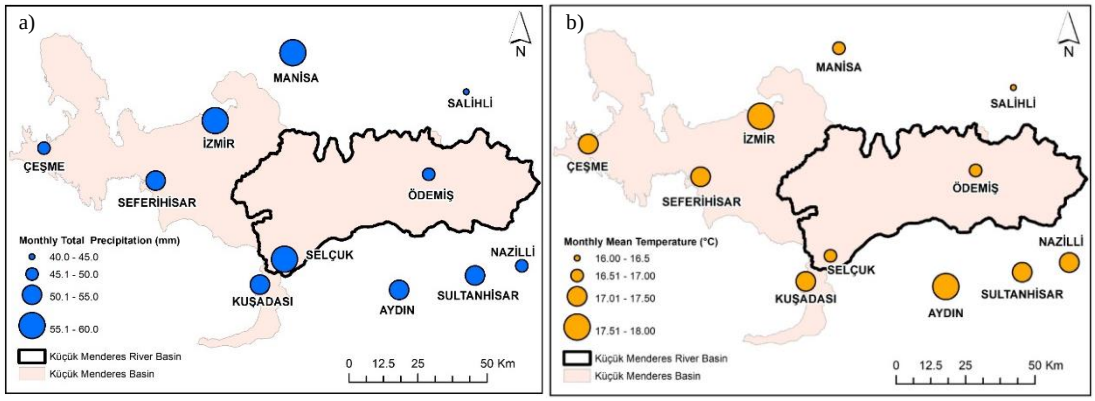


Figure 3.47 Long term average of a) total monthly precipitation (mm), b) mean monthly temperature (°C).

3.2.5.1 Statistics of Daily, Monthly and Annual Meteorological Data

Statistics of daily, monthly, and annual meteorological data included precipitation, mean temperature, minimum and maximum temperature are given by Table 3.15, Table 3.16, Table 3.17, and Table 3.18, respectively. The statistics were calculated using by R-Studio "HydroTSM" package developed by Zambrano-Bigiarini (2017).

In Tables 3.15, 3.16, 3.17 and 3.18, "Min.", "Max.", "Sd", and "Cv" represents minimum value, maximum value, standard deviation, and coefficient of variation of the series, respectively.

Table 3.15. Statistics of daily, monthly, annual precipitation series (mm).

	Prec. (mm)	Manisa	İzmir	Çeşme	Kuşadası	Aydın	Salihli	Seferihisar	Ödemiş	Sultanhisar	Selçuk	Nazilli
Daily	Min.	0.00	0.00	0.00	0.00	0.00	0.00	0.00	0.00	0.00	0.00	0.00
	Median	0.00	0.00	0.00	0.00	0.00	0.00	0.00	0.00	0.00	0.00	0.00
	Mean	1.95	1.90	1.56	1.69	1.72	1.33	1.67	1.57	1.66	1.83	1.60
	Max.	163.50	145.30	166.40	113.80	93.80	71.20	187.00	78.10	78.80	174.10	88.40
	Sd	6.81	7.06	6.41	6.24	5.80	4.56	6.75	5.33	5.54	6.61	5.41
	Cv	3.50	3.72	4.12	3.68	3.37	3.43	4.04	3.39	3.34	3.62	3.39
	Skewness	6.10	6.61	8.06	6.13	5.34	5.61	8.84	5.42	5.17	6.54	5.29
	Kurtosis	57.10	65.08	104.03	53.28	39.32	41.88	136.56	39.51	35.03	72.89	36.54
Monthly	Min.	0.00	0.00	0.00	0.00	0.00	0.00	0.00	0.00	0.00	0.00	0.00
	Median	39.75	31.95	21.85	29.90	34.45	29.75	25.90	32.40	33.90	31.30	34.00
	Mean	59.19	57.85	47.34	51.24	52.34	40.49	50.74	47.47	50.32	55.56	48.54
	Max.	393.80	354.60	286.60	336.60	344.10	196.60	308.70	333.70	321.40	326.50	300.60
	Sd	63.94	67.36	59.66	61.73	56.24	38.18	62.35	50.59	54.32	65.35	51.39
	Cv	1.08	1.16	1.26	1.20	1.07	0.94	1.23	1.07	1.08	1.18	1.06
	Skewness	1.56	1.49	1.57	1.55	1.44	1.04	1.54	1.44	1.47	1.48	1.39
	Kurtosis	2.93	2.08	2.16	2.47	2.36	0.61	2.19	2.57	2.36	2.03	1.92
Annual	Min.	406.20	339.30	210.90	349.60	359.20	294.20	314.20	371.50	360.30	342.20	346.30
	Median	684.90	685.10	590.80	611.50	661.30	464.50	599.40	551.40	595.20	672.60	554.20
	Mean	710.20	694.20	568.00	614.80	628.00	485.90	608.80	569.60	603.80	666.80	582.50
	Max.	1075.00	1086.00	869.70	914.90	946.40	669.00	979.10	876.70	1034.00	1060.00	925.90
	Sd	160.65	178.02	144.38	146.44	150.34	83.10	136.92	115.75	140.00	145.63	124.70
	Cv	0.23	0.26	0.25	0.24	0.24	0.17	0.22	0.20	0.23	0.22	0.21
	Skewness	0.31	0.28	-0.31	0.01	0.03	0.14	0.34	0.59	0.69	0.20	0.54
	Kurtosis	-0.38	-0.35	-0.55	-1.17	-0.72	-0.23	0.26	0.25	0.59	-0.17	-0.02

Table 3.16 Statistics of daily, monthly, annual mean temperature series (°C).

	Mean Temp. (°C)	Manisa	İzmir	Çeşme	Kuşadası	Aydın	Salihli	Seferihisar	Ödemiş	Sultanhisar	Selçuk	Nazilli
Daily	Min.	-4.3	-2.3	-1	-1.9	-1.7	-6.6	-2.5	-2.6	-2.5	-2.6	-3.1
	Median	16.8	17.9	17.3	17.3	17.4	16.5	16.9	16.2	17	16.8	17.1
	Mean	16.87	18.01	17.37	17.3	17.69	16.47	17.06	16.54	17.36	16.77	17.44
	Max.	39.8	35.5	31.4	34.6	35.2	37.5	35.2	35.6	35	33.9	36.4
	Sd	8.47	7.55	6.49	6.7	7.73	8.25	7.24	7.8	7.73	7.29	8.06
	cv	0.5	0.42	0.37	0.39	0.44	0.5	0.42	0.47	0.45	0.43	0.46
	Skewness	-0.06	-0.07	-0.16	-0.17	-0.05	-0.1	-0.08	-0.02	-0.01	-0.12	0.01
	Kurtosis	-1.14	-1.06	-1	-0.84	-1.1	-1.09	-0.94	-1.09	-1.12	-0.95	-1.14

Table 3.16 (continuation) Statistics of daily, monthly, annual mean temperature series (ºC).

	Mean Temp. (ºC)	Manisa	İzmir	Çeşme	Kuşadası	Aydın	Salihli	Seferihisar	Ödemiş	Sultanhisar	Selçuk	Nazilli
Monthly	Min.	3.21	5.62	6.33	5.82	4.84	2.49	4.69	3.96	4.64	4.4	4.46
	Median	16.52	17.51	17	16.84	17.12	16.22	16.28	15.86	16.85	16.21	16.69
	Mean	16.83	17.96	17.34	17.28	17.64	16.45	17.02	16.52	17.32	16.74	17.4
	Max.	30.66	30.22	28.32	28.34	30.42	29.83	29.23	29.31	30.23	29.59	30.95
	Sd	7.9	7.04	6.03	6.15	7.26	7.67	6.7	7.28	7.28	6.73	7.64
	cv	0.47	0.39	0.35	0.36	0.41	0.47	0.39	0.44	0.42	0.4	0.44
	Skewness	0.07	0.08	0.06	0.07	0.08	0.04	0.13	0.12	0.1	0.1	0.1
	Kurtosis	-1.38	-1.36	-1.36	-1.28	-1.37	-1.36	-1.31	-1.36	-1.38	-1.3	-1.38
Annual	Min.	15.44	16.66	16.43	15.57	16.4	15.06	15.76	15.41	16.2	15.44	16.02
	Median	16.83	17.82	17.24	17.09	17.54	16.25	16.83	16.54	17.22	16.52	17.22
	Mean	16.83	17.96	17.34	17.28	17.64	16.45	17.02	16.52	17.32	16.74	17.4
	Max.	18.4	19.64	19.16	19.39	19.16	18.6	19.02	18.03	18.67	19.27	18.65
	Sd	0.64	0.69	0.62	0.95	0.67	0.85	0.82	0.59	0.64	0.82	0.61
	cv	0.04	0.04	0.04	0.06	0.04	0.05	0.05	0.04	0.04	0.05	0.04
	Skewness	0.28	0.4	0.69	0.37	0.35	0.57	0.57	0.31	0.25	0.66	0.12
	Kurtosis	-0.35	-0.45	0.14	-0.96	-0.78	-0.55	-0.7	-0.6	-1.02	0.25	-0.64

Table 3.17 Statistics of daily, monthly, annual minimum temperature series (ºC).

	Min. Temp.	Manisa	İzmir	Çeşme	Kuşadası	Aydın	Salihli	Seferihisar	Ödemiş	Sultanhisar	Selçuk	Nazilli
Daily	Min.	-8.9	-5	-4	-6.9	-6	-13.5	-6.2	-10	-8.2	-8.5	-8.5
	Median	11.5	13.8	13.1	13	12.2	10.6	12.1	9.7	11	11	11
	Mean	11.54	13.89	13.07	12.76	12.05	10.39	12.01	9.41	11	10.57	11.17
	Max.	30.8	30.4	27.6	29.1	28.6	33.4	28.1	28.6	27.8	29.3	32.7
	Sd	7.42	6.91	6.39	6.5	6.68	7.04	6.75	6.43	6.53	6.46	6.91
	cv	0.64	0.5	0.49	0.51	0.55	0.68	0.56	0.68	0.59	0.61	0.62
	Skewness	-0.06	-0.11	-0.08	-0.21	-0.15	-0.14	-0.12	-0.18	-0.09	-0.22	0.01
	Kurtosis	-0.96	-0.95	-0.93	-0.71	-0.89	-0.87	-0.82	-0.83	-0.86	-0.77	-0.83
Monthly	Min.	-0.64	2.51	2.68	1.17	0.56	-2.57	0.55	-2.11	-0.17	-1.03	-0.99
	Median	11.01	13.46	12.45	12.2	11.47	9.85	11.4	8.72	10.36	10.01	10.35
	Mean	11.5	13.85	13.04	12.73	12.02	10.37	11.98	9.4	10.97	10.54	11.14
	Max.	24.23	25.45	24.08	24.48	23.63	22.81	23.56	20.27	21.92	21.95	23.28
	Sd	6.73	6.3	5.68	5.77	6.06	6.33	5.95	5.63	5.89	5.55	6.29
	cv	0.59	0.46	0.44	0.45	0.5	0.61	0.5	0.6	0.54	0.53	0.57
	Skewness	0.15	0.12	0.16	0.13	0.09	0.1	0.18	0.12	0.14	0.14	0.17
	Kurtosis	-1.27	-1.29	-1.25	-1.1	-1.26	-1.18	-1.18	-1.18	-1.25	-1.08	-1.23

Table 3.17 (continuation) Statistics of daily, monthly, annual minimum temperature series (°C).

	Min. Temp. (°C)	Manisa	İzmir	Çeşme	Kuşadası	Aydın	Salihli	Seferihisar	Ödemiş	Sultanhisar	Selçuk	Nazilli
Annual	Min.	10.09	12.54	11.91	10.12	10.63	8.57	10.32	7.75	9.76	8.8	9.27
	Median	11.37	13.78	12.87	12.52	11.88	9.99	11.6	9.17	10.9	10.47	11.15
	Mean	11.5	13.85	13.04	12.71	12.02	10.37	11.98	9.4	10.97	10.54	11.14
	Max.	13.48	15.67	15.13	15.67	13.98	13.07	14.23	11.26	12.79	13.32	12.91
	Sd	0.79	0.7	0.73	1.51	0.84	1.09	0.97	0.79	0.73	1.13	0.78
	cv	0.07	0.05	0.06	0.12	0.07	0.11	0.08	0.08	0.07	0.11	0.07
	Skewness	0.48	0.36	0.68	0.19	0.49	0.59	0.47	0.26	0.37	0.34	-0.14
	Kurtosis	-0.55	-0.12	-0.17	-1.21	-0.7	-0.7	-0.67	-0.85	-0.57	-0.88	-0.05

Table 3.18 Statistics of daily, monthly, annual maximum temperature series (°C).

	Max. Temp. (°C)	Manisa	İzmir	Çeşme	Kuşadası	Aydın	Salihli	Seferihisar	Ödemiş	Sultanhisar	Selçuk	Nazilli
Daily	Min.	-0.90	0.80	1.60	1.30	1.20	-3.00	1.20	0.50	1.20	0.60	0.60
	Median	23.00	22.80	22.00	22.10	24.60	23.40	22.00	23.80	24.50	23.50	24.50
	Mean	22.98	22.81	22.04	22.21	24.71	23.25	22.38	23.92	24.50	23.58	24.49
	Max.	45.50	43.00	40.50	42.40	44.80	44.80	42.90	44.60	44.50	44.00	46.30
	Sd	9.69	8.25	6.96	7.09	8.98	9.53	7.98	9.06	9.01	8.16	9.22
	cv	0.42	0.36	0.32	0.32	0.36	0.41	0.36	0.38	0.37	0.35	0.38
	Skewness	-0.09	-0.08	-0.18	-0.06	-0.07	-0.12	-0.03	-0.05	-0.08	-0.10	-0.09
	Kurtosis	-1.14	-1.05	-0.91	-0.80	-1.18	-1.12	-0.97	-1.13	-1.18	-1.00	-1.17
Monthly	Min.	7.62	9.08	9.40	10.15	9.95	7.23	9.67	9.08	9.88	9.98	9.11
	Median	22.81	22.55	21.78	21.97	24.49	23.25	21.68	23.42	24.26	23.41	24.31
	Mean	22.93	22.76	22.00	22.18	24.66	23.21	22.35	23.87	24.46	23.54	24.44
	Max.	38.17	35.91	32.89	33.66	38.98	38.41	35.62	38.99	39.04	36.96	39.75
	Sd	8.96	7.61	6.43	6.47	8.37	8.77	7.40	8.36	8.39	7.54	8.59
	cv	0.39	0.33	0.29	0.29	0.34	0.38	0.33	0.35	0.34	0.32	0.35
	Skewness	0.00	0.02	0.01	0.05	0.01	0.00	0.10	0.06	0.00	0.03	0.00
	Kurtosis	-1.41	-1.40	-1.41	-1.35	-1.43	-1.40	-1.36	-1.41	-1.43	-1.38	-1.41
Annual	Min.	21.46	21.46	21.10	20.16	23.17	21.58	20.80	22.45	23.44	22.20	23.08
	Median	22.93	22.69	21.99	21.99	24.65	23.07	22.26	23.78	24.39	23.47	24.33
	Mean	22.93	22.76	22.00	22.17	24.66	23.21	22.35	23.87	24.46	23.54	24.44
	Max.	24.36	24.11	23.38	23.55	26.34	25.22	24.19	25.39	25.72	26.22	26.12
	Sd	0.70	0.66	0.55	0.69	0.74	0.81	0.90	0.66	0.65	0.75	0.80
	cv	0.03	0.03	0.02	0.03	0.03	0.04	0.04	0.03	0.03	0.03	0.03
	Skewness	0.08	0.20	0.32	-0.13	0.08	0.36	0.24	0.16	0.20	0.74	0.31
	Kurtosis	-0.85	-0.92	-0.66	0.23	-0.73	-0.66	-1.23	-0.70	-1.03	1.73	-0.94

Figure 3.47 and Figure 3.50 display the annual, monthly, and daily precipitation data, as well as box-plot graphs and histograms, for the Ödemiş and Selçuk stations. Figure 3.49 and Figure 3.51 depict matrix graphs illustrating the monthly precipitation data for Ödemiş and Selçuk Stations.

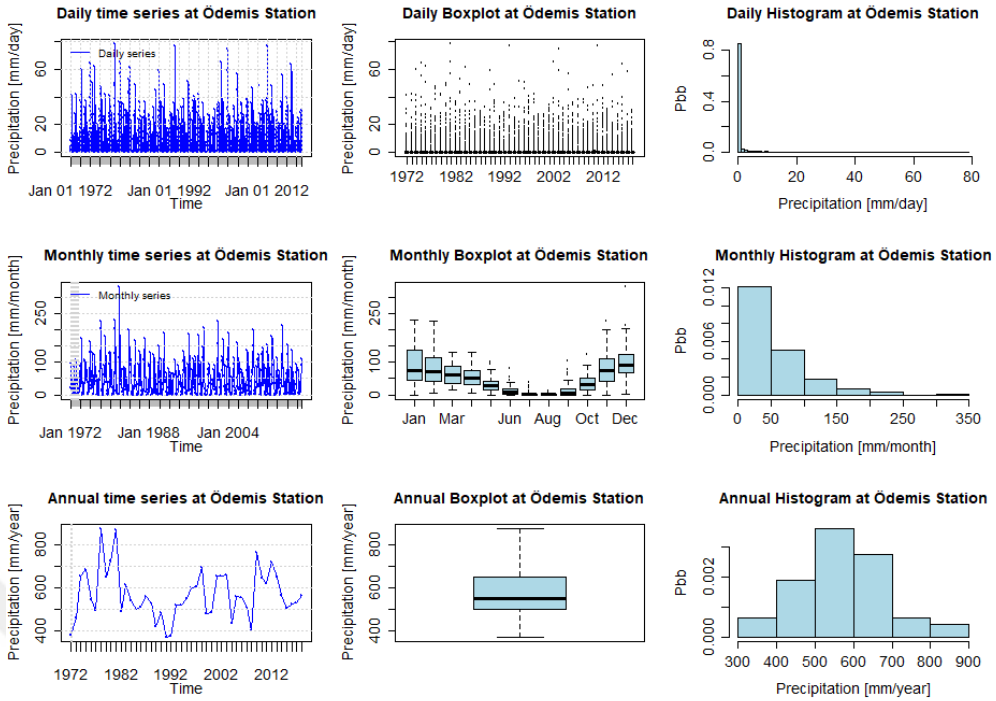


Figure 3.48 Daily, monthly, annual total precipitation graphs of Ödemiş Meteorological Station.

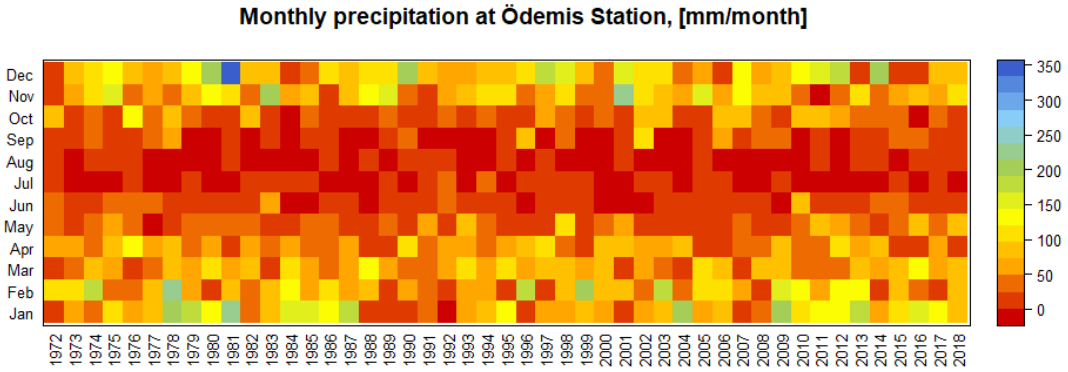


Figure 3.49 The monthly total precipitation matrix of Ödemiş Meteorological Station.

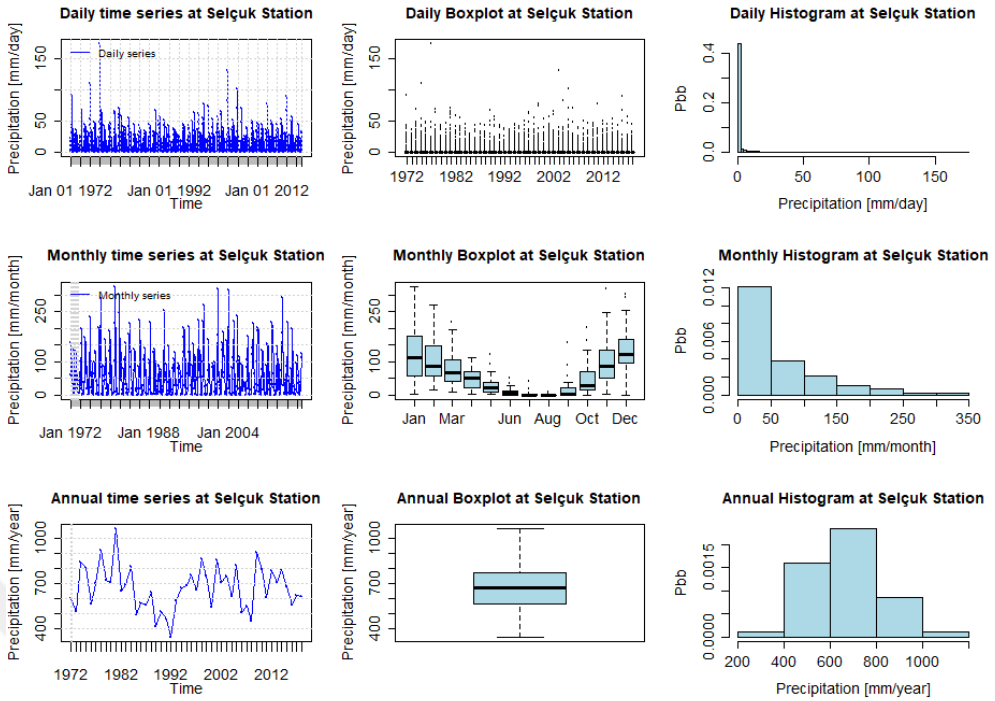


Figure 3.50 Daily, monthly, annual total precipitation graphs of Selçuk Meteorological Station.

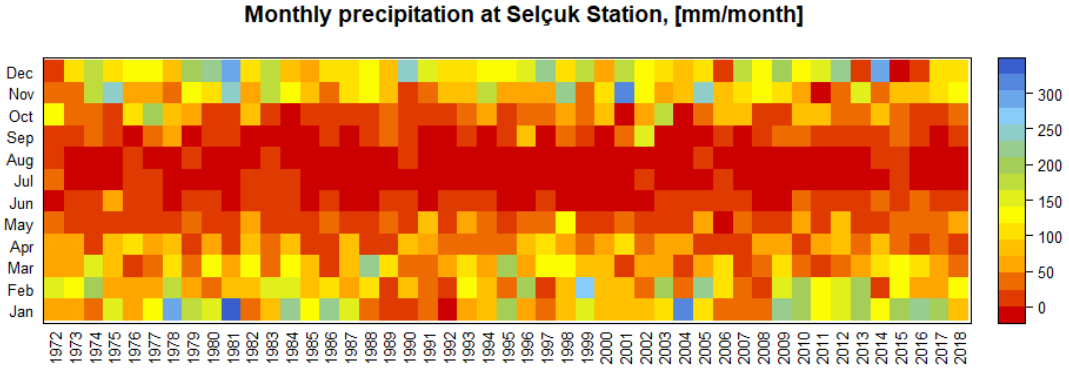


Figure 3.51 The monthly total precipitation matrix of Selçuk Meteorological Station.

Figure 3.52 and Figure 3.54 display the annual, monthly, and daily temperature data, as well as box-plot graphs and histograms, for the Ödemiş and Selçuk stations. Figure 3.53 and Figure 3.55 depict matrix graphs illustrating the monthly temperature data for Ödemiş and Selçuk Stations.

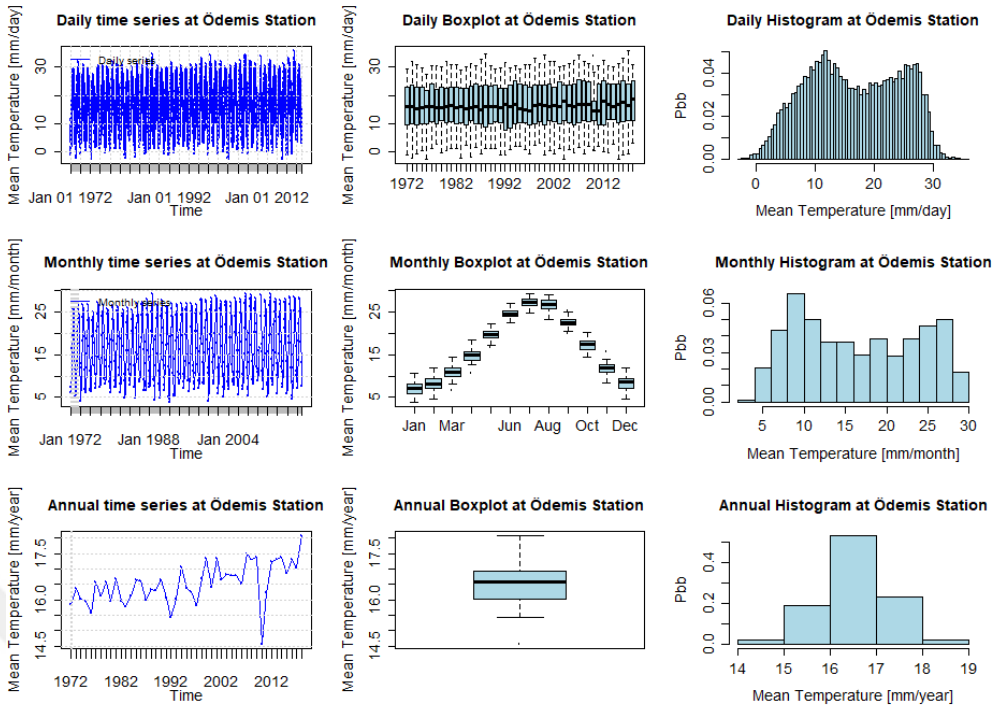


Figure 3.52 Daily, monthly, annual mean temperature graphs of Ödemiş Meteorological Station.

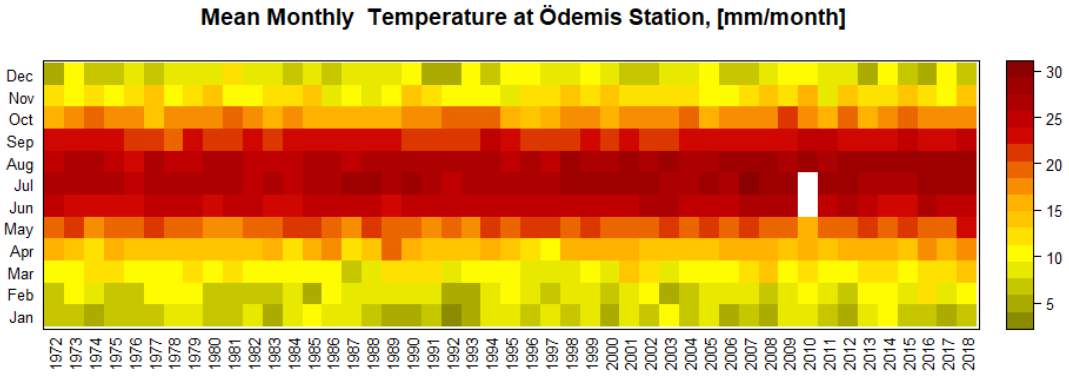


Figure 3.53 The monthly mean temperature matrix of Ödemiş Meteorological Station.

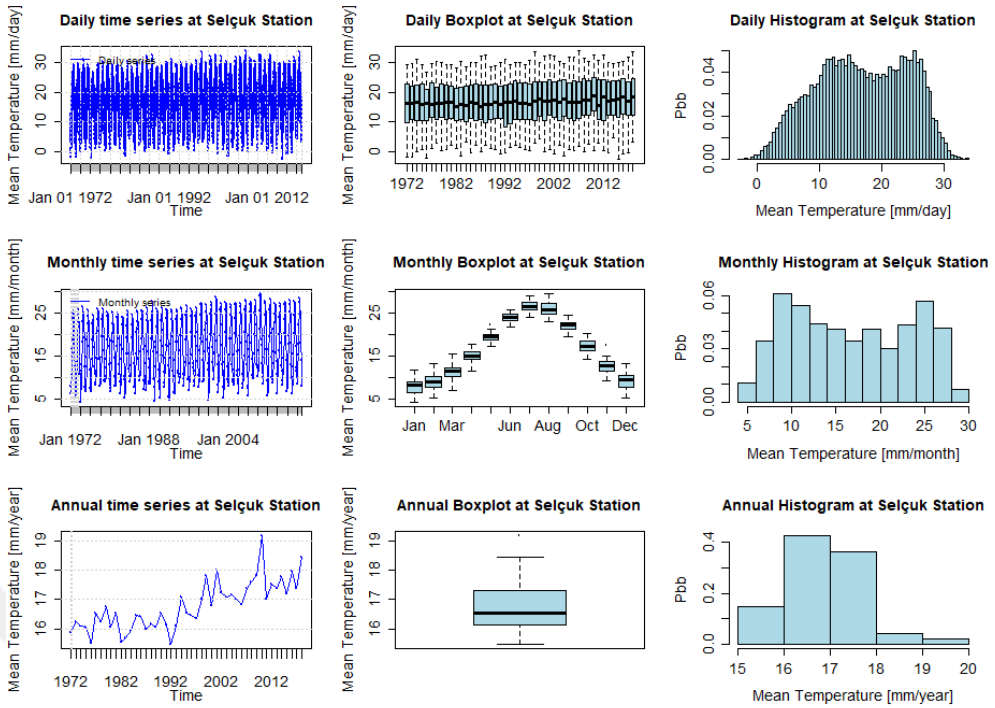


Figure 3.54 Daily, monthly, annual mean temperature graphs of Selçuk Meteorological Station.

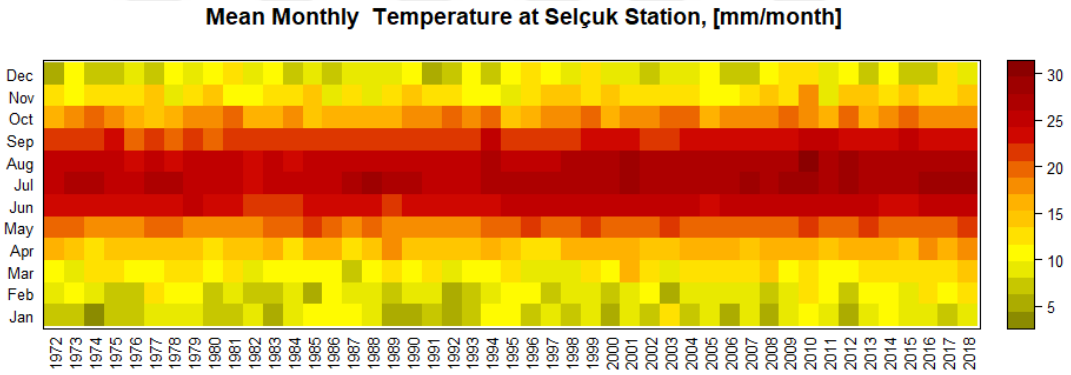


Figure 3.55 The monthly mean temperature matrix of Selçuk Meteorological Station.

3.2.5.2 Statistics of Seasonal Meteorological Data

The full periods were divided seasonally as winter (December, January, February), spring (March, April, May), summer (June, July, August) and fall (September, November, December). Statistics of seasonal meteorological data included total precipitation, mean temperature, minimum temperature and maximum temperature are given by Table 3.19, Table 3.20, Table 3.21, and Table 3.22, respectively.

Table 3.19 Statistics of seasonally precipitation series (mm).

	Prec. (mm)	Manisa	İzmir	Çeşme	Kuşadası	Aydın	Salihli	Seferihisar	Ödemiş	Sultanhisar	Selçuk	Nazilli
Seasonal (Dec-Jan-Feb)	Min.	85.60	64.80	73.80	62.80	66.00	61.00	61.50	76.40	93.20	82.30	76.80
	Median	330.80	344.50	291.00	282.50	285.30	207.80	303.50	254.70	270.00	324.00	260.40
	Mean	344.90	352.90	310.80	314.60	301.70	205.90	323.00	266.20	292.50	345.10	279.50
	Max.	622.50	657.70	698.70	621.80	552.80	400.00	618.30	507.20	512.10	628.30	497.20
	Sd	131.76	130.25	133.67	135.68	125.37	74.57	132.86	111.16	115.08	134.86	107.15
	cv	0.38	0.37	0.43	0.43	0.42	0.36	0.41	0.42	0.39	0.39	0.38
	Skewness	0.12	0.03	0.36	0.38	0.18	0.37	0.36	0.37	0.24	0.45	0.01
	Kurtosis	-0.61	-0.24	-0.20	-0.70	-0.84	-0.23	-0.60	-0.60	-0.78	-0.52	-0.75
Seasonal (Mar-Apr-May)	Min.	70.90	52.40	19.90	63.70	65.30	48.80	51.20	78.30	65.40	65.30	52.80
	Median	164.10	151.40	116.50	126.10	158.90	134.40	138.70	149.60	148.80	140.60	137.40
	Mean	171.60	154.80	121.00	138.80	162.20	133.70	134.20	148.90	151.10	150.70	146.00
	Max.	304.80	303.80	255.90	301.60	327.80	248.90	292.10	243.10	238.80	304.00	294.30
	Sd	57.23	61.64	53.53	57.81	52.73	45.42	54.35	42.05	45.66	57.07	48.58
	cv	0.33	0.40	0.44	0.42	0.33	0.34	0.41	0.28	0.30	0.38	0.33
	Skewness	0.49	0.49	0.29	0.99	0.41	0.29	0.31	0.18	0.15	0.79	0.54
	Kurtosis	-0.42	-0.42	-0.24	0.64	0.51	-0.49	-0.25	-0.83	-0.85	0.06	0.25
Seasonal (Jun-Jul-Aug)	Min.	0.10	0.00	0.00	0.00	0.00	0.80	0.00	0.00	0.00	0.00	0.00
	Median	21.80	4.60	2.10	1.70	13.70	28.60	1.60	12.00	23.90	5.30	22.40
	Mean	31.25	15.01	6.27	6.79	21.33	33.67	7.06	19.20	23.53	9.52	27.88
	Max.	141.80	87.70	69.70	56.30	98.00	175.20	79.60	81.50	73.00	49.90	110.00
	Sd	33.27	20.94	12.22	11.69	22.75	31.35	13.80	19.46	18.07	12.11	25.66
	cv	1.06	1.40	1.95	1.72	1.07	0.93	1.96	1.01	0.77	1.27	0.92
	Skewness	1.53	1.75	3.43	2.50	1.24	2.30	3.45	1.42	0.49	1.47	1.18
	Kurtosis	1.96	2.50	13.56	6.24	1.22	7.30	14.04	1.33	-0.30	1.57	0.93
Seasonal (Sep-Oct-Nov)	Min.	45.60	45.90	23.90	0.10	37.50	33.80	24.60	31.60	35.40	45.80	25.80
	Median	145.60	159.60	112.30	143.60	131.40	104.90	123.50	132.10	120.70	156.60	116.40
	Mean	160.40	168.90	126.70	152.70	140.70	110.60	142.50	133.30	134.10	159.10	126.20
	Max.	337.10	395.20	373.00	378.10	345.40	234.80	348.20	296.10	301.90	350.30	243.60
	Sd	65.21	78.93	69.42	82.77	63.45	49.36	76.09	53.94	60.19	75.58	52.42
	cv	0.41	0.47	0.55	0.54	0.45	0.45	0.53	0.40	0.45	0.48	0.42
	Skewness	0.42	0.82	1.00	0.64	0.77	0.56	0.98	0.54	0.59	0.66	0.38
	Kurtosis	-0.03	0.46	1.45	0.25	0.80	-0.48	0.46	0.44	-0.18	-0.17	-0.61

Table 3.20 Statistics of seasonally mean temperature series (ºC).

	Mean Temp. (ºC)	Manisa	İzmir	Çeşme	Kuşadası	Aydın	Salihli	Seferihisar	Ödemiş	Sultanhisar	Selçuk	Nazilli
Seasonal (Dec-Jan-Feb)	Min.	3.96	6.61	7.46	6.51	5.79	3.55	5.98	4.54	5.58	5.19	5.23
	Median	7.33	9.58	10.15	9.96	8.98	7.23	9.08	7.97	8.53	8.92	8.12
	Mean	7.23	9.52	10.14	9.97	8.80	7.07	9.18	7.81	8.48	8.73	8.07
	Max.	10.00	12.04	12.61	12.79	11.12	9.87	12.13	10.07	10.58	11.63	10.21
	Sd	1.16	1.11	1.02	1.24	1.06	1.28	1.15	1.08	0.99	1.23	0.99
	cv	0.16	0.12	0.10	0.12	0.12	0.18	0.13	0.14	0.12	0.14	0.12
	Skewness	-0.40	-0.30	-0.29	-0.35	-0.42	-0.37	-0.19	-0.64	-0.51	-0.39	-0.46
	Kurtosis	0.18	-0.14	-0.07	0.11	-0.03	0.08	0.34	0.34	-0.04	0.22	0.05
Seasonal (Mar-Apr-May)	Min.	12.53	13.61	13.03	12.99	13.72	12.64	12.48	12.46	13.58	12.51	13.54
	Median	15.47	16.30	15.64	15.49	16.18	15.26	15.14	14.97	15.85	15.39	16.18
	Mean	15.38	16.28	15.59	15.63	16.23	15.34	15.06	15.06	15.91	15.29	16.08
	Max.	18.68	19.62	18.48	19.20	19.32	19.22	18.60	18.08	18.61	18.44	18.56
	Sd	1.11	1.11	0.94	1.23	1.01	1.23	1.18	0.97	0.97	1.07	0.92
	cv	0.07	0.07	0.06	0.08	0.06	0.08	0.08	0.06	0.06	0.07	0.06
	Skewness	0.14	0.29	0.21	0.45	0.34	0.53	0.41	0.30	0.18	0.27	-0.30
	Kurtosis	0.58	0.49	1.05	0.11	0.57	0.72	0.41	1.23	0.05	0.61	0.51
Seasonal (Jun-Jul-Aug)	Min.	24.36	24.93	23.59	22.43	24.55	23.54	23.36	23.70	24.35	23.31	25.55
	Median	27.07	27.03	24.99	25.27	27.13	26.42	25.73	26.08	26.90	25.33	27.25
	Mean	27.09	27.13	25.13	25.14	27.12	26.28	25.82	26.19	26.84	25.56	27.39
	Max.	28.76	28.89	26.71	27.39	29.04	28.61	28.22	28.96	28.85	28.08	29.66
	Sd	0.95	0.94	0.74	1.25	0.99	1.20	1.16	1.07	1.02	1.14	1.04
	cv	0.04	0.03	0.03	0.05	0.04	0.05	0.04	0.04	0.04	0.04	0.04
	Skewness	-0.38	-0.27	0.04	-0.12	-0.18	-0.08	0.03	0.19	-0.11	0.07	0.39
	Kurtosis	-0.01	-0.33	-0.72	-1.13	-0.29	-0.77	-0.91	-0.04	-0.63	-0.91	-0.70
Seasonal (Sep-Oct-Nov)	Min.	15.85	17.39	17.09	15.94	16.43	14.50	16.01	15.38	16.29	15.08	16.36
	Median	17.65	18.97	18.59	18.31	18.35	17.08	17.96	17.18	18.09	17.33	18.09
	Mean	17.62	18.94	18.50	18.41	18.42	17.05	18.04	17.17	18.05	17.37	18.04
	Max.	19.93	20.85	20.38	20.75	20.35	19.75	19.79	19.14	20.05	19.81	19.93
	Sd	0.89	0.82	0.77	1.15	0.86	1.08	0.93	0.84	0.83	0.97	0.86
	cv	0.05	0.04	0.04	0.06	0.05	0.06	0.05	0.05	0.05	0.06	0.05
	Skewness	0.21	0.04	0.12	0.12	0.02	0.15	-0.14	0.02	0.13	0.09	-0.04
	Kurtosis	-0.30	-0.59	-0.58	-0.81	-0.35	-0.28	-0.72	-0.15	-0.22	-0.12	-0.51

Table 3.21 Statistics of seasonally minimum temperature series (°C).

	Min. Temp. (°C)	Manisa	İzmir	Çeşme	Kuşadası	Aydın	Salihli	Seferihisar	Ödemiş	Sultanhisar	Selçuk	Nazilli
Seasonal (Dec-Jan-Feb)	Min.	0.25	3.37	3.76	2.41	1.13	-1.06	1.93	-1.24	0.93	0.54	0.14
	Median	3.80	6.73	6.64	6.29	5.08	3.19	5.30	3.18	4.24	4.55	3.89
	Mean	3.70	6.53	6.57	6.26	4.87	3.00	5.32	2.99	4.15	4.32	3.80
	Max.	6.69	9.35	9.36	9.69	7.76	6.16	8.55	5.81	6.67	7.71	6.34
	Sd	1.26	1.20	1.08	1.53	1.26	1.46	1.25	1.39	1.18	1.45	1.25
	cv	0.34	0.18	0.16	0.25	0.26	0.49	0.24	0.46	0.28	0.33	0.33
	Skewness	-0.29	-0.33	-0.30	-0.23	-0.38	-0.36	-0.10	-0.59	-0.27	-0.38	-0.52
	Kurtosis	-0.12	-0.12	0.23	-0.28	0.20	0.03	0.23	0.22	-0.27	-0.21	0.15
Seasonal (Mar-Apr-May)	Min.	7.12	9.40	8.62	7.98	7.74	6.61	7.48	5.68	7.45	6.37	7.23
	Median	9.66	11.89	11.01	10.75	10.46	9.13	9.81	8.12	9.55	9.03	9.65
	Mean	9.69	11.89	11.03	10.96	10.53	9.17	9.82	8.12	9.48	9.09	9.61
	Max.	12.84	14.88	13.92	15.32	13.56	12.99	13.42	10.84	12.04	12.36	12.08
	Sd	1.03	1.00	0.97	1.64	1.02	1.21	1.24	0.90	0.89	1.21	0.87
	cv	0.11	0.08	0.09	0.15	0.10	0.13	0.13	0.11	0.09	0.13	0.09
	Skewness	0.34	0.25	0.44	0.34	0.24	0.55	0.47	0.05	0.10	0.17	-0.29
	Kurtosis	0.80	0.66	0.74	-0.58	0.84	0.94	0.12	1.11	0.21	-0.11	0.91
Seasonal (Jun-Jul-Aug)	Min.	17.62	19.86	18.55	16.50	17.04	15.56	17.04	14.53	16.21	14.57	16.75
	Median	20.57	22.14	20.48	20.09	19.96	18.33	19.68	16.90	18.96	17.63	19.54
	Mean	20.39	22.13	20.50	19.97	19.89	18.53	19.79	16.83	18.75	17.73	19.51
	Max.	22.46	23.74	22.71	23.09	22.00	21.53	22.05	19.24	20.83	20.59	21.91
	Sd	1.23	0.97	1.09	2.00	1.22	1.68	1.37	1.25	1.13	1.68	1.21
	cv	0.06	0.04	0.05	0.10	0.06	0.09	0.07	0.07	0.06	0.09	0.06
	Skewness	-0.30	-0.33	0.07	-0.16	-0.21	0.00	-0.12	-0.07	-0.29	-0.10	-0.02
	Kurtosis	-0.94	-0.42	-1.18	-1.34	-0.83	-1.28	-0.87	-1.05	-0.94	-1.34	-0.73
Seasonal (Sep-Oct-Nov)	Min.	10.48	13.01	12.14	10.90	10.82	8.44	10.85	7.96	9.97	8.50	9.57
	Median	12.02	14.74	14.12	13.51	12.63	10.47	12.86	9.47	11.36	10.76	11.63
	Mean	12.23	14.86	14.07	13.78	12.79	10.75	12.99	9.77	11.51	11.01	11.62
	Max.	14.68	16.91	16.24	17.15	15.21	13.63	15.19	12.33	13.70	14.01	13.93
	Sd	1.01	0.84	0.92	1.60	1.05	1.32	1.09	1.16	0.95	1.36	1.04
	cv	0.08	0.06	0.07	0.12	0.08	0.12	0.08	0.12	0.08	0.12	0.09
	Skewness	0.70	0.25	0.21	0.20	0.40	0.34	0.22	0.47	0.55	0.27	0.24
	Kurtosis	-0.20	-0.22	-0.57	-0.96	-0.39	-0.97	-0.78	-0.80	-0.48	-0.89	-0.60

Table 3.22 Statistics of seasonally maximum temperature series (ºC).

	Max. Temp. (ºC)	Manisa	İzmir	Çeşme	Kuşadası	Aydın	Salihli	Seferihisar	Ödemiş	Sultanhisar	Selçuk	Nazilli
Seasonal (Dec-Jan-Feb)	Min.	8.48	10.99	11.72	11.35	11.99	8.95	10.52	11.06	11.37	11.26	11.13
	Median	11.67	13.40	14.10	14.28	14.32	12.13	13.42	13.71	13.95	14.20	13.59
	Mean	11.69	13.32	14.14	14.30	14.15	12.20	13.48	13.57	13.91	14.25	13.59
	Max.	14.21	15.16	15.93	16.13	15.89	14.67	15.69	15.44	15.56	17.95	15.55
	Sd	1.17	1.05	0.98	1.04	1.00	1.25	1.15	1.00	0.99	1.18	1.04
	cv	0.10	0.08	0.07	0.07	0.07	0.10	0.09	0.07	0.07	0.08	0.08
	Skewness	-0.35	-0.22	-0.35	-0.43	-0.15	-0.28	-0.15	-0.35	-0.31	0.16	-0.26
	Kurtosis	-0.06	-0.78	-0.38	-0.04	-0.82	-0.14	-0.25	-0.43	-0.54	1.01	-0.60
Seasonal (Mar-Apr-May)	Min.	18.84	18.78	17.66	18.17	20.37	19.18	17.27	19.39	19.83	18.91	19.86
	Median	21.89	21.53	20.47	20.53	23.06	22.09	20.50	22.03	23.13	21.96	23.21
	Mean	21.76	21.37	20.36	20.54	23.19	22.11	20.37	22.22	23.08	21.87	23.22
	Max.	25.66	24.80	23.22	23.67	27.08	26.47	24.10	25.82	26.35	24.81	26.92
	Sd	1.33	1.24	1.04	1.08	1.29	1.42	1.34	1.23	1.22	1.18	1.36
	cv	0.06	0.06	0.05	0.05	0.06	0.06	0.07	0.06	0.05	0.05	0.06
	Skewness	0.21	0.22	-0.07	0.39	0.46	0.48	0.14	0.50	0.05	-0.01	0.15
	Kurtosis	0.09	-0.28	0.20	0.12	0.26	0.20	0.00	0.43	0.21	-0.06	0.13
Seasonal (Jun-Jul-Aug)	Min.	31.48	30.33	28.92	28.02	32.18	31.32	29.05	31.41	32.65	30.48	32.68
	Median	34.38	32.47	30.17	30.44	35.19	34.34	31.79	34.57	34.99	32.94	35.09
	Mean	34.22	32.47	30.13	30.45	35.17	34.21	31.93	34.56	34.99	33.06	35.17
	Max.	36.21	34.27	31.29	32.34	37.49	36.65	34.57	37.08	37.31	35.24	38.12
	Sd	0.99	0.88	0.57	0.90	1.10	1.17	1.23	1.21	1.07	1.13	1.20
	cv	0.03	0.03	0.02	0.03	0.03	0.03	0.04	0.04	0.03	0.03	0.03
	Skewness	-0.30	-0.22	-0.16	-0.10	-0.15	-0.24	-0.01	-0.32	0.21	-0.02	0.44
	Kurtosis	0.08	-0.37	-0.87	-0.17	0.03	-0.22	-0.75	0.22	-0.14	-0.43	-0.04
Seasonal (Sep-Oct-Nov)	Min.	21.64	22.08	21.57	21.23	23.84	21.62	21.31	23.16	23.64	22.57	23.54
	Median	24.07	24.12	23.47	23.65	26.20	24.33	23.60	25.34	25.97	24.97	25.78
	Mean	24.06	23.90	23.39	23.54	26.13	24.28	23.61	25.29	25.87	24.99	25.80
	Max.	26.60	25.42	25.23	26.38	28.21	26.91	25.55	27.26	28.13	28.95	28.37
	Sd	1.11	0.89	0.80	0.95	1.00	1.14	1.06	1.05	0.93	1.03	1.08
	cv	0.05	0.04	0.03	0.04	0.04	0.05	0.04	0.04	0.04	0.04	0.04
	Skewness	-0.06	-0.26	-0.05	0.11	-0.17	0.05	-0.37	-0.12	-0.14	0.83	0.06
	Kurtosis	-0.65	-1.05	-0.39	0.40	-0.61	-0.33	-0.78	-1.01	-0.05	3.03	-0.13

3.2.5.3 Missing Data Completion

There are no missing values in the total monthly precipitation data. Regression studies were conducted for both the Ödemiş station, which had missing mean monthly temperature data for the period June-July 2010, and the Kuşadası station, which had missing data for the month of November in 1980. The selection of stations for the regression analysis was based on their geographical locations and altitudes.

- The mean monthly temperature values of Ödemiş station (located at 111 m elevation) were completed by the mean monthly temperature values of Salihli station (located at 111 m elevation) and R^2 is calculated as 0.99.
- The mean monthly temperature values of Kuşadası station (located at 25 m elevation) were completed by the mean monthly temperature values of Selçuk station (located at 18 m elevation) and R^2 is calculated as 0.99.

After completed the missing value, the statistics of observed total monthly precipitation and mean monthly temperature series were obtained and given by Table 3.23 and Table 3.24, respectively. In Tables 3.23, 3.24, "Min.", "Max.", "SD", and "Var" represents minimum value of the series, maximum value, standard deviation, variance, respectively.

Table 3.23 Statistics of observed total monthly precipitation series (mm).

Precipitation (mm)	Mean	SD	Var	Min	Max	Median	Quantiles				
							0%	25%	50%	75%	100%
MANİSA	59.19	63.94	4088.38	0	393.8	39.75	0	7.875	39.75	93.575	393.8
İZMİR	57.85	67.36	4536.89	0	354.6	31.95	0	2.6	31.95	91.85	354.6
ÇEŞME	47.34	59.66	3559.74	0	286.6	21.85	0	0.6	21.85	73.275	286.6
KUŞADASI	51.38	61.90	3831.64	0	336.6	29.9	0	0.625	29.9	79.55	336.6
AYDIN	52.34	56.24	3163.15	0	344.1	34.45	0	4.8	34.45	77.875	344.1
SALİHLİ	40.49	38.19	1458.81	0	196.6	29.6	0	7.975	29.6	64.6	196.6
SEFERİHİSAR	50.74	62.33	3884.90	0	308.7	25.9	0	0.8	25.9	79.9	308.7
ÖDEMİŞ	47.46	50.58	2558.39	0	333.7	32.4	0	5.675	32.4	76.3	333.7
SULTANHİSAR	50.31	54.32	2951.00	0	321.4	33.9	0	6.325	33.9	74.75	321.4
SELÇUK	55.52	65.37	4273.18	0	326.5	31.15	0	1.45	31.15	86.125	326.5
NAZİLLİ	48.55	51.38	2639.50	0	300.6	34	0	5.7	34	72.4	300.6

Table 3.24 Statistics of observed mean monthly temperature series (ºC).

Temperature (ºC)	Mean	SD	Var	Min	Max	Median	Quartiles				
							0%	25%	50%	75%	100%
MANİSA	16.83	7.90	62.45	3.2	30.7	16.5	3.2	9.6	16.5	24.2	30.7
İZMİR	17.97	7.04	49.50	5.6	30.2	17.5	5.6	11.3	17.5	24.525	30.2
ÇEŞME	17.34	6.03	36.41	6.3	28.3	17	6.3	11.8	17	23.2	28.3
KUŞADASI	17.28	6.14	37.74	5.8	28.3	16.8	5.8	11.575	16.8	23	28.3
AYDIN	17.64	7.26	52.74	4.8	30.4	17.15	4.8	10.9	17.15	24.525	30.4
SALİHLİ	16.44	7.67	58.87	2.5	29.8	16.2	2.5	9.5	16.2	23.8	29.8
SEFERİHİSAR	17.02	6.70	44.85	4.7	29.2	16.3	4.7	10.875	16.3	23.225	29.2
ÖDEMİŞ	16.55	7.29	53.18	4	29.3	15.9	4	9.8	15.9	23.525	29.3
SULTANHİSAR	17.32	7.28	53.05	4.6	30.2	16.85	4.6	10.375	16.85	24.2	30.2
SELÇUK	16.74	6.73	45.24	4.4	29.6	16.2	4.4	10.5	16.2	23.1	29.6
NAZİLLİ	17.40	7.63	58.29	4.5	31	16.7	4.5	10	16.7	24.725	31

3.2.5.4 Homogeneity Analysis

Homogeneity analysis was performed using Pettitt's Test, SNHT Test and Buishand's Test to secure that the data sets employed in the study have adequate quality. Table 3.25 indicates that all the precipitation series are homogeneous since H hypothesis is accepted which means "the series is homogeneous" and rejected NH which means "non-homogeneous". For the temperature series, only Kuşadası is not homogeneous.

Table 3.25 Homogeneity test results of total monthly precipitation (mm) and mean monthly temperature (ºC) series.

Station No	**Station Name**	**Pettitt's Test, SNHT Test, Buishand's Test**			
		Monthly Total Precipitation	**Monthly Mean Temperature**	**Monthly Minimum Temperature**	**Monthly Maximum Temperature**
17186	MANİSA	H, H, H	H, H, H	H, H, H	H, H, H
17220	İZMİR	H, H, H	H, H, H	H, H, H	H, H, H
17221	ÇEŞME	H, H, H	H, H, H	H, H, H	H, H, H
17232	KUŞADASI	H, H, H	NH, NH, NH	NH, NH, NH	H, H, H
17234	AYDIN	H, H, H	H, H, H	NH, H, H	H, H, H
17792	SALİHLİ	H, H, H	H, H, H	NH, NH, NH	H, H, H
17820	SEFERİHİSAR	H, H, H	NH, H, H	NH, NH, NH	H, H, H
17822	ÖDEMİŞ	H, H, H	H, H, H	NH, H, H	H, H, H
17850	SULTANHİSAR	H, H, H	H, H, H	H, H, H	H, H, H
17854	SELÇUK	H, H, H	H, H, H	NH, NH, NH	H, H, H
17860	NAZİLLİ	H, H, H	H, H, H	H, H, H	H, H, H

3.2.5.5 Trend Analysis

Trend analyses were conducted using Mann-Kendall Trend Test for total monthly precipitation and mean monthly temperature series. Figure 3.56a illustrates that there is no trend for monthly precipitation series. In Figure 3.56b, İzmir, Kuşadası, Aydın, Salihli, Seferihisar, Sultanhisar and Selçuk stations have significant increasing trend. For Çeşme and Ödemiş, there are weak increasing trend. Manisa and Nazilli have no trends.

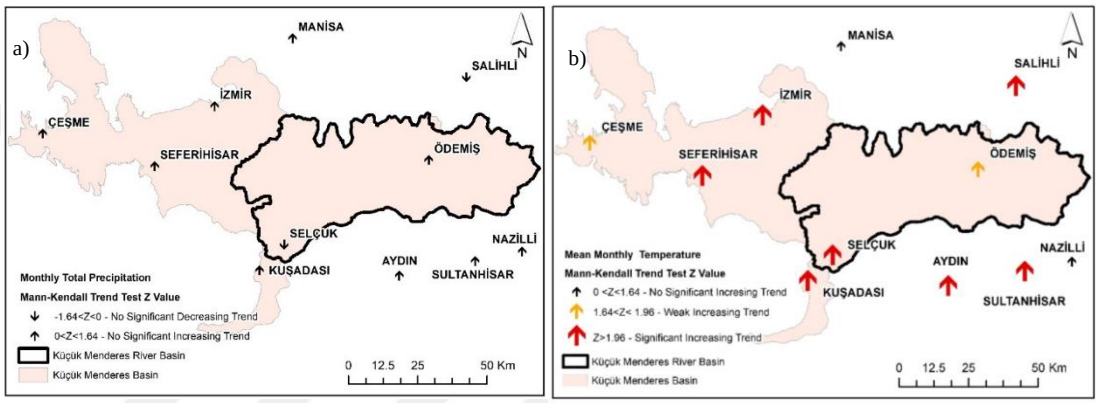


Figure 3.56 Trend maps of a) total monthly precipitation (mm), b) mean monthly temperature (ºC).

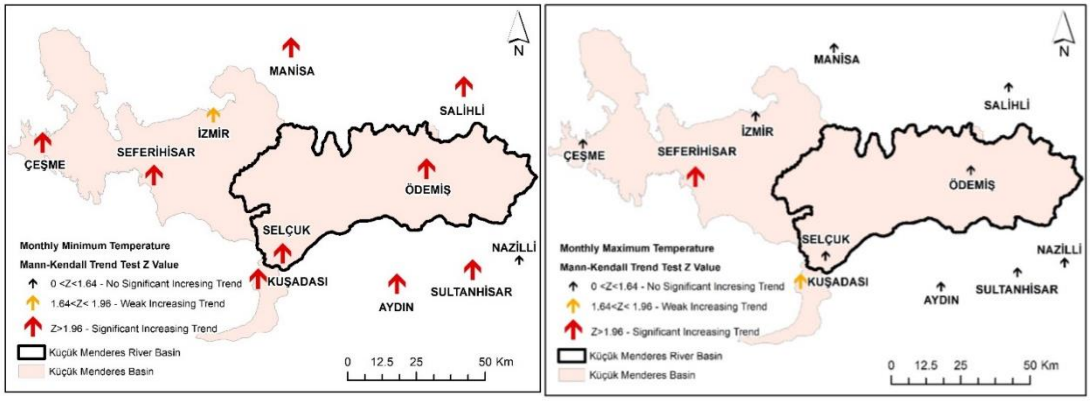


Figure 3.57 Trend maps of a) monthly minimum temperature, b) monthly maximum temperature (ºC).

Regarding the monthly minimum temperature, all stations except Nazilli exhibit an increasing trend (Figure 3.57a). However, when it comes to the maximum temperature, only Kuşadası and Seferihisar demonstrate an increasing trend (Figure 3.57b).

3.2.5.6 Decomposition of Series

Since the mean monthly temperature series have trends (Figure 3.56b), using R program "stR" package, decomposed values of series were obtained (Dokumentov and Hyndman, 2022). For Ödemiş and Selçuk stations, decomposition of total monthly precipitation series and mean monthly temperature series are given by Figure 3.58, Figure 3.59, Figure 3.60 and Figure 3.61, respectively. The procedures for the other stations are given in the appendix. In Figure 3.58, Figure 3.59, Figure 3.60, and Figure 3.61, the observed series and decomposed data components, that are seasonal predictor which, random data which contains residual of the model fit, and fit/forecast for the model, were given.

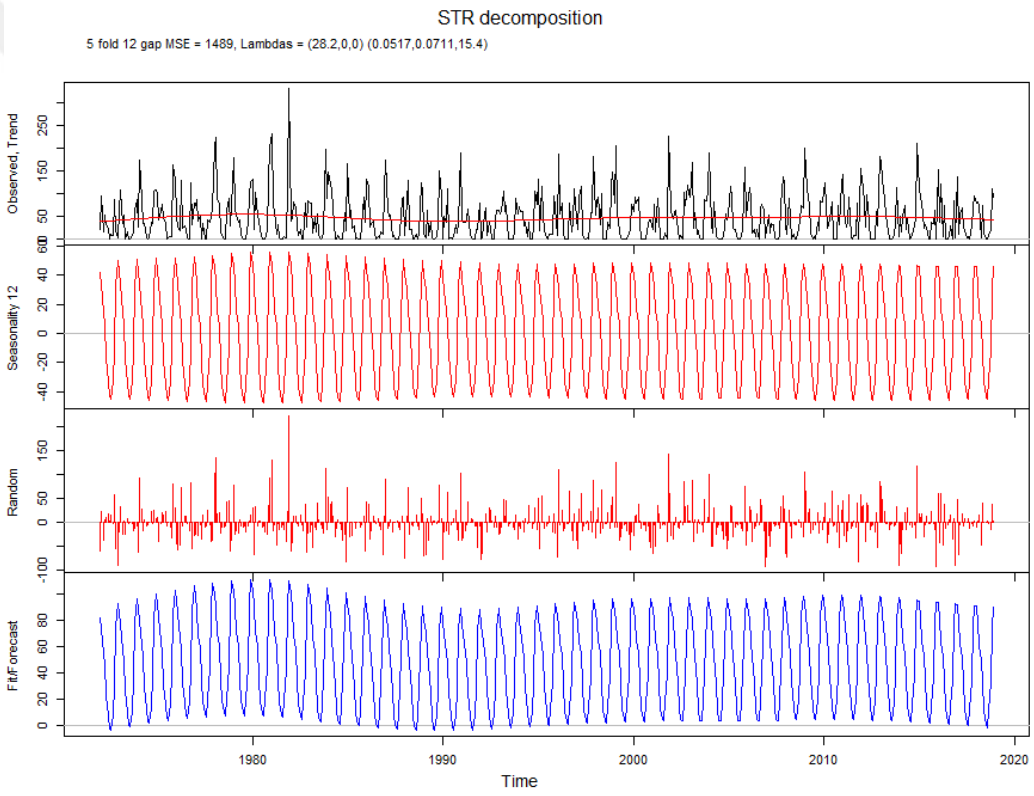


Figure 3.58 Decomposition of total monthly precipitation (mm) series for Ödemiş station.

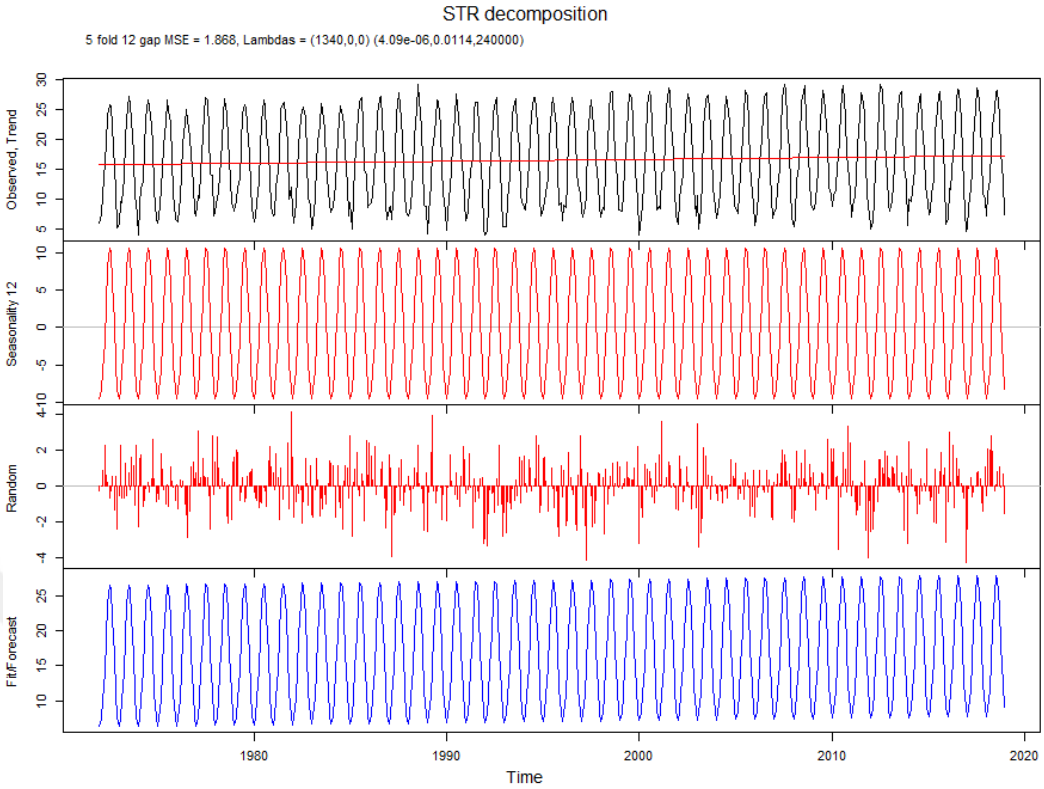


Figure 3.59 Decomposition of mean monthly temperature (ºC) series for Ödemiş station.

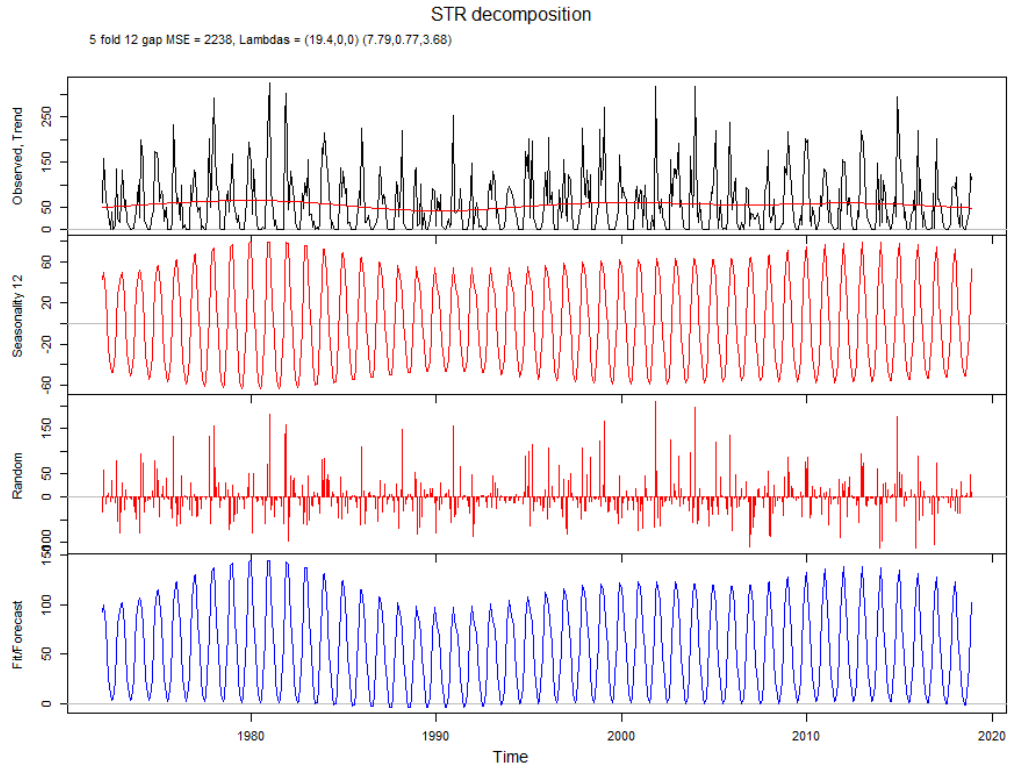


Figure 3.60 Decomposition of total monthly precipitation (mm) series for Selçuk station.

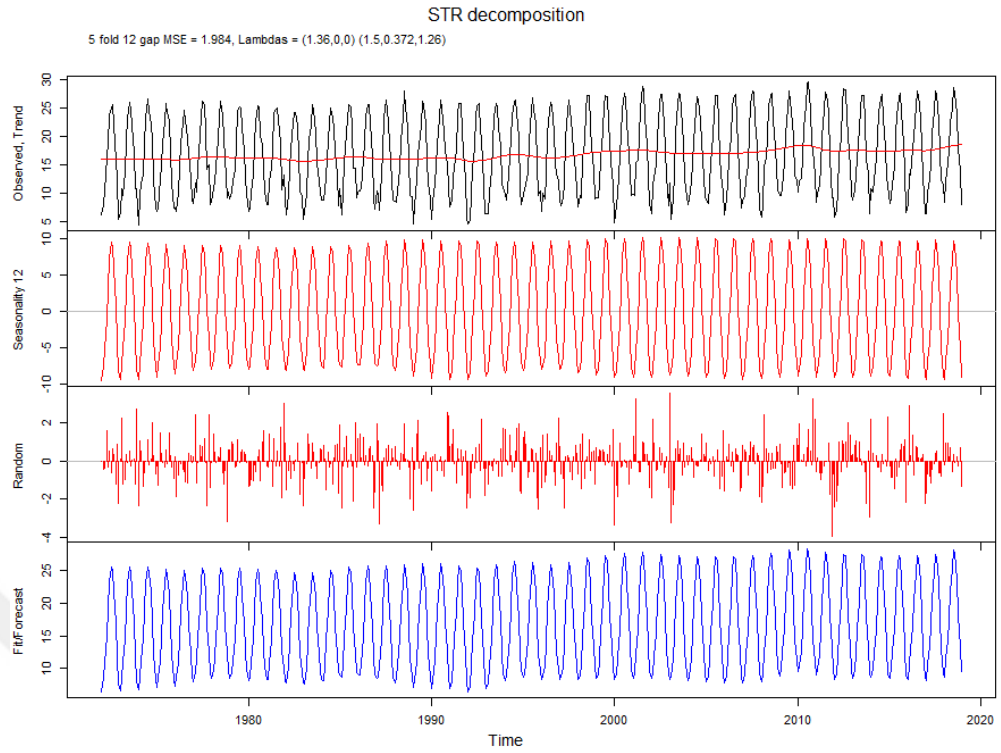


Figure 3.61 Decomposition of mean monthly temperature (°C) series for Selçuk station.

3.2.5.7 Distribution Functions

The best fit distributions were selected for total monthly precipitation and mean monthly temperature for each station by using Chi-Squared and Kolmogorov Simirnov test and given by Table 3.26.

Table 3.26 Best fit distributions of total monthly precipitation and mean monthly mean temperature.

Station No	Station Name	Total Monthly Precipitation (mm)	Mean Monthly Temperature (^{0}C)
17186	MANİSA	Generalized Pareto	Johnson's SB
17220	İZMİR		
17221	ÇEŞME		
17232	KUŞADASI		
17234	AYDIN		
17792	SALİHLİ		
17820	SEFERİHİSAR		
17822	ÖDEMİŞ		
17850	SULTANHİSAR		
17854	SELÇUK		
17860	NAZİLLİ		

CHAPTER FOUR
RESULTS AND CONCLUSIONS

4.1 VIC Modeling

The study area for the VIC model was created on a grid basis with 1/16^{o} resolution as given by Schaperow et al. (2021). Model inputs were prepared using the same grid areas. Parameters for calibration were selected as variable infiltration curve parameter (INFILT), fraction of maximum velocity of baseflow where non-linear baseflow begins (Ds) and fraction of maximum soil moisture where non-linear baseflow occurs (Ws). Model calibration (Figure 4.1) was performed for the period 2000-2003 and validation (Figure 4.2) for the period 2004-2005. Potential evapotranspiration for SWAT model and baseflow parameters for HEC-HMS model were calculated.

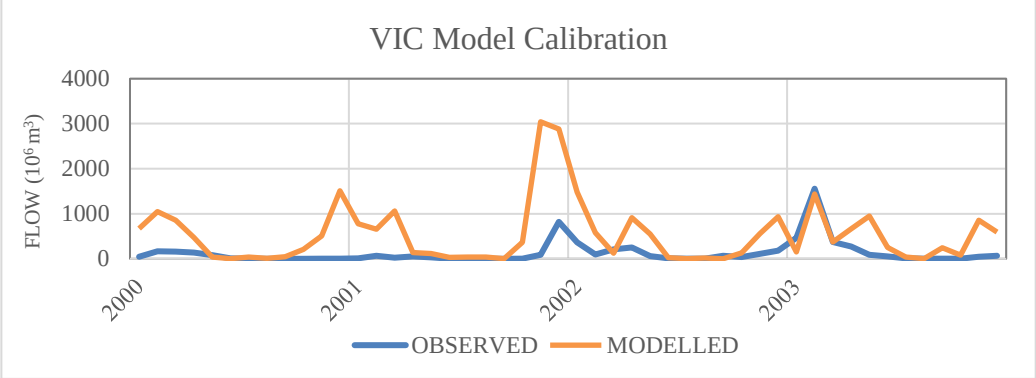


Figure 4.1 Model calibration of VIC Model.

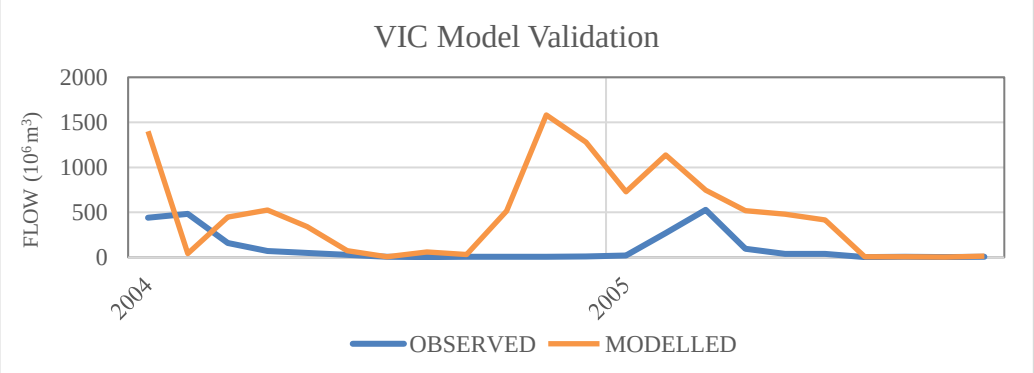


Figure 4.2 Model validation of VIC Model.

4.2 SWAT Modeling

The flowchart depicted in Figure 4.3 outlines the SWAT modeling process. Initially, the SWAT model was run covering the timeframe from 2000 to 2012. Subsequently, utilizing the generated outputs, sensitivity analysis, calibration, and validation procedures were sequentially conducted through SWAT-CUP. Employing the optimized parameter values derived from these processes, the SWAT model underwent individual runs for the periods as the reference period (1971-2004), the near future (2025-2049), the middle future (2050-2074) and the far future (2075-2099) (Figure 4.4).

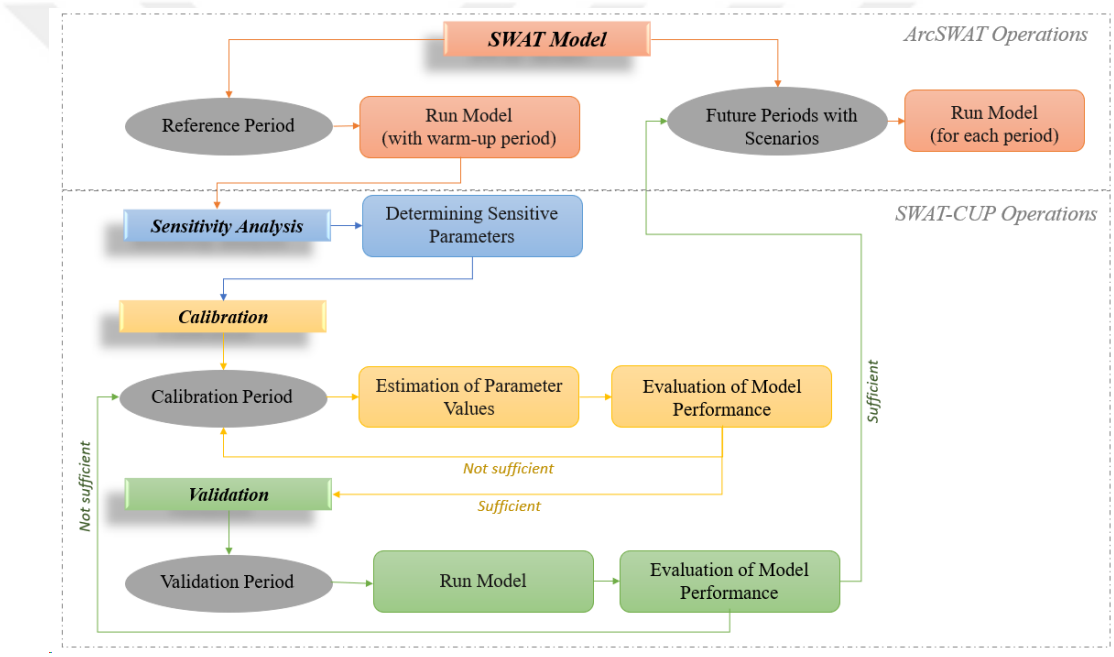


Figure 4.3 The process of SWAT and SWAT-CUP modeling.

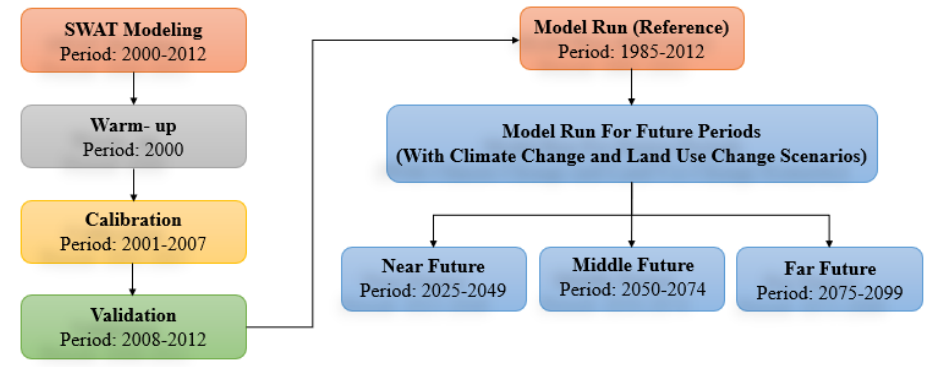


Figure 4.4 Selected periods for modelling.

4.2.1 Basin Modeling

To initiate the modeling procedures in ArcSWAT, the "Watershed Delineation" tool was employed as the first step. The Digital Elevation Model (DEM) specific to the Küçük Menderes basin (depicted in Figure 4.5a) was input into the model. Subsequently, the flow direction (Figure 4.5b) and various basin characteristics, including subbasins, reaches, outlets, etc. (Figure 4.5c), were derived through this tool.

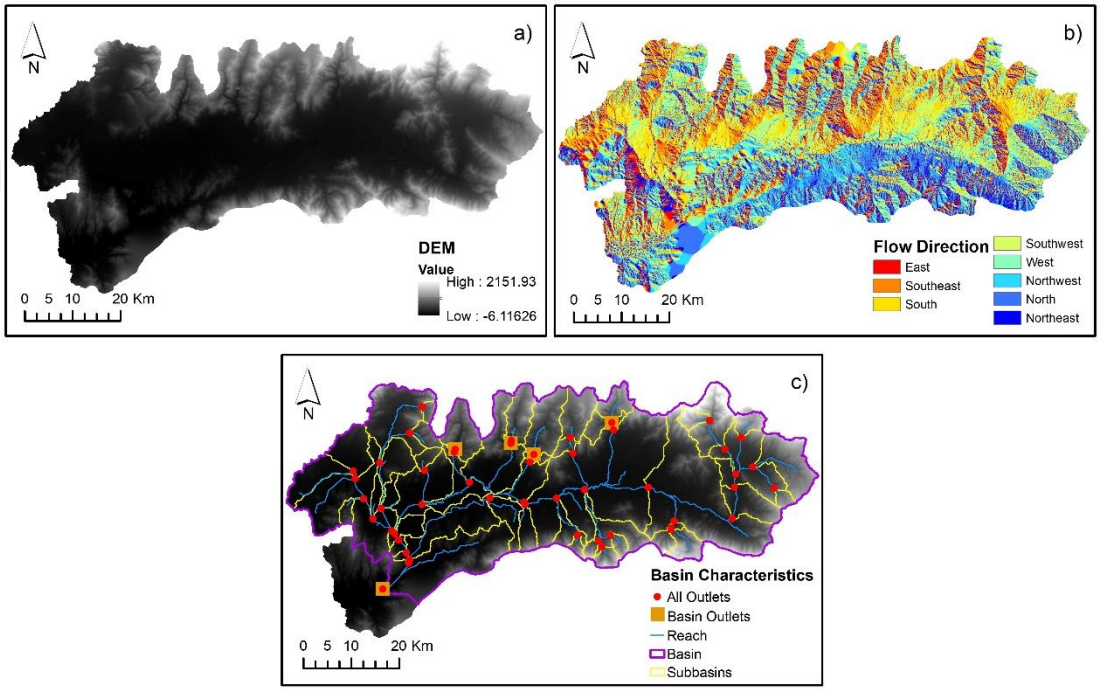


Figure 4.5 The maps of a) DEM, b) flow direction, c) basin characteristics.

Following the determination of flow direction and accumulation through the DEM of the basin, the stream network was established. In the SWAT model, outlet points were designated at river confluences to delineate sub-basins. Specifically, 12 flow observation stations and 13 storage structures (comprising dams and ponds) were chosen as outlet points within the basin. It's worth noting that the model permits definitions exclusively at the selected outlet points. Due to the absence of any storage structure implementation from 2000 to 2012, which corresponds to the study period for SWAT, the reservoir operation data was not incorporated into the SWAT model for the period. In this study, 18 outlet points were assigned to the junctions of the rivers

where 18-point discharge points were located. After the overlapping points were identified, the total number of outfall points was defined as 50.

As part of the study, five flow observation stations (E06A001, D06A011, D06A013, D06A025, and D06A027) were identified as watershed outlets due to their sufficient observations during the period 2000-2012. Among these, station E06A001, positioned at the outlet of the Küçük Menderes River Basin, was specifically designated as the outlet for the entire basin.

For the SWAT model during the 2000-2012 study period, CORINE data from 2006 served as the basis for land use information. A lookup table, illustrated in Figure 4.6a, facilitated the alignment of CORINE land use classes with SWAT land uses. Subsequently, the matched land use data was incorporated into the model, as depicted in Figure 4.6b. The analysis revealed that 51.05% of the study area is dedicated to agriculture, 18.23% to natural areas, 17.76% to mixed forest, and 8.43% to olive cultivation. The corresponding land use map is presented in Figure 4.9a.

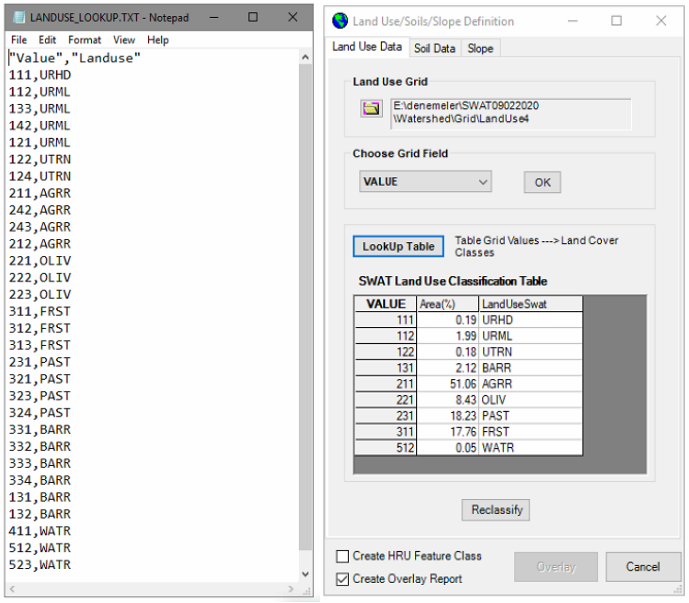


Figure 4.6 a) The look-up table for land use. a) Identifying the land use data.

The soil map was prepared in 1 km resolution and on grid basis with the scope of the study. The SWAT model retrieves the soil types and parameter values defined for

the Küçük Menderes River Basin and shown as each pixel in the soil map from the "usersoil" table in the "SWAT2012.mdb" file (Figure 4.7b) through the lookup table shown in Figure 4.7a. The soil map is given by Figure 4.9b.

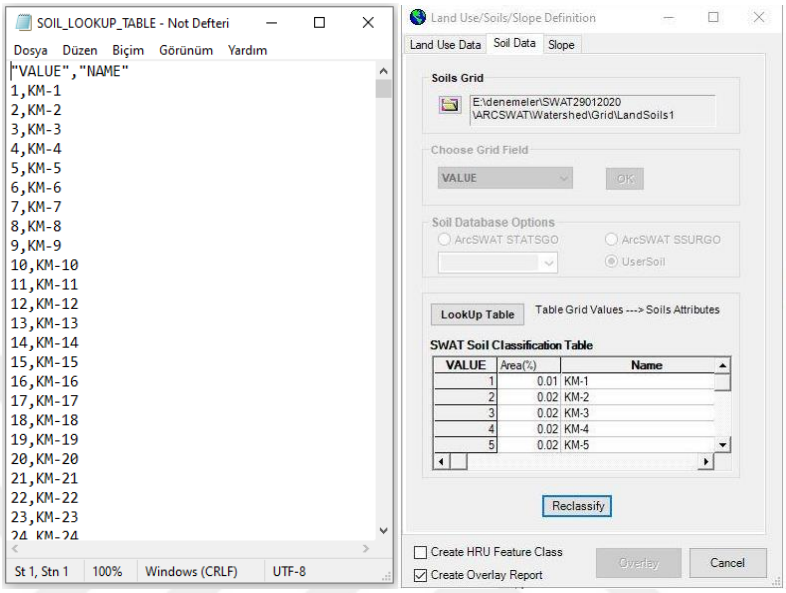


Figure 4.7 a) The look-up table for soil b) Identifying the soil database.

To characterize the study area, a slope map was generated utilizing the "Slope" tool within the "Spatial Analysis Tool," incorporating the percentage rise option. Given the SWAT model's constraint of accommodating up to five slope classes in the multiple slope option, a specific classification approach was adopted for the study area. The "natural breaks (jenks)" method was employed, resulting in the identification of five distinct slope classes. The lower and upper limits obtained through this process were manually rounded to the nearest fifth or tenth value, as detailed in Table 4.1 and Figure 4.8. The resulting slope map is visually represented in Figure 4.9c.

Table 4.1 Determination of slope classes (%)

Natural Breaks Method			Manuel Adjustment		
0	-	8.6	0	-	10
8.6	-	25.81	10	-	25
25.81	-	43.01	25	-	45
43.01	-	60.13	45	-	60
60.13	-	94.62	60	-	100

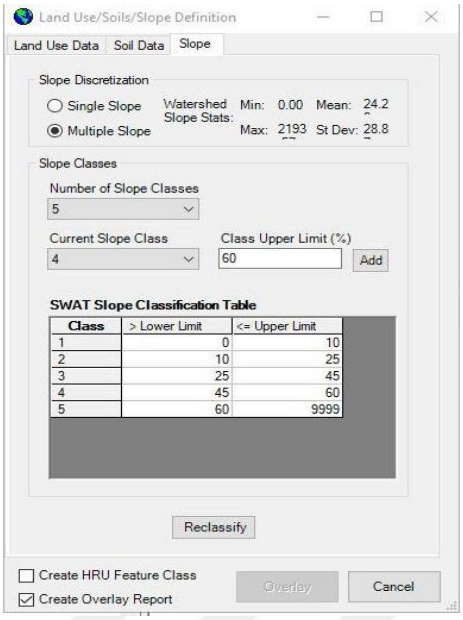


Figure 4.8 Identifying the slope (%) classification.

Hydrological processing units (HRUs) were generated employing a multiple HRU methodology resulting in a total of 1088 HRUs across 50 sub-basins. This generation process involved applying specific thresholds: 5% for land use, 10% for soil, and 5% for slope combinations.

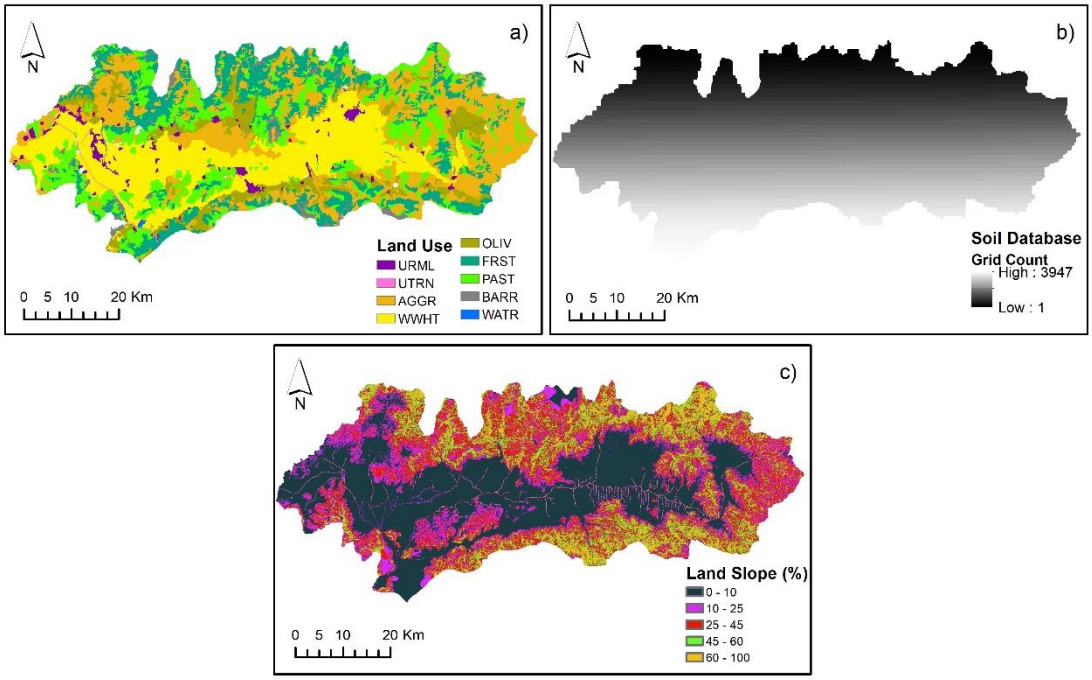


Figure 4.9 The maps of a) land use, b) soil database, c) land slope.

The data and locations of 10 meteorological stations (Figure 1.2 and Figure 3.36) located in and around the basin, including long-term measurements, were included into the model.

In order to overcome the gaps in the meteorological data observed during the research period, a user table for the Küçük Menderes Basin weather generator was developed and included in the model (Figure 4.10). The text file containing the geographical coordinates of the meteorological stations was transferred to the model (Figure 4.11a). Meteorological data including precipitation, maximum temperature, minimum temperature, relative humidity, wind speed and solar radiation were included in the folder entered into the model (Figure 4.11b). The SWAT model retrieves data files from directories containing location files.

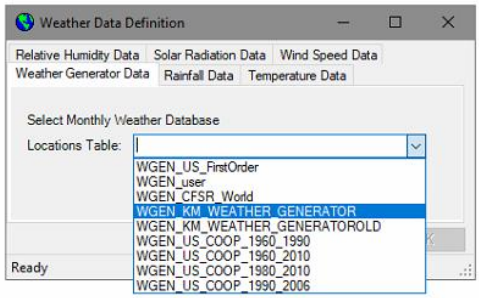


Figure 4.10 Selecting Weather Generator Data for Küçük Menderes.

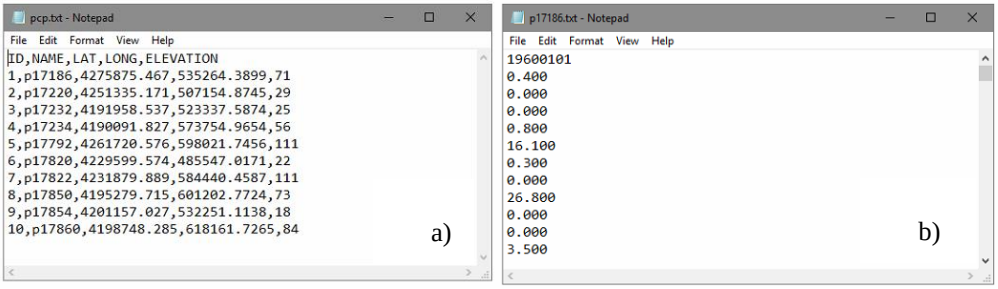


Figure 4.11 Meteorological input files for SWAT model, a) Station locations, b) Input data.

The model was supplemented with agricultural irrigation data as given by Figure 4.12. The prior planning studies have identified groundwater as the source of agricultural irrigation in Küçük Menderes during the research period, and this has been defined as such in the model. The model incorporates specific provisions for crops

within agricultural regions, organizing agricultural practices under the "Operations" tab, as illustrated in Figure 4.13. This section outlines the sequential steps involved in crop cultivation: initial planting, subsequent fertilization, irrigation based on the crop's water stress, and, ultimately, harvesting at the designated time. Notably, the model stipulates that all Hydrological Processing Units (HRUs) engaged in agricultural activities are irrigated using groundwater sourced from their respective sub-basins. The irrigation process assumes an average efficiency of 60%, reflecting the extraction of water from underground sources.

After all inputs were added to the SWAT model, the SWAT model database was updated with the "Rewrite Input Files" option. SWAT model was run monthly by selecting the period 2000-2012 for Küçük Menderes River Basin.

Figure 4.14 depicts "NYSKIP" as the duration of years during which no output will be generated and it is called as “warm-up period”. In the study, the year 2000 as the timeframe for "NYSKIP".

The output files generated by the SWAT model, as depicted in Figure 4.15, were transferred to the output database. To assess the functionality of the SWAT model, an analysis was conducted using the "Run Swat Check" option.

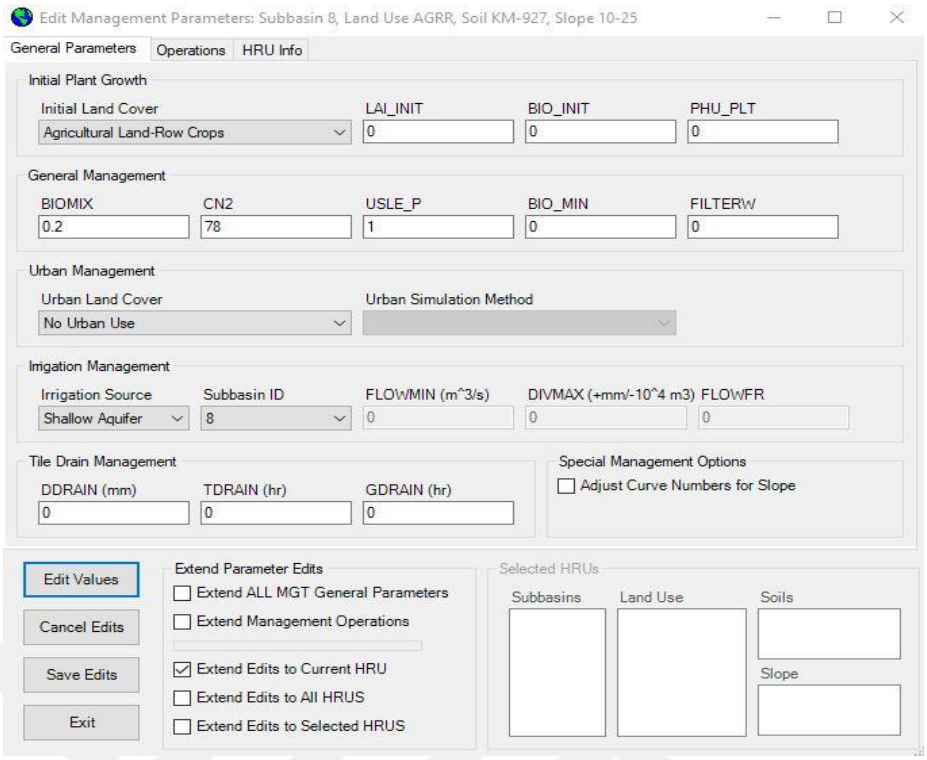


Figure 4.12 Introducing the application principles to SWAT model in HRUs to be irrigated.

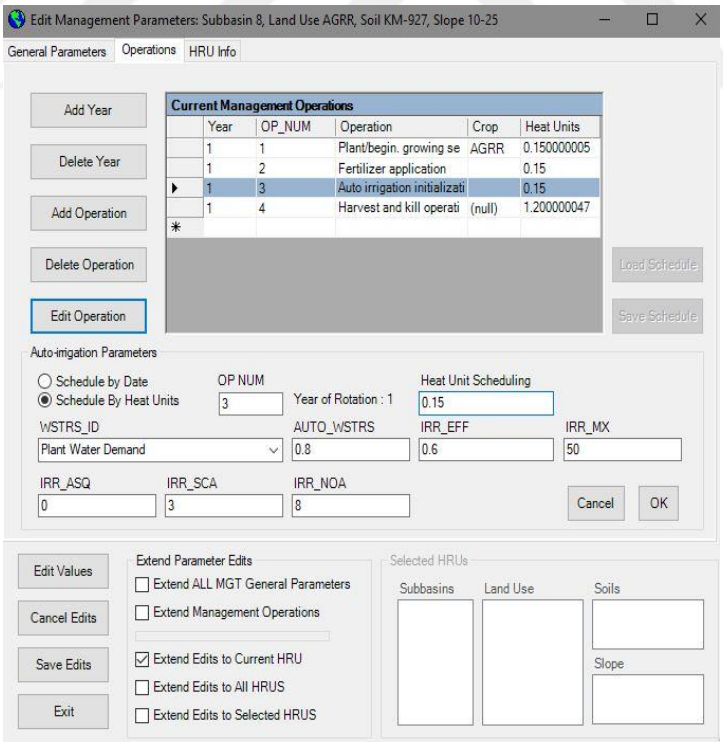


Figure 4.13 Agricultural operation.

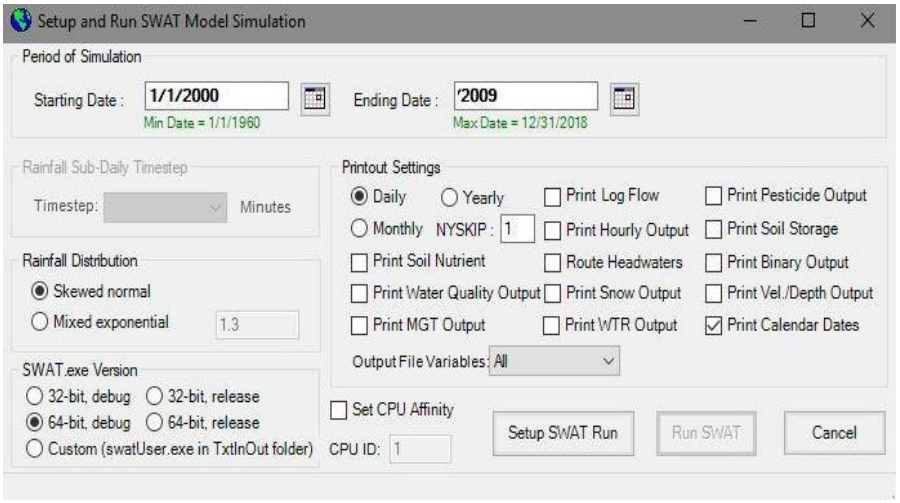


Figure 4.14 SWAT model running.

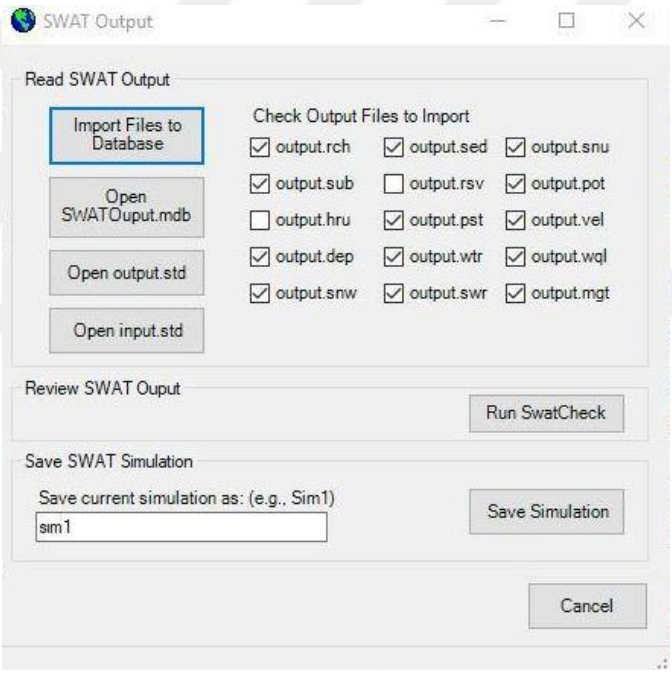


Figure 4.15 SWAT model outputs.

4.2.2 The SWAT-CUP Processing

The data from 5 flow observation stations, designated as basin outlets, were utilized for the purposes of the sensitivity analyses, the calibration, and the validation.

4.2.2.1 The Sensitivity Analyses

Both "One-at-a-time" and "Global" sensitivity analysis methodologies were employed for all regarding parameters examined in the study. In order to perform the Global Sensitivity analysis, 500 simulations were run in a single iteration for the 46 parameters shown in Figure 4.16. For the Global sensitivity analysis, parameters with $p<0.05$ according to t-test are considered sensitive (Abbaspour, 2015). The p-value and t-statistic obtained for each parameter according to the global sensitivity analysis are given in Figure 4.16.



Figure 4.16 One-at-a-time sensitivity analysis the parameters.

The One-at-a-time sensitivity analysis involved three iterations for each parameter. Graphical comparisons were made of the simulation results obtained for different

values of each parameter. The presence of any noticeable variation in the simulation outputs indicated the sensitivity of the respective parameter. Figure 4.17 presents the results of the One-at-a-time sensitivity analysis for a selection of parameters. In the procedures, the "absolute" method, employing addition-subtraction, was utilized for parameters with a value of "0", while the "relative" method, involving multiplication, was applied for other parameters. Both Global and One-at-a-time sensitivity analyses were performed to identify parameters for use in calibration and validation procedures. A total of 14 parameters were identified and are listed in Table 4.2.

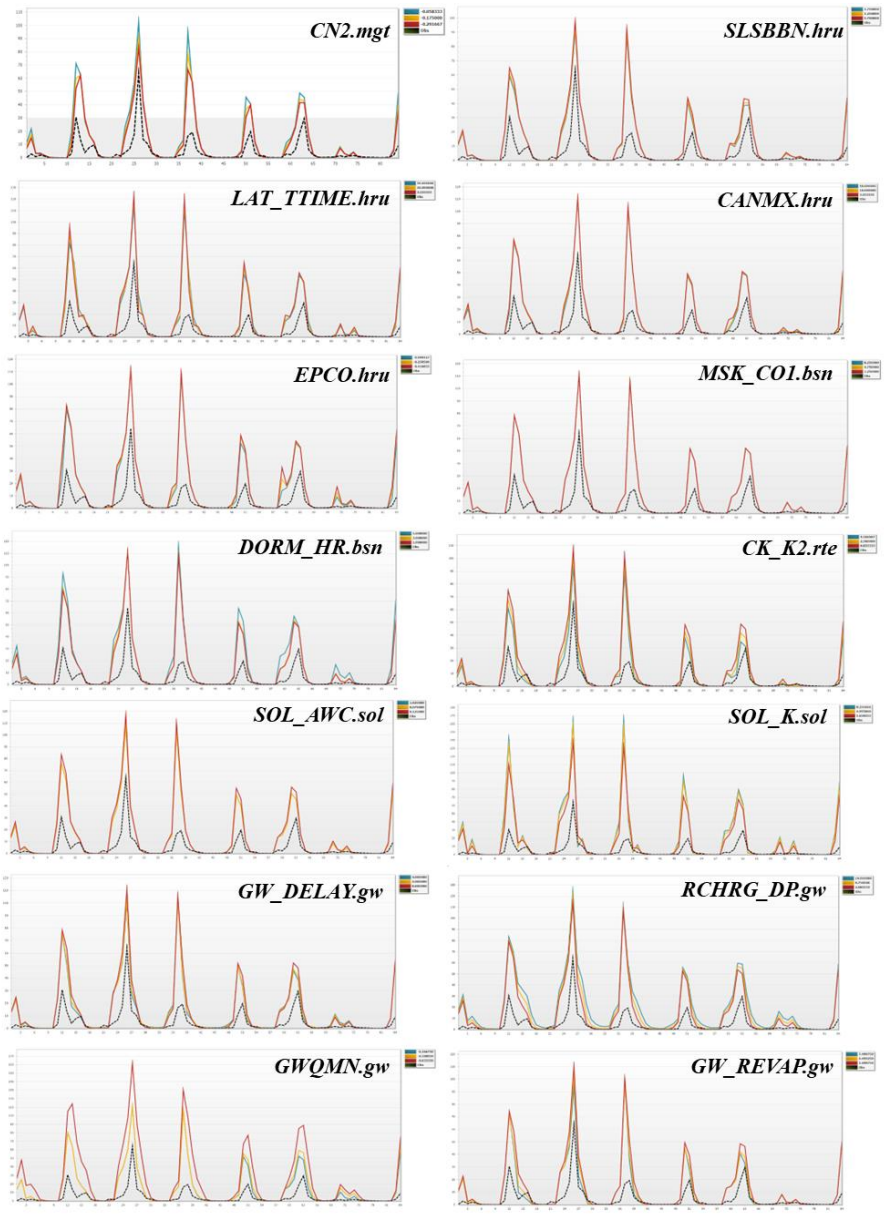


Figure 4.17 One-at-a-time sensitivity analysis the parameters.

Table 4.2 The sensitive parameters.

Parameter	***Group***	***Description***
CN2.mgt	Management	Initial SCS curve number for moisture condition II
SLSUBBSN.hru	HRU	Average slope length (m)
LAT_TTIME.hru	HRU	Lateral flow travel time (days)
CANMX.hru	HRU	Maximum canopy storage (mm H_2O)
EPCO.hru	HRU	Plant uptake compensation factor
MSK_CO1.bsn	Basin	Calibration coefficient used to control impact of the storage time constant (Km) for normal flow
DORM_HR.bsn	Basin	Time threshold used to define dormancy (hours)
CH_K2.rte	Transport	Effective hydraulic conductivity in main channel alluvium (mm/hr)
SOL_AWC.sol	Soil	Available water capacity of the soil layer (mm H_2O/mm soil).
SOL_K.sol	Soil	Saturated hydraulic conductivity (mm/hr)
GW_DELAY.gw	Groundwater	Groundwater delay time (days)
RCHRG_DP.gw	Groundwater	Deep aquifer percolation fraction
GWQMN.gw	Groundwater	Threshold depth of water in the shallow aquifer required for return flow to occur (mm H_2O)
GW_REVAP.gw	Groundwater	Groundwater "revap" coefficient

4.2.2.2 The Calibration and the Validation

The calibration phase focused on the period from 2001 to 2007, with validation carried out for the subsequent period from 2008 to 2012. Within the Küçük Menderes Basin, 50 sub-basins were established, and five specific outlets were identified. To ensure the availability of relevant flow data, a thorough examination was conducted for the flow observation stations at these basin outlets, covering the years 2000 to 2012. The calibration process utilized sensitive parameters outlined in Table 4.2. For efficiency, it was determined that calibration procedures would be conducted using flow data obtained from four basin outlets: the 3rd, 9th, 14th, and 50th sub-basins. Correspondingly, the flow stations identified as D06A011, D06A027, D06A013, and E06A001 (as detailed in Table 3.10) were associated with these sub-basins. Flows measured in 50 sub-basins are representative of the whole basin. Monthly flow data (in cubic meters per second, m^3/s) from the specified stations were employed for the monthly calibration process. Consequently, multiple calibration iterations were carried out to enhance the accuracy of the model for the Küçük Menderes Basin.

This study involved conducting five iterations, each consisting of 500 simulations. Following each iteration, a thorough examination of the updated parameter ranges was carried out. Values falling outside the predetermined ranges for the SWAT model parameters were adjusted accordingly, guiding the commencement of a new iteration based on the revised parameter ranges. The techniques employed in parameterization using SWAT-CUP are as outlined below (Abbaspour,2015):

- Replace (v__): The new value is inserted instead of the existing one.
- Absolute (a__): The addition-subtraction operation is carried out between the prior parameter value and the new parameter value.
- Relative (r__): The preceding parameter value is multiplied by the sum of 1 and the provided value of the parameter.

The evaluation of the model's calibration effectiveness relies significantly on two statistical metrics: "p-factor" and the "r-factor". The "p factor" represents the proportion of measured data falling inside the 95 % uncertainty (95PPU), while the "r factor" quantifies the average width of the 95PPU band relative to the standard deviation of the measured data (Abbaspour, 2015). The p factor, with a range of 0-100%, has a value of 100% or unity. The r factor, with a range of 0-∞, has a value close to zero in an ideal case when the observed and simulated results perfectly match (Abbaspour, 2015).

The objective function was selected as MNS. The performance of the model for each iteration are given in Table 4.3. Upon analyzing the NS values during calibration iterations, slight modifications were found during the second iteration. Furthermore, while analyzing the p and r variables, it was determined that the most optimal statistical values were achieved during the third iteration. The parameter estimations derived from the selected iteration were considered optimal for the study.

Following the calibration process, the evaluation of model performance involves the utilization of model efficiency coefficients like R^2, Nash Sutcliffe Efficiency

(NSE), PBIAS, and Modified Nash Sutcliffe Efficiency (MNS). These coefficients were computed using the SWAT-CUP model.

As a result of the calibration, it is seen that the NSE value is 0.81 and the PBIAS value is -10.4 considering the station at the outlet of the basin. Referring to the model evaluation criteria presented in Table 3.3 and established by Moriasi et al. (2007), it is observed that the multiple calibration is categorized as "very good" based on the NSE value and "good" based on the PBIAS value.

Table 4.3 The calibration results.

Monthly based model calibration	***Period***	***Goal Function***	***Iteration Number***	***Simulation Number***	***R^2***	***NSE***	***MNS***	***PBIAS***	***p***	***r***
Subbasin 3	2001-2007	MNS	1	500	0.71	0.6	0.69	34.8	0.67	0.8
			2		0.77	0.69	0.79	22.9	0.73	0.86
			3		0.8	0.66	0.75	25.9	0.65	0.79
			4		0.79	0.73	0.84	15.7	0.5	0.55
			5		0.77	0.72	0.82	17.5	0.39	0.31
Subbasin 9	2001-2007	MNS	1	500	0.65	0.6	0.67	30.1	0.78	1.21
			2		0.7	0.67	0.76	21.8	0.78	1.12
			3		0.73	0.71	0.81	21.5	0.65	0.99
			4		0.73	0.72	0.82	11.3	0.53	0.79
			5		0.73	0.71	0.82	12.9	0.37	0.38
Subbasin 14	2001-2007	MNS	1	500	0.63	0.61	0.79	16.2	0.77	1.17
			2		0.68	0.65	0.86	-5	0.81	1.16
			3		0.64	0.63	0.79	6.4	0.75	1.04
			4		0.64	0.62	0.81	-11.6	0.63	0.79
			5		0.65	0.64	0.82	-9.3	0.42	0.45
Subbasin 50	2001-2007	MNS	1	500	0.75	0.74	0.88	-0.1	0.75	2.4
			2		0.82	0.81	0.93	2	0.92	1.29
			3		0.81	0.81	0.94	-10.4	0.81	1.11
			4		0.81	0.81	0.93	-10.8	0.62	1.05
			5		0.83	0.83	0.94	-4.9	0.5	0.42

The relative (r) and absolute (a) values of the parameters obtained as a result of calibration and intended to be used in the validation phase are presented in Table 4.4.

Accordingly, the parameter values (ranges) to be used in modelling are obtained and presented in Table 4.4.

Table 4.4 Relevant best parameter values according to calibration and validation.

Parameter	***Method***	***Method Value***	***Parameter Values***	
			Minimum	***Maximum***
CN2.mgt	r	-0.39	36.6	59.79
SLSUBBSN.hru	r	1.253	20.28	135.78
LAT_TTIME.hru	a	13.656	13.66	13.66
CANMX.hru	a	17.395	17.4	17.4
EPCO.hru	r	-0.164	0.84	0.84
MSK_CO1.bsn	r	1.628	1.97	1.97
DORM_HR.bsn	a	9.062	9.06	9.06
CH_K2.rte	a	4.287	4.29	4.29
SOL_AWC.sol	r	0.478	0.38	0.61
SOL_K.sol	r	0.004	0.14	0.69
GW_DELAY.gw	r	0.849	57.33	57.33
RCHRG_DP.gw	r	3.77	0.24	0.24
GWQMN. gw	r	-0.002	998.26	4991.31
GW_REVAP.gw	r	5.144	0.12	0.12

During the validation period spanning from 2008 to 2012, the ArcSWAT model was executed with the optimal parameter values outlined in Table 4.4. The NSE value for the outlet station, determined as 0.86 during this validation period, is indicative of strong model performance. Table 3.3 indicates that the model performs “very good” during the validation period.

The observed and modelled flows for both the calibration and the validation periods for the 4 sub-basins (sub-basins 3, 9, 14 and 50) are depicted in Figures 4.18, 4.19, 4.20, 4.21, respectively.

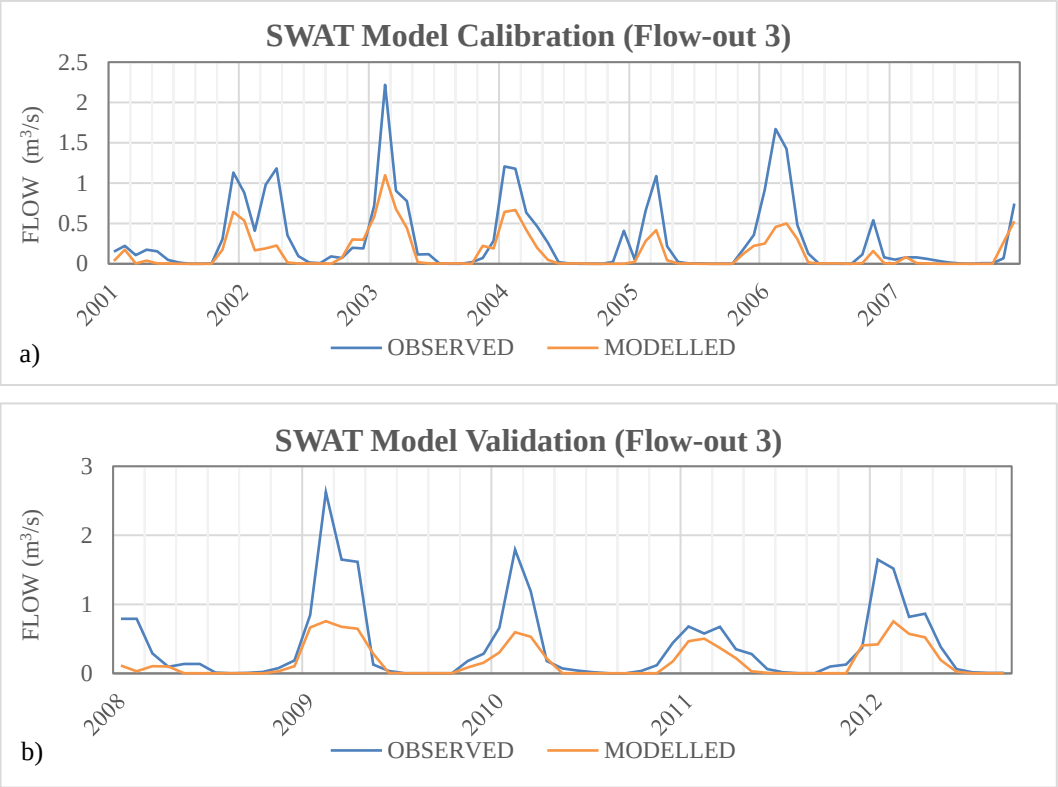


Figure 4.18 For Subbasin 3: SWAT Model a) calibration and b) validation.

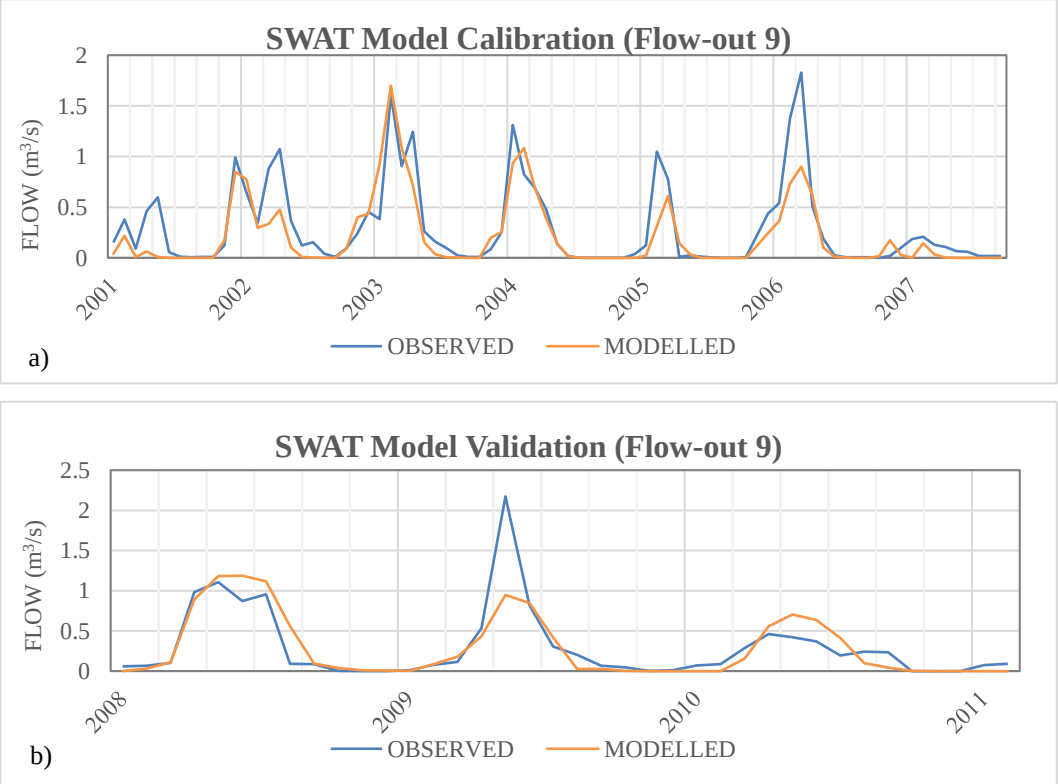


Figure 4.19 For Subbasin 9: SWAT Model a) calibration and b) validation.

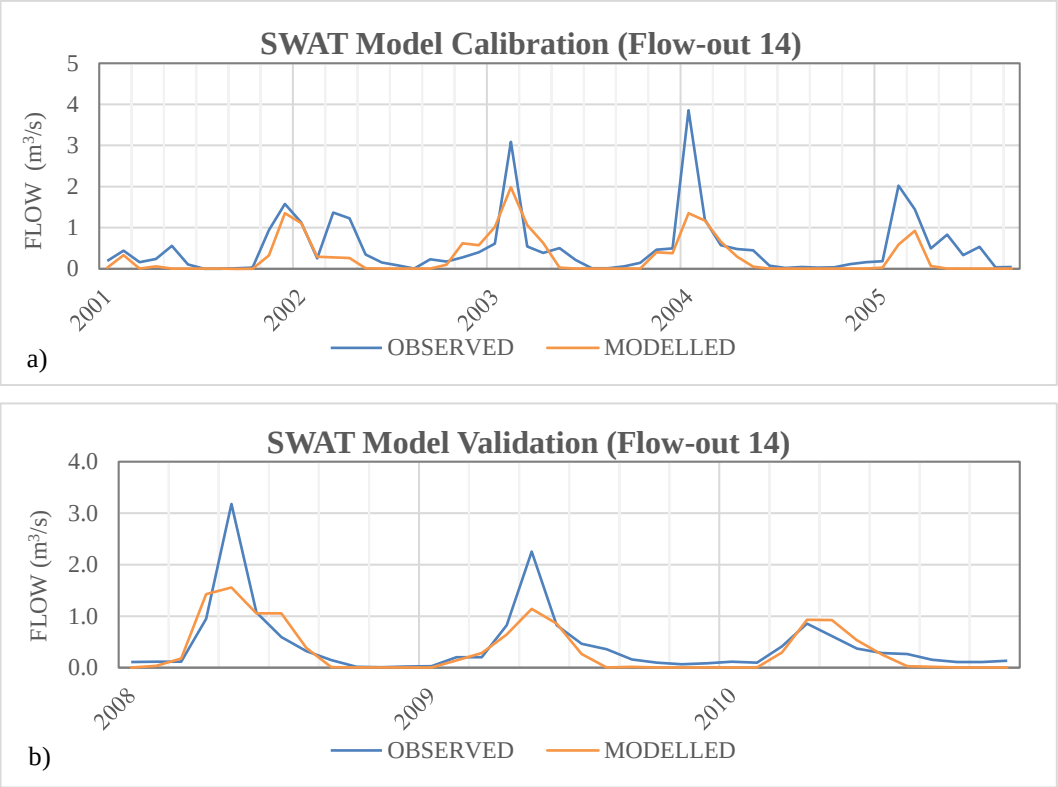


Figure 4.20 For Subbasin 14: SWAT Model a) calibration and b) validation.

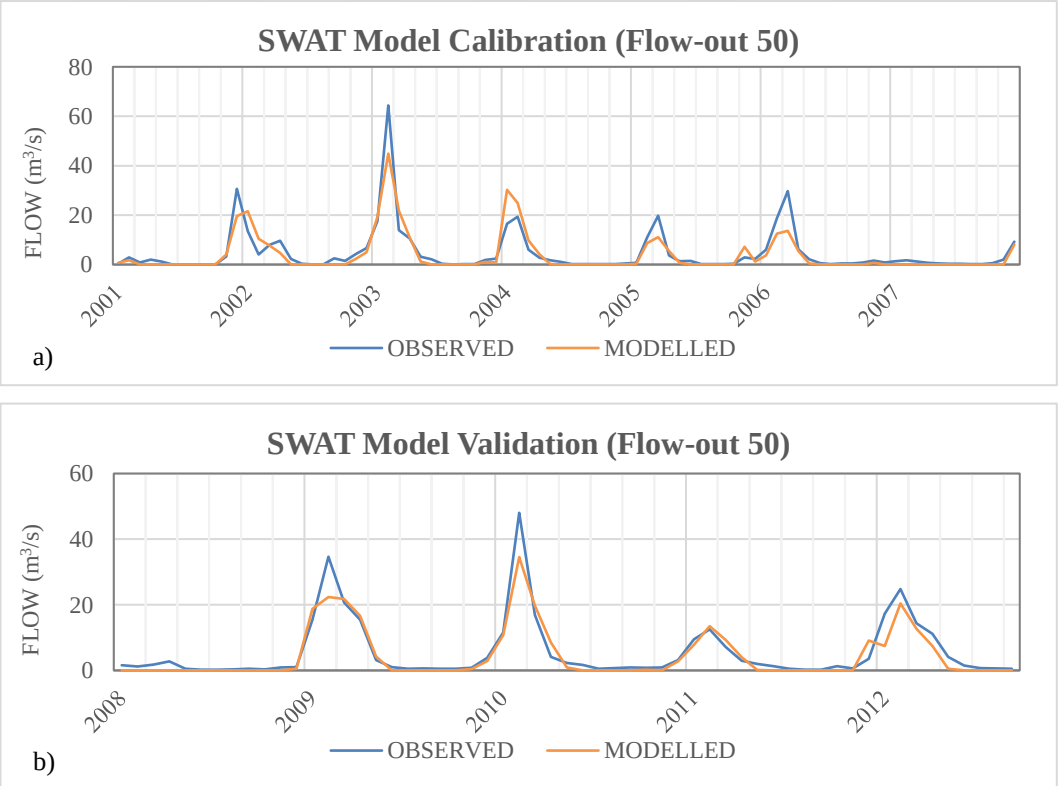


Figure 4.21 For Subbasin 50: SWAT Model a) calibration and b) validation.

4.2.3 SWAT Modeling for Future Period

The reference period was selected as 1985-2012 considering the observation periods of the stations. The future period (2025-2099) was segmented into three distinct periods: near future (2025-2049), middle future (2050-2074), and far future (2075-2099). The modeling studies were conducted for each of these periods, incorporating considerations for climate and land use changes. For the future periods, both the climate data and the land use data derived in İKLİMRİSK (2019-2021) project were used for modeling basin.

The assessment of climate change impact was derived from the outputs of the MPI-ESM-MR model with RCP 8.5 scenario. Land use change maps for the years 2035, 2065, and 2085 were employed as input data. The basin modelling for the future period utilized the land use maps of 2035, 2065, and 2085, which correspond to the near future (2025-2049), middle future (2050-2074), and far future (2075-2099), respectively. Consequently, projections were conducted for both the basin flow and the actual evapotranspiration under various scenarios, considering changes in climate and land use. In addition, averaged rainfall data for each subbasin were also obtained for these periods.

Upon evaluating the combined impact of land use and climate scenarios, it was observed that monthly average flows (m^3/s) are anticipated to decrease in the future periods relative to the reference period. In each sub-basin, climate and land use changes affected the hydrological cycle at different rates. For instance, the decrease in flows at the basin outlet (subbasin 50) was estimated to be 2% for the near future, while it was projected to exceed 80% for the far future.

4.3 Drought Analyses

4.3.1 Drought Analysis by Using Observed Data

The meteorological stations located in and around the basin given by Figure 1.2 and Figure 3.36 were evaluated. Çeşme station was excluded from drought research because of its considerable distance from the river basin, except for regional frequency

analysis. Utilizing data from 10 stations, the SPI and SPEI indices were computed for 1-, 3-, 6-, and 12-month periods. Figures 4.22 and 4.23 present the SPI – 12 month and SPEI – 12 month series for Ödemiş and Selçuk stations, respectively. It is observed that the periods 1986-1994, 2000-2002, 2008-2010 and 2016-2018 were characterized by prolonged and severe drought conditions.

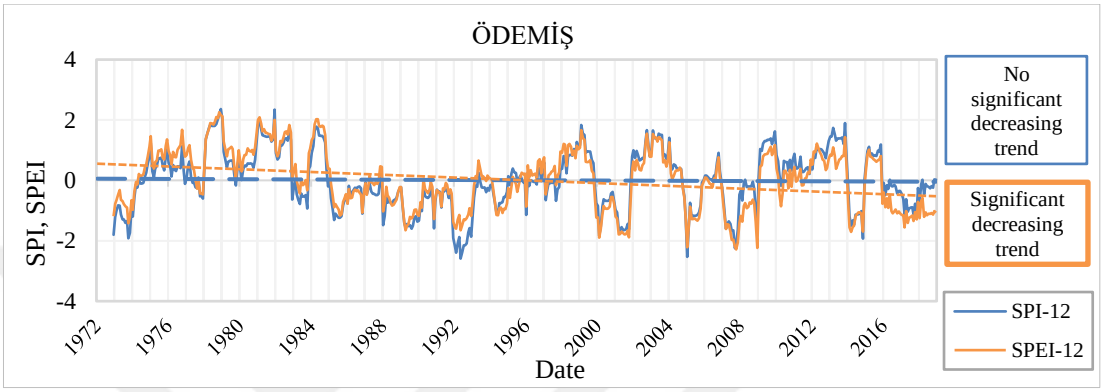


Figure 4.22 SPI-12 month and SPEI-12 month series for Ödemiş Station.

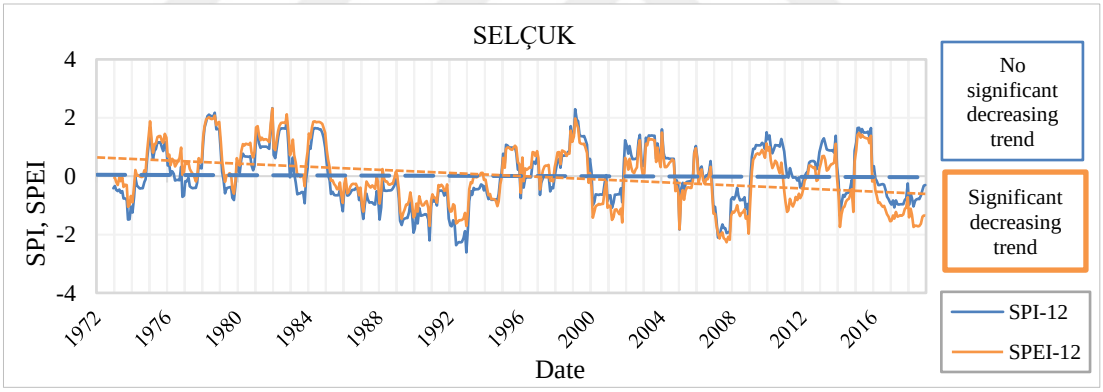


Figure 4.23 SPI – 12 month and SPEI – 12 month series for Selçuk Station.

4.3.1.1 Homogeneity and Trend Tests

The Pettit test, the SNHT test, and the Buishand test were conducted to analyze the homogeneity using the SPI and SPEI series derived from observed data and the results of these tests are presented in Table 4.5 and Table 4.6, respectively. As shown in Table 4.5, all SPI-1 month series are considered homogeneous (H). For SPI - 3 month, although the Çeşme and Nazilli stations show homogeneity according to the SNHT test, additional tests indicate that these stations are not homogeneous. Salihli station is considered homogenous for the SPI - 3 month analysis based on the results of Petttitt's

and SNHT tests. All stations did not exhibit homogeneity for both the 6-month and 12-month SPI. In the case of SPI - 6 month, Nazilli exhibits homogeneity according to the SNHT test, although other tests indicate that these stations are not homogeneous. All stations did not exhibit homogeneity for SPEI series (Table 4.6).

Table 4.5 Homogeneity test results of SPI series.

Station	SPI - 1 month			SPI – 3 month		
	Pettitt's Test	Buishand's Test	SNHT	Pettitt's Test	Buishand's Test	SNHT
Manisa	H	NH	H	NH	NH	NH
İzmir	H	H	H	NH	NH	NH
Çeşme	H	H	H	NH	NH	H
Kuşadası	H	H	H	NH	NH	NH
Aydın	H	H	H	NH	NH	NH
Salihli	H	H	H	H	NH	H
Seferihisar	H	H	H	NH	NH	NH
Ödemiş	H	H	H	NH	NH	NH
Sultanhisar	H	H	H	NH	NH	NH
Selçuk	H	H	H	NH	NH	NH
Nazilli	H	H	H	NH	NH	H
Station	SPI – 6 month			SPI – 12 month		
	Pettitt's Test	Buishand's Test	SNHT	Pettitt's Test	Buishand's Test	SNHT
Manisa	NH	NH	NH	NH	NH	NH
İzmir	NH	NH	NH	NH	NH	NH
Çeşme	NH	NH	NH	NH	NH	NH
Kuşadası	NH	NH	NH	NH	NH	NH
Aydın	NH	NH	NH	NH	NH	NH
Salihli	NH	NH	NH	NH	NH	NH
Seferihisar	NH	NH	NH	NH	NH	NH
Ödemiş	NH	NH	NH	NH	NH	NH
Sultanhisar	NH	NH	NH	NH	NH	NH
Selçuk	NH	NH	NH	NH	NH	NH
Nazilli	NH	NH	H	NH	NH	NH

Table 4.6 Homogeneity test results of SPEI series.

Station	SPEI - 1, 3, 6, 12 month		
	Pettitt's Test	Buishand's Test	SNHT
Manisa	NH	NH	NH
İzmir	NH	NH	NH
Çeşme	NH	NH	NH
Kuşadası	NH	NH	NH
Aydın	NH	NH	NH
Salihli	NH	NH	NH
Seferihisar	NH	NH	NH
Ödemiş	NH	NH	NH
Sultanhisar	NH	NH	NH
Selçuk	NH	NH	NH
Nazilli	NH	NH	NH

Mann- Kendall trend analysis was applied to SPI and SPEI series. Accordingly, when the SPI-1 month series were analysed, a weak increasing trend was observed only at Seferihisar station (Figure 4.24a). In SPI-3 month series, significant increasing trend was observed at Izmir Region, Seferihisar, Aydın and Sultanhisar stations, while no significant trend was observed at other stations (Figure 4.24b). For SPI-6 month series, significant increasing trend was observed at Izmir Region, Seferihisar, Aydın and Sultanhisar stations and weak increasing trend was observed at Kuşadası and Nazilli stations (Figure 4.24c). For SPI-12 month, significant increasing trend was observed for Izmir Region, Seferihisar, Kuşadası, Aydın and Sultanhisar and weak increasing trend was observed for Nazilli (Figure 4.24d). A significant decreasing trend was observed for all SPEI series (Figure 4.24e). It should be noted that negative values for SPI and SPEI indices indicate drought, drought progression increases for decreasing trends and decreases for increasing trends.

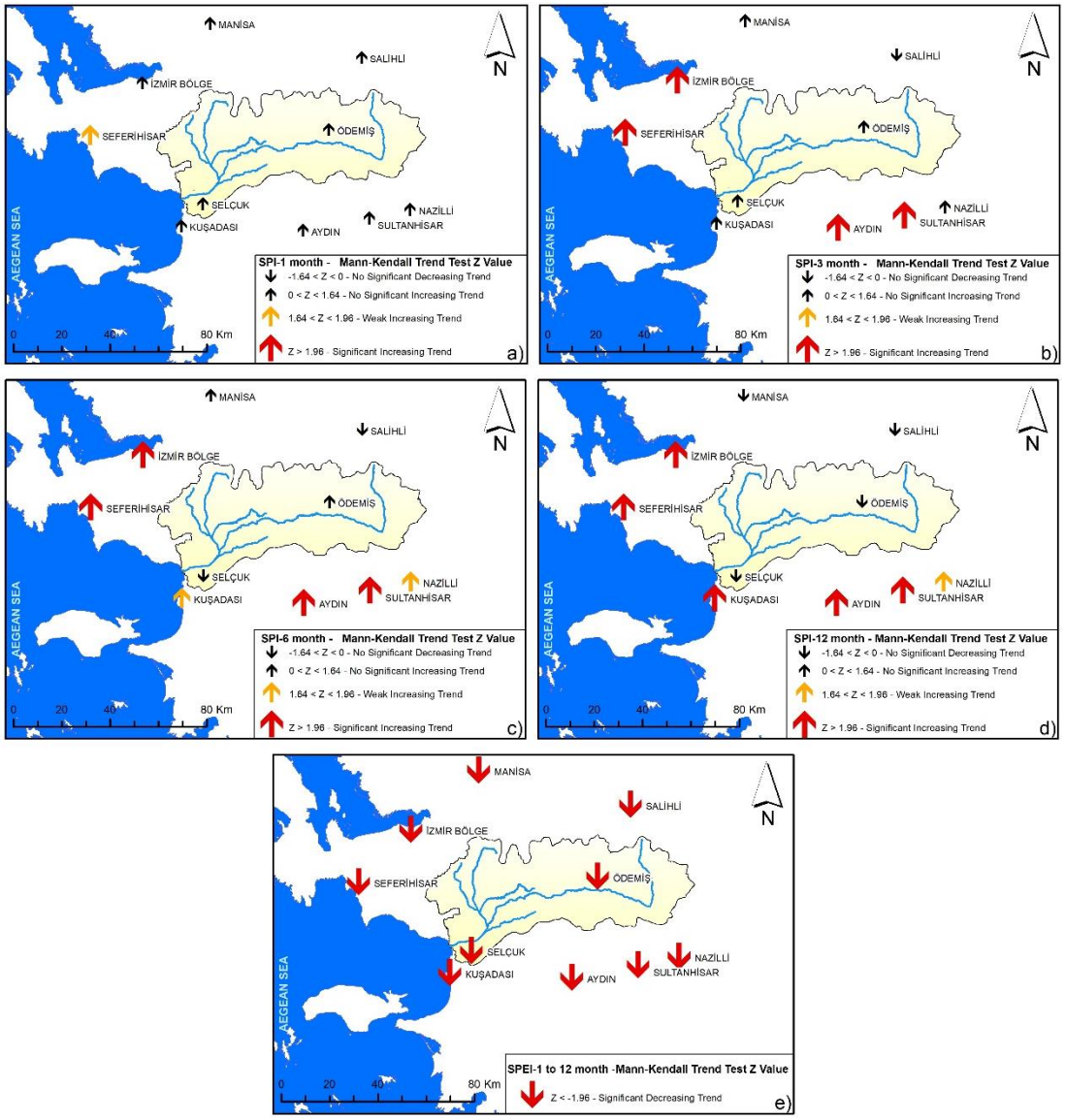


Figure 4.24 Trend in drought indices series for a) SPI-1 month, b) SPI-3 month, c) SPI-6 month, d) SPI-12 month, e)SPEI for 1-month to12-month.

4.3.1.2 Regional Frequency Analysis

A regional assessment of drought risk was conducted for the Küçük Menderes basin. This assessment was based on the analysis of the frequency of annual drought severity, using the 6-month Standardized Precipitation Index (SPI) series. In the regional frequency analysis, all stations including Çeşme station were evaluated. The L-moment ratios were computed by utilizing the annual drought severities and durations for each site, as presented in Table 4.7 and Table 4.8, respectively. By classifying 11 sites as a unified region, we calculated the discordancy statistics (D_i)

and compared them to the critical value of D_i for each site. None of the sites were deemed discordant.

Table 4.7 The L-moment statistics of regional frequency analysis for annual drought severities derived from SPI-6 month series.

Station	N (year)	Mean	L-CV	L-skewness	L-kurtosis	t5	D_i
Manisa	42	4.68	0.49	0.34	0.22	0.06	0.84
İzmir	43	4.42	0.53	0.36	0.17	0.10	0.32
Çeşme	44	4.38	0.57	0.41	0.23	0.15	2.61
Kuşadası	43	4.55	0.48	0.27	0.15	0.12	1.05
Aydın	41	4.65	0.49	0.32	0.15	0.09	0.08
Salihli	44	4.66	0.52	0.31	0.05	-0.03	1.95
Seferihisar	44	4.11	0.51	0.39	0.16	0.02	1.74
Ödemiş	42	4.46	0.52	0.33	0.12	0.05	0.26
Sultanhisar	44	4.26	0.48	0.27	0.13	0.10	0.78
Selçuk	44	4.26	0.46	0.30	0.19	0.15	0.95
Nazilli	44	4.37	0.50	0.34	0.15	0.09	0.4

Table 4.8 The L-moment statistics of regional frequency analysis for annual drought durations derived from SPI-6 month series.

Station	N (year)	Mean	L-CV	L-skewness	L-kurtosis	t5	Di
Manisa	42	5.24	0.33	0.13	0.11	0.04	1.99
İzmir	43	4.91	0.36	0.17	0.07	0.02	0.82
Çeşme	44	4.52	0.38	0.20	0.04	0.02	1.49
Kuşadası	43	5.42	0.34	0.13	0.06	0.01	0.15
Aydın	41	5.17	0.31	0.10	0.09	0.05	0.86
Salihli	44	4.84	0.38	0.20	0.06	0.02	0.85
Seferihisar	44	4.59	0.36	0.19	0.07	0.04	1.02
Ödemiş	42	4.71	0.33	0.09	0.05	0.10	0.69
Sultanhisar	44	4.57	0.32	0.08	0.07	0.11	0.76
Selçuk	44	5.09	0.35	0.11	0.04	0.02	1.28
Nazilli	44	4.73	0.32	0.11	0.08	0.06	1.1

The relationship between L-moment skewness (L-skew) and L-moment coefficient of variation (L-Cv) are given by Figure 4.25. Given that the computed values for H_1, specifically -1.36 for annual drought severity and -1.03 for annual drought duration, are both less than 2, the region is considered homogeneous.

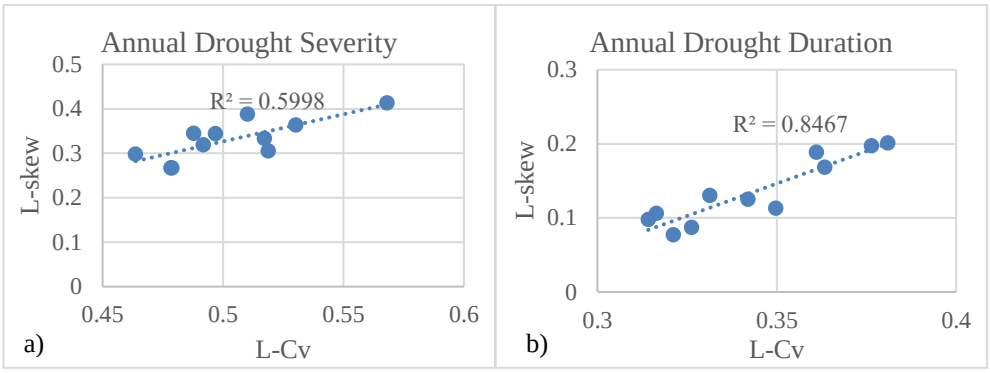


Figure 4.25 The relationship between L-skewness and L-CV for a) annual drought severity, b) annual drought duration.

Both the Generalized Pareto and Pearson Type III distributions were considered suitable for the regional frequency distribution of annual drought severity, as the magnitudes of Z_{DIST} were below 1.64. The goodness of fit measures (Z values) for annual drought severities were 0.41 and 0.37 for the Pearson Type III and Generalized Pareto distributions, respectively. Furthermore, the Generalized Pareto distribution was deemed suitable for representing the regional frequency distribution of annual drought duration. The goodness of fit measure (Z value) for annual drought severities was calculated to be -1.48. The Generalized Pareto distribution was selected for the regional frequency distribution.

4.3.1.3 Drought Maps

Maps depicting indicators such as annual drought severity and duration were generated based on SPI-1 month, SPI-3 month, SPEI-1 month and SPEI-3 month series, as illustrated in Figure 4.26 and Figure 4.27. Trend analyses of these indicators were conducted using Sen's trend test, and the spatial changes in the results were visually presented through maps in Figure 4.28 and Figure 4.29. An examination of the trends reveals a decreasing pattern in the annual severity and duration of drought determined from the SPI series, whereas the opposite trend is observed for the SPEI series. Comprehensive details, including annual maximum drought durations, severities, and the onset dates for each drought condition (moderate, severe, and extreme), are provided in Appendices through Table Ap.1 to Table Ap.24.

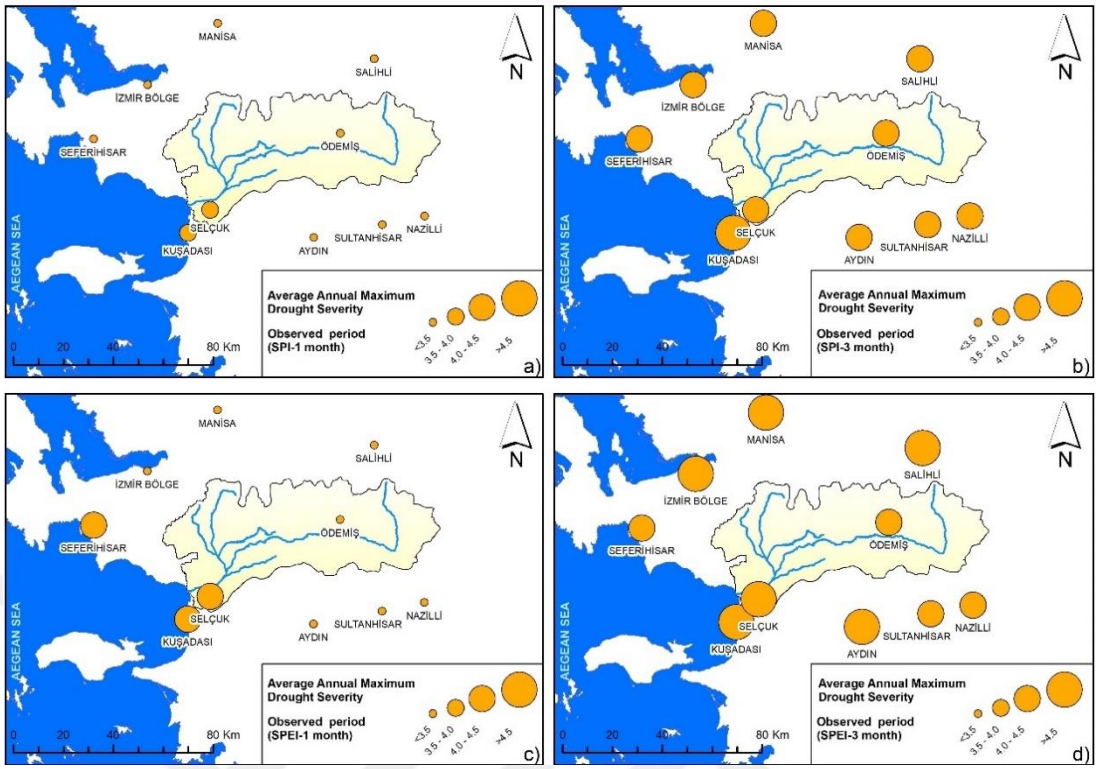


Figure 4.26 Average annual maximum drought severity for the observed period a) SPI-1 month, b) SPI-3 month, c) SPEI-1 month, d) SPEI-3 month.

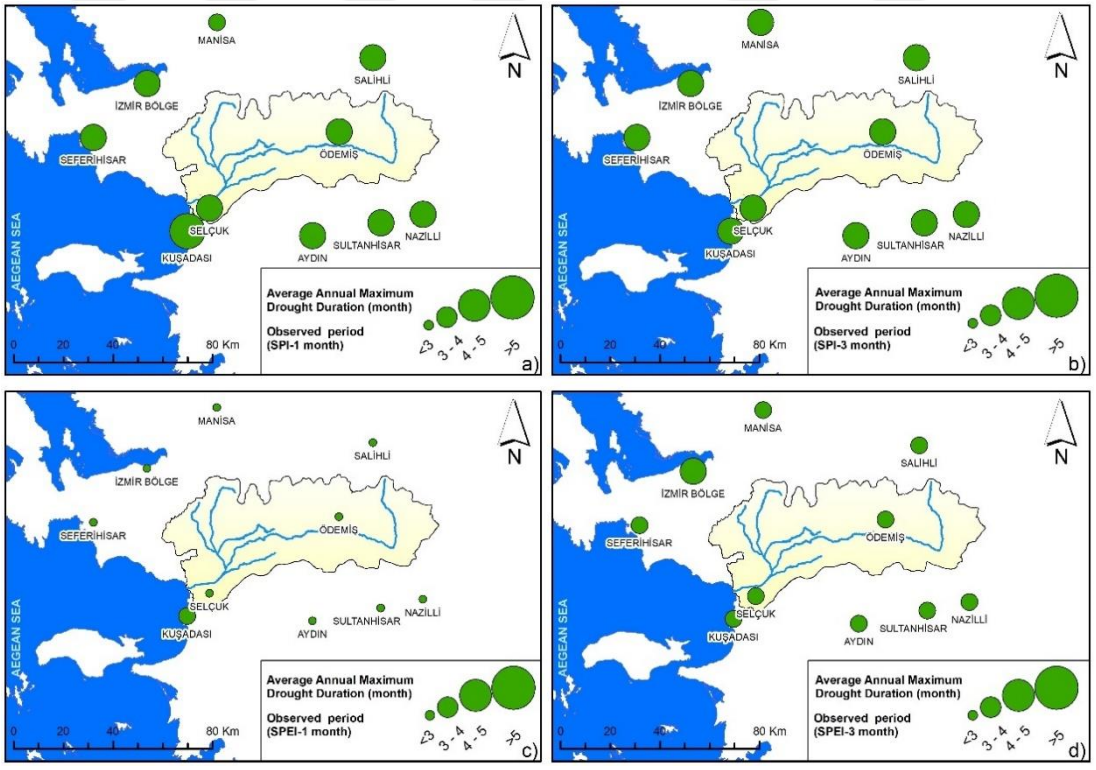


Figure 4.27 Average annual maximum drought duration for the observed period a) SPI-1 month, b) SPI-3 month, c) SPEI-1 month, d) SPEI-3 month.

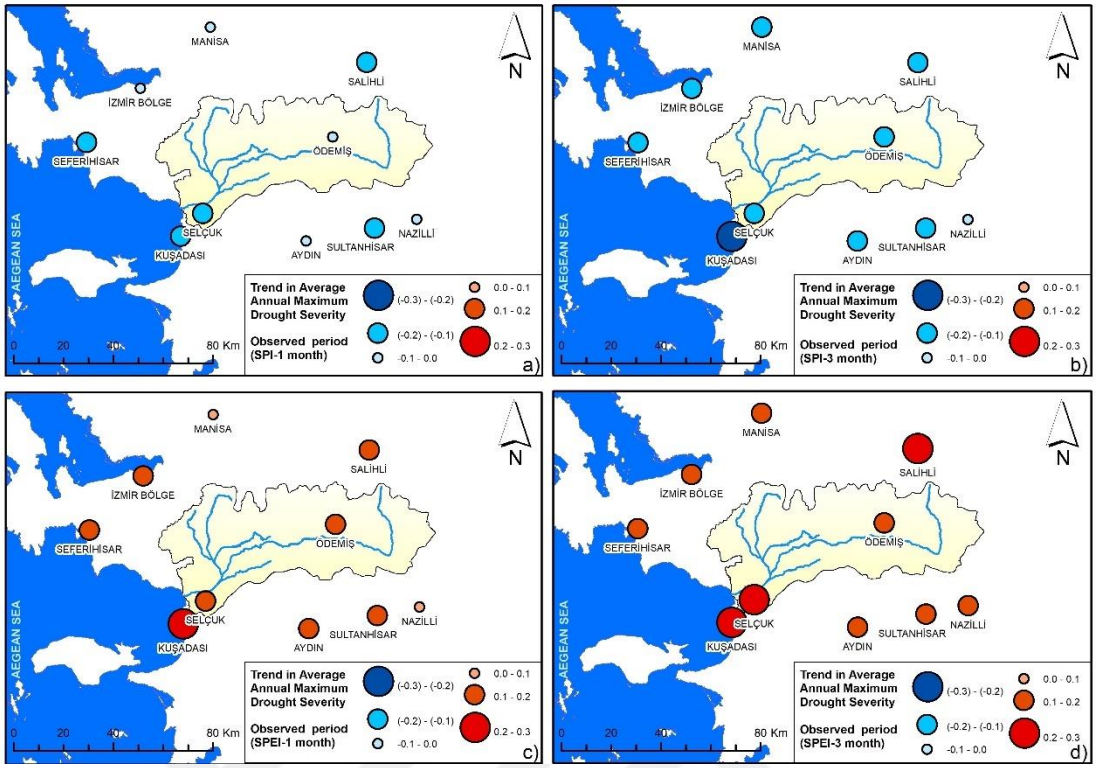


Figure 4.28 Trend in average annual maximum drought severity for the observed period a) SPI-1 month, b) SPI-3-month, c) SPEI-1 month, d) SPEI-3 month.

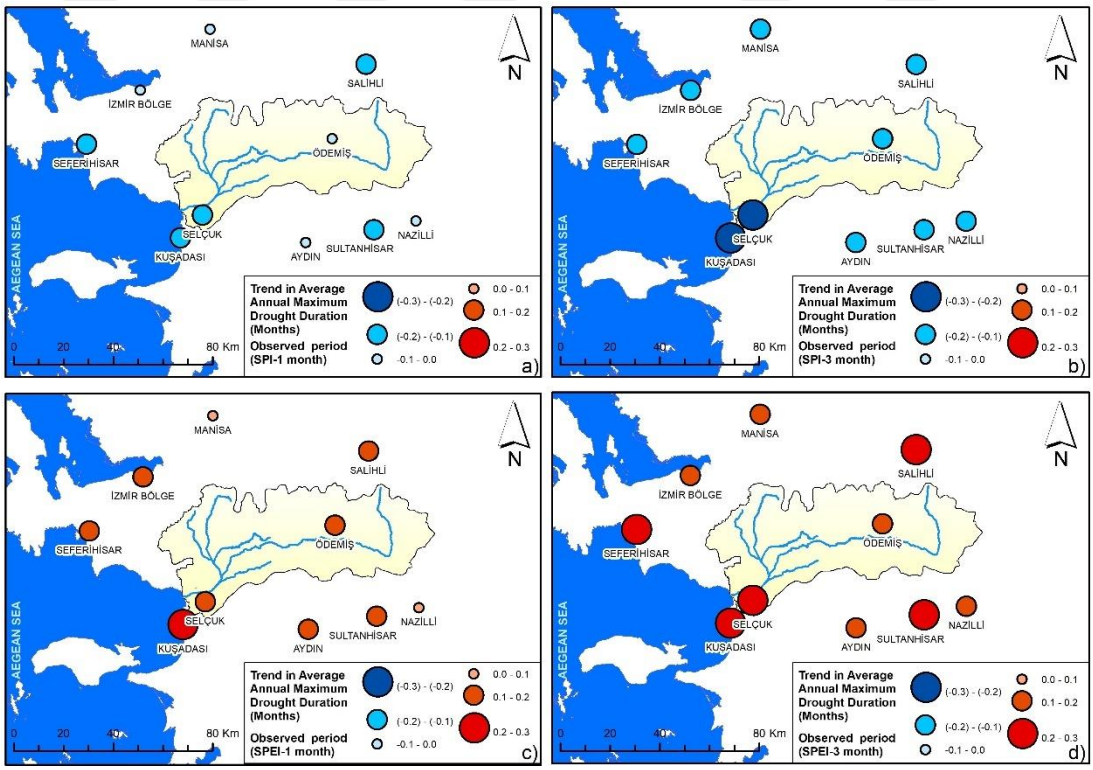


Figure 4.29 Trend in average annual maximum drought duration for the observed period a) SPI-1 month, b) SPI-3-month, c) SPEI-1 month, d) SPEI-3 month.

4.3.2 Drought Analysis by Using Climate Data

SPI-30 day and SPI-90 day series were computed from daily total precipitation data, while SPI-1 month and SPI-3 month series were derived from monthly total precipitation data. Additionally, SPEI-1 month and SPEI-3 month series were generated using both monthly total precipitation and monthly average temperature data through grid-based climate data. Following the grid-based calculations, the Python script was employed to compute the average values of the micro-watersheds for each index.

Maps of annual drought severity, duration, magnitude, and time of drought onset were derived. Trend analyses of these indicators were carried out according to Sen's trend test, and the spatial changes of the results were also shown with maps. The maps were created for four distinct time periods: the reference era (1971-2004), the near future (2025-2049), the middle future (2050-2074), and the far future (2075-2099).

4.3.2.1 Monthly Drought Maps

Average annual maximum drought severities, durations, magnitudes, and median days of the drought start values for the observed period were calculated and mapped for the series of SPI-1 month, SPI-3 month (Figure 4.30 – Figure 4.37) and SPEI-1 month and SPEI-3 month (Figure 4.38 - Figure 4.45). Maps of number of drought events for each drought conditions including moderate, severe, and extreme are given by Figure Ap.55 – Figure Ap.70 in Appendices.

Figure 4.30 and Figure 4.31 display the average annual maximum drought severities from SPI-1 and SPI-3 for the whole time periods examined. The data shows a shift in drought conditions from less severe to more severe as we approach the year 2100. There is also evidence of increased variation in the upstream region of the basin, which is further away from the coastal areas that receive more precipitation. The calculation of high drought severities relies, which amplifies the significance of signals when translating meteorological drought conditions into subsequent hydrologic consequences. The analysis was conducted on the durations of annual maximum

drought severities, revealing persistent increases in the average lengths of the most severe droughts for all indices (Figure 4.32, Figure 4.33, Figure 4.40, Figure 4.41).

Annual maximum droughts by calculating using SPI-1 month, that last normally for 3-5 months arrive in longer durations with 6-8 months in the far future period (Figure 4.32). In the near and middle future period, it is seen that drought will be longer in the upstream (eastern) and southern parts of the basin. Annual maximum droughts by calculating using SPI-1 month, that last normally for 3-4 months arrive in longer durations with 6-7 months in the far future period (Figure 4.32). Annual maximum droughts by calculating using SPI-3 month, that last normally for 5-6 months arrive in longer durations with 8-9 months in the far future period (Figure 4.33). When the annual maximum drought magnitudes calculated from the SPI-1 month indices are analyzed, drought is generally not observed in the basin during the reference period (Figure 4.34). In the near future, middle future and far future, moderate drought will prevail in the basin. When the annual maximum drought magnitudes calculated from the SPI-3 month indices are analyzed, it is seen that there is a similar situation with the SPI-1 month series, but severe drought is expected in the far future period around Selçuk district, which is downstream of the basin (Figure 4.35).

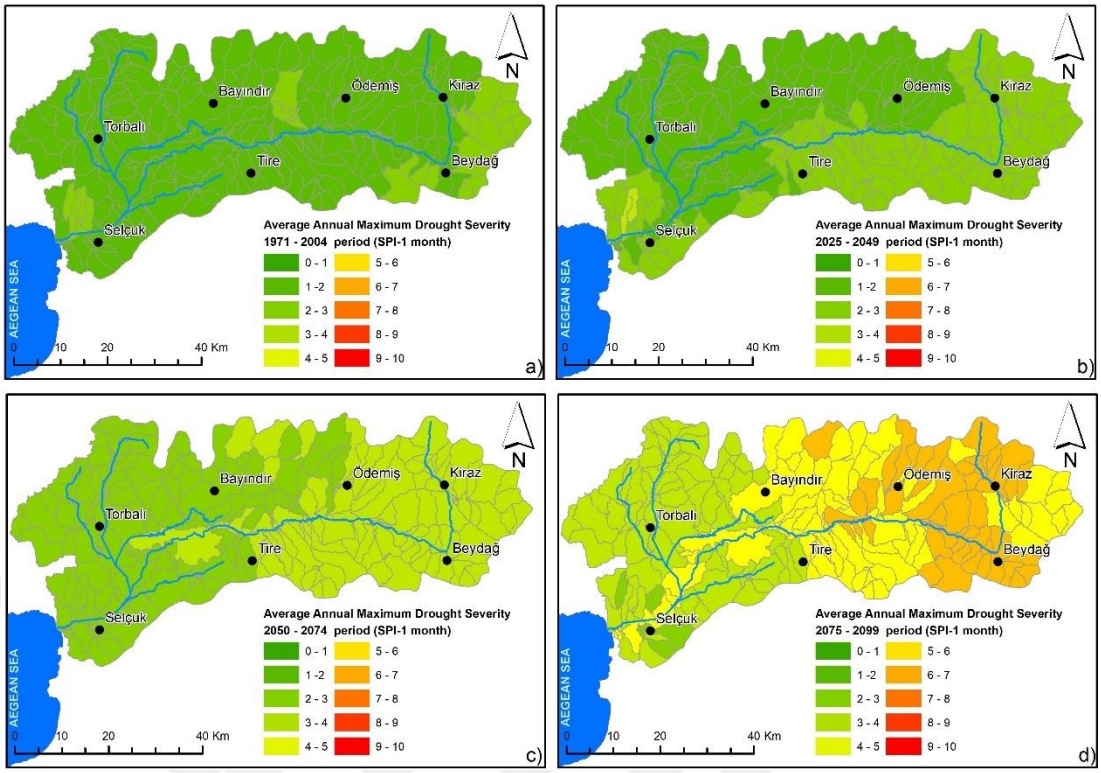


Figure 4.30 Average annual maximum drought severity of SPI-1 month for the period a)1971-2004, b)2025-2049, c)2050-2074, d)2075-2099.

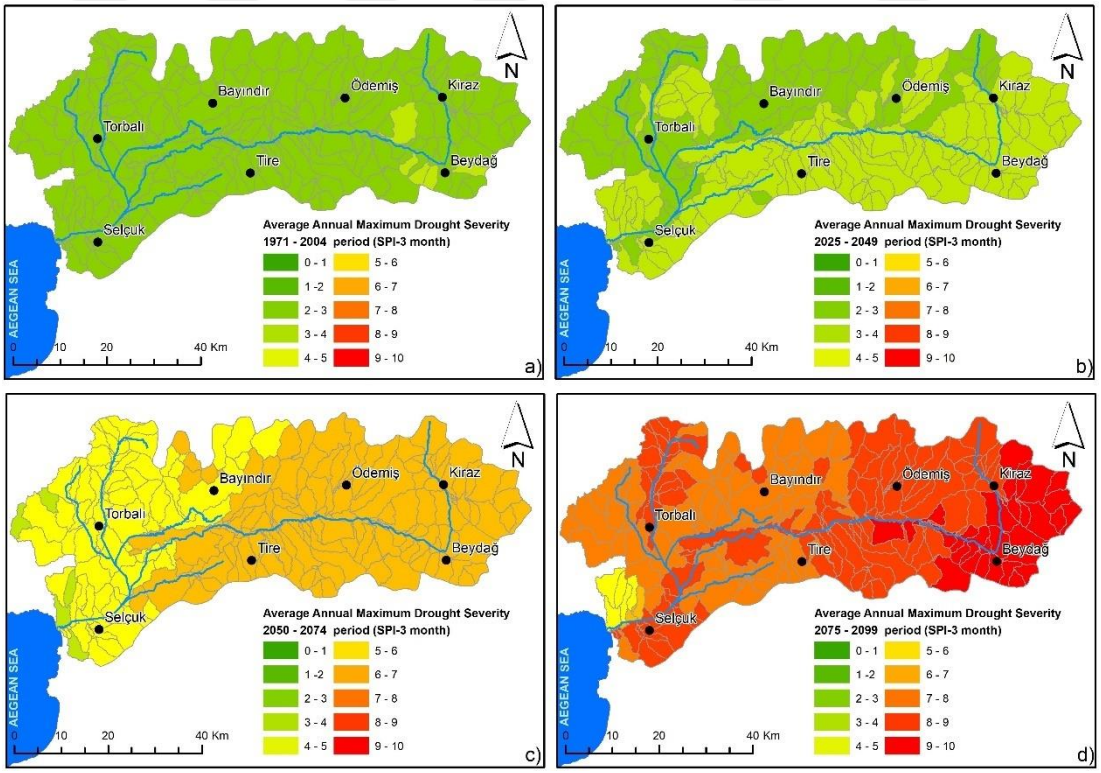


Figure 4.31 Average annual maximum drought severity of SPI-3 month for the period a)1971-2004, b)2025-2049, c)2050-2074, d)2075-2099.

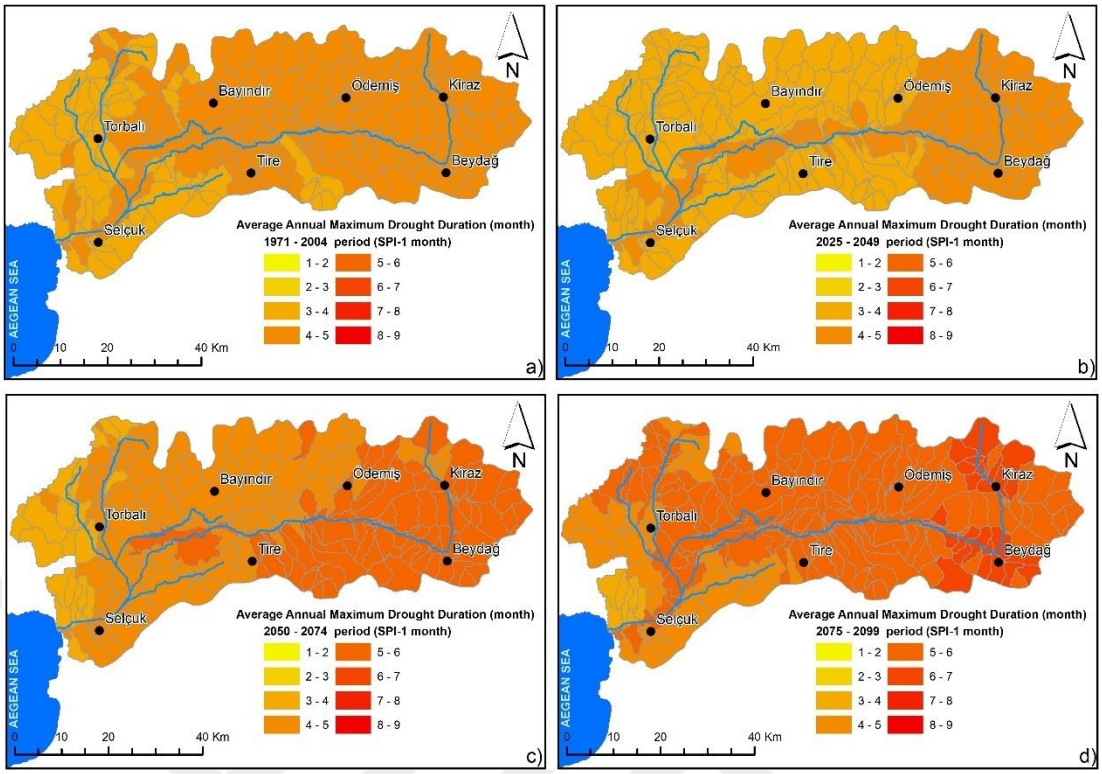


Figure 4.32 Average annual maximum drought duration of SPI-1 month for the period a)1971-2004, b)2025-2049, c)2050-2074, d)2075-2099.

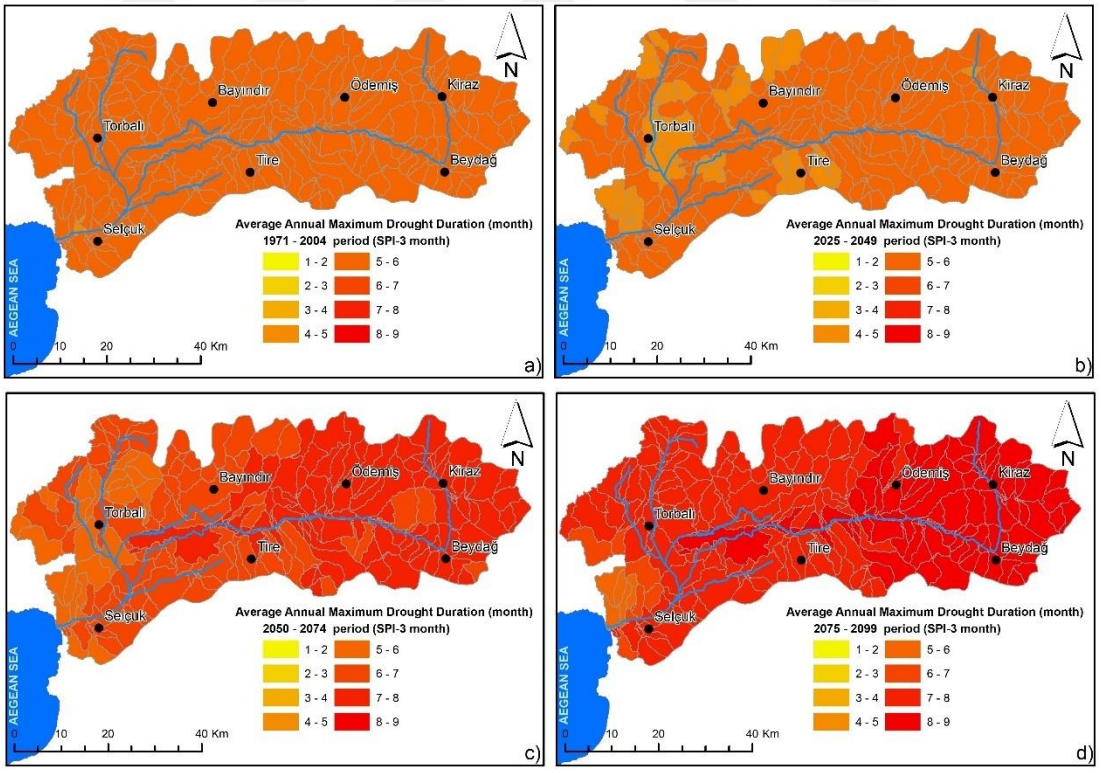


Figure 4.33 Average annual maximum drought duration of SPI-3 month for the period a)1971-2004, b)2025-2049, c)2050-2074, d)2075-2099.

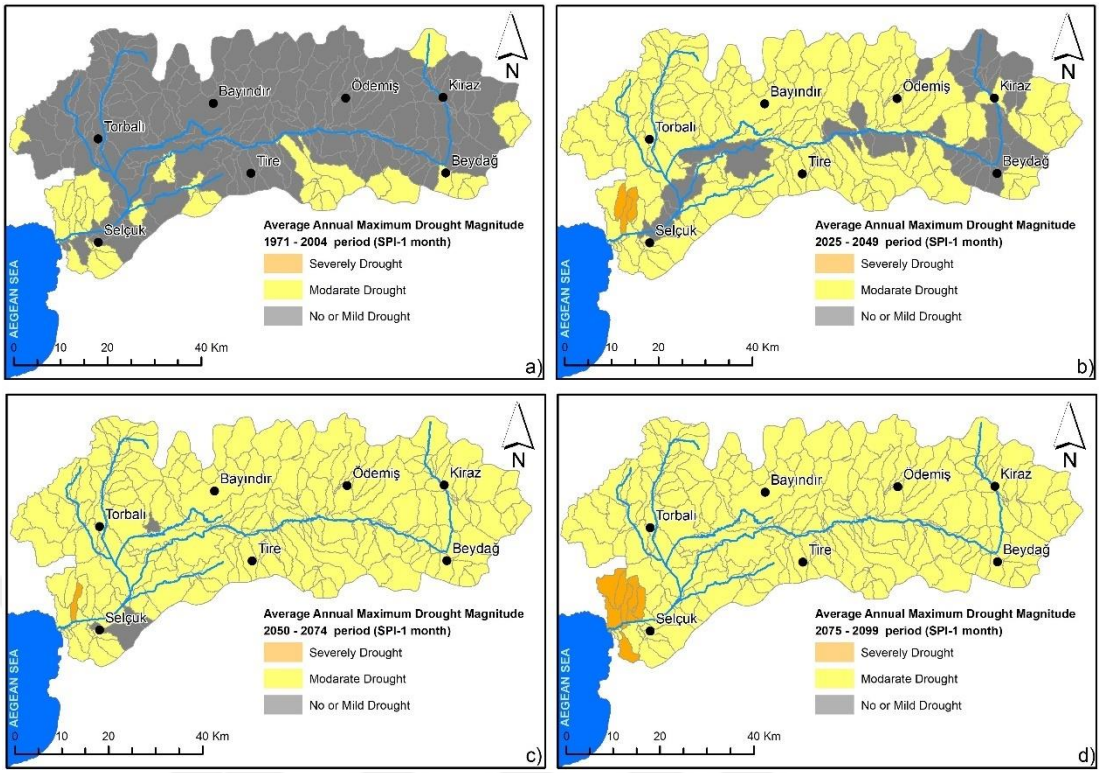


Figure 4.34 Average annual maximum drought magnitude of SPI-1 month for the period a)1971-2004, b)2025-2049, c)2050-2074, d)2075-2099.

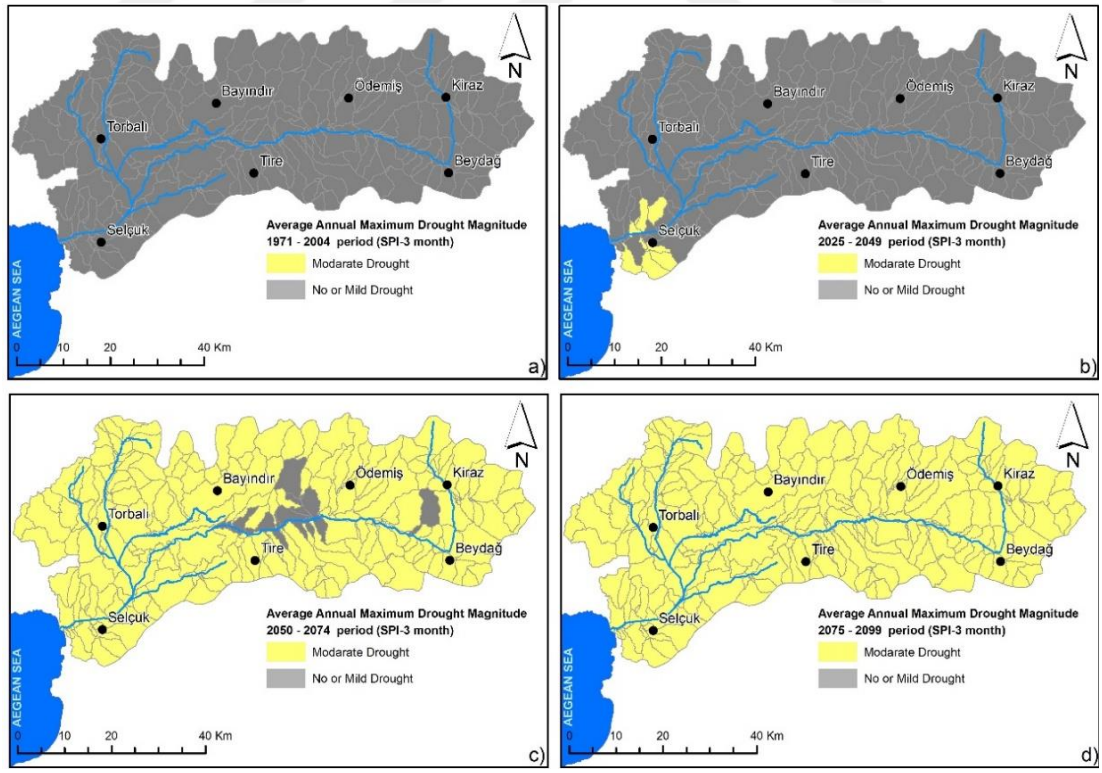


Figure 4.35 Average annual maximum drought magnitude of SPI-3 month for the period a)1971-2004, b)2025-2049, c)2050-2074, d)2075-2099.

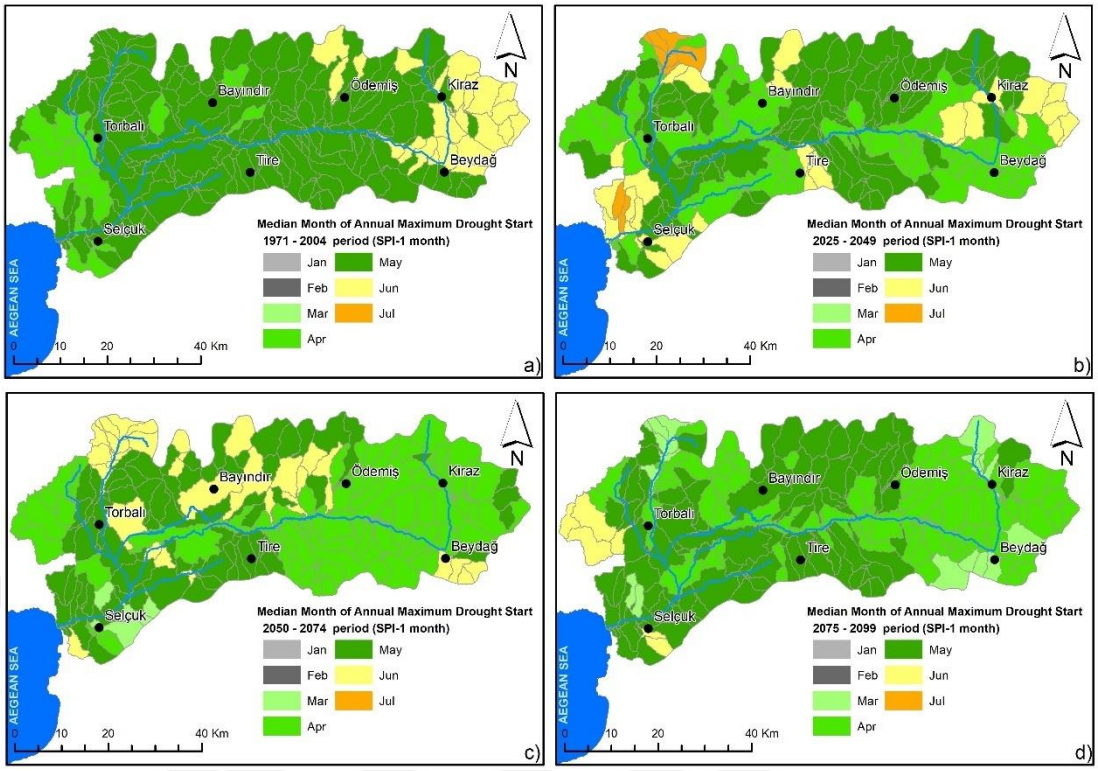


Figure 4.36 Median month of annual drought start of SPI-1 month for the period a)1971-2004, b)2025-2049, c)2050-2074, d)2075-2099.

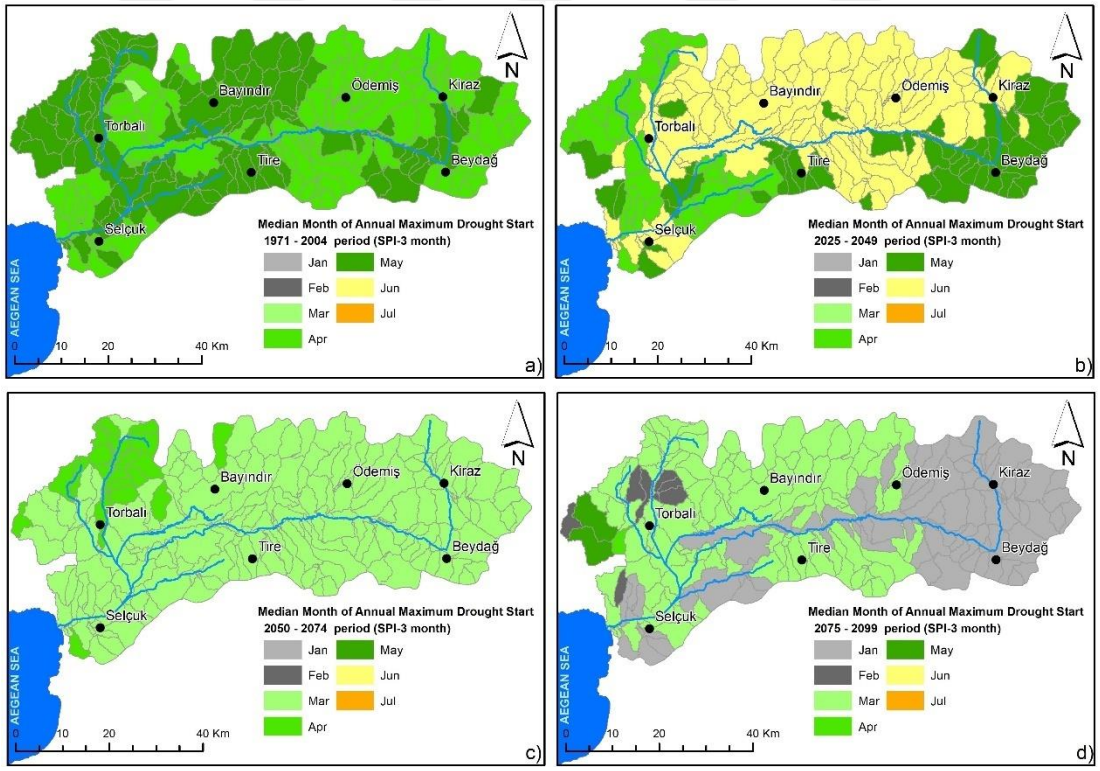


Figure 4.37 Median month of annual drought start of SPI-3 month for the period a)1971-2004, b)2025-2049, c)2050-2074, d)2075-2099.

When the maps derived from SPI-1 month series and showing the onset period of drought are examined, it is observed that drought initiates in May during the reference period. However, this period gradually advances to April in future periods, as illustrated in Figure 4.36. Examining the maps derived from SPI-3 month series and depicting the onset of drought, it is noted that the onset in the reference period is in April-May. In the near future, this initiation shifts to June, followed by a further shift to March in the medium future period, and ultimately advances to January in the far future period, especially in the upstream part as depicted in Figure 4.37.

The General Circulation Models (GCMs) generally concur on the projected rise in temperatures above the average regional values along the Aegean-Mediterranean transects in Türkiye. These trends are expected to continue in future climate conditions. Temperature anomalies are the primary factor influencing perceptions of drought, leading to notable variations in the severity of drought conditions. The SPEI analyses indicate swift fluctuations in the average severity of conditions between consecutive periods, underscoring the significance of temperature anomalies in forecasting droughts.

The significant patterns in the views represented by the SPEI indices become noticeable when considering the magnitudes of annual maximum drought severities averaged within their associated drought periods.

In the annual maximum drought magnitudes derived from the SPEI-1 month and SPEI 3- month indices, the basin typically does not experience drought during the reference period (refer to Figure 4.38 and Figure 4.39). The differences between the investigated periods, which include the 1 and 3-month accumulation periods and yield SPEI-1 month and SPEI-3 month values, are particularly evident when comparing the reference times of 1971–2004 to the furthest time horizon of 2075–2099. According to drought classification schemes using SPEI, the most concerning observations are seen across the entire basin, with gradual transitions between different levels of drought. Initially characterized by no or mild drought conditions in the reference period, the region progresses toward extreme drought conditions by the year 2100.

The evolving non-stationary nature of meteorological variables significantly impacts drought characteristics, including severity, duration, and magnitude. The onset of drought periods may also exhibit temporal variations within the years. The study also examined the potential influence of changing climatic conditions on the occurrence of annual maximum drought events in comparison to the reference period.

In the far future period, annual maximum droughts, calculated using SPEI-1 month and typically lasting 5-6 months, extend to longer durations of 11-12 months (Figure 4.40). Similarly, annual maximum droughts computed with SPEI-3 month, which usually endure for 6-7 months, exhibit extended durations of 11-12 months in the far future (Figure 4.41).

Upon analyzing the annual maximum drought magnitudes derived from the SPI-1 month and SPEI-3 month indices, it is generally observed that drought is not present in the basin during the reference period (Figure 4.42 and Figure 4.43). Expecting moderate, severe, and extreme droughts in the near, middle, and far future, respectively.

When the maps derived from SPEI-1 month series and showing the onset period of drought are examined, it is observed that drought started in April-May-Jun in the reference period, shifted to May in the near future period, shifted to April in the medium future period, and shifted to February in the far future period, especially in the upstream part (Figure 4.44). When the maps derived from SPEI-3 month series and showing the onset period of drought are examined, it is seen that drought started in April-May in the reference period, shifted to May in the near future period, shifted to March in the medium future period, and shifted to January in the far future period, especially in the upstream part (Figure 4.45).

Considering the temperature variable, this emerging perspective suggests that predicted temperature increases due to regional climate change will have a substantial impact on the severity of droughts.

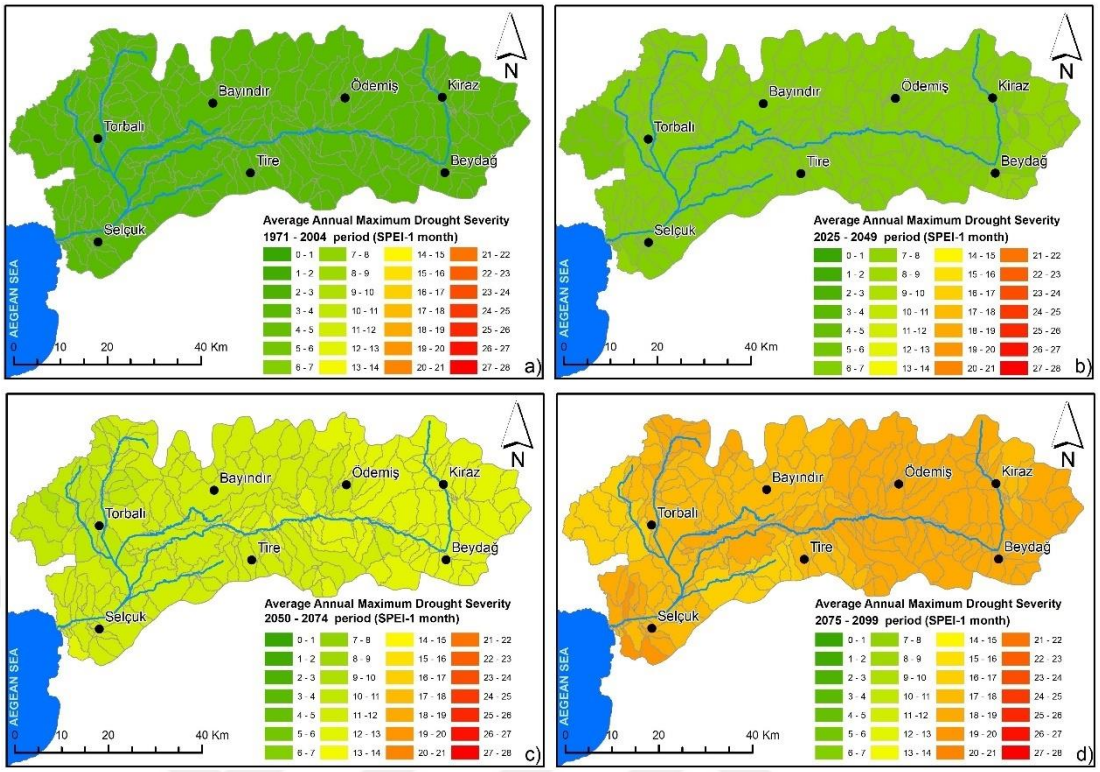


Figure 4.38 Average annual maximum drought severity of SPEI-1 month for the period a)1971-2004, b)2025-2049, c)2050-2074, d)2075-2099.

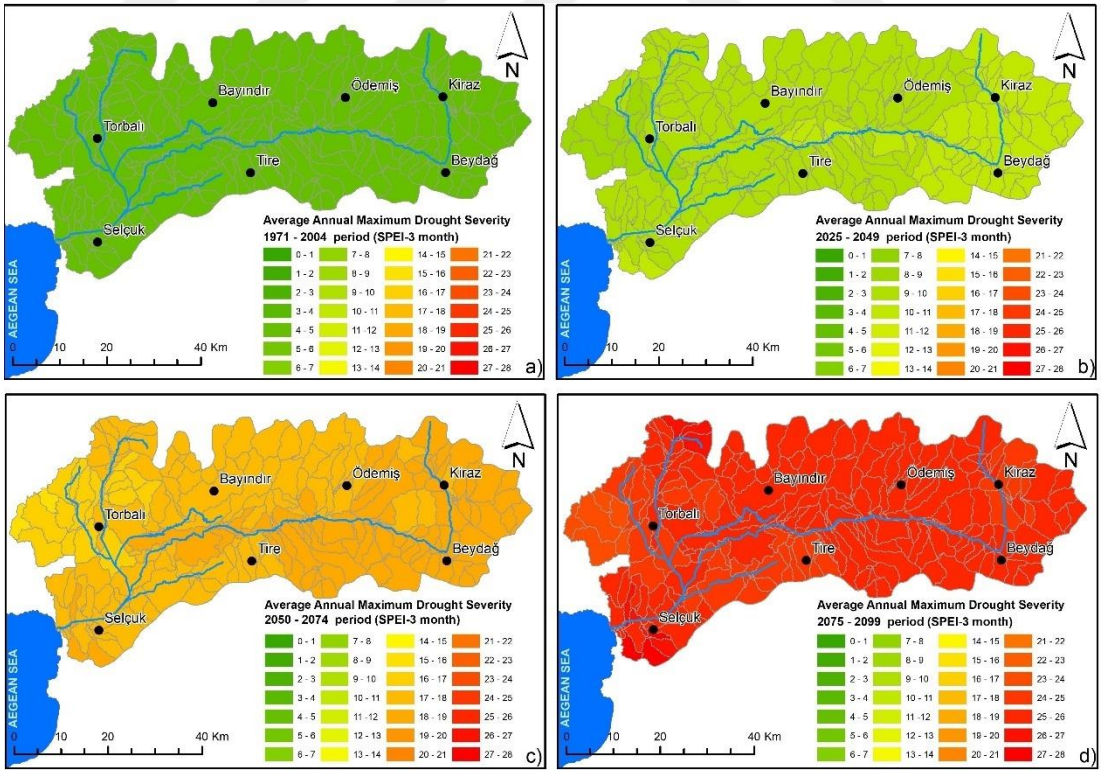


Figure 4.39 Average annual maximum drought severity of SPEI-3 month for the period a)1971-2004, b)2025-2049, c)2050-2074, d)2075-2099.

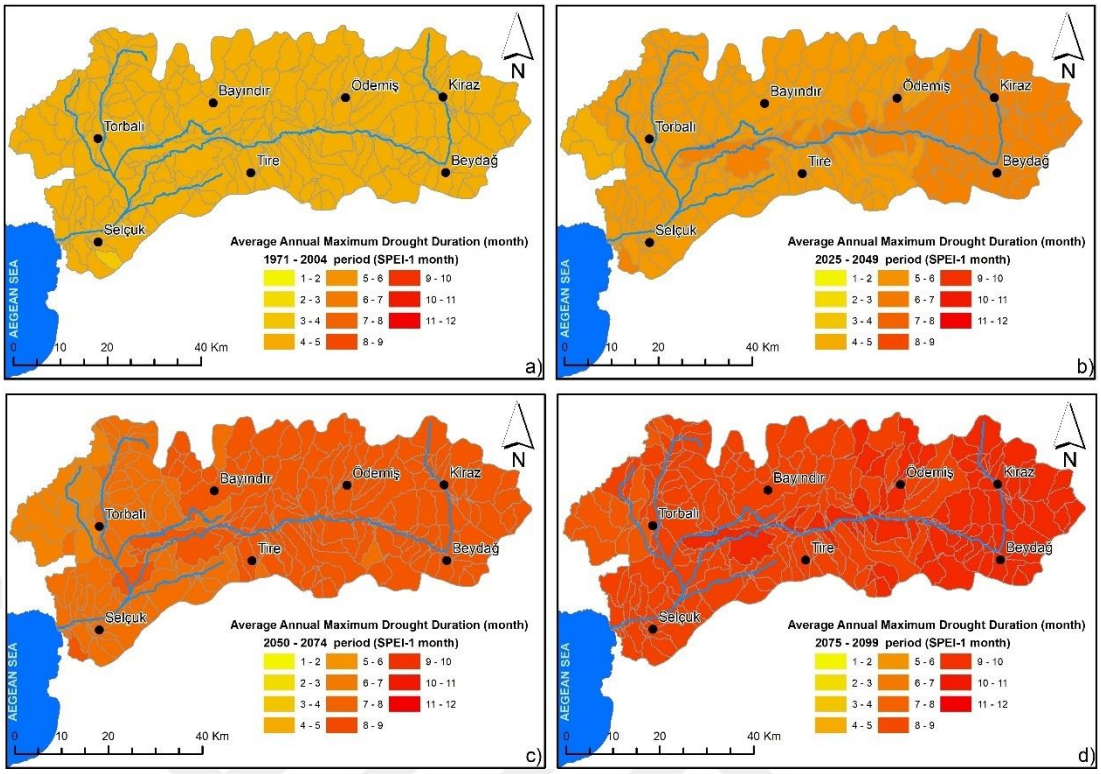


Figure 4.40 Average annual maximum drought duration of SPEI-1 month for the period a)1971-2004, b)2025-2049, c)2050-2074, d)2075-2099.

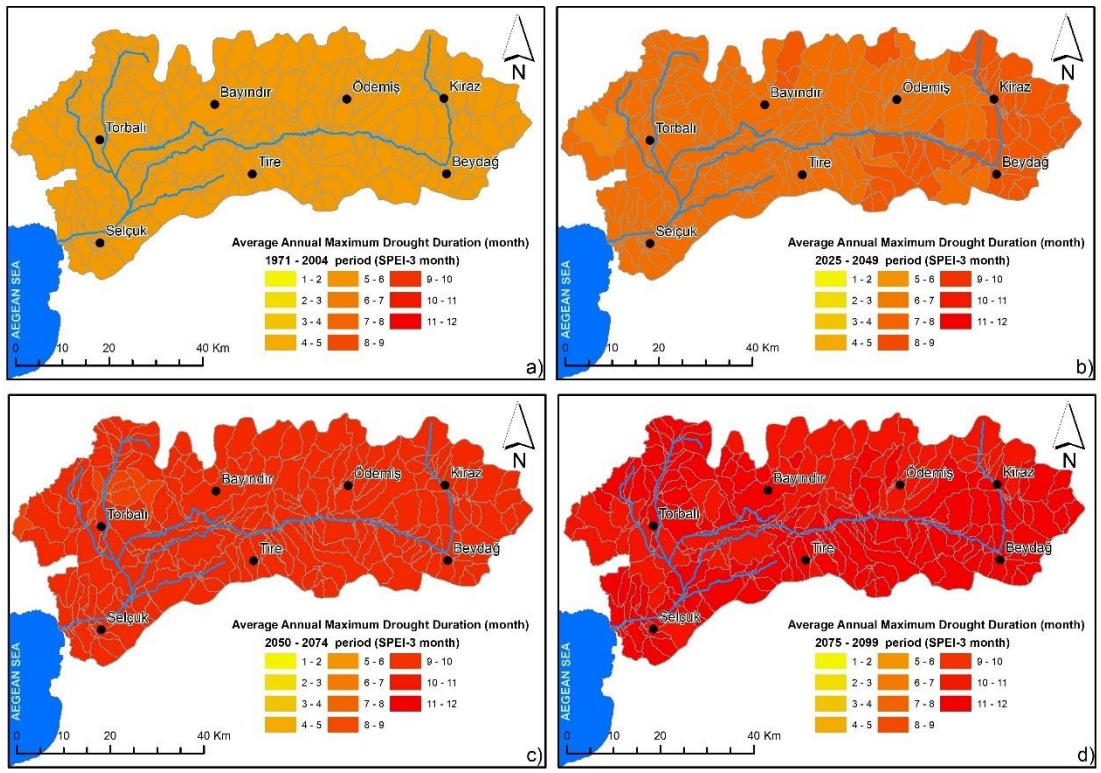


Figure 4.41 Average annual maximum drought duration of SPEI-3 month for the period a)1971-2004, b)2025-2049, c)2050-2074, d)2075-2099.

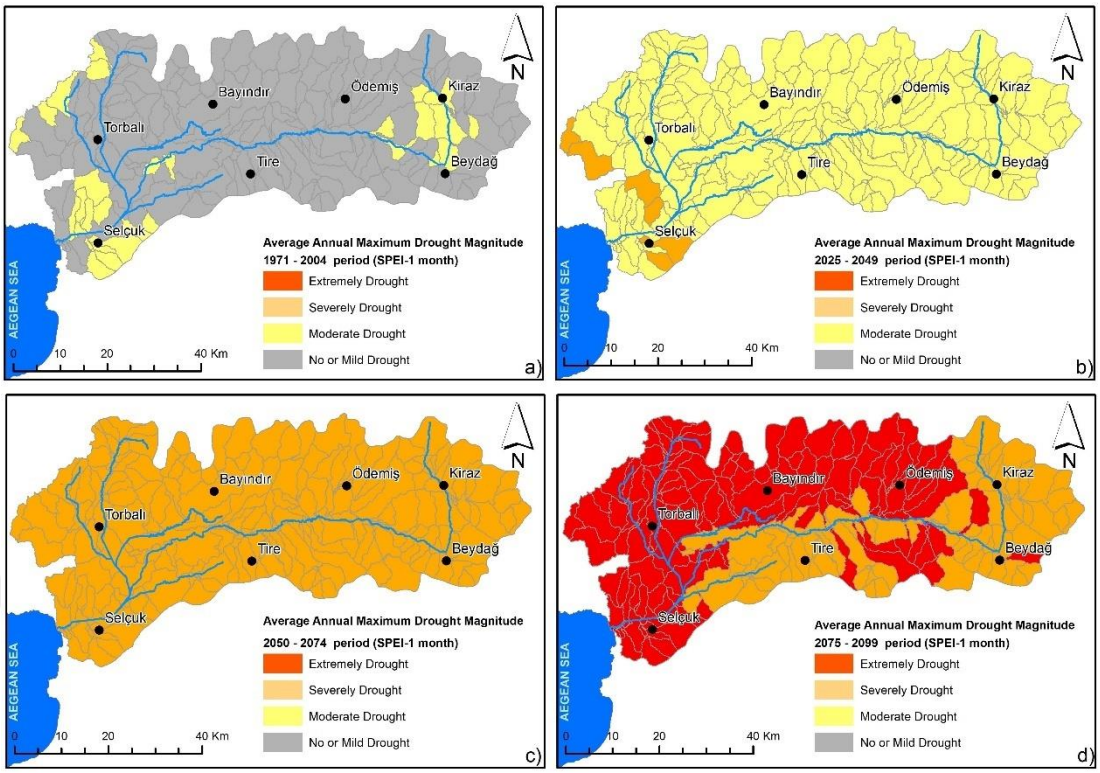


Figure 4.42 Average annual maximum drought magnitude of SPEI-1 month for the period a)1971-2004, b)2025-2049, c)2050-2074, d)2075-2099.

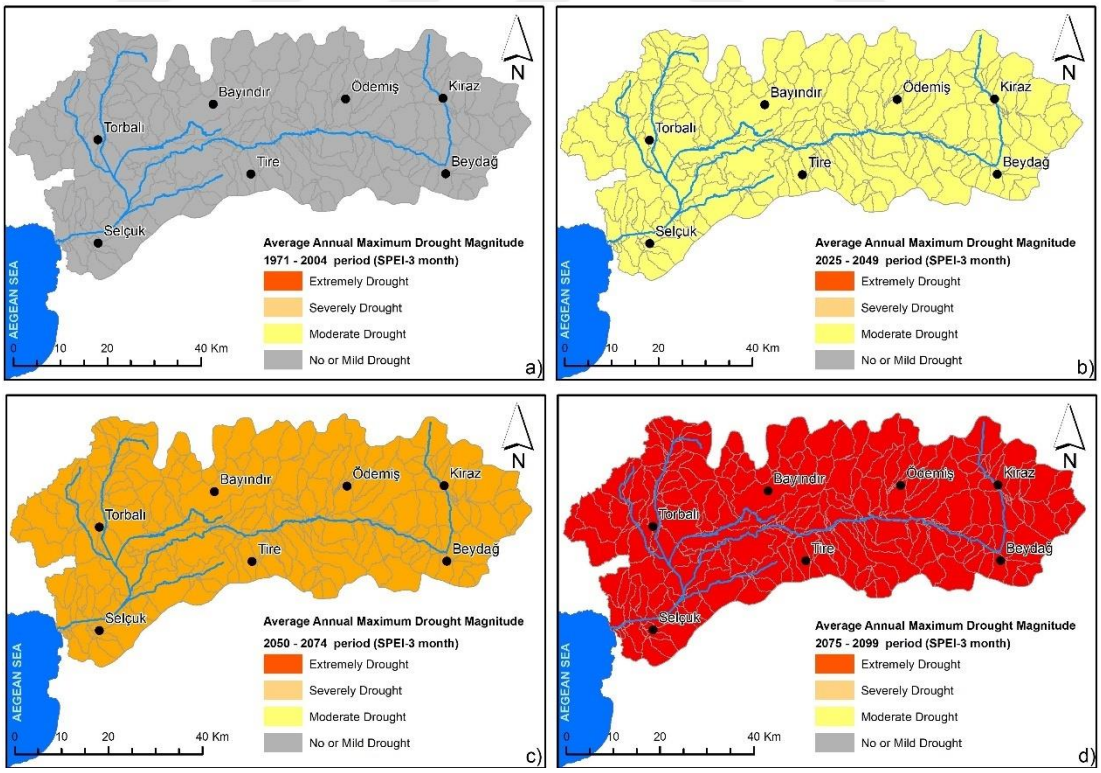


Figure 4.43 Average annual maximum drought magnitude of SPEI-3 month for the period a)1971-2004, b)2025-2049, c)2050-2074, d)2075-2099.

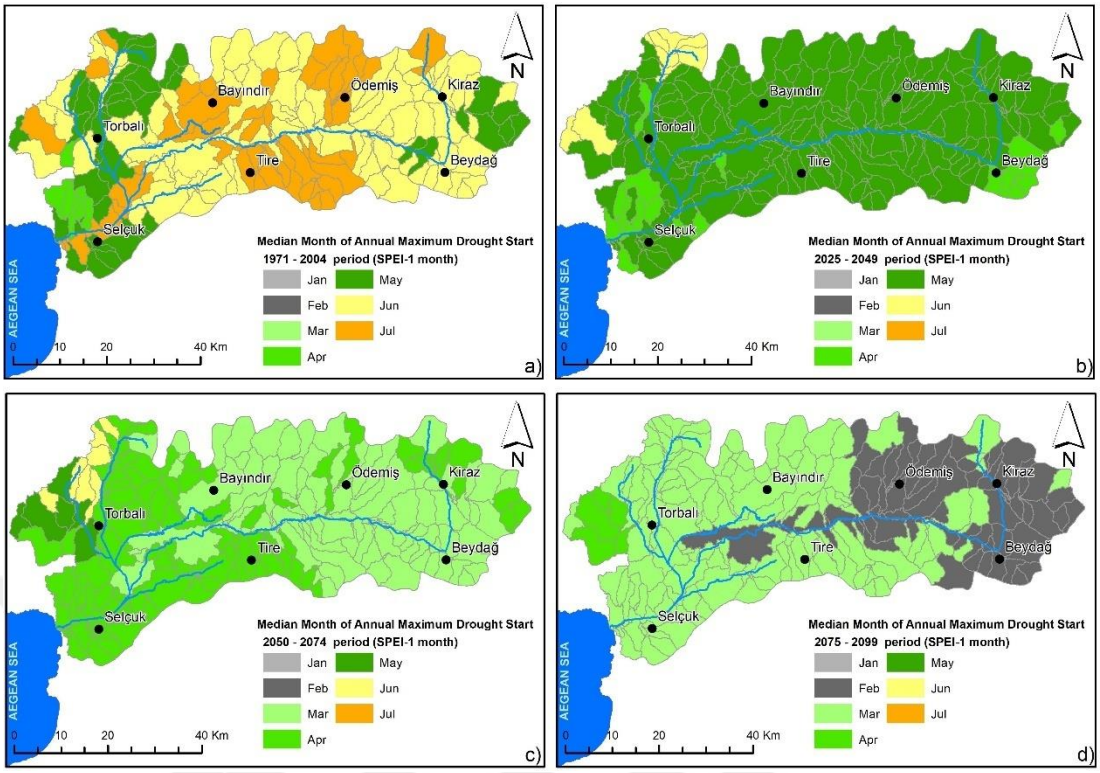


Figure 4.44 Median month of annual maximum drought start of SPEI-1 month for the period a)1971-2004, b)2025-2049, c)2050-2074, d)2075-2099.

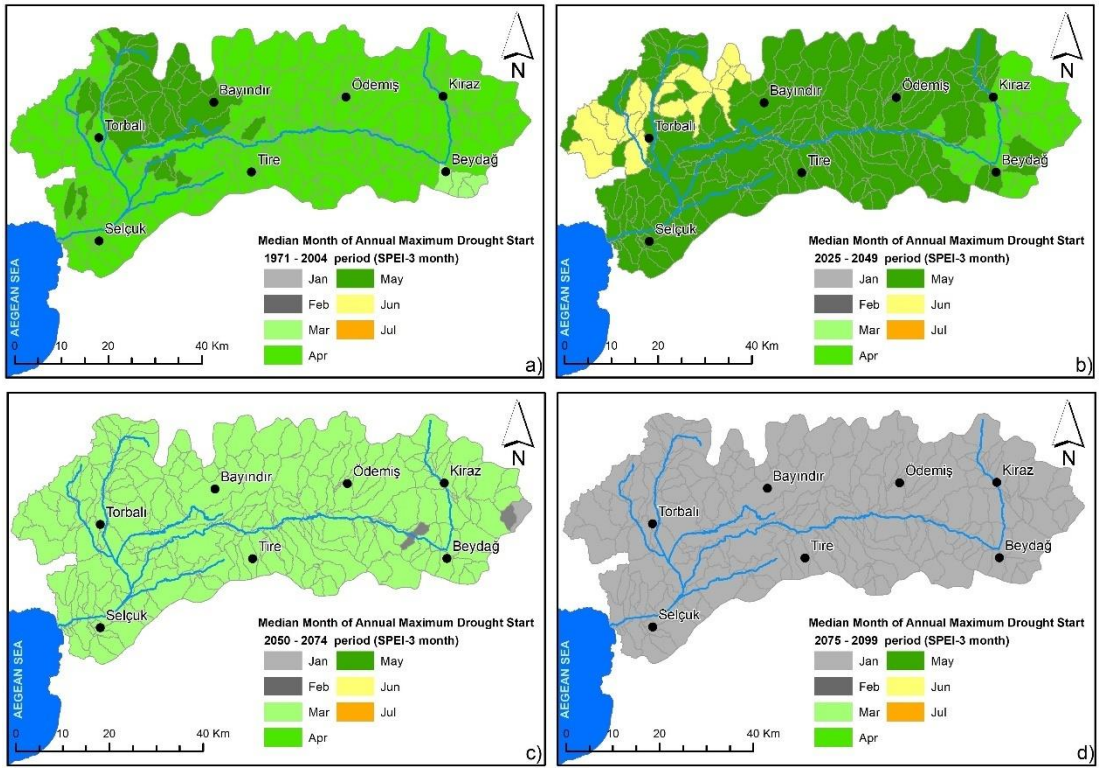


Figure 4.45 Median month of annual maximum drought start of SPEI-3 month for the period a)1971-2004, b)2025-2049, c)2050-2074, d)2075-2099.

The basin predominantly exhibited a negative trend in average annual maximum drought severities (Figure 4.46 and Figure 4.47). The lower part of the basin exhibited a declining pattern, whereas the upper part displayed an increasing pattern during the period from 2075 to 2099. Nevertheless, there was a consistent upward trend in the average duration of maximum droughts across all time periods (Figure 4.47 and Figure 4.49). The trend in the average annual maximum drought magnitude for the SPI-1 month exhibited similar results to drought severity, while the trend in the series of SPI-3 month was comparable to durations (Figure 4.50 and Figure 4.51). During the period from 2025 to 2049, there was a noticeable upward trend in the starting month of annual maximum droughts for the SPI series (Figure 4.52 and Figure 4.53). The significantly increasing trend was observed in the period 2050-2074 for the series of average annual maximum drought severities, durations, and magnitudes for SPEI (Figure 4.54- Figure 4.59). The start month of drought for the SPEI series exhibited a prominent increasing trend in the western part of the basin, whereas the same trend was not observed in the eastern part (Figure 4.60-Figure 4.61).

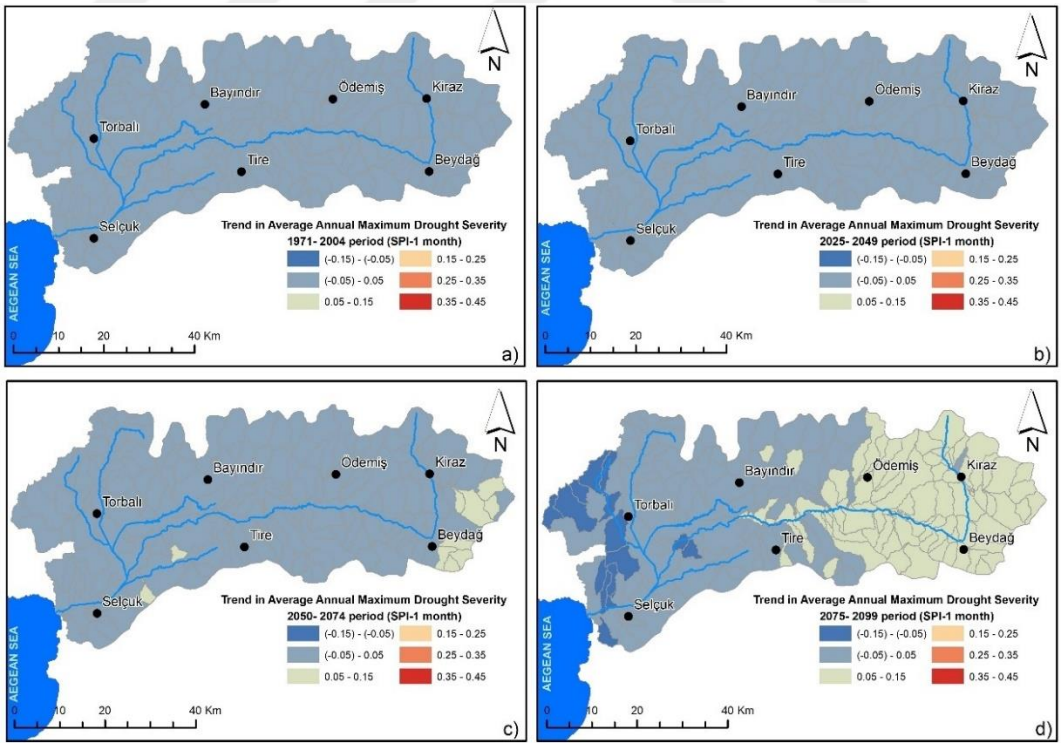


Figure 4.46 Trend in average annual maximum drought severity of SPI-1 month for the period a)1971-2004, b)2025-2049, c)2050-2074, d)2075-2099.

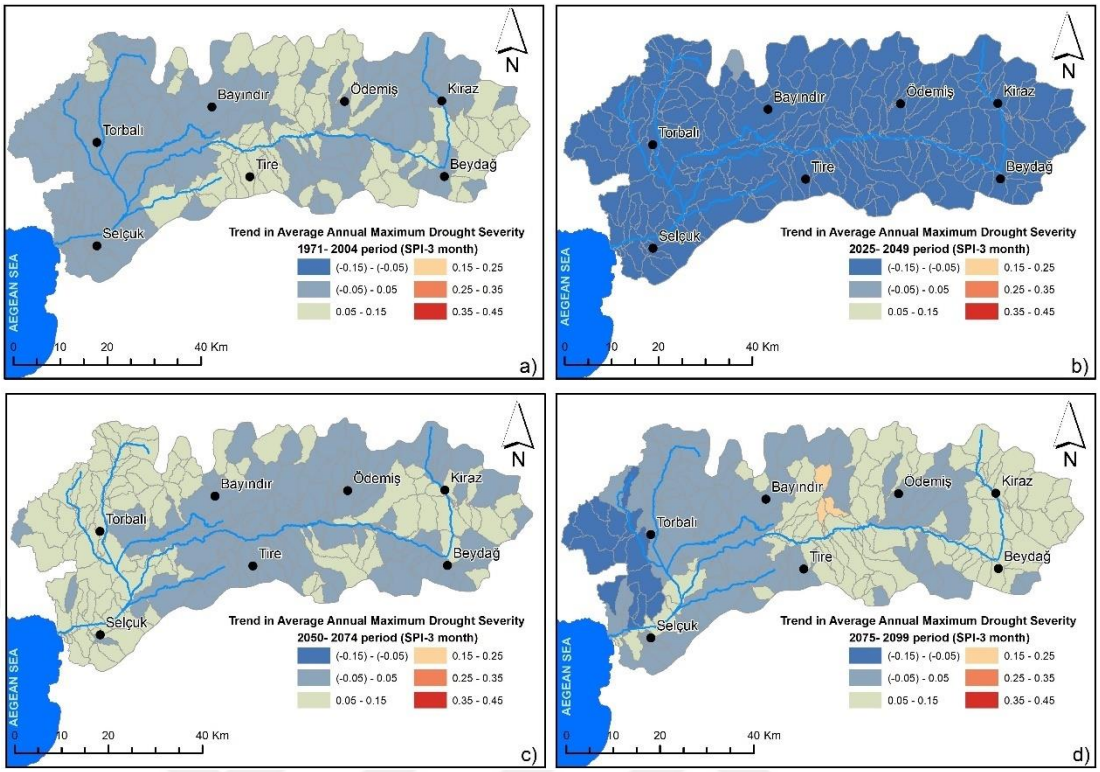


Figure 4.47 Trend in average annual maximum drought severity of SPI-3 month for the period a)1971-2004, b)2025-2049, c)2050-2074, d)2075-2099.

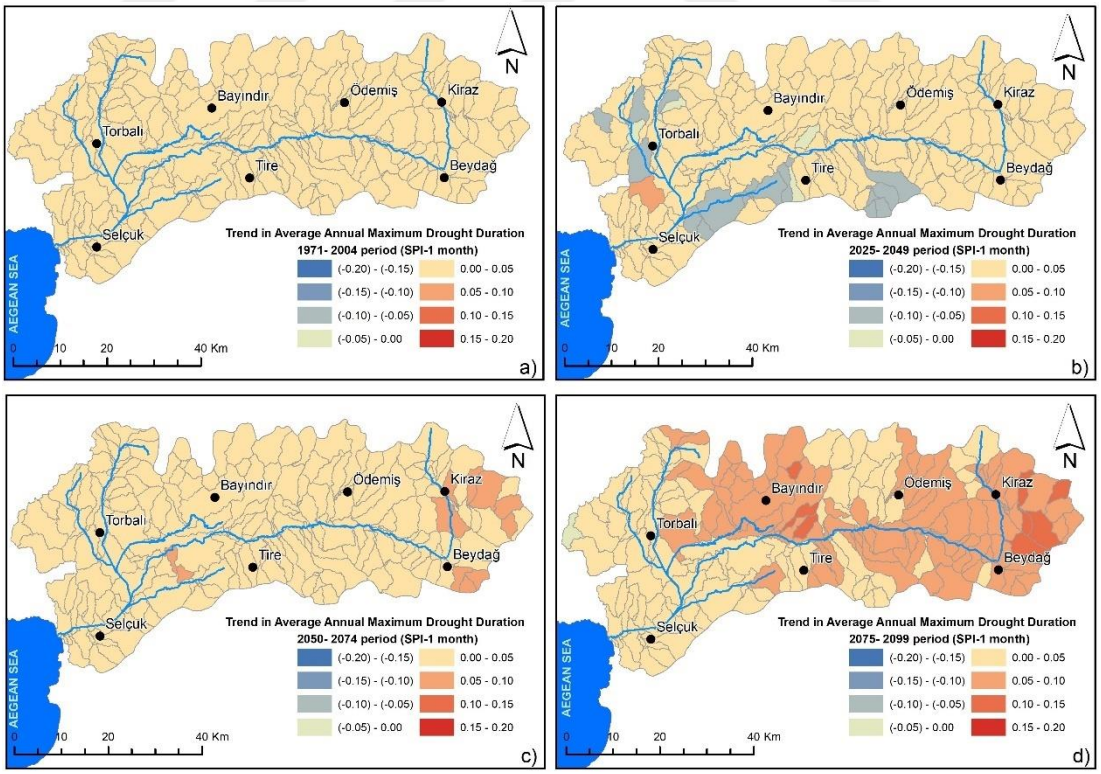


Figure 4.48 Trend in average annual maximum drought duration of SPI-1 month for the period a)1971-2004, b)2025-2049, c)2050-2074, d)2075-2099.

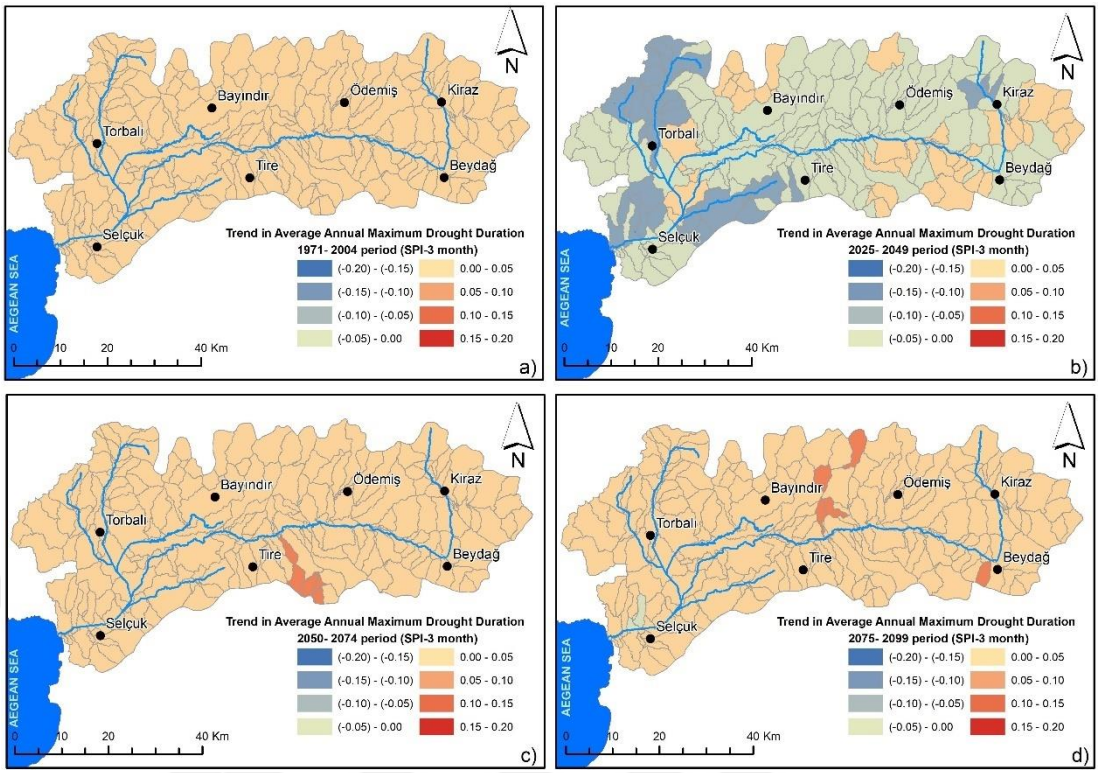


Figure 4.49 Trend in average annual maximum drought duration of SPI-3 month for the period a)1971-2004, b)2025-2049, c)2050-2074, d)2075-2099.

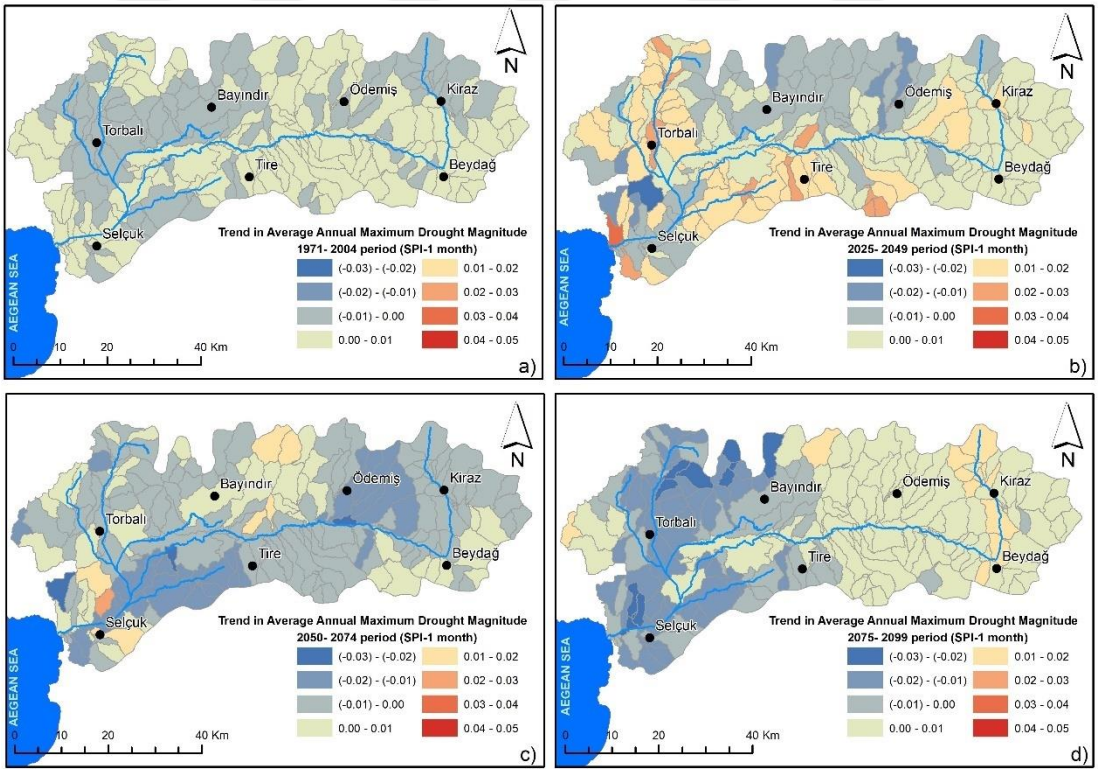


Figure 4.50 Trend in average annual maximum drought magnitude of SPI-1 month for the period a)1971-2004, b)2025-2049, c)2050-2074, d)2075-2099.

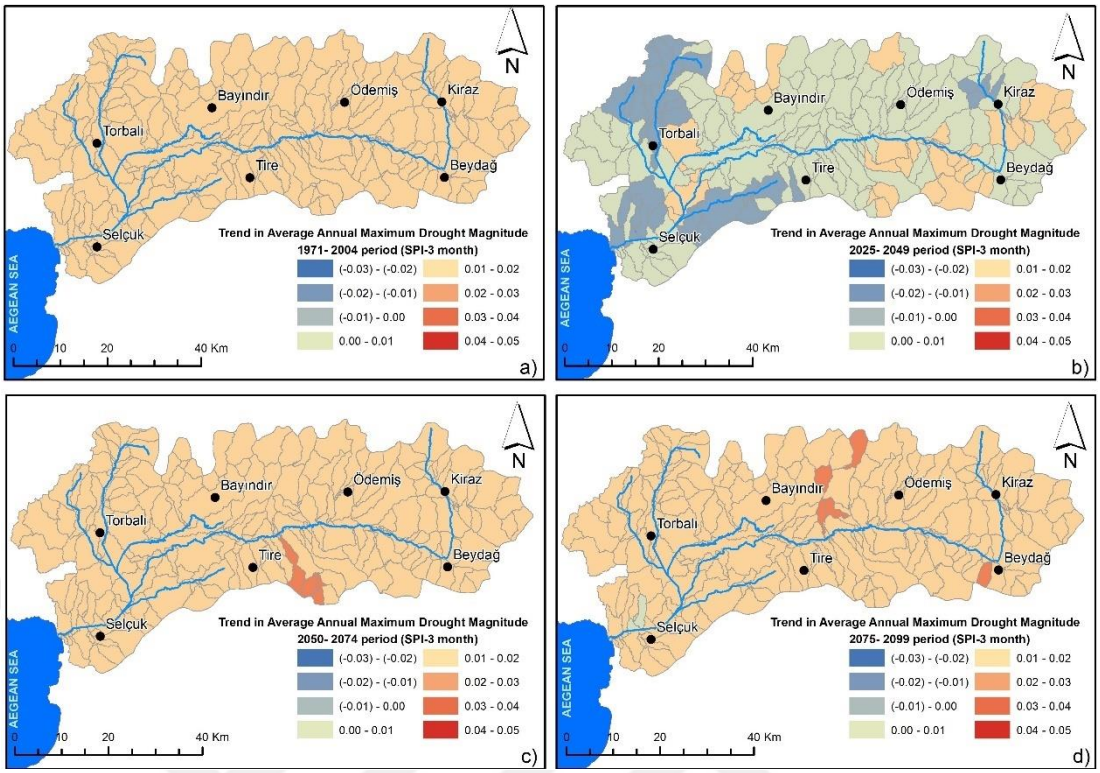


Figure 4.51 Trend in average annual maximum drought magnitude of SPI-3 month for the period a)1971-2004, b)2025-2049, c)2050-2074, d)2075-2099.

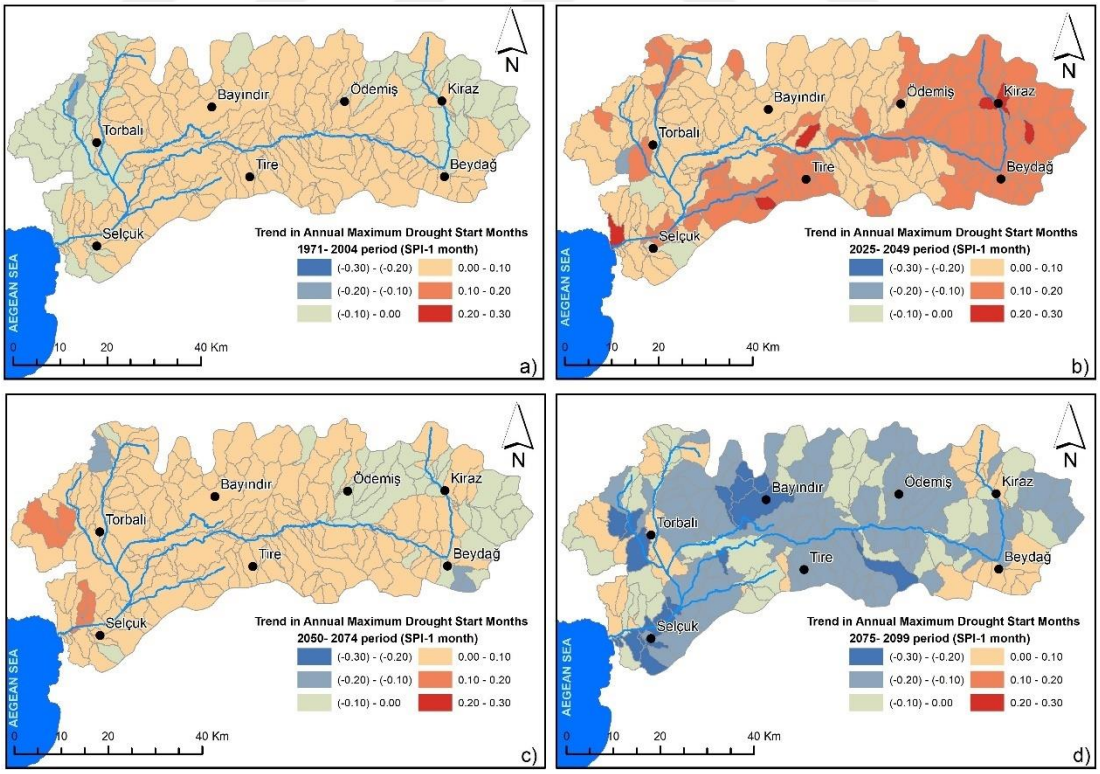


Figure 4.52 Trend in annual maximum drought start month of SPI-1 month for the period a)1971-2004, b)2025-2049, c)2050-2074, d)2075-2099.

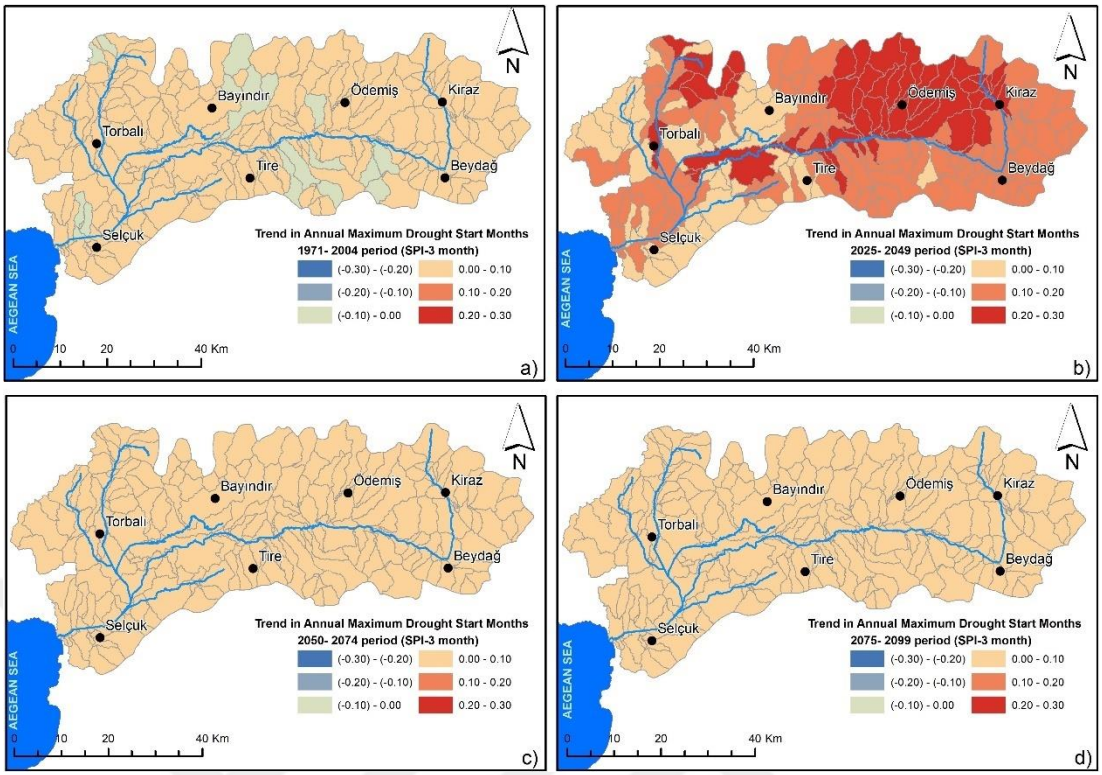


Figure 4.53 Trend in annual maximum drought start month of SPI-3 month for the period a)1971-2004, b)2025-2049, c)2050-2074, d)2075-2099.

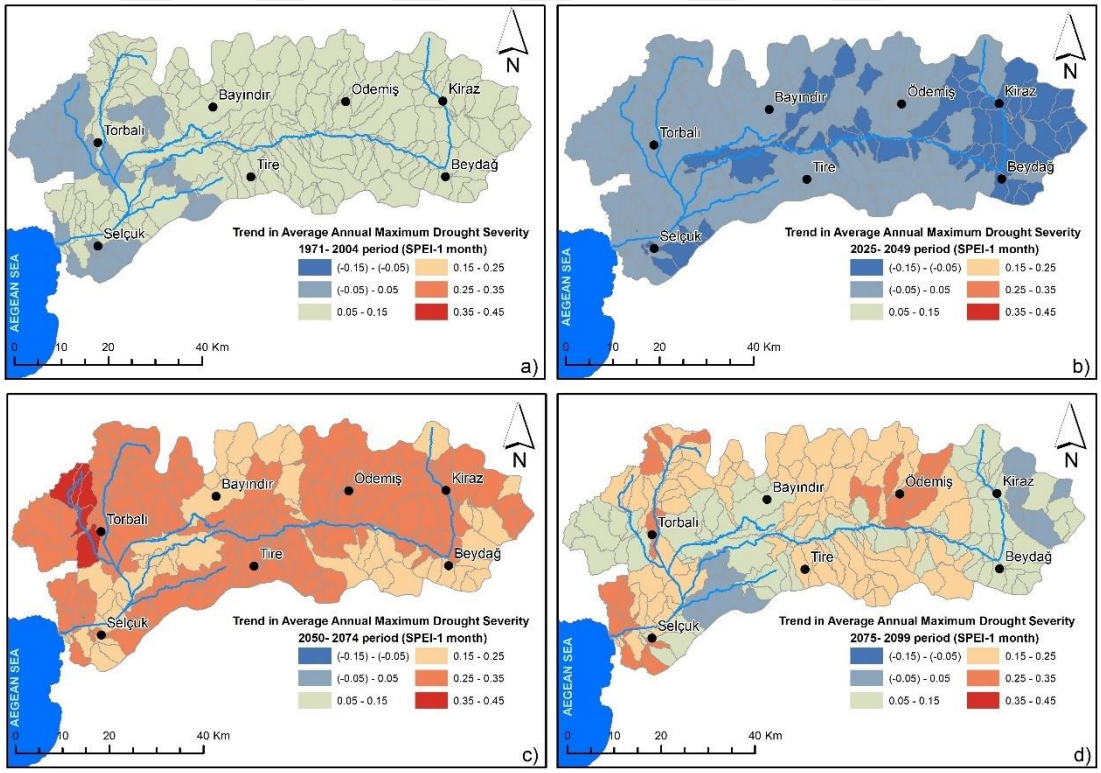


Figure 4.54 Trend in average annual maximum drought severity of SPEI-1 month for the period a)1971-2004, b)2025-2049, c)2050-2074, d)2075-2099.

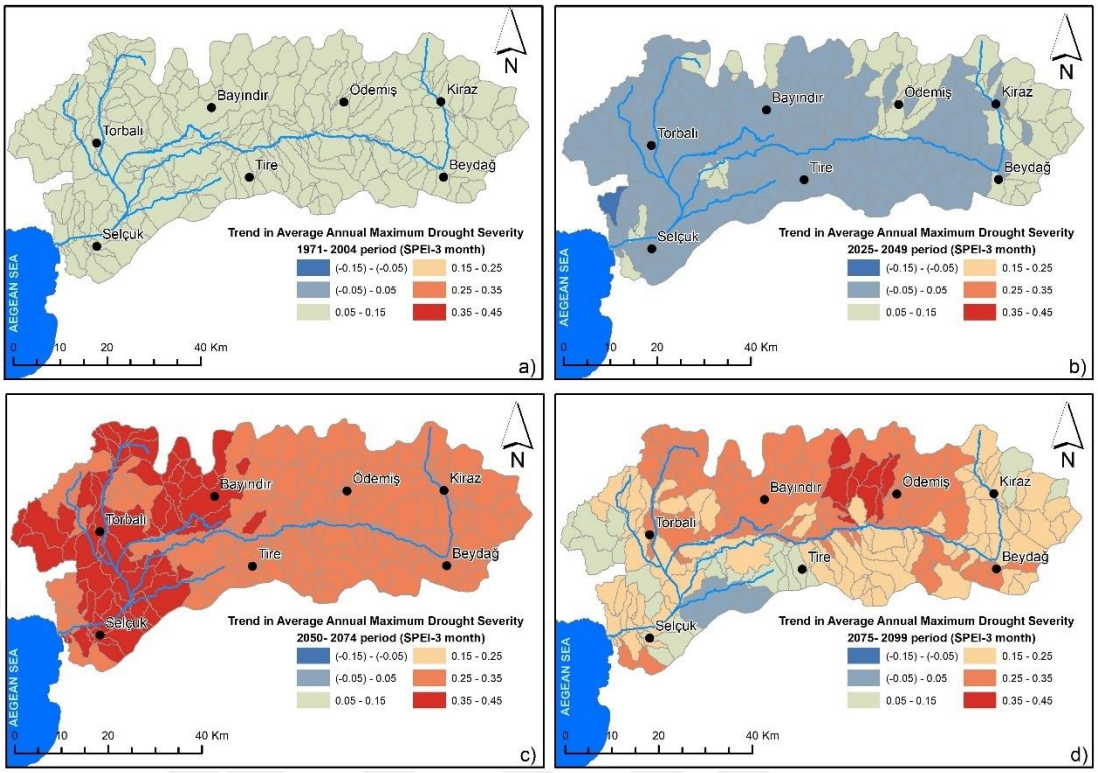


Figure 4.55 Trend in average annual maximum drought severity of SPEI-3 month for the period a)1971-2004, b)2025-2049, c)2050-2074, d)2075-2099.

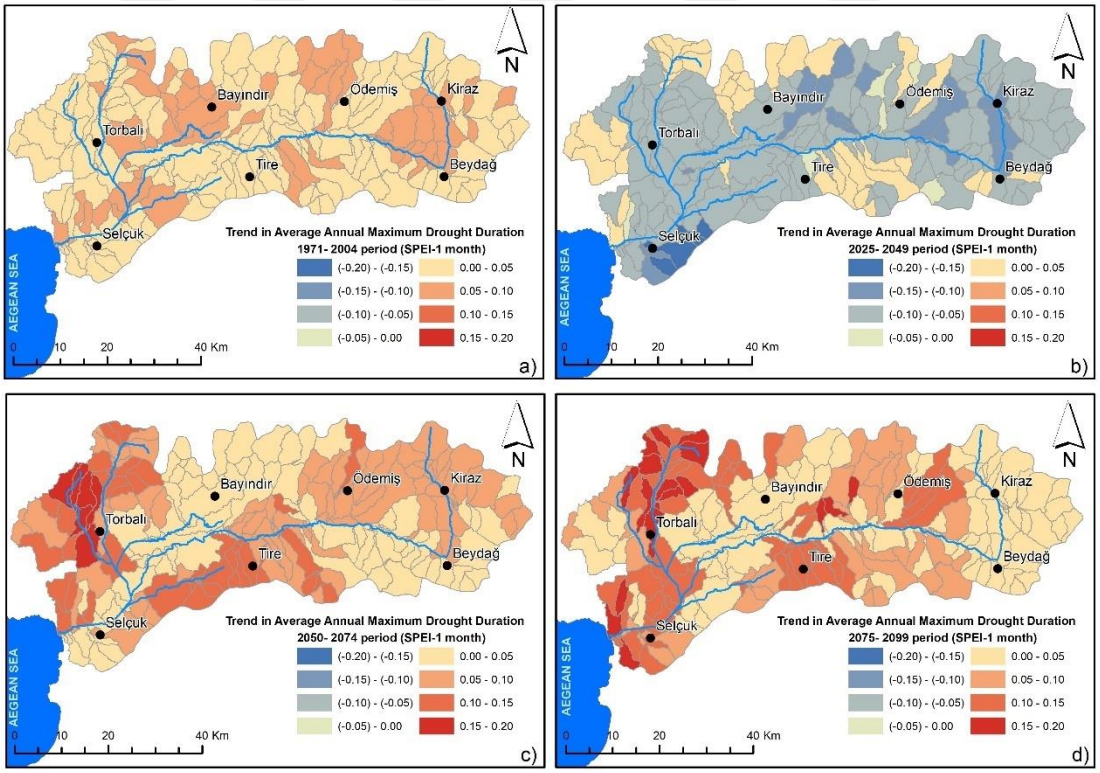


Figure 4.56 Trend in average annual maximum drought duration of SPEI-1 month for the period a)1971-2004, b)2025-2049, c)2050-2074, d)2075-2099.

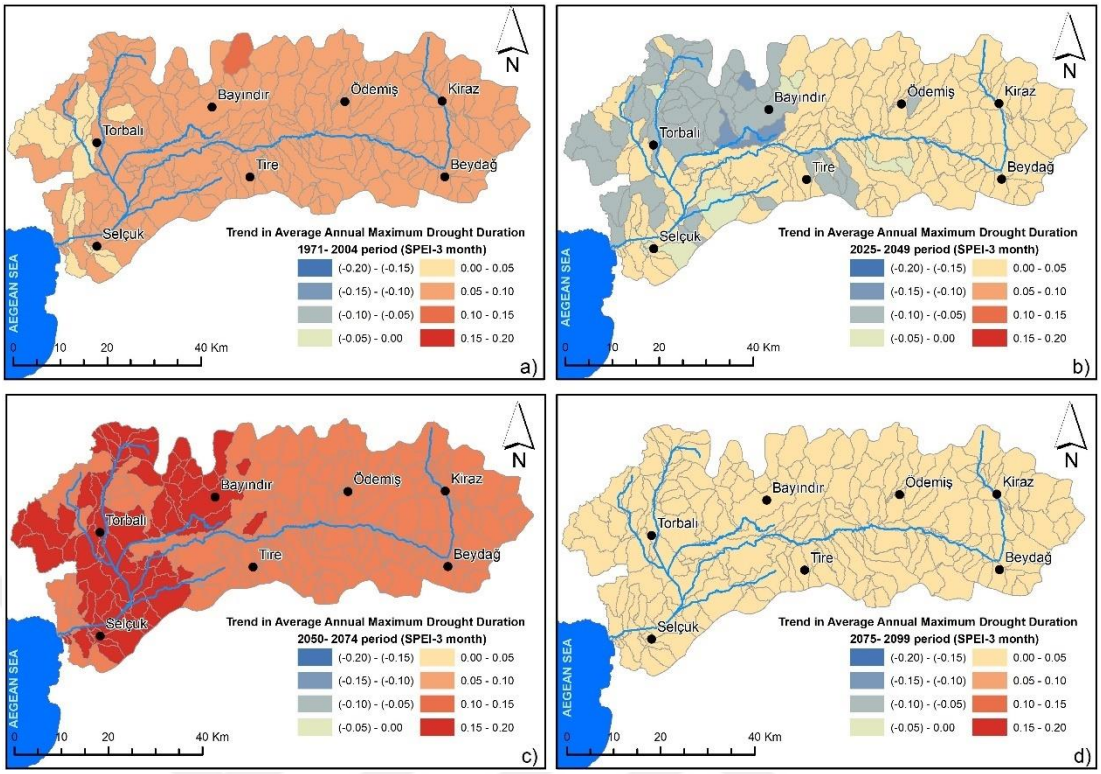


Figure 4.57 Trend in average annual maximum drought duration of SPEI-3 month for the period a)1971-2004, b)2025-2049, c)2050-2074, d)2075-2099.

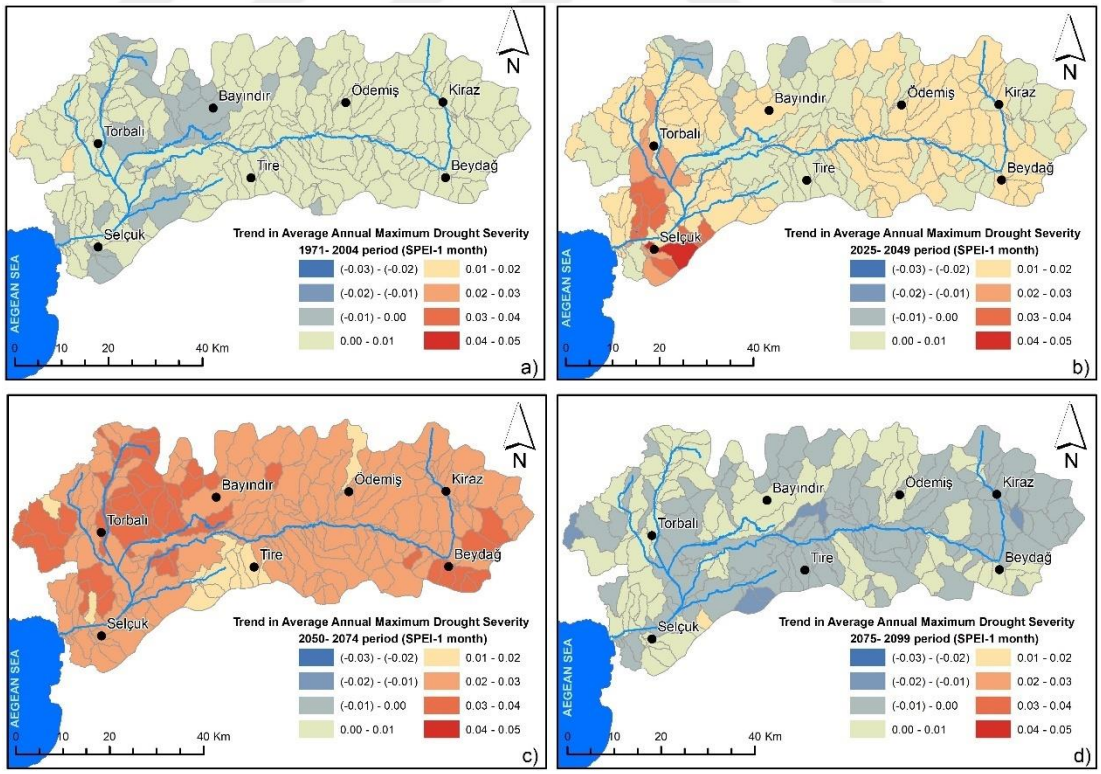


Figure 4.58 Trend in average annual maximum drought magnitude of SPEI-1 month for the period a)1971-2004, b)2025-2049, c)2050-2074, d)2075-2099.

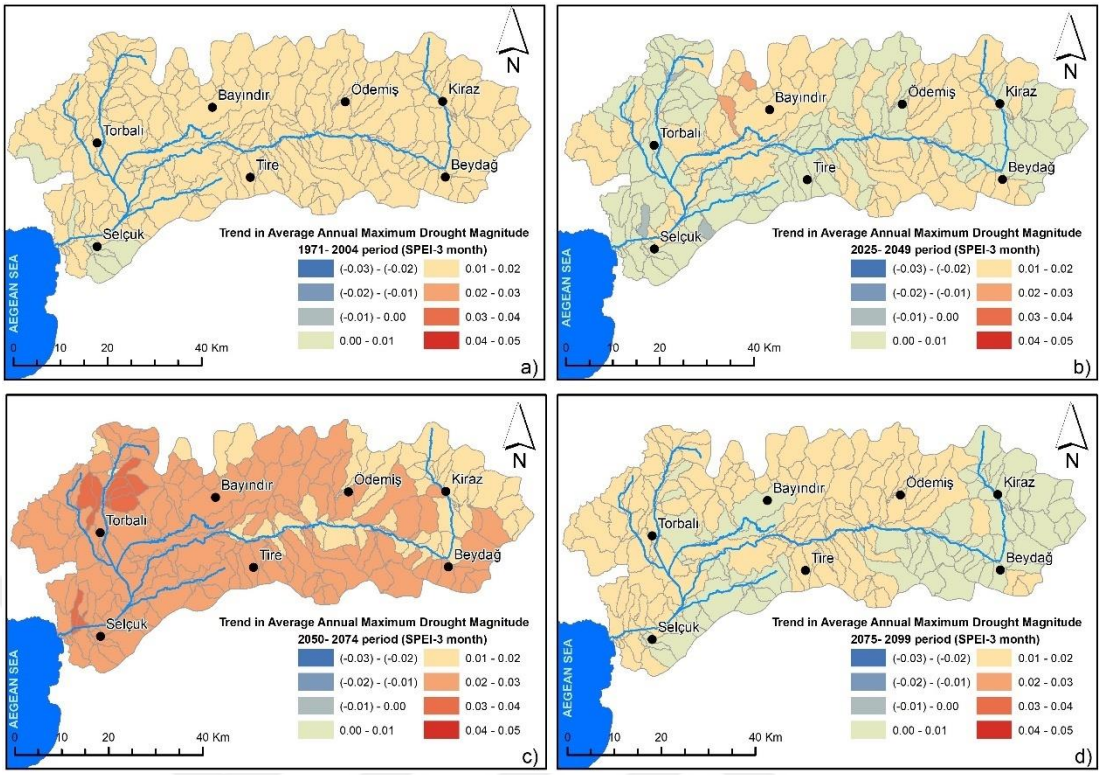


Figure 4.59 Trend in average annual maximum drought magnitude of SPEI-3 month for the period a)1971-2004, b)2025-2049, c)2050-2074, d)2075-2099.

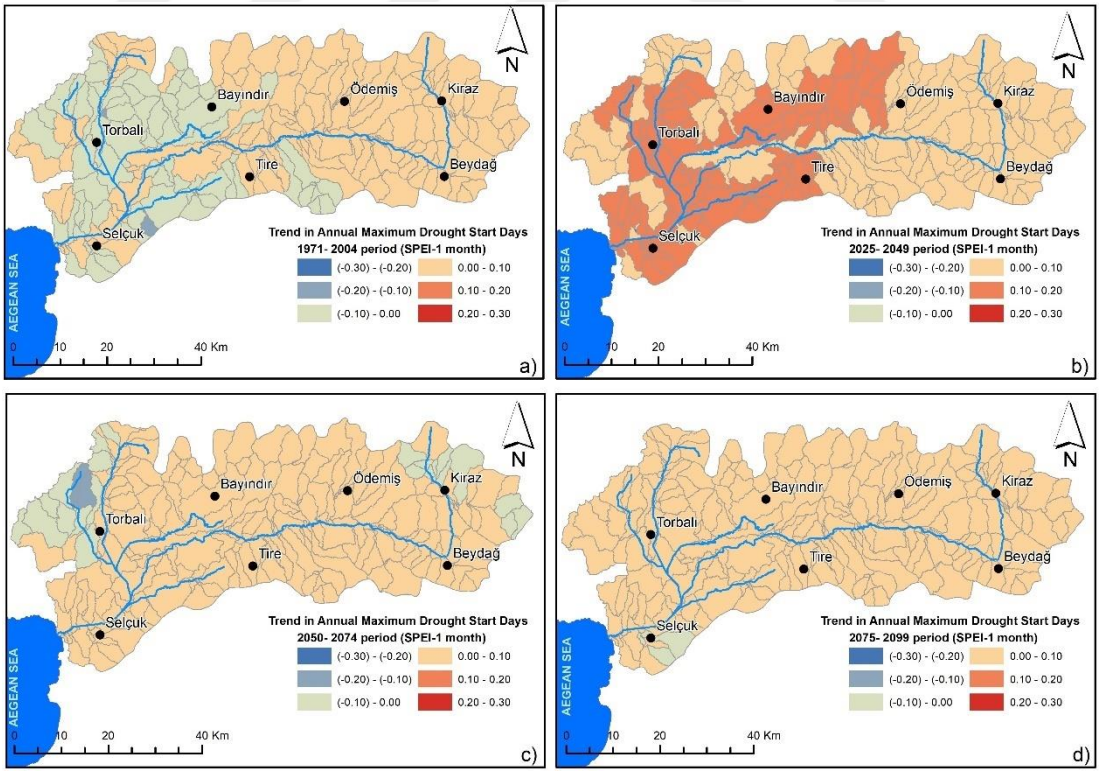


Figure 4.60 Trend in annual maximum drought start months of SPEI-1 month for the period a)1971-2004, b)2025-2049, c)2050-2074, d)2075-2099.

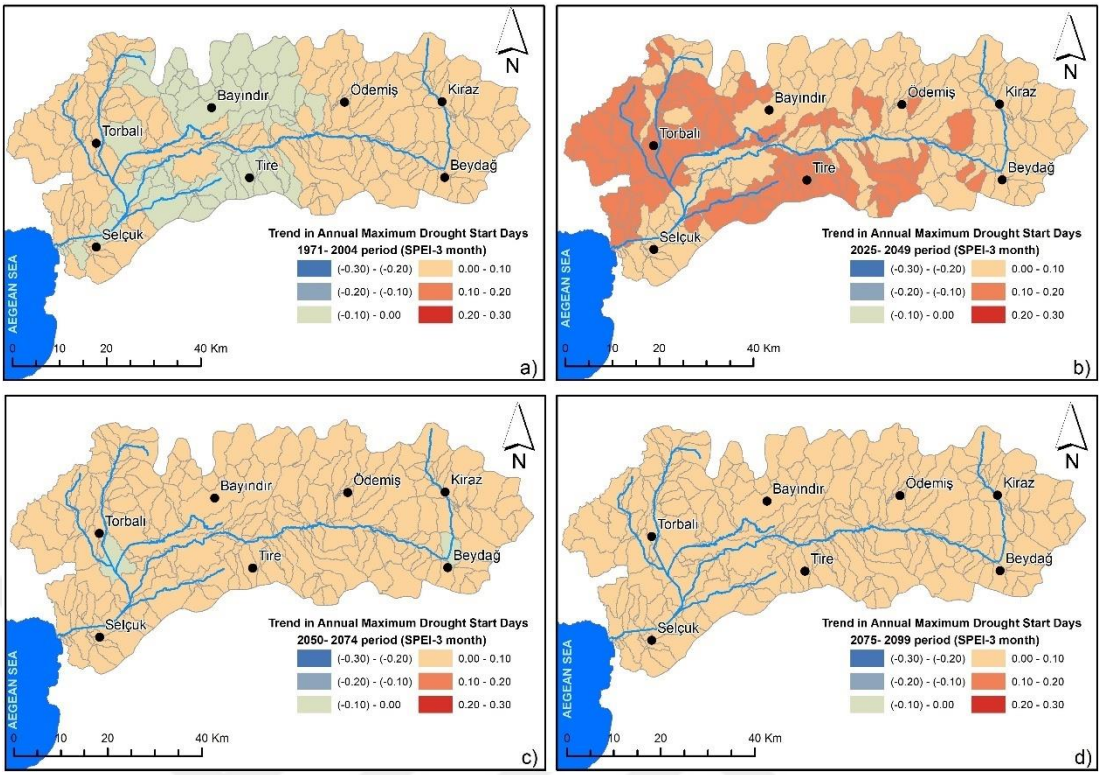


Figure 4.61 Trend in annual maximum drought start months of SPEI-3 month for the period a)1971-2004, b)2025-2049, c)2050-2074, d)2075-2099.

4.3.2.2 Daily Drought Maps

Average annual maximum drought severities, durations, magnitudes and median days of the drought start values for the observed period were calculated and mapped for the series of SPI-30 day SPI-90 day (Figure 4.62- Figure 4.69). Additionally, Appendices provide maps illustrating the number of drought events for various conditions, encompassing moderate, severe, and extreme categories (see Figure Ap.71 to Figure Ap.78).

The change map of annual maximum drought severities derived from SPI-30 day and SPI-90-day series from the baseline period to the climate-induced scenario futures are given in Figure 4.62 and Figure 4.63, respectively. The severity figures based on daily data attain higher values compared to the annual maximum severities calculated from monthly index definitions. This is because the aggregations include daily drought index values more frequently. Drought severities estimated based on SPI-3 month (or SPI-90 day) values indicate more rapid changes in larger quantities. Although it is not

expected to occur that rapidly as seen in the predictions through the SPEI index based on monthly meteorological variables, shifts to earlier times are still estimated considering the start times of annual maximum drought events.

Upon analysis of the annual maximum drought periods, it is evident that these periods will extend from the reference period to the distant future period, reaching approximately 145-155 days. Furthermore, it is observed that the duration of drought periods will be greater in the upstream region of the basin, specifically in the eastern part (Figure 4.64 and Figure 4.65). When analyzing the annual maximum drought magnitudes derived from the SPI-30 day series, the basin consistently experiences moderate drought across all time periods. However, when evaluating the annual maximum drought magnitudes calculated from the SPI-90 day series, the basin shows drought magnitudes that suggest a normal condition throughout all time periods (Figure 4.66 and Figure 4.67). While it may appear that there is no drought in this situation, this can be attributed to the diminished influence of drought severity caused by prolonged periods of drought. Analyzing the maps generated from the SPI-30 day series, which indicate the initiation of drought, reveals that in the reference period, drought onset occurred in May. However, in the far future period, particularly in the upstream region, the drought initiation month shifted to March, with an anticipated start in February (Figure 4.68). In the case of SPI-90 day series, the onset month for drought is projected to be January in the far future period (Figure 4.69).

Regarding the trends in average annual maximum drought severities and durations, the basin exhibited a predominantly decreasing trend during the period 2025-2049 for SPI-90 day. Conversely, a dominant increasing trend was observed for the period 2075-2099 for SPI-90 day. Additionally, for the period 2025-2049, there were increasing trend in annual maximum drought start month for SPI-30 day series. Upon examining the annual maximum drought severity maps obtained from the SPI-30 day and SPI-90 day series, we observe a decline in the reference period, while an increased trend is appears in other periods (Figure 4.70 - Figure 4.71). When drought durations are assessed, a similar situation is observed in terms of drought severity (Figure 4.72 and Figure 4.73). There are also trends in annual maximum drought

magnitudes (Figure 4.74 and Figure 4.75). A decreasing trend is observed in the onset months of drought, indicating that drought will occur in earlier months (Figure 4.76 and Figure 4.77).

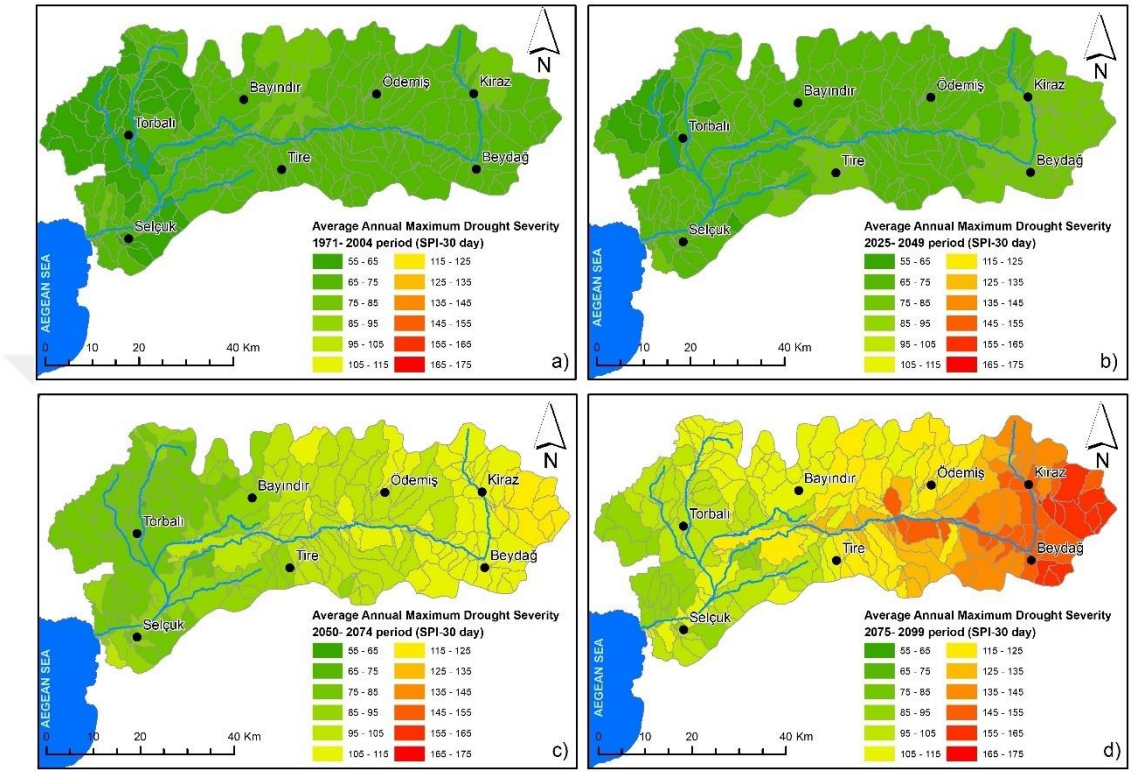


Figure 4.62 Average annual maximum drought severity of SPI-30 day for the period a)1971-2004, b)2025-2049, c)2050-2074, d)2075-2099.

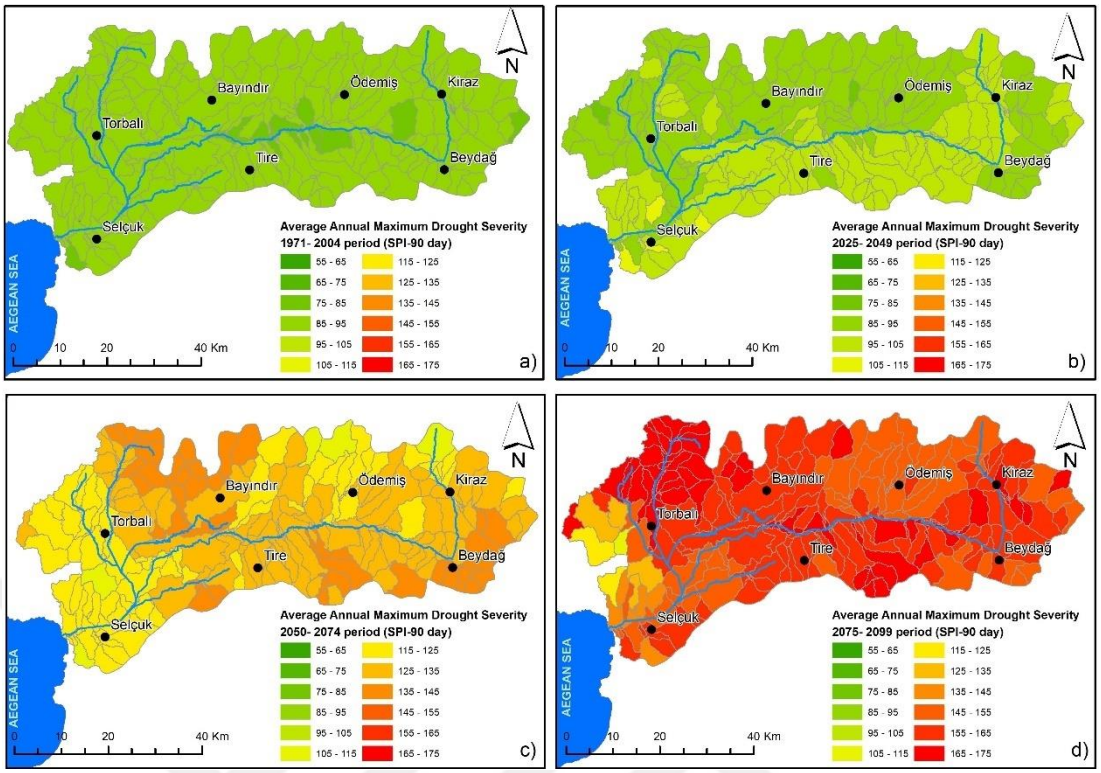


Figure 4.63 Average annual maximum drought severity of SPI-90 day for the period a)1971-2004, b)2025-2049, c)2050-2074, d)2075-2099.

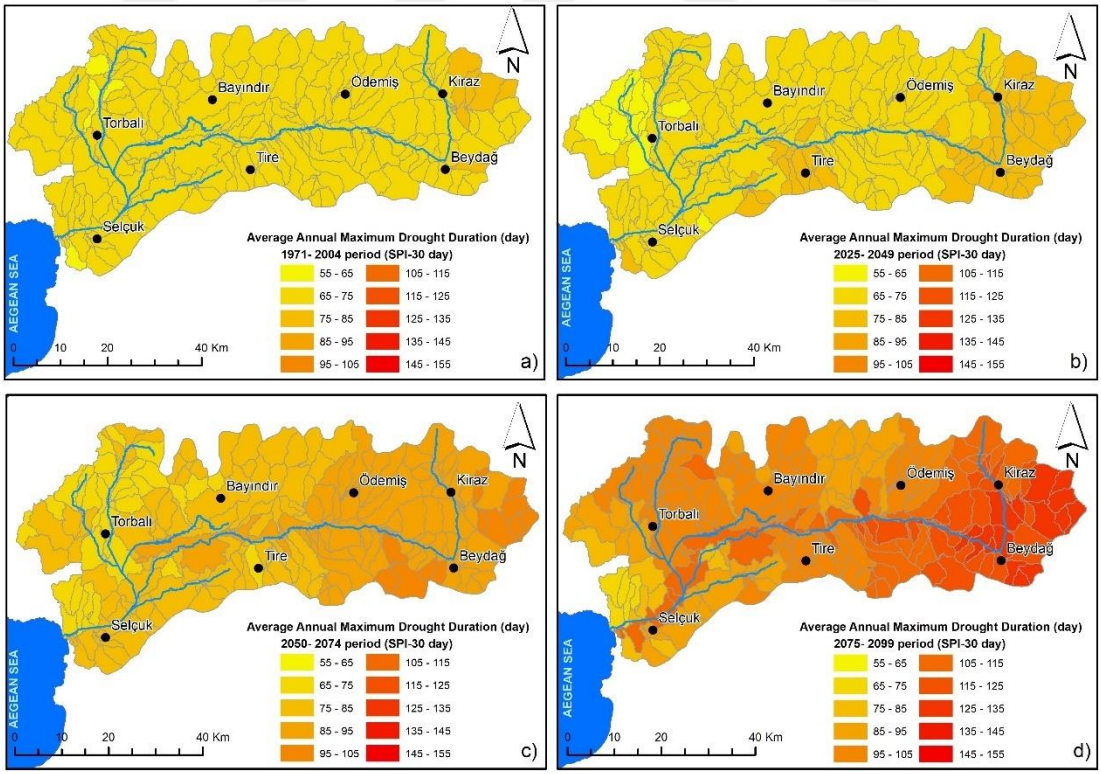


Figure 4.64 Average annual maximum drought duration of SPI-30 day for the period a)1971-2004, b)2025-2049, c)2050-2074, d)2075-2099.

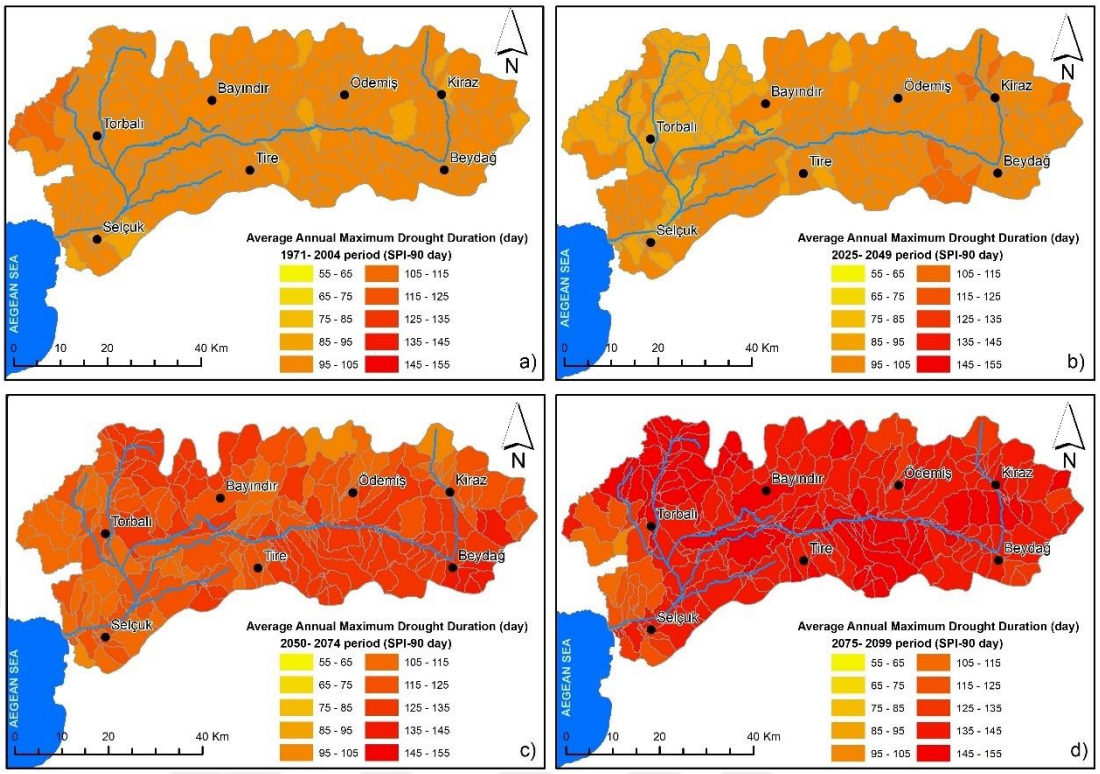


Figure 4.65 Average annual maximum drought duration of SPI-90 day for the period a)1971-2004, b)2025-2049, c)2050-2074, d)2075-2099.

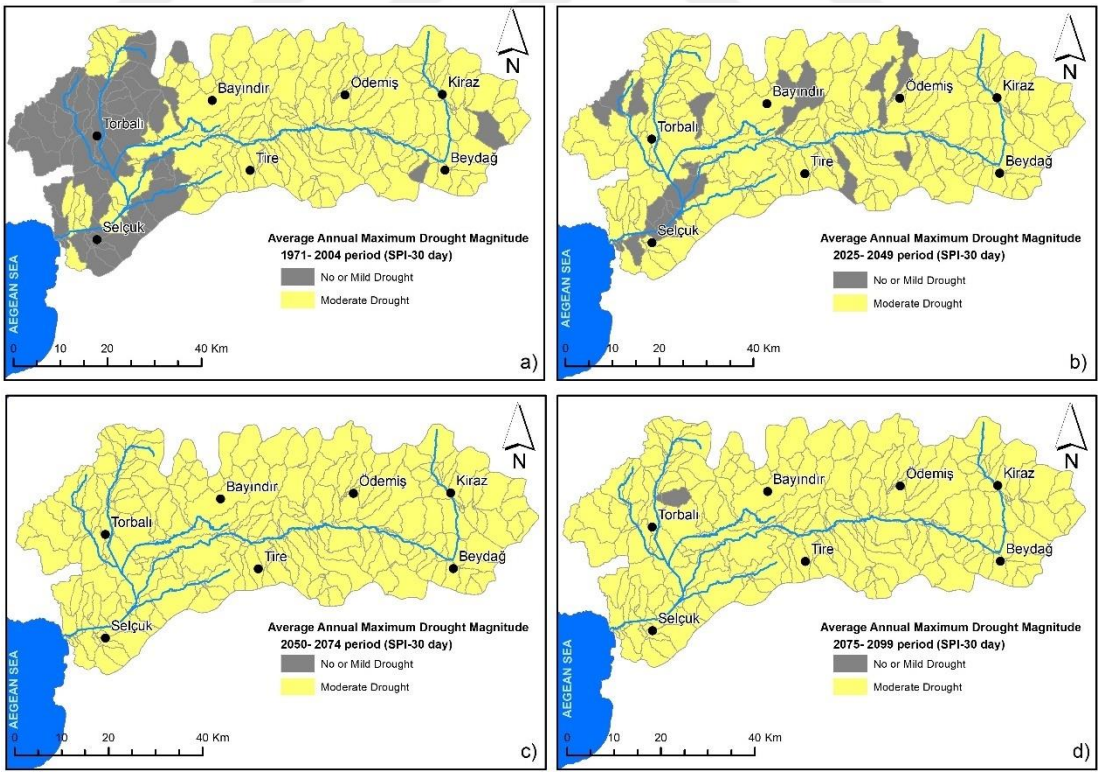


Figure 4.66 Average annual maximum drought magnitude of SPI-30 day for the period a)1971-2004, b)2025-2049, c)2050-2074, d)2075-2099.

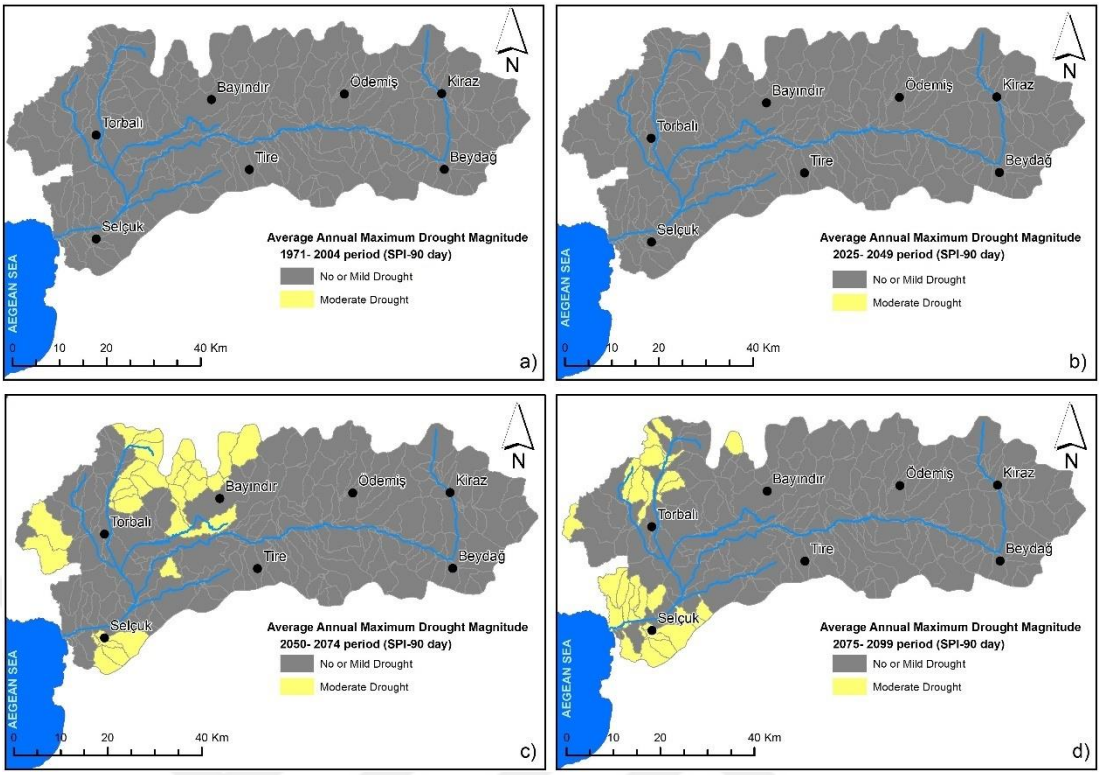


Figure 4.67 Average annual maximum drought magnitude of SPI-90 day for the period a)1971-2004, b)2025-2049, c)2050-2074, d)2075-2099.

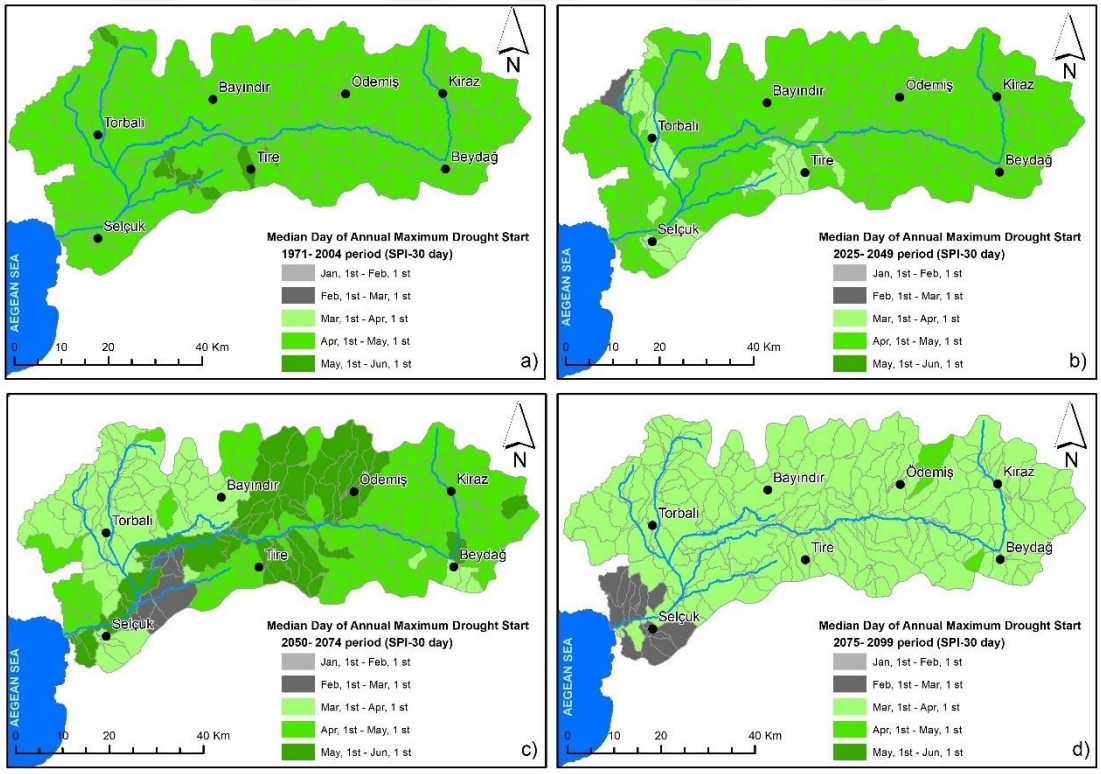


Figure 4.68 Median day of annual drought start of SPI-30 day for the period a)1971-2004, b)2025-2049, c)2050-2074, d)2075-2099.

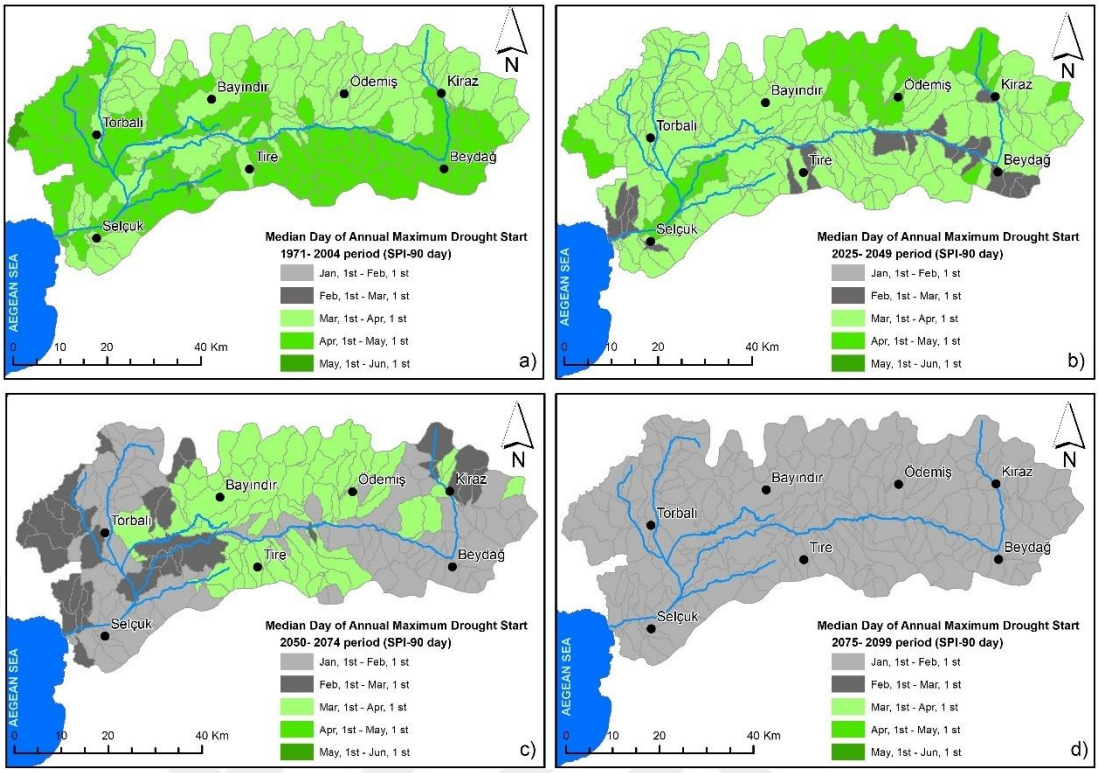


Figure 4.69 Median day of annual drought start of SPI-90 day for the period a)1971-2004, b)2025-2049, c)2050-2074, d)2075-2099.

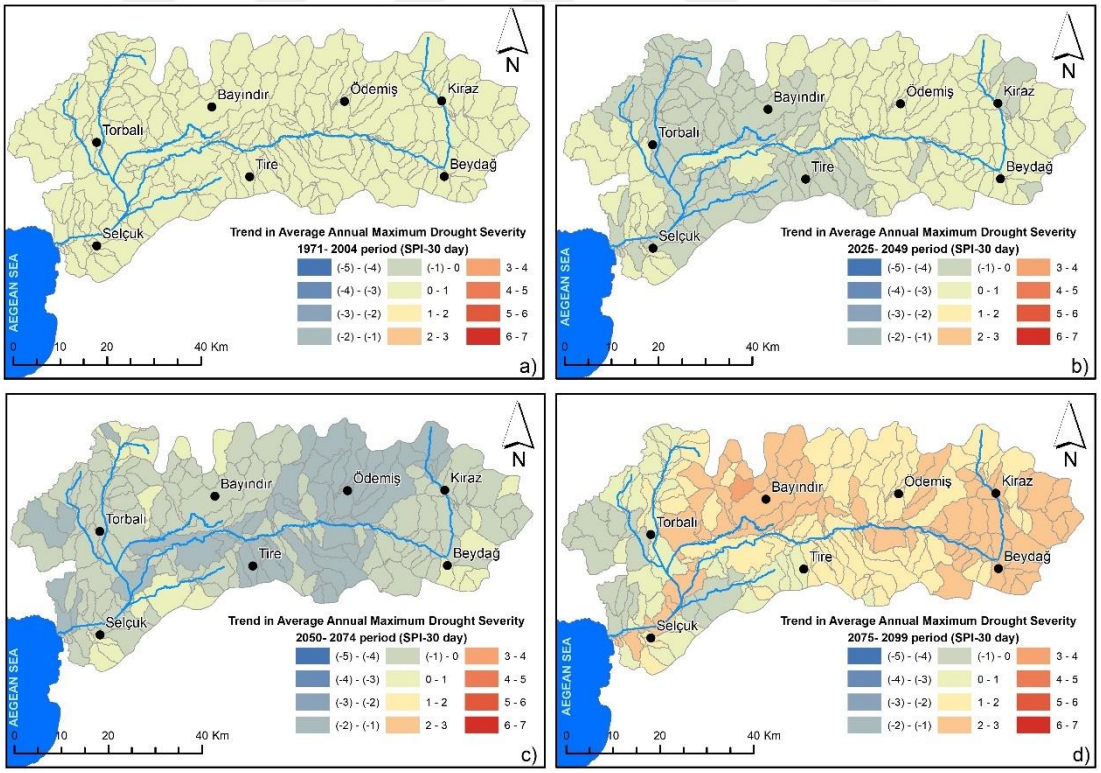


Figure 4.70 Trend in average annual maximum drought severity of SPI-30 day for the period a)1971-2004, b)2025-2049, c)2050-2074, d)2075-2099.

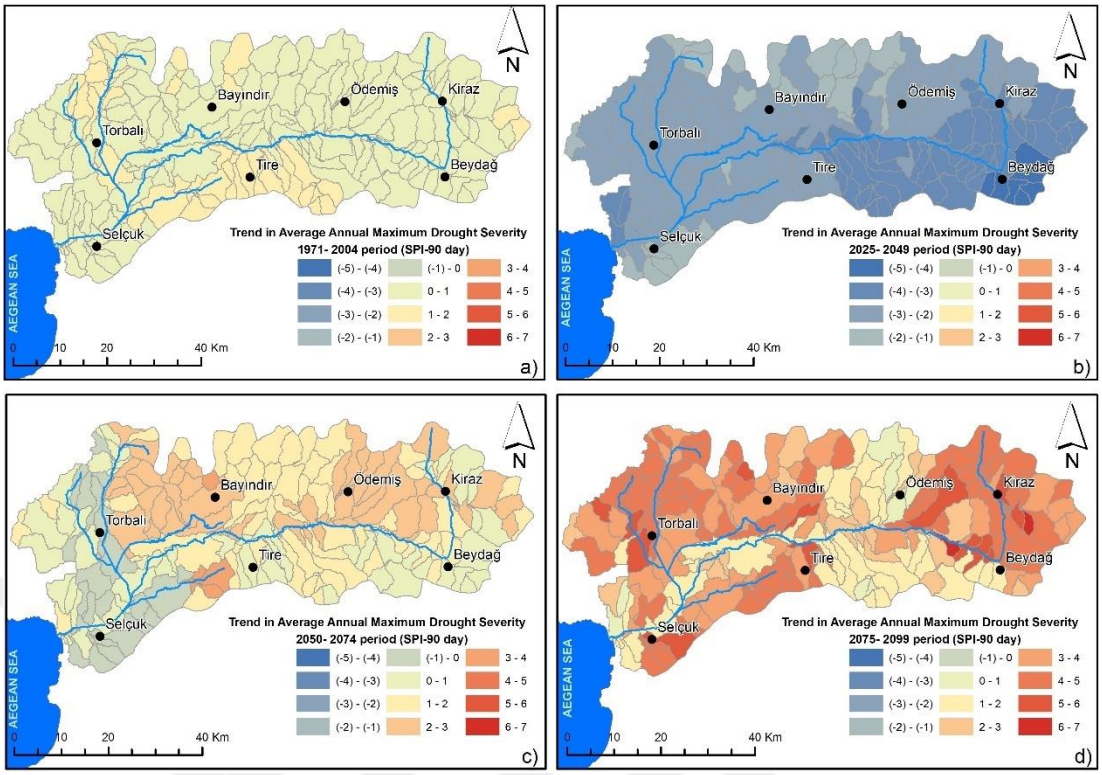


Figure 4.71 Trend in average annual maximum drought severity of SPI-90 day for the period a)1971-2004, b)2025-2049, c)2050-2074, d)2075-2099.

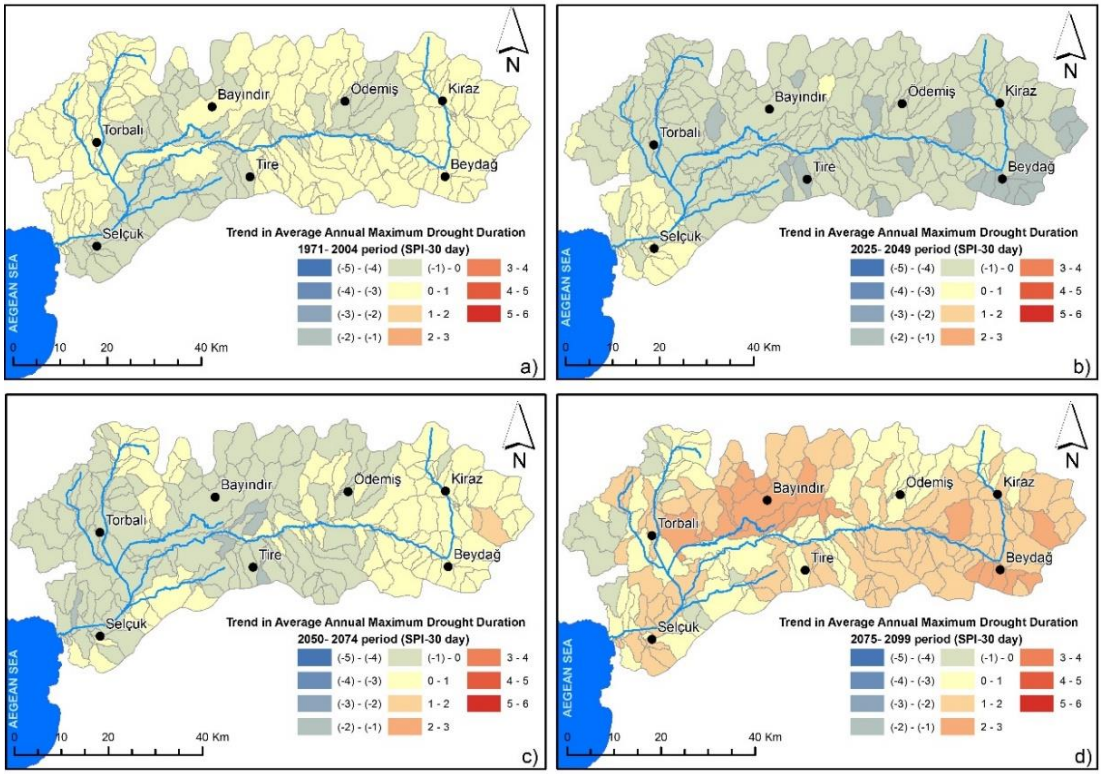


Figure 4.72 Trend in average annual maximum drought duration of SPI-30 day for the period a)1971-2004, b)2025-2049, c)2050-2074, d)2075-2099.

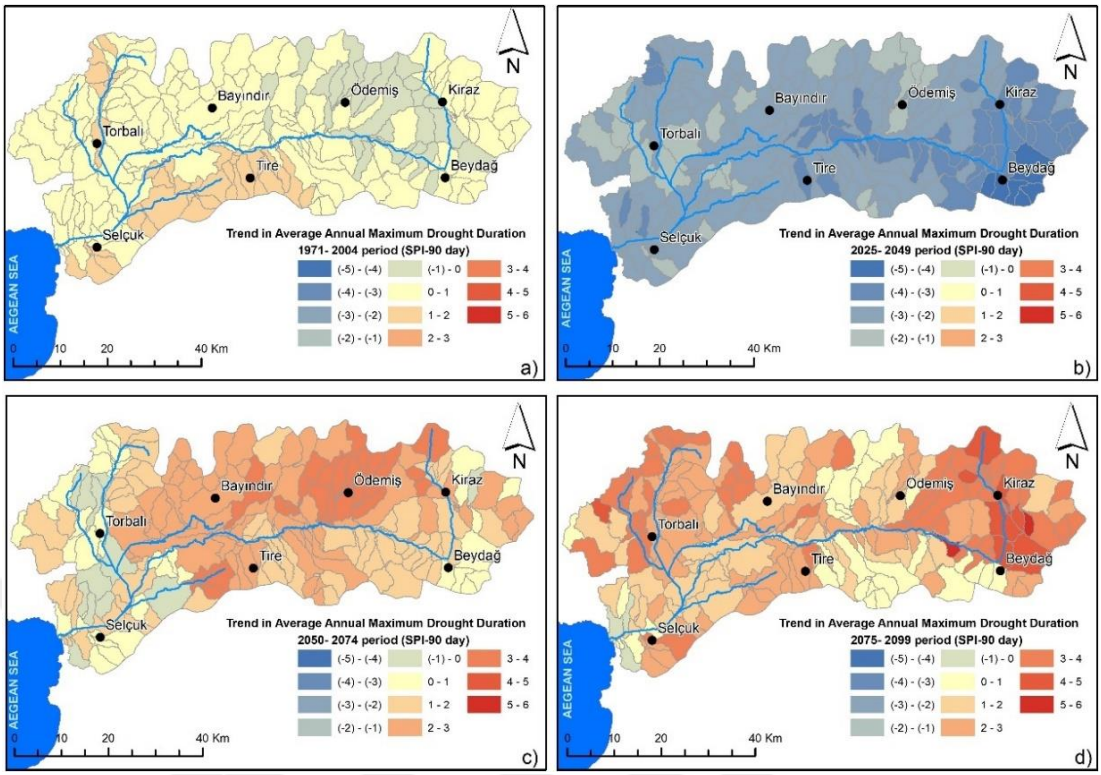


Figure 4.73 Trend in average annual maximum drought duration of SPI-90 day for the period a)1971-2004, b)2025-2049, c)2050-2074, d)2075-2099.

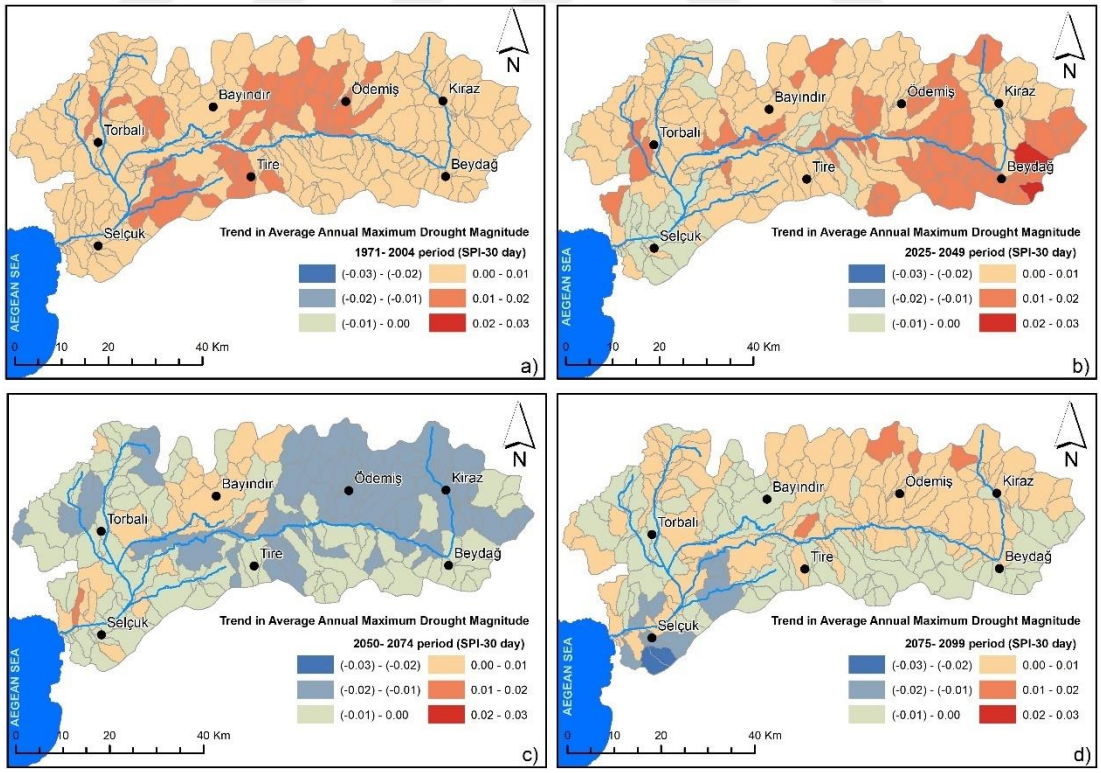


Figure 4.74 Trend in average annual maximum drought magnitude of SPI-30 day for the period a)1971-2004, b)2025-2049, c)2050-2074, d)2075-2099.

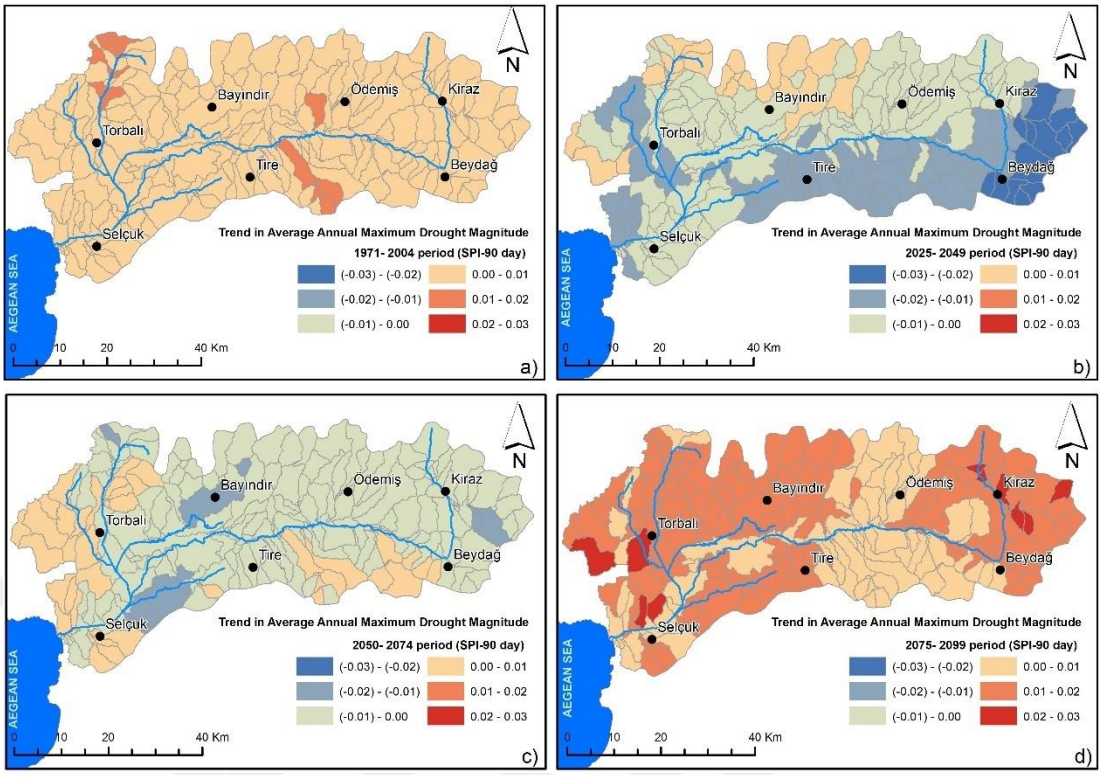


Figure 4.75 Trend in average annual maximum drought magnitude of SPI-90 day for the period a)1971-2004, b)2025-2049, c)2050-2074, d)2075-2099.

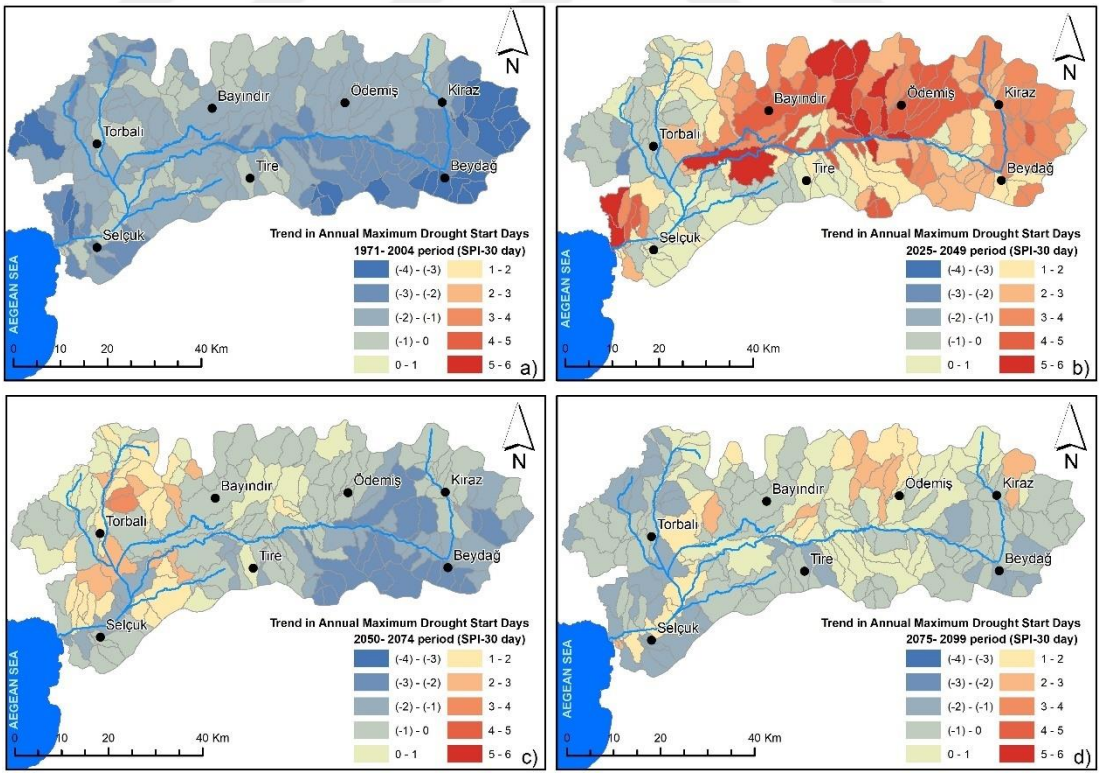


Figure 4.76 Trend in annual maximum drought start days of SPI-30 day for the period a)1971-2004, b)2025-2049, c)2050-2074, d)2075-2099.

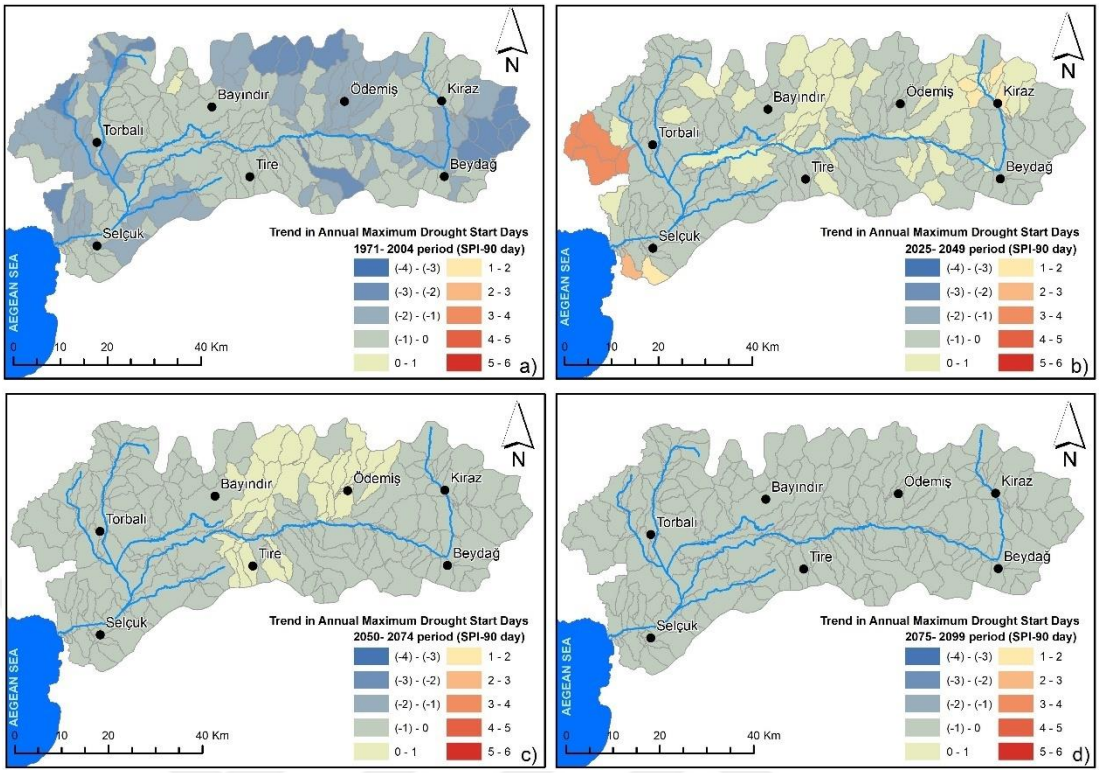


Figure 4.77 Trend in annual maximum drought start days of SPI-90 day for the period a)1971-2004, b)2025-2049, c)2050-2074, d)2075-2099.

4.3.3 Drought Analysis by Using SWAT Model Outputs

The Küçük Menderes Basin was modeled for both reference and future periods utilizing coupled VIC (Chapter 4.1) and SWAT (Chapter 4.2) models. The model outputs, including streamflow and actual evapotranspiration, were derived for each subbasin. Additionally, averaged precipitation and potential evapotranspiration values for each subbasin were obtained from the model outputs. Subsequently, pivotal hydrological indices, namely Standardized Precipitation Index (SPI), Standardized Precipitation Evapotranspiration Index (SPEI), and Standardized Stream Flow Index (SSFI), were computed for each subbasin. The indices were calculated over varying time intervals ranging from 1 month to 12 months. Furthermore, the SPEI was estimated separately with respect to potential evapotranspiration (PET) and actual evapotranspiration (ET_a). This comprehensive modeling approach and drought index calculation strategy contribute to a detailed understanding of the hydrological dynamics in the Küçük Menderes Basin across different temporal scales.

In this investigation, the correlations among SPI, SPEI (with ET_a and PET, individually), and SSFI were systematically examined. The study aimed to evaluate the compatibility of various drought indices, examining potential interrelationships, and providing insights into their collective usefulness in describing drought situations. Table 4.9 clearly demonstrates that as the period is extended, there is a noticeable increase in the correlation between the indices. When 12-month drought indices are compared, the highest correlation is observed between SPI and SPEI- ET_a. However, SSFI and SPEI-PET demonstrated the higher correlation than SPEI-ET_a. SSFI showed the highest correlation between SPI.

Table 4.9 The correlations between SPI, SPEI and SSFI drought indices.

Drought Indices	*Statistics*	*1-month*	*3-month*	*6-month*	*12-month*
SPI – SPEI-ET_a	NSE	0.73	0.76	0.87	0.94
	R^2	0.75	0.77	0.88	0.94
SPI – SPEI-PET	NSE	0.76	0.79	0.84	0.90
	R^2	0.78	0.80	0.84	0.90
SPEI-ET_a – SPEI-PET	NSE	0.76	0.79	0.87	0.90
	R^2	0.78	0.81	0.87	0.91
SPI - SSFI	NSE	-0.27	-0.07	0.30	0.70
	R^2	0.10	0.19	0.42	0.72
SSFI – SPEI-ET_a	NSE	-0.65	-0.27	0.16	0.57
	R^2	0.07	0.17	0.38	0.64
SSFI – SPEI-PET	NSE	-0.62	-0.26	0.26	0.70
	R^2	0.08	0.18	0.43	0.74

Drought Mapping: Average annual maximum drought severity, average annual maximum drought duration, average annual maximum drought magnitude were mapping to demonstrate the droughts with modelled series for the reference (1985-2012), near future (2025-2049), middle future (2050-2074) and far future period (2075-2099) and given by Figure 4.78-4.141.

4.3.3.1 Drought Maps Generated Using SPI

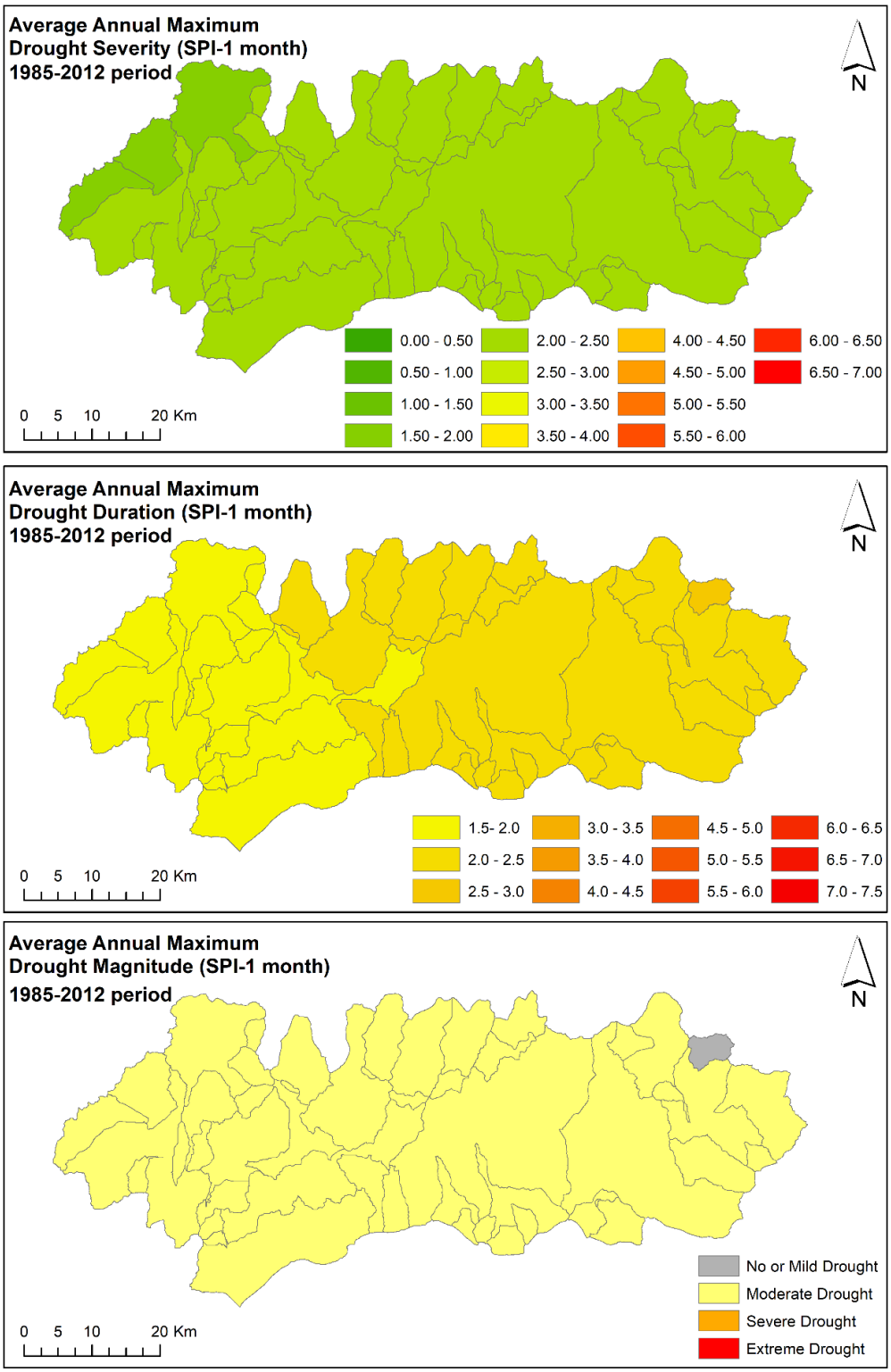


Figure 4.78 Maps obtained using SPI-1 month series for the reference period: a) average annual maximum drought severity, b) duration and c) magnitude.

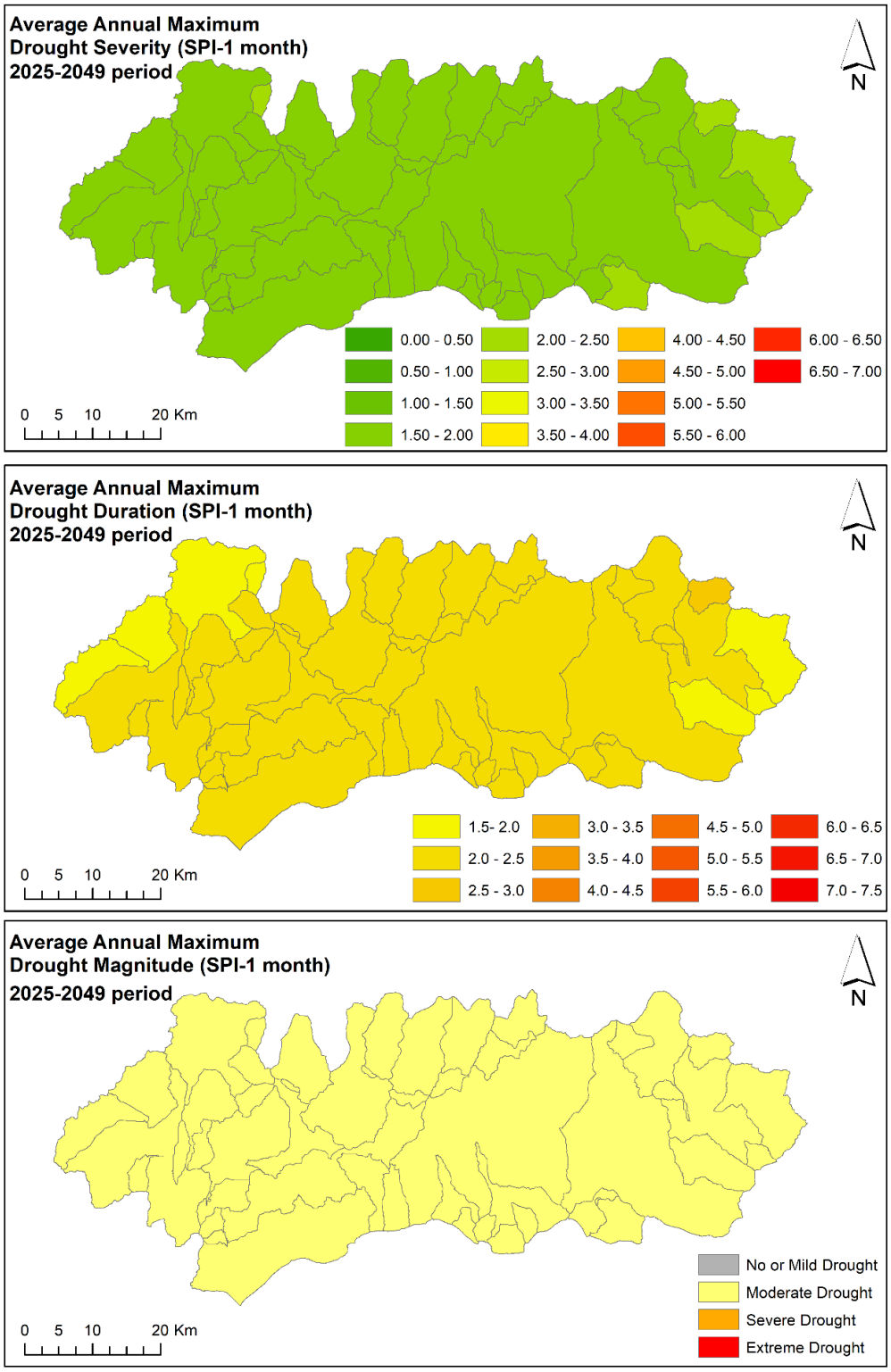


Figure 4.79 Maps obtained using SPI-1 month series for the near future period: a) average annual maximum drought severity, b) duration and c) magnitude.

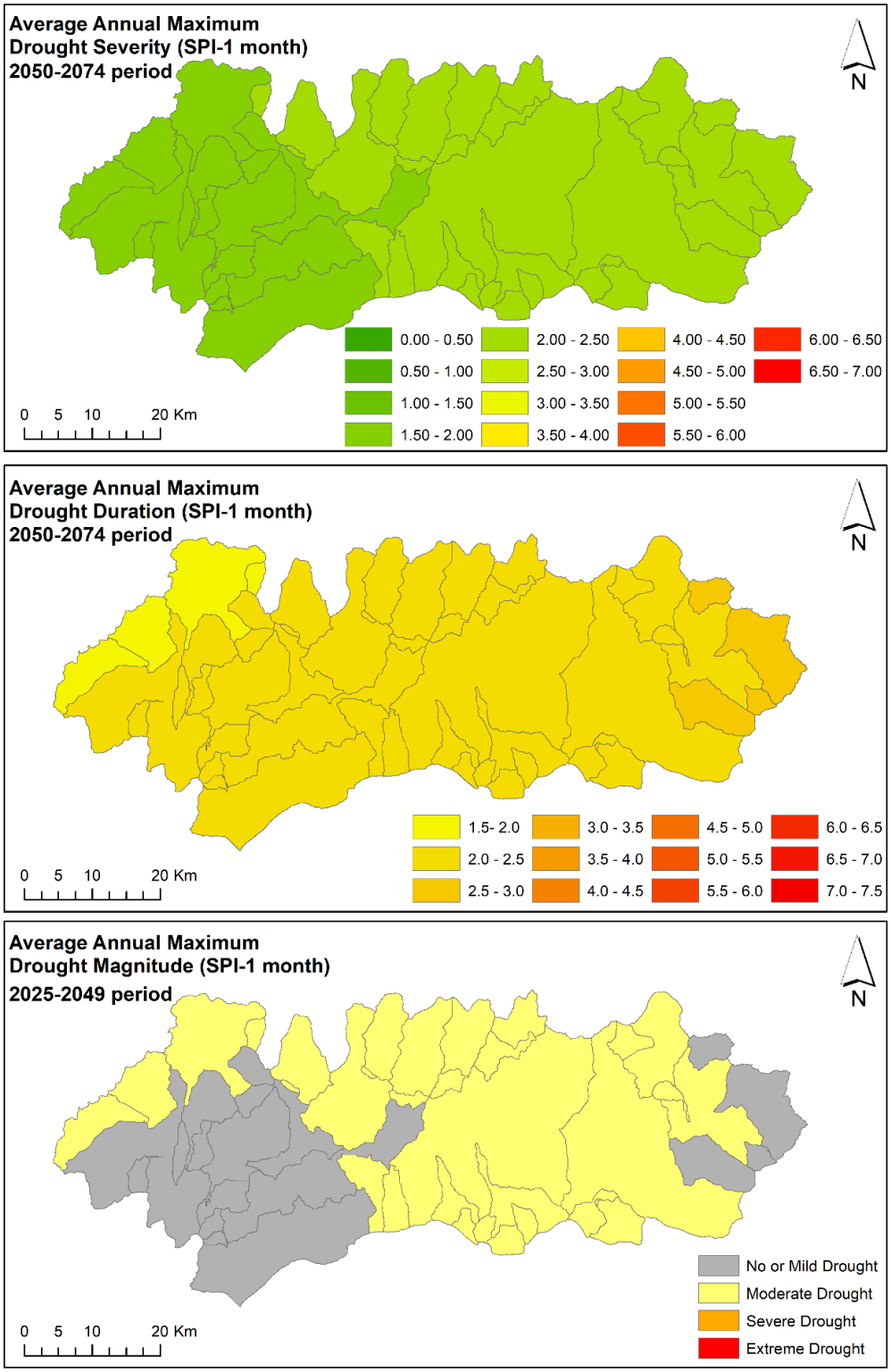


Figure 4.80 Maps obtained using SPI-1 month series for the middle future period: a) average annual maximum drought severity, b) duration and c) magnitude.

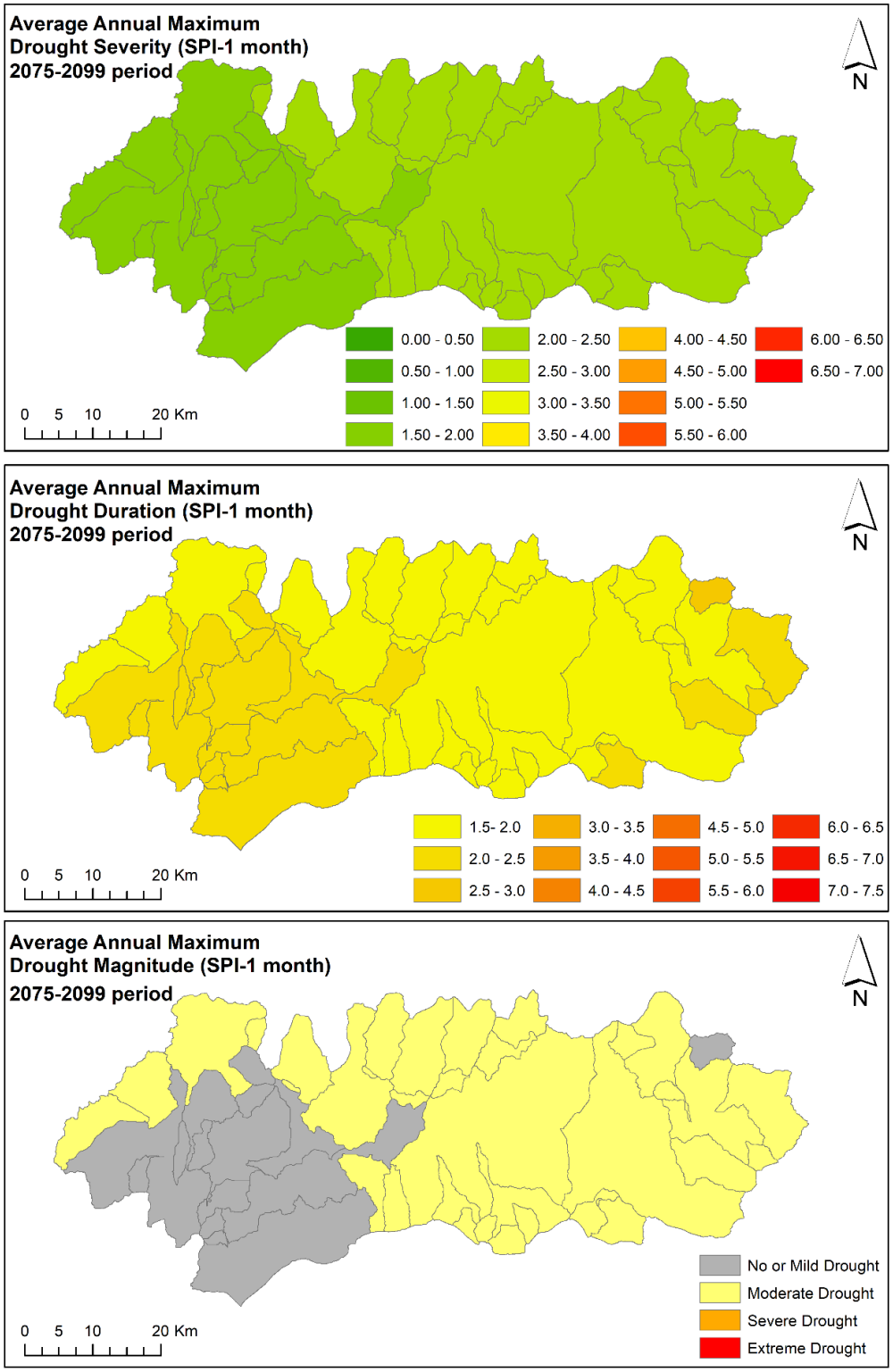


Figure 4.81 Maps obtained using SPI-1 month series for the far future period: a) average annual maximum drought severity, b) duration and c) magnitude.

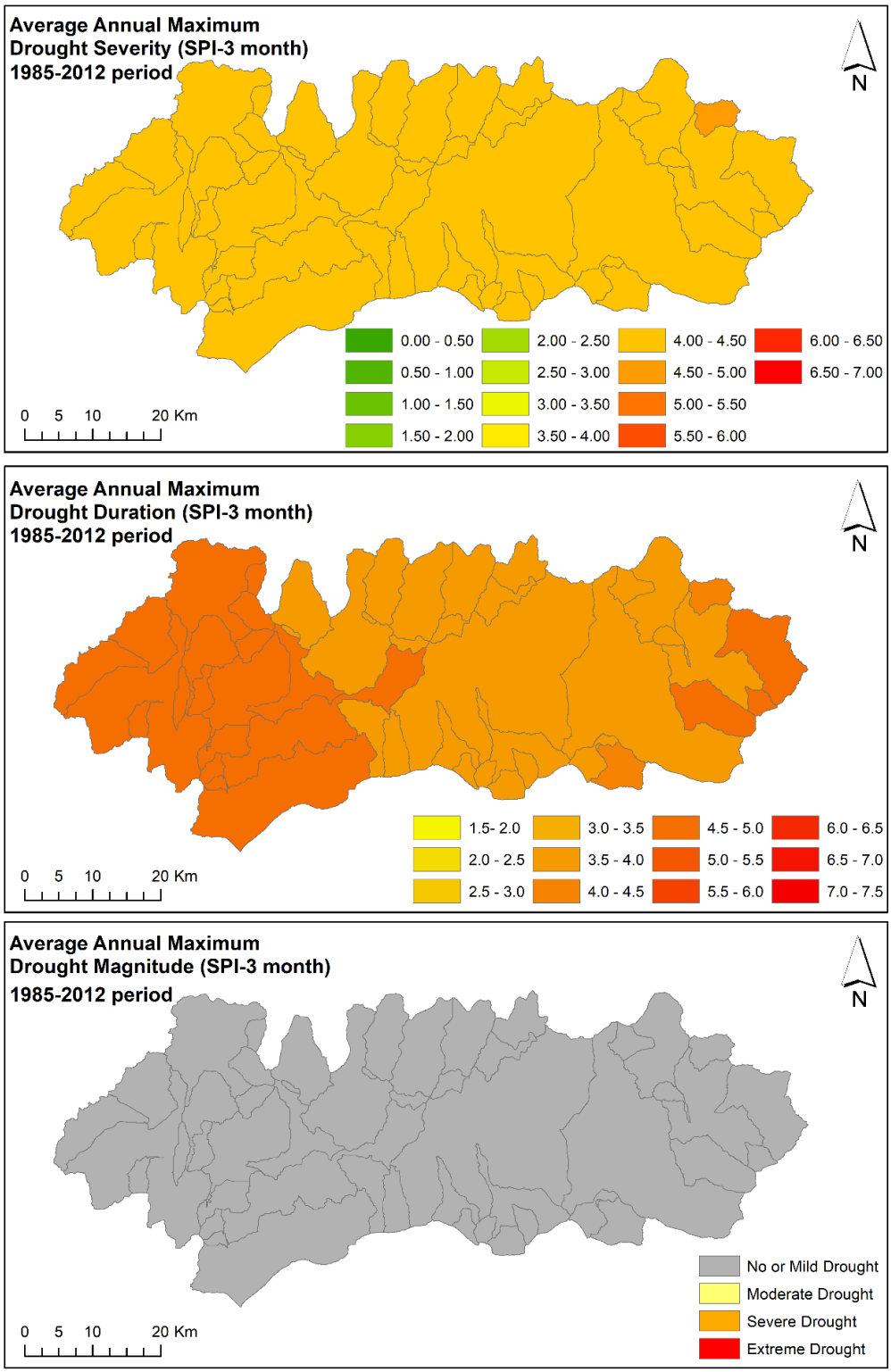


Figure 4.82 Maps obtained using SPI-3 month series for the reference period: a) average annual maximum drought severity, b) duration and c) magnitude.

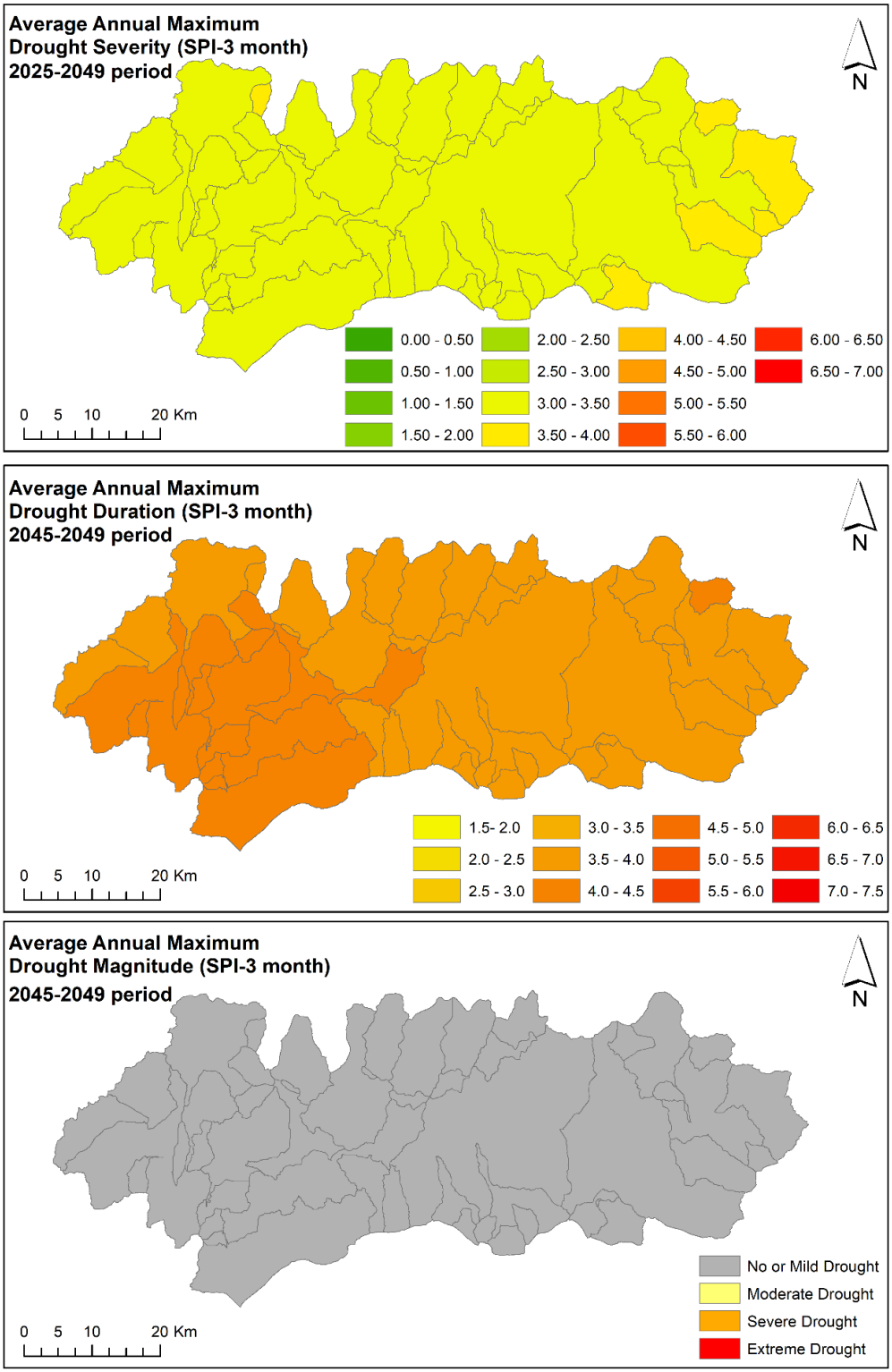


Figure 4.83 Maps obtained using SPI-3 month series for the near future period: a) average annual maximum drought severity, b) duration and c) magnitude.

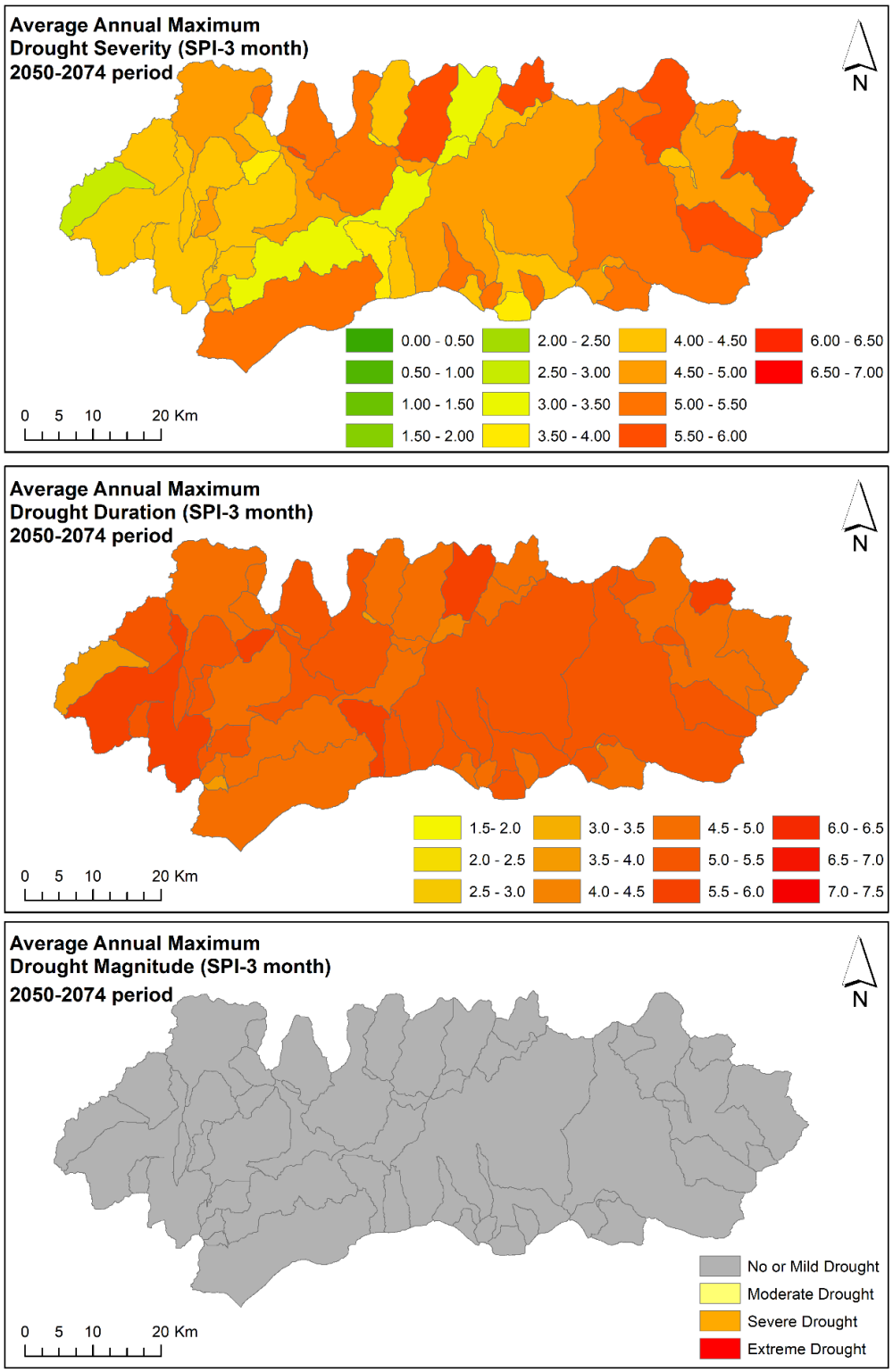


Figure 4.84 Maps obtained using SPI-3 month series for the middle future period: a) average annual maximum drought severity, b) duration and c) magnitude.

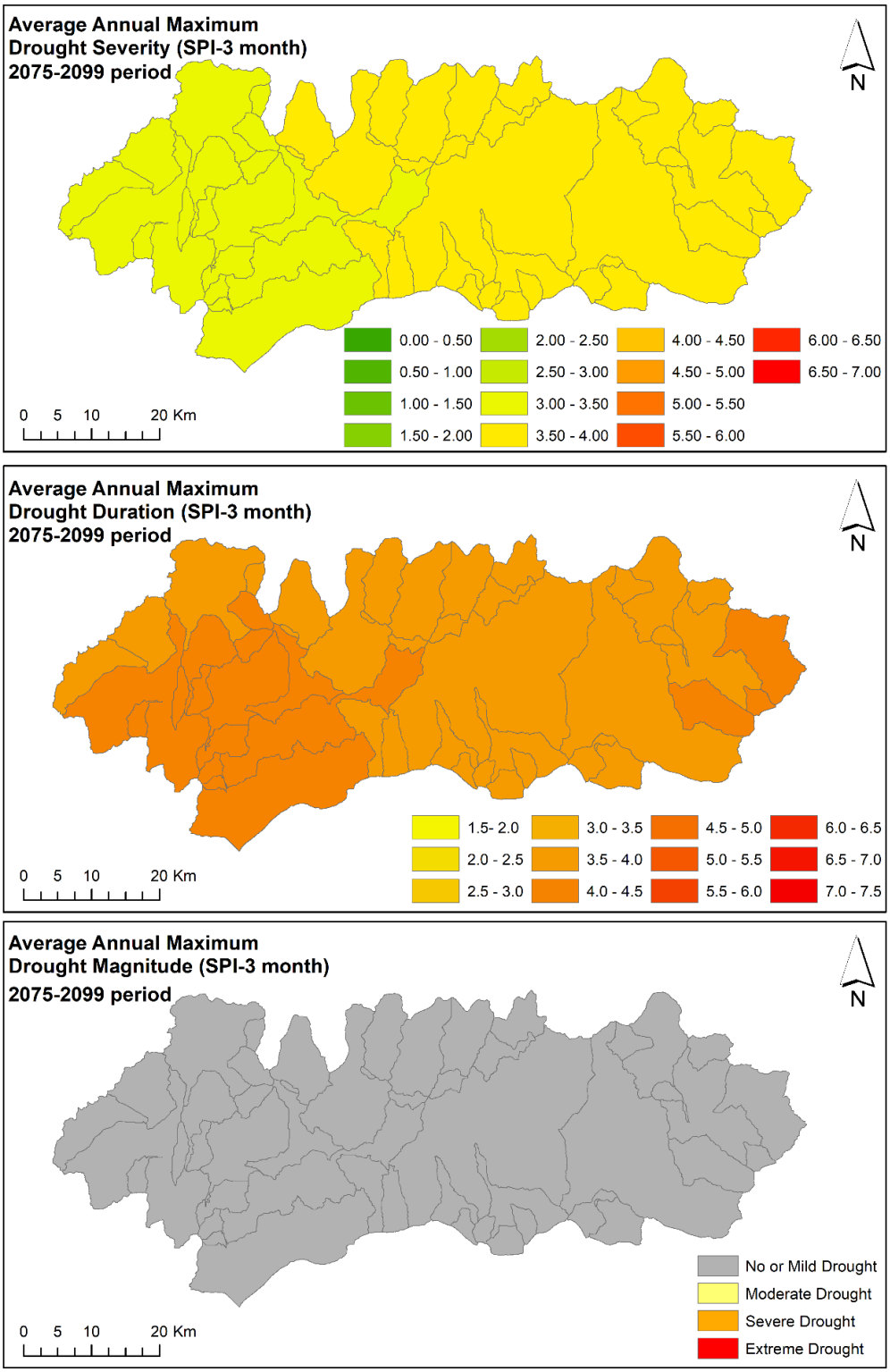


Figure 4.85 Maps obtained using SPI-3 month series for the far future period: a) average annual maximum drought severity, b) duration and c) magnitude.

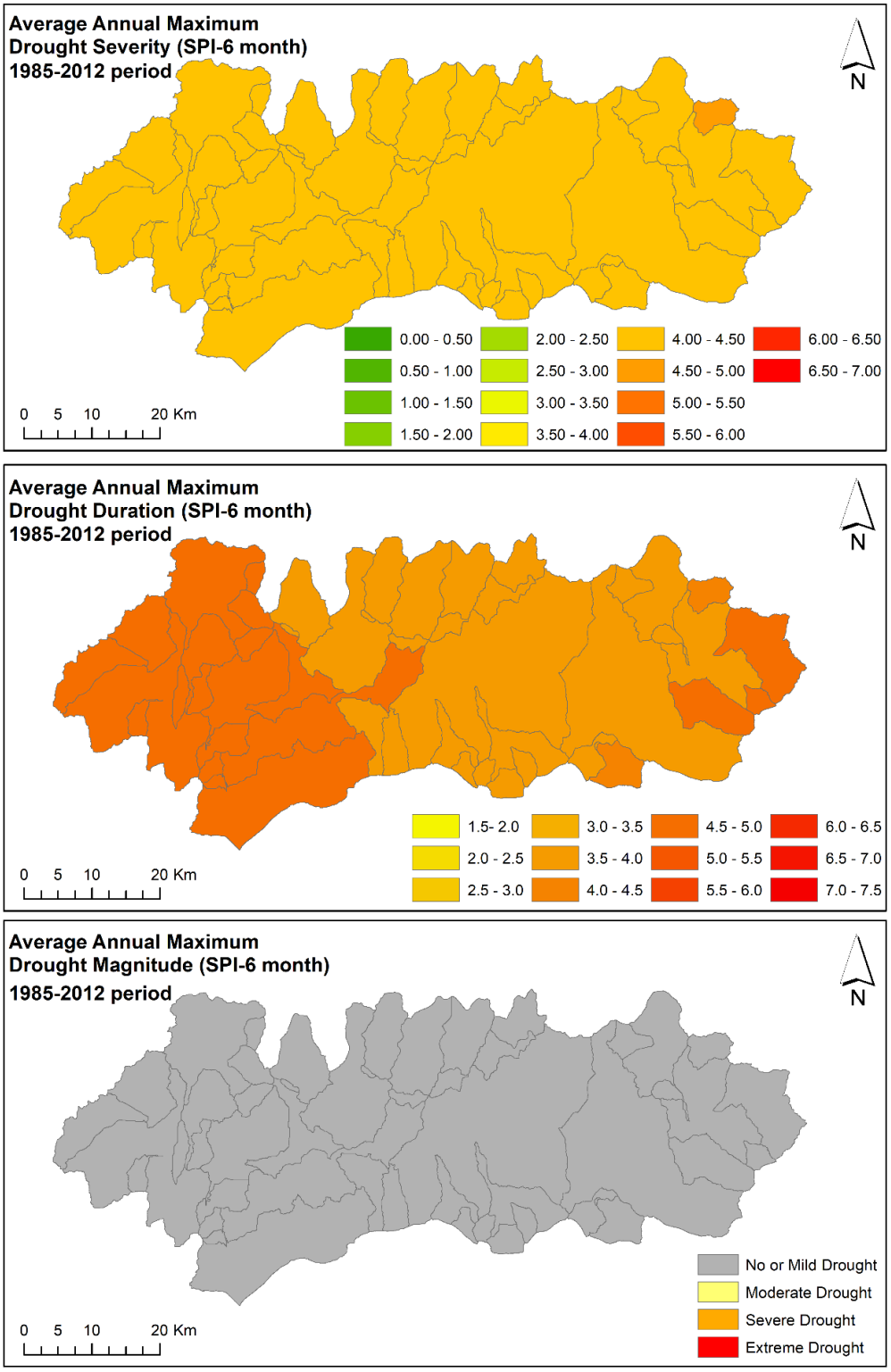


Figure 4.86 Maps obtained using SPI-6 month series for the reference period: a) average annual maximum drought severity, b) duration and c) magnitude.

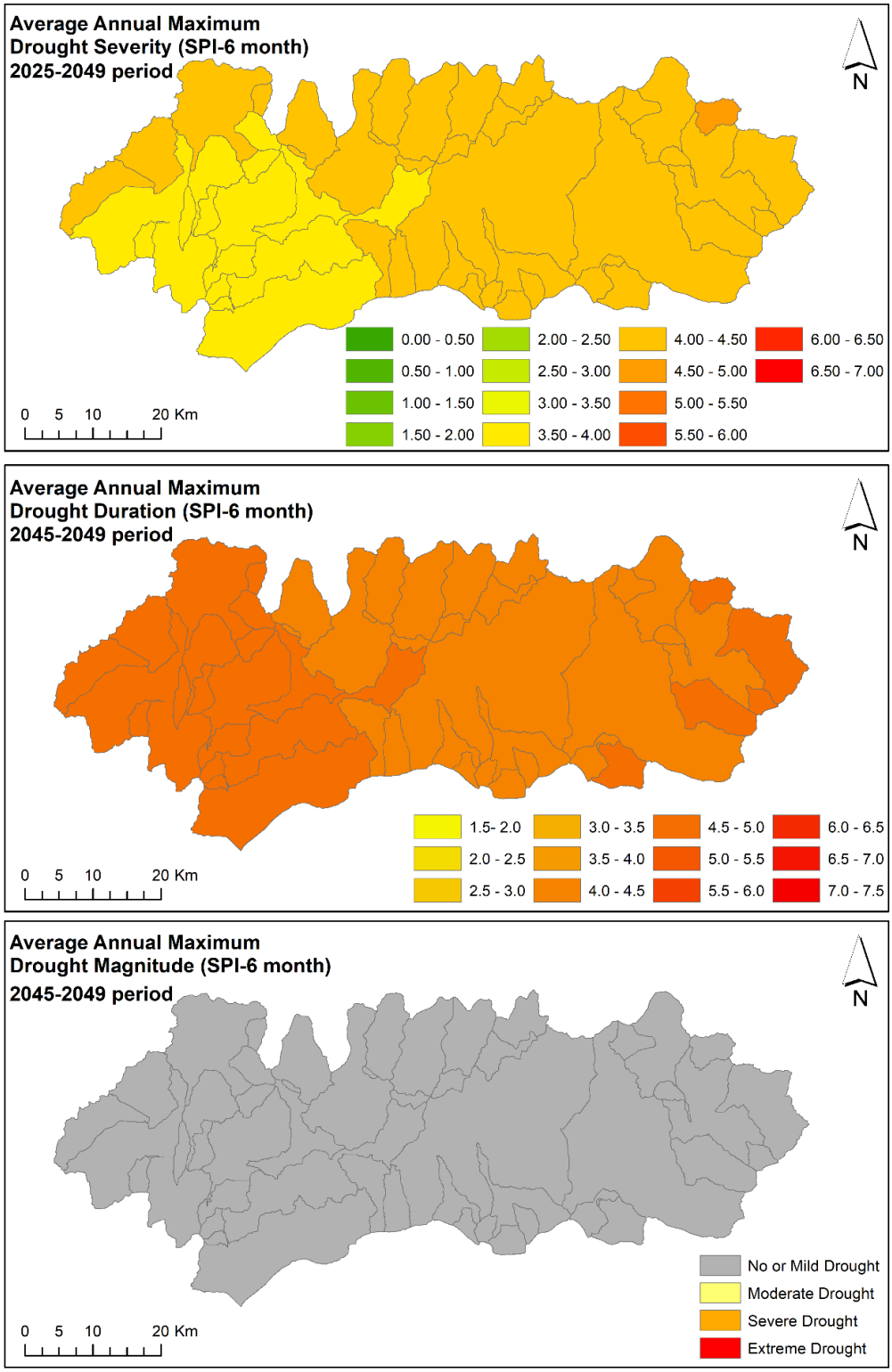


Figure 4.87 Maps obtained using SPI-6 month series for the near future period: a) average annual maximum drought severity, b) duration and c) magnitude.

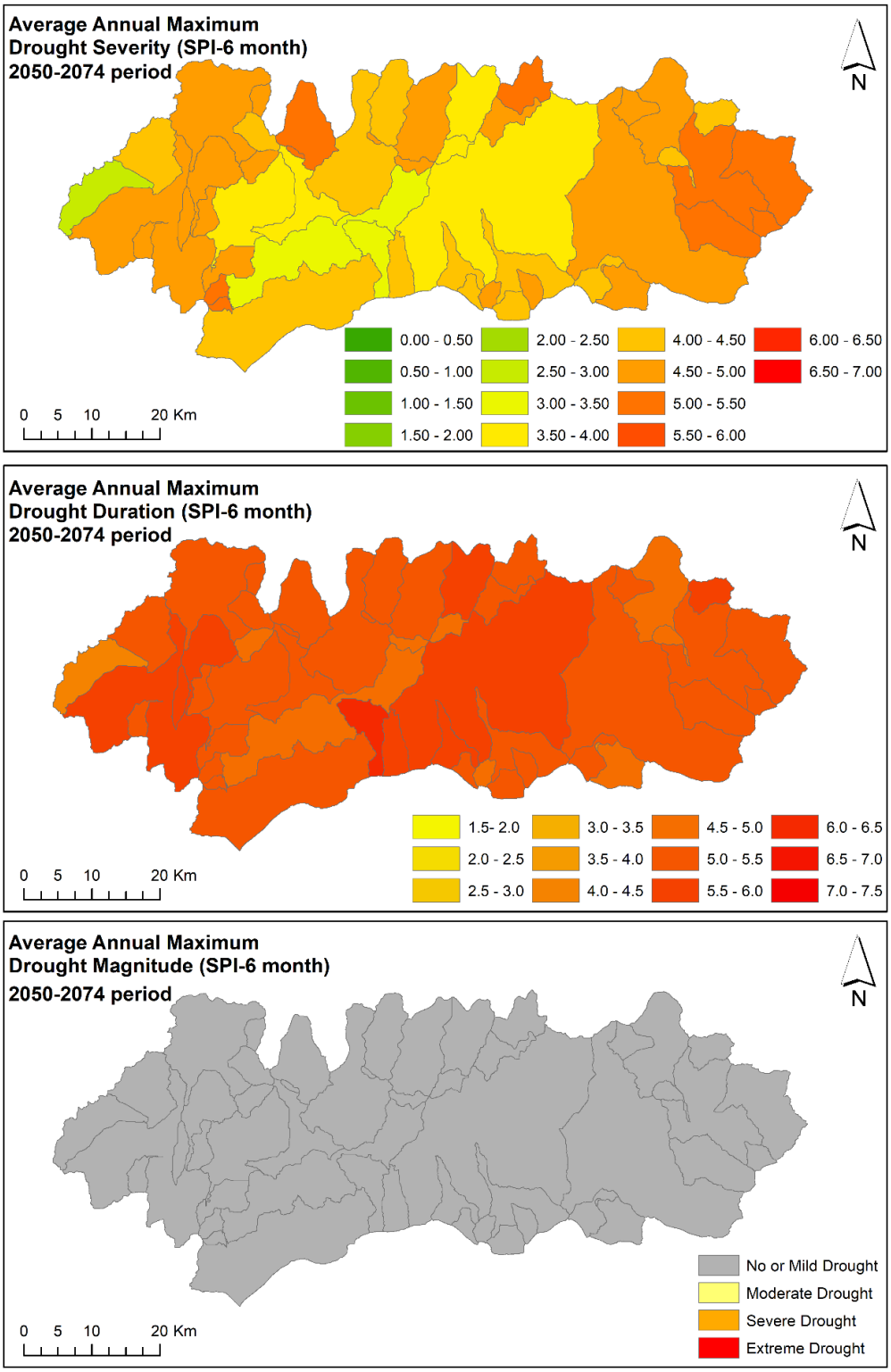


Figure 4.88 Maps obtained using SPI-6 month series for the middle future period: a) average annual maximum drought severity, b) duration and c) magnitude.

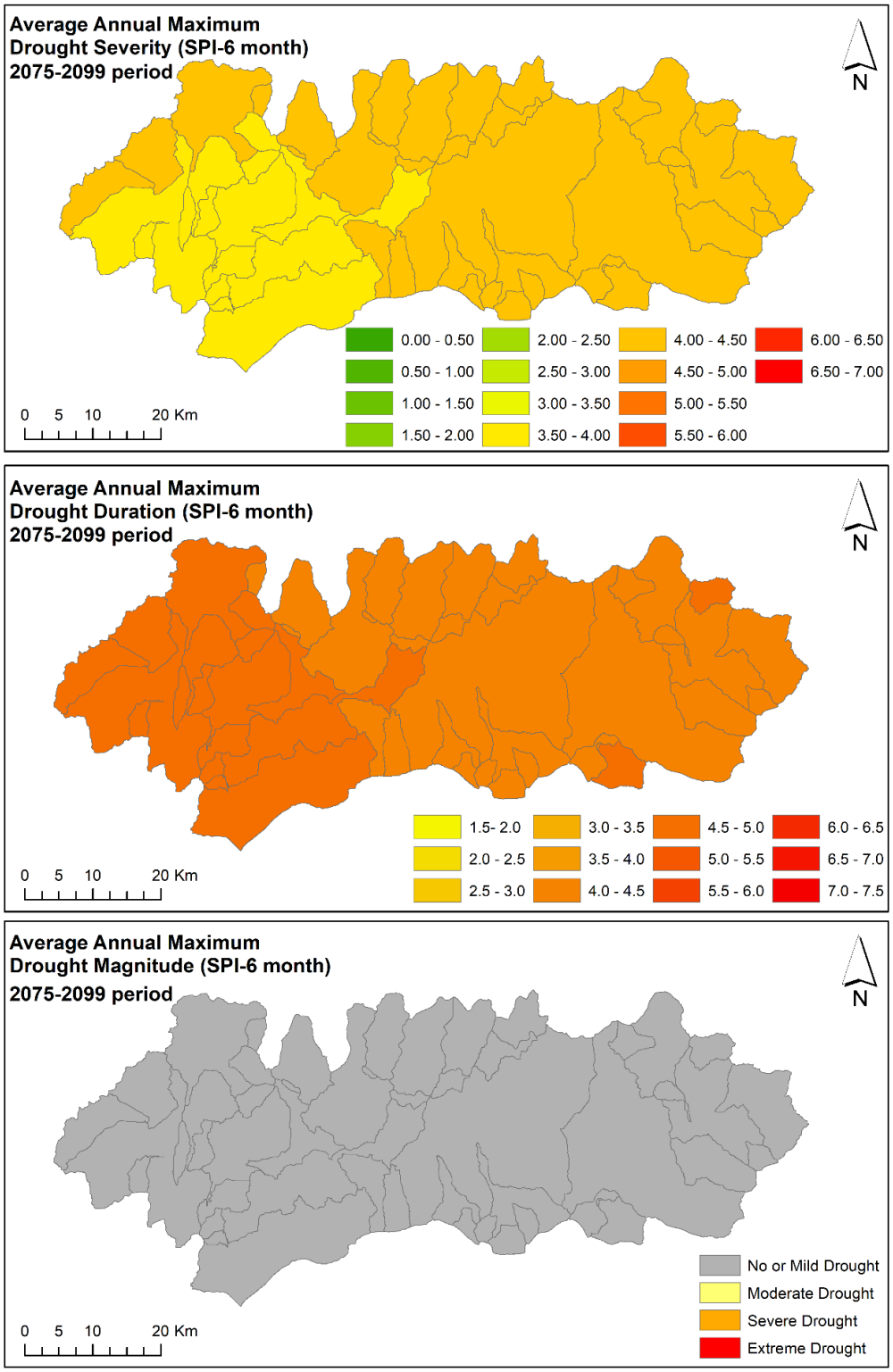


Figure 4.89 Maps obtained using SPI-6 month series for the far future period: a) average annual maximum drought severity, b) duration and c) magnitude.

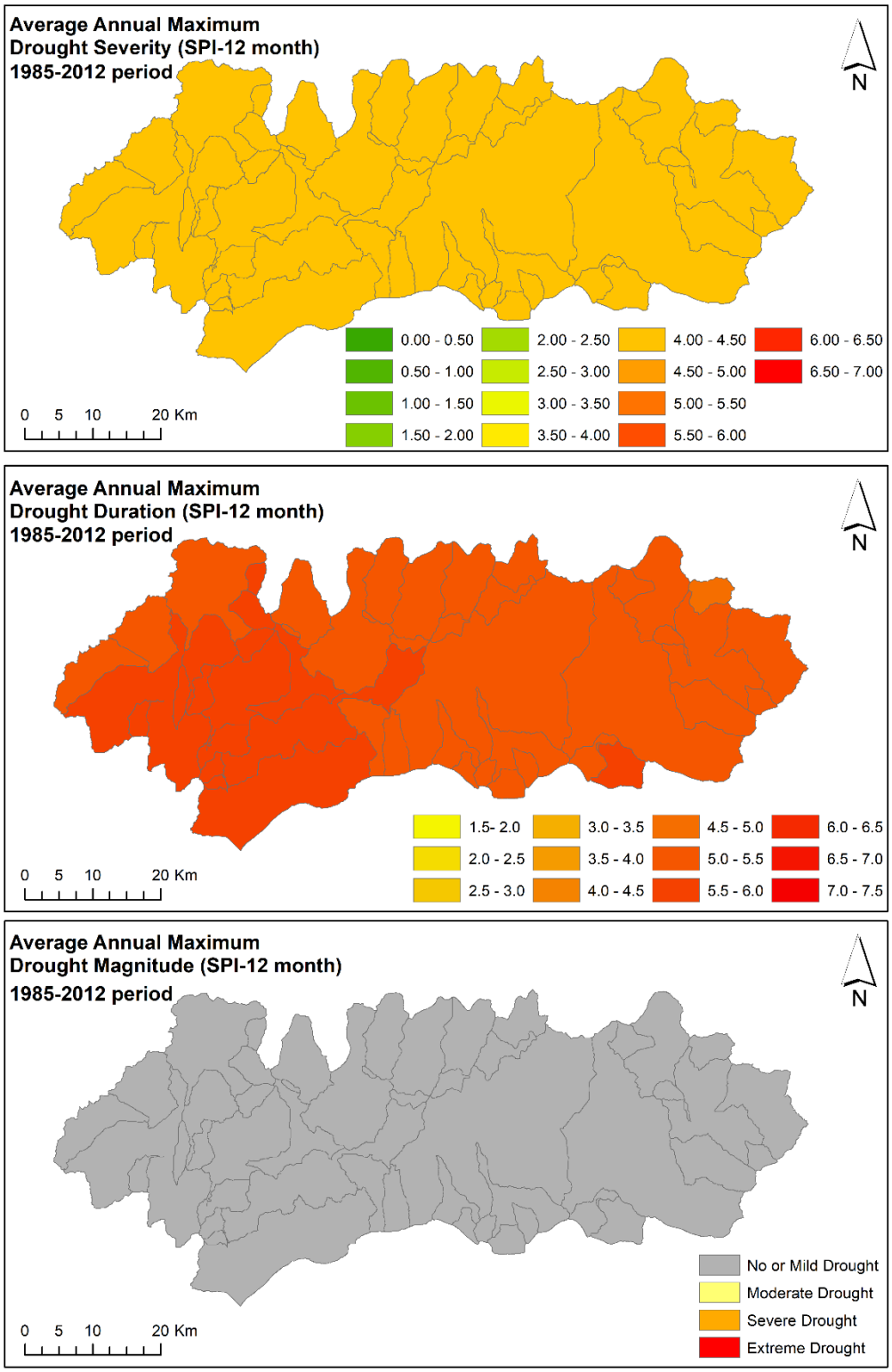


Figure 4.90 Maps obtained using SPI-12 month series for the reference period: a) average annual maximum drought severity, b) duration and c) magnitude.

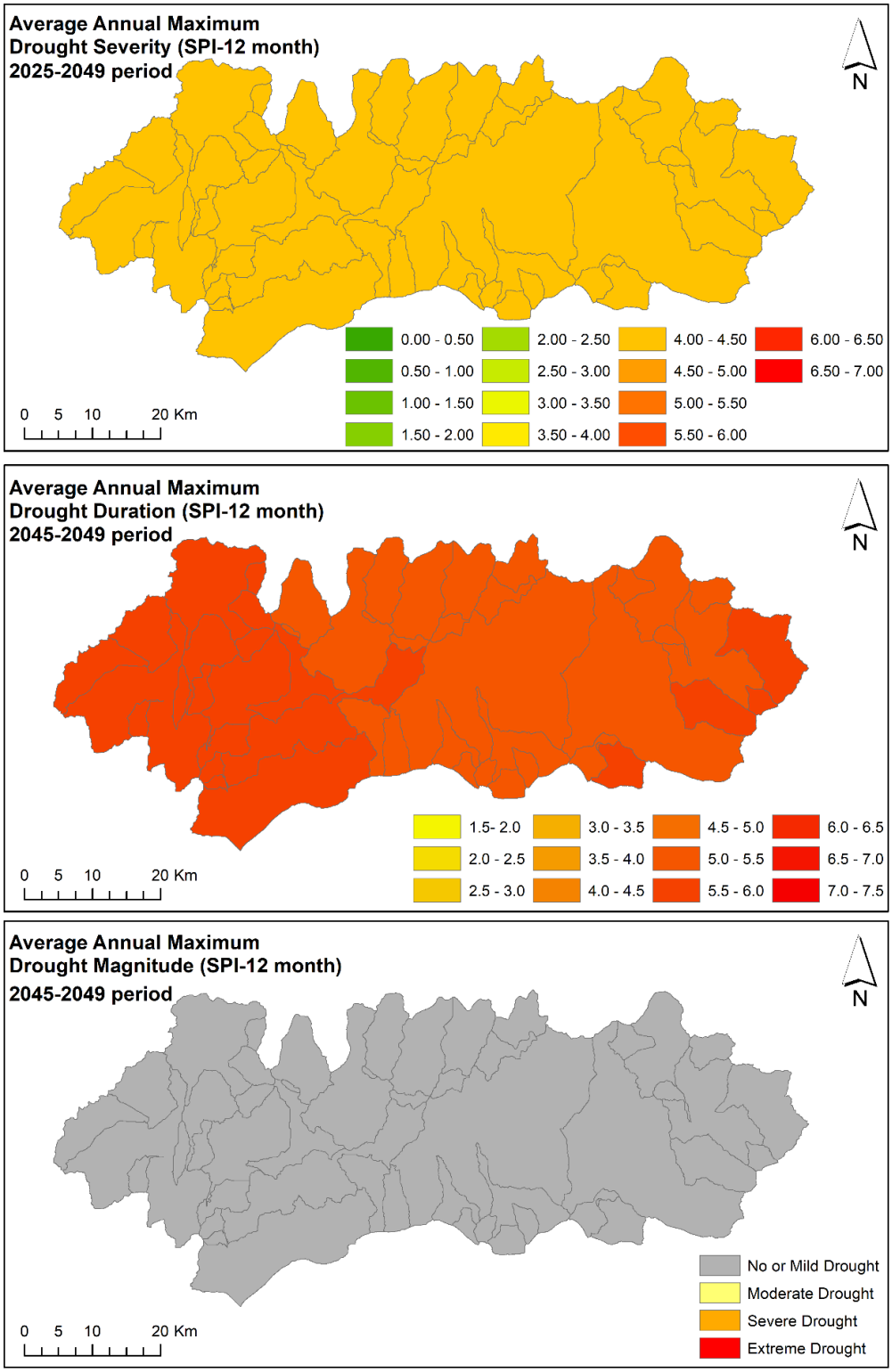


Figure 4.91 Maps obtained using SPI-12 month series for the near future period: a) average annual maximum drought severity, b) duration and c) magnitude.

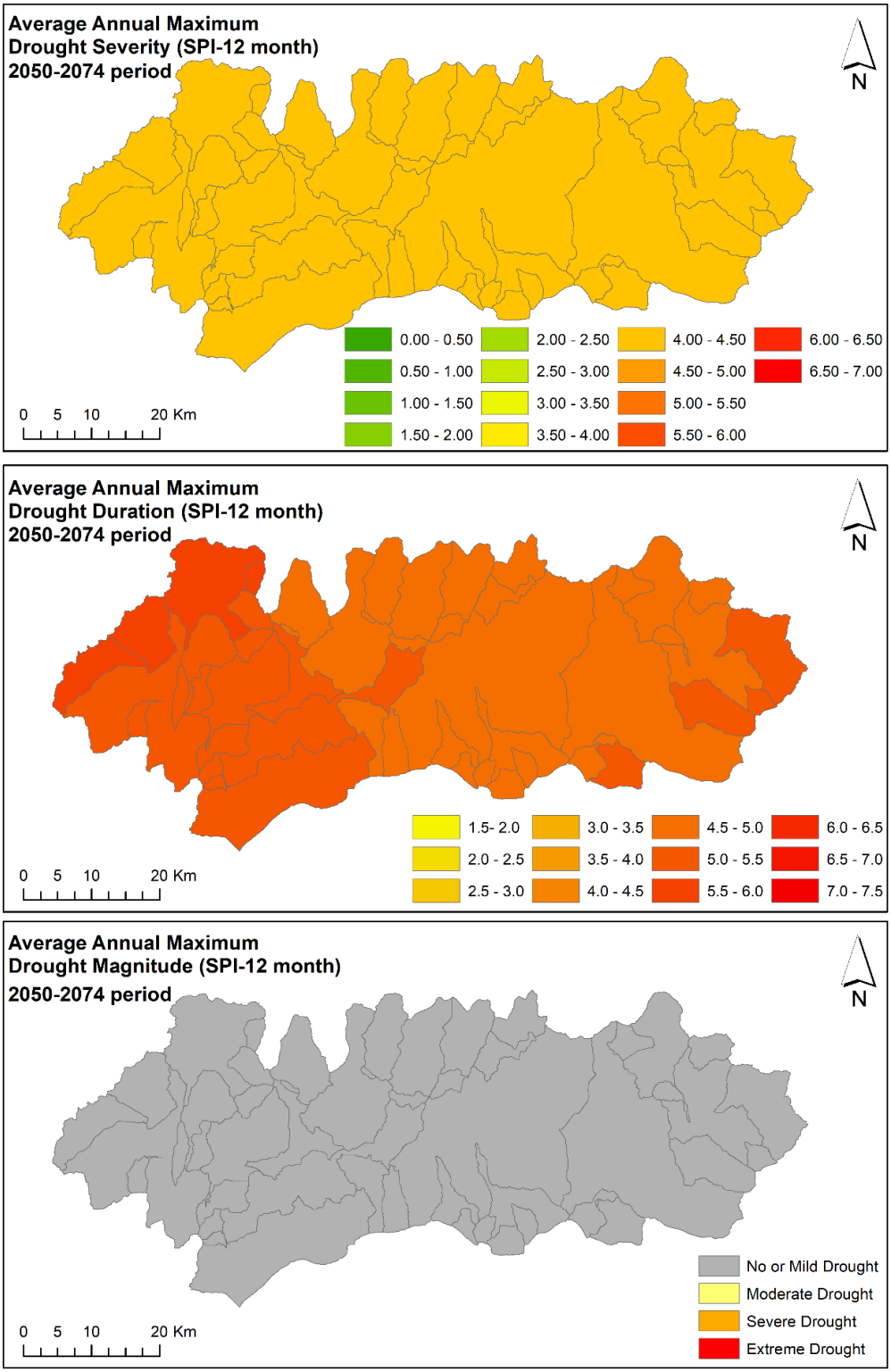


Figure 4.92 Maps obtained using SPI-12 month series for the middle future period: a) average annual maximum drought severity, b) duration and c) magnitude.

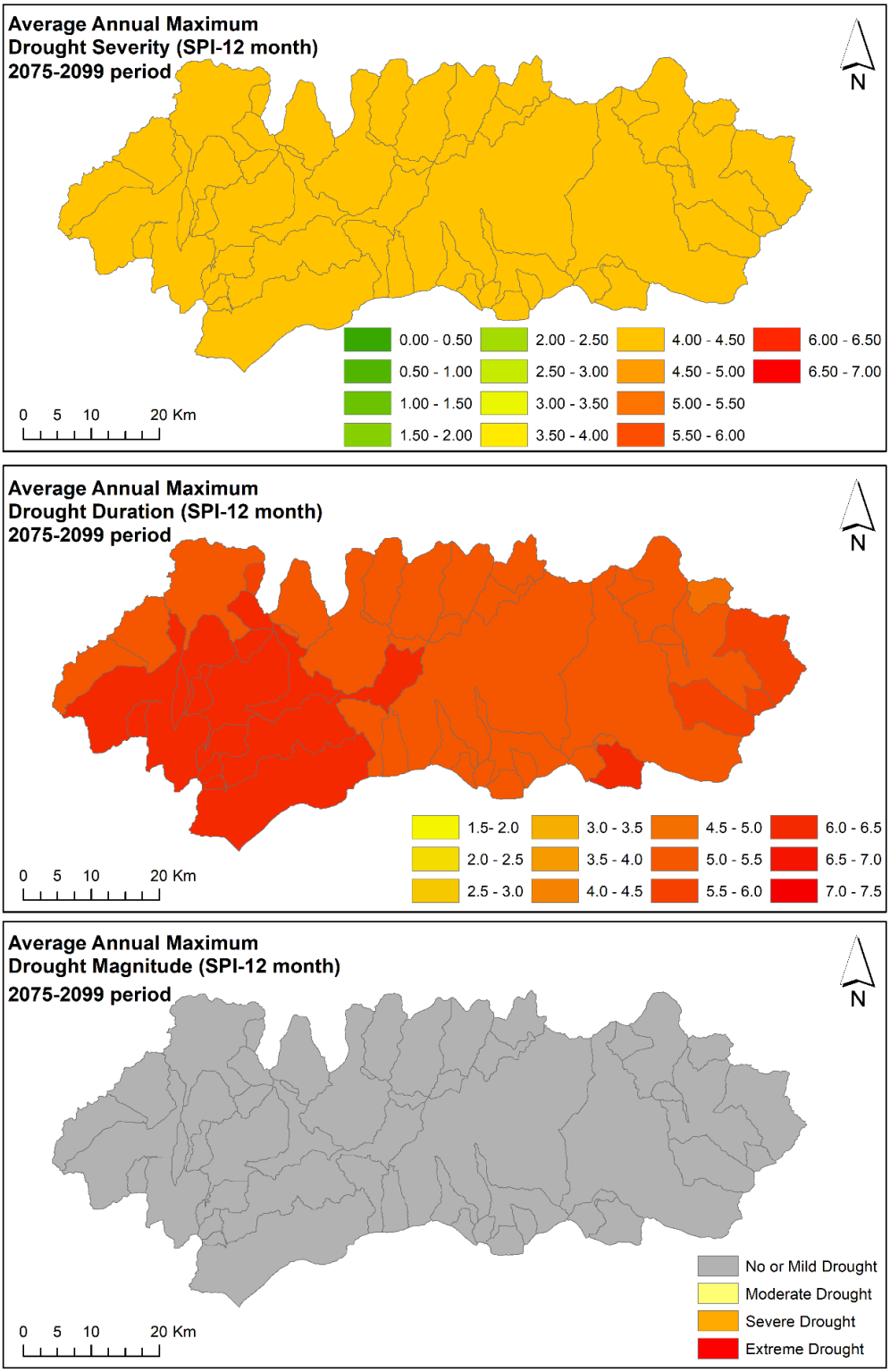


Figure 4.93 Maps obtained using SPI-12 month series for the far future period: a) average annual maximum drought severity, b) duration and c) magnitude.

4.3.3.2 Drought Maps Generated Using SPEI (with ETa)

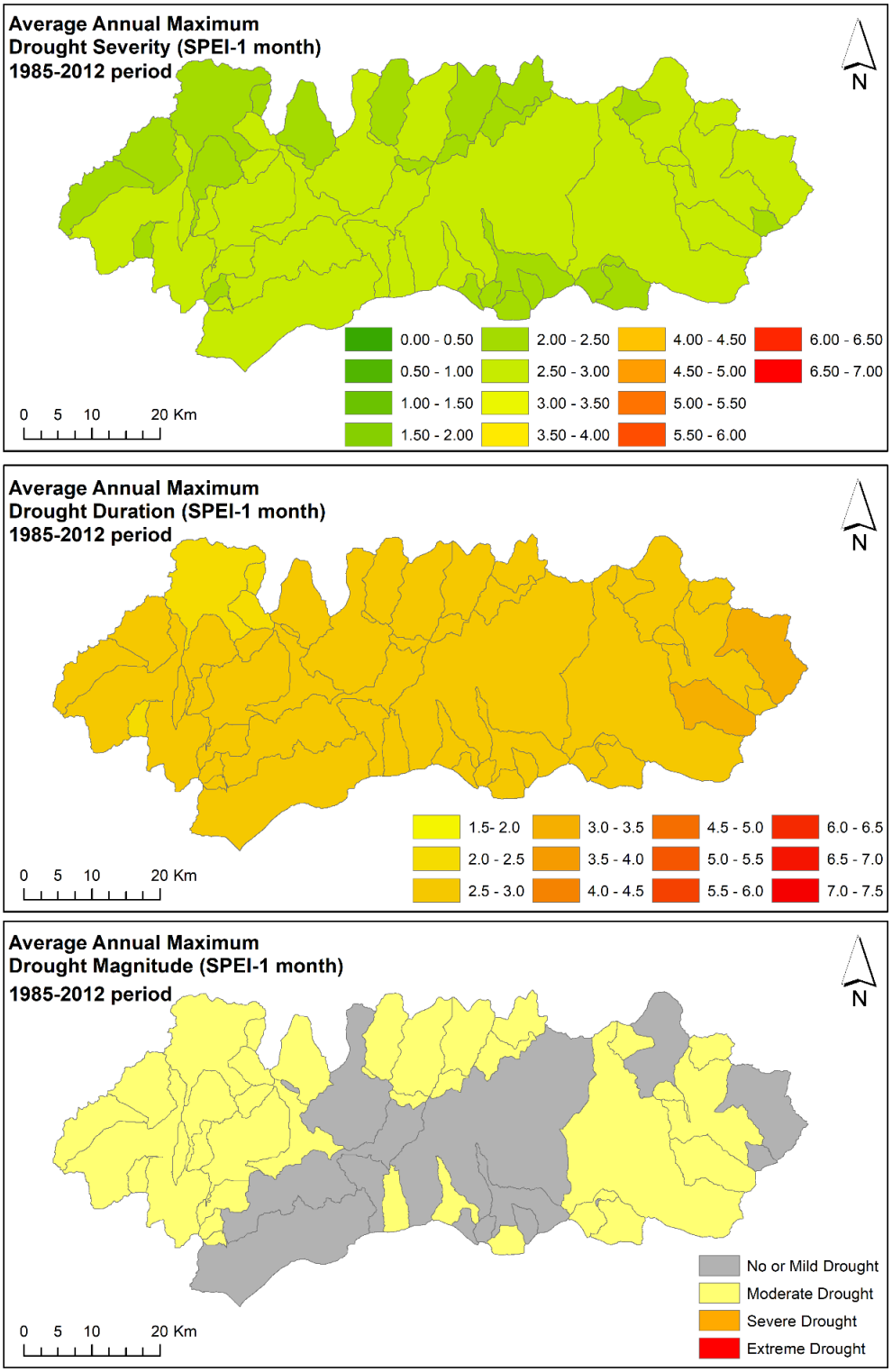


Figure 4.94 Maps obtained using SPEI-1 month series (with ET_a) for the reference period: a) average annual maximum drought severity, b) duration and c) magnitude.

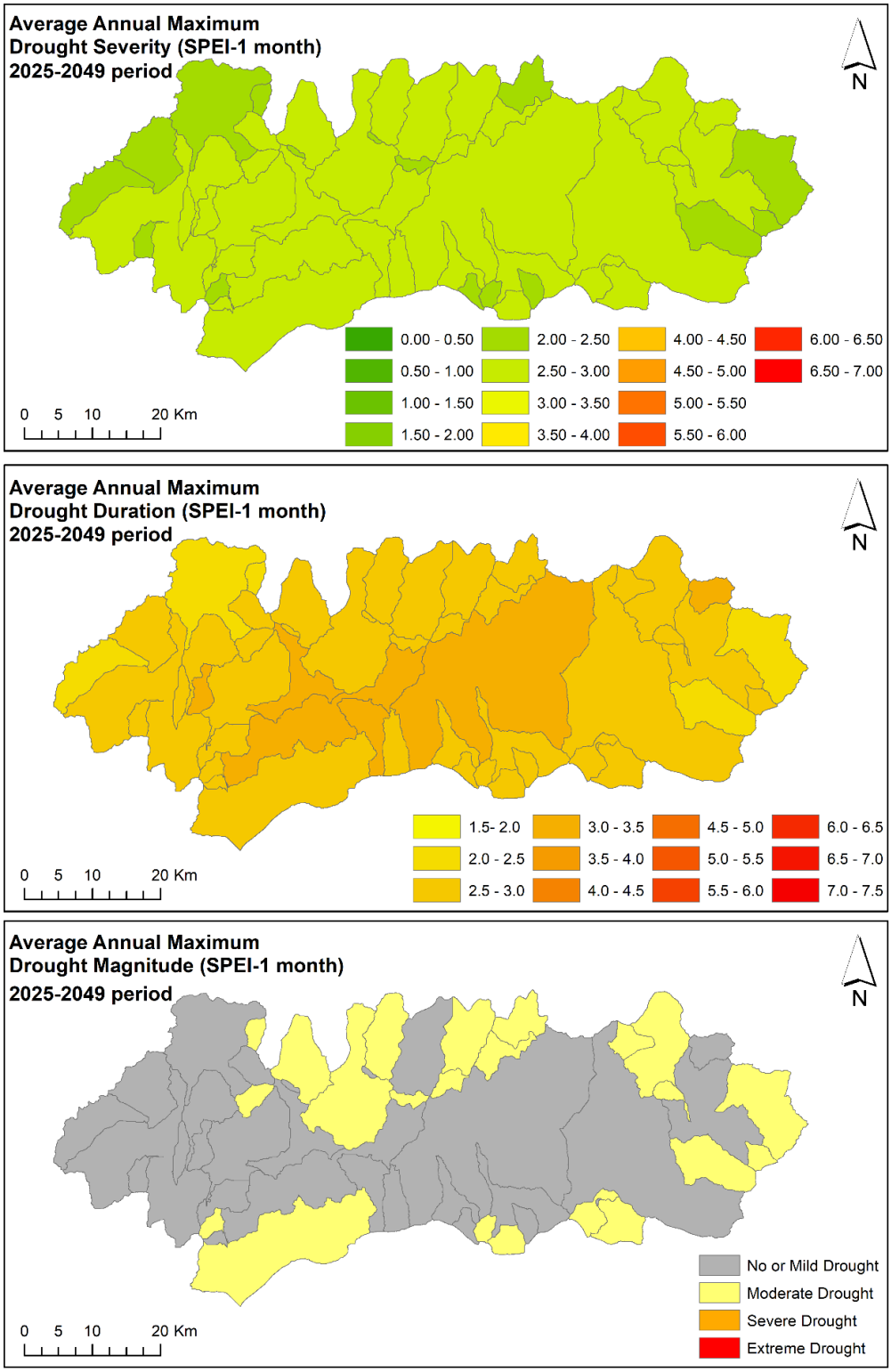


Figure 4.95 Maps obtained using SPEI-1 month series (with ET_a) for the near future period: a) average annual maximum drought severity, b) duration and c) magnitude.

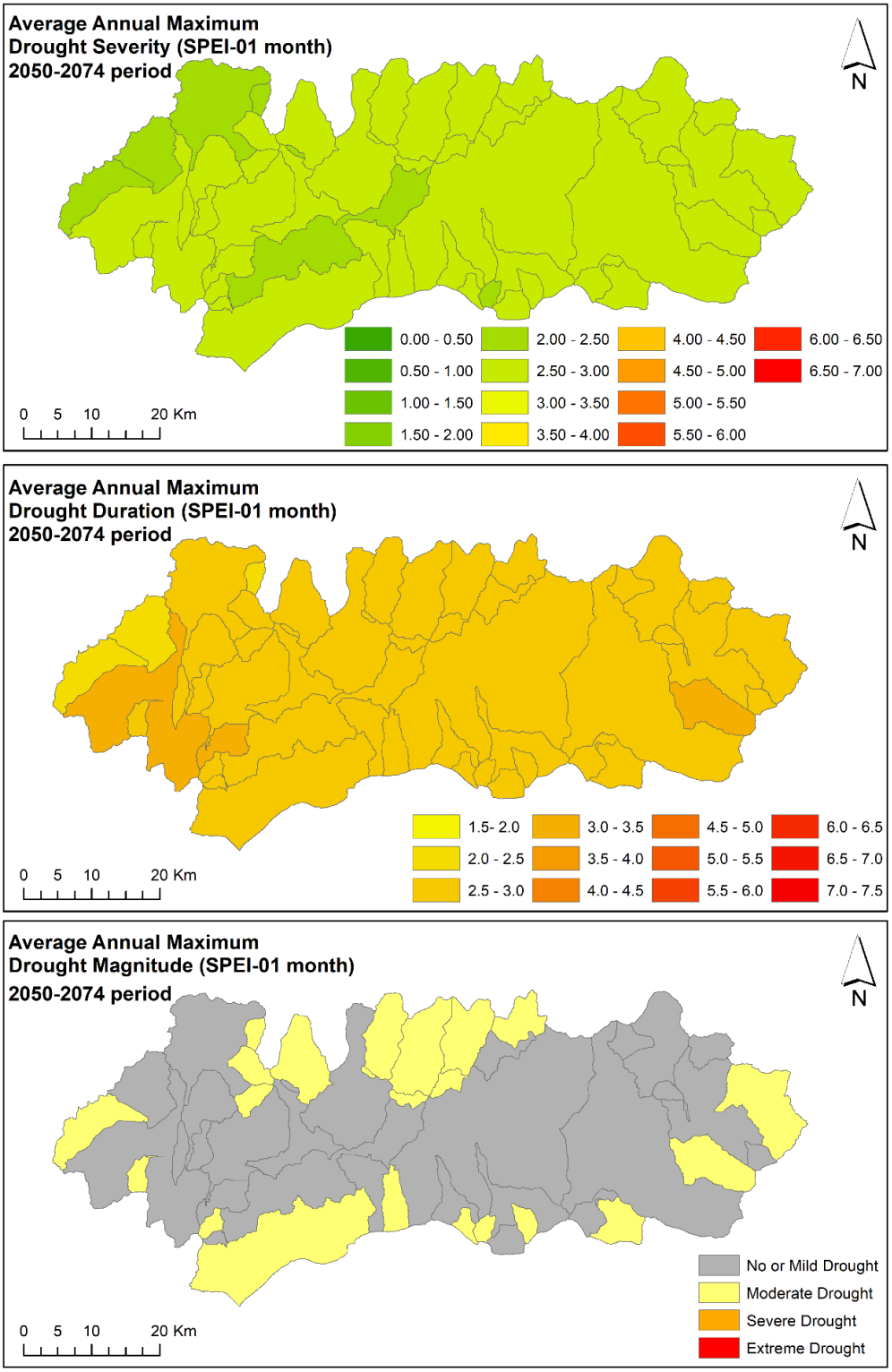


Figure 4.96 Maps obtained using SPEI-1 month series (with ET_a) for the middle future period: a) average annual maximum drought severity, b) duration and c) magnitude.

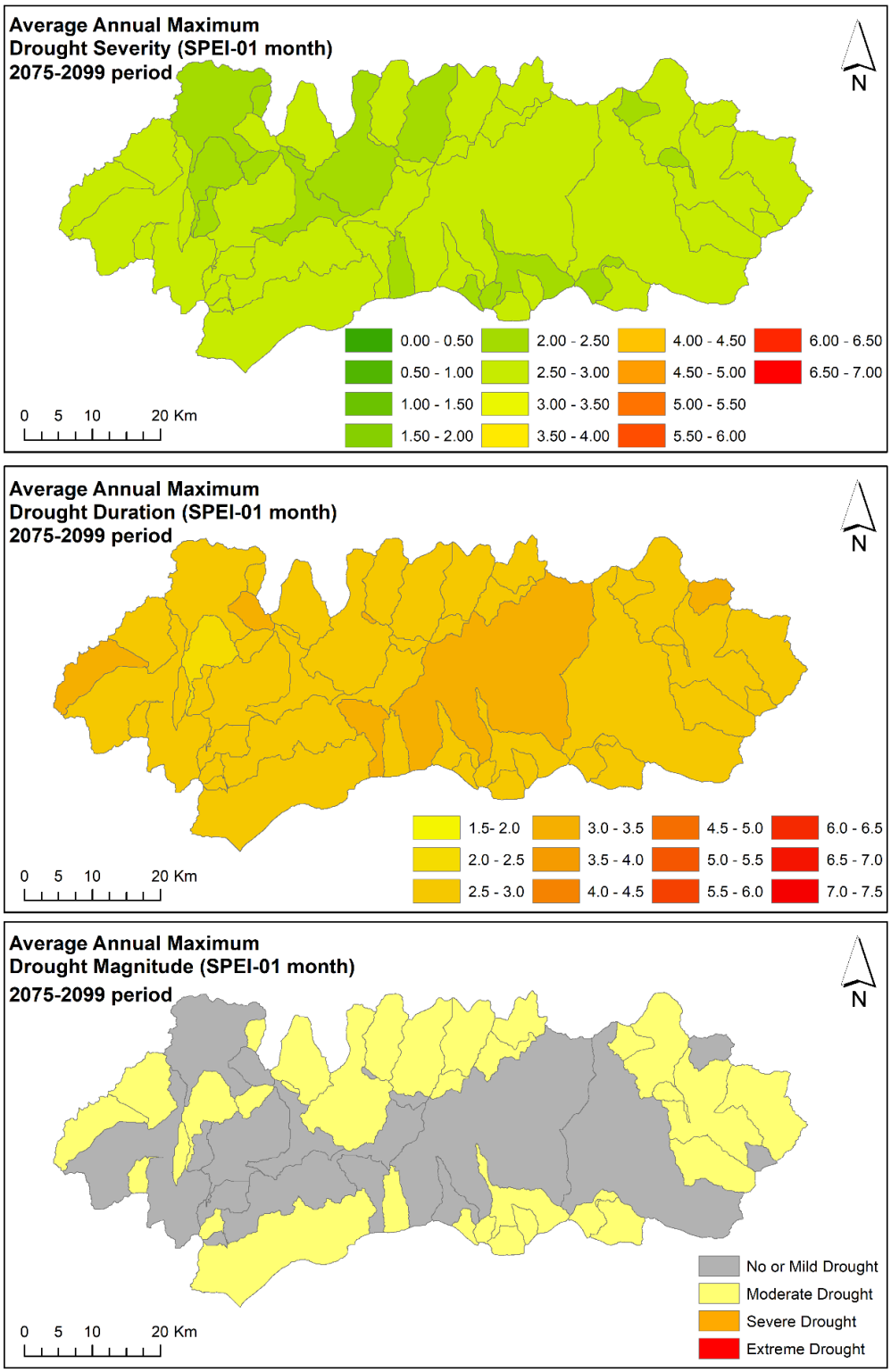


Figure 4.97 Maps obtained using SPEI-1 month series (with ET_a) for the far future period: a) average annual maximum drought severity, b) duration and c) magnitude.

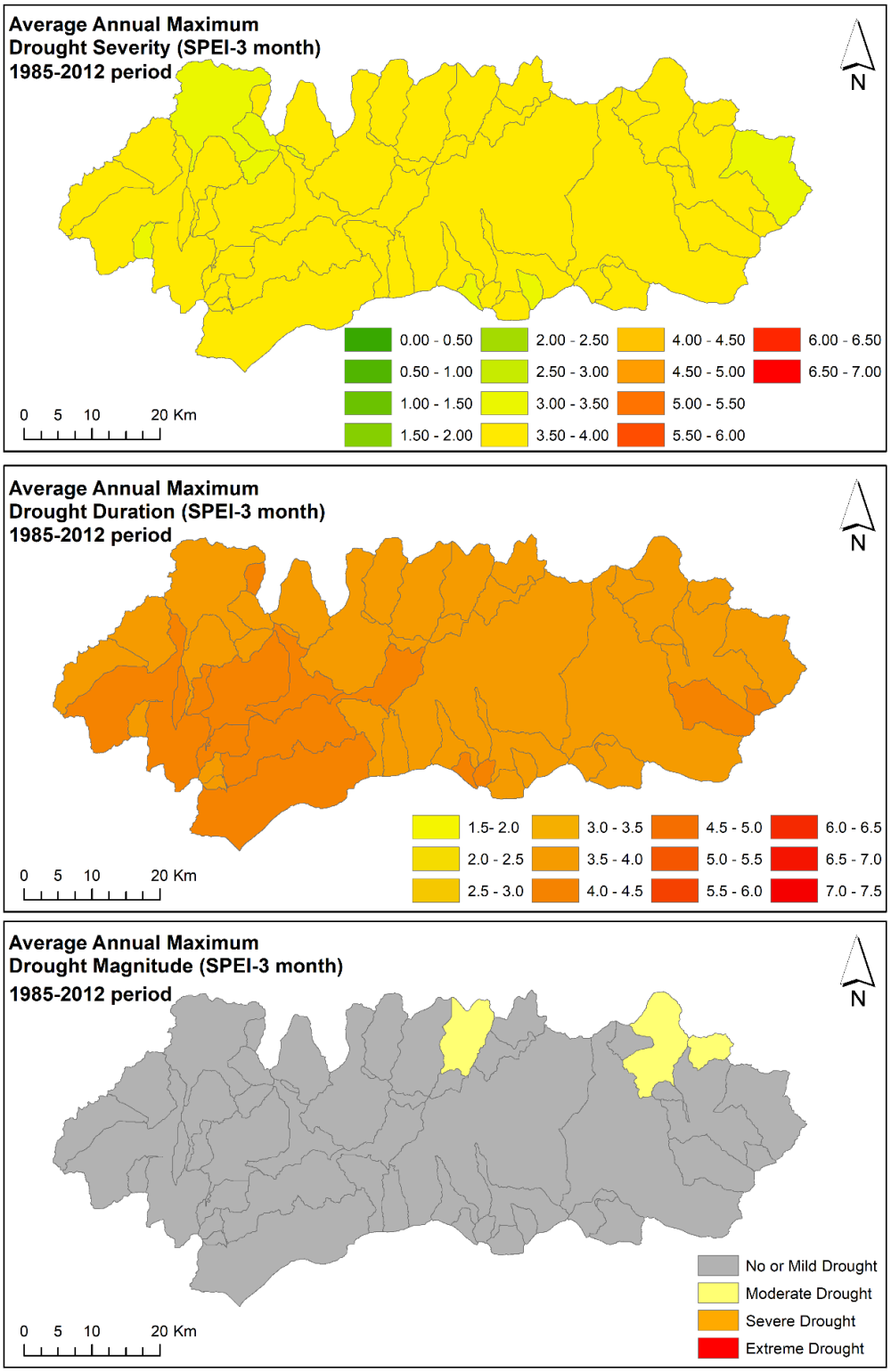


Figure 4.98 Maps obtained using SPEI-3 month series (with ET_a) for the reference period: a) average annual maximum drought severity, b) duration and c) magnitude.

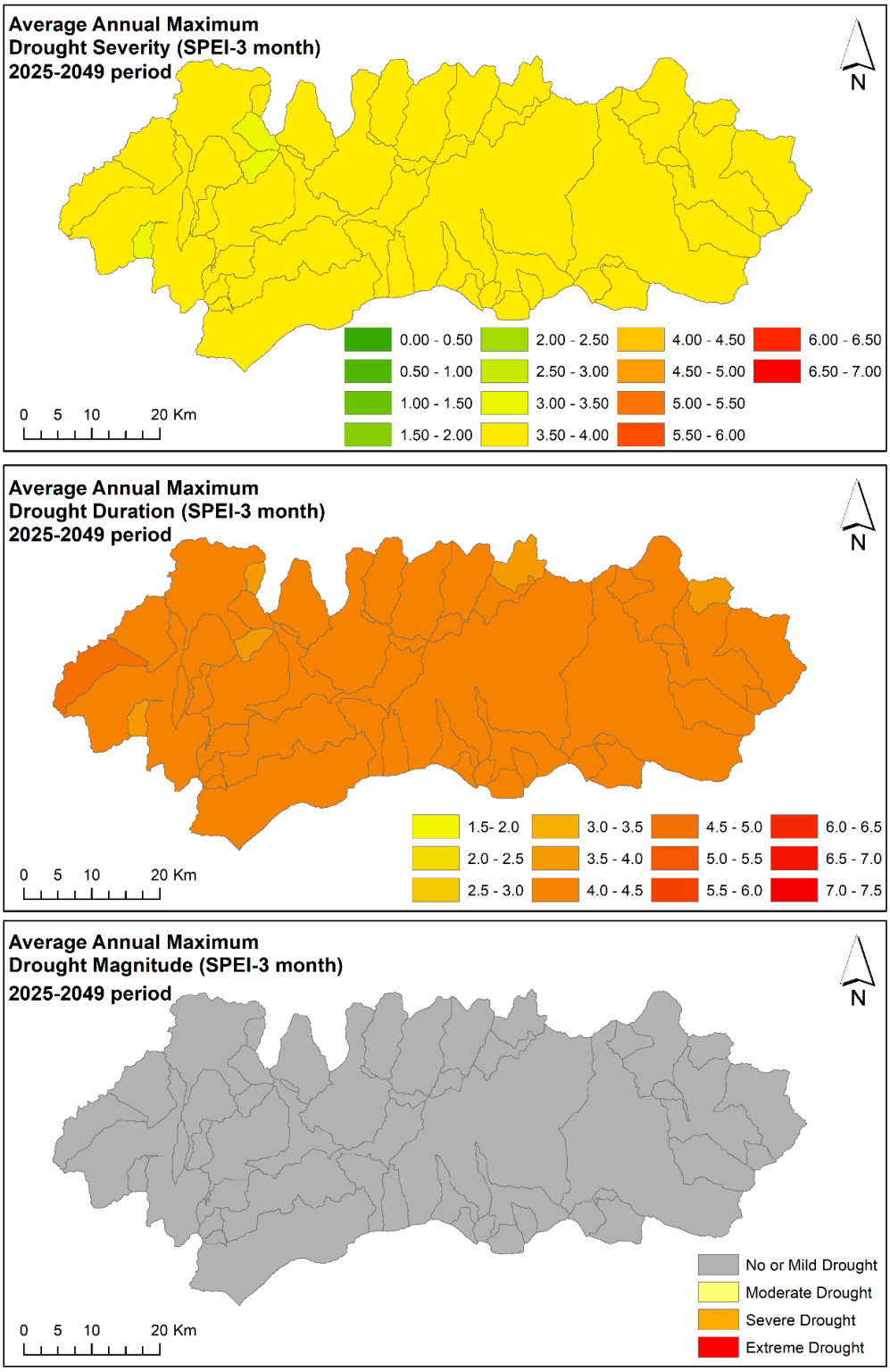


Figure 4.99 Maps obtained using SPEI-3 month series (with ET_a) for the near future period: a) average annual maximum drought severity, b) duration and c) magnitude.

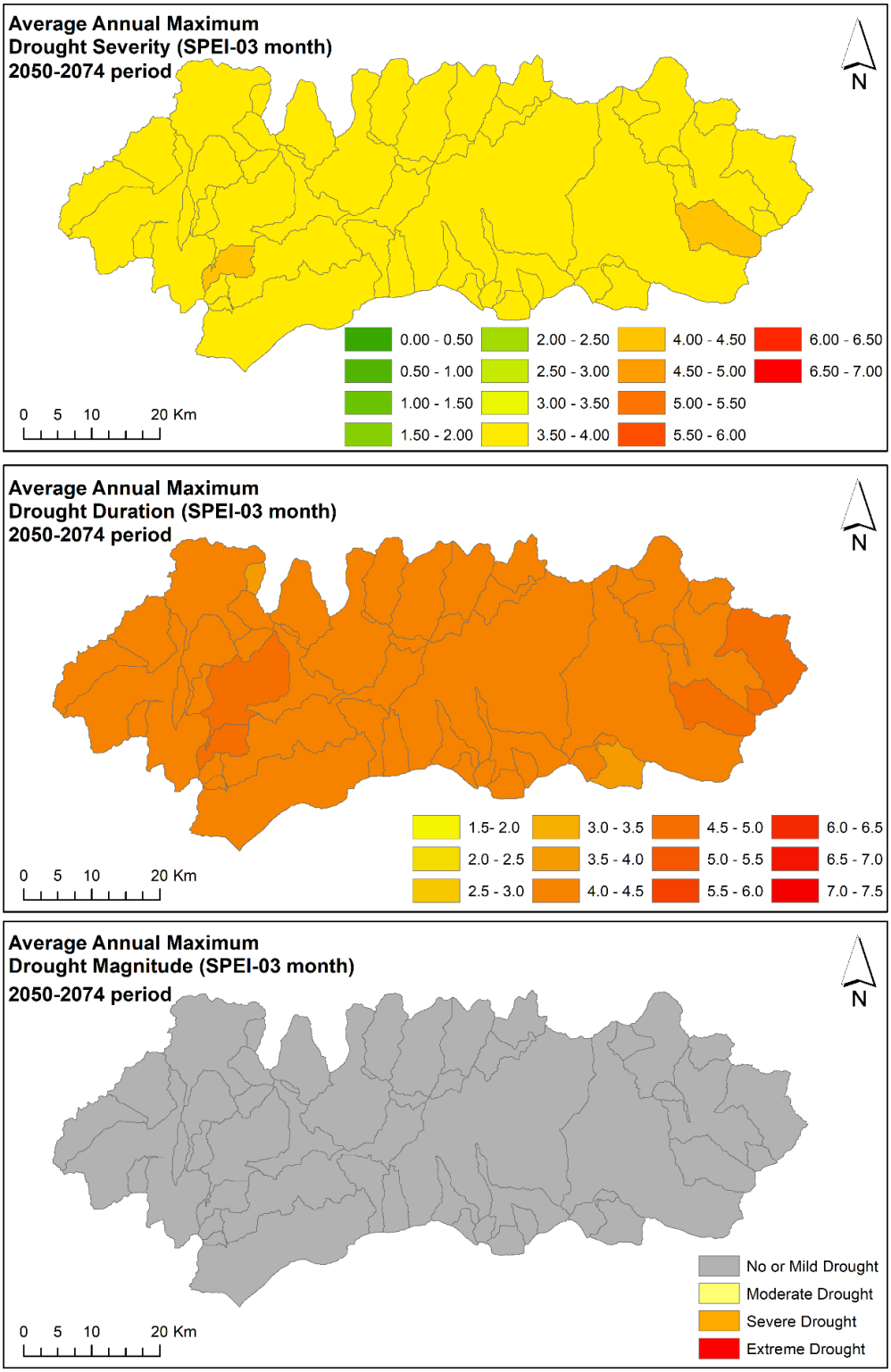


Figure 4.100 Maps obtained using SPEI-3 month series (with ET_a) for the middle future period: a) average annual maximum drought severity, b) duration and c) magnitude.

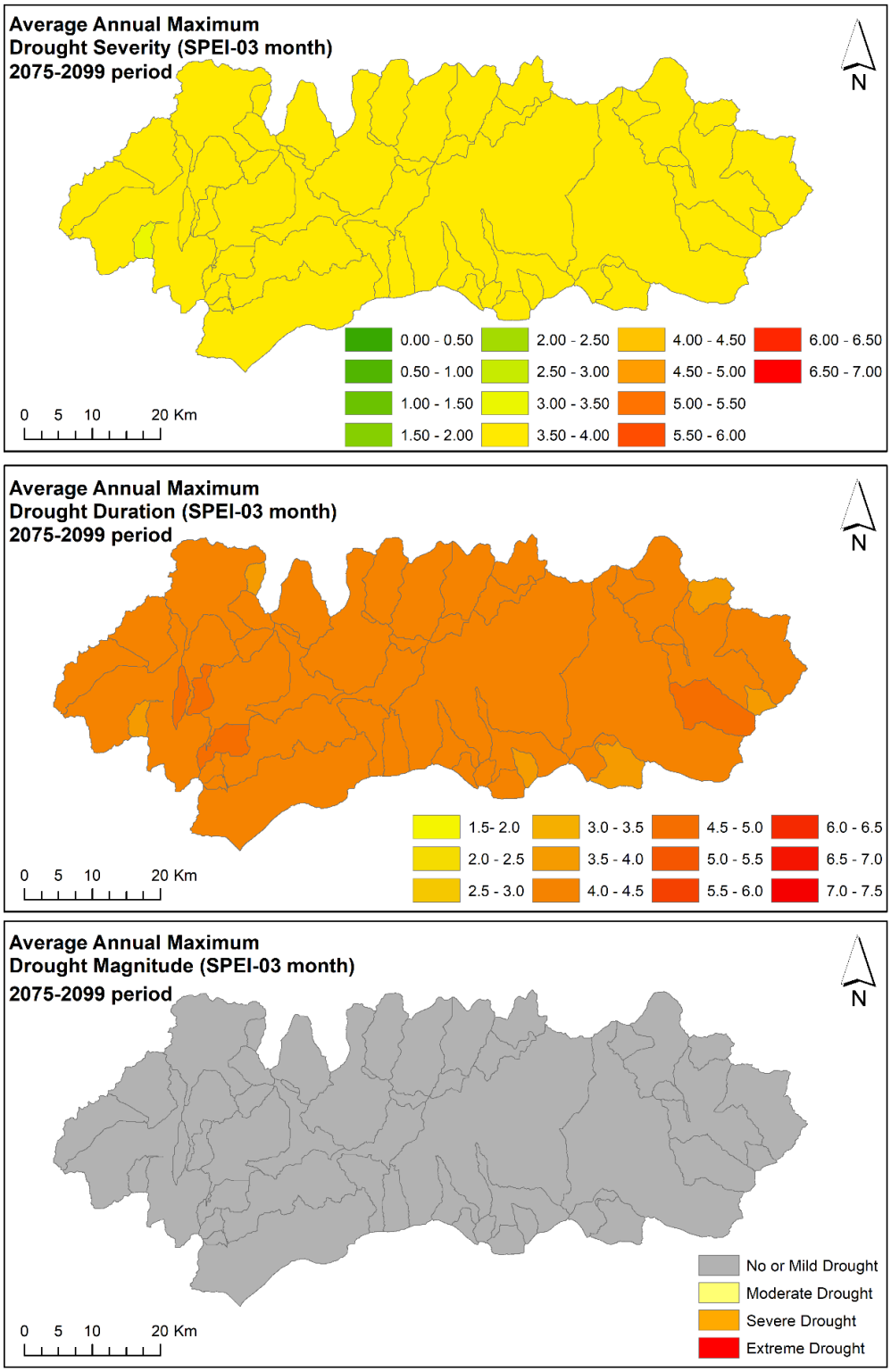


Figure 4.101 Maps obtained using SPEI-3 month series (with ET_a) for the far future period: a) average annual maximum drought severity, b) duration and c) magnitude.

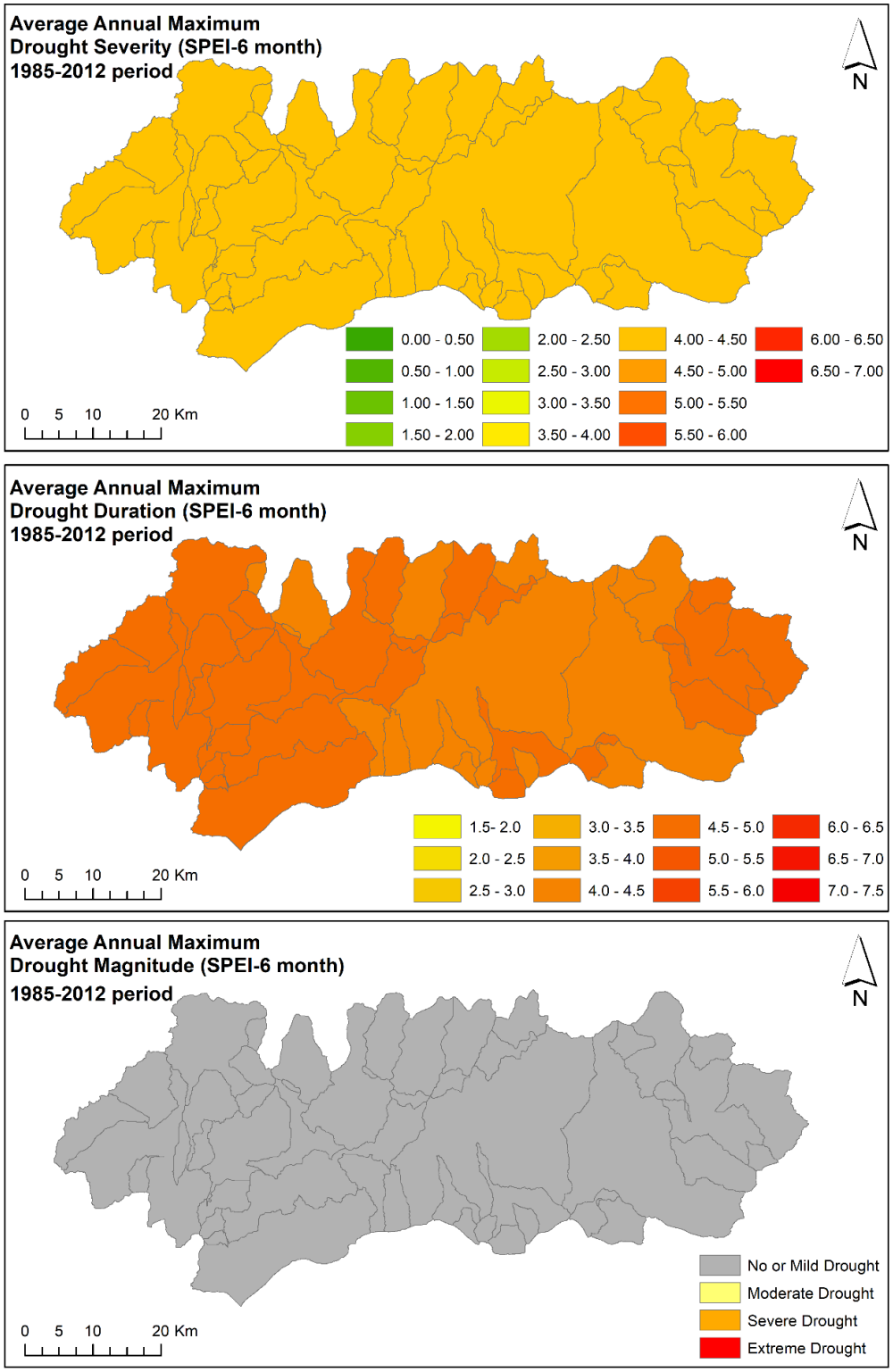


Figure 4.102 Maps obtained using SPEI-6 month series (with ET_a) for the reference period: a) average annual maximum drought severity, b) duration and c) magnitude.

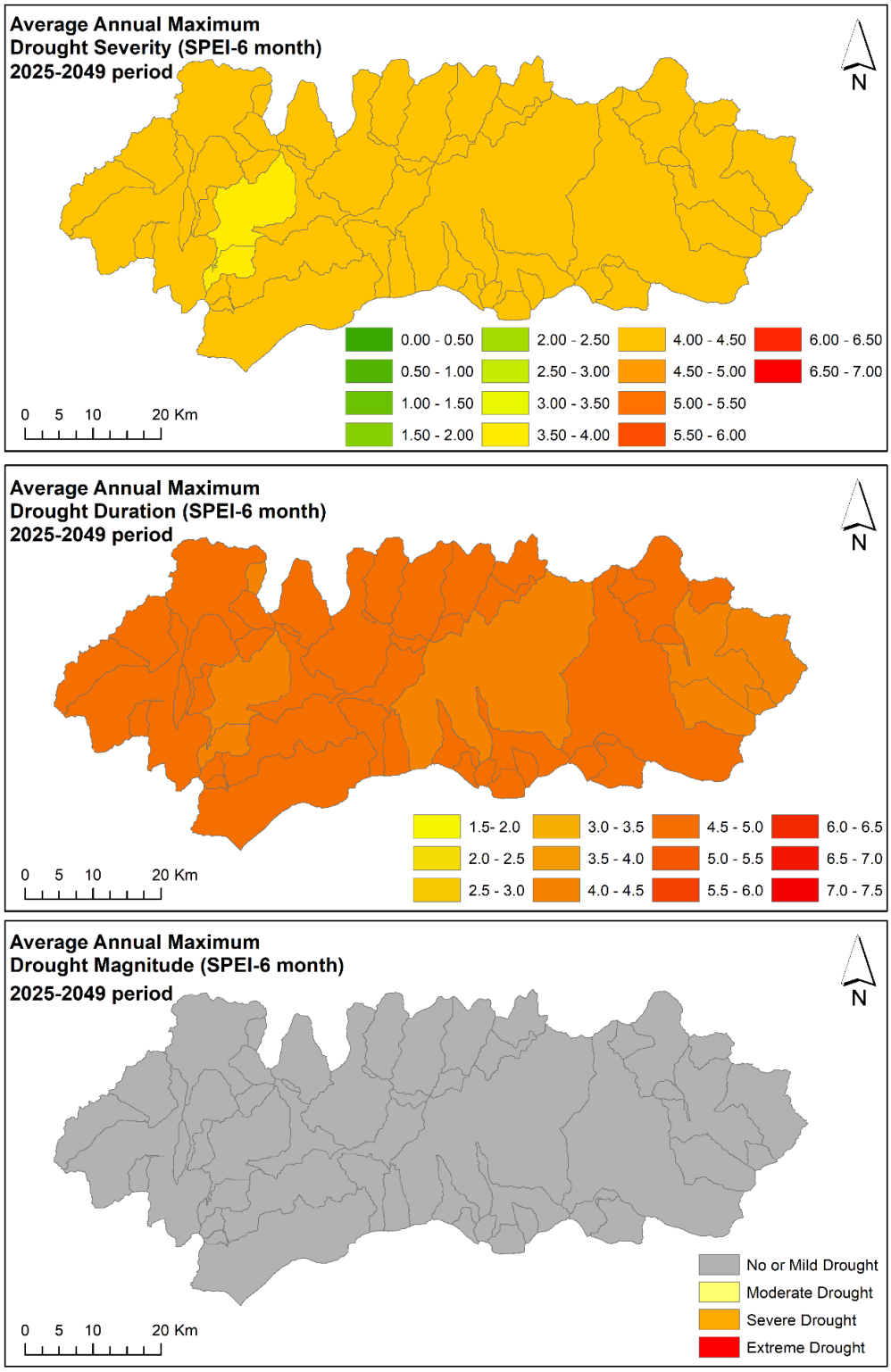


Figure 4.103 Maps obtained using SPEI-6 month series (with ET_a) for the near future period: a) average annual maximum drought severity, b) duration and c) magnitude.

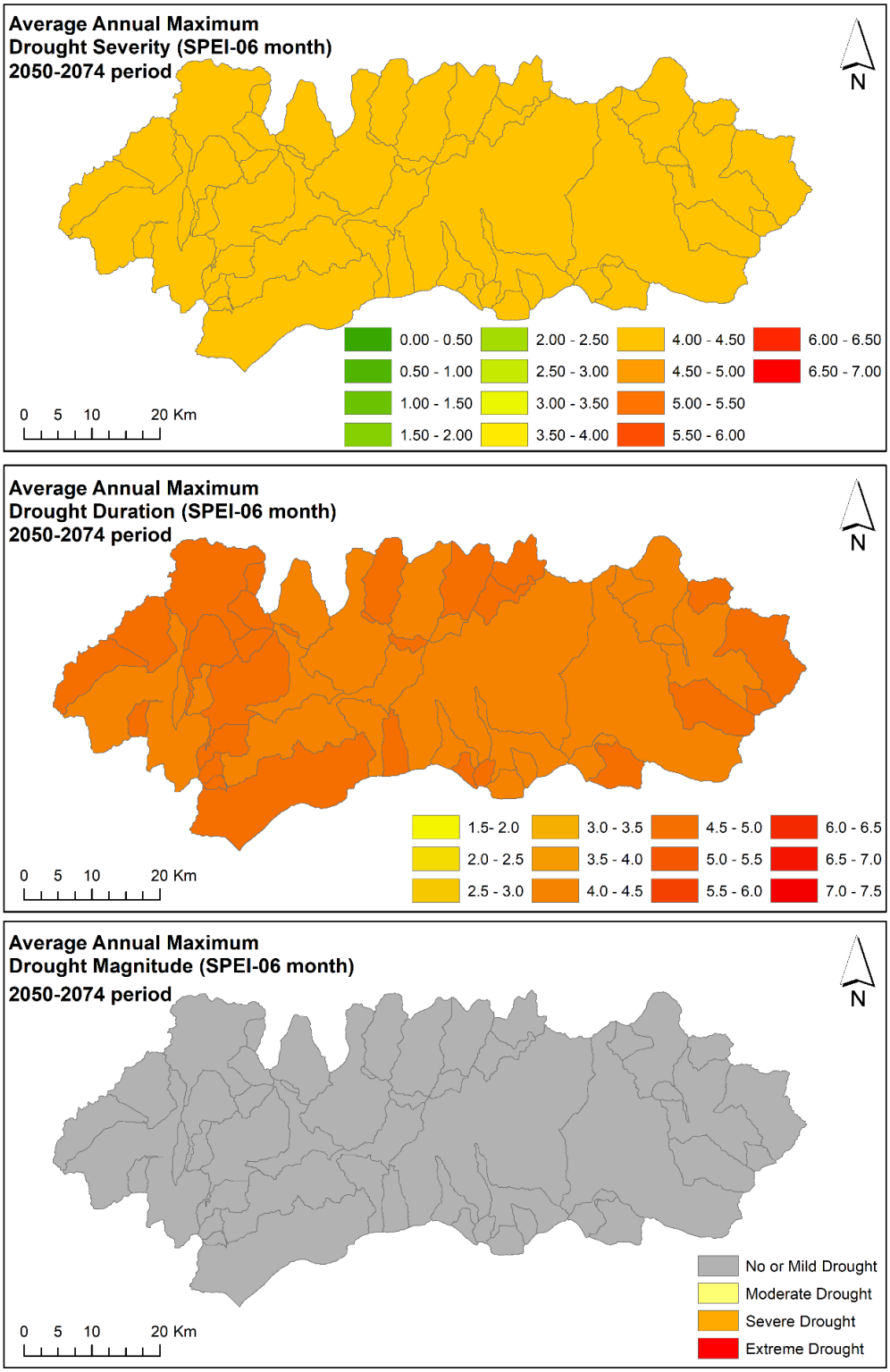


Figure 4.104 Maps obtained using SPEI-6 month series (with ET_a) for the middle future period: a) average annual maximum drought severity, b) duration and c) magnitude.

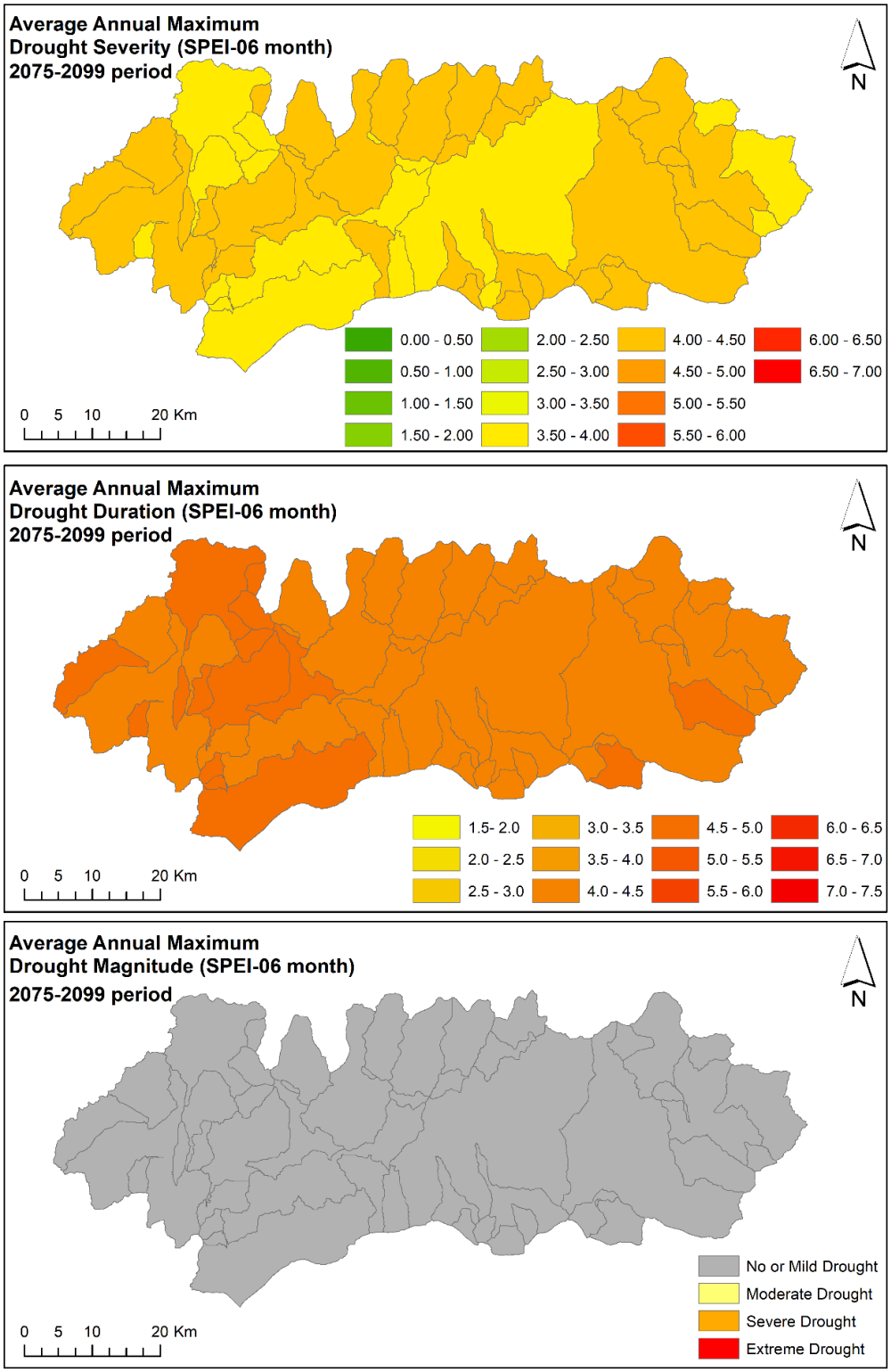


Figure 4.105 Maps obtained using SPEI-6 month series (with ET_a) for the far future period: a) average annual maximum drought severity, b) duration and c) magnitude.

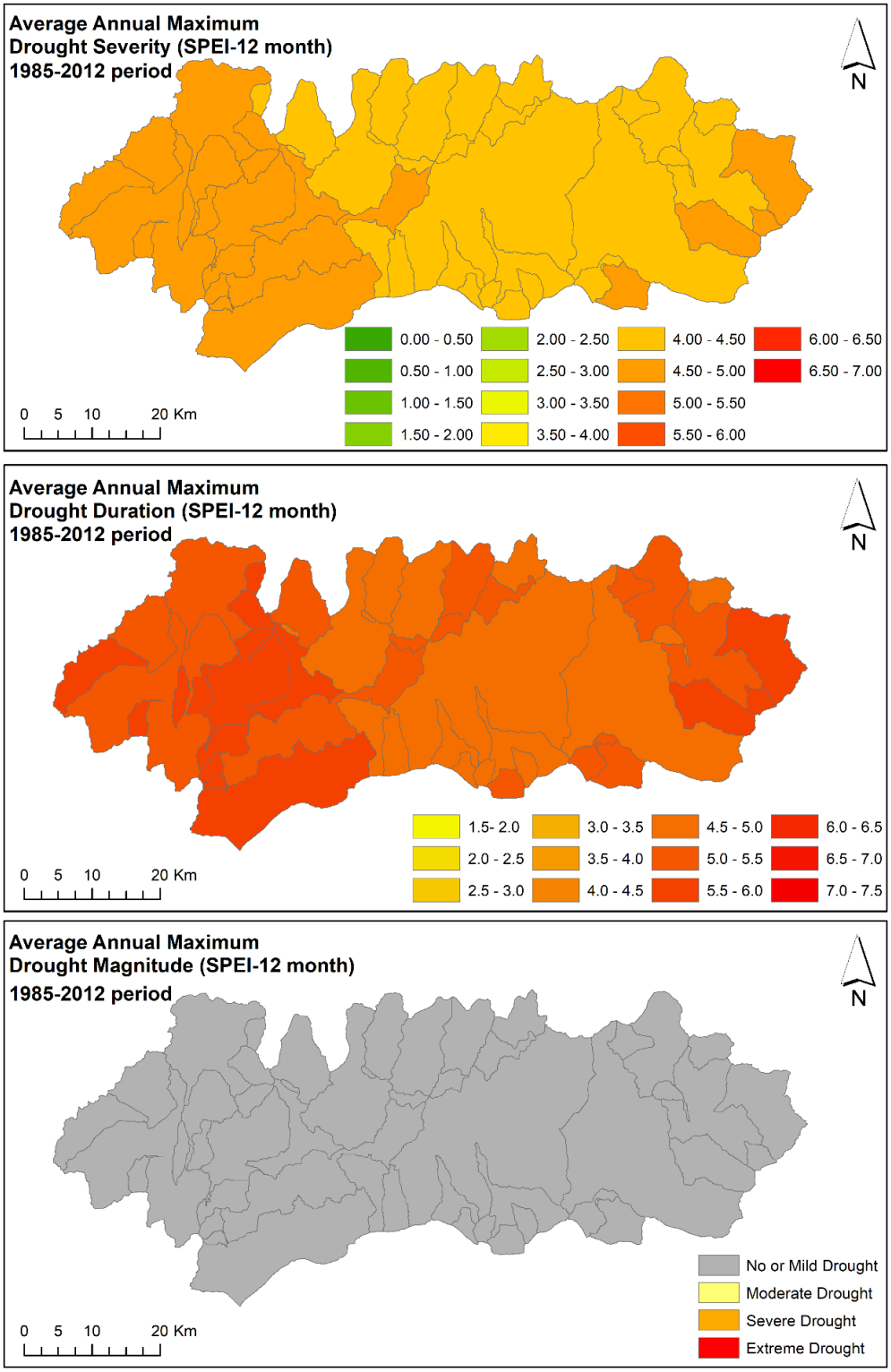


Figure 4.106 Maps obtained using SPEI-12 month series (with ET_a) for the reference period: a) average annual maximum drought severity, b) duration and c) magnitude.

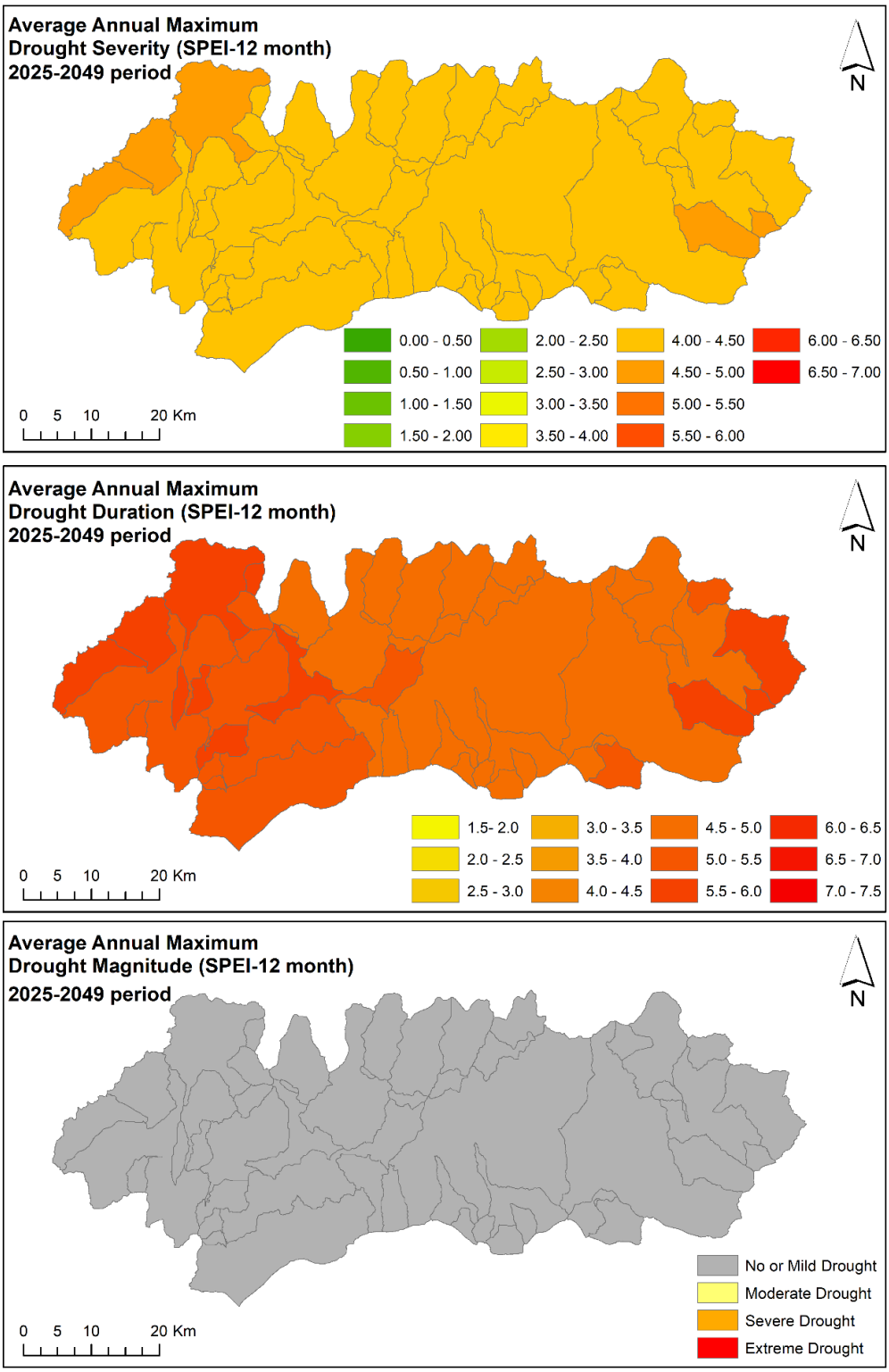


Figure 4.107 Maps obtained using SPEI-12 month series (with ET_a) for the near future period: a) average annual maximum drought severity, b) duration and c) magnitude.

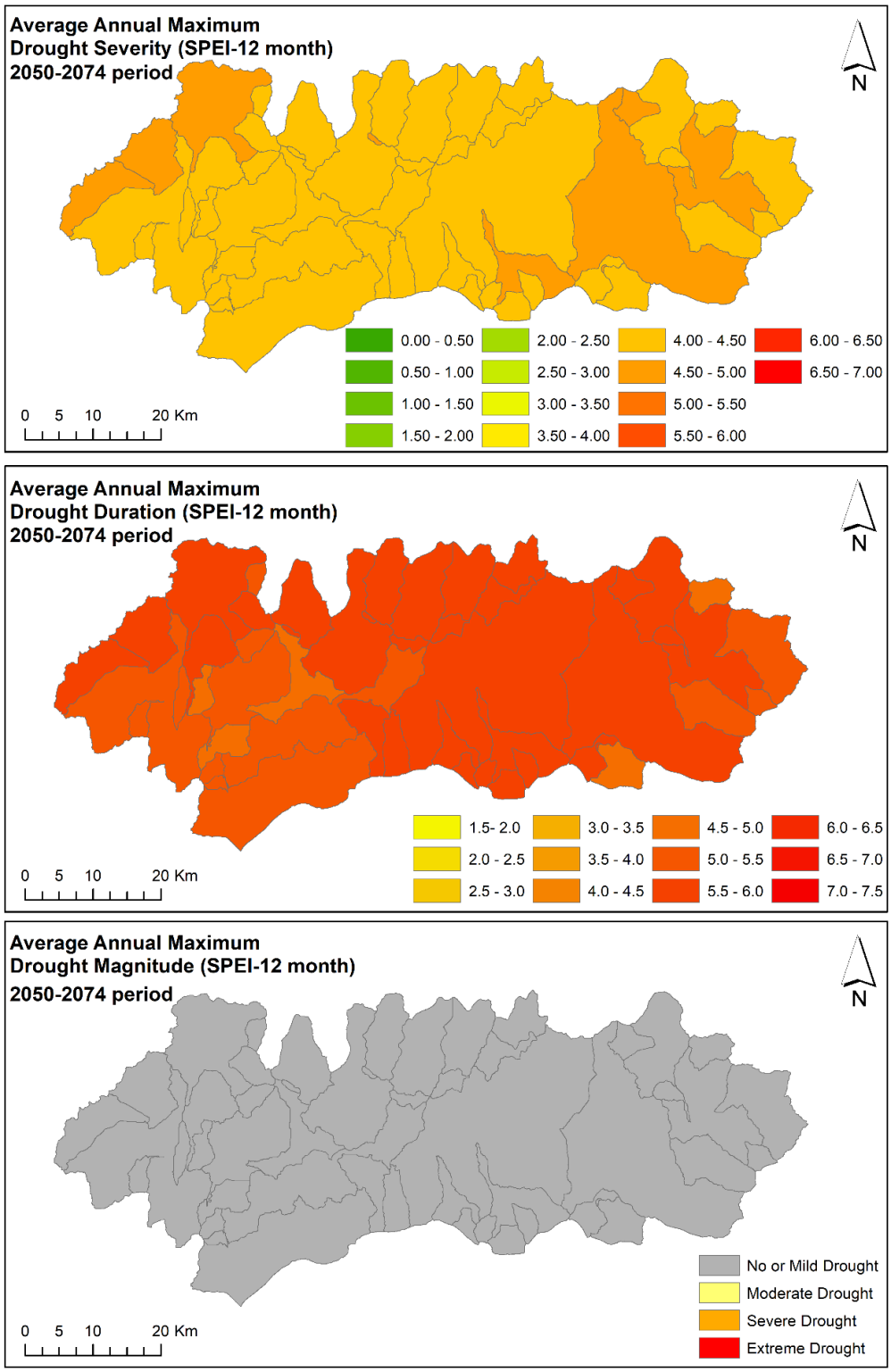


Figure 4.108 Maps obtained using SPEI-12 month series (with ET_a) for the middle future period: a) average annual maximum drought severity, b) duration and c) magnitude.

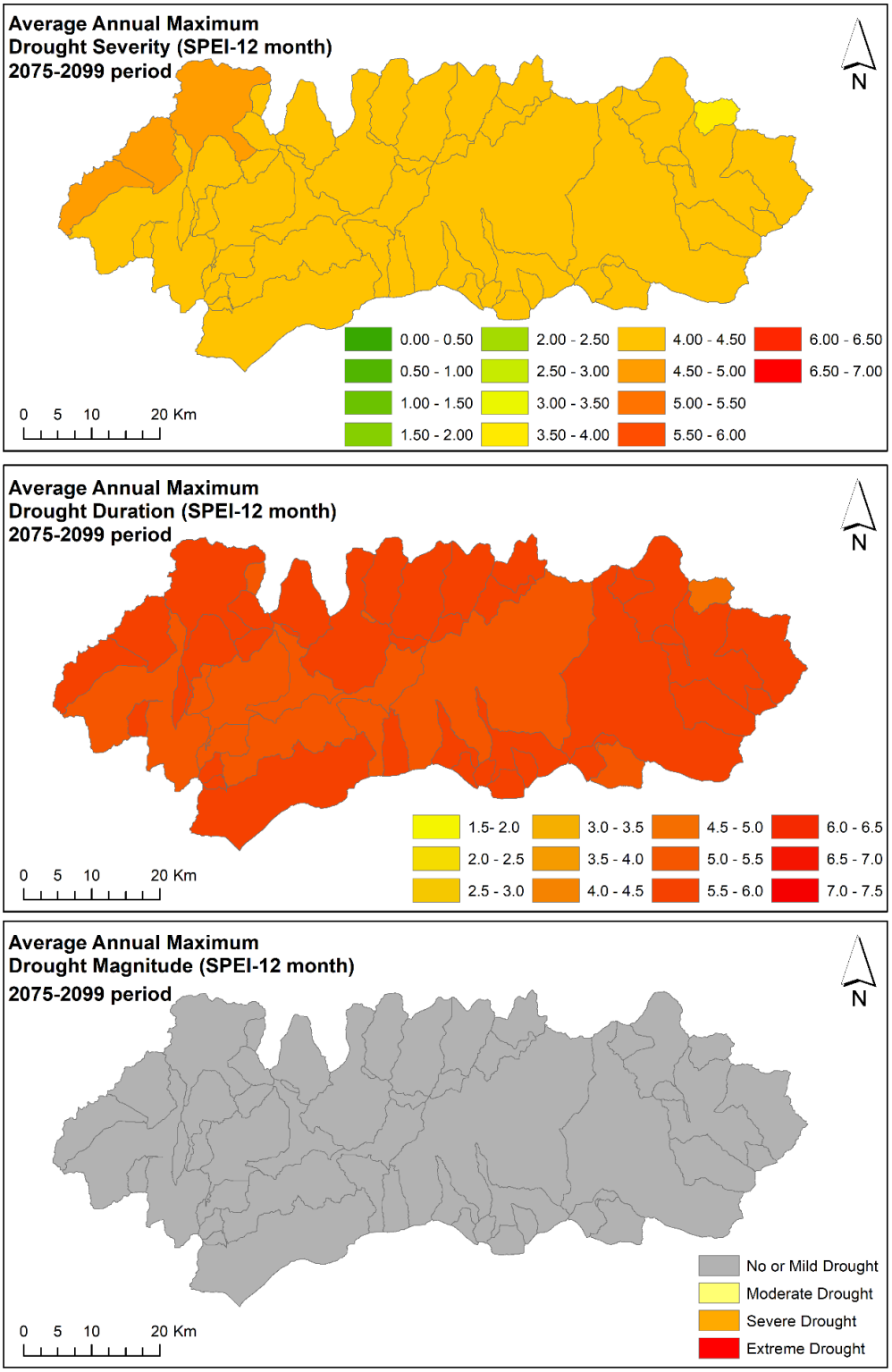


Figure 4.109 Maps obtained using SPEI-12 month series (with ET_a) for the far future period: a) average annual maximum drought severity, b) duration and c) magnitude.

4.3.3.3 Drought Maps Generated Using SPEI (with PET)

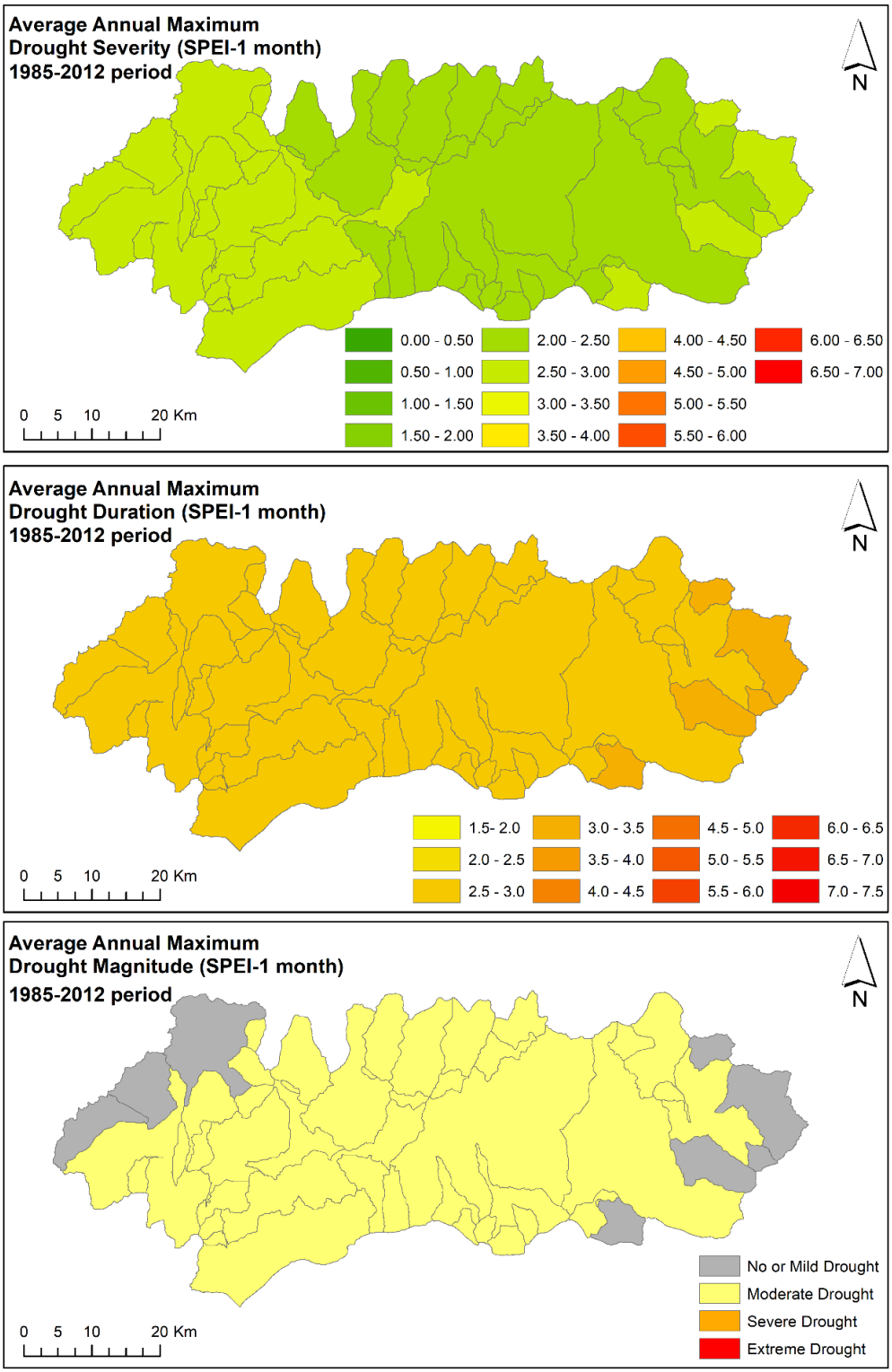


Figure 4.110 Maps obtained using SPEI-1 month series (with PET) for the far future period: a) average annual maximum drought severity, b) duration and c) magnitude.

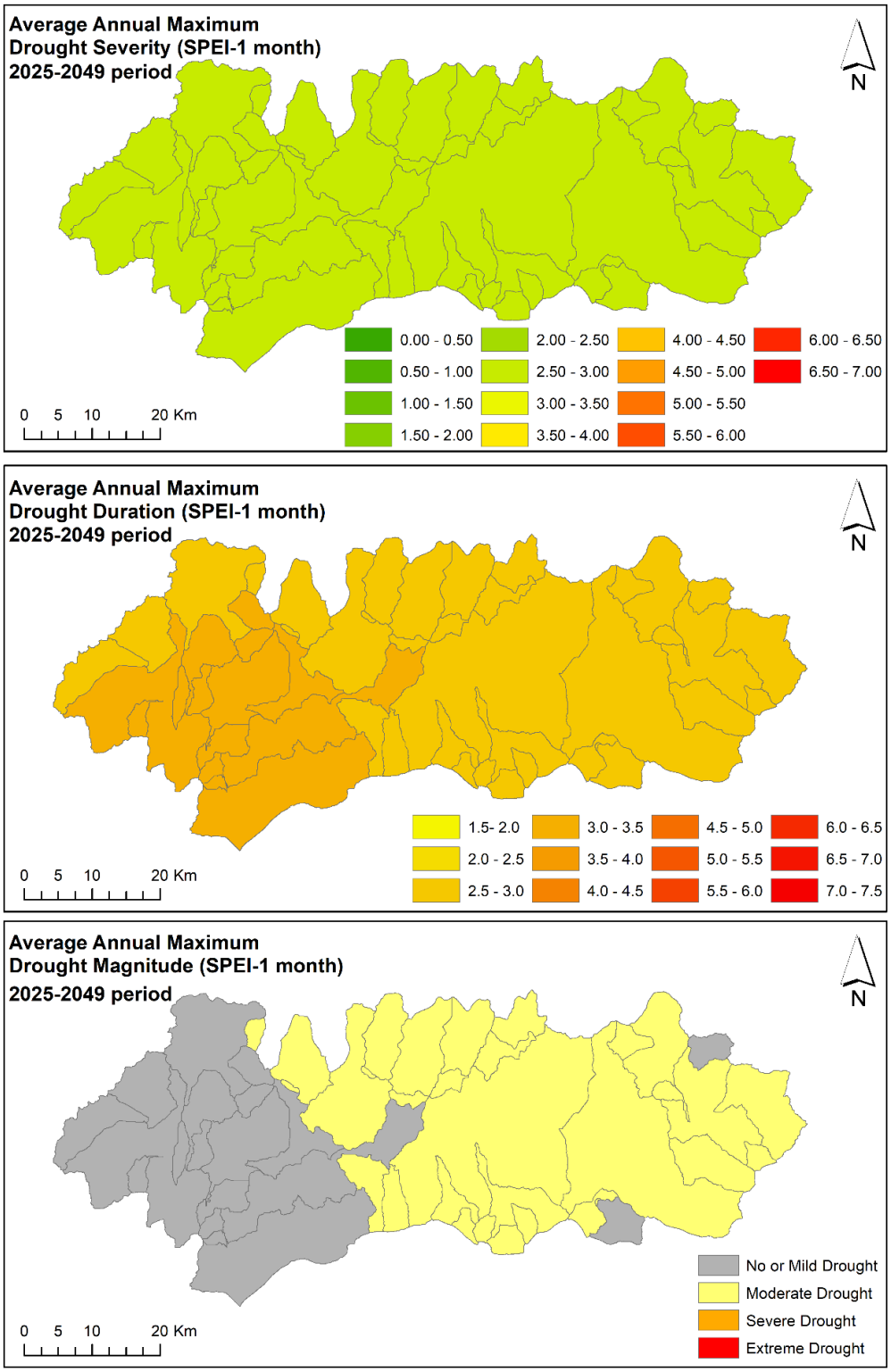


Figure 4.111 Maps obtained using SPEI-1 month series (with PET) for the near future period: a) average annual maximum drought severity, b) duration and c) magnitude.

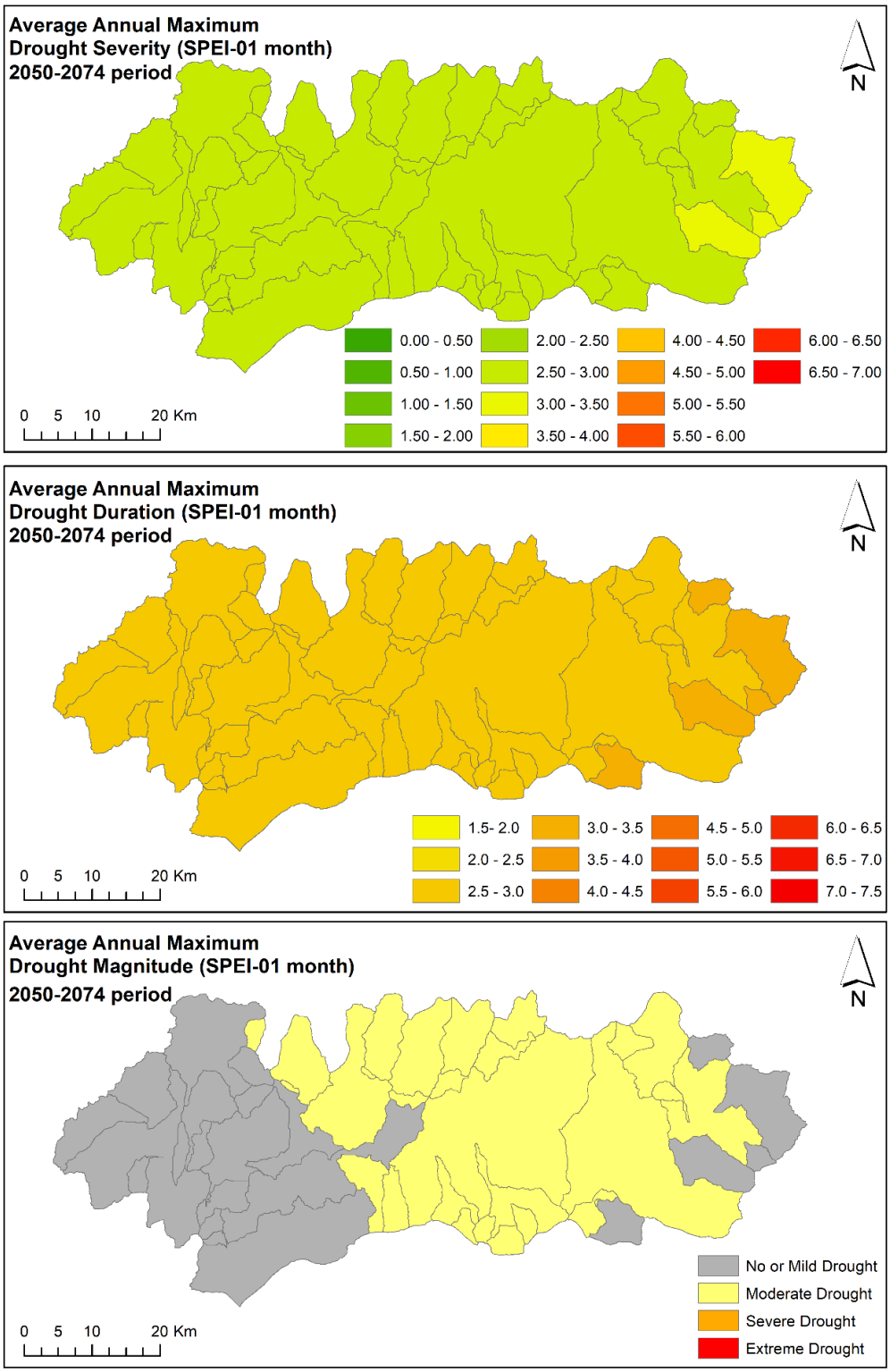


Figure 4.112 Maps obtained using SPEI-1 month series (with PET) for the middle future period: a) average annual maximum drought severity, b) duration and c) magnitude.

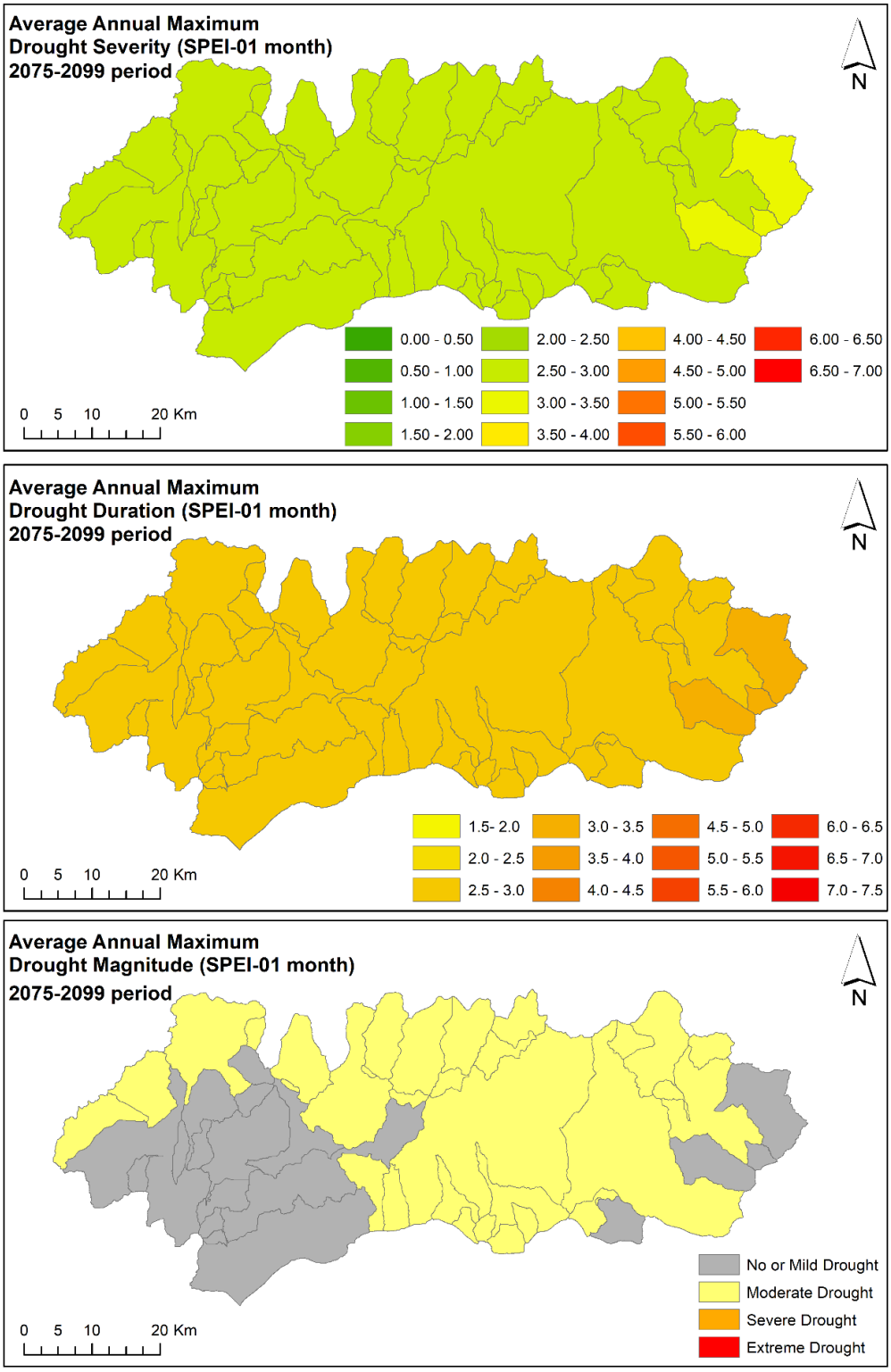


Figure 4.113 Maps obtained using SPEI-1 month series (with PET) for the far future period: a) average annual maximum drought severity, b) duration and c) magnitude.

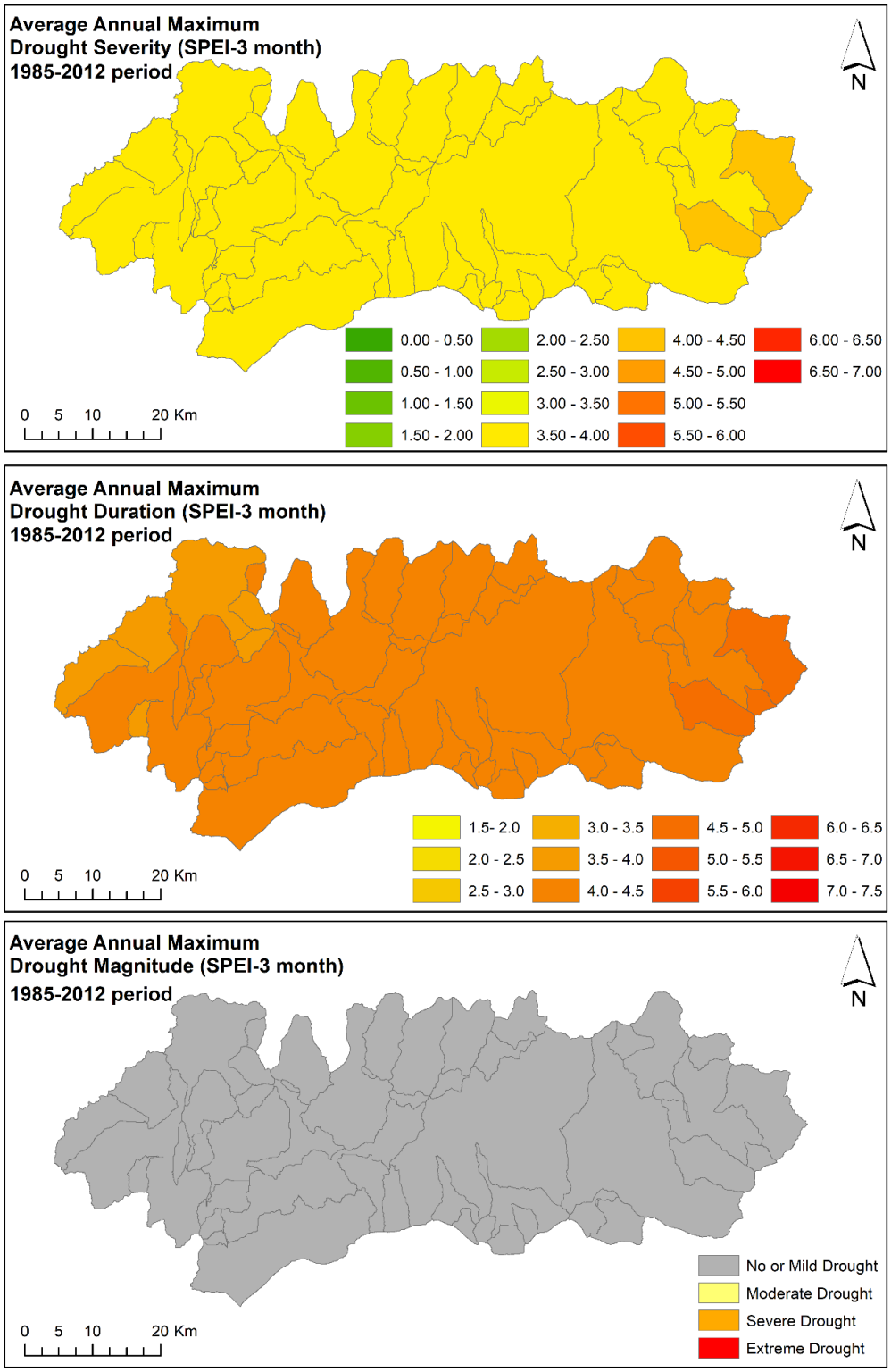


Figure 4.114 Maps obtained using SPEI-3 month series (with PET) for the reference period: a) average annual maximum drought severity, b) duration and c) magnitude.

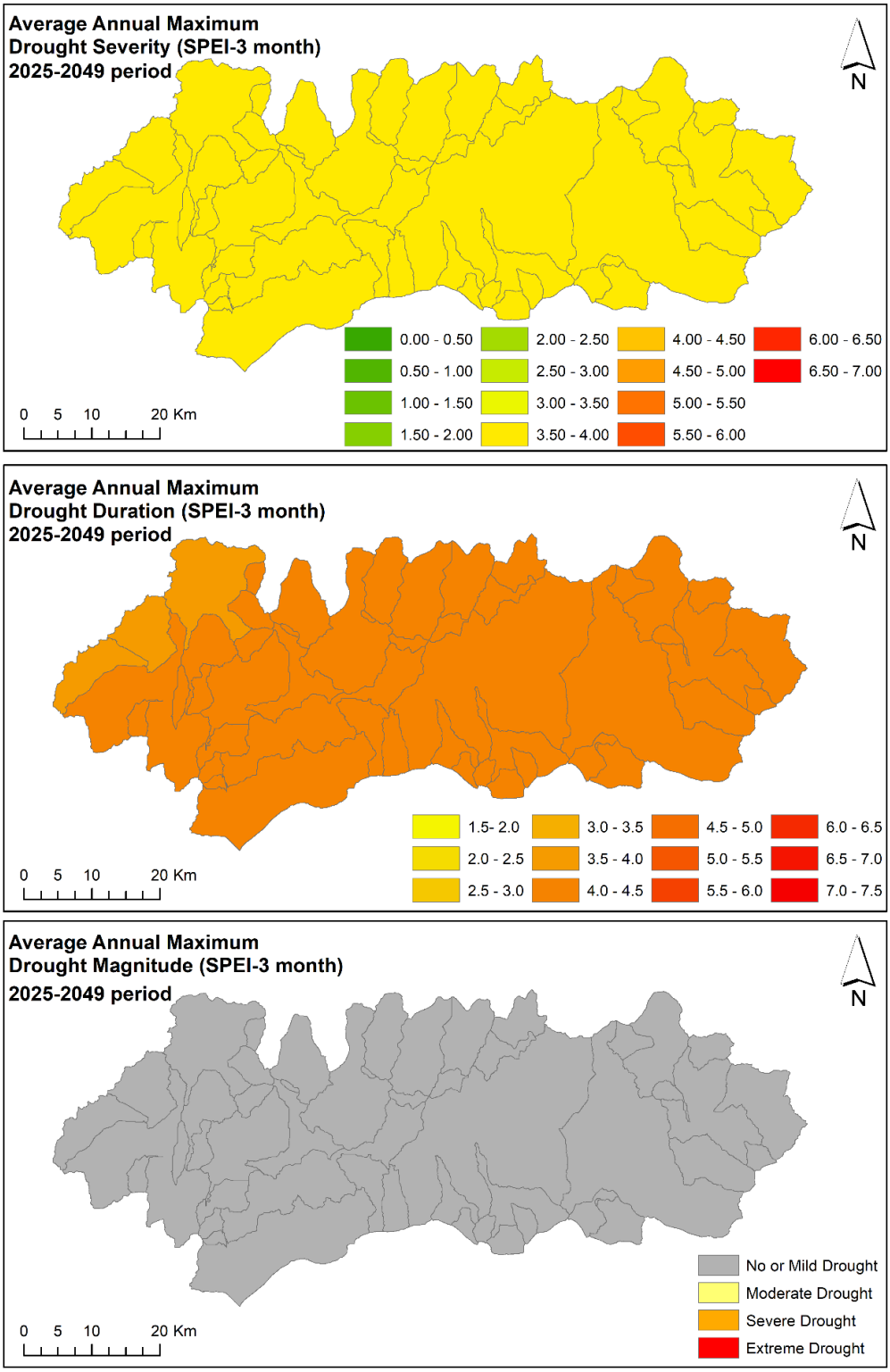


Figure 4.115 Maps obtained using SPEI-3 month series (with PET) for the near future period: a) average annual maximum drought severity, b) duration and c) magnitude.

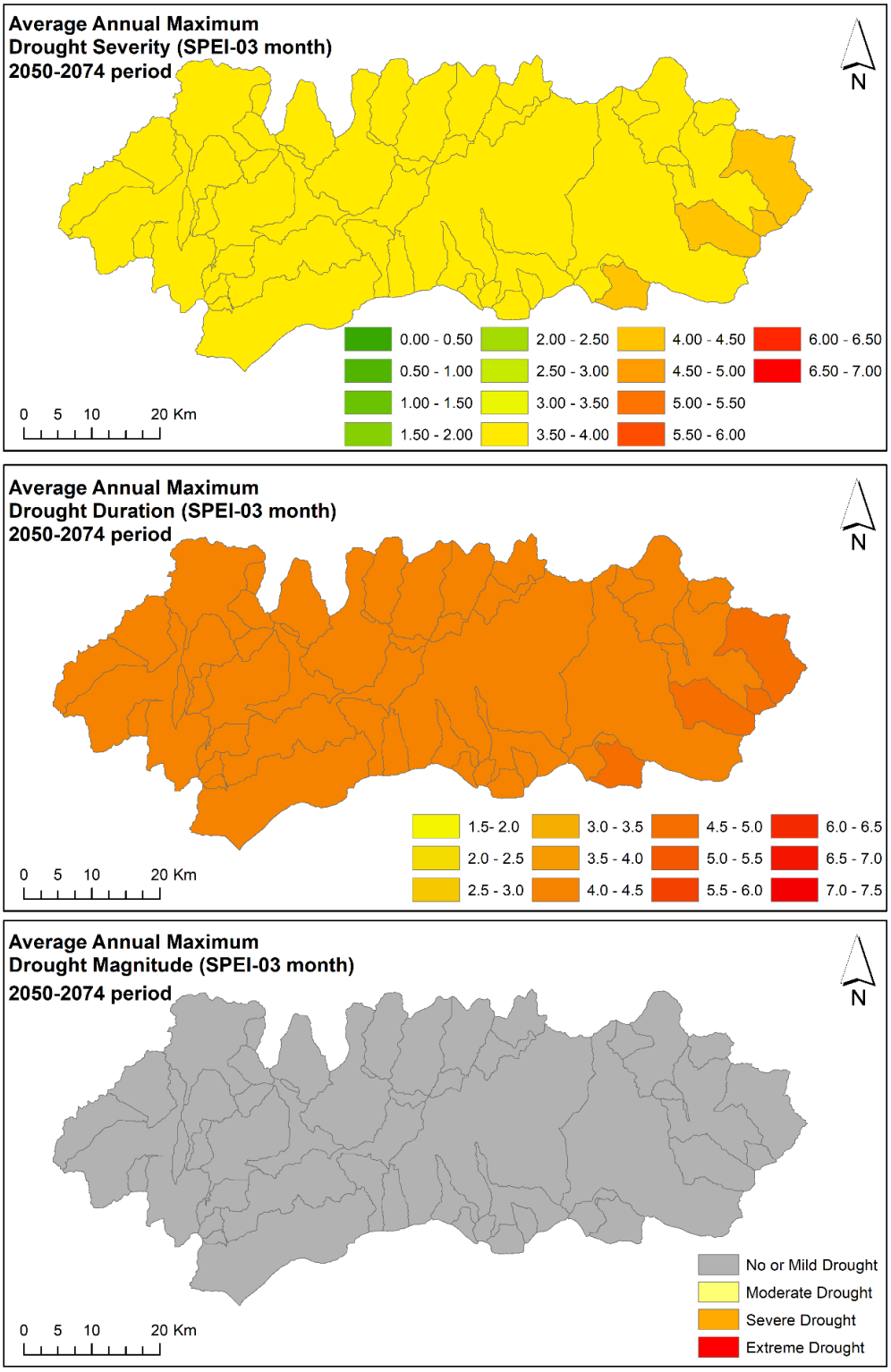


Figure 4.116 Maps obtained using SPEI-3 month series (with PET) for the middle future period: a) average annual maximum drought severity, b) duration and c) magnitude.

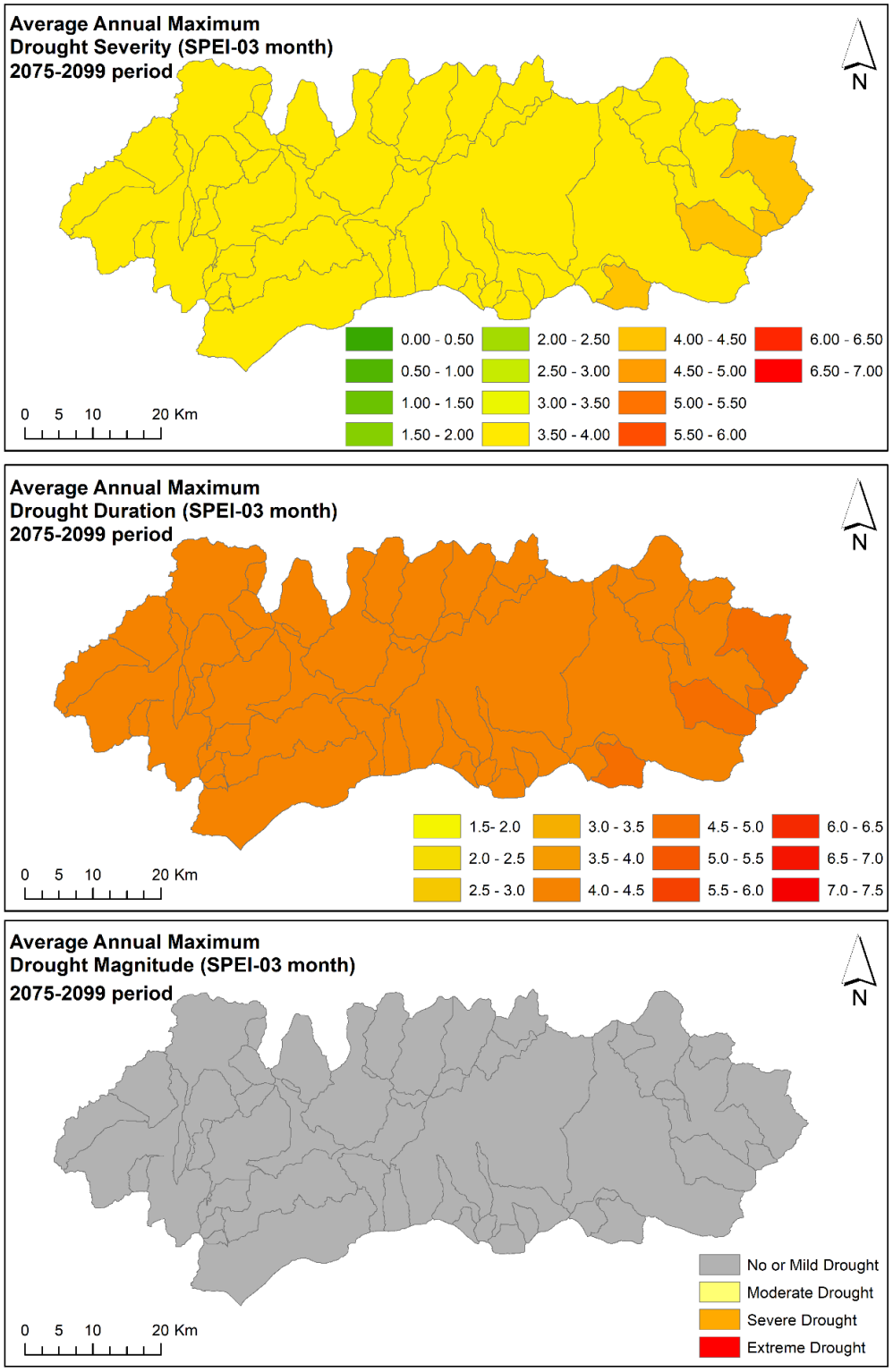


Figure 4.117 Maps obtained using SPEI-3 month series (with PET) for the far future period: a) average annual maximum drought severity, b) duration and c) magnitude.

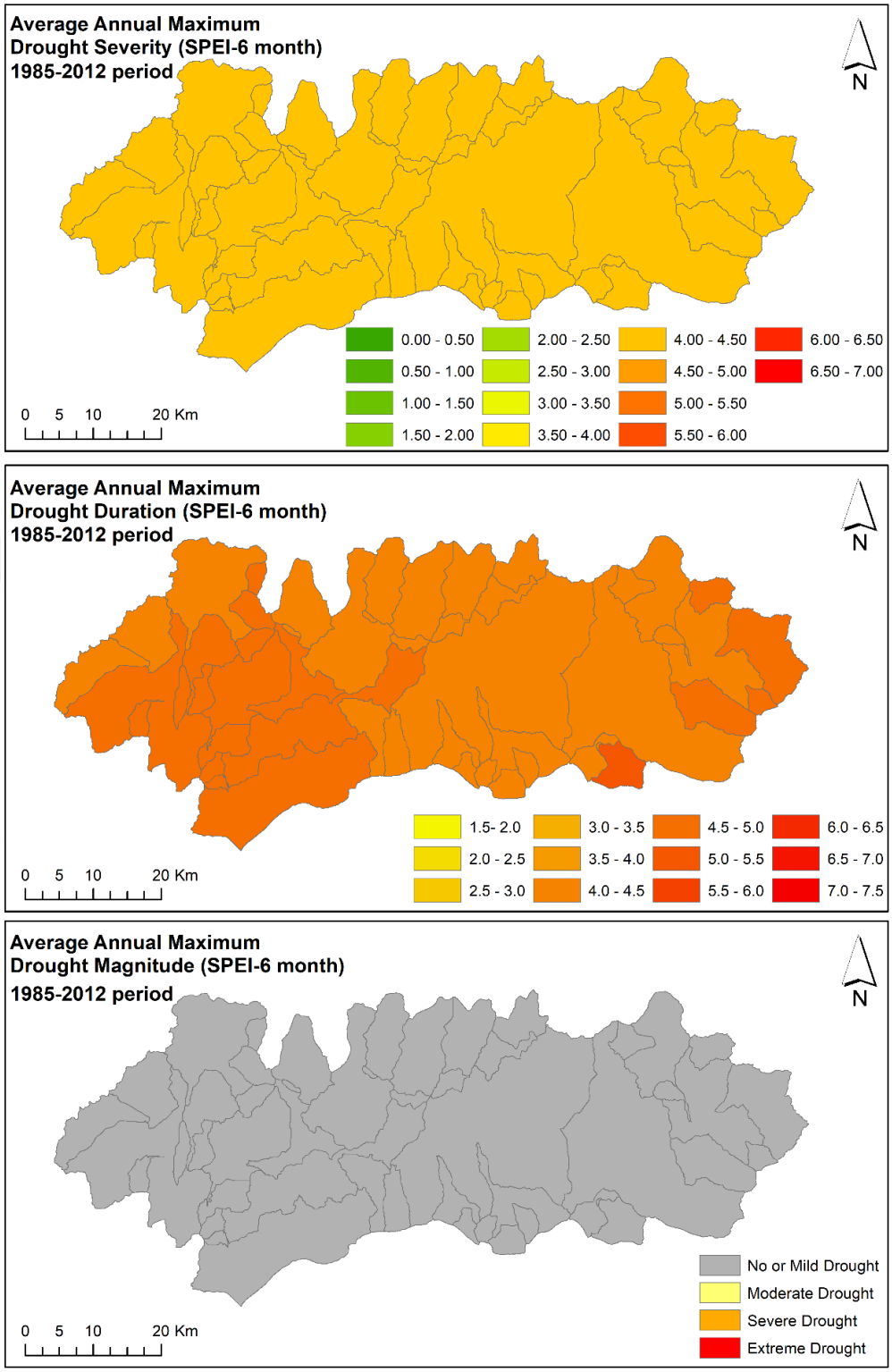


Figure 4.118 Maps obtained using SPEI-6 month series (with PET) for the reference period: a) average annual maximum drought severity, b) duration and c) magnitude.

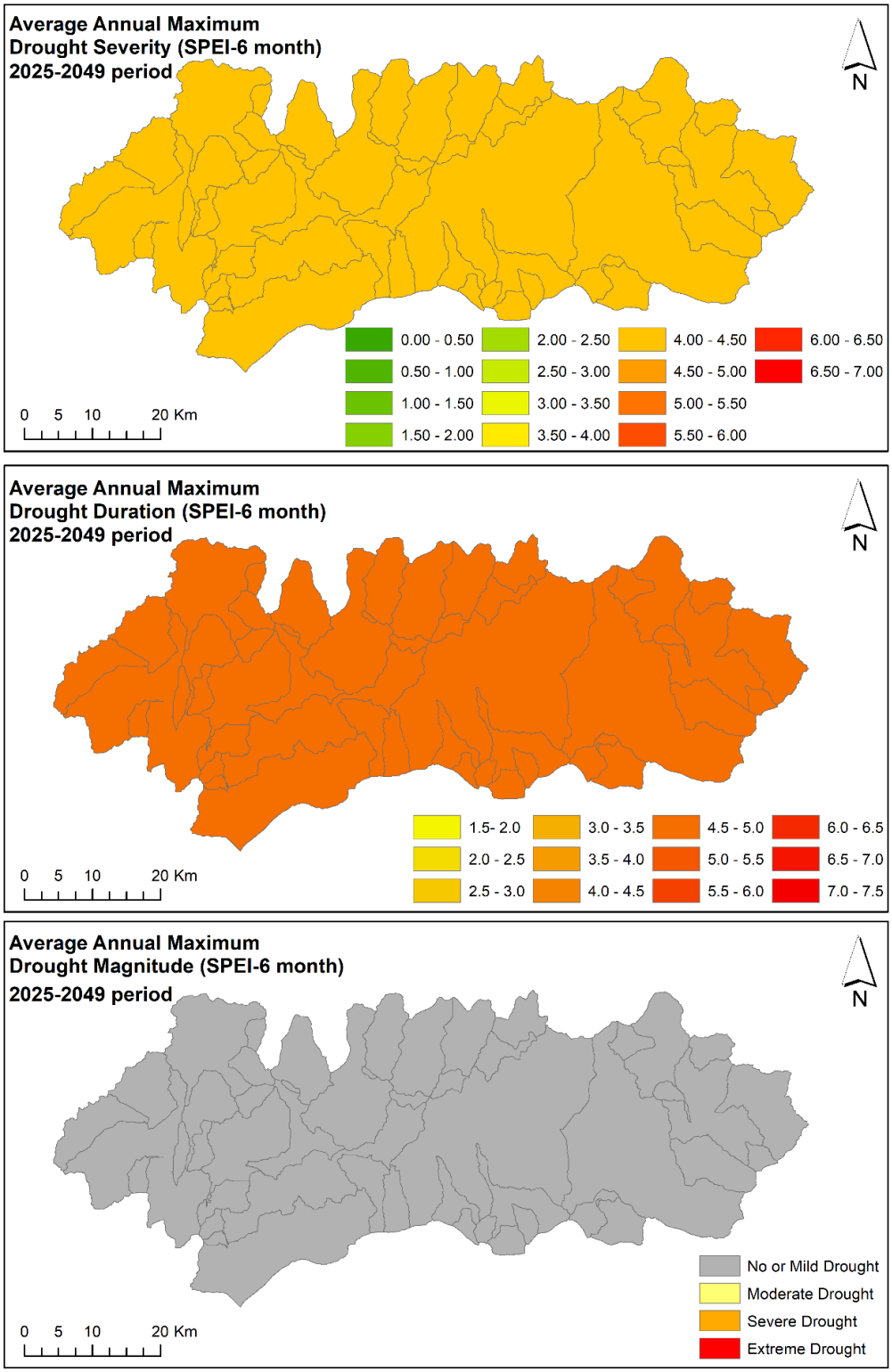


Figure 4.119 Maps obtained using SPEI-6 month series (with PET) for the near future period: a) average annual maximum drought severity, b) duration and c) magnitude.

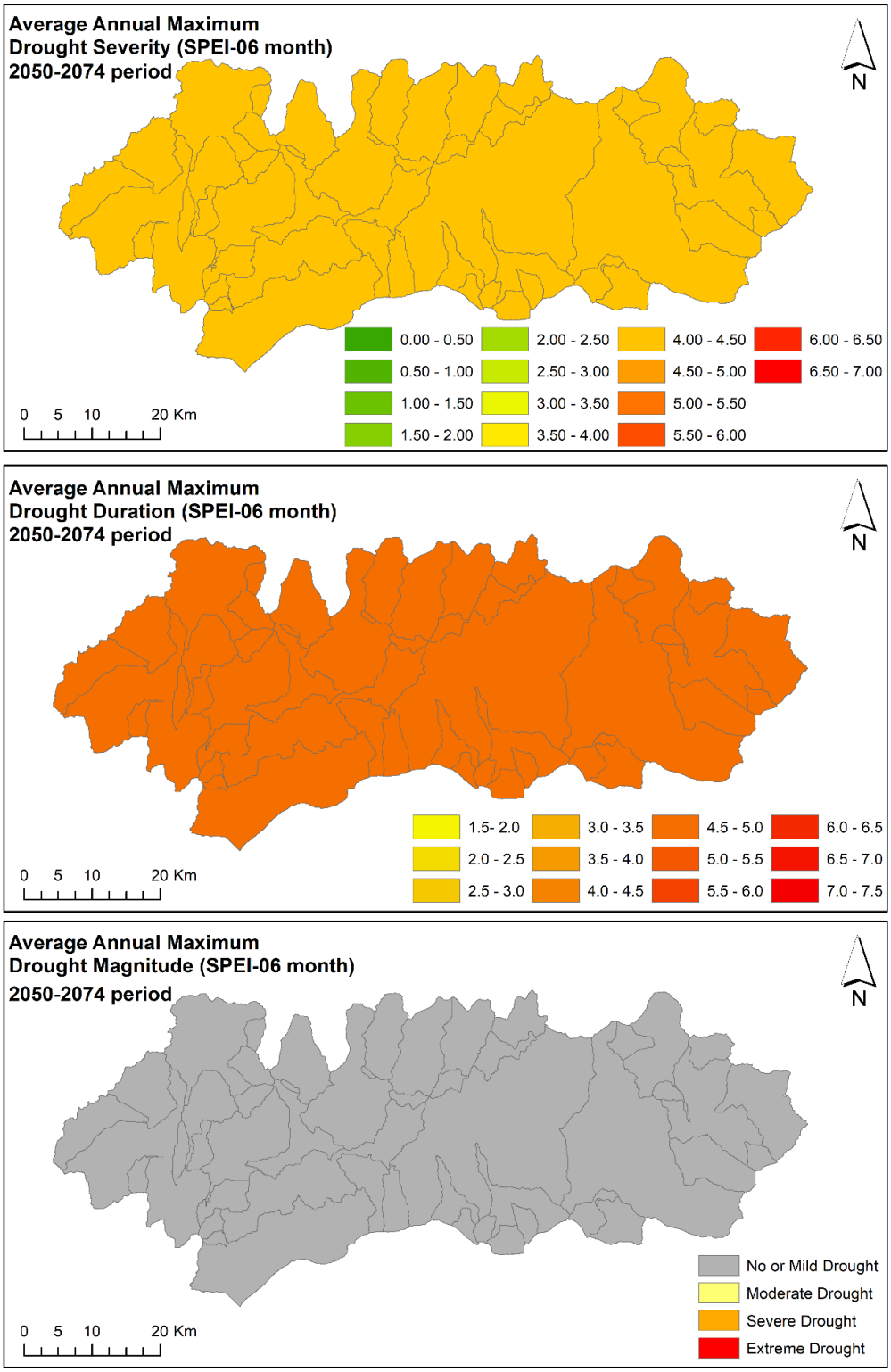


Figure 4.120 Maps obtained using SPEI-6 month series (with PET) for the middle future period: a) average annual maximum drought severity, b) duration and c) magnitude.

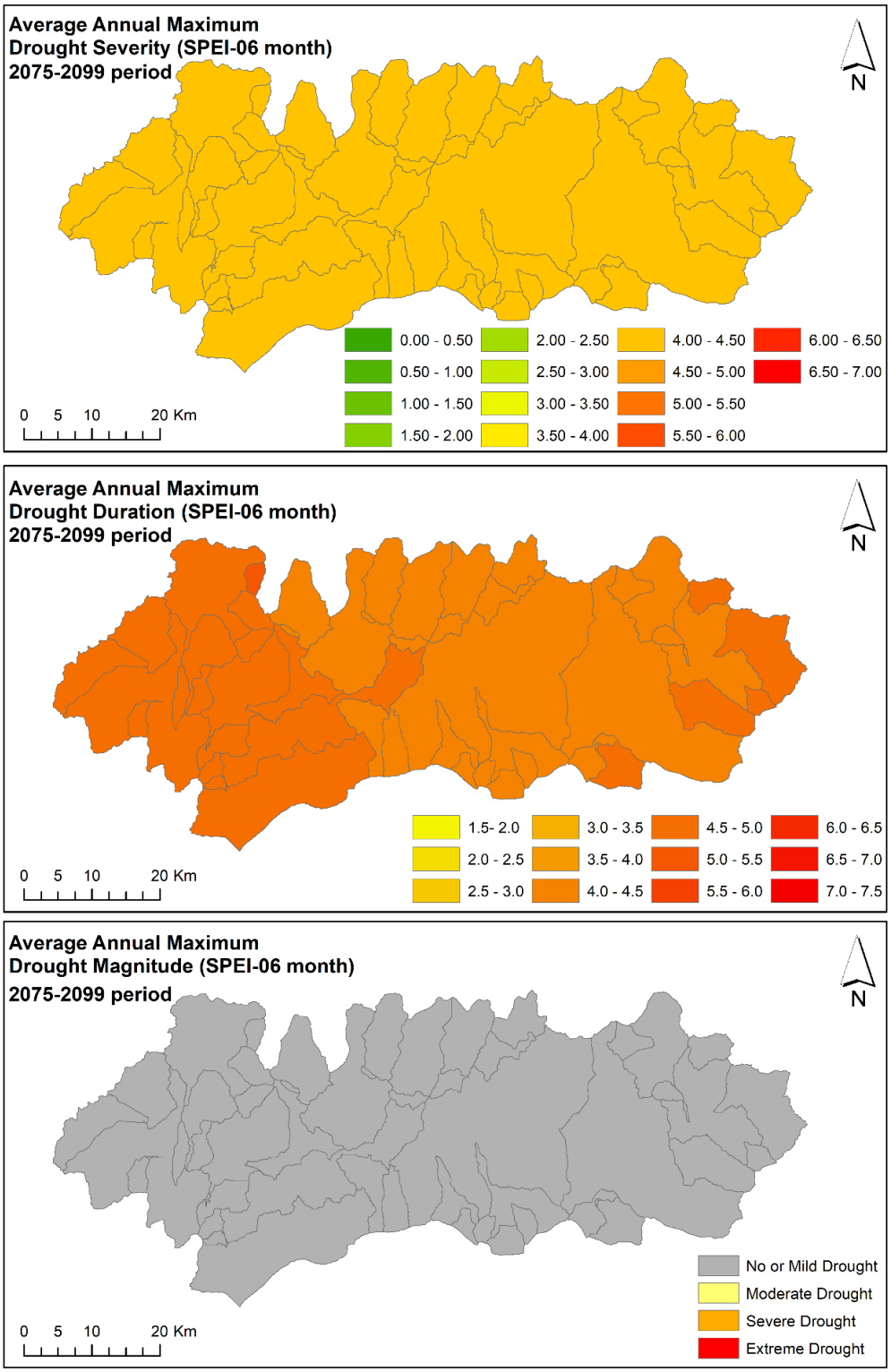


Figure 4.121 Maps obtained using SPEI-6 month series (with PET) for the far future period: a) average annual maximum drought severity, b) duration and c) magnitude.

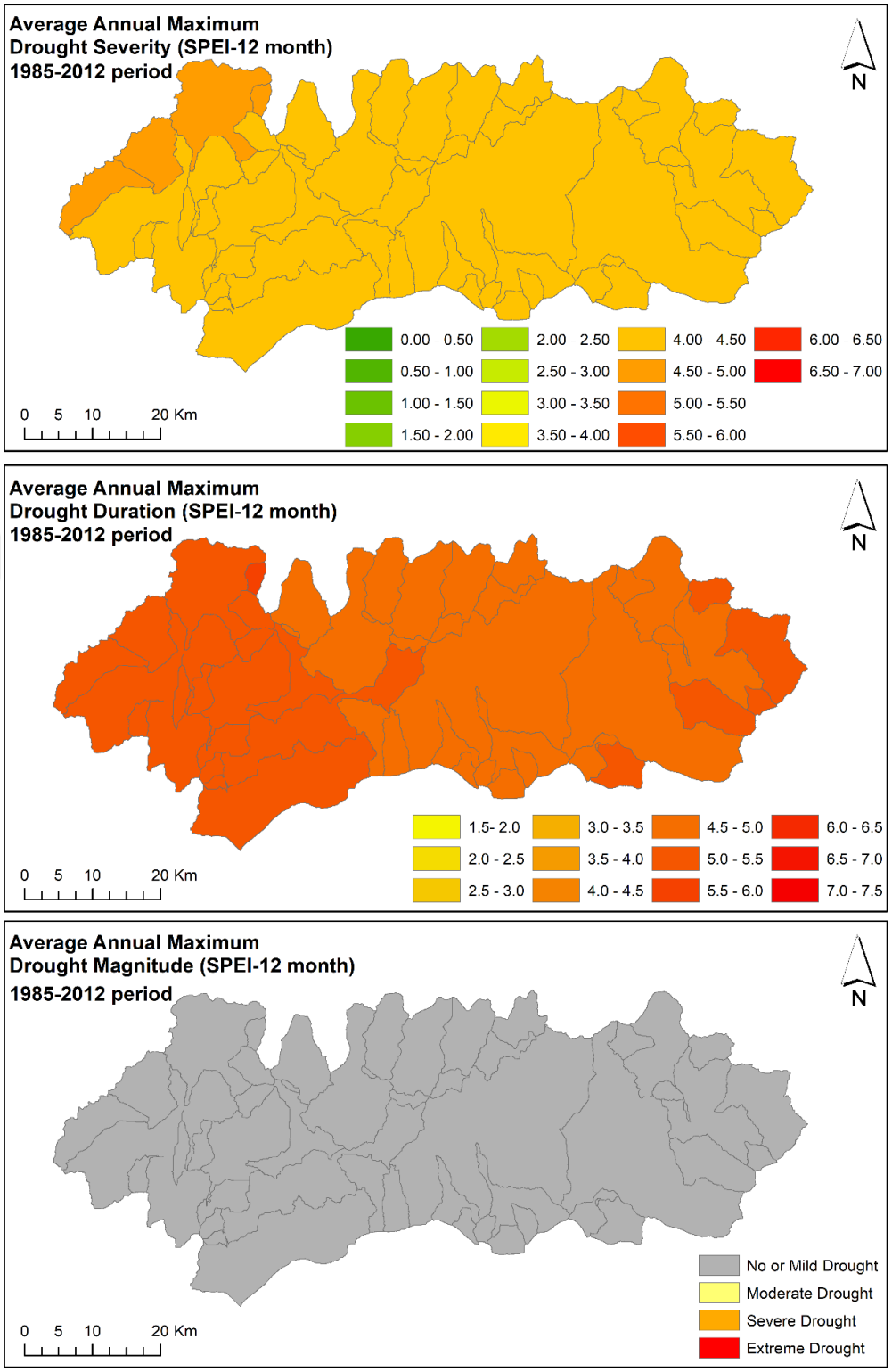


Figure 4.122 Maps obtained using SPEI-12 month series (with PET) for the reference period: a) average annual maximum drought severity, b) duration and c) magnitude.

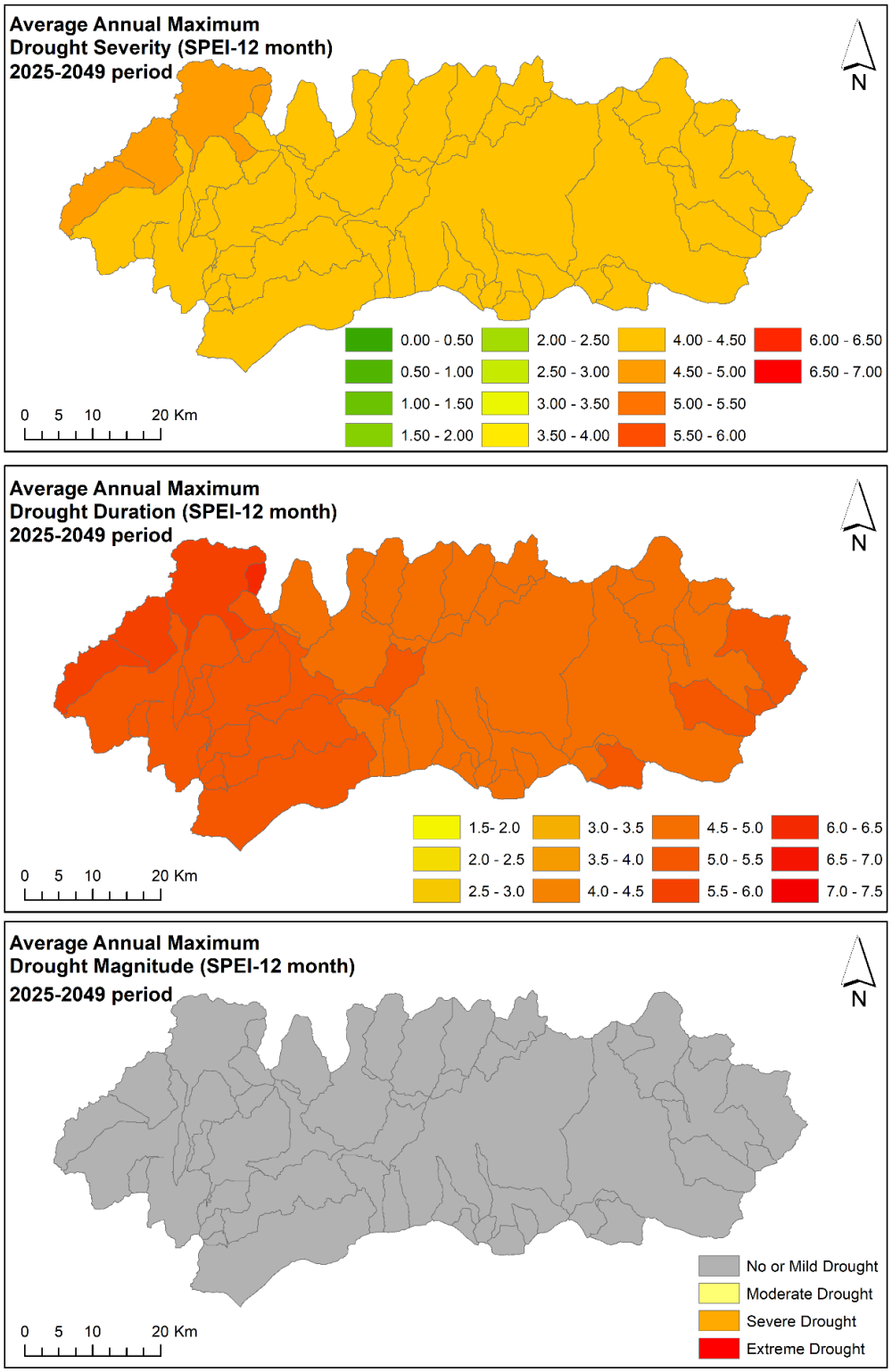


Figure 4.123 Maps obtained using SPEI-12 month series (with PET) for the near future period: a) average annual maximum drought severity, b) duration and c) magnitude.

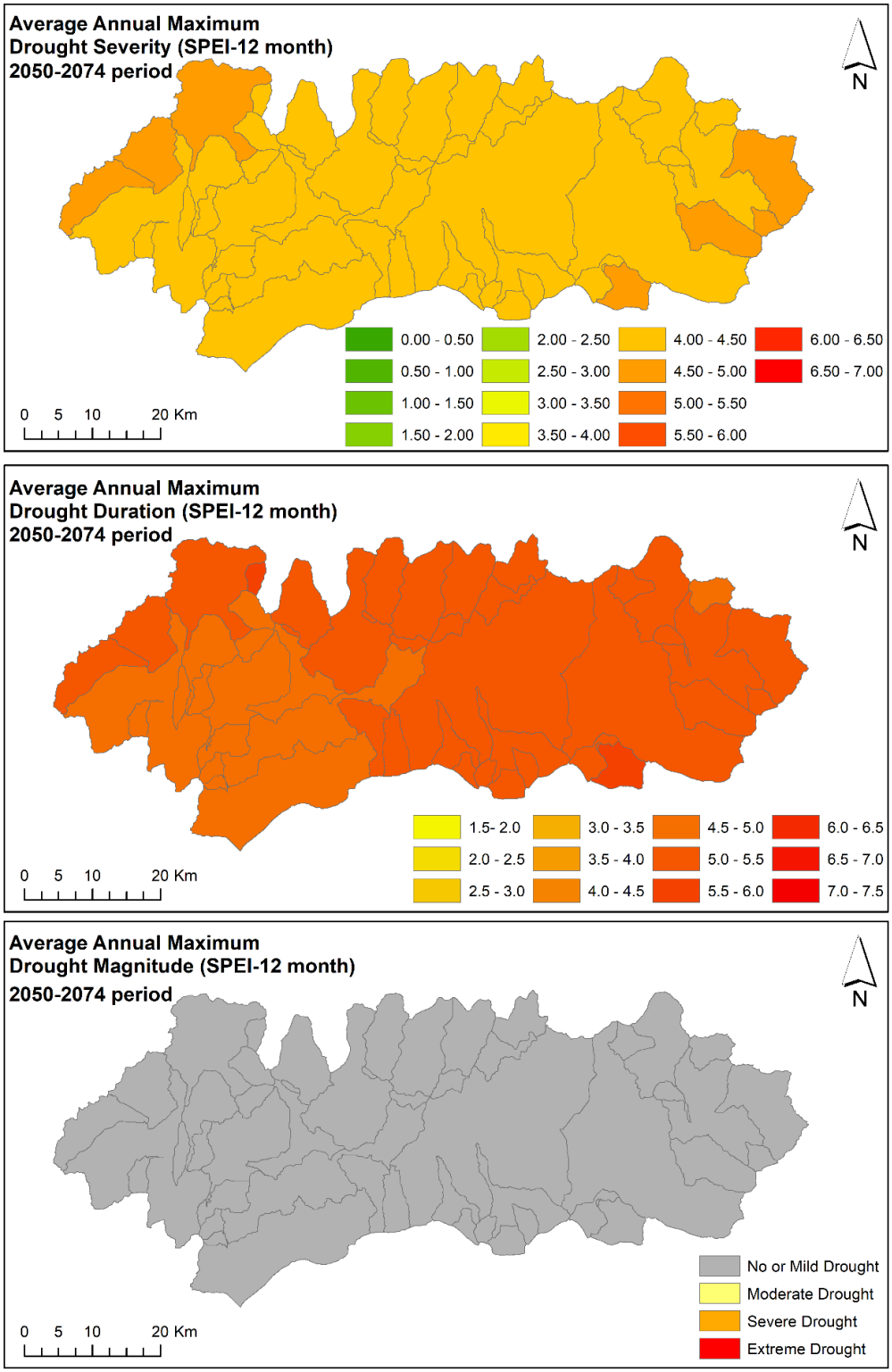


Figure 4.124 Maps obtained using SPEI-12 month series (with PET) for the middle future period: a) average annual maximum drought severity, b) duration and c) magnitude.

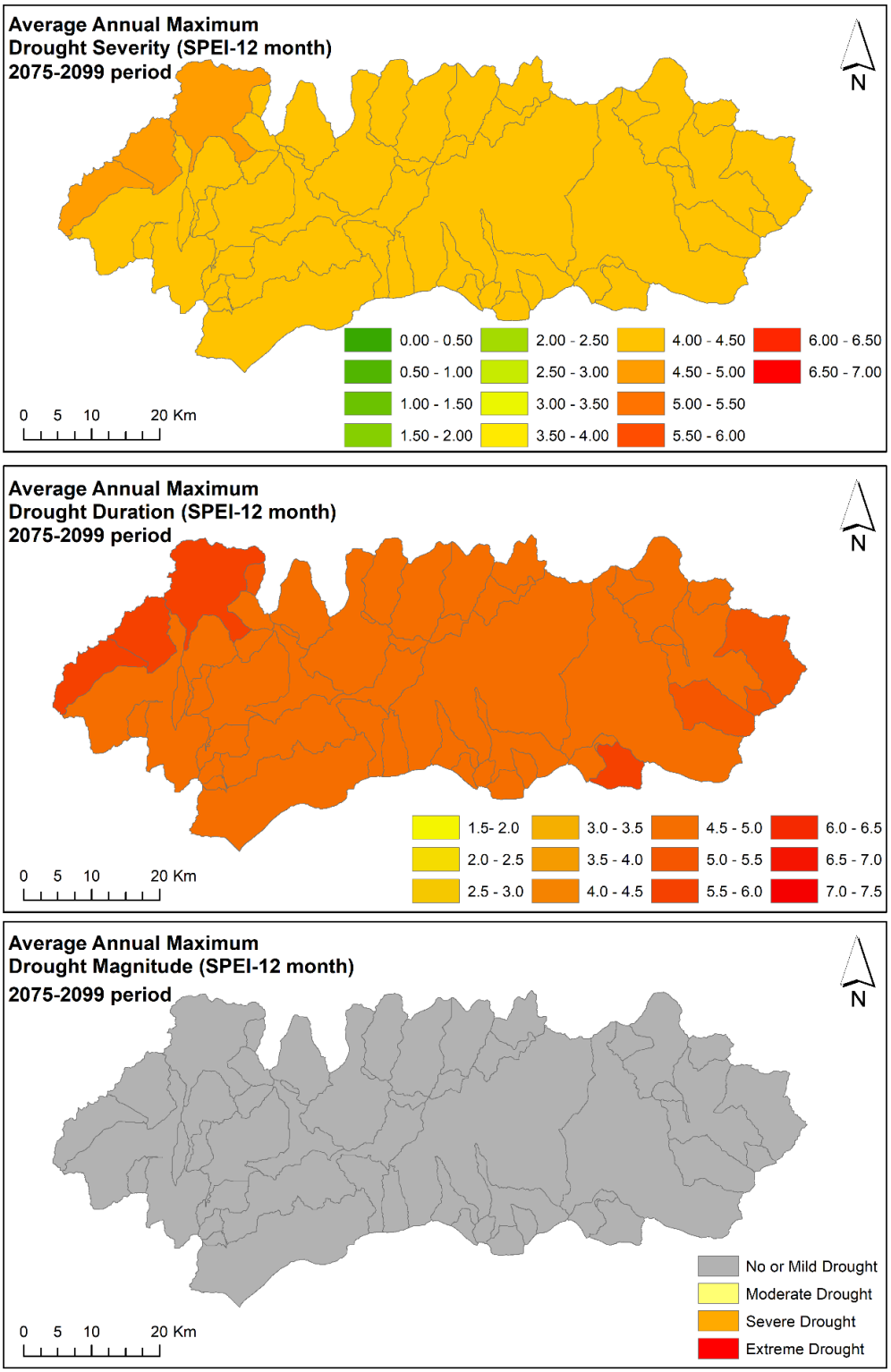


Figure 4.125 Maps obtained using SPEI-12 month series (with PET) for the far future period: a) average annual maximum drought severity, b) duration and c) magnitude.

4.3.3.4 Drought Maps Generated Using SSFI

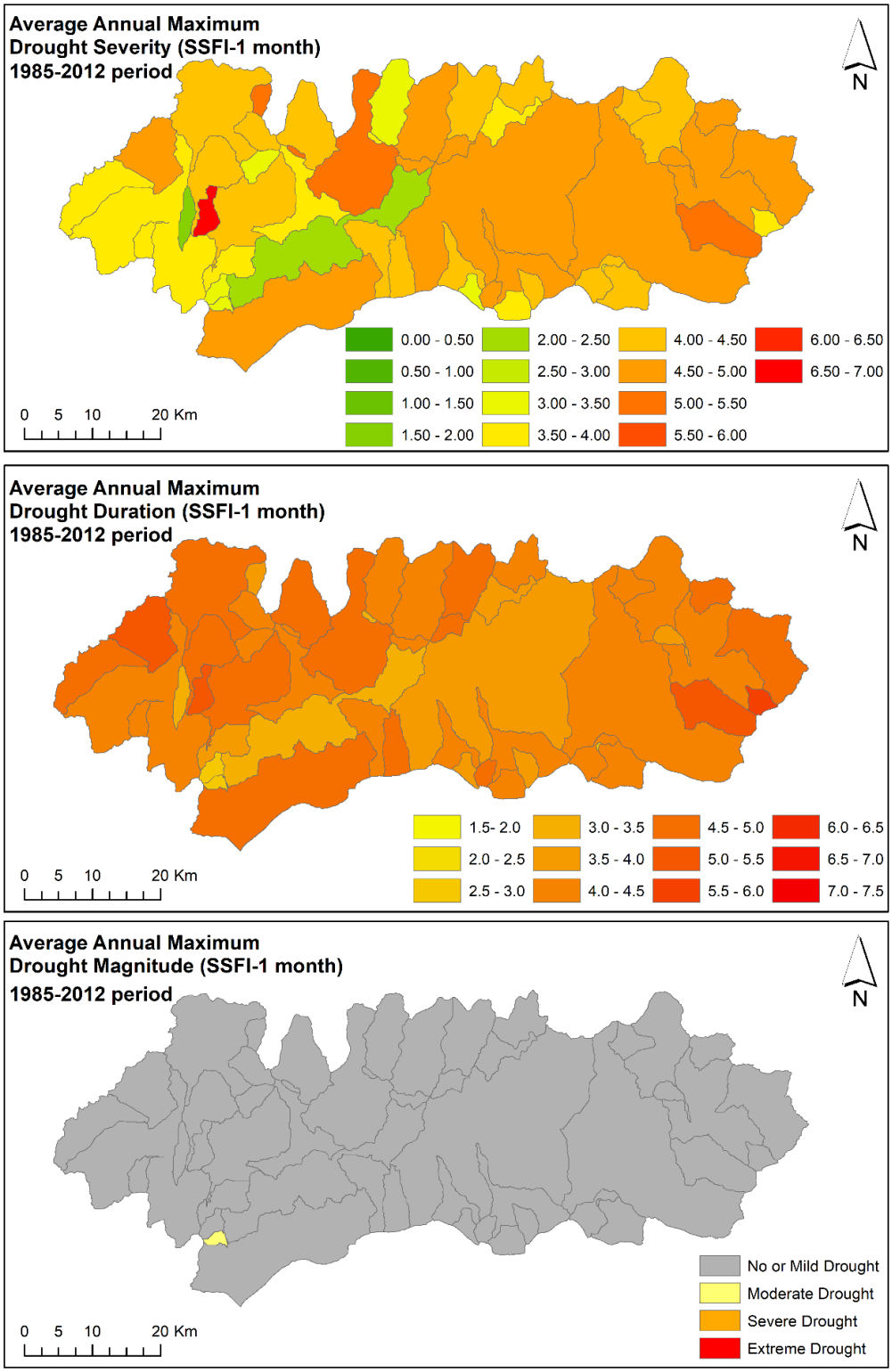


Figure 4.126 Maps obtained using SSFI-1 month series for the reference period: a) average annual maximum drought severity, b) duration and c) magnitude.

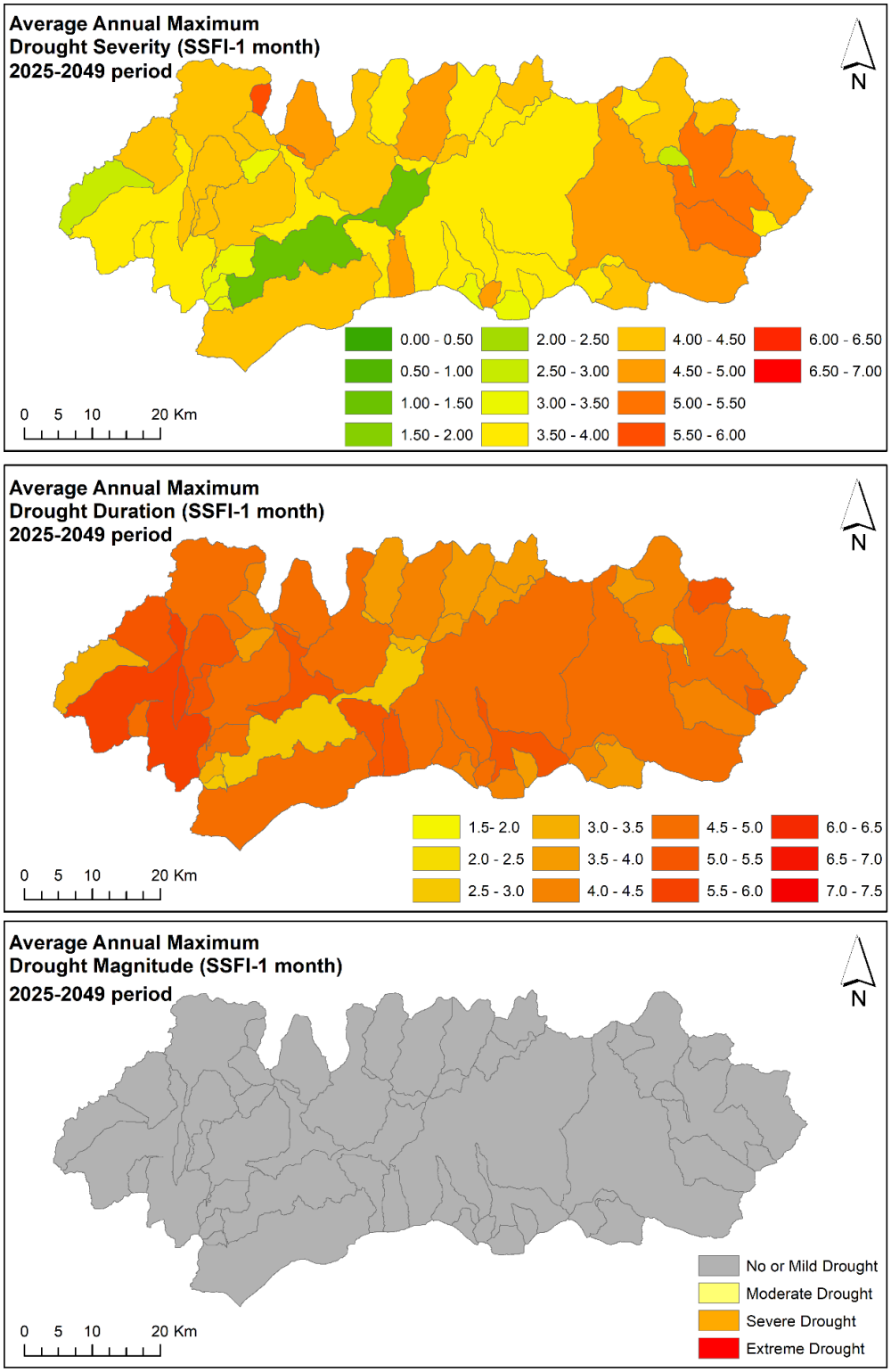


Figure 4.127 Maps obtained using SSFI-1 month series for the near future period: a) average annual maximum drought severity, b) duration and c) magnitude.

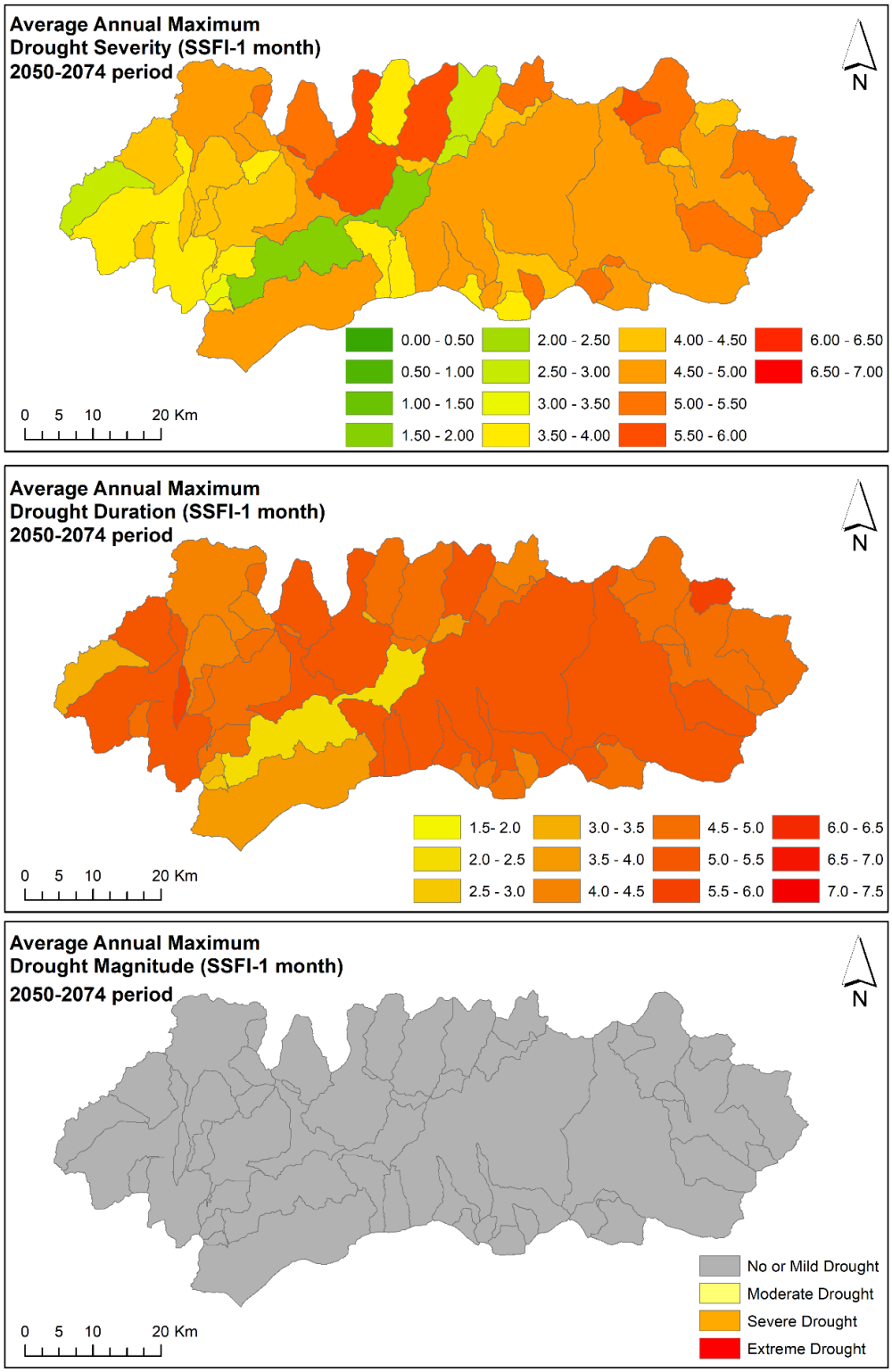


Figure 4.128 Maps obtained using SSFI-1 month series for the middle future period: a) average annual maximum drought severity, b) duration and c) magnitude.

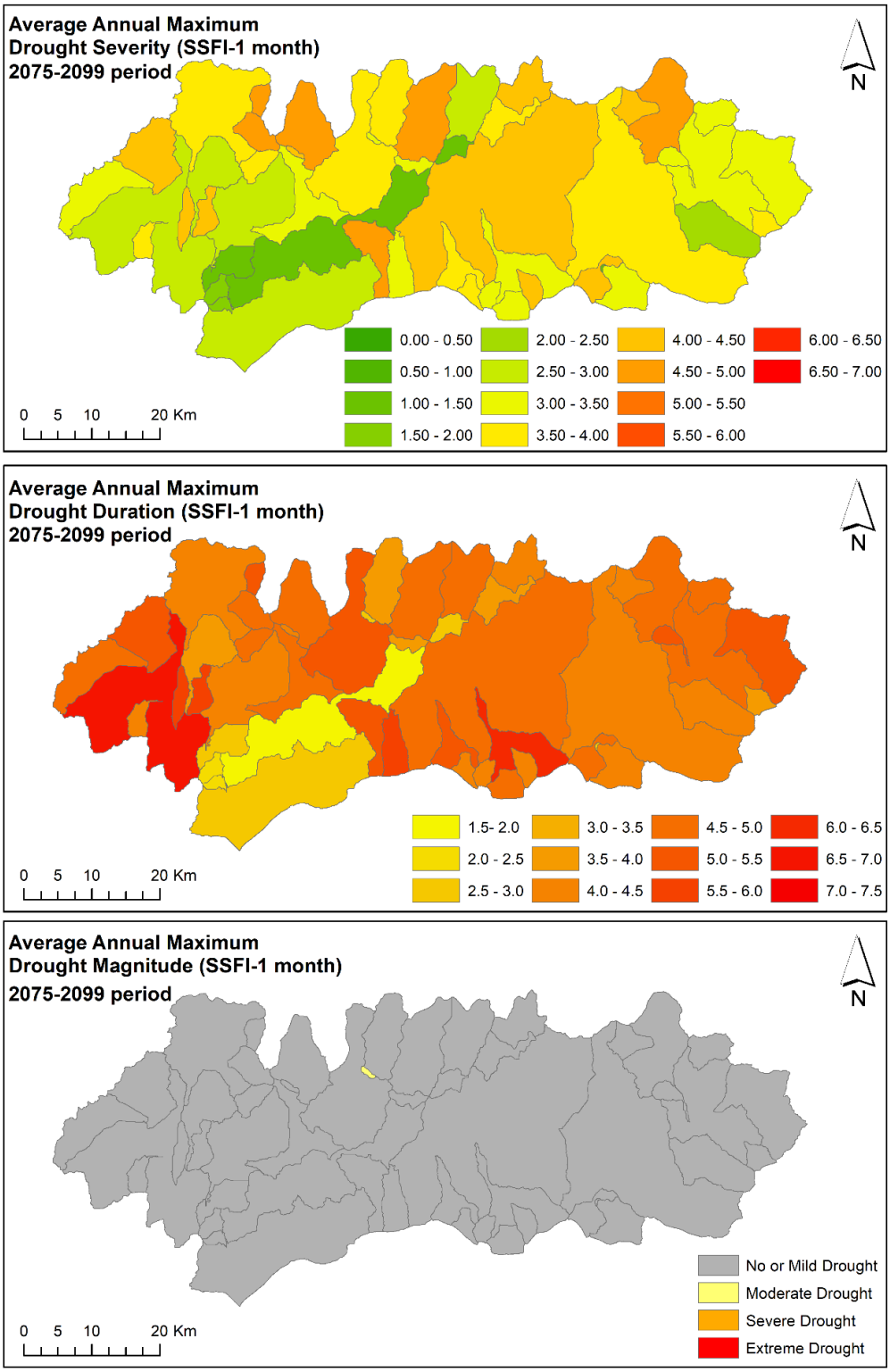


Figure 4.129 Maps obtained using SSFI-1 month series for the far future period: a) average annual maximum drought severity, b) duration and c) magnitude.

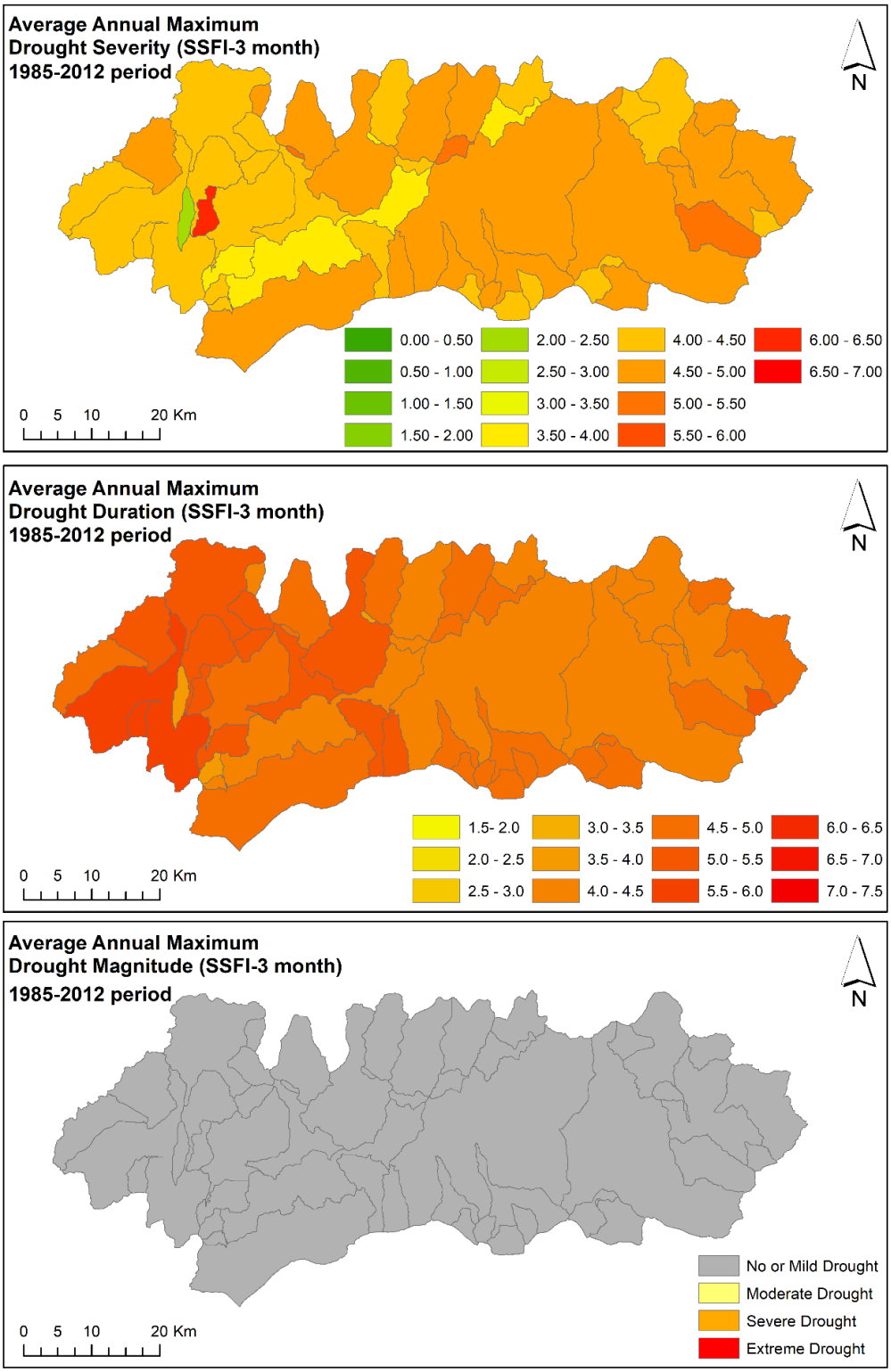


Figure 4.130 Maps obtained using SSFI-3 month series for the reference period: a) average annual maximum drought severity, b) duration and c) magnitude.

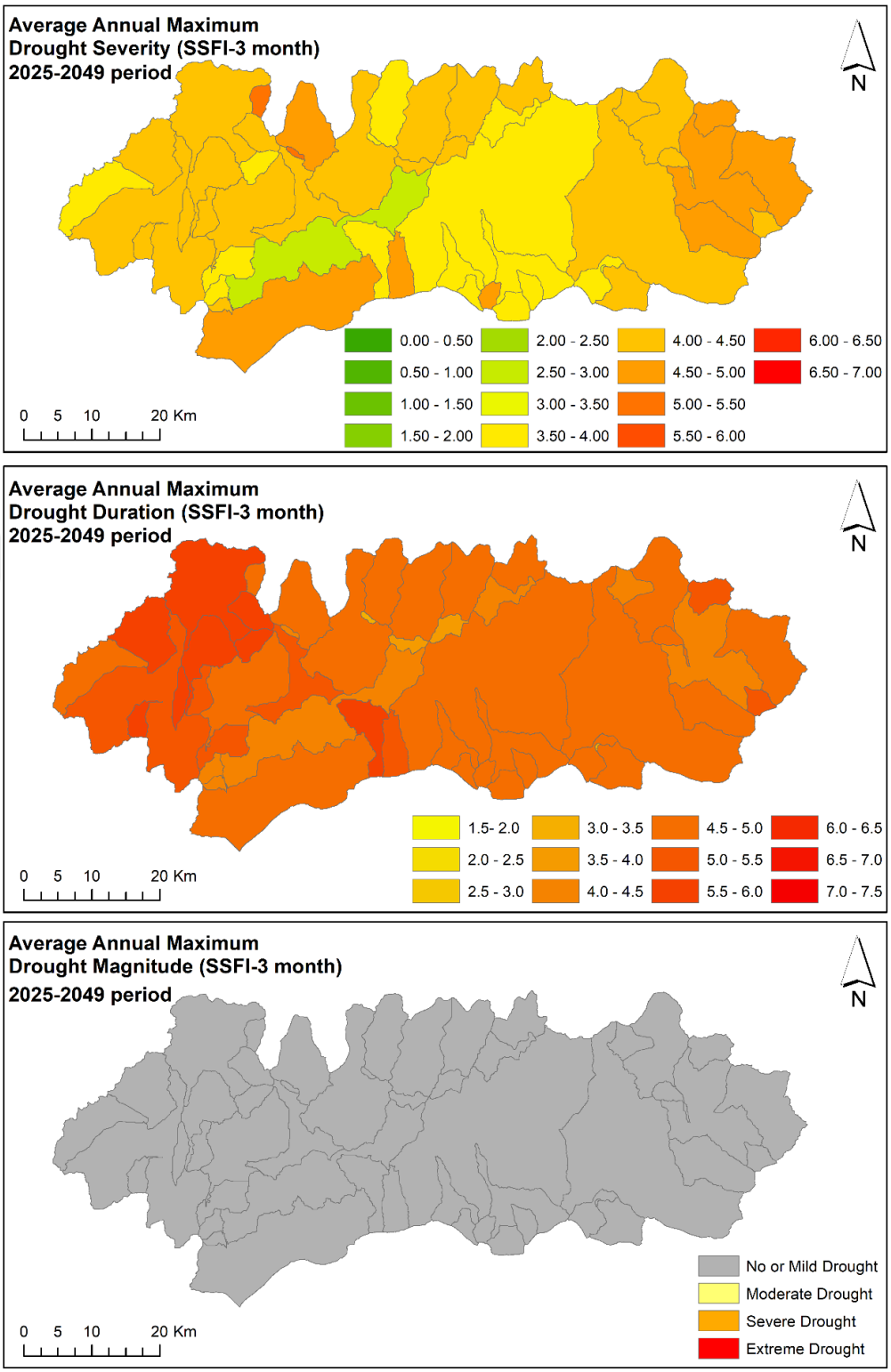


Figure 4.131 Maps obtained using SSFI-3 month series for the near future period: a) average annual maximum drought severity, b) duration and c) magnitude.

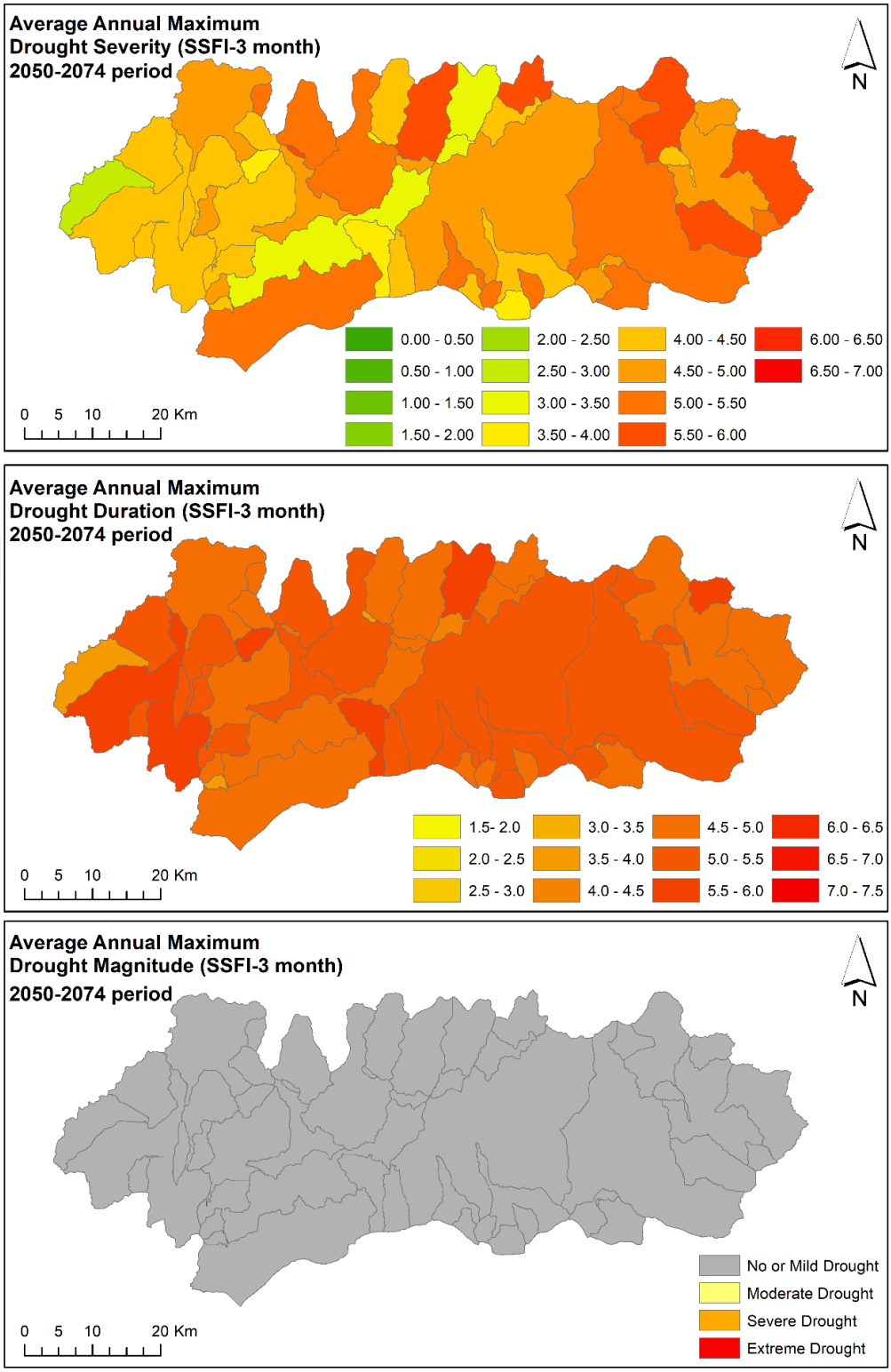


Figure 4.132 Maps obtained using SSFI-3 month series for the middle future period: a) average annual maximum drought severity, b) duration and c) magnitude.

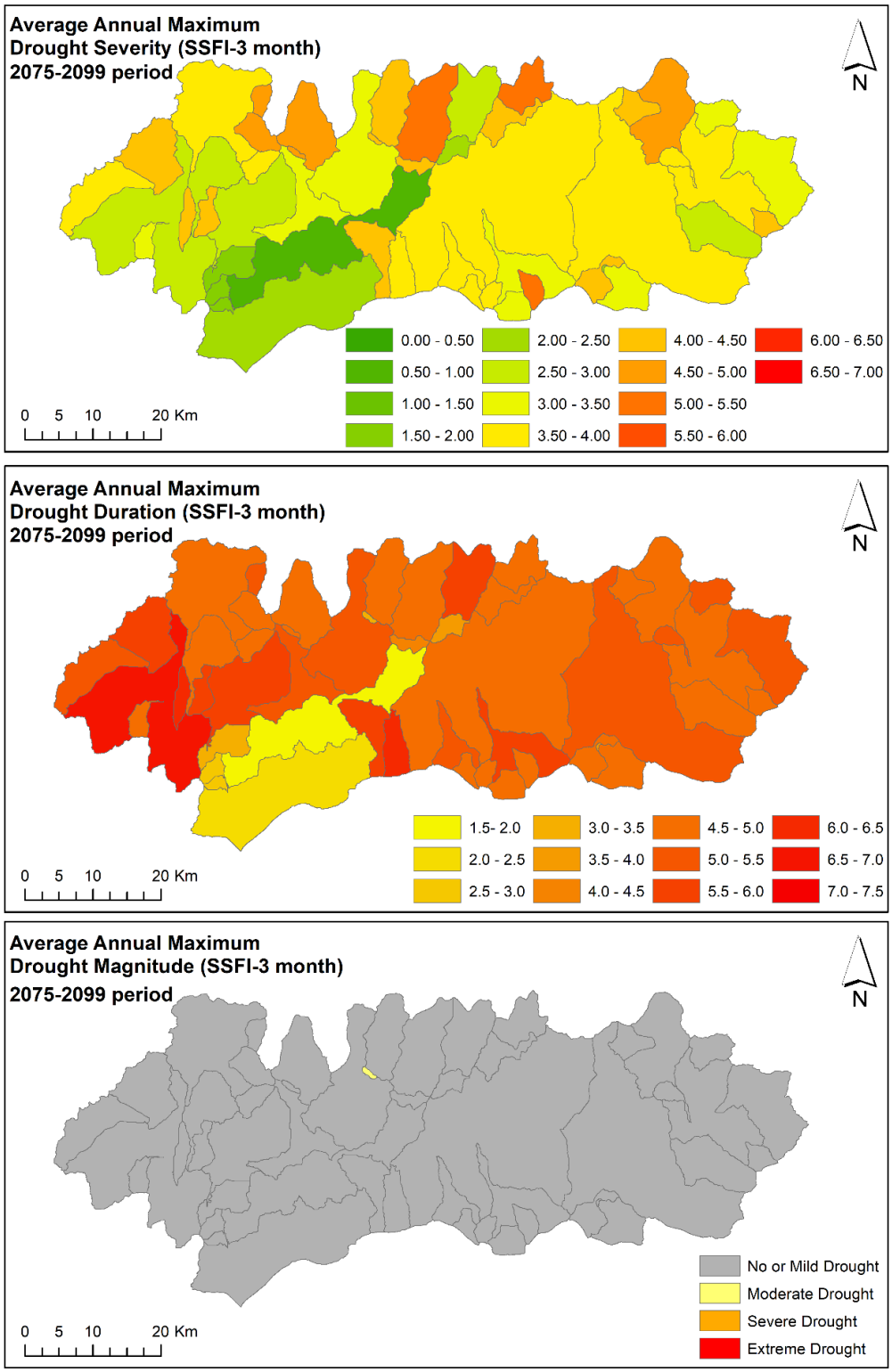


Figure 4.133 Maps obtained using SSFI-3 month series for the far future period: a) average annual maximum drought severity, b) duration and c) magnitude.

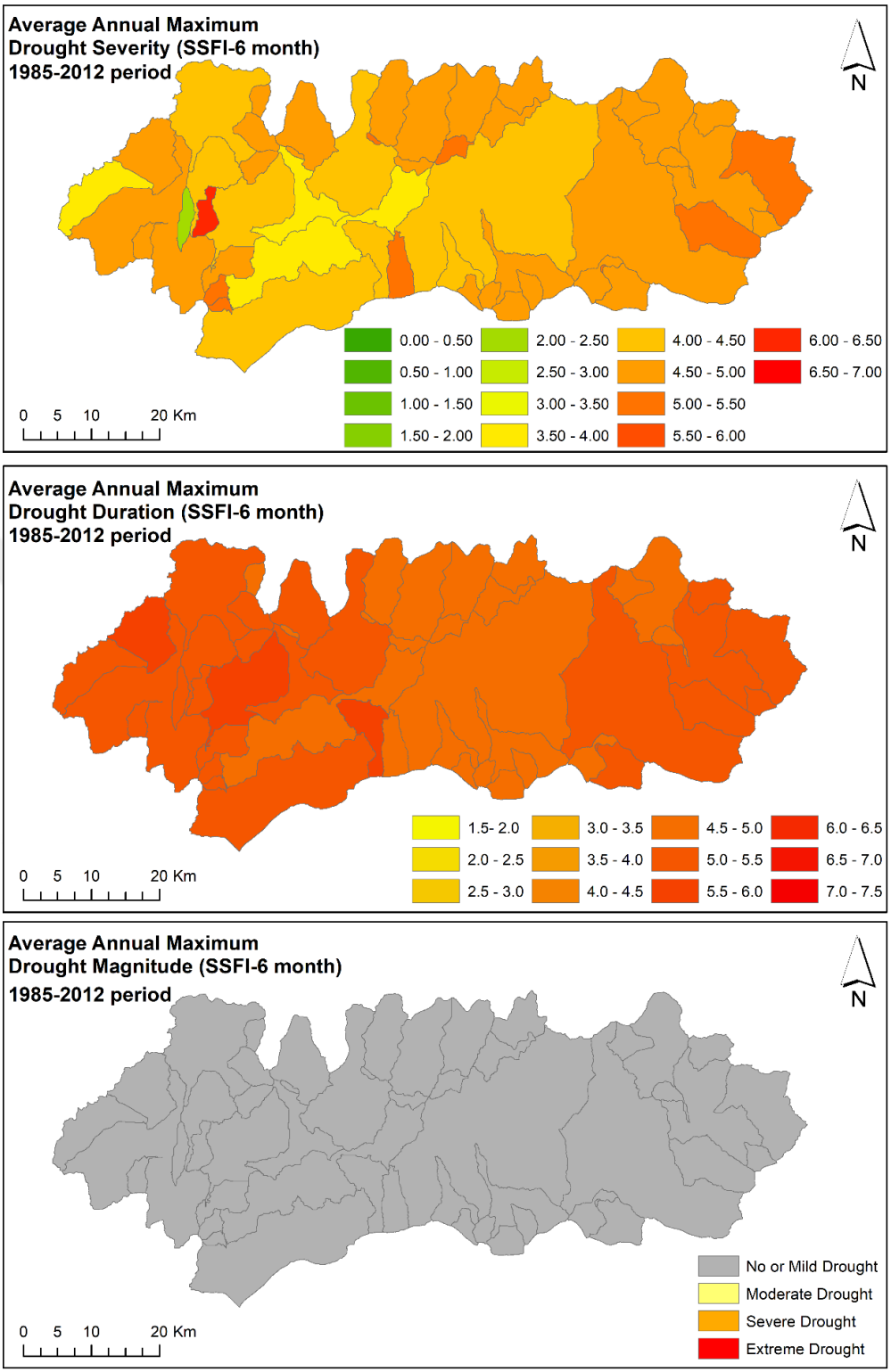


Figure 4.134 Maps obtained using SSFI-6 month series for the reference period: a) average annual maximum drought severity, b) duration and c) magnitude.

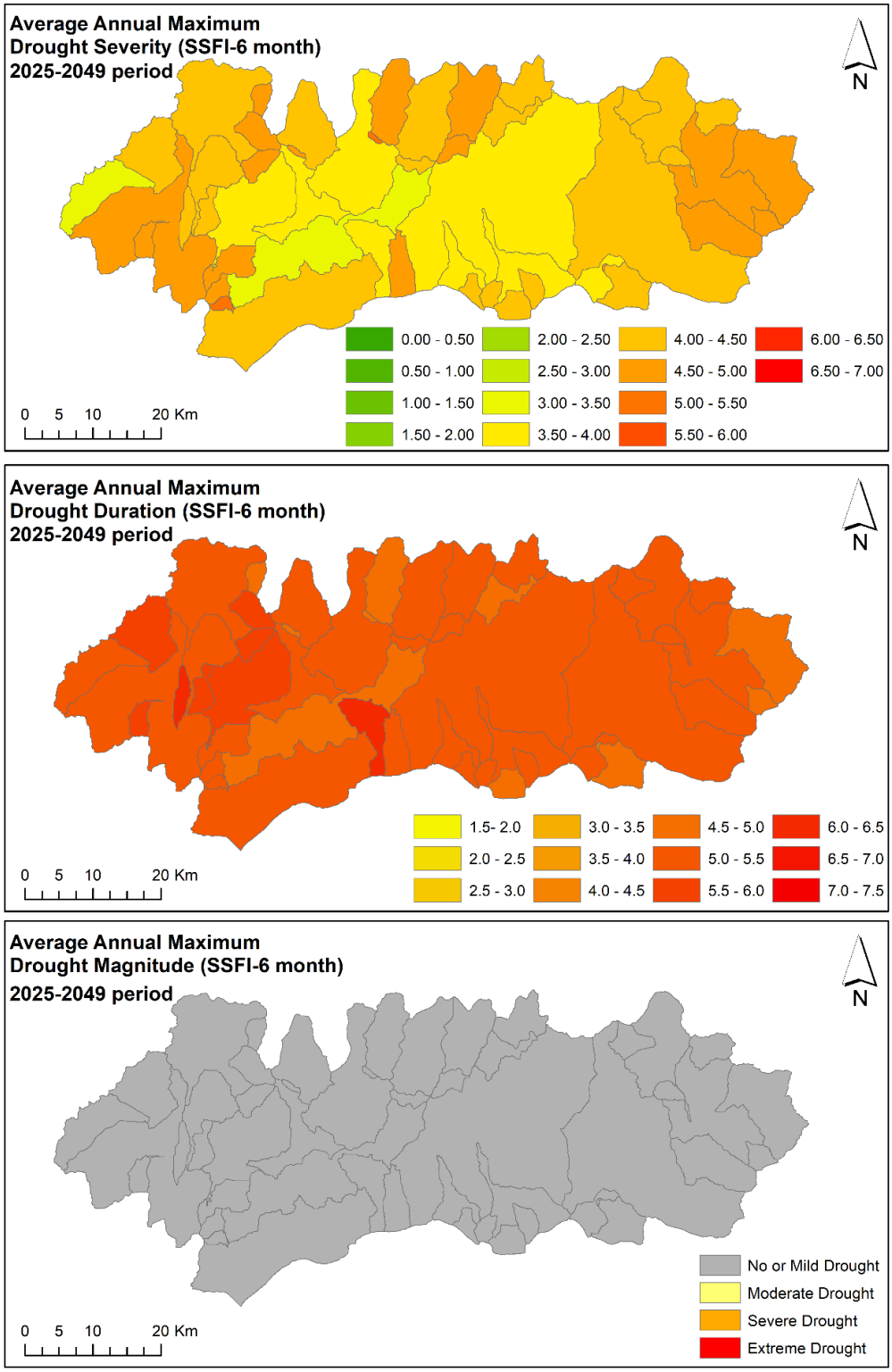


Figure 4.135 Maps obtained using SSFI-6 month series for the near future period: a) average annual maximum drought severity, b) duration and c) magnitude.

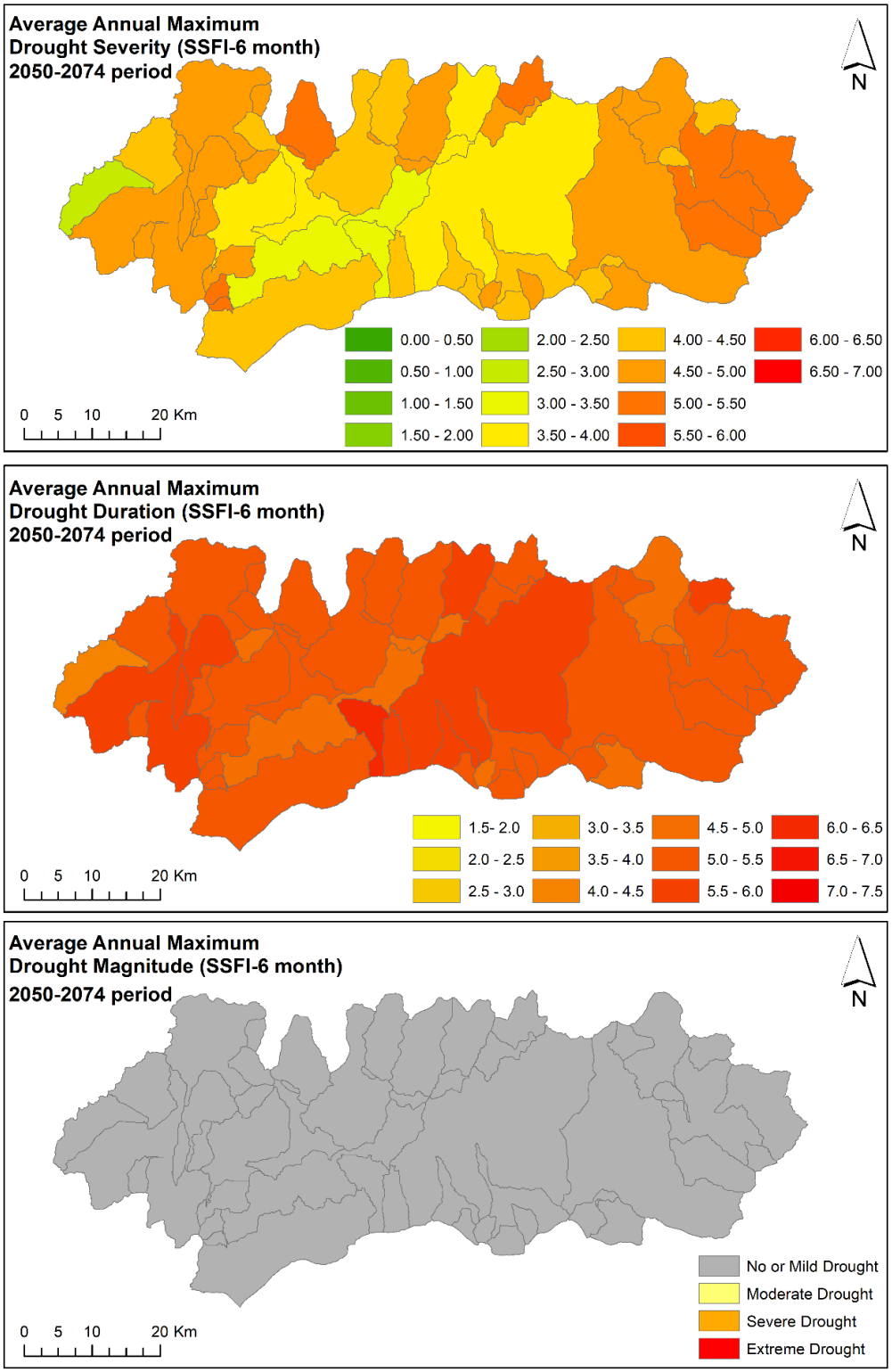


Figure 4.136 Maps obtained using SSFI-6 month series for the middle future period: a) average annual maximum drought severity, b) duration and c) magnitude.

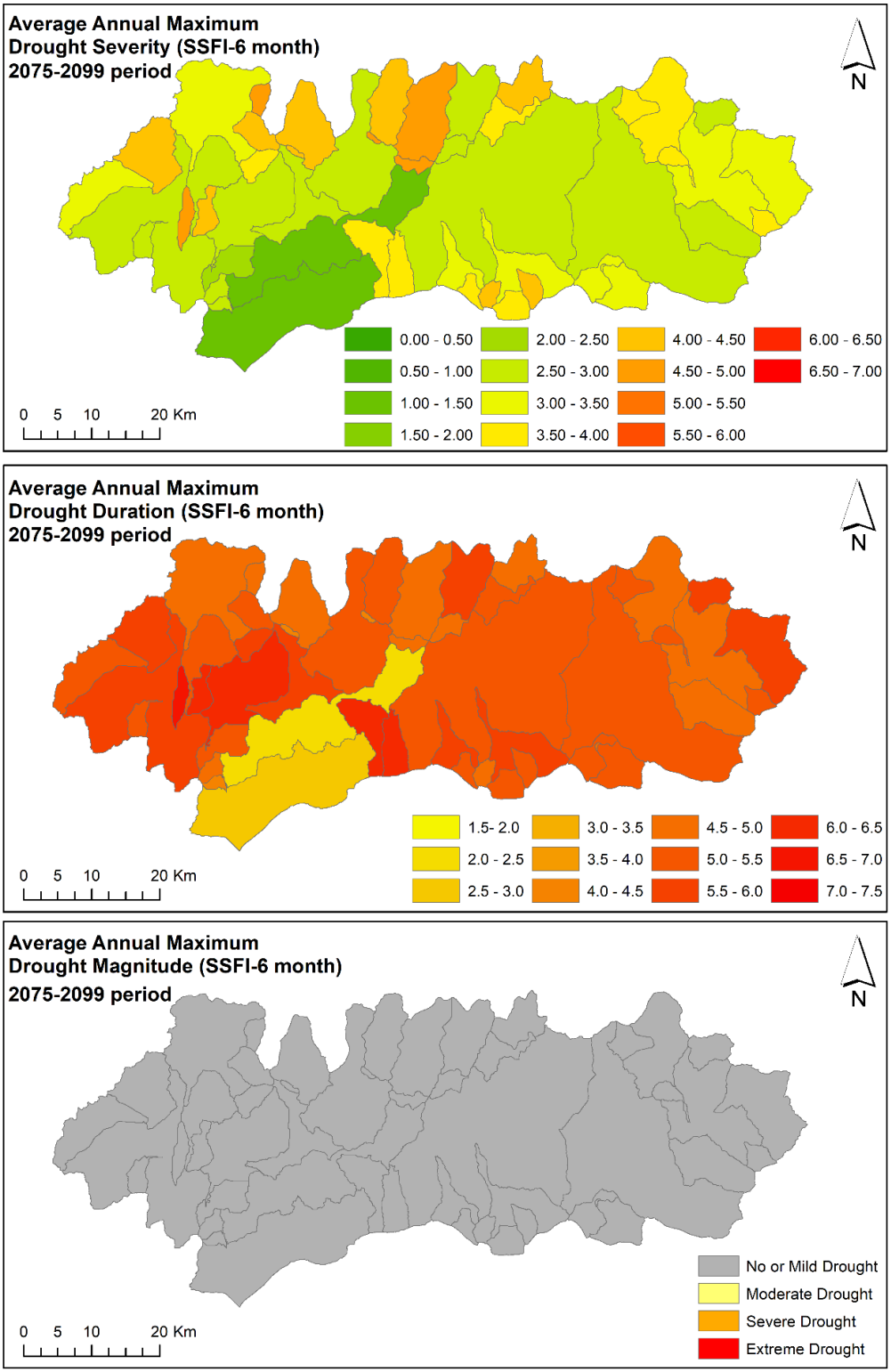


Figure 4.137 Maps obtained using SSFI-6 month series for the far future period: a) average annual maximum drought severity, b) duration and c) magnitude.

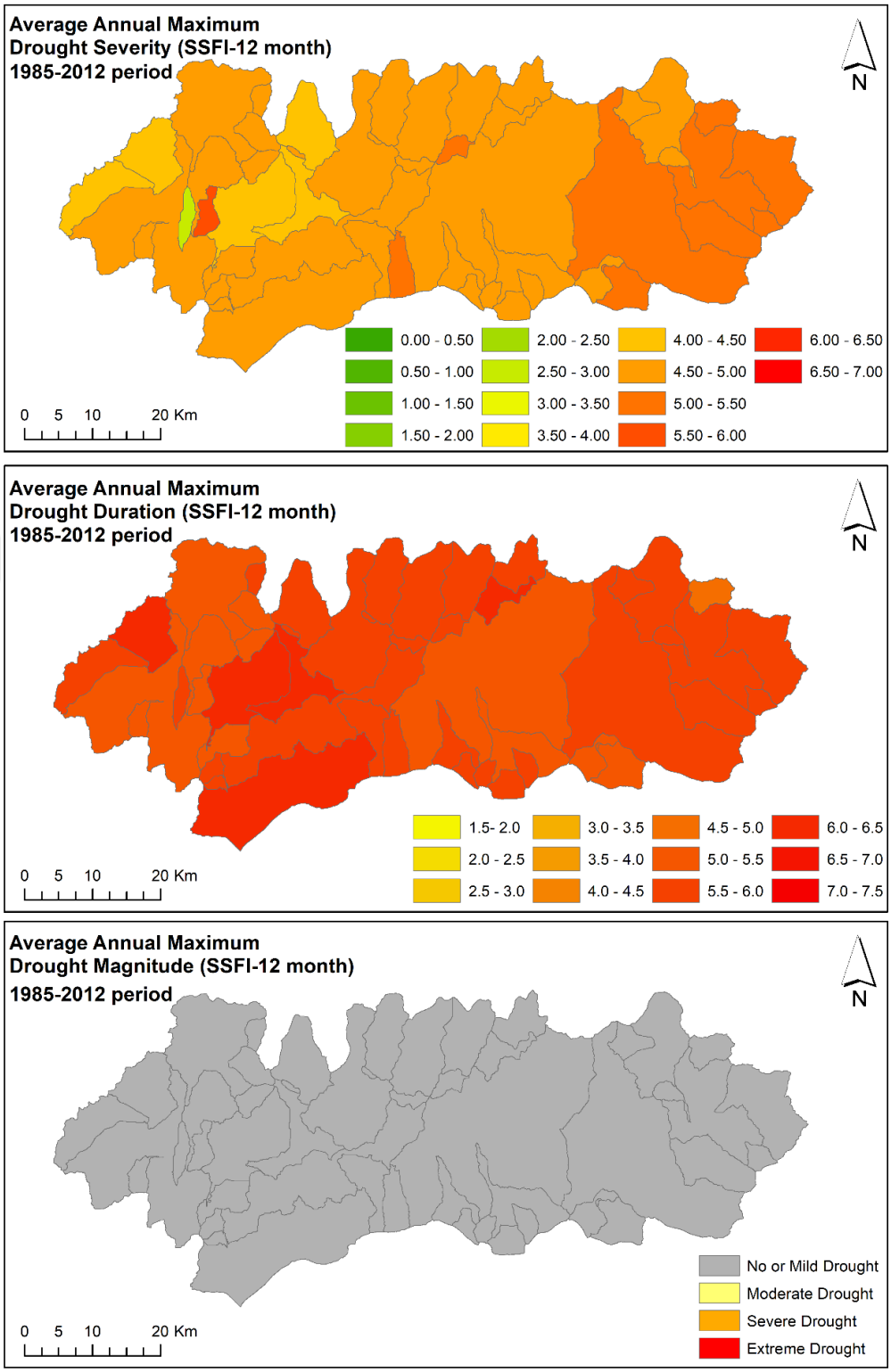


Figure 4.138 Maps obtained using SSFI-12 month series for the reference period: a) average annual maximum drought severity, b) duration and c) magnitude.

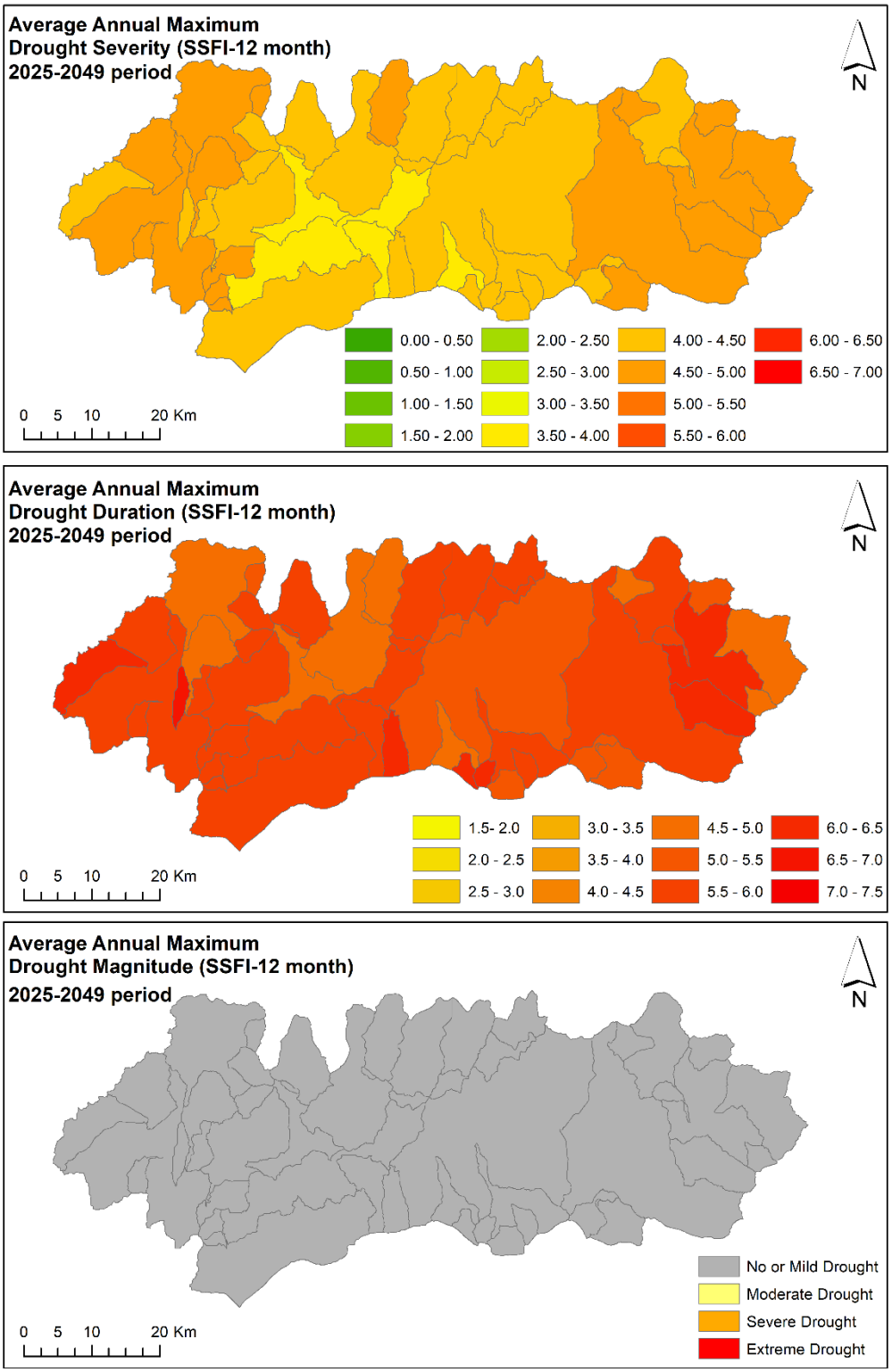


Figure 4.139 Maps obtained using SSFI-12 month series for the near future period: a) average annual maximum drought severity, b) duration and c) magnitude.

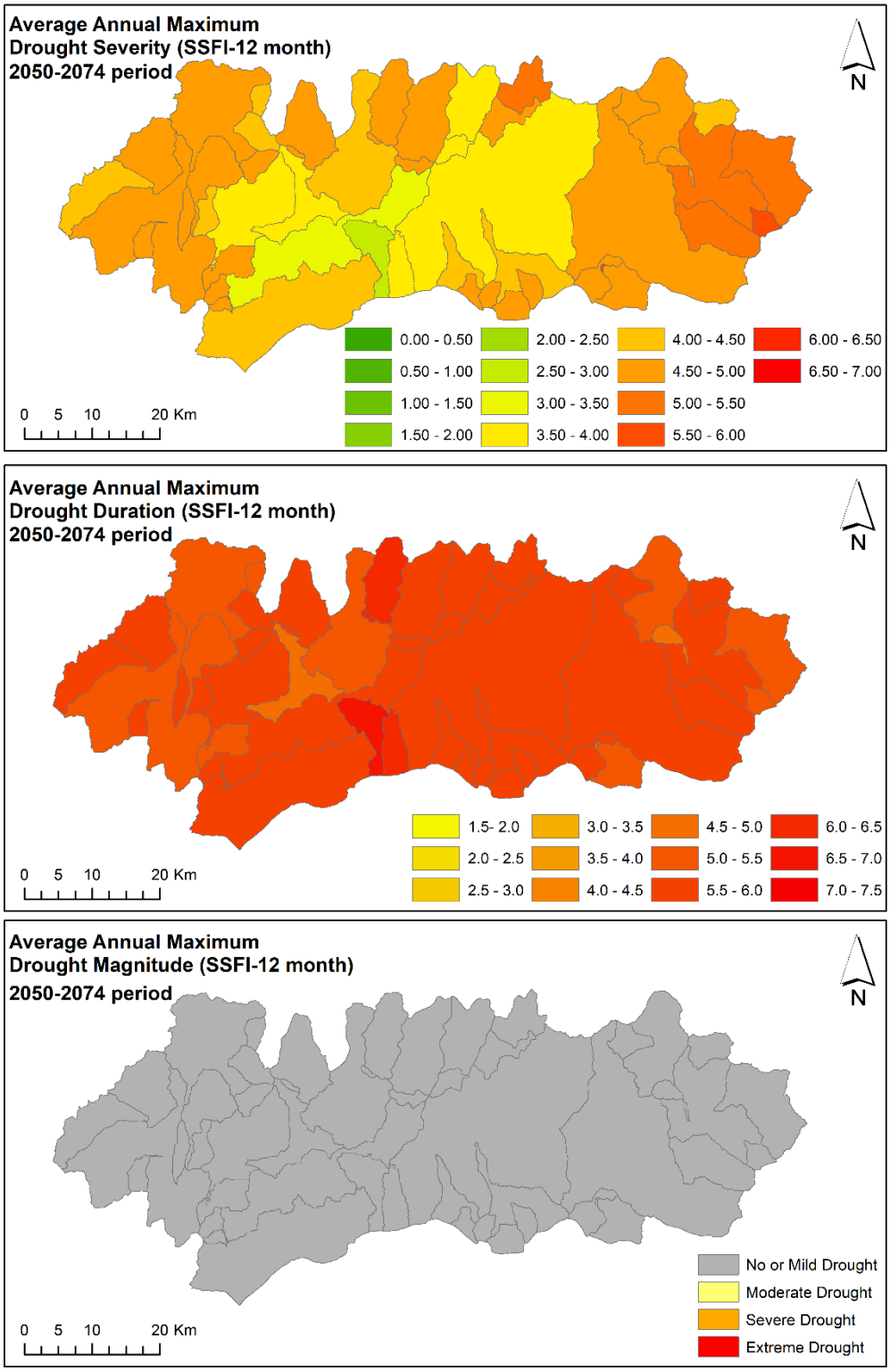


Figure 4.140 Maps obtained using SSFI-12 month series for the middle future period: a) average annual maximum drought severity, b) duration and c) magnitude.

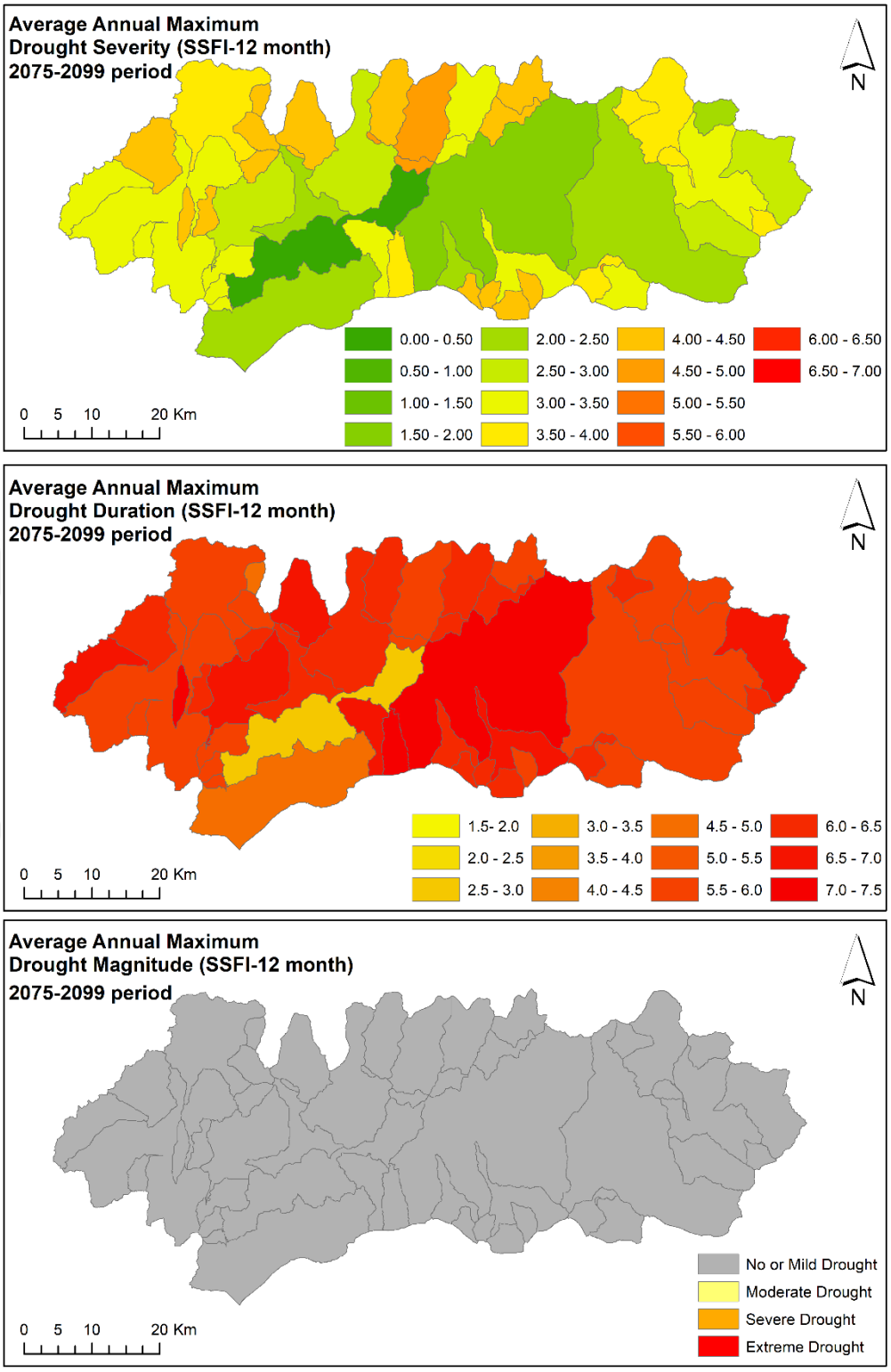


Figure 4.141 Maps obtained using SSFI-12 month series for the far future period: a) average annual maximum drought severity, b) duration and c) magnitude.

4.4 Flood Analyses

4.4.1 Obtaining IDF Curves

To derive recurrent flood hydrographs, instantaneous hyetographs were computed. The first step of these calculations is to obtain rainfall intensity-duration recurrence curves. Standard duration rainfall measured at Ödemiş Meteorological Station (17822) is given in Table 4.10. The rainfall intensities are given by Table 4.11. Employing statistical tests such as Kolmogorov-Simirnov, Anderson Darling and Chi-Square, an investigation was conducted to identify the most appropriate statistical distribution for each rainfall duration. The results indicated that the rainfall data for all durations fit to the Generalized Extreme Value (GEV) distribution, with Table 4.12 displaying the GEV distribution parameters for a 24-hour rainfall duration as an illustrative example.

Table 4.10 Maximum rainfall values (mm) observed at standard times.

Maximum Rainfall Values (mm) Observed at Standard Times														
PERIOD	**MINUTE**				**HOUR**									
INTERVAL	**5**	**10**	**15**	**30**	**1**	**2**	**3**	**4**	**5**	**6**	**8**	**12**	**18**	**24**
2 YEARS	4.77	7.13	8.56	11.35	13.99	17.23	19.18	20.45	21.3	22.21	23.43	25.37	28.44	44.36
5 YEARS	6.82	9.88	11.99	15.63	19.64	24.28	27.44	29.59	30.82	32.18	34.14	37.61	41.88	56.8
10 YEARS	8.1	11.54	14.2	18.38	23.41	28.96	32.92	35.72	37.19	38.77	41.08	45.62	50.14	63.67
25 YEARS	9.63	13.48	16.93	21.76	28.19	34.87	39.84	43.56	45.3	47.09	49.67	55.64	59.92	71.04
50 YEARS	10.7	14.81	18.91	24.21	31.76	39.26	44.98	49.45	51.37	53.25	55.92	63.01	66.72	75.7
100 YEARS	11.72	16.05	20.83	26.59	35.32	43.63	50.09	55.34	57.44	59.36	62.02	70.26	73.12	79.75
250 YEARS	12.99	17.56	23.31	29.64	40.02	49.39	56.81	63.19	65.49	67.39	69.91	79.71	81.02	84.31
500 YEARS	13.9	18.62	25.14	31.89	43.59	53.74	61.9	69.19	71.62	73.45	75.75	86.78	86.63	87.25
1000 YEARS	14.76	19.61	26.93	34.09	47.17	58.09	66.98	75.24	77.79	79.5	81.49	93.79	91.94	89.83

Table 4.11 Maximum rainfall intensity values (mm/hr) observed at standard times.

Maximum Rainfall Intensity Values (mm/hr) Observed at Standard Times														
PERIOD	**MINUTE**				**HOUR**									
INTERVAL	**5**	**10**	**15**	**30**	**1**	**2**	**3**	**4**	**5**	**6**	**8**	**12**	**18**	**24**
2 YEARS	57.25	42.8	34.24	22.7	13.99	8.62	6.39	5.11	4.26	3.7	2.93	2.11	1.58	1.85
5 YEARS	81.89	59.26	47.96	31.26	19.64	12.14	9.15	7.4	6.16	5.36	4.27	3.13	2.33	2.37
10 YEARS	97.22	69.24	56.8	36.76	23.41	14.48	10.97	8.93	7.44	6.46	5.14	3.8	2.79	2.65
25 YEARS	115.54	80.88	67.72	43.52	28.19	17.44	13.28	10.89	9.06	7.85	6.21	4.64	3.33	2.96
50 YEARS	128.41	88.87	75.64	48.42	31.76	19.63	14.99	12.36	10.27	8.88	6.99	5.25	3.71	3.15
100 YEARS	140.62	96.29	83.32	53.18	35.32	21.82	16.7	13.84	11.49	9.89	7.75	5.86	4.06	3.32
250 YEARS	155.86	105.36	93.24	59.28	40.02	24.7	18.94	15.8	13.1	11.23	8.74	6.64	4.5	3.51
500 YEARS	166.76	111.71	100.6	63.78	43.59	26.87	20.63	17.3	14.32	12.24	9.47	7.23	4.81	3.64
1000 YEARS	177.18	117.65	107.7	68.18	47.17	29.05	22.33	18.81	15.56	13.25	10.19	7.82	5.11	3.74

Table 4.12 Parameters of GEV distribution for each duration.

Time (min)	Distribution	ξ	σ	ɱ
5	GEV	-0.0016	8.8087	18.987
10		-0.09376	2.6405	6.1826
15		-0.02798	3.1055	7.427
30		-0.03072	3.8808	9.9389
60		0.00607	4.963	12.165
120		0.00164	6.2097	14.956
180		8.5824E-4	7.2847	16.51
240		0.01389	7.9615	17.522
300		0.01014	8.3234	18.24
360		-0.0016	8.8087	18.987
480		-0.02345	9.6581	19.904
720		-0.01185	10.919	21.372
1080		-0.07775	12.742	23.837
1440		-0.19231	13.11	39.72

The IDF relationship for Ödemiş station is obtained by graphical method expressed as Equation 4.1, where i represents rainfall intensity, R is reccurrence, T_d denotes rainfall duration, and the constants 13.414 and 0.176 have been derived. IDF curves are given by Figure 4.142.

$$i_{mm/hr} = \frac{13.414\ x\ R^{0.176}}{T_d^{0.668}} \tag{4.1}$$

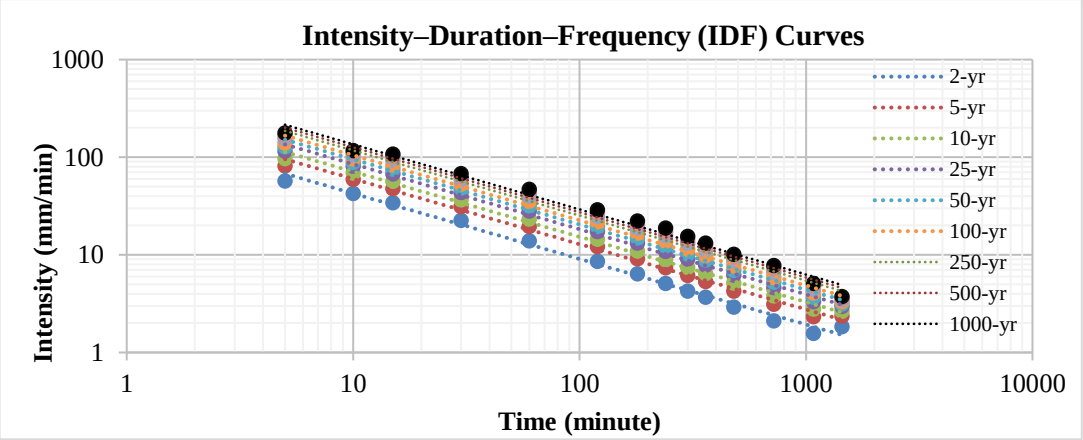


Figure 4.142 Rainfall IDF curves for Ödemiş Station

4.4.2 Obtaining Hyetographs

Table 4.13 provides the 24-hour instantaneous rainfall hyetograph, while Figure 4.143 presents the design hyetographs derived for return periods for 2, 5, 10, 25, 50, 50, 100, 250, 500 and 1000 years.

Table 4.13 Obtaining instantaneous hyetograph of 24-hour precipitation with 100-year recurrence for Ödemiş Station.

Time	t_a, t_b	T_d	*Rainfall Intensity*	*Incremental Rainfall*
(hour)	(hour)	(hour)	(mm/hour)	(mm)
0	12	24	1.79	0
1	11	22	1.9	1.85
2	10	20	2.02	1.96
3	9	18	2.17	2.1
4	8	16	2.35	2.26
5	7	14	2.57	2.46
6	6	12	2.85	2.71
7	5	10	3.22	3.03
8	4	8	3.73	3.47
9	3	6	4.52	4.13
10	2	4	5.93	5.23
11	1	2	9.42	7.68
11.5	0.5	1	14.97	6.1
11.75	0.25	0.5	23.79	4.85
11.9	0.1	0.2	43.87	5.07
11.95	0.05	0.1	69.7	2.84
12.05	0.05	0.1	69.7	6.97
12.1	0.1	0.2	43.87	2.84
12.25	0.25	0.5	23.79	5.07
12.5	0.5	1	14.97	4.85
13	1	2	9.42	6.1
14	2	4	5.93	7.68
15	3	6	4.52	5.23
16	4	8	3.73	4.13
17	5	10	3.22	3.47
18	6	12	2.85	3.03
19	7	14	2.57	2.71
20	8	16	2.35	2.46
21	9	18	2.17	2.26
22	10	20	2.02	2.1
23	11	22	1.9	1.96
24	12	24	1.79	1.85

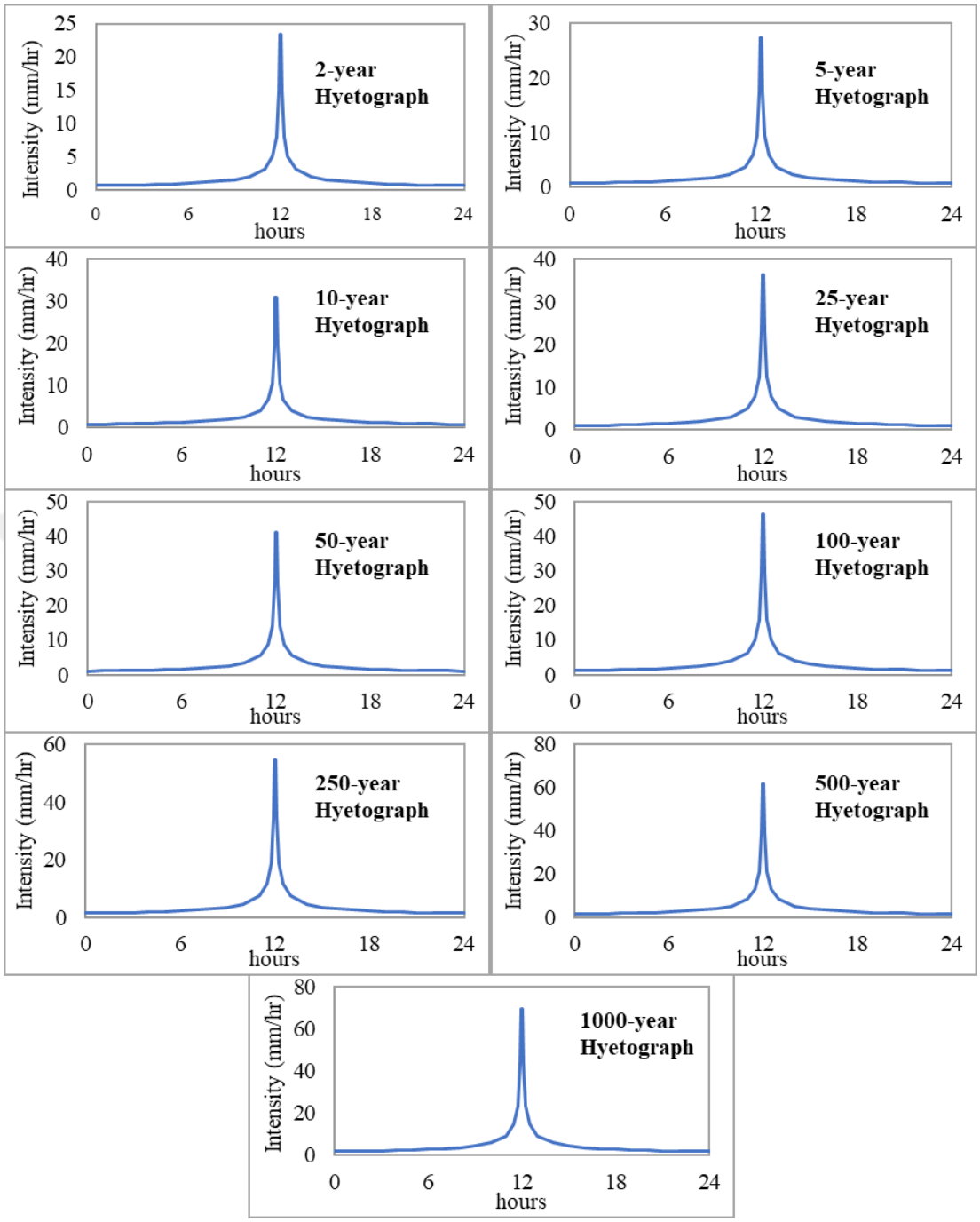


Figure 4.143 24-hour hyetographs of Ödemiş Station.

4.4.3 HEC-HMS modeling

The HEC-GeoHMS model for Ergenli Basin occurred as a 1 km^2 grid-based. The geographical extent of the project area is depicted in Figure 4.144 while the model diagram is provided in Figure 4.145. Then, the model was migrated to HEC-HMS. The modeling process involved the use of the Mod Clark method for precipitation-runoff

transformation, Muskingum method for channel routing, gridded SCS Curve Number method for loss, Recession method for base flow and gridded Hamon method for evapotranspiration (refer to Figure 4.145). The model was run with observed hourly meteorological data given in Section 3.2.3 for both calibration and validation period (Figure 4.146). All gridded data encompassing precipitation, temperature, and CN curve number were incorporated into the model in DSS format.

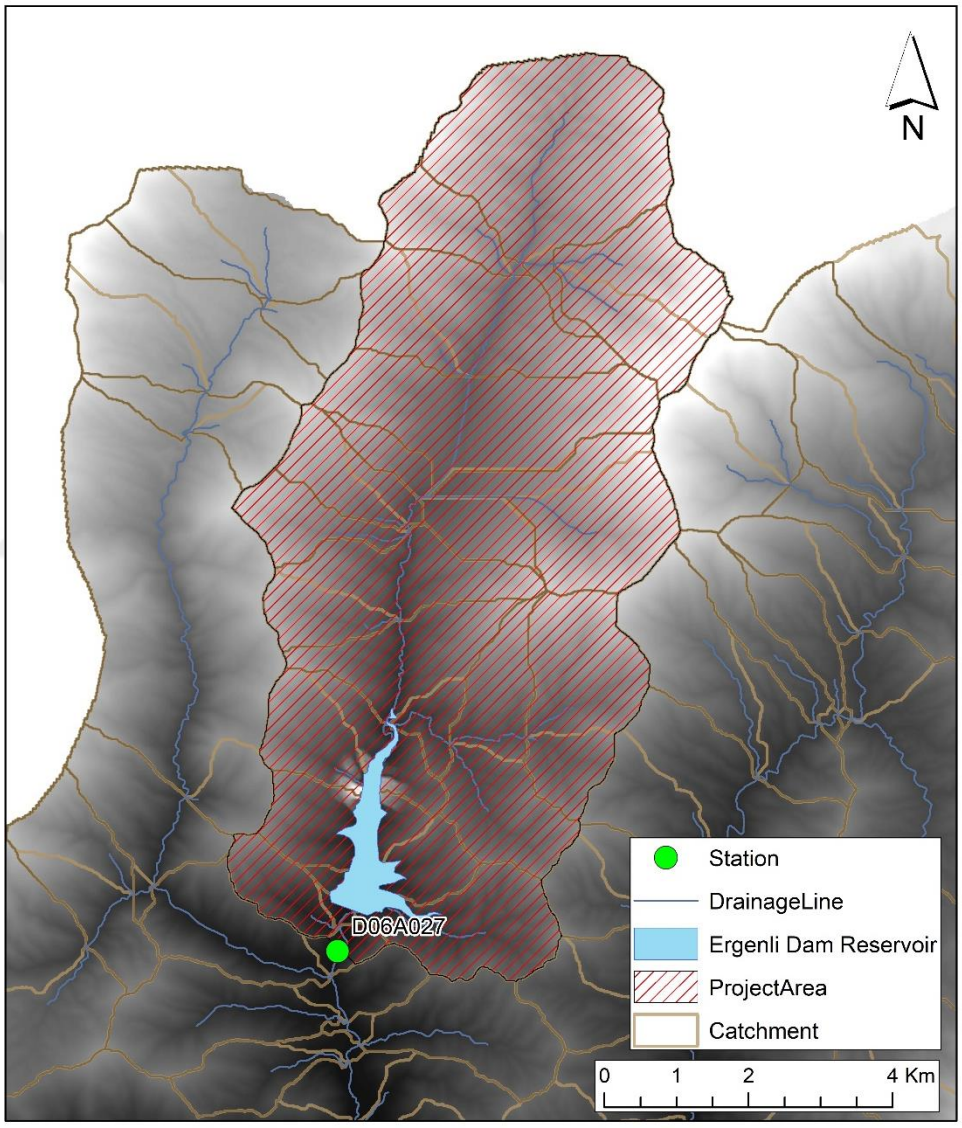


Figure 4.144 Project area of Ilıca (Ergenli) Basin for HEC-HMS model.

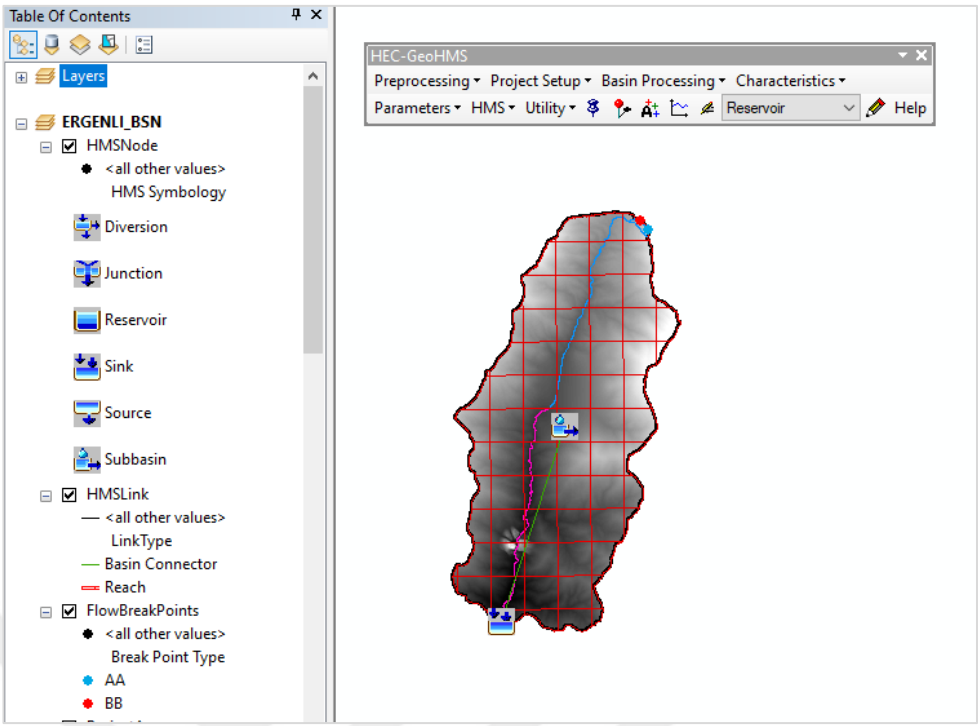


Figure 4.145 HEC-GeoHMS model schematic representation of Ilıca (Ergenli) Basin.

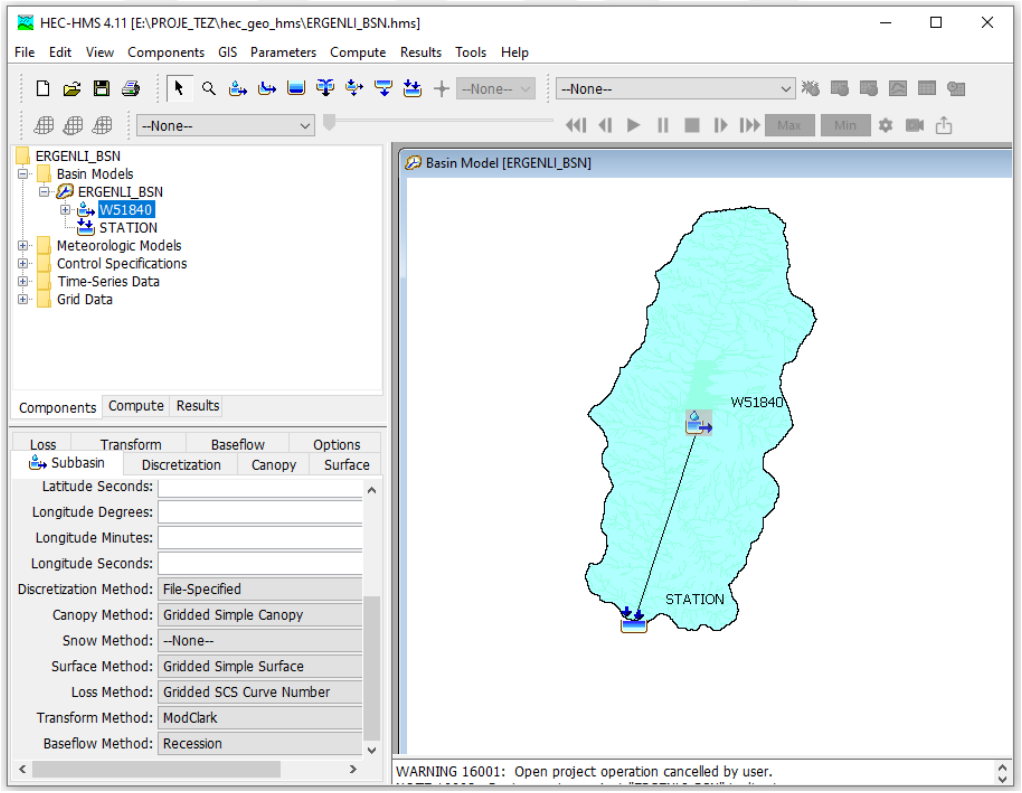


Figure 4.146 HECHMS model schematic representation of Ilıca (Ergenli) Basin.

4.4.3.1 The Calibration and The Validation of The Model

For calibration and validation, the specified periods outlined in Table 4.14 were considered. The calibration and validation results are given by Figure 4.147 and Figure 4.149, respectively. Figures 4.148 and 4.150 provide a comparison between observed and modeled flows with corresponding rainfall depths. Validation was performed using the calibrated parameter values. The final calibrated parameter set and statistical values showing the performance of the model are presented in Table 4.15. The Nash-Sutcliffe Efficiency (NSE) values were computed as 0.93 for the calibration period and 0.75 for the validation period. In conclusion, the model demonstrated excellent performance during both the calibration and validation periods.

Table 4.14 Calibration and validation periods for HEC-HMS modeling.

Period	***Begin***		***End***	
	Date	*Hour*	*Date*	*Hour*
Calibration	1/28/2011	10:00	1/30/2011	10:00
Validation	2/22/2011	2:00	2/24/2011	16:00

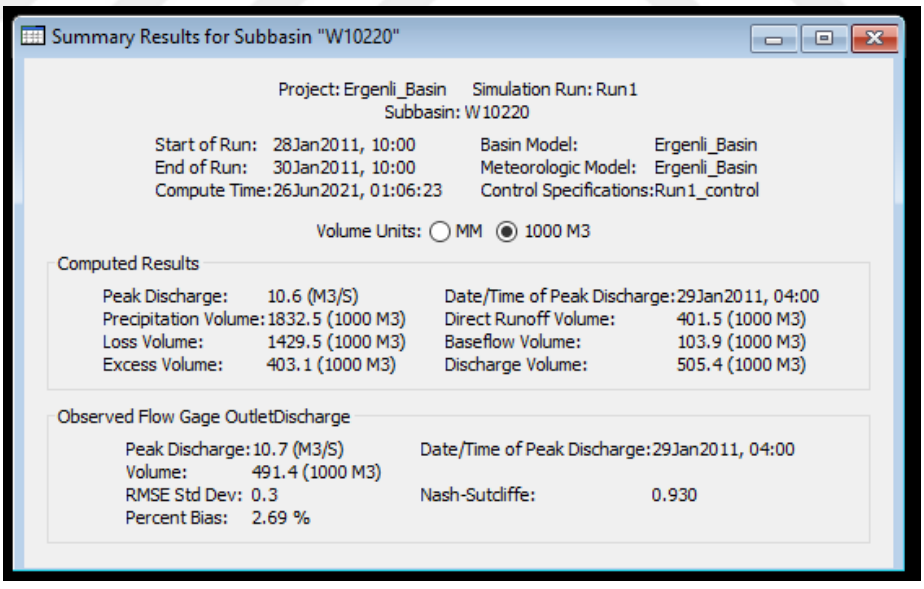


Figure 4.147 Model results for calibration period.

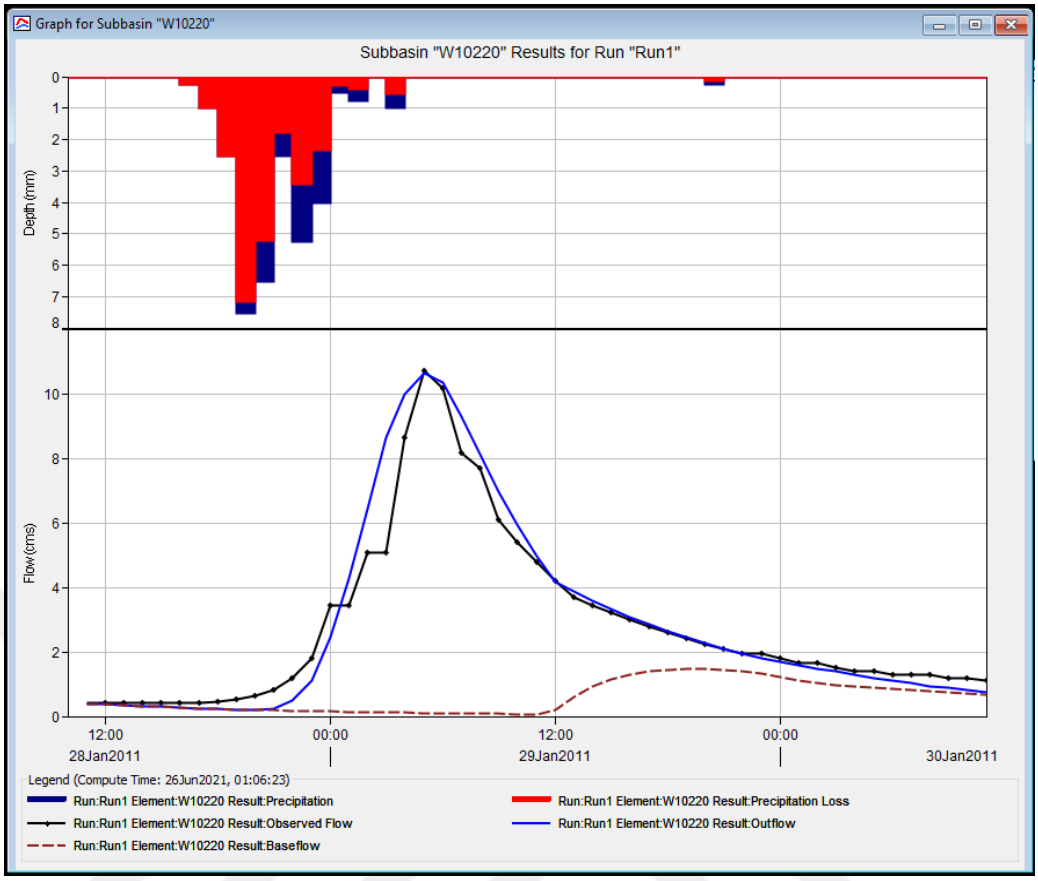


Figure 4.148 Rainfall depth (mm) and flood hydrograph (m^3/s) for calibration period.

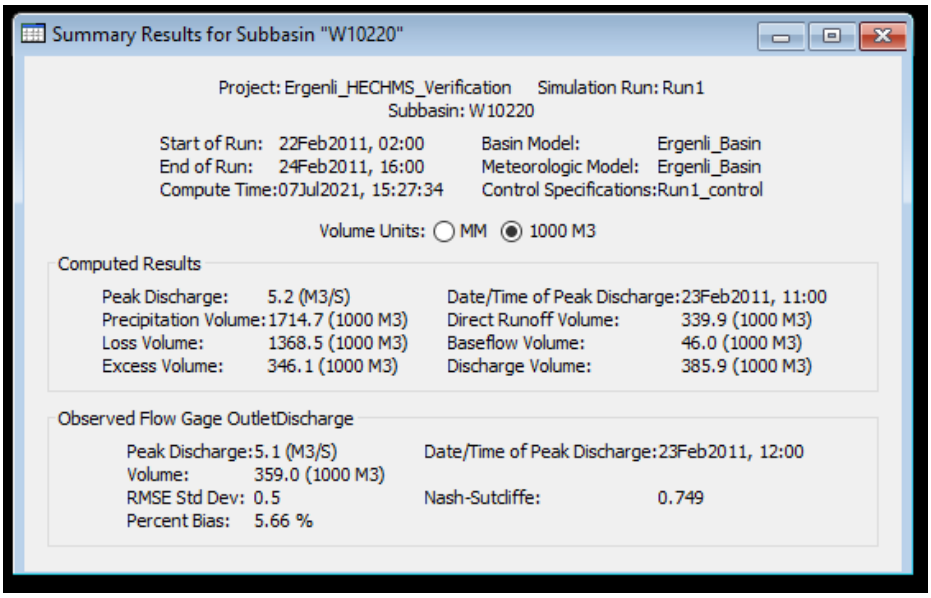


Figure 4.149 Model results for validation period.

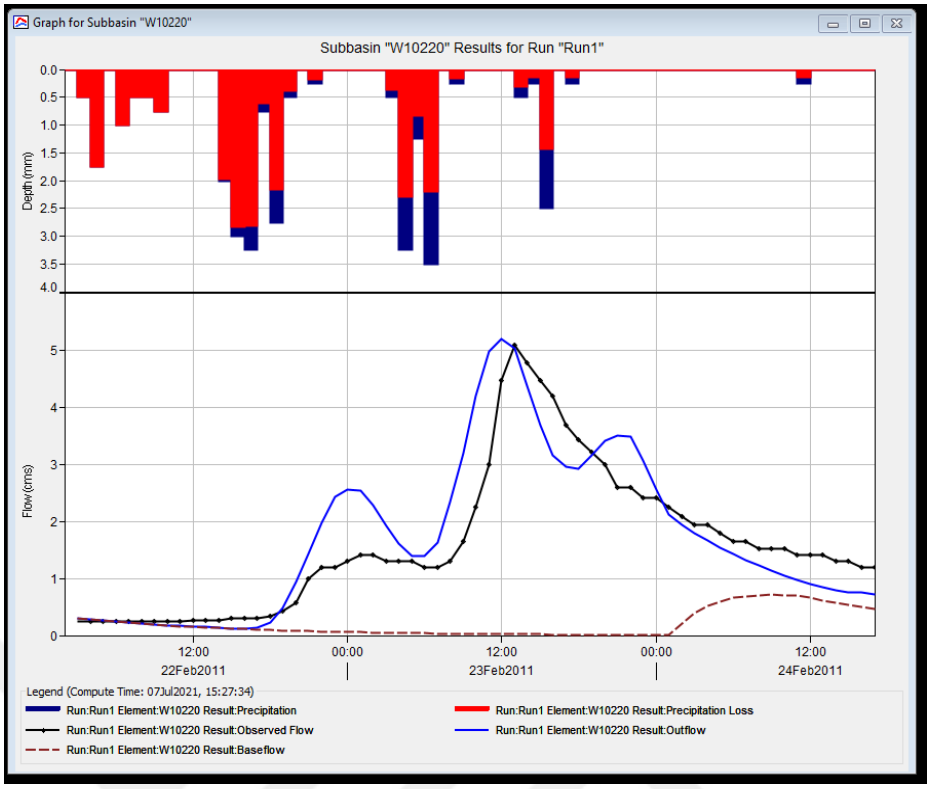


Figure 4.150 Rainfall depth (mm) and flood hydrograph (m^3/s) for validation period.

Table 4.15 HEC-HMS model calibration results.

PARAMETERS	***Calibration Period***	***Validation Period***
Mod Clark - Time of concentration	7	7
Mod Clark - Storage Coefficient	5	5
Gridded SCS Curve Number - Abstraction Ratio	0.1	0.1
Gridded SCS Curve Number - Scale Factor	0.5	0.5
Baseflow - Initial Discharge	0.4	0.3
Baseflow - Recession Constant	0.16	0.16
Baseflow - Ratio	0.4	0.4
Precipitation Time Shift	-	-
OBSERVED VALUES AND MODEL OUTPUTS		
Observed Peak Discharge (m^3/s)	10.7	5.1
Modelled Peak Discharge (m^3/s)	10.6	5.2
Observed Discharge Volume (1000 m^3)	505.4	359
Modelled Discharge Volume (1000 m^3)	491.4	385.9
STATISTICS		
Nash Sutcliffe Efficiency (NSE)	0.93	0.749
Percent BIAS (PBIAS) (%)	2.69	5.66
Standard Deviation of the Root Mean Square Errors	0.3	0.5

4.4.3.2 Flow Modelling for Floods with Specific Recurrence

As a result of the calibration, the best parameters were obtained (Table 4.15), and flood modeling was performed using the hyetographs given in Figure 4.143 and flood hydrographs with a recurrence interval from 2 years to 1000 years were obtained.

In the HEC-HMS model, which has been calibrated and validated, 24-hour design hyetographs for rainfall corresponding to return periods of 2, 5, 10, 25, 50, 100, 250, 500, and 1000 years were incorporated, and the models were subsequently rerun. Hydrographs for the current situation are given in Figure 4.151. Based on these results, the peak discharge for the 1000-year flood hydrograph is determined to be 117.9 m^3/s.

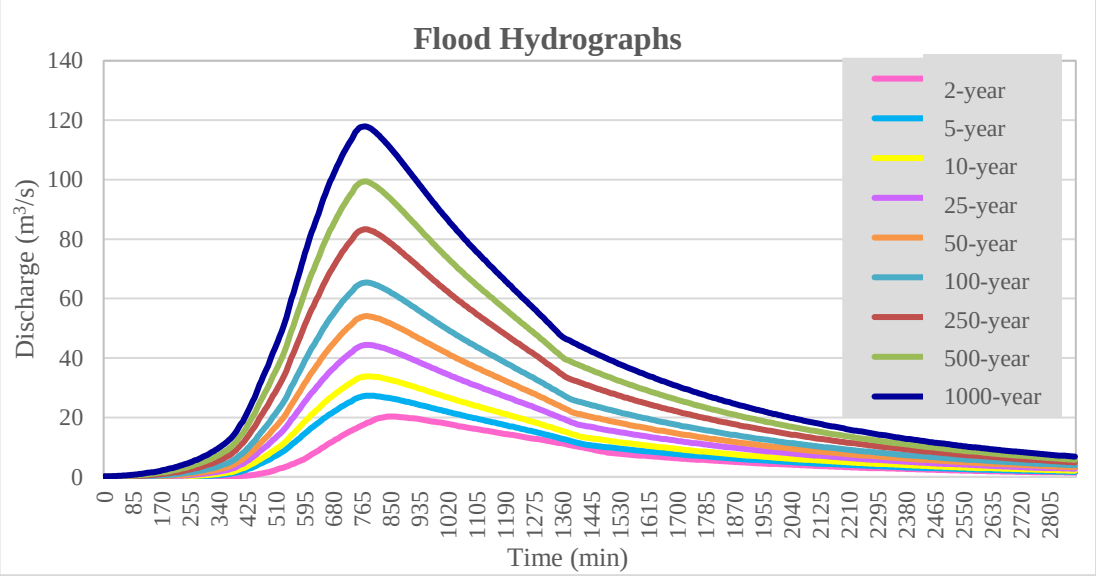


Figure 4.151 Rainfall depth (mm) and flood hydrograph (m^3/s) for validation period.

In the study, which included the effect of Ergenli Dam, the flood was offset in the dam reservoir. The reservoir was assumed to be at its normal water level of 242.5 m. Parameters such as spillway threshold elevation (242.5 m), spillway length (55 m) and elevation-volume information (Figure 4.152) were extracted from İzmir Bayındır Project Ergenli Dam and Irrigation Planning Report (DSİ, 2008). The weir coefficient was determined to be 2.66 $m^{0.5}/s$.

In the modeling conducted for January 2011 using observed data, the peak inflow into the dam reservoir was calculated as 10.6 m^3/s, and the peak outflow was 7.5 m^3/s (see Figure 4.153).

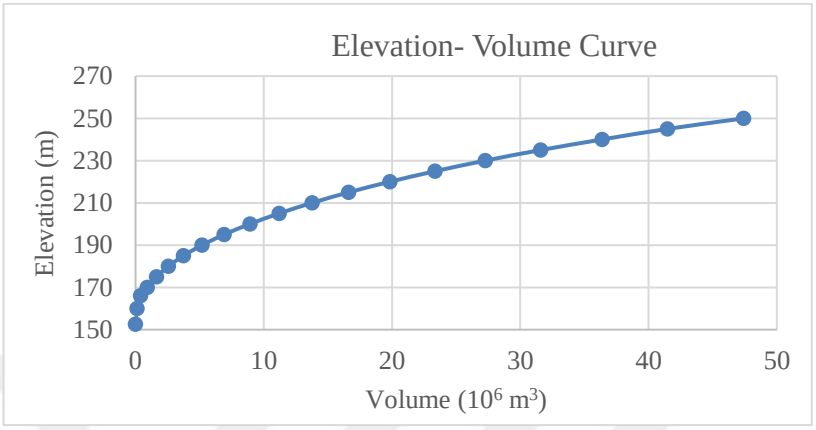


Figure 4.152 Elevation – Volume Curve for Ergenli Basin.

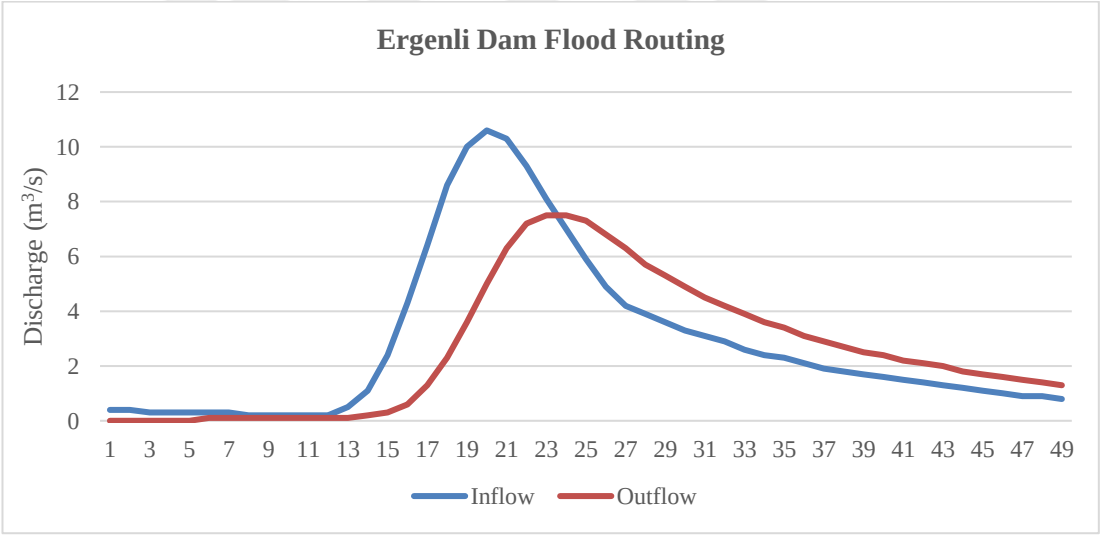


Figure 4.153 Ergenli Dam flood routing for observed flows of Jan-2011.

Considering the presence of the dam, 24-hour design hyetographs for precipitation with return periods of 2, 5, 10, 25, 50, 100, 250, 500, and 1000 years were input into the HEC-HMS model. The resulting hydrographs are presented in Figure 4.154. Consequently, the peak discharge for a 1000-year flood hydrograph is determined to be 107.1 m^3/s (refer to Figure 4.154).

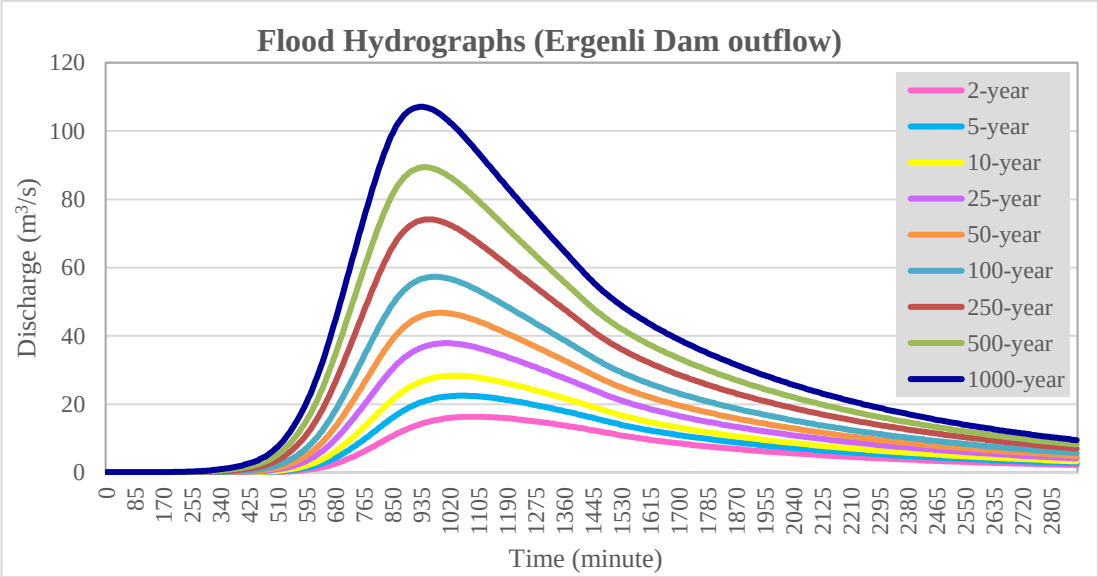


Figure 4.154 Flood hydrographs obtained by flow routing.

4.5 HEC-RAS Modeling

The HEC-RAS model was employed to assess both the current and operational conditions of Ergenli Dam separately. The model interface is given by Figure 4.155.

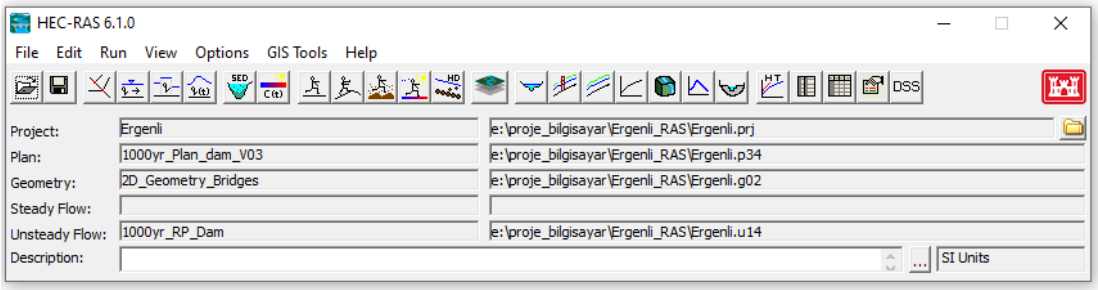


Figure 4.155 HEC-RAS Modeling interface for Ergenli Basin.

The hydraulic modeling of the flood was carried out by considering the flood hydrographs that are given by Figure 4.151 and Figure 4.154. Topographical data was provided to the HEC-RAS model from the HEC-HMS model, boundary layers were determined, and the study area was determined by creating 10m*10m meshes (Figure 4.156 and Figure 4.157). Stream sections and bridges and culverts on the stream were also created using the "geometric data" tool in the HEC-RAS model (Figure 4.158). Mesh sizes around the bridge and culvert were selected as 0.5m * 0.5m.

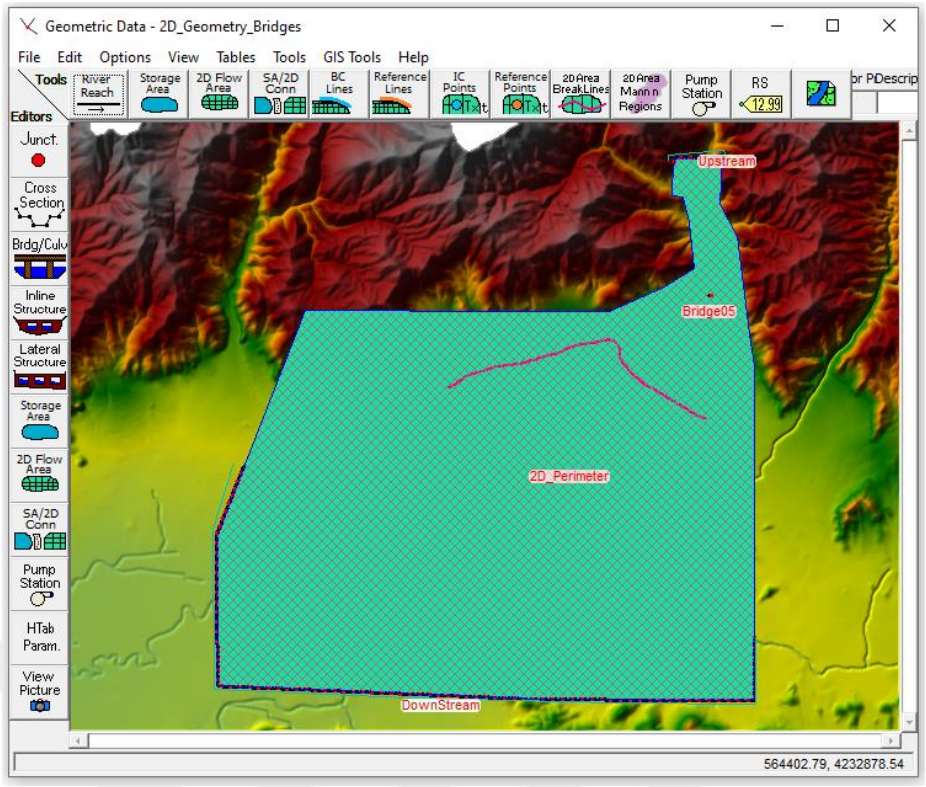


Figure 4.156 2D Flow Area

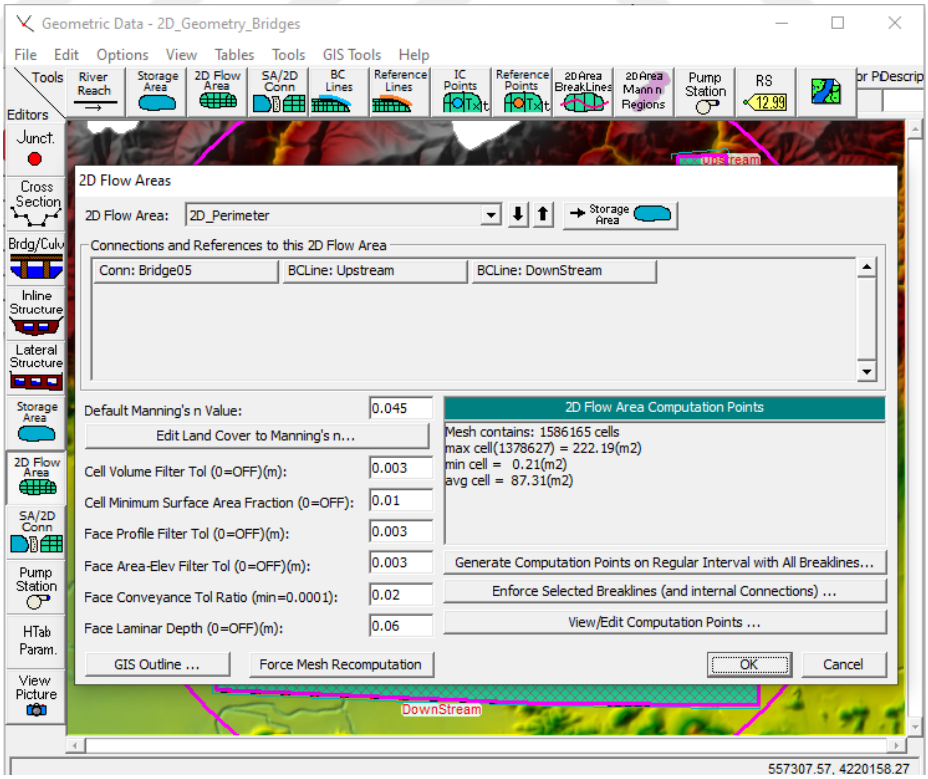


Figure 4.157 2D Flow area parameters.

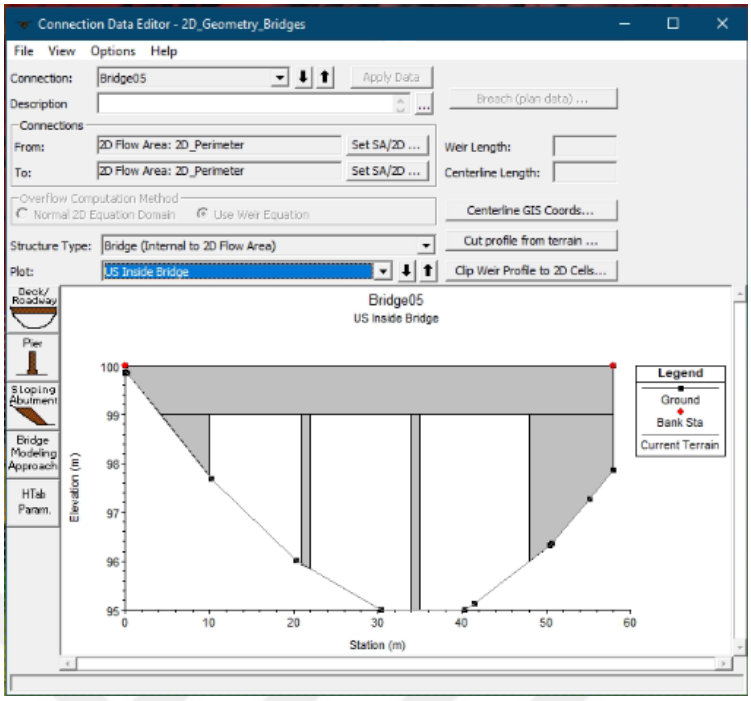


Figure 4.158 Defining the bridges.

As part of the study, 2D unsteady flow calculations were executed, depicted in Figure 4.159. The flow hydrograph is illustrated in Figure 4.160, and the outcomes were generated utilizing RAS-Mapper, presented in Figure 4.161.

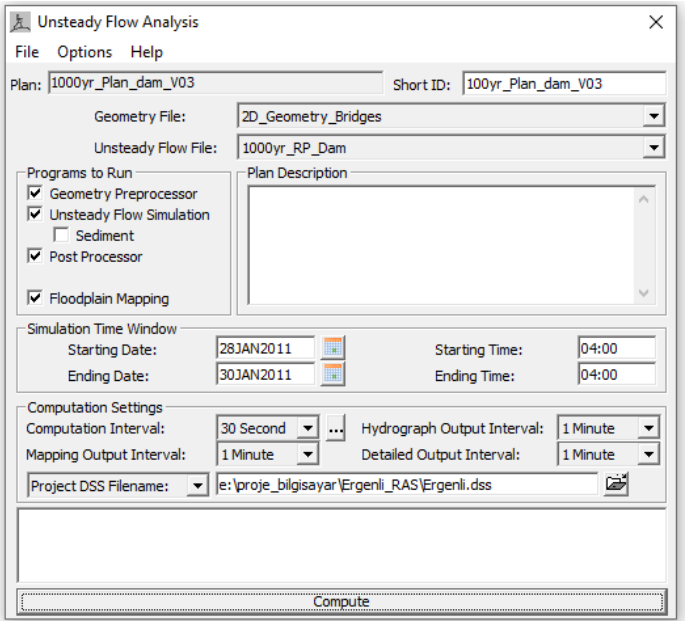


Figure 4.159 Unsteady flow data.

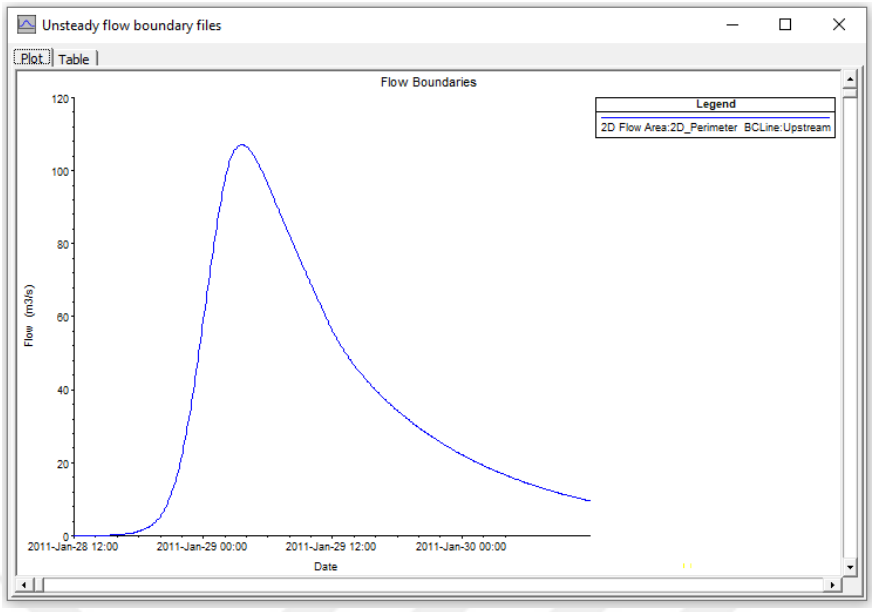


Figure 4.160 The hydrograph of Q_{1000} - Ergenli Dam in operation.

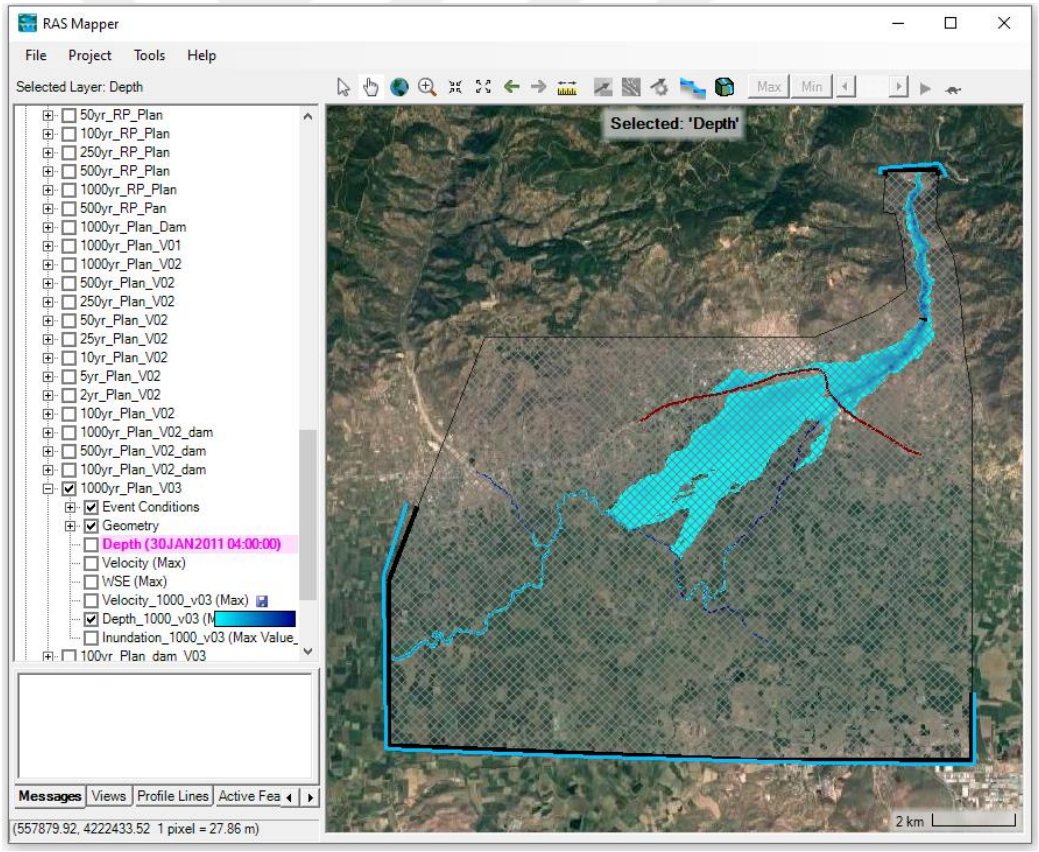


Figure 4.161 RAS Mapper and the flow depth for Q_{1000} - Ergenli Dam in operation.

Under the existing conditions, maps depicting maximum depths for floods with return periods of 2, 5, 10, 25, 25, 50, 100, 250, 500, and 1000 years are presented in

Figures 4.162 through 4.170. Correspondingly, maximum velocity maps are displayed in Figures 4.171 through 4.179. Flood inundation maps are provided in Figure 4.180 through Figure 4.183. Additionally, Table 4.16 outlines the flood inundation area and rate for the Ergenli Basin.

Table 4.16 Flood inundation area and rate for Ergenli Basin.

	2-year	5-year	10-year	25-year	50-year	100-year	250-year	500-year	1000-year
Flood Inundation Area (km^2)	6.97	7.53	8.89	8.92	9.89	10.48	10.40	10.87	14.02
Flood Inundation Rate (%)	-	7.98	27.46	27.91	41.87	50.30	49.20	55.86	101.06

Under the operational status of the dam, maps illustrating maximum depths for floods with return periods of 100, 500, and 1000 years are presented in Figures 4.184 through 4.186. Correspondingly, maximum velocity maps can be found in Figures 4.187 through 4.189. The flood inundation map is provided in Figure 4.190. Additionally, Table 4.17 outlines the flood inundation area and rate for the Ergenli Basin.

Table 4.17 Flood inundation area and rate for Ergenli Basin.

	2-year	5-year	10-year	25-year	50-year	100-year	250-year	500-year	1000-year
Flood Inundation Area (km^2)	6.75	7.62	7.88	8.44	8.88	9.55	9.89	11.61	12.68
Flood Inundation Rate (%)	-	12.9	16.76	25.01	31.5	41.45	46.46	71.93	87.88

Since the Ergenli Dam is not designed for flood control purposes, the impact of the dam in the event of a 1000-year flood is relatively limited. Following the hydrological modelling, hydraulic modelling was carried out to assess the potential flood-affected areas under various scenarios. Accordingly, it is observed that some parts of Dereköy and Ergenli Village, as well as portions of Furunlı and Karahalilli settlements, are susceptible to flooding. The impact is predominantly observed in agricultural lands.

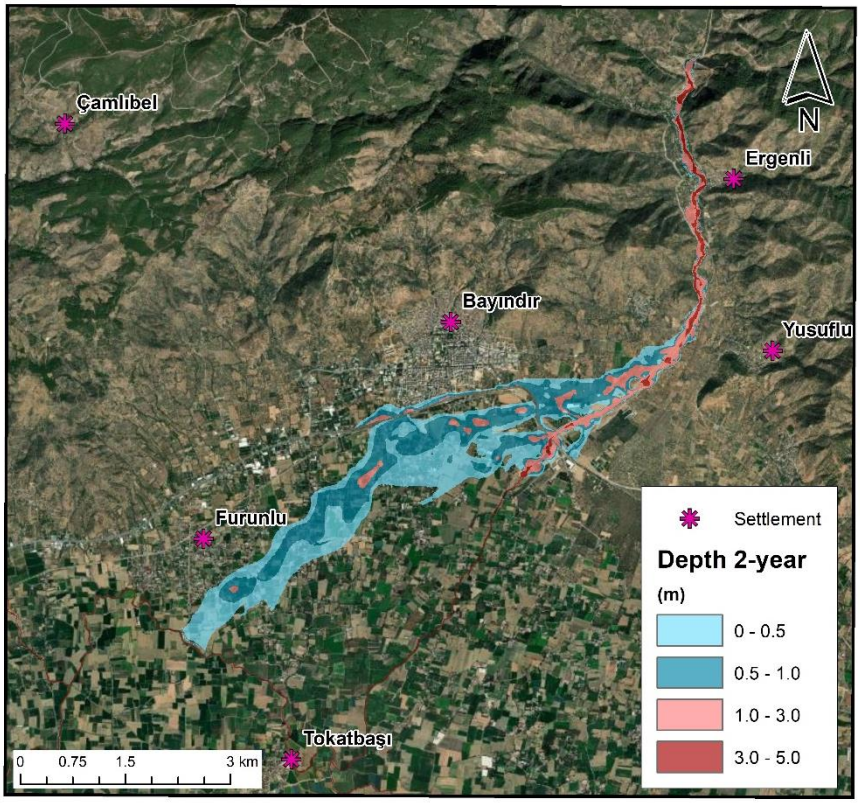


Figure 4.162 The flow depth map for 2-year flood.

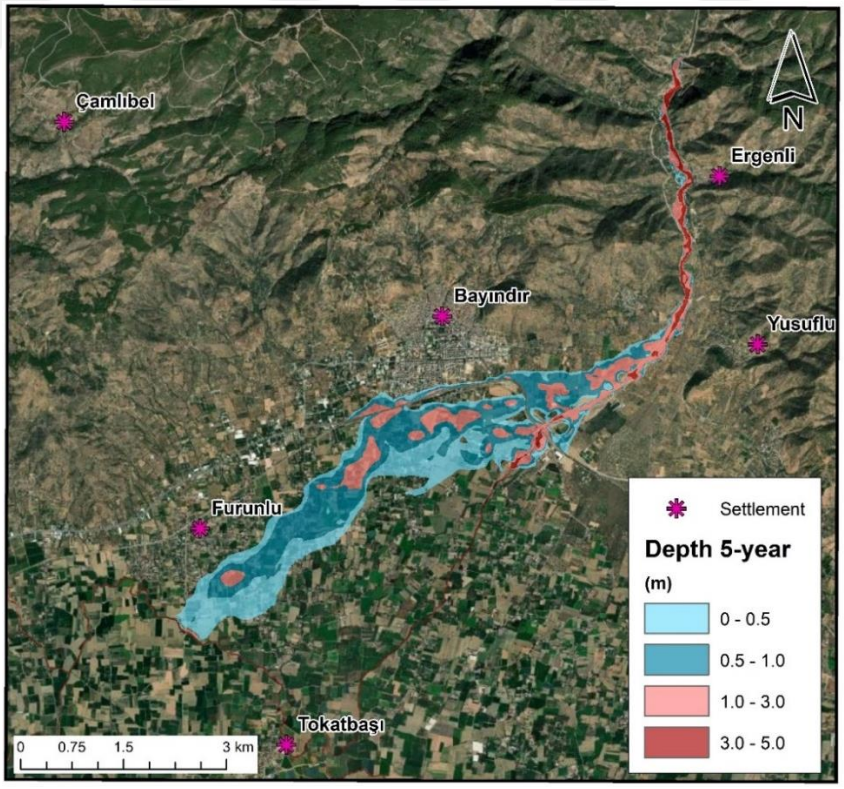


Figure 4.163 The flow depth map for 5-year flood.

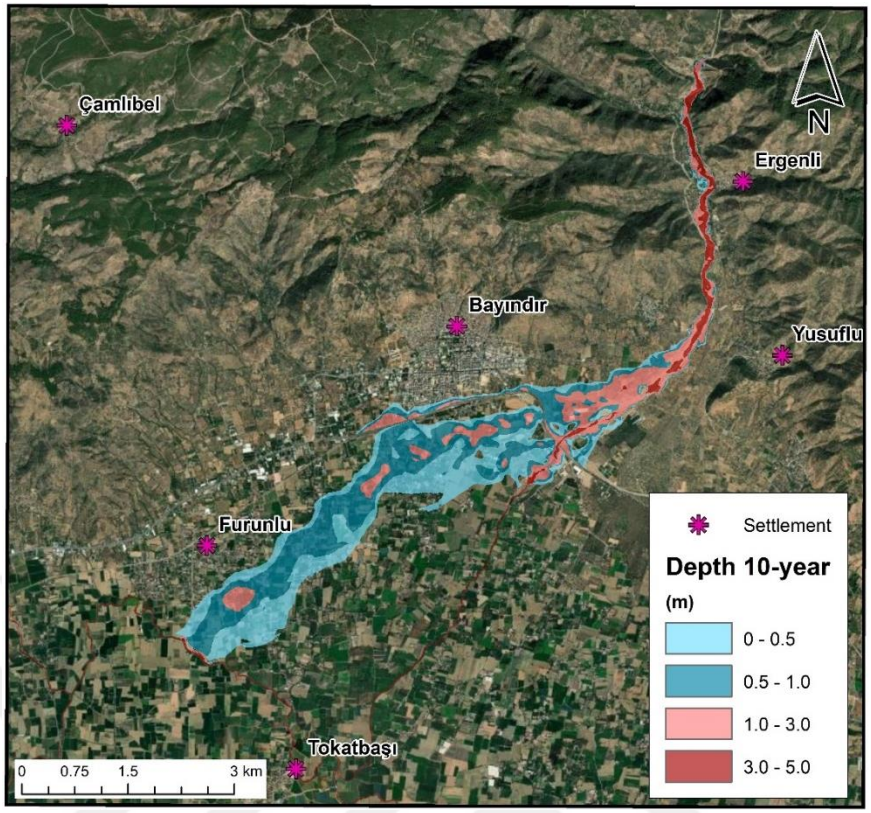


Figure 4.164 The flow depth map for 10-year flood.

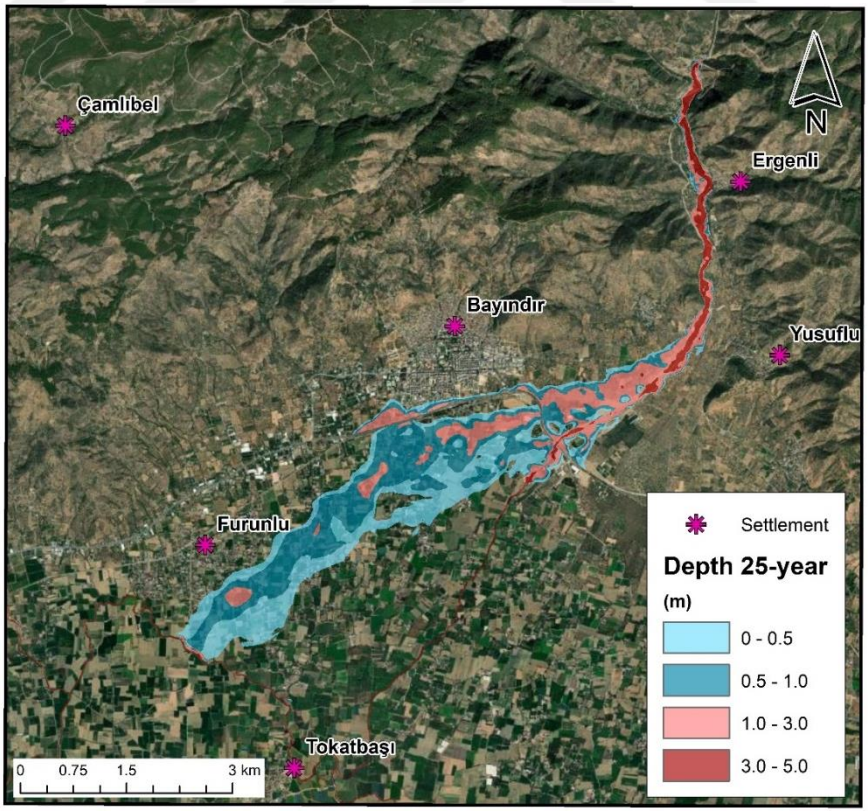


Figure 4.165 The flow depth map for 25-year flood.

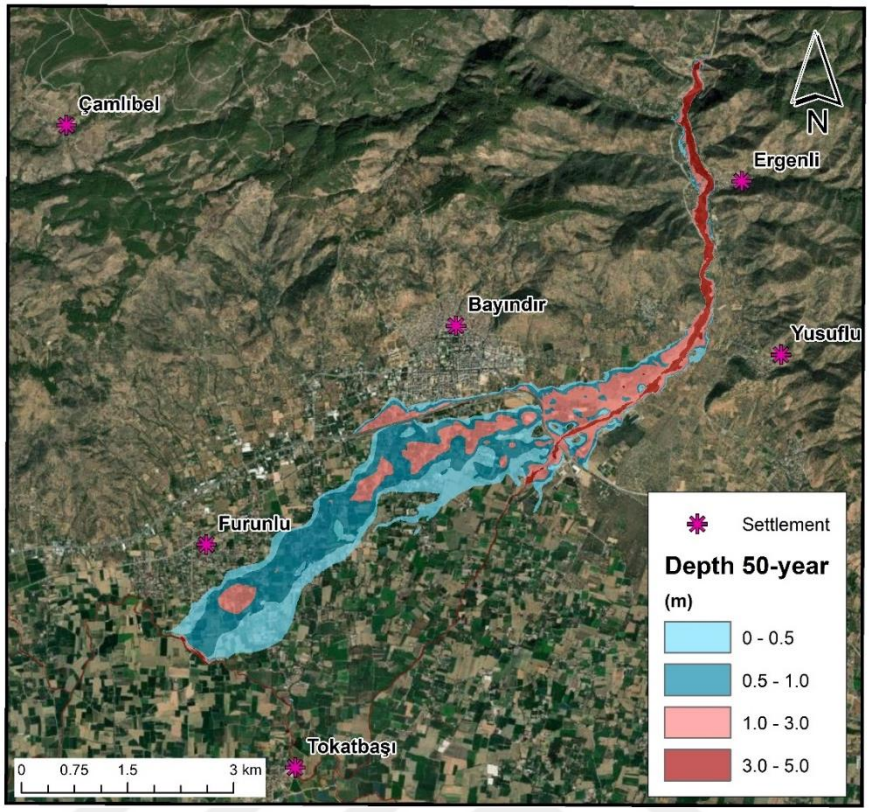


Figure 4.166 The flow depth map for 50-year flood.

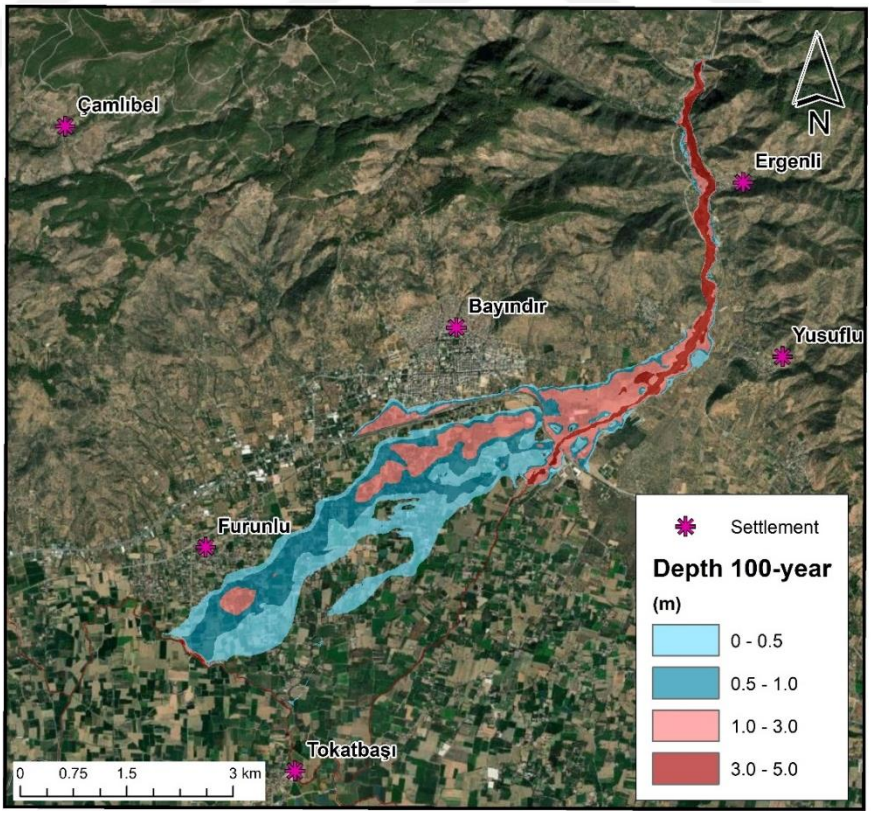


Figure 4.167 The flow depth map for 100-year flood.

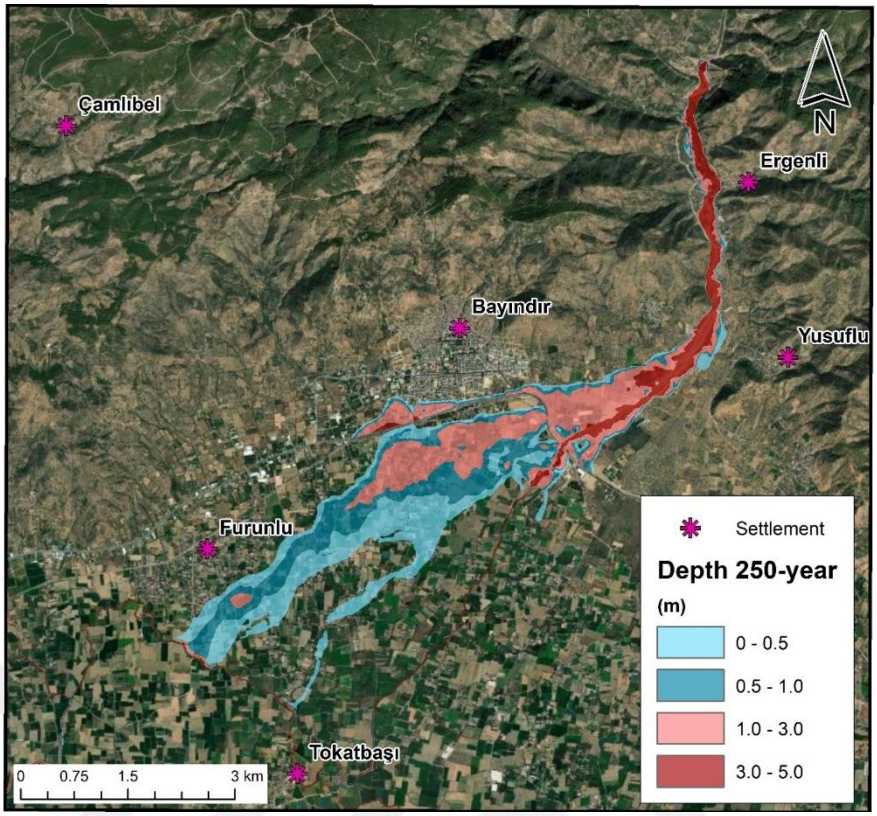


Figure 4.168 The flow depth map for 250-year flood.

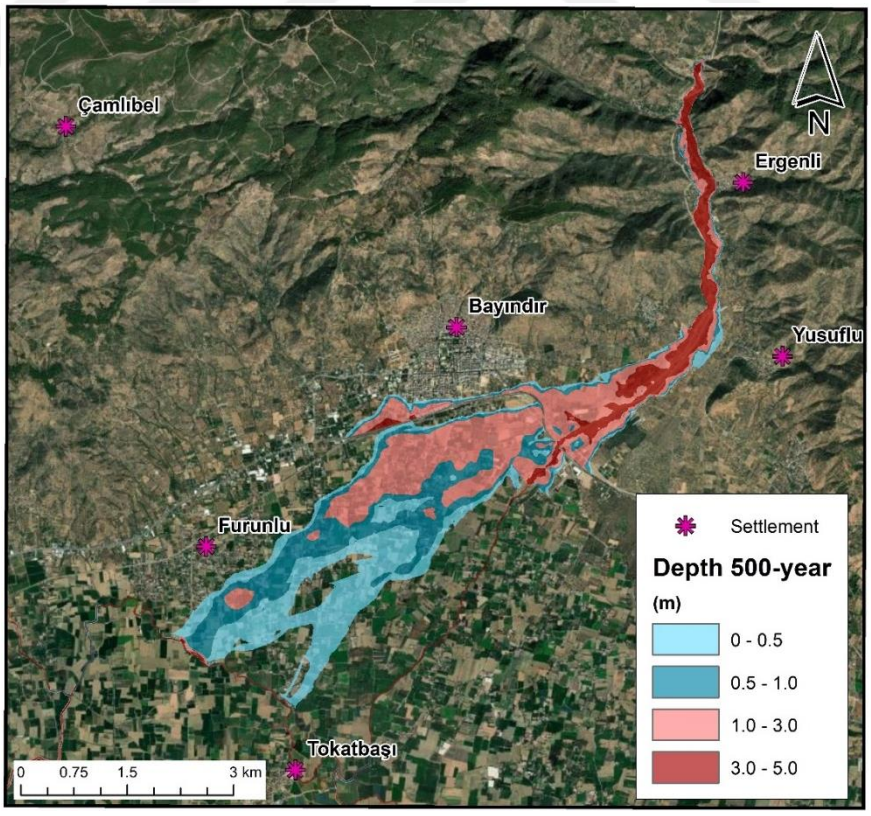


Figure 4.169 The flow depth map for 500-year flood.

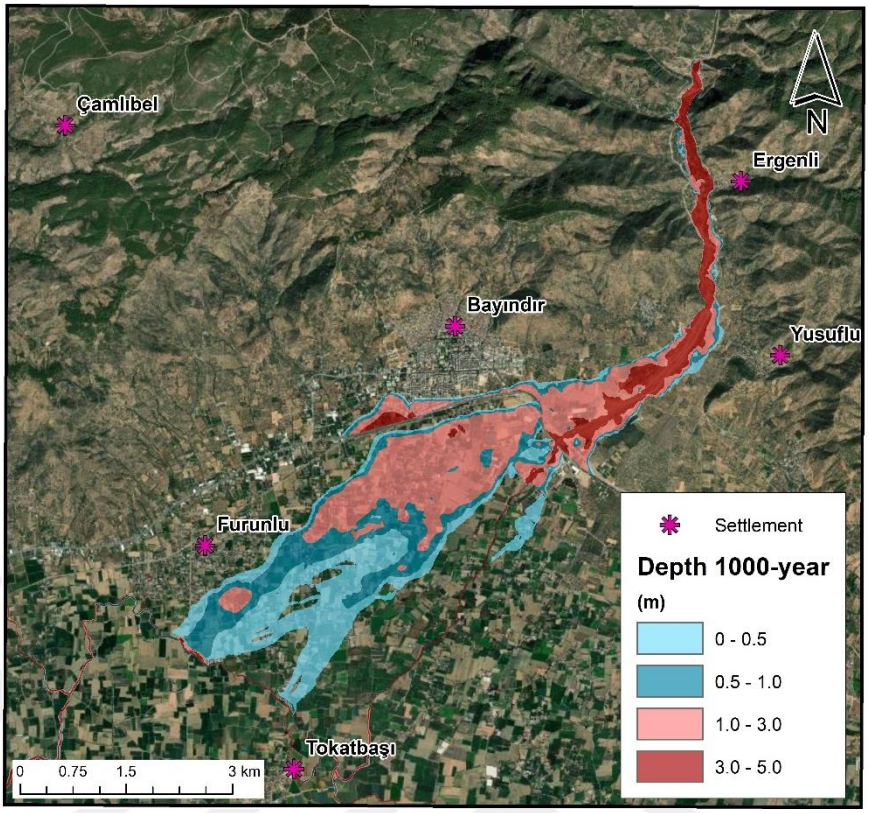


Figure 4.170 The flow depth map for 1000-year flood.

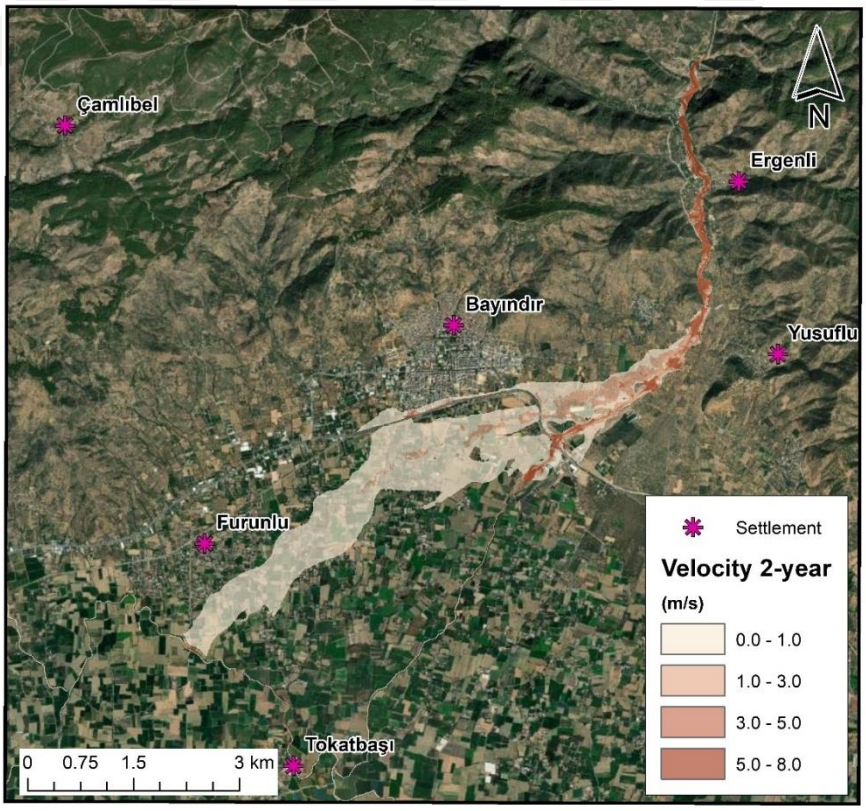


Figure 4.171 The flow velocity map for 2-year flood.

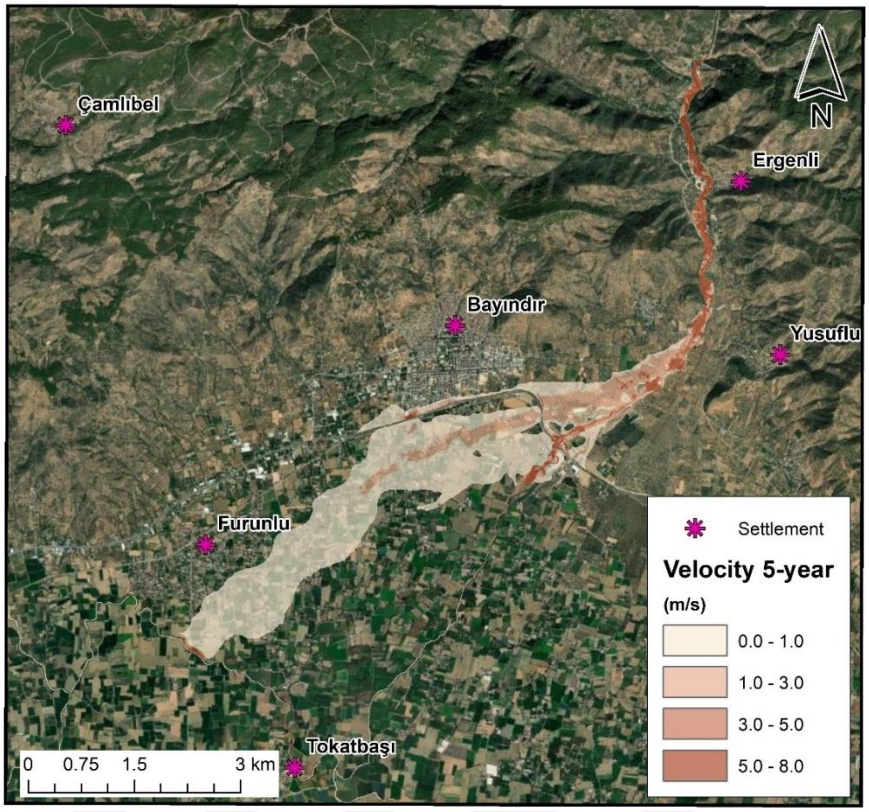


Figure 4.172 The flow velocity map for 5-year flood.

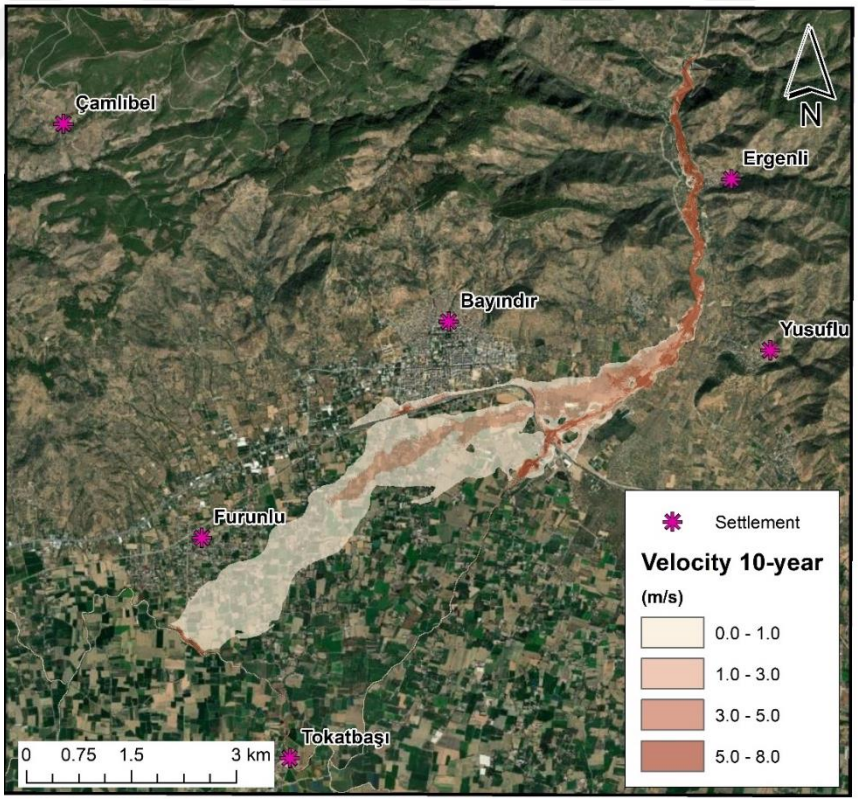


Figure 4.173 The flow velocity map for 10-year flood.

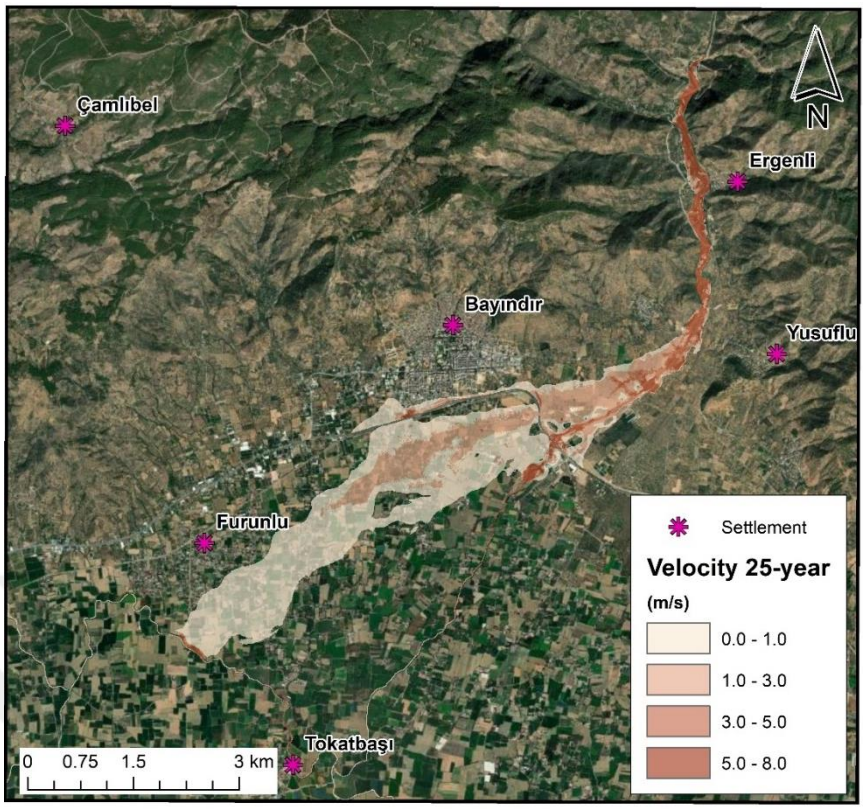


Figure 4.174 The flow velocity map for 25-year flood.

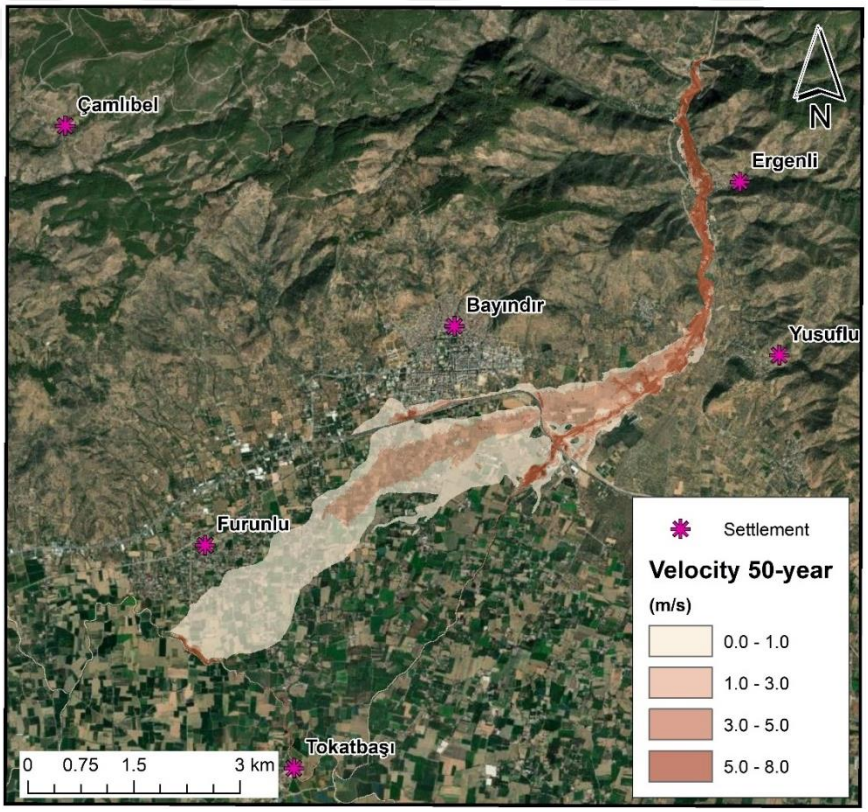


Figure 4.175 The flow velocity map for 50-year flood.

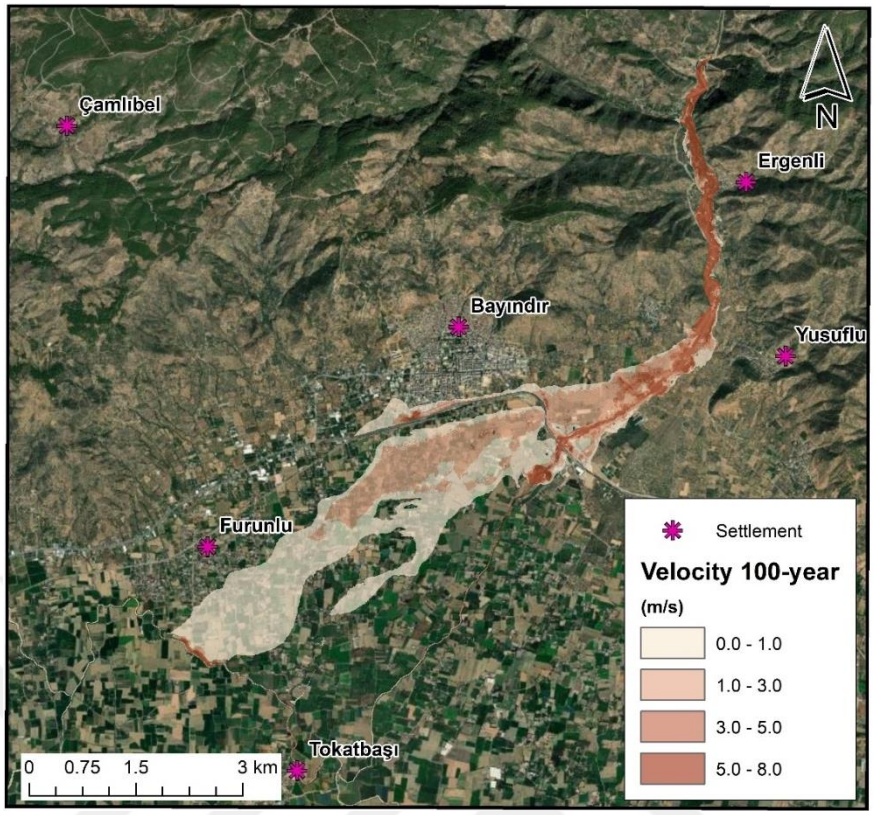


Figure 4.176 The flow velocity map for 100-year flood.

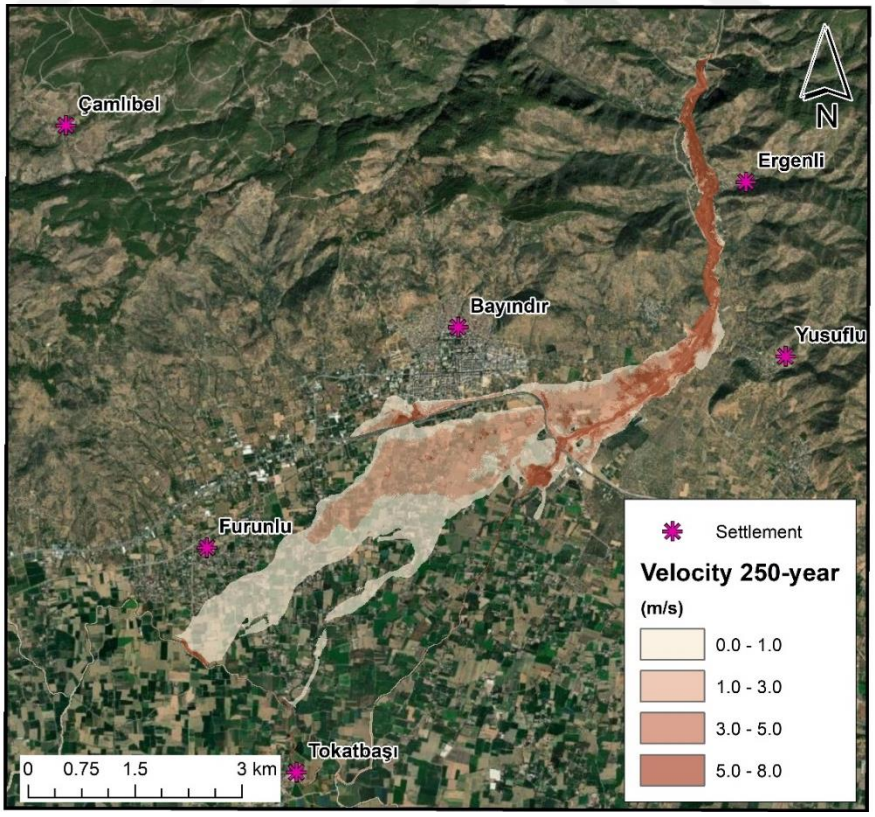


Figure 4.177 The flow velocity map for 250-year flood.

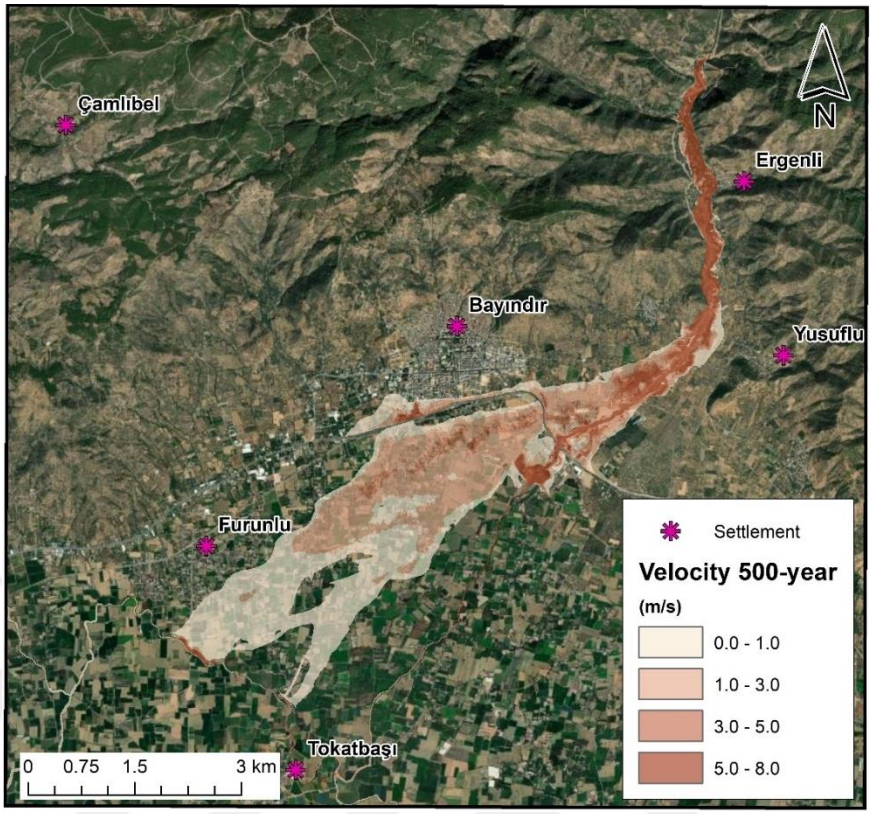


Figure 4.178 The flow velocity map for 500-year flood.

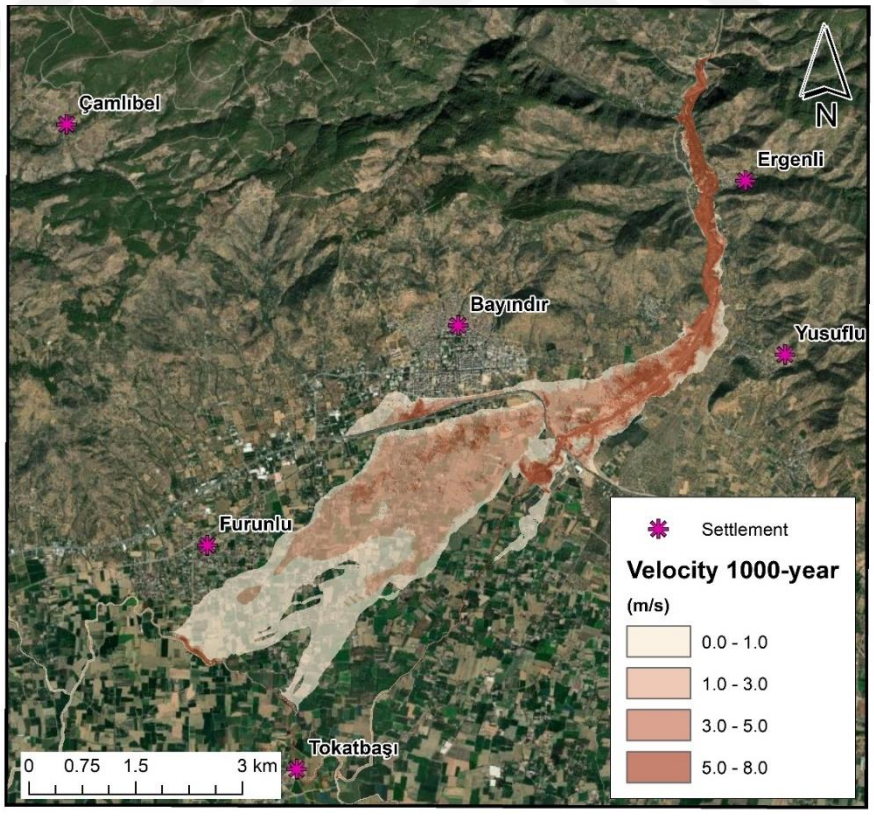


Figure 4.179 The flow velocity map for 1000-year flood.

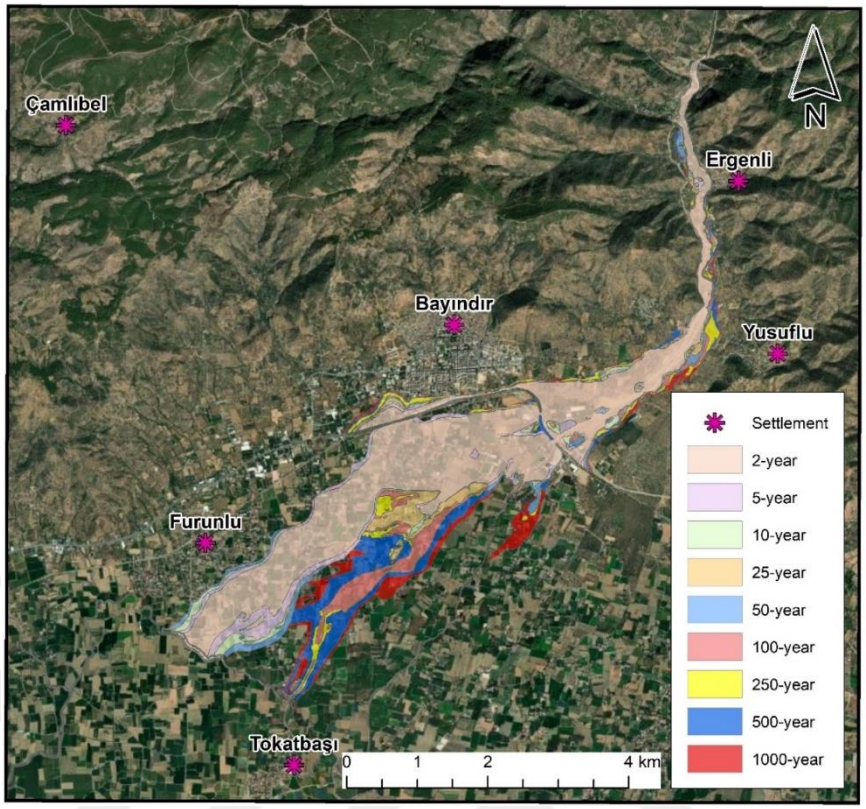


Figure 4.180 The flood inundation map.

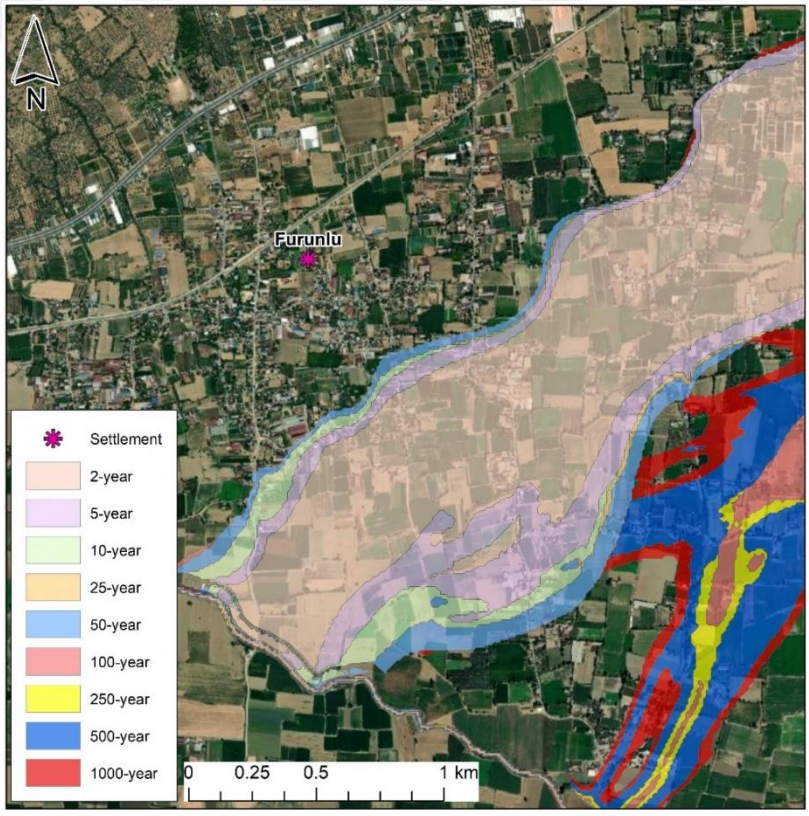


Figure 4.181 The flood inundation map for Furunlu region.

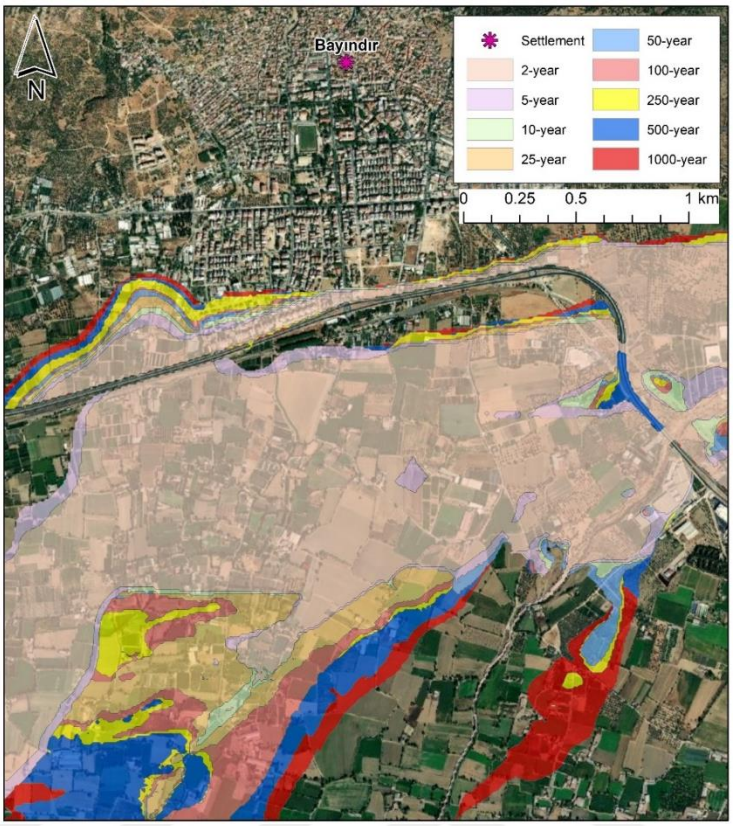


Figure 4.182 The flood inundation map for Bayındır region.

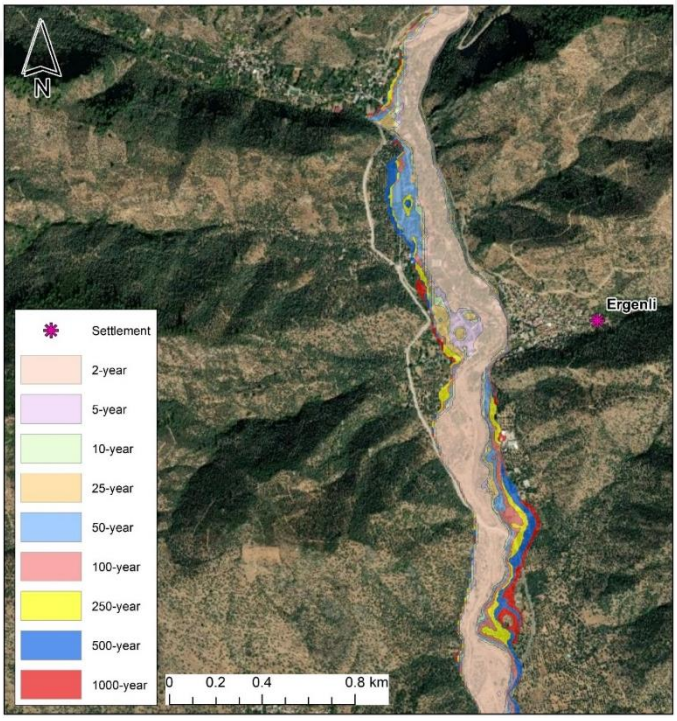


Figure 4.183 The flood inundation map for Ergenli region.

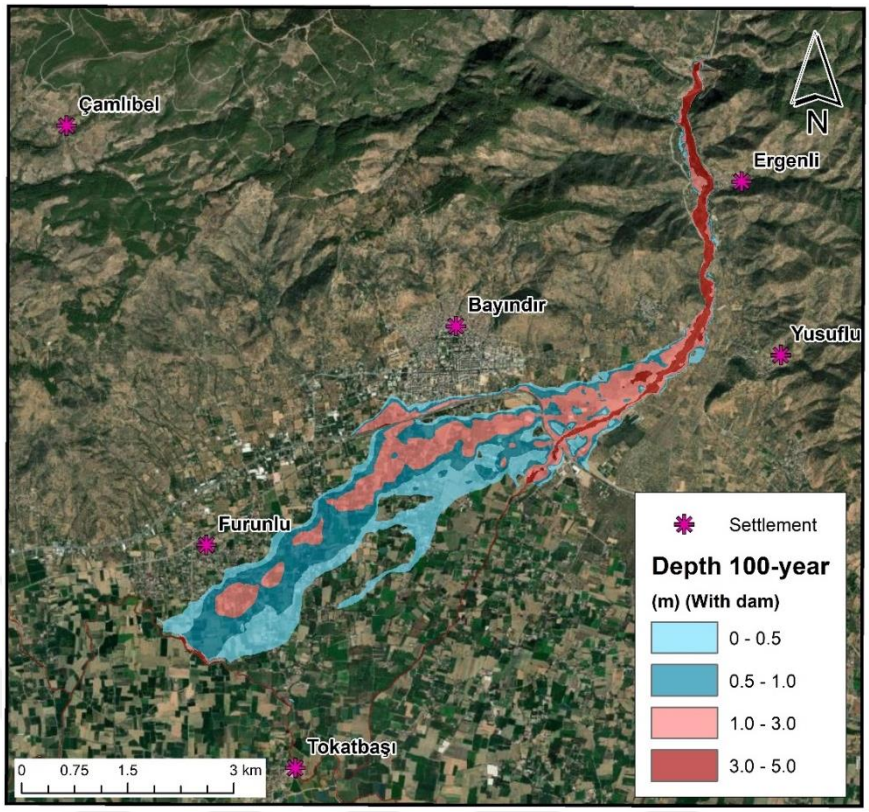


Figure 4.184 The flow depth map for 100-year flood in case the dam in operation.

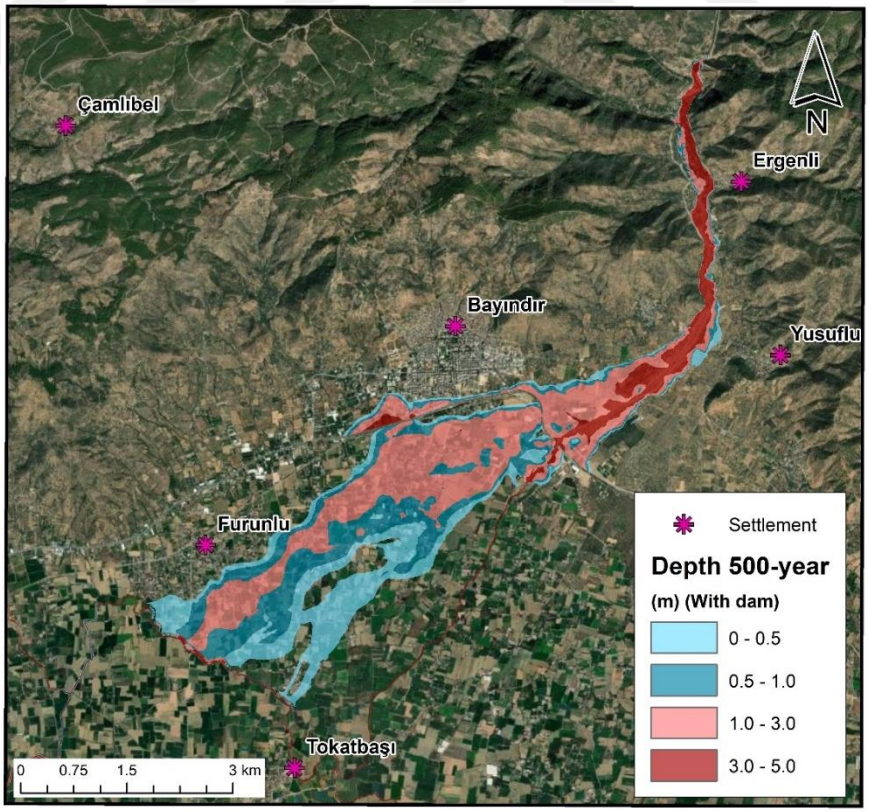


Figure 4.185 The flow depth map for 500-year flood in case the dam in operation.

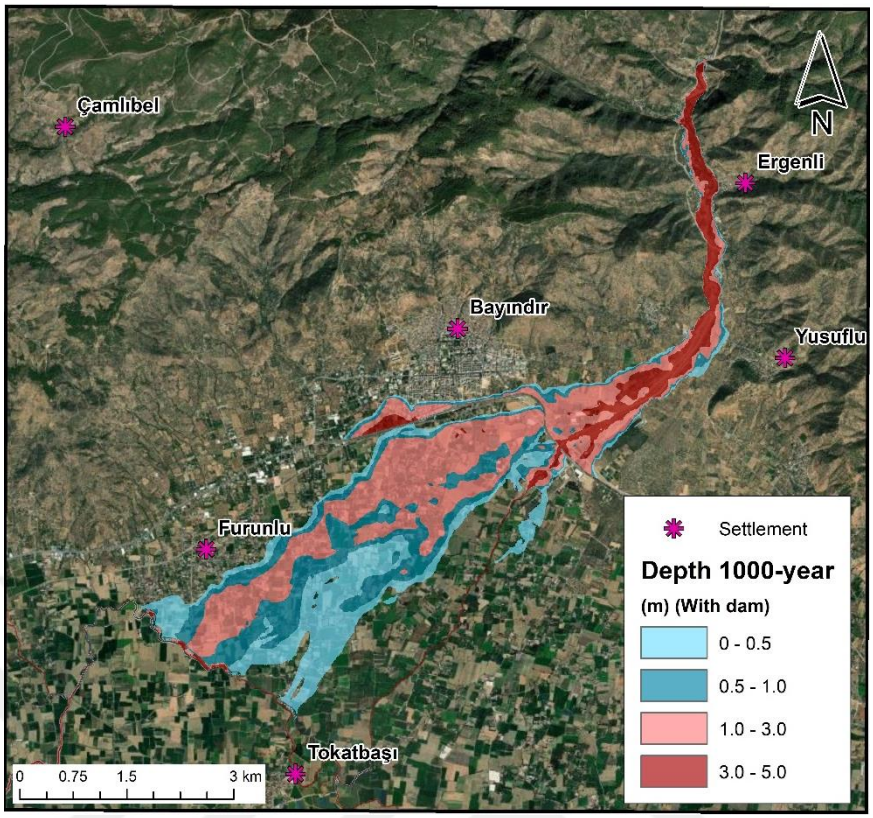


Figure 4.186 The flow depth map for 1000-year flood in case the dam in operation.

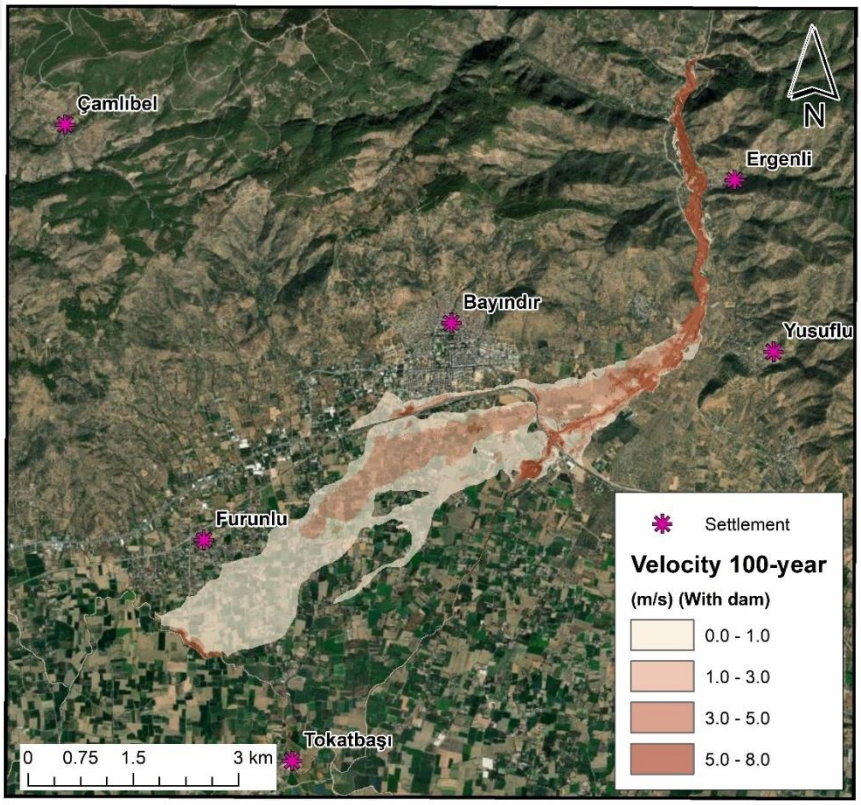


Figure 4.187 The flow velocity map for 100-year flood in case the dam in operation.

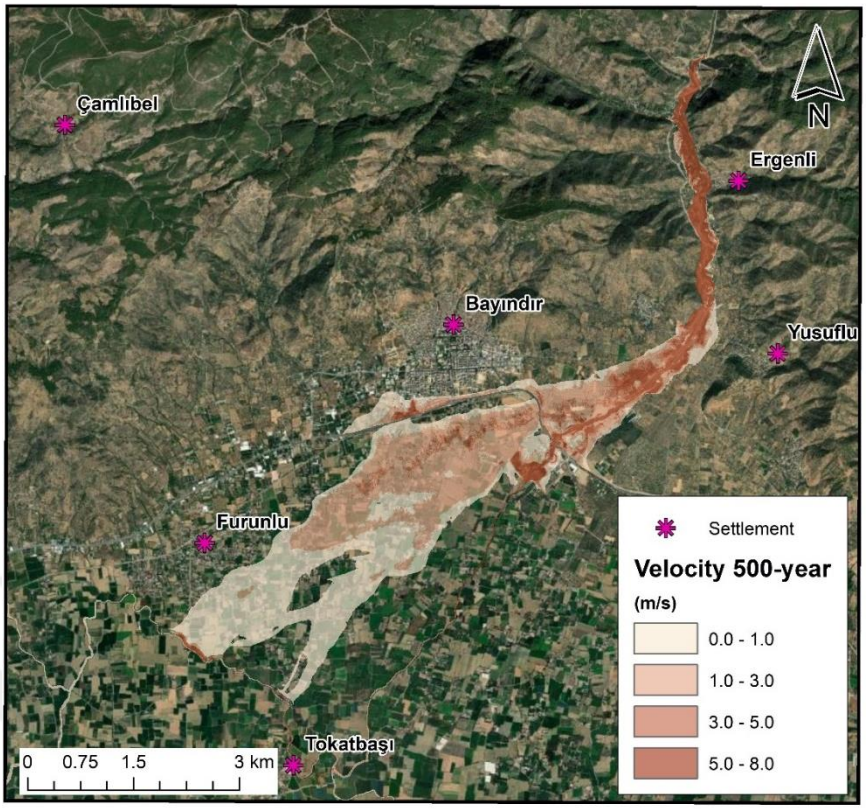


Figure 4.188 The flow velocity map for 500-year flood in case the dam in operation.

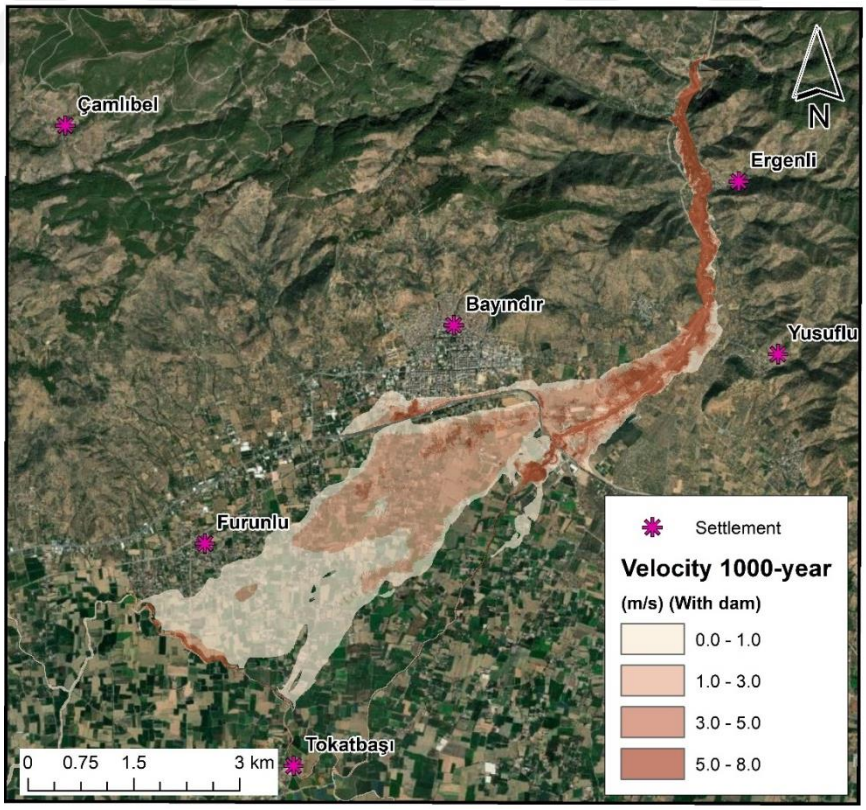


Figure 4.189 The flow velocity map for 1000-year flood in case the dam in operation.

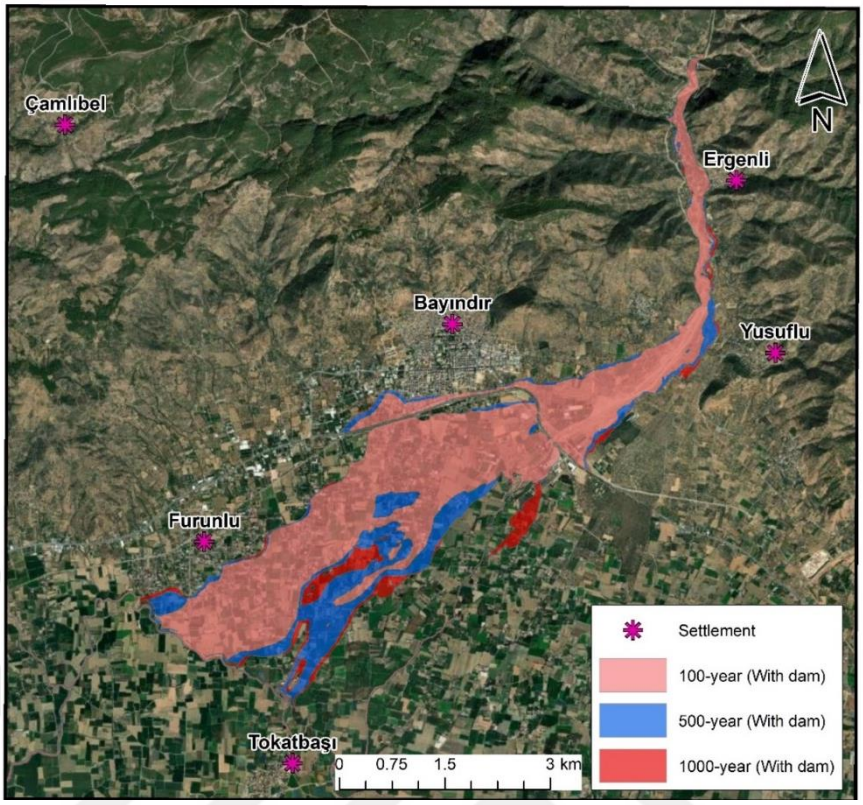


Figure 4.190 The flood inundation map in case the dam in operation.

4.6 Conclusion

This study makes significant contributions to the climate and disaster resilience literature by coupling the VIC land surface model with hydrological models SWAT and HEC-HMS to simulate droughts and floods under various climate and land use change scenarios. Through this coupling procedure, the study provides a comprehensive approach to understanding the challenges faced by smart cities in terms of drought and flooding, helping to plan and adaptation strategies. In particular, the SPI values were calculated daily and grid-based using climate data together with modelling studies. There is no comparable study conducted in Turkey, making this study distinct and unique.

In the conducted study, information essential for the implementation of smart planning tools in the pre-disaster phase of smart cities, specifically addressing flood and drought disasters with observed increases in magnitude and frequency due to climate change, has been comprehensively developed through hydrological/hydraulic and statistical analyses.

Performing of flood and drought simulations through the integration of coupled land surface and hydrologic models represents a significant step towards the development of climate and disaster-resilient smart cities. The comprehensively created daily and monthly drought maps, along with flood inundation maps, will serve as tools guiding urban planning, risk management, and emergency response strategies.

The drought maps derived from the analyses, which contain indicators of the temporal and spatial distribution of the severity, duration and magnitude of drought, are of critical importance in terms of enabling urban planning, the formulation of water resources management strategies, agricultural planning and the development of infrastructure practices that consider potential drought scenarios. Drought maps created on a monthly and daily basis further enhance our understanding of evolving drought patterns and offer a more detailed approach to resilient-urban planning.

Flood inundation maps created for different scenarios are one of the unique tools that represent the visual expression of potential areas that are likely to be inundated. This information is critical for urban planners and emergency responders, essential for identifying high-risk areas, planning evacuation routes, and design resilient infrastructure capable of withstanding flood events. Through the integration of flood propagation maps into the urban planning framework, smart cities can enhance their adaptive capacity and mitigate the socio-economic and environmental impacts associated with floods.

As a result, combining sophisticated modeling techniques for flood and drought simulations provides strong and reliable technical support for climate- and disaster-resilient smart cities. The results of the studies will enable decision-makers to develop proactive strategies, rapidly identify disasters, quickly predict risks and make effective decisions, and contribute to smart city solutions to build resilient cities to the effects of climate change and possible disasters.

REFERENCES

Abbaspour, K. C. (2015). *SWAT calibration and uncertainty programs. A user manual*, *103*, pp.17-66.

Abbaspour, K. C., Rouholahnejad, E., Vaghefi, S., Srinivasan, R., Yang, H., & Kløve, B. (2015). A continental-scale hydrology and water quality model for Europe: Calibration and uncertainty of a high-resolution large-scale SWAT model.*Journal of hydrology,524*, pp. 733-752. https://doi.org/10.1016/j.jhydrol.2015.03.027

Adams, J. (2017). *Climate indices: An open source Python library providing reference implementations of commonly used climate indices*. Climate indices in Python. https://climate-indices.readthedocs.io/en/latest/

Aditya, F., Gusmayanti, E., & Sudrajat, J. (2021). Rainfall trend analysis using Mann-Kendall and Sen's slope estimator test in West Kalimantan. In *IOP Conference Series: Earth and Environmental Science*, Vol. 893, No. 1, p. 012006. IOP Publishing. https://doi.org/10.1088/1755-1315/893/1/012006

AFAD (2022). *Türkiye Afet Azaltma Planı (TARAP) 2022-2030*, 104 s. https://www.afad.gov.tr/kurumlar/afad.gov.tr/e_Kutuphane/Planlar/28032022-TARAP-kitap_V6.pdf

Akiyanova, F., Ongdas, N., Zinabdin, N., Karakulov, Y., Nazhbiyev, A., Mussagaliyeva, Z., & Atalikhova, A. (2023). Operation of Gate-Controlled Irrigation System Using HEC-RAS 2D for Spring Flood Hazard Reduction. *Computation*, *11*(2), 27. MDPI AG. https://doi.org/10.3390/computation11020027

Arabi, M., Frankenberger, J. R., Engel, B. A., & Arnold, J. G. (2008). Representation of agricultural conservation practices with SWAT. *Hydrological Processes: An International Journal*, *22*(16), pp.3042-3055. https://doi.org/10.1002/hyp.6890

Arnold, J. G., Kiniry, J. R., Srinivasan, R., Williams, J. R., Haney, E. B., & Neitsch, S. L. (2011). *Soil and water assessment tool input/output file documentation version 2009*. Texas Water Resources Institute. https://swat.tamu.edu/media/69296/swat-io-documentation-2012.pdf

Arnold, J. G., Moriasi, D. N., Gassman, P. W., Abbaspour, K. C., White, M. J., Srinivasan, R., ... & Jha, M. K. (2012). SWAT: Model use, calibration, and validation. *Transactions of the ASABE*, *55*(4), pp. 1491-1508. https://doi.org/10.13031/2013.42256

ASCE, Task Committee on Hydraulic Modeling, Environmental and Water Resources Institute. (2000, May). Hydraulic modeling: Concepts and Practice. American Society of Civil Engineers.

Bakir, M., & Zhang, X. (2008). GIS-based hydrological modelling: a comparative study of HEC-HMS and the Xinanjiang model. *IAHS Publications-Series of Proceedings and Reports*, *319*, pp.124-133. Twelfth International Water Technology Conference, IWTC12 2008 Alexandria, Egypt

Beguería, S., Vicente-Serrano, S. M., Reig, F., & Latorre, B. (2014). Standardized precipitation evapotranspiration index (SPEI) revisited: parameter fitting, evapotranspiration models, tools, datasets and drought monitoring. *International journal of climatology*, *34*(10), pp.3001-3023. https://doi.org/10.1002/joc.3887

Benra, F. K., Dohmen, H. J., Pei, J., Schuster, S., & Wan, B. (2011). A comparison of one-way and two-way coupling methods for numerical analysis of fluid-structure interactions. *Journal of applied mathematics*, 2011. https://doi.org/10.1155/2011/853560

Berger, H. E., & Van D Langemheen, H. E. L. M. U. S. (2007). Rhine Floods And Low Flows. In *Extreme Hydrological Events: New Concepts for Security* , pp. 47-

58. Dordrecht: Springer Netherlands. https://link.springer.com/chapter/10.1007/978-1-4020-5741-0_3

Bergström, S., & Lindström, G. (2015). Interpretation of runoff processes in hydrological modelling—experience from the HBV approach. *Hydrological Processes*, *29*(16), pp.3535-3545. https://doi.org/10.1002/hyp.10510

Bernard, M. M. (1932). Formulas for rainfall intensities of long duration. *Transactions of the American Society of Civil Engineers*, *96*(1), pp.592-606.

Best, M. J., Pryor, M., Clark, D. B., Rooney, G. G., Essery, R., Ménard, C. B., ... & Harding, R. J. (2011). The Joint UK Land Environment Simulator (JULES), model description–Part 1: energy and water fluxes. *Geoscientific Model Development*, *4*(3), pp.677-699. https://doi.org/10.5194/gmd-4-677-2011

Beven, K. (1997). TOPMODEL: a critique. *Hydrological processes*, *11*(9), pp.1069-1085.https://doi.org/10.1002/(SICI)1099-1085(199707)11:9<1069::AID-HYP545>3.0.CO;2-O

Beven, K., Lamb, R., Quinn, P., Romanowicz, R., & Freer, J. (1995). Topmodel. *Computer models of watershed hydrology.*, pp.627-668. ISBN 9780918334916

Bohn, T. J., Podest, E., Schroeder, R., Pinto, N., McDonald, K. C., Glagolev, M., ... & Lettenmaier, D. P. (2013). Modeling the large-scale effects of surface moisture heterogeneity on wetland carbon fluxes in the West Siberian Lowland. *Biogeosciences*, *10*(10), pp.6559-6576. https://doi.org/10.5194/bg-10-6559-2013

Boithias, L., Sauvage, S., Lenica, A., Roux, H., Abbaspour, K. C., Larnier, K., ... & Sánchez-Pérez, J. M. (2017). Simulating flash floods at hourly time-step using the SWAT model. *Water*, *9*(12), 929. https://doi.org/10.3390/w9120929

Bonan, G. B. (2008). Forests and climate change: forcings, feedbacks, and the climate benefits of forests. *science*, *320*(5882), pp.1444-1449. https://doi.org/10.1126/science.115512

Brouziyne, Y., Abouabdillah, A., Bouabid, R., Benaabidate, L., & Oueslati, O. (2017). SWAT manual calibration and parameters sensitivity analysis in a semi-arid watershed in North-western Morocco. *Arabian Journal of Geosciences*, *10*, pp.1-13. https://doi.org/10.1007/s12517-017-3220-9

Brunner, G. W. (1994). *HEC river analysis system (HEC-RAS)* (No. 147). US Army Corps of Engineers, Hydrologic Engineering Center.

Brunner, G. W. (2016). HEC-RAS River Analysis System: Hydraulic Reference Manual, Version 5.0. *US Army Corps of Engineers–Hydrologic Engineering Center*, *547*.

Buishand, T. A. (1982). Some methods for testing the homogeneity of rainfall records. *Journal of hydrology*, *58*(1-2), pp.11-27. https://doi.org/10.1016/0022-1694(82)90066-X

Chaney, N. W. (2015). *Land Surface Models in Hydrologic Monitoring Systems: Addressing the Sources of Uncertainty*, [Doctoral dissertation]. Princeton University. https://www.proquest.com/openview/e1f515889ef4f588a0585ceb0b8e88b0/1?pq-origsite=gscholar&cbl=18750

Chen, W., Wu, H., Kimball, J. S., Alfieri, L., Nanding, N., Li, X., ... & Zhong, W. (2022). A Coupled River Basin-Urban Hydrological Model (DRIVE-Urban) for Real-Time Urban Flood Modeling. *Water Resources Research*, *58*(11), e2021WR031709. https://doi.org/10.1029/2021WR031709

Cheng, C., Yang, Y. E., Ryan, R., Yu, Q., & Brabec, E. (2017). Assessing climate change-induced flooding mitigation for adaptation in Boston's Charles River watershed, USA. *Landscape and Urban Planning*, *167*, pp.25-36. https://doi.org/10.1016/j.landurbplan.2017.05.019

Cherkauer, K. A., & Lettenmaier, D. P. (2003). Simulation of spatial variability in snow and frozen soil. *Journal of Geophysical Research: Atmospheres*, *108*(D22). https://doi.org/10.1029/2003JD003575

Chu, X., & Steinman, A. (2009). Event and continuous hydrologic modeling with HEC-HMS. *Journal of Irrigation and Drainage Engineering*, *135*(1), pp.119-124. https://doi.org/10.1061/(ASCE)0733-9437(2009)135:1(119)

Clark, D. B., Mercado, L. M., Sitch, S., Jones, C. D., Gedney, N., Best, M. J., ... & Cox, P. M. (2011). The Joint UK Land Environment Simulator (JULES), model description–Part 2: carbon fluxes and vegetation dynamics. *Geoscientific Model Development*, *4*(3), pp.701-722. https://doi.org/10.5194/gmd-4-701-2011

Dai, A. (2011). Characteristics and trends in various forms of the Palmer Drought Severity Index during 1900–2008. *Journal of Geophysical Research: Atmospheres*, *116*(D12). https://doi.org/10.1029/2010JD015541

Deardorff, J. (1977). A parameterization of ground-surface moisture content for use in atmospheric prediction models. *Journal of Applied Meteorology (1962-1982)*, pp.1182-1185. https://www.jstor.org/stable/26178222

Devia, G. K., Ganasri, B. P., & Dwarakish, G. S. (2015). A review on hydrological models. Aquatic procedia, 4, pp.1001-1007. https://doi.org/10.1016/j.aqpro.2015.02.126

Dhondia, J. F., & Stelling, G. S. (2004). Sobek one dimensional–two dimensional integrated hydraulic model for flood simulation–its capabilities and features

explained. *Hydroinformatics: V2*, pp.1867-1874. https://doi.org/10.1142/9789812702838_0230

Dikici, M. (2020). *Drought analysis with different indices for the Asi Basin (Turkey).* Scientific Reports, 10(1), 20739. https://doi.org/10.1038/s41598-020-77827-z

Dokumentov, A., & Hyndman, R. J. (2022). STR: Seasonal-trend decomposition using regression. *INFORMS Journal on Data Science*, *1*(1), pp.50-62. https://doi.org/10.1287/ijds.2021.0004

Douglas-Mankin, K. R., Srinivasan, R., & Arnold, J. G. (2010). Soil and Water Assessment Tool (SWAT) model: Current developments and applications. *Transactions of the ASABE*, *53*(5), pp.1423-1431. https://doi.org/10.13031/2013.34915

DSİ (2008). *İzmir Bayındır project Ergenli Dam and irrigation planning report.*

Erena, S. H., Worku, H., & De Paola, F. (2018). Flood hazard mapping using FLO-2D and local management strategies of Dire Dawa city, Ethiopia. *Journal of Hydrology: Regional Studies*, *19*, pp. 224-239. https://doi.org/10.1016/j.ejrh.2018.09.005

Erkan, B. B. B., & Hasgul, E. (2015, May). *Turkish Disaster Data Bank (TABB).* International Institute of Earthquake Engineering and Seismology (IIEES) , pp.441-442. http://www.iiees.ac.ir/fa/wp-content/uploads/2016/04/00019-RL.pdf

Franchini, M., & Pacciani, M. (1991). Comparative analysis of several conceptual rainfall-runoff models. Journal of hydrology, 122(1-4), pp 161-219. https://doi.org/10.1016/0022-1694(91)90178-K

Fung, K. F., Huang, Y. F., Koo, C. H., & Soh, Y. W. (2020). Drought forecasting: A review of modelling approaches 2007–2017. *Journal of Water and Climate Change, 11*(3), pp.771-799. https://doi.org/10.2166/wcc.2019.236

Getirana, A., Kumar, S. V., Konapala, G., & Ndehedehe, C. E. (2021). Impacts of fully coupling land surface and flood models on the simulation of large wetlands' water dynamics: The case of the Inner Niger Delta. *Journal of Advances in Modeling Earth Systems, 13*(5), e2021MS002463. https://doi.org/10.1029/2021MS002463

Goll, D. S., Vuichard, N., Maignan, F., Jornet-Puig, A., Sardans, J., Violette, A., ... & Ciais, P. (2017). A representation of the phosphorus cycle for ORCHIDEE (revision 4520). *Geoscientific Model Development*, *10*(10), pp.3745-3770. https://doi.org/10.5194/gmd-10-3745-2017

Gosain, A. K., Rao, S., & Basuray, D. (2006). Climate change impact assessment on hydrology of Indian river basins. *Current science*, pp.346-353. https://www.jstor.org/stable/24091868

Gouveia, C. M., Trigo, R. M., Beguería, S., & Vicente-Serrano, S. M. (2017). Drought impacts on vegetation activity in the Mediterranean region: An assessment using remote sensing data and multi-scale drought indicators. *Global and Planetary Change, 151*, pp.15-27. https://doi.org/10.1016/j.gloplacha.2016.06.011

Graham, D. N., & Butts, M. B. (2005). *Flexible, integrated watershed modelling with MIKE SHE*. Watershed models, 849336090, CRC Press. ISBN: 0849336090, pp.245-272.

Guimberteau, M., Zhu, D., Maignan, F., Huang, Y., Yue, C., Dantec-Nédélec, S., ... & Ciais, P. (2018). ORCHIDEE-MICT (v8. 4.1), a land surface model for the high latitudes: model description and validation. *Geoscientific Model Development, 11*(1), pp.121-163. https://doi.org/10.5194/gmd-11-121-2018

Günaçtı, M. C., Onuşluel Gül, G., Benzeden, E., Kuzucu, A., Çetinkaya, C. P., & Baran, T. (2018, September 5-9). *Forecasting Drought Based On The Standardized Precipitation Index (SPI) In Küçük Menderes Basin, Turkey.* 4th International Conference Water resources and wetlands. Tulcea, Romania. https://www.limnology.ro/wrw2018/Proceedings/24_Gunacti.pdf

Halwatura, D., & Najim, M. M. M. (2013). Application of the HEC-HMS model for runoff simulation in a tropical catchment. *Environmental modelling & software*, *46*, pp.155-162. https://doi.org/10.1016/j.envsoft.2013.03.006

Hamman, J. J., Nijssen, B., Bohn, T. J., Gergel, D. R., & Mao, Y. (2018). The Variable Infiltration Capacity model version 5 (VIC-5): Infrastructure improvements for new applications and reproducibility. *Geoscientific Model Development*, *11*(8), pp.3481-3496. https://doi.org/10.5194/gmd-11-3481-2018

Homdee, T., Pongput, K., & Kanae, S. (2016). A comparative performance analysis of three standardized climatic drought indices in the Chi River basin, Thailand. *Agriculture and Natural Resources*, *50*(3), pp. 211-219. https://doi.org/10.1016/j.anres.2016.02.002

Hosking, J. R. M. (2009). *Regional frequency analysis using L-moments, lmomRFA R package, version 2.2*. https://cran.r-project.org/web/packages/lmomRFA/index.html

Hosking, J. R. M., & Wallis, J. R. (1997). *Regional frequency analysis*. pp 240. ISBN 0521430453. Cambridge, UK: Cambridge University Press.

Huang, S., Krysanova, V., & Hattermann, F. (2015). Projections of climate change impacts on floods and droughts in Germany using an ensemble of climate change scenarios. *Regional Environmental Change*, *15*, pp.461-473. https://doi.org/10.1007/s10113-014-0606-z

ICLE (2015, April 8-12). *ICLEI World Congress 2015 Report. 25 years of impact - one world of local action A high-level congress of partnerships and advocacy, with a focus on new and existing themes, highlighting ICLEI's growing presence and priorities in Asia. Sustainable Solutions for an Urban Area.* ICLEI World Congress .Seoul, Republic of Korea. https://e-lib.iclei.org/wp-content/uploads/2015/09/World-Congress-2015-Report.pdf

ICLEI (2023, October 10). *Join ICLEI at the Smart City Expo World Congress*. https://iclei.europe.org/news/?Join_ICLEI_at_the_Smart_City_Expo_World_Congress_&newsID=T9XDdLBM

IPCC (2012). *Managing the risks of extreme events and disasters to advance climate change adaptation. A special report of working groups I and II of the Intergovernmental Panel on Climate Change*. Cambridge University Press, Cambridge, UK / New York, NY, USA. https://www.ipcc.ch/site/assets/uploads/2018/03/SREX_Full_Report-1.pdf

IPCC (2022). *Climate Change 2022: Impacts, Adaptation and Vulnerability. Contribution of Working Group II to the Sixth Assessment Report of the Intergovernmental Panel on Climate Change*. Cambridge University Press. Cambridge University Press, Cambridge, UK and New York, NY, USA, 3056 pp. https://doi.org/10.1017/9781009325844.

IPCC (2023). *Climate Change 2023: Synthesis Report. Contribution of Working Groups I, II and III to the Sixth Assessment Report of the Intergovernmental Panel on Climate Change*. IPCC, Geneva, Switzerland, (pp. 35-115), doi: https://doi.org/10.59327/IPCC/AR6-9789291691647

ISRIC World Soil Information, (2020). *SoilGrids - global gridded soil information*, 2020-05-04. https://soilgrids.org/

İKLİM RİSK (2021). *Hydrological risks and water quality change for sustainable water management under the impact of climate change final report.* TÜBİTAK Project 2018-2021, Project No: 116Y423.

Jehanzaib, M., Sattar, M. N., Lee, J. H., & Kim, T. W. (2020). Investigating effect of climate change on drought propagation from meteorological to hydrological drought using multi-model ensemble projections. *Stochastic Environmental Research and Risk Assessment, 34*, pp.7-21. https://doi.org/10.1007/s00477-019-01760-5

Jeong, J., Kannan, N., Arnold, J. G., Glick, R., Gosselink, L., Srinivasan, R., & Harmel, R. D. (2011). Development of sub-daily erosion and sediment transport algorithms for SWAT. *Transactions of the ASABE*, *54*(5), pp.1685-1691. https://doi.org/10.13031/2013.39841

Joetzjer, E., Douville, H., Delire, C., Ciais, P., Decharme, B., & Tyteca, S. (2012). Evaluation of drought indices at interannual to climate change timescales: a case study over the Amazon and Mississippi river basins. Hydrology & Earth System Sciences Discussions, 9(11). https://doi.org/10.5194/hessd-9-13231-2012

Kadam, P., & Sen, D. (2012). Flood inundation simulation in Ajoy River using MIKE-FLOOD. ISH Journal of Hydraulic Engineering, 18(2), pp.129-141. https://doi.org/10.1080/09715010.2012.695449

Kang, H. M., & Yusof, F. (2012). Homogeneity tests on daily rainfall series. *Int. J. Contemp. Math. Sciences*, *7*(1), pp.9-22. https://www.m-hikari.com/ijcms/ijcms-2012/1-4-2012/kangIJCMS1-4-2012.pdf

Kauffeldt, A., Wetterhall, F., Pappenberger, F., Salamon, P., & Thielen, J. (2016). Technical review of large-scale hydrological models for implementation in operational flood forecasting schemes on continental level. *Environmental Modelling & Software, 75*, pp.68-76. https://doi.org/10.1016/j.envsoft.2015.09.009

Kendall, M. G. (1948). *Rank correlation methods*. 4th Edition, Griffin, London.

Khoi, D. N. (2016). Comparison of the HEC-HMS and SWAT hydrological models in simulating the stream flow. *Journal of Science and Technology*, *53*(5A), pp.189-195.

Kim, S., Paik, J., & Kim, K. S. (2013). Run-out modeling of debris flows in Mt. Umyeon using FLO-2D. *KSCE Journal of Civil and Environmental Engineering Research*, *33*(3), pp.965-974. https://doi.org/10.12652/Ksce.2013.33.3.965

Koster, R. D., & Suarez, M. J. (1996). *Energy and water balance calculations in the Mosaic LSM*. National Aeronautics and Space Administration, Goddard Space Flight Center, Laboratory for Atmospheres, Data Assimilation Office.

Krysanova, V., & Arnold, J. G. (2008). Advances in ecohydrological modelling with SWAT—a review. *Hydrological Sciences Journal*, *53*(5), pp.939-947. https://doi.org/10.1623/hysj.53.5.939

Krysanova, V., & White, M. (2015). Advances in water resources assessment with SWAT—an overview. Hydrological Sciences Journal, 60(5), pp.771-783. https://doi.org/10.1080/02626667.2015.1029482

Krysanova, V., & White, M. (2015). Advances in water resources assessment with SWAT—an overview. *Hydrological Sciences Journal*, *60*(5), pp.771-783. https://doi.org/10.1080/02626667.2015.1029482

Kundzewicz, Z. W., Budhakooncharoen, S., Bronstert, A., Hoff, H., Lettenmaier, D., Menzel, L., & Schulze, R. (2001, December). *Floods and droughts: Coping with variability and climate change*. In Thematic Background Paper presented at the International Conference on Freshwater, Bonn. https://es.ircwash.org/sites/default/files/Kundzewicz-2001-Floods.pdf

Kuzucu, A., & Onuşluel Gül, G. (2023). Analysis of Drought Dynamics over Annual Maximum Drought Severity Series Based on Daily Index Definitions. *Water Resources Management, 37*(3), pp.1421-1436. https://doi.org/10.1007/s11269-023-03434-y

Kuzucu, A., Najar, M., Gül, A., Onuşluel Gül, G., & Çetinkaya, C. P., (2023, June 27-July 1). *An approach for assessing the sustainability of Mediterranean wetlands through a tailored handling of drought indices*. The 12th World Congress of the European Water Resources Association - EWRA2023: "Managing Water-Energy-Land-Food under Climatic, Environmental and Social Instability".Thessaloniki, Greece.

Lawrence, D. M., Fisher, R. A., Koven, C. D., Oleson, K. W., Swenson, S. C., Bonan, G., ... & Zeng, X. (2019). The Community Land Model version 5: Description of new features, benchmarking, and impact of forcing uncertainty. *Journal of Advances in Modeling Earth Systems*, *11*(12), pp.4245-4287. https://doi.org/10.1029/2018MS001583

Lawrence, P. J., & Chase, T. N. (2007). Representing a new MODIS consistent land surface in the Community Land Model (CLM 3.0). *Journal of Geophysical Research: Biogeosciences*, *112*(G1). https://doi.org/10.1029/2006JG000168

Lee, M. H., Im, E. S., & Bae, D. H. (2019). A comparative assessment of climate change impacts on drought over Korea based on multiple climate projections and multiple drought indices. *Climate dynamics, 53*, pp.389-404. https://doi.org/10.1007/s00382-018-4588-2

Li, H. Y., Leung, L. R., Getirana, A., Huang, M., Wu, H., Xu, Y., ... & Voisin, N. (2015). Evaluating global streamflow simulations by a physically based routing model coupled with the community land model. *Journal of Hydrometeorology*, *16*(2), pp.948-971. https://doi.org/10.1175/JHM-D-14-0079.1

Liang, X., Lettenmaier, D. P., Wood, E. F., & Burges, S. J. (1994). A simple hydrologically based model of land surface water and energy fluxes for general circulation models. *Journal of Geophysical Research: Atmospheres*, *99*(D7), pp.14415-14428. https://doi.org/10.1029/94JD00483

Lohmann, D. A. G., Nolte-Holube, R. A. L. P. H., & Raschke, E. (1996). A large-scale horizontal routing model to be coupled to land surface parametrization schemes. *Tellus A*, *48*(5), pp.708-721.

Lohmann, D., Raschke, E., Nijssen, B., & Lettenmaier, D. P. (1998). Regional scale hydrology: I. Formulation of the VIC-2L model coupled to a routing model. *Hydrological sciences journal*, *43*(1), pp.131-141. https://doi.org/10.1080/02626669809492107

Manabe, S. (1969). Climate and the ocean circulation: I. The atmospheric circulation and the hydrology of the earth's surface. *Monthly weather review*, *97*(11), pp.739-774. https://doi.org/10.1175/1520-0493(1969)097<0739:CATOC>2.3.CO;2

Mann, H. B. (1945). Nonparametric tests against trend. *Econometrica: Journal of the econometric society*, pp.245-259. https://doi.org/10.2307/1907187

McKee, T. B., Doesken, N. J., & Kleist, J. (1993, January). The relationship of drought frequency and duration to time scales. In *Proceedings of the 8th Conference on Applied Climatology* (Vol.17, No.22, pp.179-183. https://climate.colostate.edu/pdfs/relationshipofdroughtfrequency.pdf

Min, L., Zhao-Hui, L., Chuan-Guo, Y., & Quan-Xi, S. (2014). Application of a coupled land surface-hydrological model to flood simulation in the Huaihe River Basin of China. *Atmospheric and Oceanic Science Letters*, *7*(6), pp.493-498. https://doi.org/10.3878/AOSL20140050

Mitchell, K. (2005). The community Noah land-surface model (LSM). *User's Guide Public Release Version, 2*(1). https://www.academia.edu/download/42046380/THE_COMMUNITY_Noah_LAND-SURFACE_MODEL_L20160204-7785-1jpbaav.pdf

Modarres, R. (2007). Streamflow drought time series forecasting. *Stochastic Environmental Research and Risk Assessment, 21*, pp.223-233. https://doi.org/10.1007/s00477-006-0058-1

Modi, P. A., Czuba, J. A., & Easton, Z. M. (2022). Coupling a land surface model with a hydrodynamic model for regional flood risk assessment due to climate change: Application to the Susquehanna River near Harrisburg, Pennsylvania. Journal of Flood Risk Management, 15(1), e12763. https://doi.org/10.1111/jfr3.12763

Moriasi, D. N., Arnold, J. G., Van Liew, M. W., Bingner, R. L., Harmel, R. D., & Veith, T. L. (2007). Model evaluation guidelines for systematic quantification of accuracy in watershed simulations. *Transactions of the ASABE, 50*(3), pp.885-900. https://doi.org/10.13031/2013.23153

Najar, M. (2021). *Production and Assessment of Hazard Maps for Dam-Break Connected Floods In The Case of Embankment Dams Through GIS and Mathematical Models* [Doctoral dissertation]. Dokuz Eylül University.

Namara, W. G., Damisse, T. A., & Tufa, F. G. (2022). Application of HEC-RAS and HEC-GeoRAS model for flood inundation mapping, the case of Awash bello flood plain, upper Awash River Basin, oromiya regional state, Ethiopia. *Modeling Earth Systems and Environment, 8*(2), pp.1449-1460. https://doi.org/10.1007/s40808-021-01166-9

Narsimlu, B., Gosain, A. K., & Chahar, B. R. (2013). Assessment of future climate change impacts on water resources of Upper Sind River Basin, India using SWAT

model. *Water resources management, 27*, pp.3647-3662. https://doi.org/10.1007/s11269-013-0371-7

Ndayiragije, J. M., & Li, F. (2022). Effectiveness of drought indices in the assessment of different types of droughts, managing and mitigating their effects. *Climate*, *10*(9), 125. https://doi.org/10.3390/cli10090125

Neitsch, S. L., Arnold, J. G., Kiniry, J. R., & Williams, J. R. (2011). *Soil and water assessment tool theoretical documentation version 2009*. Texas Water Resources Institute. https://swat.tamu.edu/media/99192/swat2009-theory.pdf

New South Wales Department of Planning and Environment (2023). *Flood risk management manual. The policy and manual for the management of flood liable land.* ISBN 978-1-923076-17-4. https://www.environment.nsw.gov.au/-/media/OEH/Corporate-Site/Documents/Water/Floodplains/flood-risk-management-manual-2023-230220.pdf

Niu, G. Y., Yang, Z. L., Mitchell, K. E., Chen, F., Ek, M. B., Barlage, M., ... & Xia, Y. (2011). The community Noah land surface model with multiparameterization options (Noah-MP): 1. Model description and evaluation with local-scale measurements. *Journal of Geophysical Research: Atmospheres*, *116*(D12). https://doi.org/10.1029/2010JD015139

Onuşluel Gül, G., Gül, A., & Najar, M. (2022). Historical evidence of climate change impact on drought outlook in river basins: analysis of annual maximum drought severities through daily SPI definitions. *Natural Hazards*, pp.1-16. https://doi.org/10.1007/s11069-021-04995-0

Onuşluel Gül, G., Gül, A., Kuzucu, A. (2017, September 21-22). Analysis of drought in küçük menderes river basin using SPI and SPEI drought indices, STAHY 2017 Workshop.Warsaw,Poland. https://meetingorganizer.copernicus.org/STAHY2017/STAHY2017-33.pdf

Onuşluel Gül, G., Harmancıoğlu, N., & Gül, A. (2010). A combined hydrologic and hydraulic modeling approach for testing efficiency of structural flood control measures. *Natural hazards*, *54*, pp.245-260. https://doi.org/10.1007/s11069-009-9464-2

Orth, R., Dutra, E., Trigo, I. F., & Balsamo, G. (2017). Advancing land surface model development with satellite-based Earth observations. *Hydrology and Earth System Sciences*, *21*(5), pp.2483-2495. https://doi.org/10.5194/hess-21-2483-2017

Overgaard, J., Rosbjerg, D., & Butts, M. B. (2006). Land-surface modelling in hydrological perspective–a review. *Biogeosciences*, *3*(2), pp.229-241. https://doi.org/10.5194/bg-3-229-2006

Önöz, B. & Bayazit, M. (2003). The power of statistical tests for trend detection. *Turkish journal of engineering and environmental sciences*, *27*(4), pp.247-251. https://dergipark.org.tr/en/download/article-file/126634

Pappenberger, F., Dutra, E., Wetterhall, F., & Cloke, H. L. (2012). Deriving global flood hazard maps of fluvial floods through a physical model cascade. *Hydrology and Earth System Sciences*, *16*(11), pp.4143-4156. https://doi.org/10.5194/hess-16-4143-2012

Patel, D. P., Ramirez, J. A., Srivastava, P. K., Bray, M., & Han, D. (2017). Assessment of flood inundation mapping of Surat city by coupled 1D/2D hydrodynamic modeling: a case application of the new HEC-RAS 5. *Natural Hazards*, *89*, pp.93-130. https://doi.org/10.1007/s11069-017-2956-6

Patro, S., Chatterjee, C., Mohanty, S., Singh, R., & Raghuwanshi, N. S. (2009). Flood inundation modeling using MIKE FLOOD and remote sensing data. *Journal of the Indian Society of Remote Sensing*, *37*, pp.107-118. https://doi.org/10.1007/s12524-009-0002-1

Phillips, B. C., Yu, S., Thompson, G. R., & De Silva, N. (2005, August). 1D and 2D modelling of urban drainage systems using XP-SWMM and TUFLOW. In *10th international conference on urban drainage* , pp. 21-26. Copenhagen, Denmark.

Phyo, A. P., Yabar, H., & Richards, D. (2023). Managing dam breach and flood inundation by HEC-RAS modeling and GIS mapping for disaster risk management. *Case Studies in Chemical and Environmental Engineering*, *8*, 100487. https://doi.org/10.1016/j.cscee.2023.100487

Pitman, A. J. (2003). The evolution of, and revolution in, land surface schemes designed for climate models. *International Journal of Climatology: A Journal of the Royal Meteorological Society*, *23*(5), pp.479-510. https://doi.org/10.1002/joc.893

Pohlert, T., Pohlert, M. T., & Kendall, S. (2016). *Package 'trend'. Title non-parametric trend tests and change-point detection*. https://cran.r-project.org/web/packages/trend/index.html

Rossi, L., Wens, M., De Moel, H., Cotti, D., Sabino Siemons, A.-S., Toreti, A., Maetens,W., Masante, D., Van Loon, A., Hagenlocher, M., Rudari, R., Meroni, M., Isabellon, M., Avanzi, F., Naumann, G. & Barbosa P. (2023).*European Drought Risk Atlas*. Publications Office of the European Union, Luxembourg. https://publications.jrc.ec.europa.eu/repository/handle/JRC135215

Samuel, J., Coulibaly, P., & Metcalfe, R. A. (2011). Estimation of continuous streamflow in Ontario ungauged basins: Comparison of regionalization methods. *Journal of Hydrologic Engineering*, *16*(5), pp.447-459. https://doi.org/10.1061/(ASCE)HE.1943-5584.0000338

Santos, J. F., Portela, M. M., & Pulido-Calvo, I. (2011). Regional frequency analysis of droughts in Portugal. *Water Resources Management*, *25*, pp.3537-3558. https://doi.org/10.1007/s11269-011-9869-z

Sato, N., Sellers, P. J., Randall, D. A., Schneider, E. K., Shukla, J., Kinter III, J. L., ... & Albertazzi, E. (1989). *Implementing the Simple Biosphere Model (SiB) in a general circulation model: Methodologies and results* (No. NASA-CR-185509). https://ntrs.nasa.gov/api/citations/19890017917/downloads/19890017917.pdf

Schaperow, J. R. & Li, D. (2021). *VICGlobal: soil and vegetation parameters for the Variable Infiltration Capacity hydrological model (1.6d)* [Data set]. Zenodo. https://doi.org/10.5281/zenodo.5038653

Schaperow, J. R., Li, D., Margulis, S. A., & Lettenmaier, D. P. (2021). A near-global, high resolution land surface parameter dataset for the variable infiltration capacity model. *Scientific Data*, *8*(1), 216. https://doi.org/10.1038/s41597-021-00999-4

Sellers, P. J., & Dorman, J. L. (1987). Testing the simple biosphere model (SiB) using point micrometeorological and biophysical data. *Journal of Applied Meteorology and Climatology*, *26*(5), pp.622-651. https://doi.org/10.1175/1520-0450(1987)026<0622:TTSBMU>2.0.CO;2

Sellers, P. J., Dickinson, R. E., Randall, D. A., Betts, A. K., Hall, F. G., Berry, J. A., ... & Henderson-Sellers, A. (1997). Modeling the exchanges of energy, water, and carbon between continents and the atmosphere. Science, 275(5299), pp.502-509. https://doi.org/10.1126/science.275.5299.502

Sen, P. K. (1968). Estimates of the regression coefficient based on Kendall's tau. *Journal of the American statistical association*, pp.1379-1389. https://doi.org/10.2307/2285891

Shin, J. Y., Chen, S., Lee, J. H., & Kim, T. W. (2018). Investigation of drought propagation in South Korea using drought index and conditional probability. *Terrestrial, Atmospheric & Oceanic Sciences*, *29*(2). https://pdfs.semanticscholar.org/795f/f57cb80ed2fbdf0f0e540cebb73c881e1425.pdf

SYGM, (2016). *Impact of climate change on water resources project final report.* https://www.tarimorman.gov.tr/SYGM/Belgeler/iklim%20de%C4%9Fi%C5%9Fikli%C4%9Finin%20su%20kaynaklar%C4%B1na%20etkisi/Iklim_NihaiRapor.pdf

SYGM (2017). *Flood management report.* https://www.tarimorman.gov.tr/SYGM/Belgeler/Ta%C5%9Fk%C4%B1n%20Dairesi%20Sunum/Ta%C5%9Fk%C4%B1n_kitap.pdf

SYGM, (2018a). *Küçük Menderes Basin drought management plan.* https://www.tarimorman.gov.tr/SYGM/Belgeler/KURAKLIK%20Y%C3%96NET%C4%B0M%20PLANLARI%2009.01.2023/K%C3%BC%C3%A7%C3%BCk%20Menderes%20Havzas%C4%B1%20Kurakl%C4%B1k%20Y%C3%B6netim%20Plan%C4%B1%20Cilt%201.pdf

SYGM, (2018b). *Küçük Menderes river basin management plan. strategic environmental assessment scoping report.* https://www.tarimorman.gov.tr/SYGM/Belgeler/K%C3%BC%C3%A7%C3%BCk%20Menderes%20NHYP%20Kapsamla%C5%9Ft%C4%B1rma%20Raporlar%C4%B1.pdf

SYGM, (2019). *North Aegean, Gediz and Küçük Menderes Basins flood management plan preparation project, Küçük Menderes Basin flood management plan.* https://www.tarimorman.gov.tr/SYGM/Belgeler/Ta%C5%9Fk%C4%B1n%20Y%C3%B6netim%20Planlar%C4%B1/K%C3%9C%C3%87%C3%9CK%20MENDERES%20HAVZASI%20TA%C5%9EKIN%20Y%C3%96NET%C4%B0M%20PLANI.pdf

Syme, W. J. (2001). *TUFLOW-Two & Onedimensional unsteady flow Software for rivers, estuaries and coastal waters*. In IEAust Water Panel Seminar and Workshop on 2d Flood Modelling, Sydney. https://tuflow.com/media/4985/2001-tuflow-two-

and-one-dimensional-unsteady-flow-software-for-rivers-estuaries-and-coastal-waters-syme.pdf

Şen, G. (2021). *An Overview Of Disaster Resilience*. Turkish Journal of Health Science and Life, 4(3), pp.106-115. https://dergipark.org.tr/en/pub/tjhsl/issue/67114/996871

Tassew, B. G., Belete, M. A., & Miegel, K. (2019). Application of HEC-HMS model for flow simulation in the Lake Tana basin: The case of Gilgel Abay catchment, upper Blue Nile basin, Ethiopia. *Hydrology*, *6*(1), 21. https://doi.org/10.3390/hydrology6010021

Tatar, T. (2020). Understanding of Natural Disaster Risk Management and Where Türkiye Stands in the Picture. *Academic Platform Journal of Natural Hazards and Disaster Management, 1(2),* pp.110-121. https://dergipark.org.tr/en/pub/apjhad/issue/58261/832498

Te Chow, V., Maidment, D. R., & Mays, L. W. (1988). *Applied hydrology*. International Edition, McGraw-Hill Book Company, New York.

The World Bank & GFDDR (2013). *Building Resilince. Integrating Climate and Disaster Risk into Development.* World Bank Publications https://documents1.worldbank.org/curated/es/653931468340471918/pdf/826480WP0v20Bu0130Box37986200OUO090.pdf

Thom, H.C.S. (1966). *Some methods of climatological analysis*. Secretariat of the World Meteorological Organization.

Thompson, J. R., Sørenson, H. R., Gavin, H., & Refsgaard, A. (2004). Application of the coupled MIKE SHE/MIKE 11 modelling system to a lowland wet grassland in southeast England. *Journal of Hydrology*, *293*(1-4), pp.151-179. https://doi.org/10.1016/j.jhydrol.2004.01.017

Tobin, K. J., & Bennett, M. E. (2017). Constraining SWAT calibration with remotely sensed evapotranspiration data. *JAWRA Journal of the American Water Resources Association*, *53*(3), pp.593-604. https://doi.org/10.1111/1752-1688.12516

Todini, E. (1996). The ARNO rainfall—runoff model. *Journal of hydrology*, *175*(1-4), pp.339-382. https://doi.org/10.1016/S0022-1694(96)80016-3

Trambauer, P., Maskey, S., Winsemius, H., Werner, M., & Uhlenbrook, S. (2013). A review of continental scale hydrological models and their suitability for drought forecasting in (sub-Saharan) Africa. *Physics and Chemistry of the Earth, Parts* A/B/C, 66, pp.16-26. https://doi.org/10.1016/j.pce.2013.07.003

Tsakiris, G., & Vangelis, H. (2004). Towards a drought watch system based on spatial SPI. *Water resources management*, *18*, pp.1-12. https://doi.org/10.1023/B:WARM.0000015410.47014.a4

Türkeş, M. (2022). IPCC'nin Yeni Yayımlanan İklim Değişikliğinin Etkileri, Uyum ve Etkilenebilirlik Raporu Bize Neler Söylüyor?. Resilience, 6(1), pp.197-207. https://doi.org/10.32569/resilience.1098946

U.S. Army Corps of Engineers, Hydrologic Engineering Center (2000). *HEC-HMS Hydrologic Modeling System, Technical Reference Manual, CPD-74B*. Hydrologic Engineering Center, Davis, CA. https://www.hec.usace.army.mil/software/hec-hms/documentation/HEC-HMS_Technical%20Reference%20Manual_(CPD-74B).pdf

UNDR (2021). *United Nations Office for Disaster Risk Reduction*. Annual Report 2021. https://www.undrr.org/publication/undrr-annual-report-2021

United Nations (2017). *New Urban Agenda. Habitat III.* Quito 17-20 October216. ISBN: 978-92-1-132731-1. https://habitat3.org/wp-content/uploads/NUA-English.pdf

University of Washington Computational Hydrology Group (2021). *VIC Model Overview*. https://vic.readthedocs.io/en/master/Overview/ModelOverview/

Uniyal, B., Jha, M. K., & Verma, A. K. (2015). Assessing climate change impact on water balance components of a river basin using SWAT model. *Water resources management*, *29*, pp.4767-4785. https://doi.org/10.1007/s11269-015-1089-5

Van Loon, A. F., Stahl, K., Di Baldassarre, G., Clark, J., Rangecroft, S., Wanders, N., ... & Van Lanen, H. A. (2016). Drought in a human-modified world: reframing drought definitions, understanding, and analysis approaches. Hydrology and Earth System Sciences, 20(9), pp.3631-3650. https://doi.org/10.5194/hess-20-3631-2016

Vanderkimpen, P., Melger, E., & Peeters, P. (2009). Flood modeling for risk evaluation–a MIKE FLOOD vs. SOBEK 1D2D benchmark study. *Flood risk management: research and practice*, p77-84. 2009 Taylor & Francis Group, London, ISBN 978-0-415-48507-4.

Vicente-Serrano, S. M., Beguería, S., López-Moreno, J. I., Angulo, M., & El Kenawy, A. (2010). A new global 0.5 gridded dataset (1901–2006) of a multiscalar drought index: comparison with current drought index datasets based on the Palmer Drought Severity Index. *Journal of Hydrometeorology*, *11*(4), pp.1033-1043. https://doi.org/10.1175/2010JHM1224.1

Vicente-Serrano, S. M., Cabello, D., Tomás-Burguera, M., Martín-Hernández, N., Beguería, S., Azorin-Molina, C., & El Kenawy, A. (2015). Drought variability and land degradation in semiarid regions: Assessment using remote sensing data and drought indices (1982–2011). *Remote Sensing*, *7*(4), pp.4391-4423. https://doi.org/10.3390/rs70404391

Vu, M. T., Raghavan, S. V., & Liong, S. Y. (2012). SWAT use of gridded observations for simulating runoff–a Vietnam river basin study. *Hydrology and Earth System Sciences*, *16*(8), pp.2801-2811. https://doi.org/10.5194/hess-16-2801-2012

Ward R.C. (1975). Principles of hydrology. McGraw- Hill Book Company (UK) Limited London.

Wijngaard, J. B., Klein Tank, A. M. G., & Können, G. P. (2003). Homogeneity of 20th century European daily temperature and precipitation series. *International Journal of Climatology: A Journal of the Royal Meteorological Society*, *23*(6), pp.679-692. https://doi.org/10.1002/joc.906

Winchell, M., Srinivasan, R., Di Luzio, M., & Arnold, J. (2007). ArcSWAT interface for SWAT 2005. *User's guide*, 1-436. https://www.researchgate.net/profile/Xiangdong-Li-5/post/Who_can_assist_in_hydrologic_modeling_using_the_SWAT_tool/attachment/59d635e4c49f478072ea39f4/AS%3A273668666527744%401442259103080/download/ArcSWAT2009English+textbook.pdf

Wipfler, E. L., Metselaar, K., Van Dam, J. C., Feddes, R. A., Van Meijgaard, E., Van Ulft, L. H., ... & Bastiaanssen, W. G. M. (2011). Seasonal evaluation of the land surface scheme HTESSEL against remote sensing derived energy fluxes of the Transdanubian region in Hungary. *Hydrology and earth system sciences*, *15*(4), pp.1257-1271. https://doi.org/10.5194/hess-15-1257-2011

WMO & GWP (2016*). Handbook of drought indicators and indices*. Geneva: World Meteorological Organization (WMO) and Global Water Partnership (GWP). https://www.droughtmanagement.info/literature/GWP_Handbook_of_Drought_Indicators_and_Indices_2016.pdf

WMO (2012) *Strengthening Multi-Hazard Early Warning Systems and Risk Assessment in the Western Balkans and Turkey: Assessment of Capacities, Gaps and Needs. Regional Programme on Disaster Risk Reduction in South East Europe Activity 2 (WMO): Regional Cooperation in South Eastern Europe for Meteorological, Hydrological and Climate Data Management and Exchange to Support Disaster Risk Reduction (IPA/2009/199-922).* https://climate-

adapt.eea.europa.eu/en/metadata/publications/strengthening-multi-hazard-early-warning-systems-and-risk-assessment-in-the-western-balkans-and-turkey/11292615/@@download/file/11292615.pdf

Xiong, K., Sharifi, A., & He, B. J. (2022). Resilient-smart cities: theoretical insights. In Resilient Smart Cities: Theoretical and Empirical Insights, pp. 93-118. Cham: Springer International Publishing. Print ISSN 2365-757X.

Xu, Y. P., Zhang, X., Ran, Q., & Tian, Y. (2013). Impact of climate change on hydrology of upper reaches of Qiantang River Basin, East China. *Journal of Hydrology*, *483*, pp.51-60. https://doi.org/10.1016/j.jhydrol.2013.01.004

Xue, Y., Zeng, F. J., Mitchell, K. E., Janjic, Z., & Rogers, E. (2001). The impact of land surface processes on simulations of the US hydrological cycle: A case study of the 1993 flood using the SSiB land surface model in the NCEP Eta regional model. *Monthly weather review*, *129*(12), pp.2833-2860. https://doi.org/10.1175/1520-0493(2001)129<2833:TIOLSP>2.0.CO;2

Yang, R., Cohn, S. E., da Silva, A., Joiner, J., & Houser, P. R. (2003). Tangent linear analysis of the Mosaic land surface model. *Journal of Geophysical Research: Atmospheres*, *108*(D2). https://doi.org/10.1029/2002JD002410

Yang, Z. L., Niu, G. Y., Mitchell, K. E., Chen, F., Ek, M. B., Barlage, M., ... & Xia, Y. (2011). The community Noah land surface model with multiparameterization options (Noah-MP): 2. Evaluation over global river basins. *Journal of Geophysical Research: Atmospheres*, *116*(D12). https://doi.org/10.1029/2010JD015140

Yu, D., Xie, P., Dong, X., Hu, X., Liu, J., Li, Y., ... & Xu, S. (2018). Improvement of the SWAT model for event-based flood simulation on a sub-daily timescale. *Hydrology and Earth System Sciences*, *22*(9), pp.5001-5019. https://doi.org/10.5194/hess-22-5001-2018

Yu, D., Yin, J., & Liu, M. (2016). Validating city-scale surface water flood modelling using crowd-sourced data. *Environmental Research Letters*, *11*(12), 124011. https://doi.org/10.1088/1748-9326/11/12/124011

Yue, S., & Wang, C. (2004). The Mann-Kendall test modified by effective sample size to detect trend in serially correlated hydrological series. *Water resources management*, *18*(3), pp.201-218. https://doi.org/10.1023/B:WARM.0000043140.61082.60

Zambrano-Bigiarini, M. (2017). *hydroTSM: Time Series Management, Analysis and Interpolation for Hydrological Modelling, R package version 0.5-1*, 2017. https://CRAN.R-project.org/package=hydroTSM

Zeiger, S. J., & Hubbart, J. A. (2021). Measuring and modeling event-based environmental flows: An assessment of HEC-RAS 2D rain-on-grid simulations. *Journal of Environmental Management*, *285*, 112125. https://doi.org/10.1016/j.jenvman.2021.112125

Zhu, Y., Lin, Z., Zhao, Y., Li, H., He, F., Zhai, J., ... & Wang, Q. (2017). Flood simulations and uncertainty analysis for the pearl river basin using the coupled land surface and hydrological model system. *Water*, *9*(6), 391. https://doi.org/10.3390/w9060391

Zhong, R., Kong, D., Chen, X., Wang, Z., & Lai, C. (2023). *VIC5: The Variable Infiltration Capacity (VIC) Hydrological Model. R package version 0.2.6.* https://CRAN.R-project.org/package=VIC5

APPENDICES

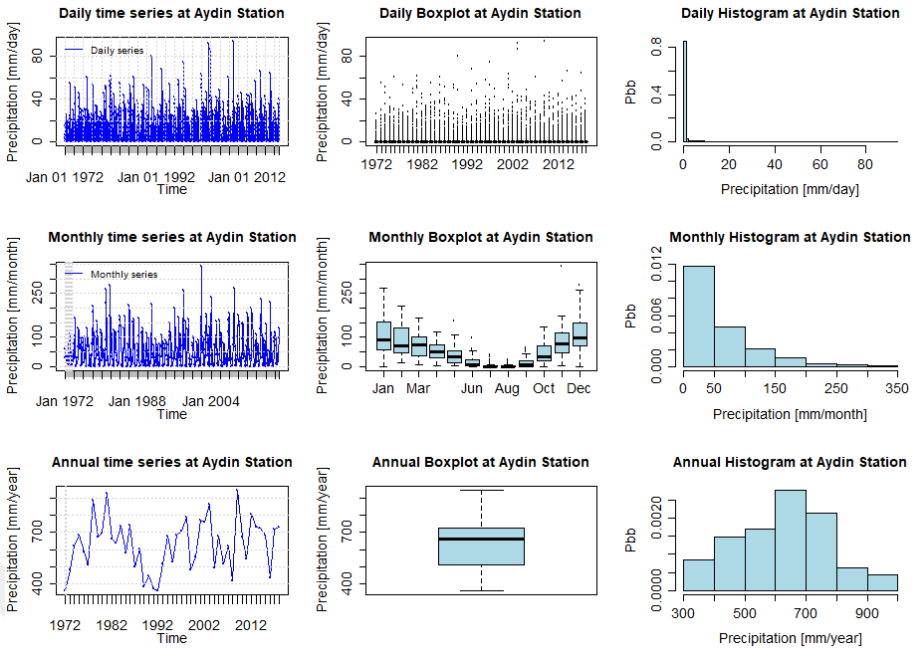


Figure Ap.1 Daily, monthly, annual total precipitation graphs of Aydın Station (mm).

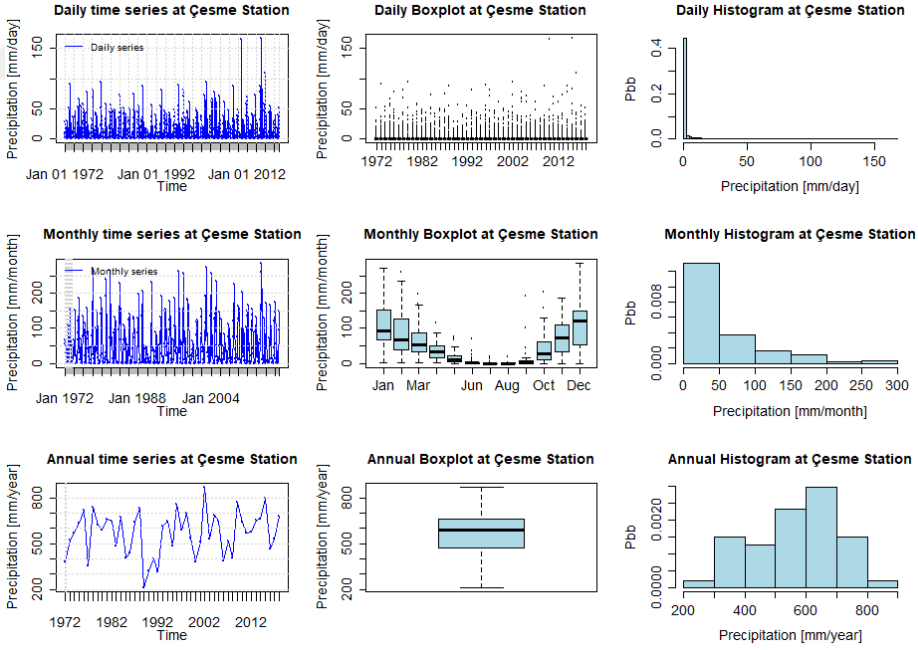


Figure Ap.2 Daily, monthly, annual total precipitation graphs of Çeşme Station (mm).

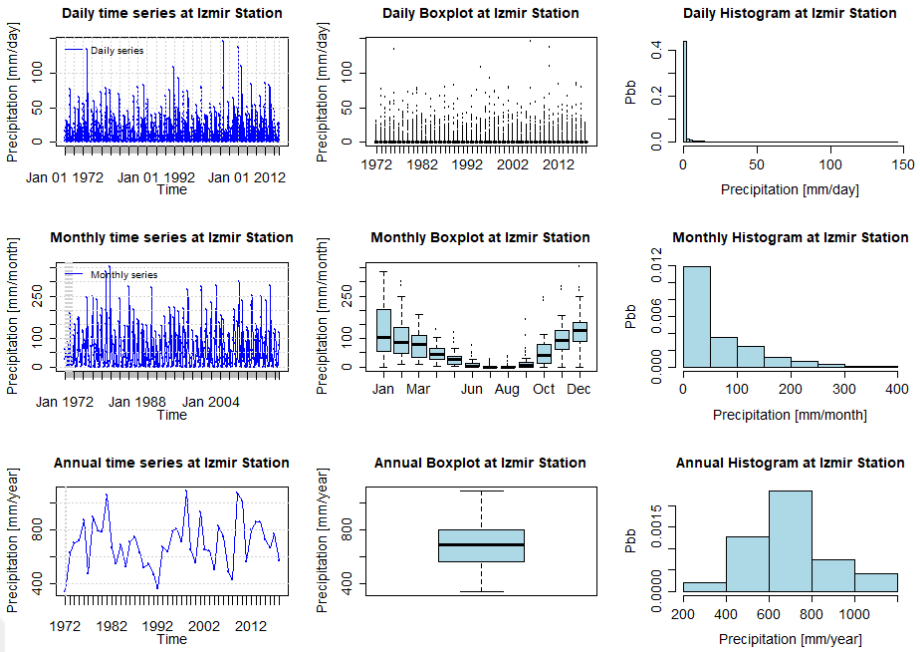


Figure Ap.3 Daily, monthly, annual total precipitation graphs of İzmir Station (mm).

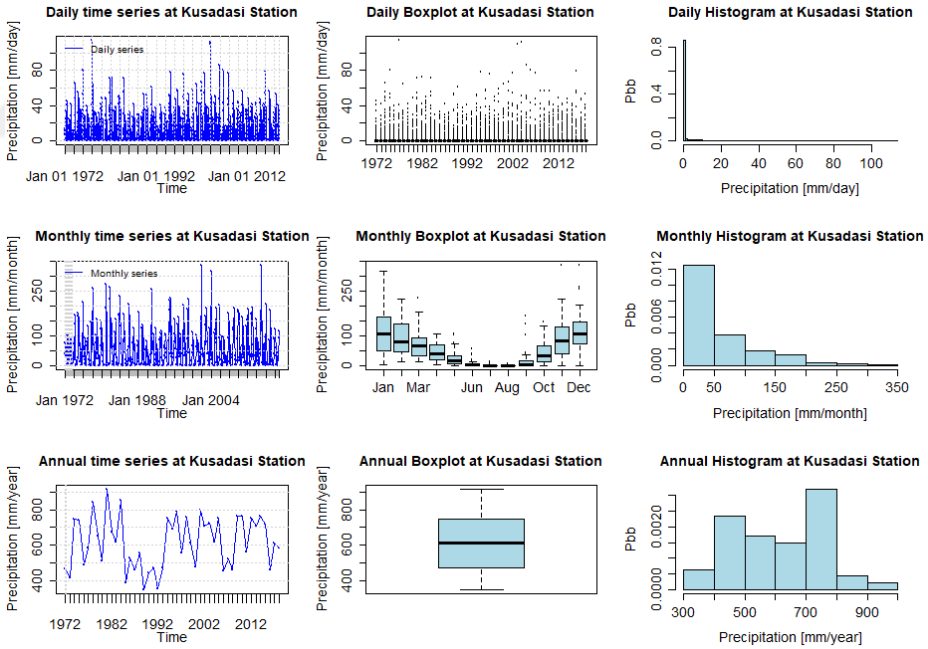


Figure Ap.4 Daily, monthly, annual total precipitation graphs of Kuşadası Station (mm).

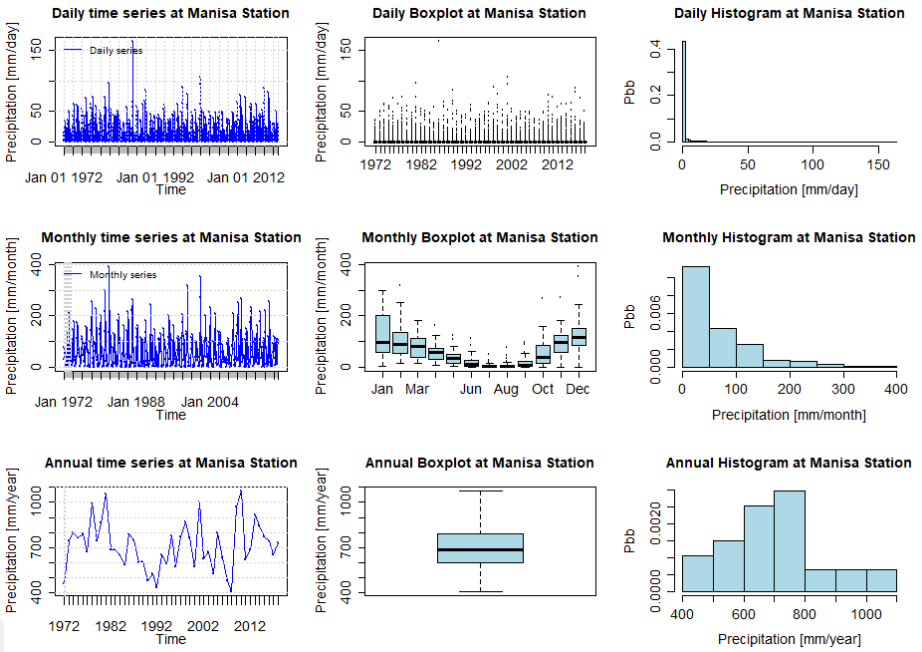


Figure Ap.5 Daily, monthly, annual total precipitation graphs of Manisa Station (mm).

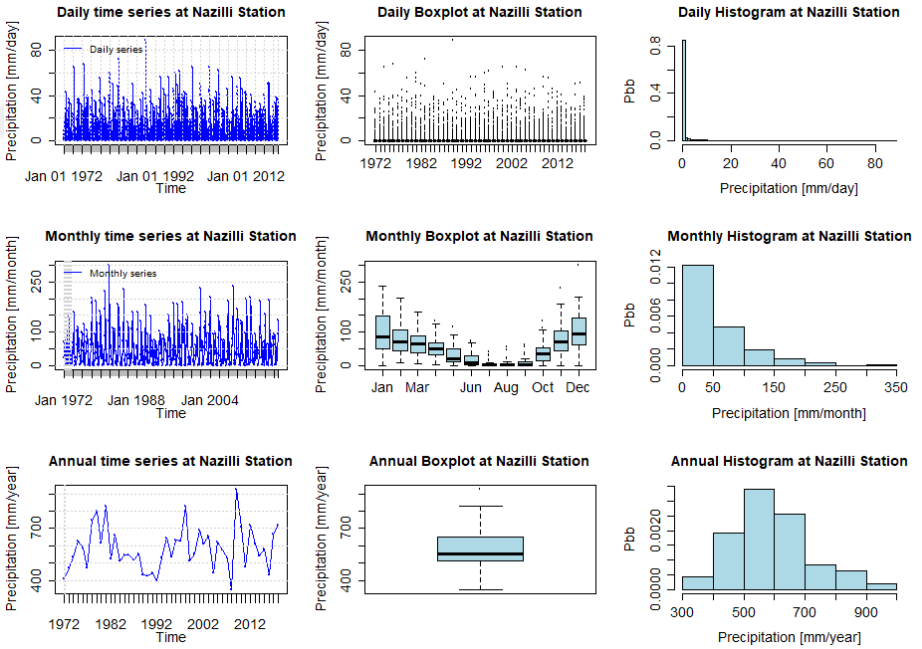


Figure Ap.6 Daily, monthly, annual total precipitation graphs of Nazilli Station (mm).

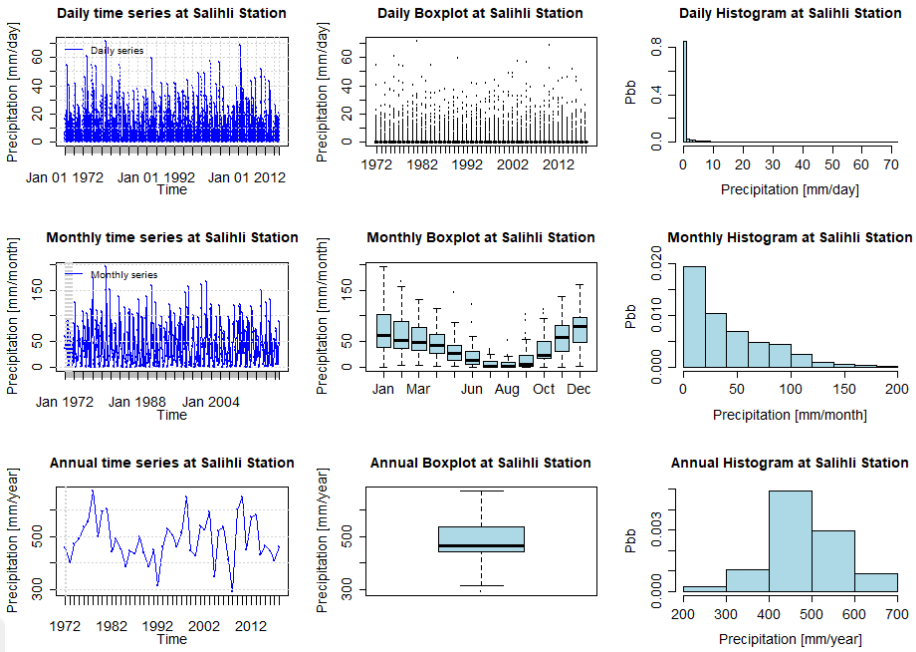


Figure Ap.7 Daily, monthly, annual total precipitation graphs of Salihli Station (mm).

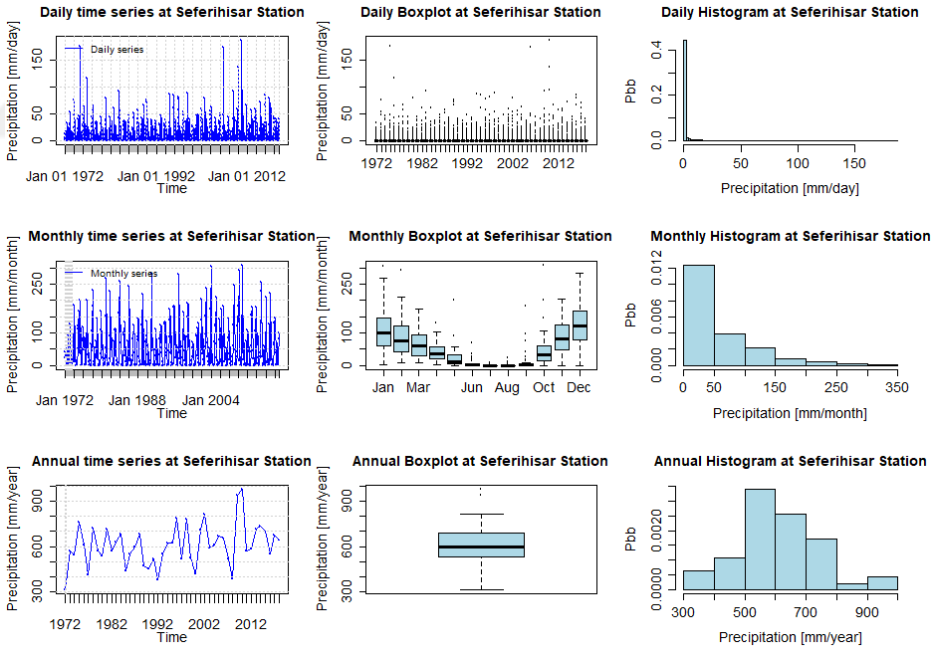


Figure Ap.8 Daily, monthly, annual total precipitation graphs of Seferihisar Station (mm).

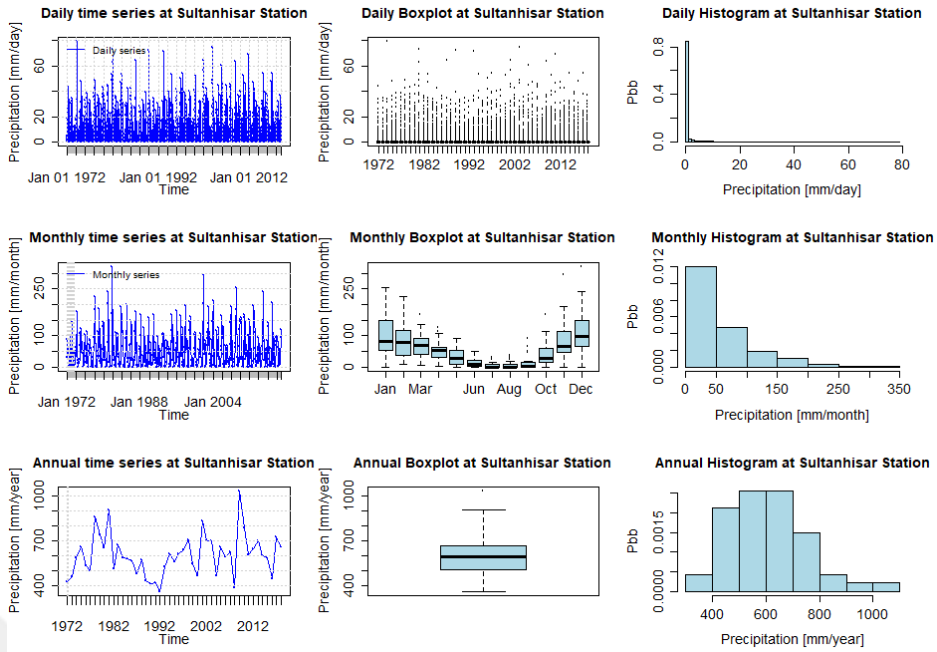


Figure Ap.9 Daily, monthly, annual total precipitation graphs of Sultanhisar Station (mm).

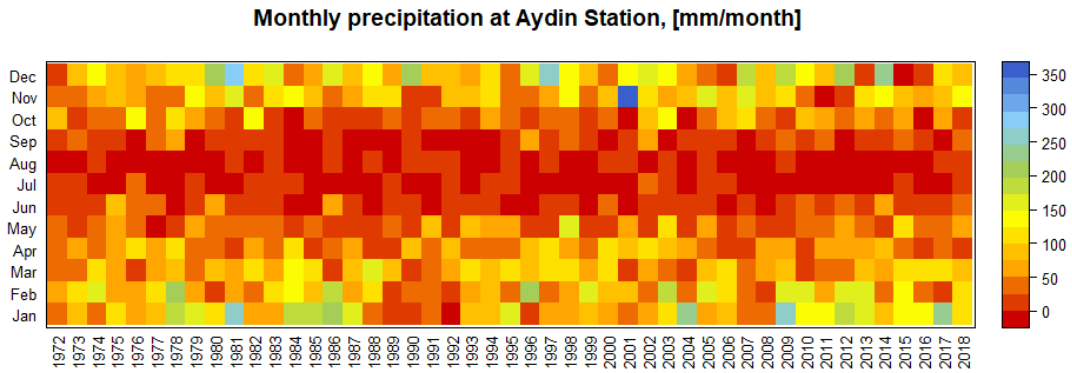


Figure Ap.10 The monthly total precipitation matrix of Aydın Station (mm).

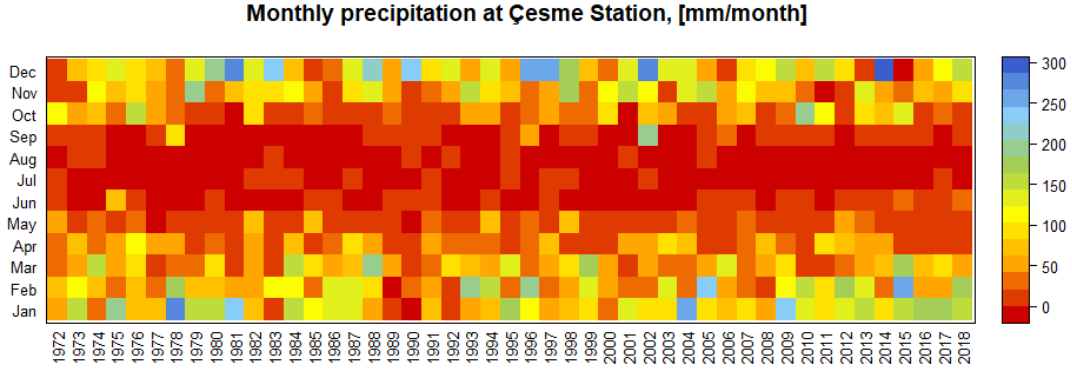


Figure Ap.11 The monthly total precipitation matrix of Çeşme Station (mm).

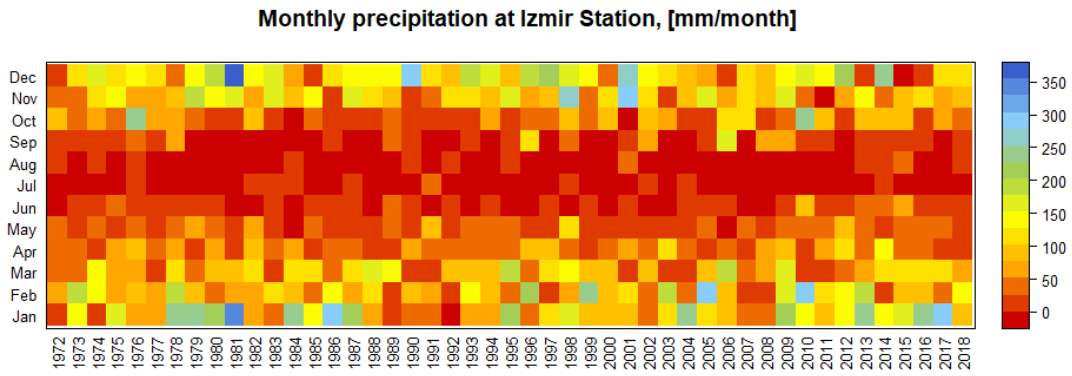


Figure Ap.12 The monthly total precipitation matrix of İzmir Station (mm).

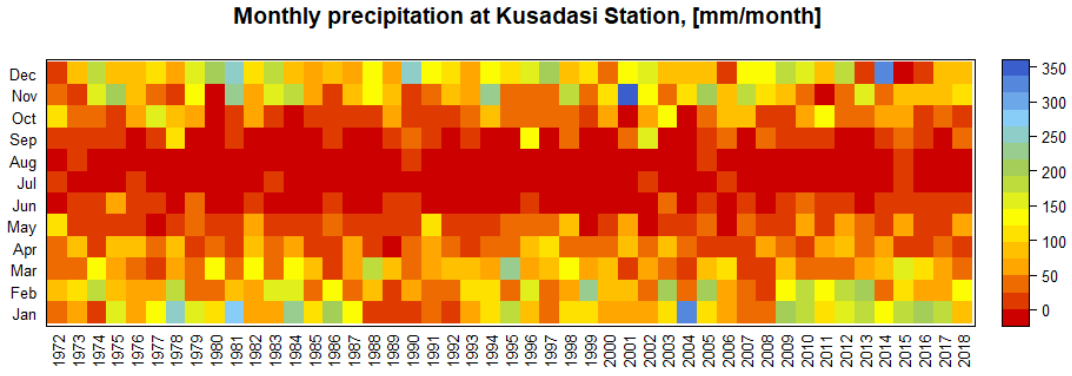


Figure Ap.13 The monthly total precipitation matrix of Kuşadası Station (mm).

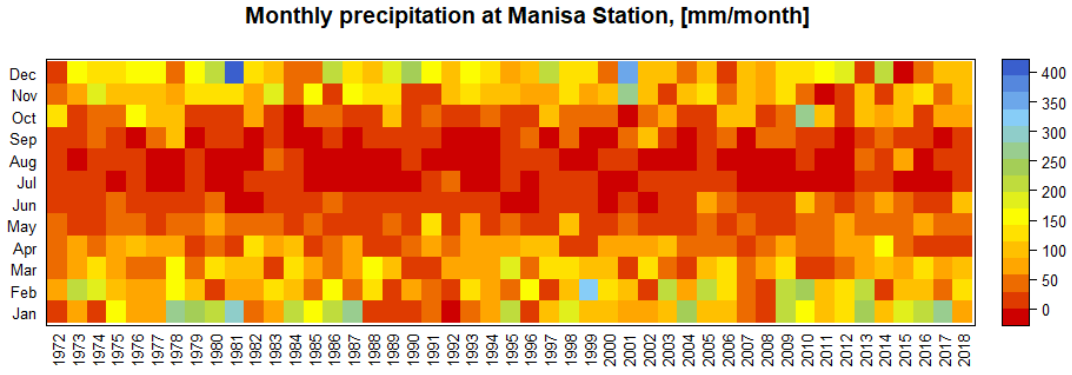


Figure Ap.14 The monthly total precipitation matrix of Manisa Station (mm).

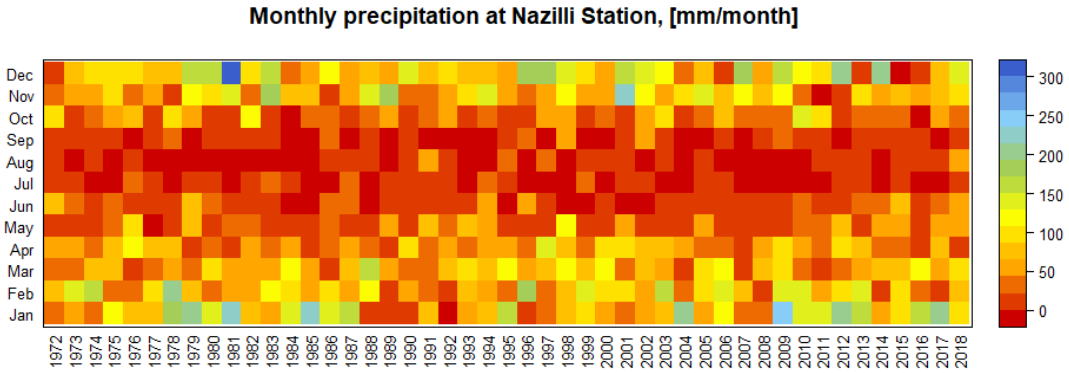


Figure Ap.15 The monthly total precipitation matrix of Nazilli Station (mm).

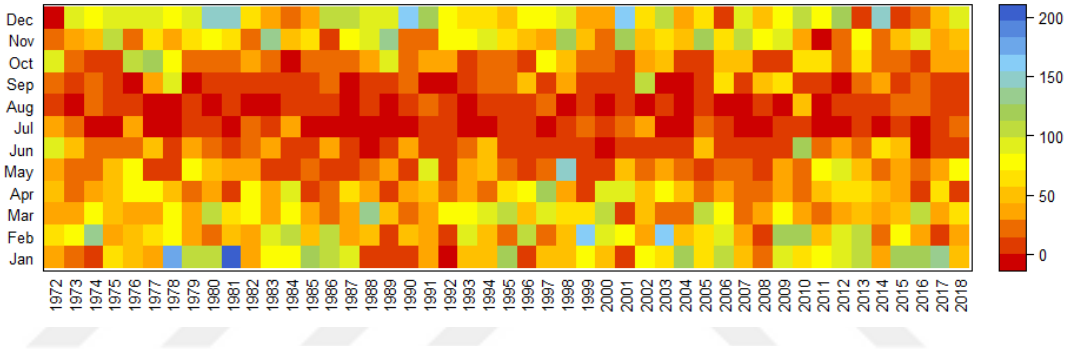


Figure Ap.16 The monthly total precipitation matrix of Salihli Station (mm).

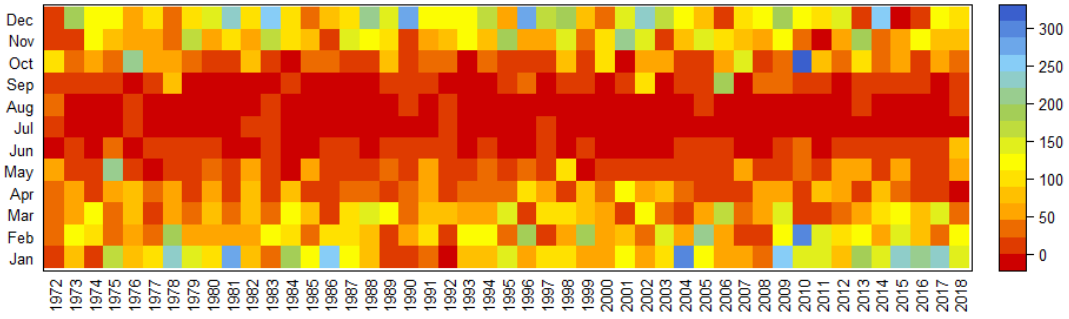


Figure Ap 17 The monthly total precipitation matrix of Seferihisar Station (mm).

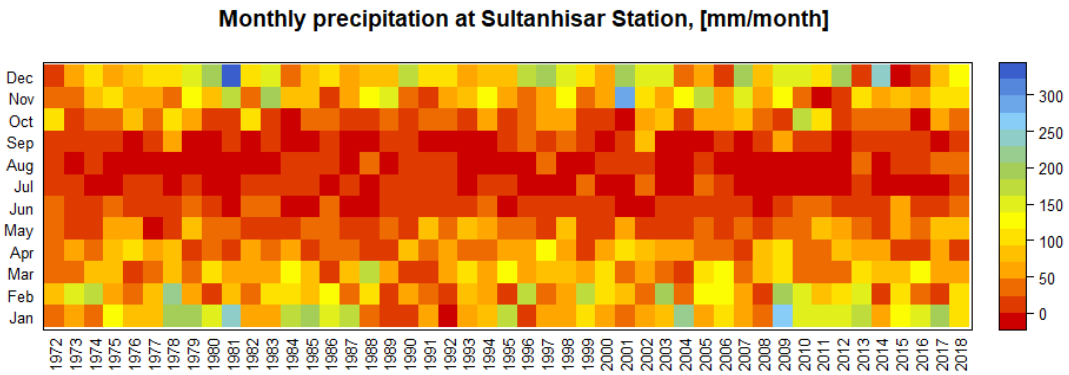


Figure Ap.18 The monthly total precipitation matrix of Sultanhisar Station (mm).

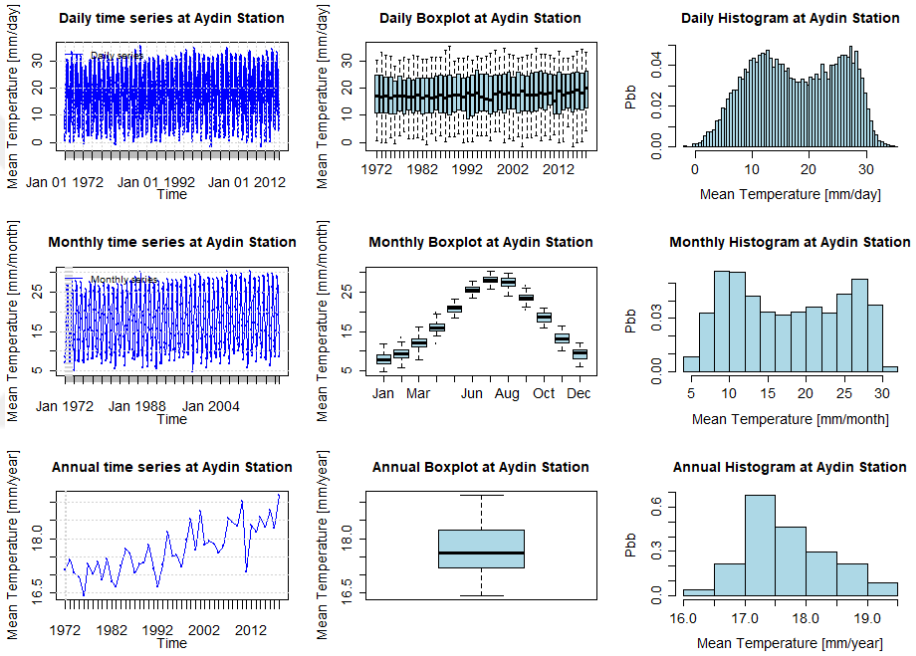


Figure Ap.19 Daily, monthly, annual mean temperature graphs of Aydın Station (ºC).

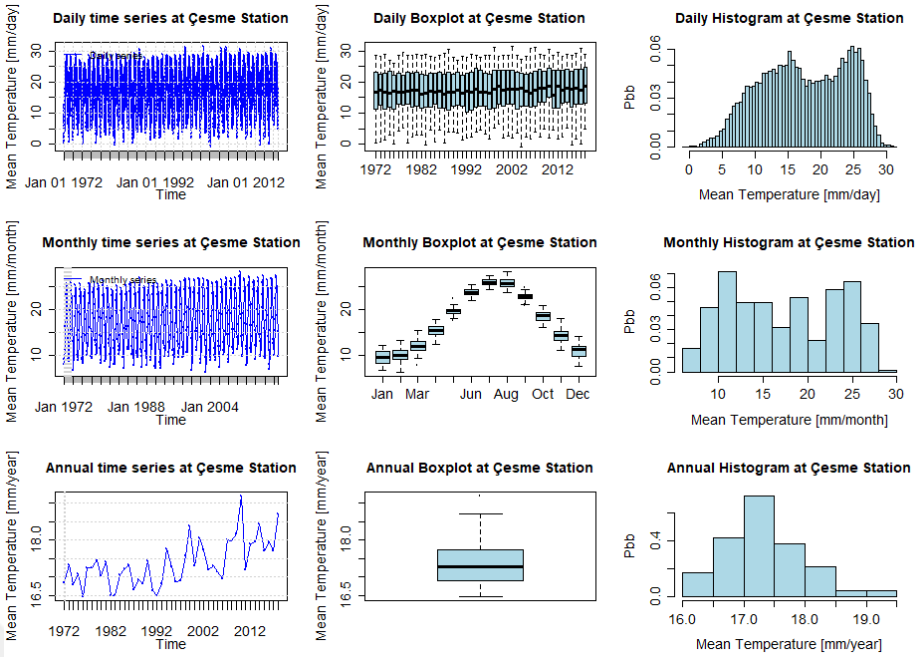


Figure Ap.20 Daily, monthly, annual mean temperature graphs of Çeşme Station (ºC).

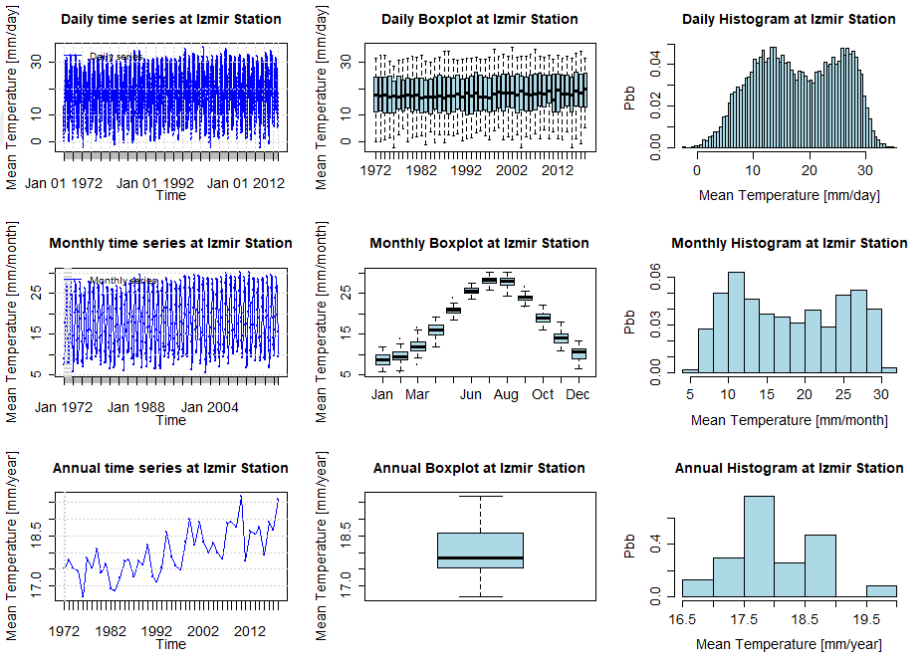


Figure Ap.21 Daily, monthly, annual mean temperature graphs of İzmir Station (ºC).

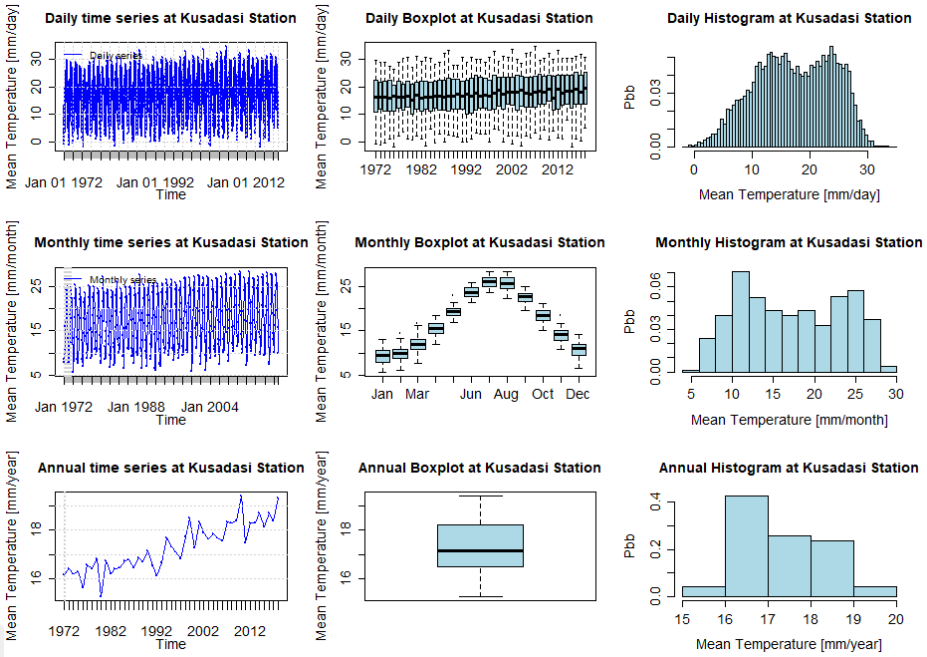


Figure Ap.22 Daily, monthly, annual mean temperature graphs of Kuşadası Station (ºC).

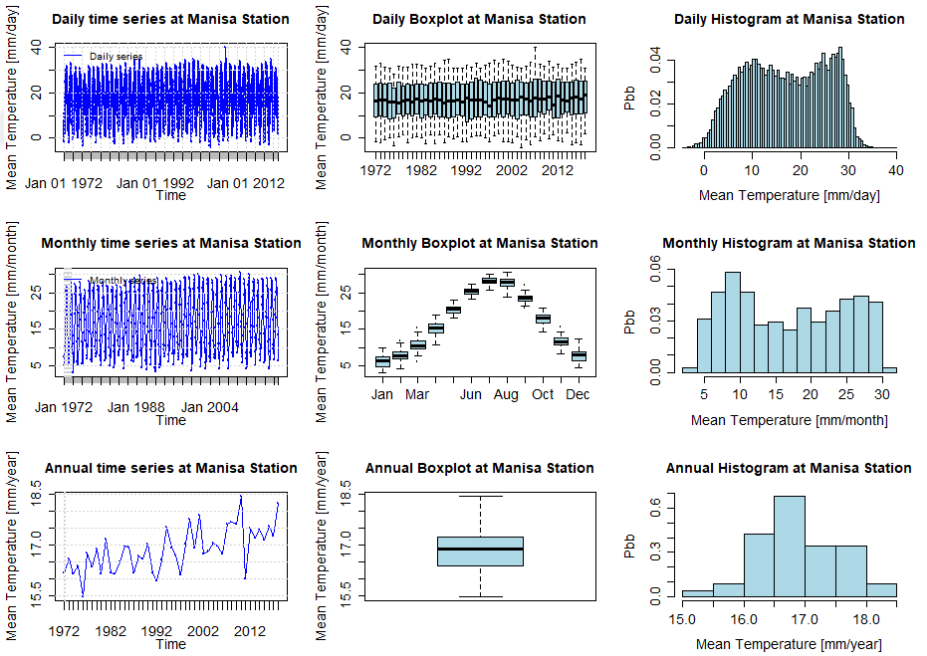


Figure Ap.23 Daily, monthly, annual mean temperature graphs of Manisa Station (ºC).

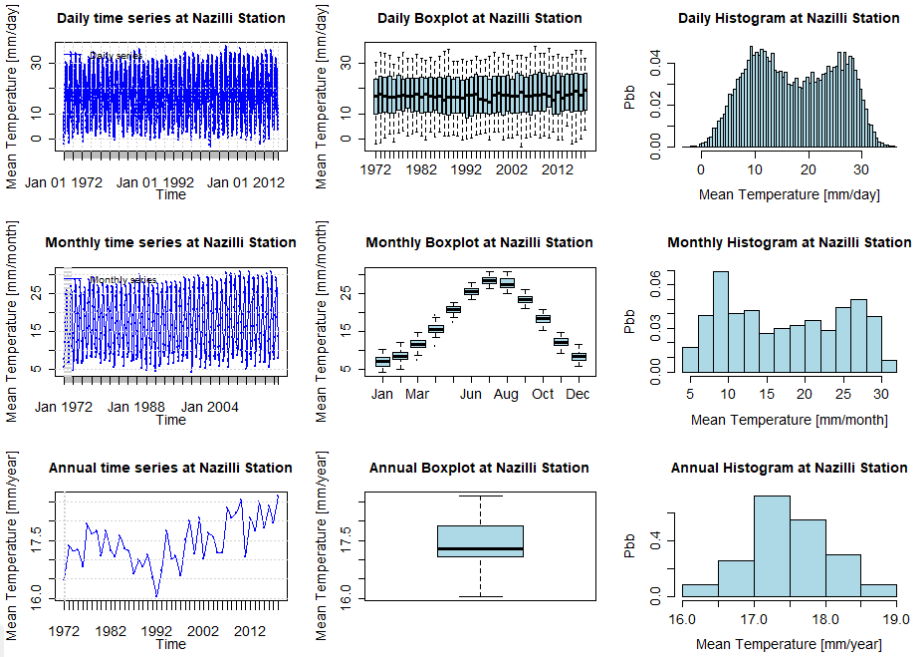


Figure Ap.24 Daily, monthly, annual mean temperature graphs of Nazilli Station (ºC).

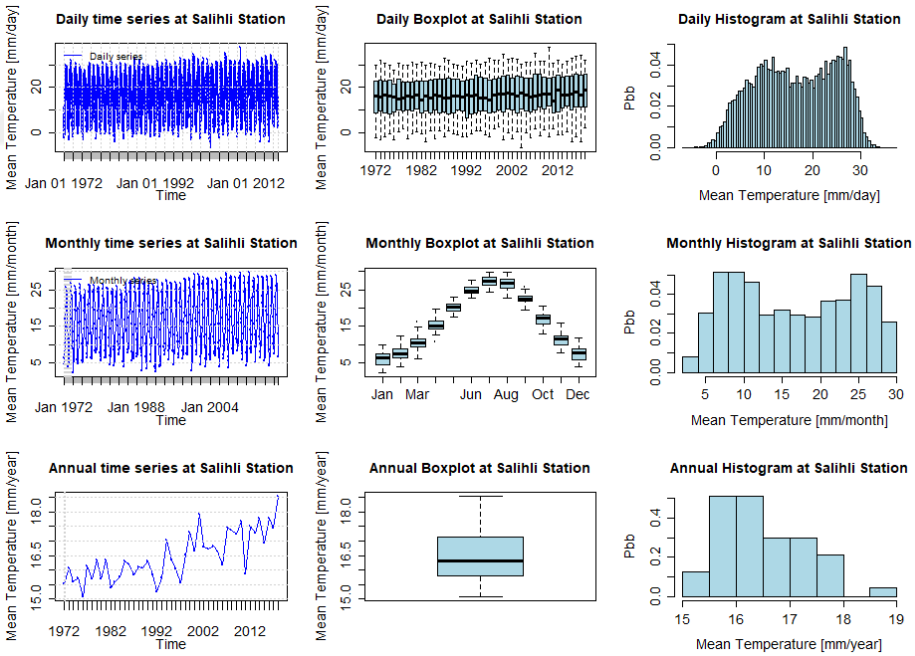


Figure Ap.25 Daily, monthly, annual mean temperature graphs of Salihli Station (ºC).

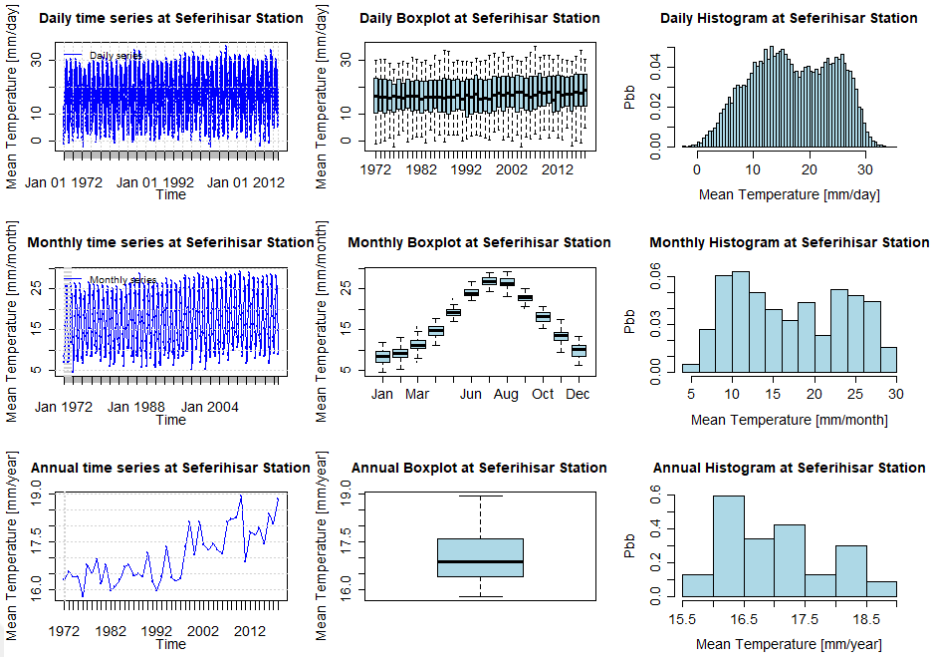


Figure Ap.26 Daily, monthly, annual mean temperature graphs of Seferihisar Station (ºC).

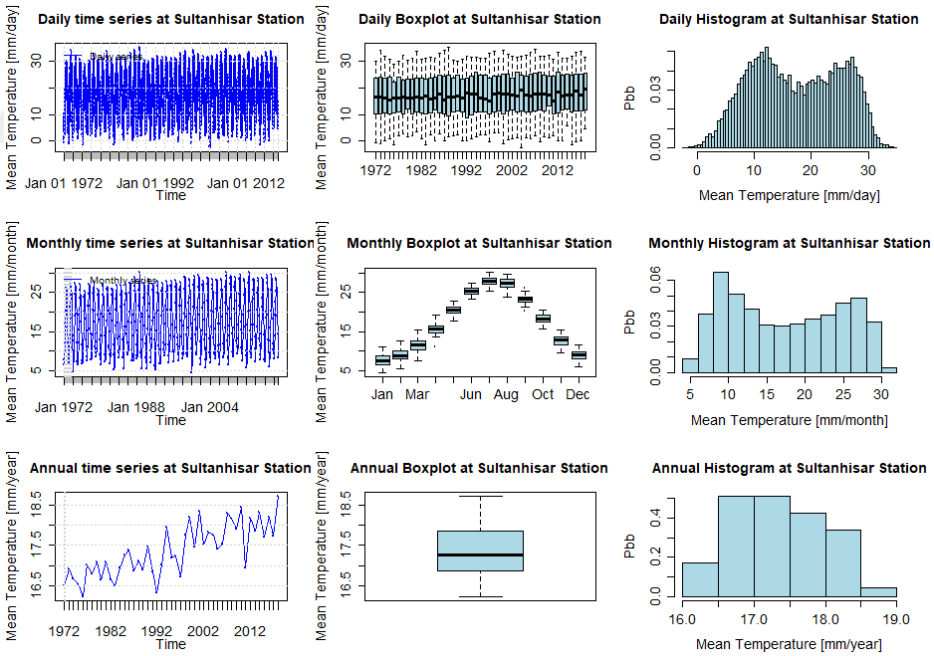


Figure Ap.27 Daily, monthly, annual mean temperature graphs of Sultanhisar Station (ºC).

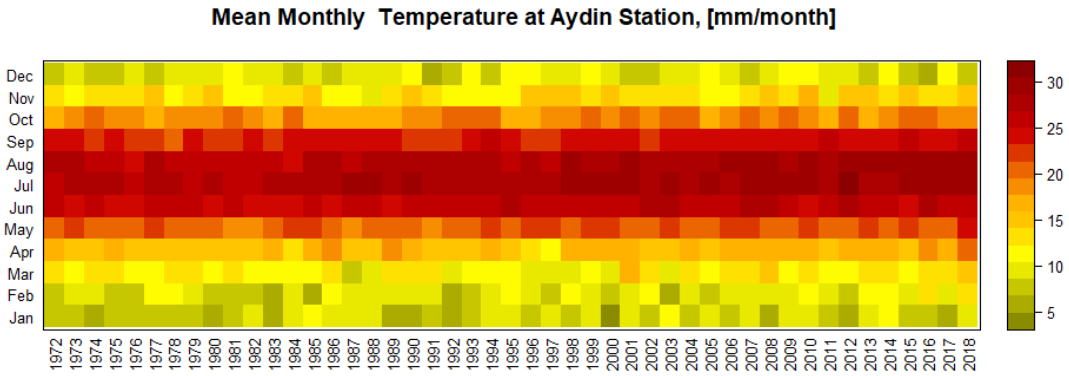


Figure Ap.28 The monthly mean temperature matrix of Aydın Station (ºC).

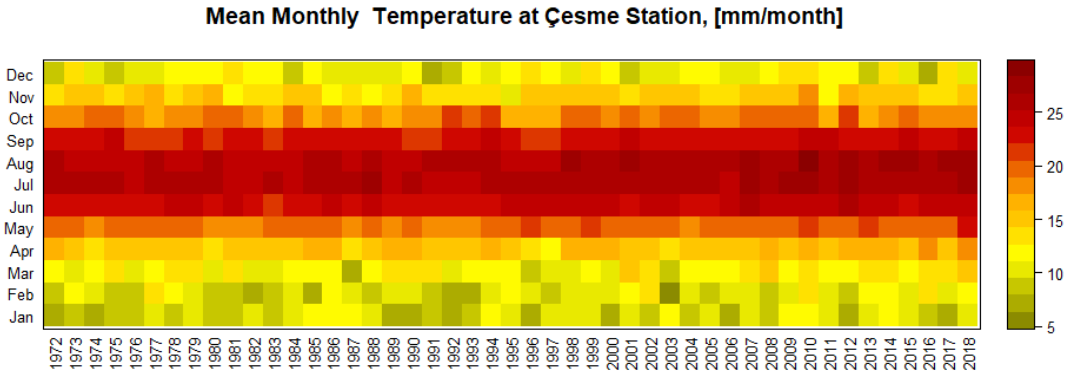


Figure Ap.29 The monthly mean temperature matrix of Çeşme Station (ºC).

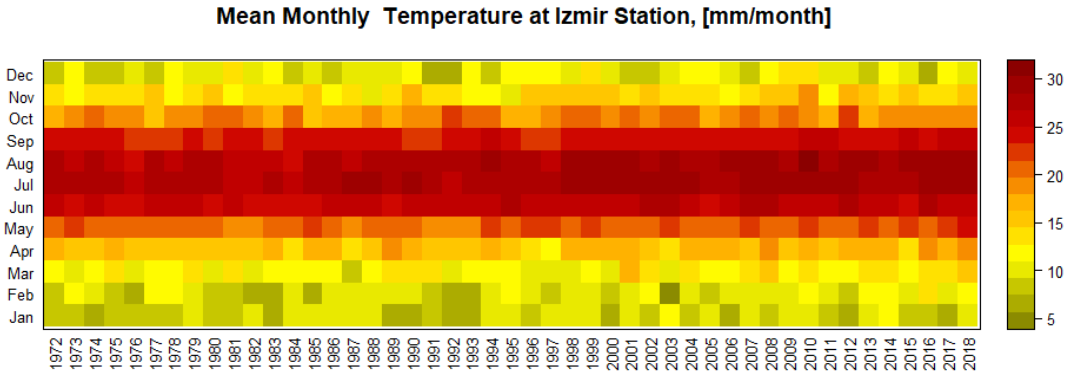


Figure Ap.30 The monthly mean temperature matrix of İzmir Station (ºC).

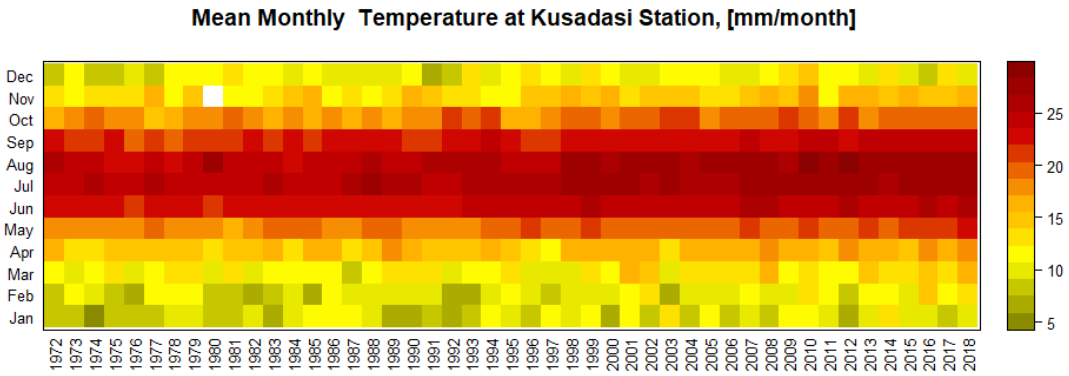


Figure Ap.31 The monthly mean temperature matrix of Kuşadası Station (ºC).

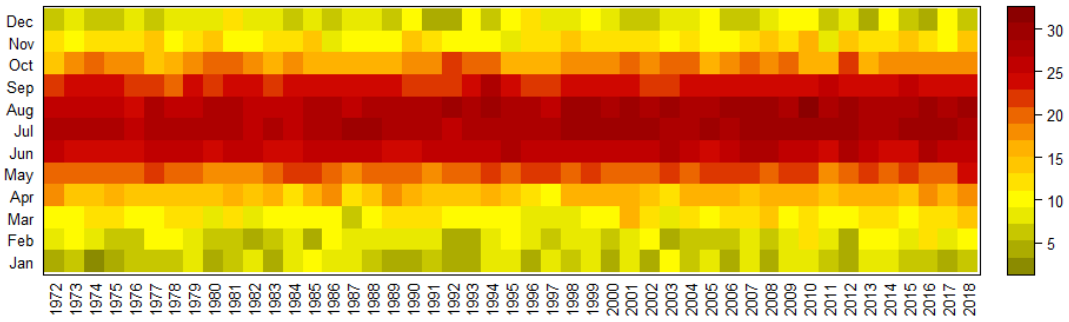


Figure Ap.32 The monthly mean temperature matrix of Manisa Station (ºC).

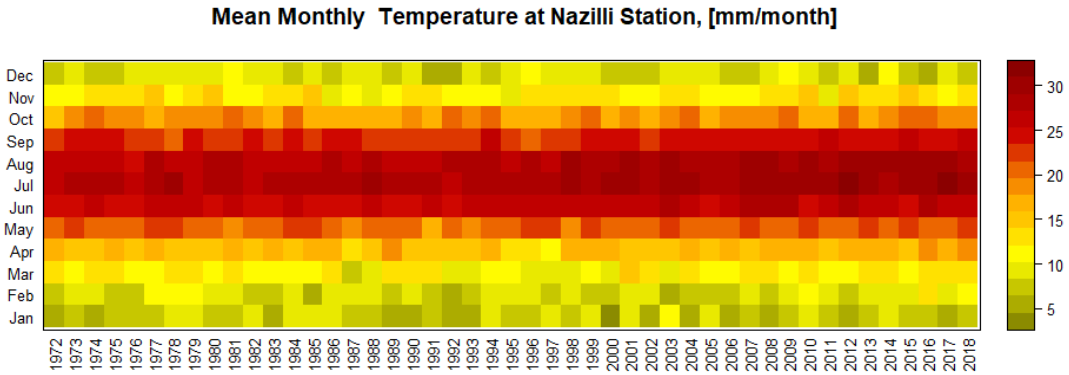


Figure Ap.33 The monthly mean temperature matrix of Nazilli Station (ºC)..

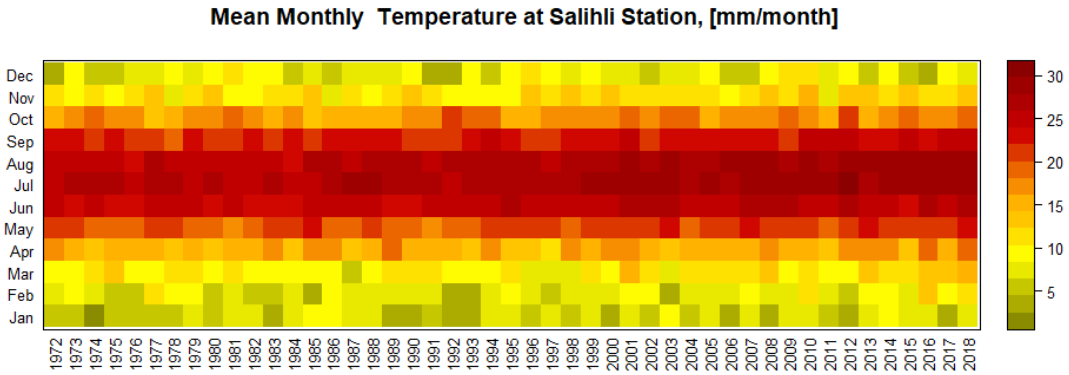


Figure Ap.34 The monthly mean temperature matrix of Salihli Station (ºC).

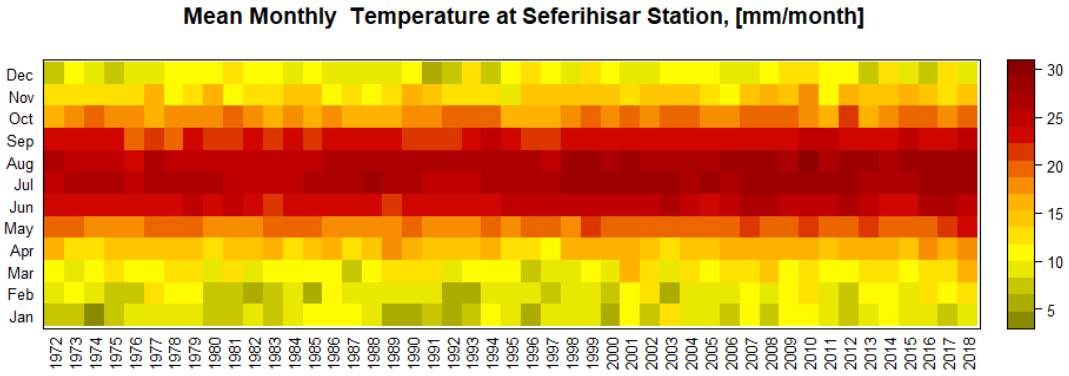


Figure Ap.35 The monthly mean temperature matrix of Seferihisar Station (ºC).

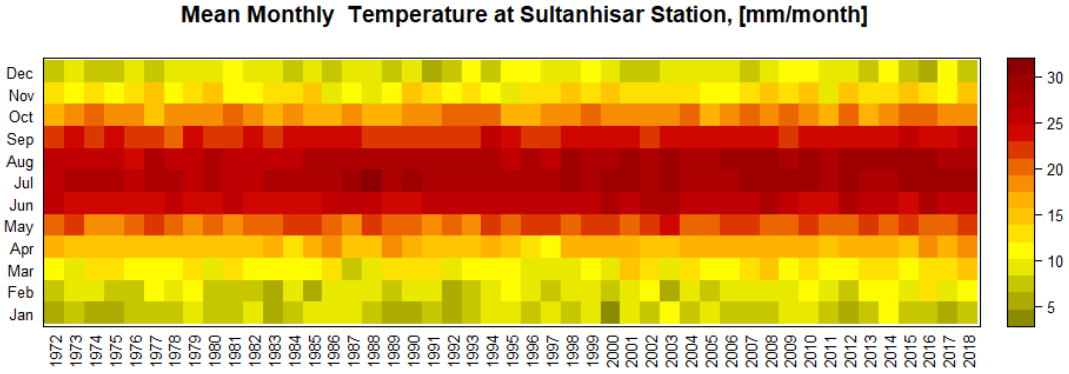


Figure Ap.36 The monthly mean temperature matrix of Sultanhisar Station (ºC).

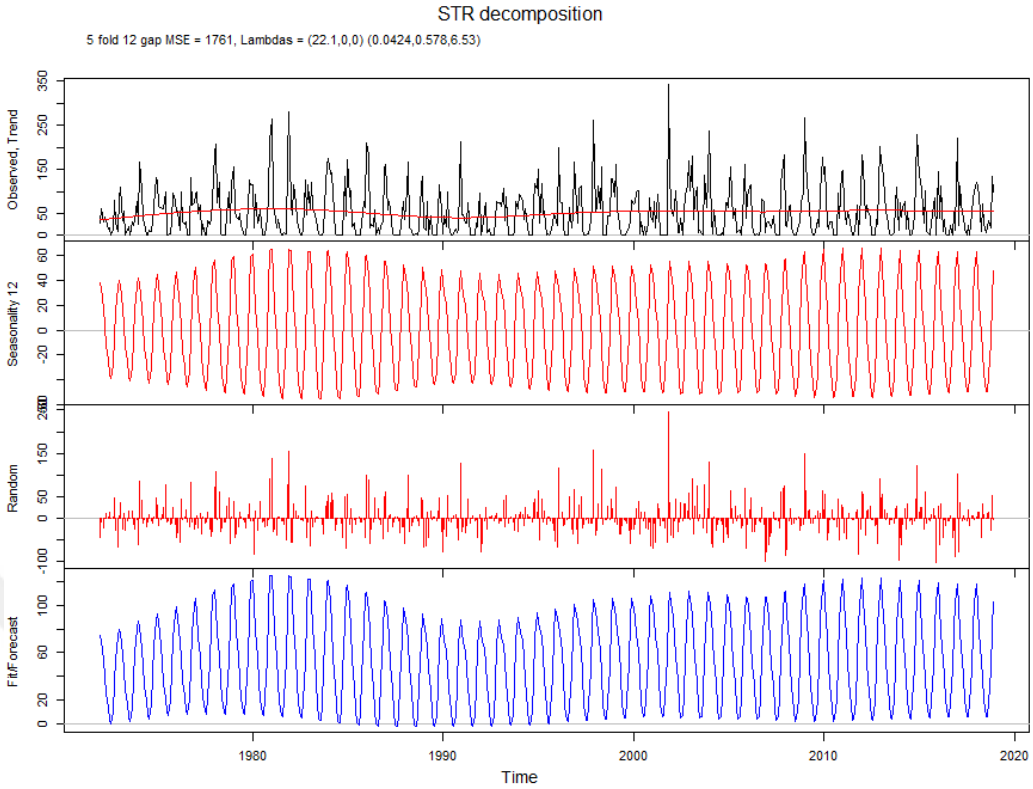


Figure Ap.37 Decomposition of total monthly precipitation (mm) series for Aydın Station.

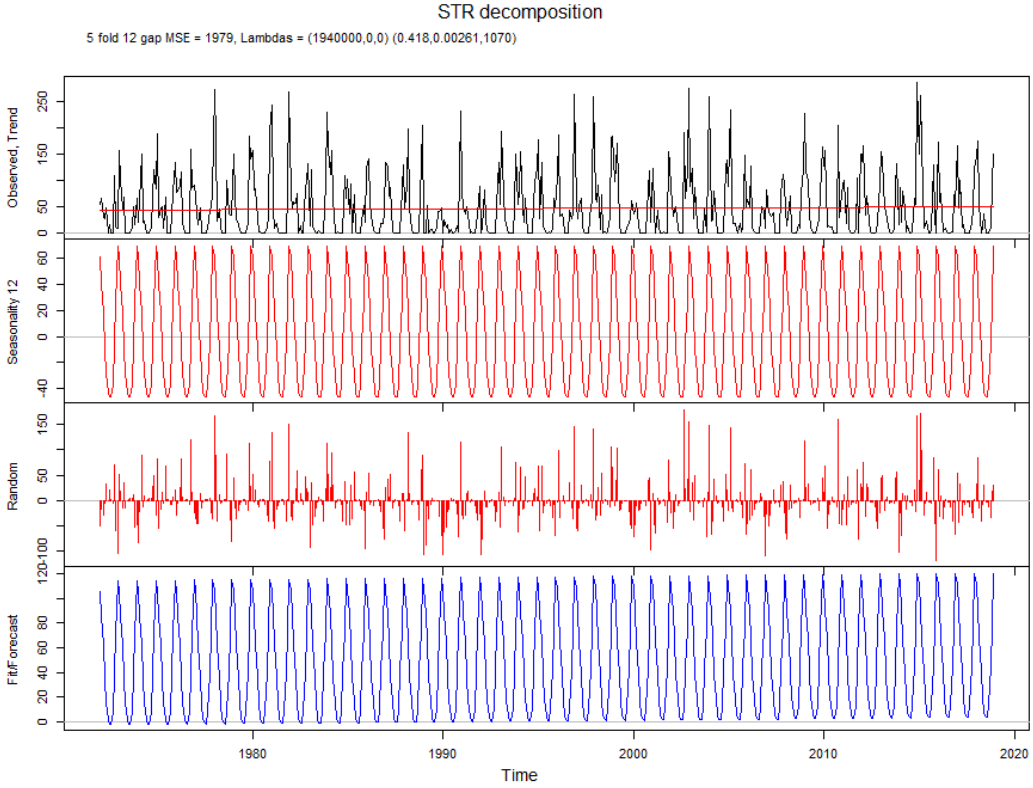


Figure Ap.38 Decomposition of total monthly precipitation (mm) series for Çeşme Station.

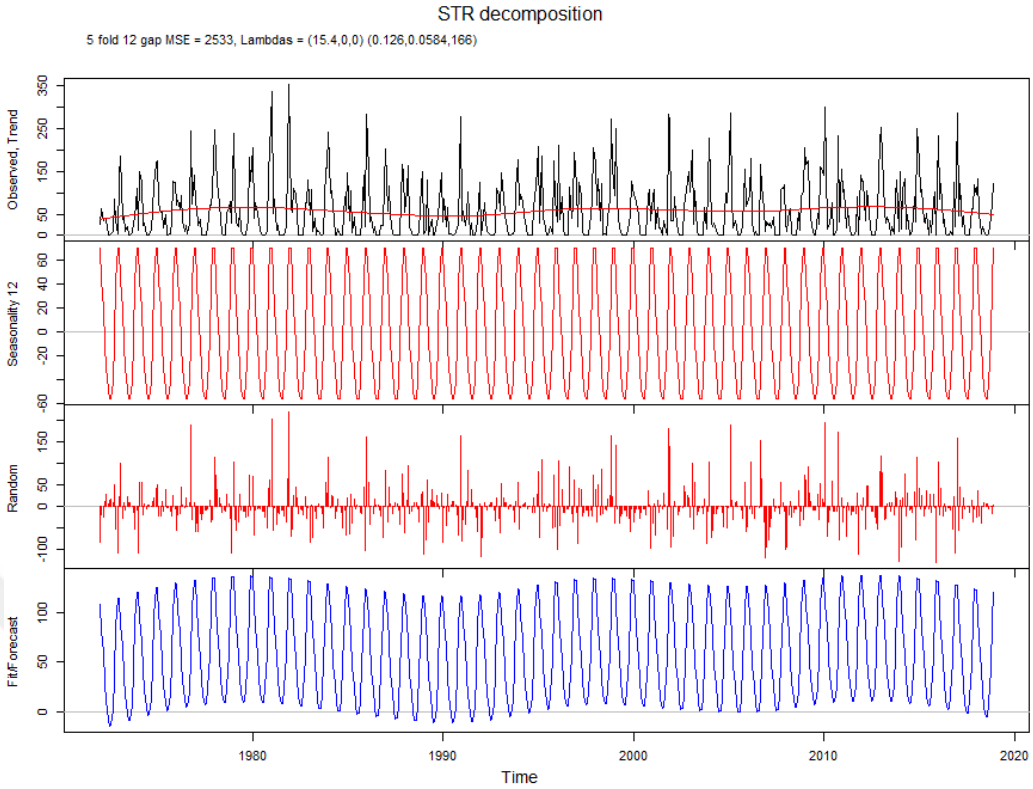


Figure Ap.39 Decomposition of total monthly precipitation (mm) series for İzmir Station.

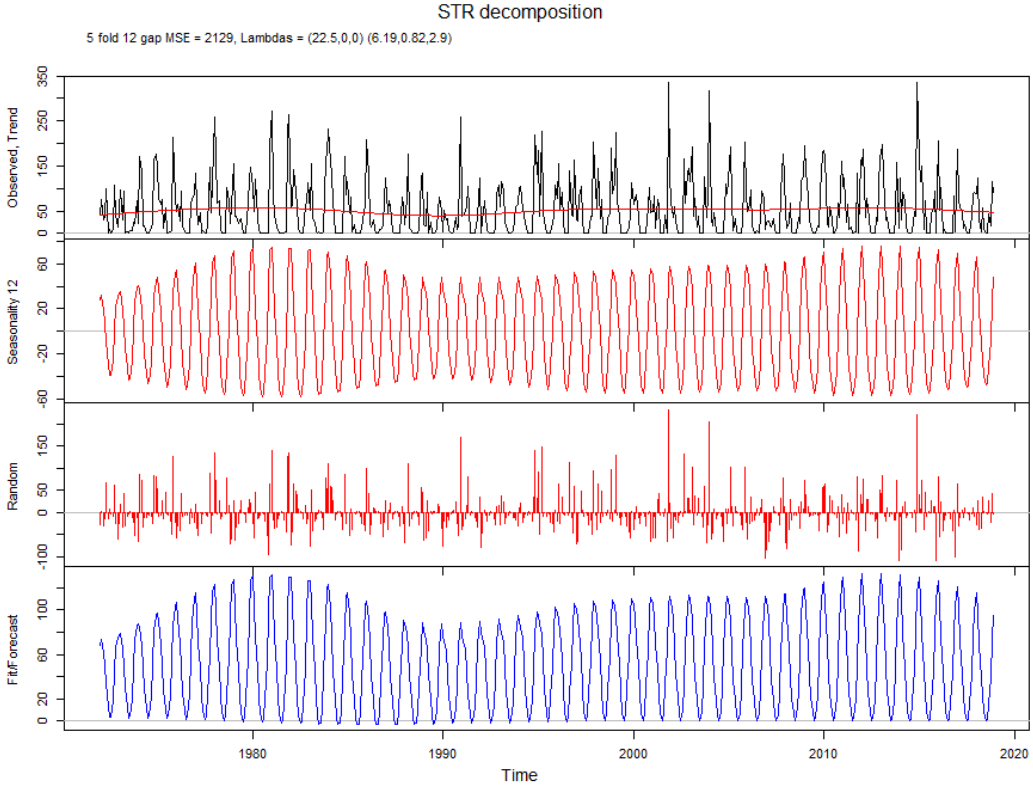


Figure Ap.40 Decomposition of total monthly precipitation (mm) series for Kuşadası Station.

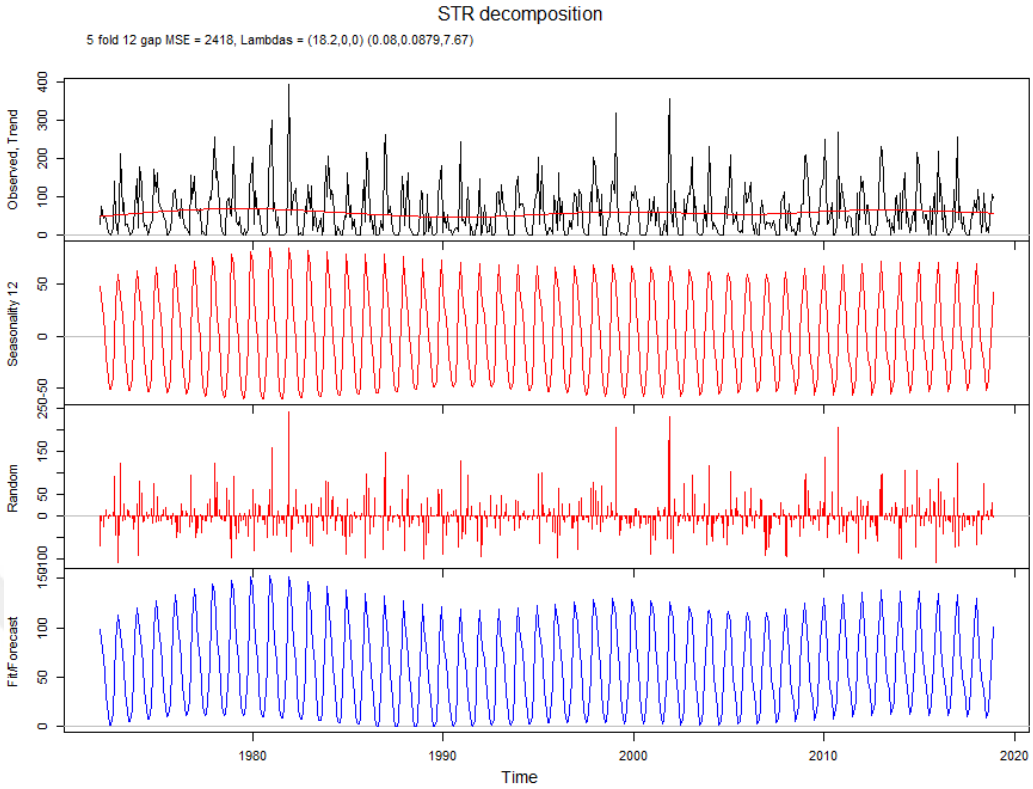


Figure Ap.41 Decomposition of total monthly precipitation (mm) series for Manisa Station.

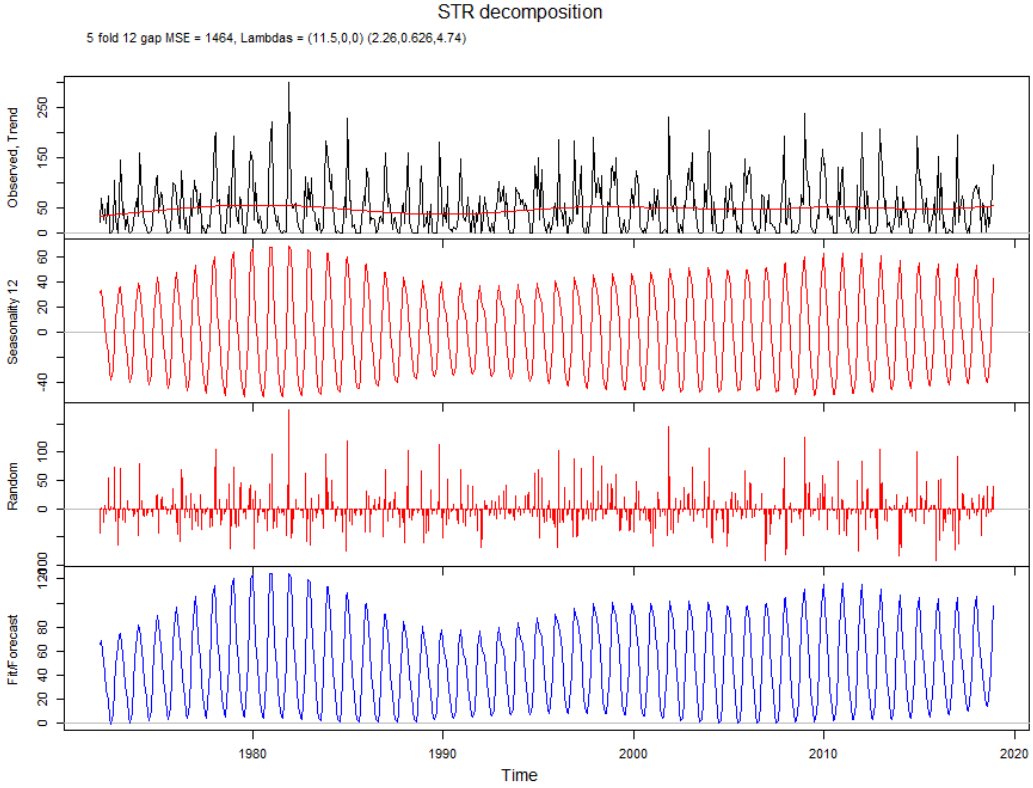


Figure Ap.42 Decomposition of total monthly precipitation (mm) series for Nazilli Station.

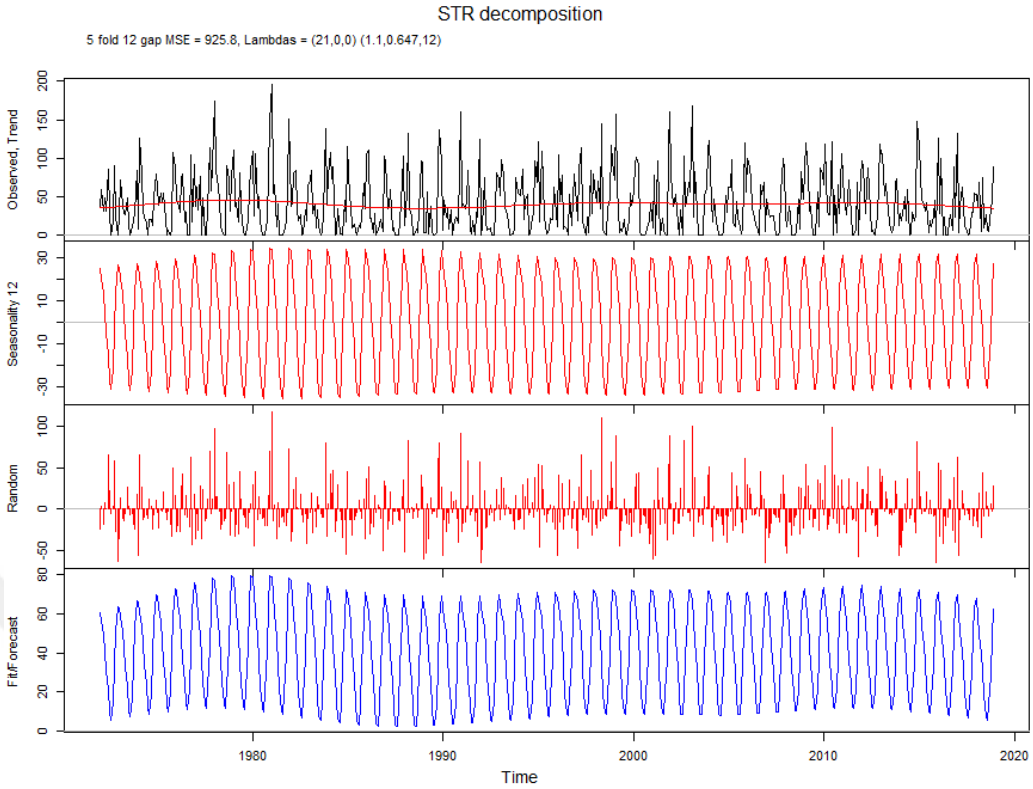


Figure Ap.43 Decomposition of total monthly precipitation (mm) series for Salihli Station.

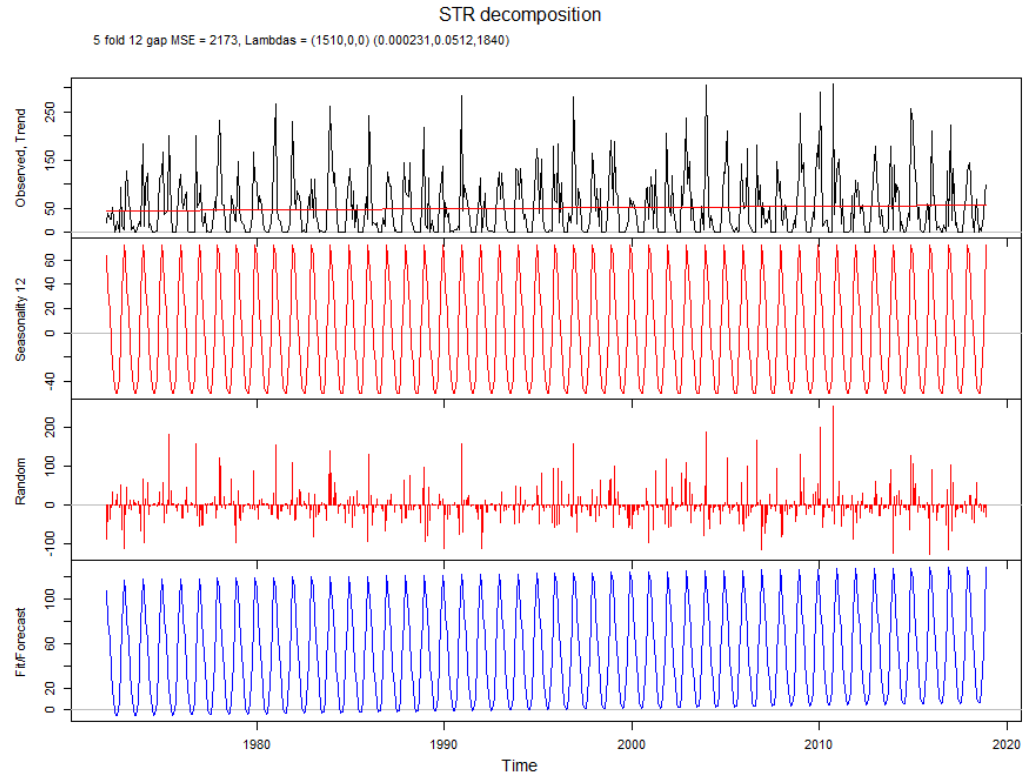


Figure Ap.44 Decomposition of total monthly precipitation (mm) series for Seferihisar Station.

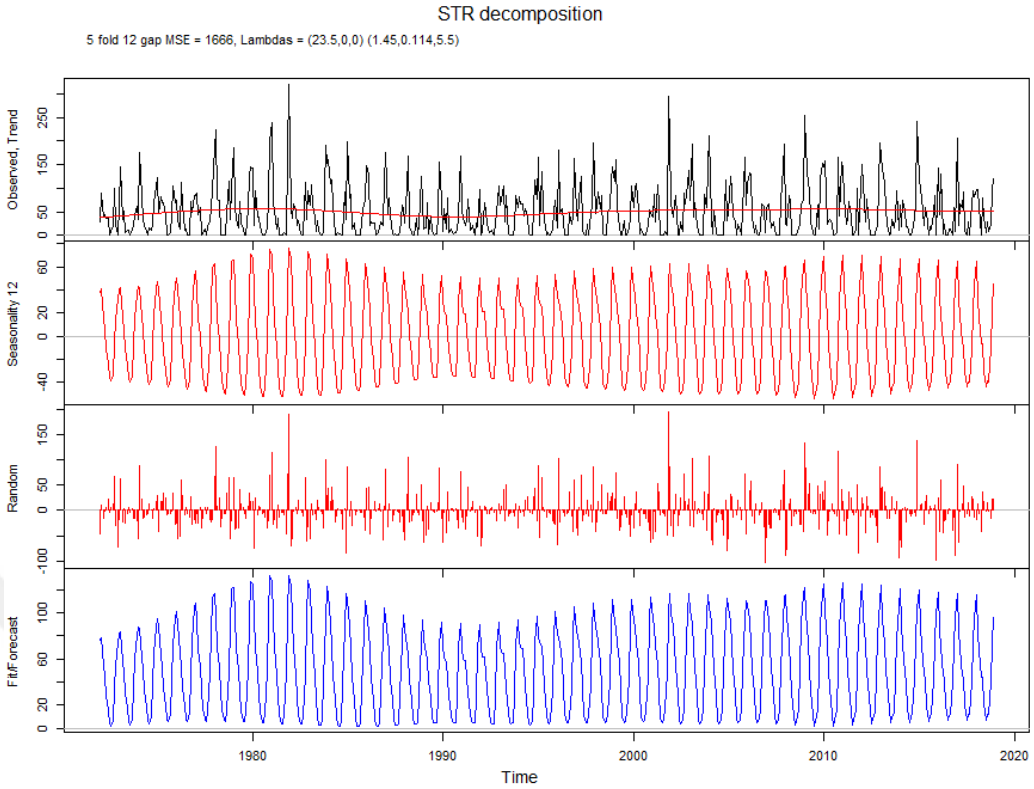


Figure Ap.45 Decomposition of total monthly precipitation (mm) series for Sultanhisar Station.

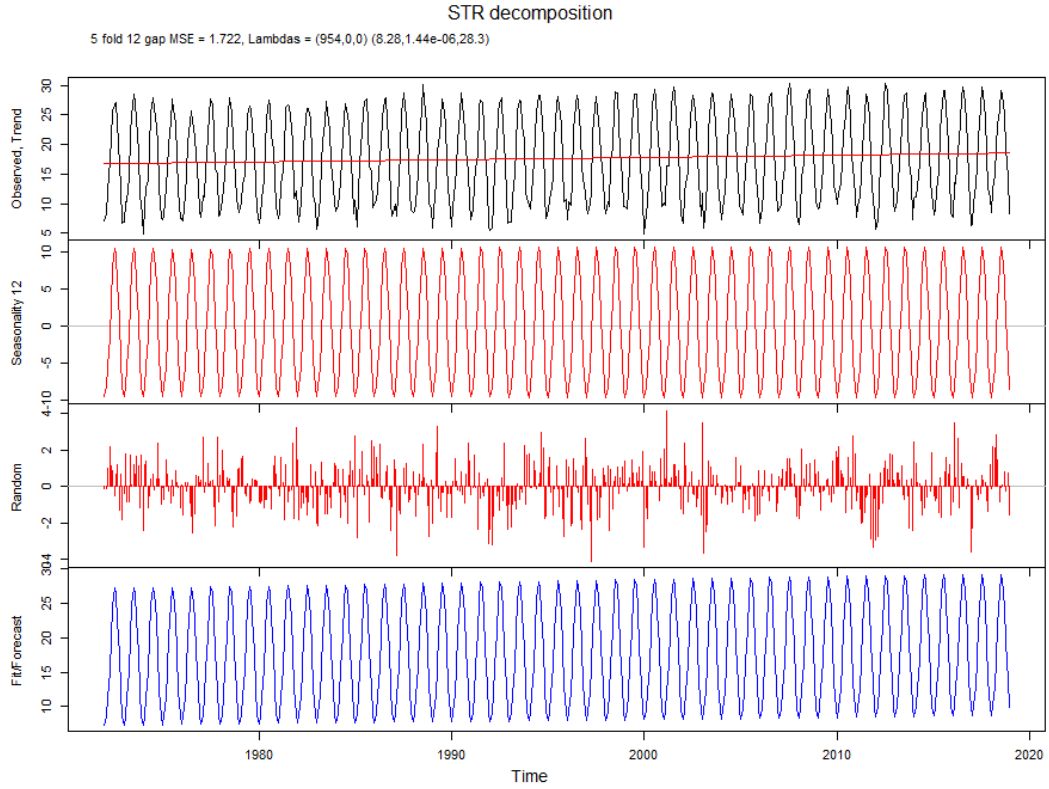


Figure Ap.46 Decomposition of mean monthly temperature (oC) series for Aydın Station.

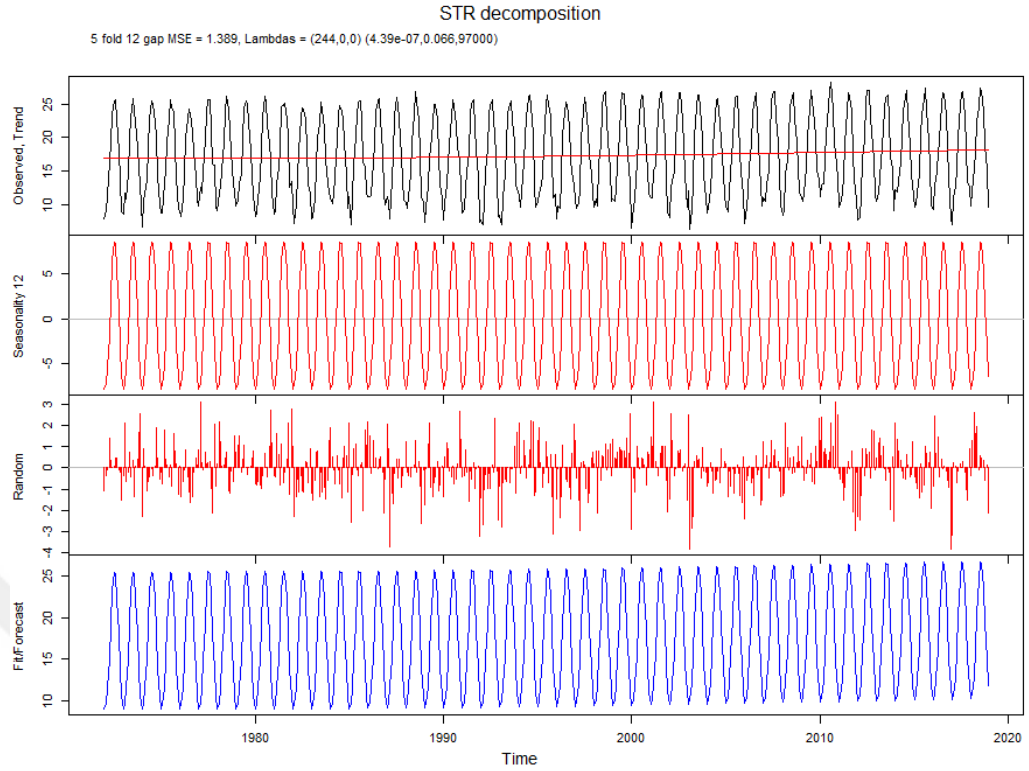


Figure Ap.47 Decomposition of mean monthly temperature (ºC) series for Çeşme Station.

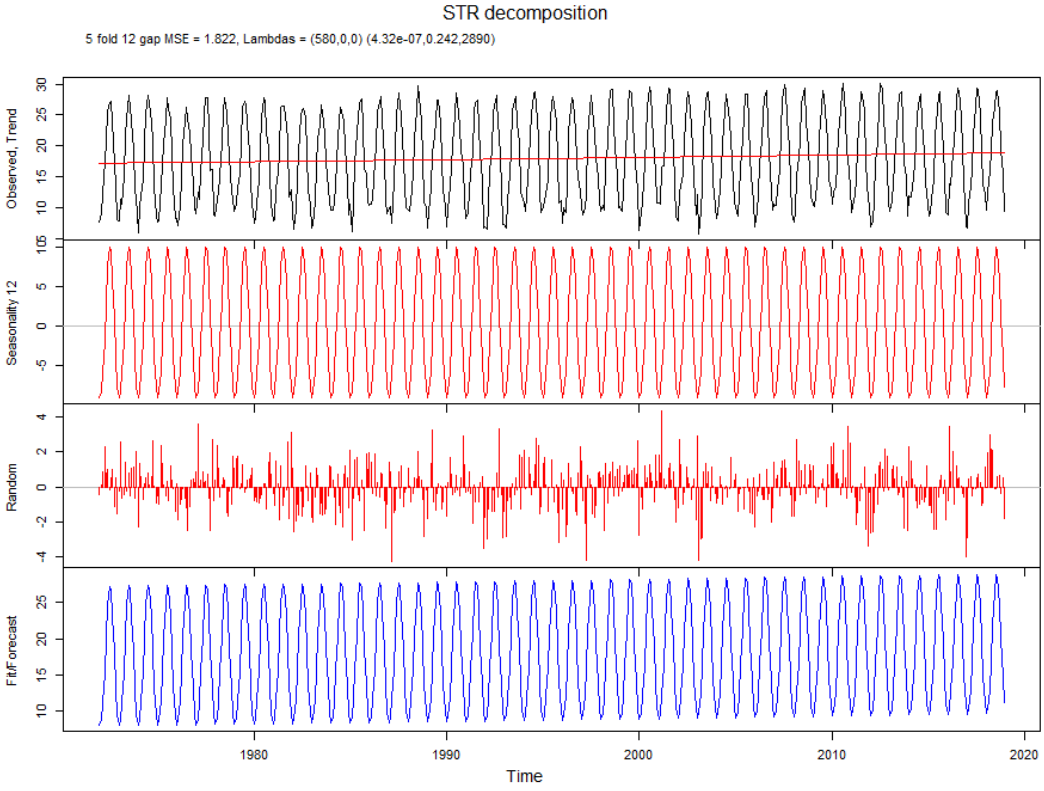


Figure Ap.48 Decomposition of mean monthly temperature (ºC) series for İzmir Station.

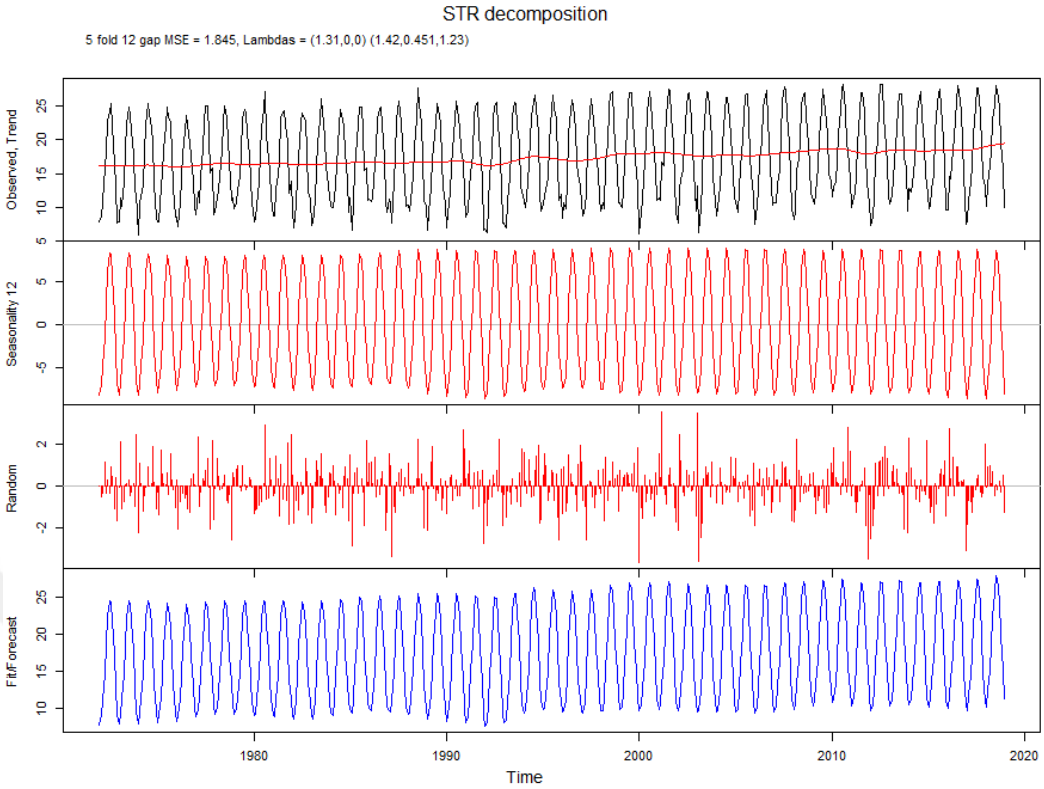


Figure Ap.49 Decomposition of mean monthly temperature (ºC) series for Kuşadası Station.

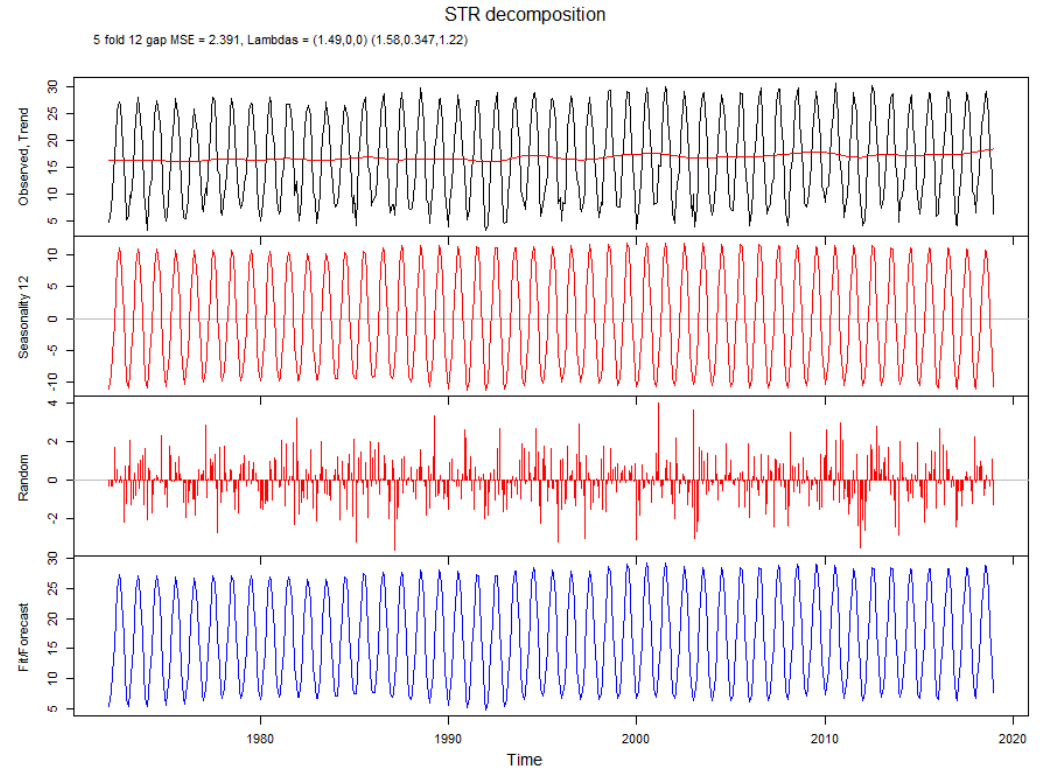


Figure Ap.50 Decomposition of mean monthly temperature (ºC) series for Manisa Station.

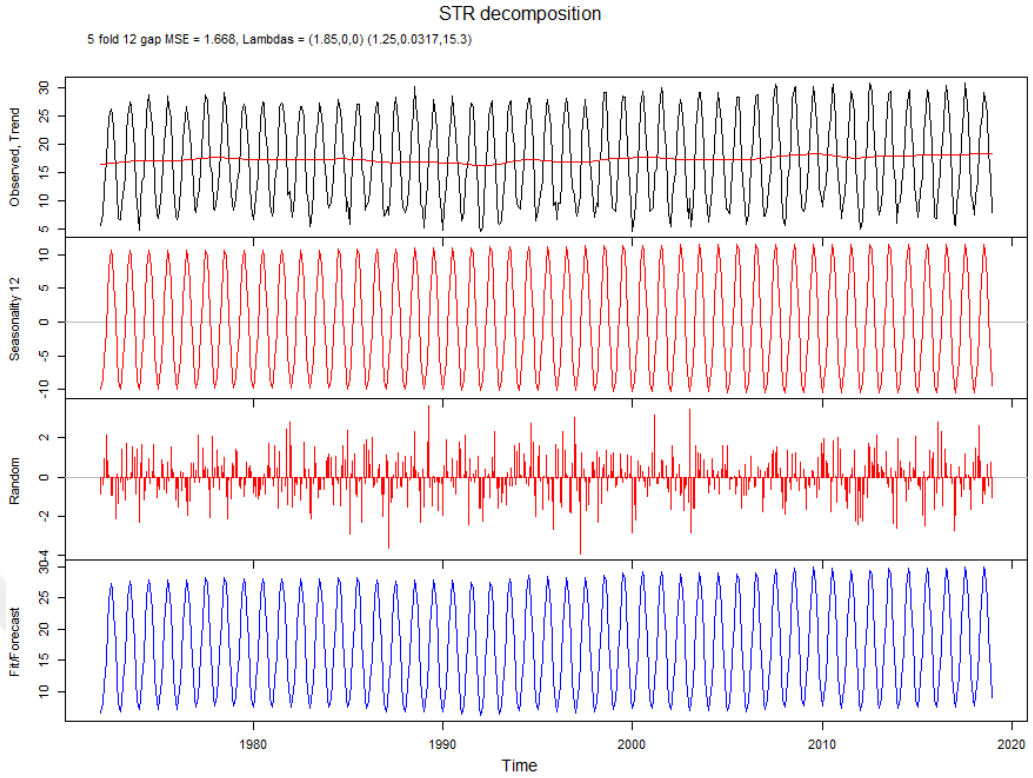


Figure Ap.51 Decomposition of mean monthly temperature (°C) series for Nazilli Station.

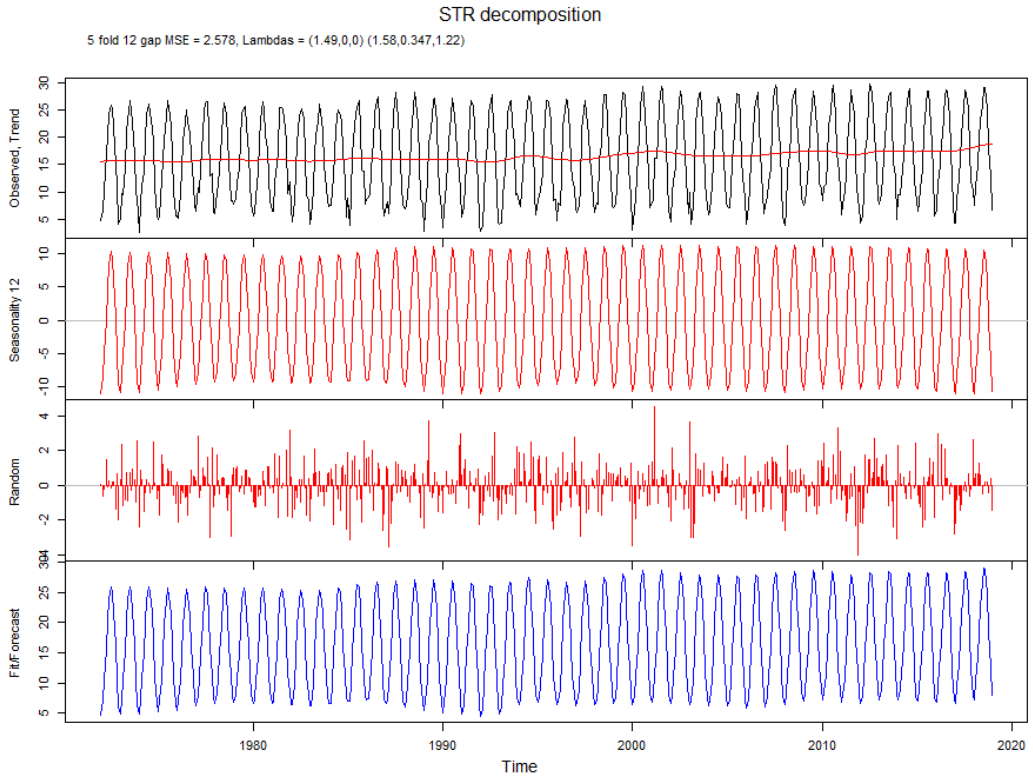


Figure Ap.52 Decomposition of mean monthly temperature (°C) series for Salihli Station.

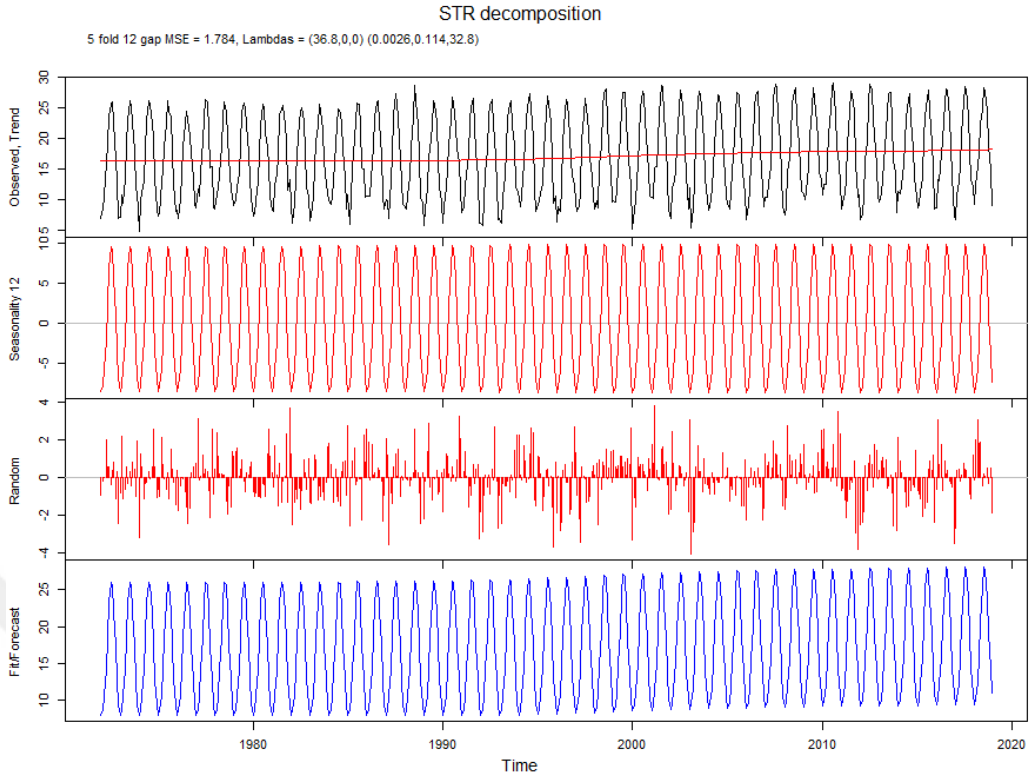


Figure Ap.53 Decomposition of mean monthly temperature (ºC) series for Seferihisar Station.

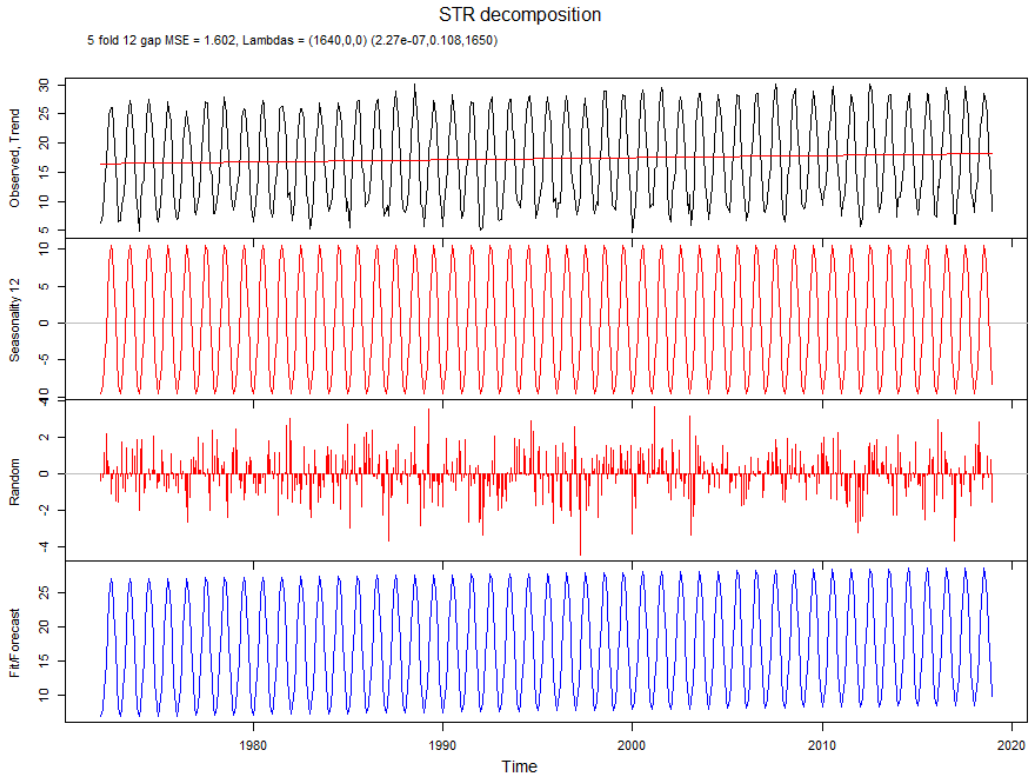


Figure Ap.54 Decomposition of mean monthly temperature (ºC) series for Sultanhisar Station.

Table Ap.1 Annual maximum drought durations and severities for moderate drought conditions for Manisa, İzmir, Kuşadası, Aydın and Salihli Stations (for SPI-1 and SPI-3 month).

		Moderate Drought									
Station	**Period**	**SPI1**					**SPI3**				
		Total Event	**Max Severity**	**Max Duration**	**Beginning Date**	**End Date**	**Total Event**	**Max Severity**	**Max Duration**	**Beginning Date**	**End Date**
MANİSA (17186)	1972-1979	3	1.257	1	Jan-72	Jan-72	2	2.090	2	Apr-79	May-79
	1980-1987	8	1.375	4	Sep-85	Dec-85	8	2.770	2	Sep-87	Oct-87
	1988-1995	8	2.179	4	Mar-88	Jun-88	9	2.090	2	Sep-88	Oct-88
	1996-2003	7	1.447	6	Oct-00	Mar-01	8	3.348	3	Dec-00	Feb-01
	2004-2011	5	4.595	7	Oct-06	Apr-07	8	1.481	1	Dec-04	Dec-04
	2012-2018	3	1.477	1	Apr-17	Apr-17	5	1.298	1	Apr-17	Apr-17
	1972-2018	**34**	**4.595**	**7**	**Oct-06**	**Apr-07**	**40**	**3.348**	**3**	**Dec-00**	**Feb-01**
İZMİR (17220)	1972-1979	4	1.394	1	Jan-72	Jan-72	7	2.421	2	Mar-77	Apr-77
	1980-1987	3	1.397	3	Feb-81	Apr-81	7	2.518	2	Nov-84	Dec-84
	1988-1995	9	1.358	4	Dec-89	Mar-90	12	2.416	2	Mar-89	Apr-89
	1996-2003	7	1.497	5	Aug-00	Dec-00	6	2.278	2	Jul-03	Aug-03
	2004-2011	7	3.551	3	Jan-07	Mar-07	5	2.394	2	Jun-06	Jul-06
	2012-2018	1	1.376	7	May-14	Nov-14	3	2.686	2	May-18	Jun-18
	1972-2018	**31**	**3.551**	**3**	**Jan-07**	**Mar-07**	**40**	**2.686**	**2**	**May-18**	**Jun-18**
KUŞADASI (17232)	1972-1979	5	1.483	2	Dec-73	Jan-74	7	2.430	2	Apr-77	May-77
	1980-1987	9	2.266	2	Mar-86	Apr-86	8	2.693	2	Nov-85	Dec-85
	1988-1995	4	1.458	1	Nov-90	Nov-90	11	3.872	3	Feb-89	Apr-89
	1996-2003	5	2.462	2	Jan-97	Feb-97	5	3.202	3	Jan-01	Mar-01
	2004-2011	6	4.898	6	Nov-06	Apr-07	4	1.484	1	Apr-08	Apr-08
	2012-2018	4	1.442	1	Apr-15	Apr-15	3	1.228	1	Feb-14	Feb-14
	1972-2018	**33**	**4.898**	**6**	**Nov-06**	**Apr-07**	**38**	**3.872**	**3**	**Feb-89**	**Apr-89**
AYDIN (17324)	1972-1979	6	1.331	1	Jan-74	Jan-74	7	2.165	2	Apr-72	May-72
	1980-1987	6	1.486	3	Aug-81	Oct-81	6	2.618	2	Aug-85	Sep-85
	1988-1995	7	1.294	5	Jun-93	Oct-93	10	2.380	2	Dec-87	Jan-88
	1996-2003	7	2.380	6	Aug-95	Jan-96	7	4.041	3	Jan-01	Mar-01
	2004-2011	7	5.017	8	Sep-06	Apr-07	4	2.456	2	Jul-08	Aug-08
	2012-2018	2	1.448	2	Jan-17	Feb-17	4	1.476	1	Nov-12	Nov-12
	1972-2018	**35**	**5.017**	**8**	**Sep-06**	**Apr-07**	**38**	**4.041**	**3**	**Jan-01**	**Mar-01**
SALİHLİ (17792)	1972-1979	5	1.367	1	Nov-76	Nov-76	6	2.503	2	Jul-78	Aug-78
	1980-1987	8	1.483	3	Mar-86	May-86	9	1.455	1	Nov-84	Nov-84
	1988-1995	7	1.500	1	Jun-88	Jun-88	8	2.446	2	Aug-89	Sep-89
	1996-2003	8	1.436	1	Jun-01	Jun-01	6	2.537	2	Sep-00	Oct-00
	2004-2011	7	2.341	2	Sep-04	Oct-04	8	1.338	1	May-07	May-07
	2012-2018	5	1.497	0	Jan-17	Dec-16	4	2.032	2	Nov-17	Dec-17
	1972-2018	**40**	**2.341**	**2**	**Sep-04**	**Oct-04**	**41**	**2.537**	**2**	**Sep-00**	**Oct-00**

Table Ap.2 Annual maximum drought durations and severities for moderate drought conditions for Seferihisar, Ödemiş, Sultanhisar, Selçuk and Nazilli Stations (for SPI-1 and SPI-3 month).

		Moderate Drought									
Station	**Period**	**SPI1**					**SPI3**				
		Total Event	**Max Severity**	**Max Duration**	**Beginning Date**	**End Date**	**Total Event**	**Max Severity**	**Max Duration**	**Beginning Date**	**End Date**
SEFERİHİSAR (17820)	1972-1979	2	1.298	1	Apr-74	Apr-74	6	3.380	3	Jan-77	Mar-77
	1980-1987	4	1.392	2	Sep-87	Oct-87	4	1.450	1	Apr-81	Apr-81
	1988-1995	3	1.258	1	Oct-88	Oct-88	6	2.379	2	Mar-89	Apr-89
	1996-2003	5	1.469	3	Dec-96	Feb-97	3	2.475	2	Jun-00	Jul-00
	2004-2011	6	1.421	1	Mar-11	Mar-11	5	1.489	1	Feb-08	Feb-08
	2012-2018	3	1.206	1	Oct-16	Oct-16	4	1.397	1	Jan-12	Jan-12
	1972-2018	**23**	**1.469**	**3**	**Dec-96**	**Feb-97**	**28**	**3.380**	**3**	**Jan-77**	**Mar-77**
ÖDEMİŞ (17822)	1972-1979	5	1.214	1	Jan-72	Jan-72	5	1.385	1	Dec-72	Dec-72
	1980-1987	7	1.264	4	Aug-82	Nov-82	6	2.473	2	Sep-87	Oct-87
	1988-1995	5	1.439	8	Apr-91	Nov-91	7	3.769	3	Aug-93	Oct-93
	1996-2003	8	1.300	10	Jul-98	Apr-99	11	3.799	3	Aug-99	Oct-99
	2004-2011	8	1.326	1	Oct-04	Oct-04	10	2.544	2	Jun-08	Jul-08
	2012-2018	4	1.422	10	May-13	Feb-14	4	2.502	2	Aug-12	Sep-12
	1972-2018	**37**	**1.439**	**8**	**Apr-91**	**Nov-91**	**43**	**3.799**	**3**	**Aug-99**	**Oct-99**
SULTANHİSAR (17850)	1972-1979	6	1.330	1	Apr-79	Apr-79	8	2.665	2	Dec-73	Jan-74
	1980-1987	7	1.497	1	Mar-86	Mar-86	7	2.320	2	Sep-80	Oct-80
	1988-1995	4	2.305	8	Oct-87	May-88	6	3.686	3	Aug-93	Oct-93
	1996-2003	3	1.251	10	Aug-99	May-00	6	4.674	4	Dec-00	Mar-01
	2004-2011	6	2.747	4	Nov-07	Feb-08	6	1.488	1	May-10	May-10
	2012-2018	3	1.384	1	Feb-17	Feb-17	5	1.246	1	Sep-04	Sep-04
	1972-2018	**29**	**2.747**	**4**	**Nov-07**	**Feb-08**	**38**	**4.674**	**4**	**Dec-00**	**Mar-01**
SELÇUK (17854)	1972-1979	6	1.383	1	Jan-74	Jan-74	6	2.475	2	Nov-73	Dec-73
	1980-1987	8	1.495	5	Jun-81	Oct-81	5	1.459	1	Dec-86	Dec-86
	1988-1995	5	1.333	10	May-94	Feb-95	8	2.861	2	Jan-92	Feb-92
	1996-2003	3	1.437	2	Apr-00	May-00	2	1.263	1	Nov-99	Nov-99
	2004-2011	3	3.480	3	Jan-07	Mar-07	5	2.698	2	Apr-04	May-04
	2012-2018	3	1.296	6	May-16	Oct-16	2	1.228	1	Nov-12	Nov-12
	1972-2018	**28**	**3.480**	**3**	**Jan-07**	**Mar-07**	**28**	**2.861**	**2**	**Jan-92**	**Feb-92**
NAZİLLİ (17860)	1972-1979	4	1.353	1	Jan-72	Jan-72	8	3.435	3	Nov-73	Jan-74
	1980-1987	7	2.530	4	Mar-84	Jun-84	9	2.273	2	Apr-81	May-81
	1988-1995	7	1.434	1	Jan-88	Jan-88	6	2.318	2	Aug-89	Sep-89
	1996-2003	7	2.339	2	May-02	Jun-02	5	2.452	2	Jan-01	Feb-01
	2004-2011	6	1.441	1	Mar-11	Mar-11	8	2.790	2	Apr-11	May-11
	2012-2018	3	1.454	9	Jun-16	Feb-17	6	2.639	2	Aug-12	Sep-12
	1972-2018	**34**	**2.530**	**4**	**Mar-84**	**Jun-84**	**42**	**3.435**	**3**	**Nov-73**	**Jan-74**

Table Ap.3 Annual maximum drought durations and severities for moderate drought conditions for Manisa, İzmir, Kuşadası, Aydın and Salihli Stations (for SPI-6 and SPI-12 month).

		Moderate Drought									
Station	**Period**	**SPI6**					**SPI12**				
		Total Event	**Max Severity**	**Max Duration**	**Beginning Date**	**End Date**	**Total Event**	**Max Severity**	**Max Duration**	**Beginning Date**	**End Date**
MANİSA (17186)	1972-1979	5	2.102	2	Jul-77	Aug-77	1	1.411	1	Jan-73	Jan-73
	1980-1987	4	4.942	4	Jan-85	Apr-85	3	1.496	1	May-85	May-85
	1988-1995	7	2.956	2	Mar-89	Apr-89	6	5.232	4	Jan-91	Apr-91
	1996-2003	9	7.686	6	Dec-00	May-01	5	7.848	6	May-01	Oct-01
	2004-2011	5	3.659	3	Feb-08	Apr-08	6	3.847	3	Mar-08	May-08
	2012-2018	5	1.247	1	Dec-16	Dec-16	2	2.178	2	Apr-18	May-18
	1972-2018	**35**	**7.686**	**6**	**Dec-00**	**May-01**	**23**	**7.848**	**6**	**May-01**	**Oct-01**
İZMİR (17220)	1972-1979	4	2.243	2	Apr-77	May-77	5	3.141	3	Jun-74	Aug-74
	1980-1987	8	5.023	4	Dec-84	Mar-85	4	7.539	6	May-83	Oct-83
	1988-1995	11	5.029	4	Mar-89	Jun-89	6	5.944	5	Jun-90	Oct-90
	1996-2003	7	1.438	1	Nov-99	Nov-99	2	9.035	8	Feb-00	Sep-00
	2004-2011	5	3.349	3	Feb-08	Apr-08	7	7.977	7	Apr-04	Oct-04
	2012-2018	2	2.636	2	Aug-18	Sep-18	-	-	-	-	-
	1972-2018	**37**	**5.029**	**4**	**Mar-89**	**Jun-89**	**24**	**9.035**	**8**	**Feb-00**	**Sep-00**
KUŞADASI (17232)	1972-1979	5	3.565	3	Mar-73	May-73	4	1.445	1	Dec-73	Dec-73
	1980-1987	8	3.646	3	Jan-87	Mar-87	5	7.011	6	May-87	Oct-87
	1988-1995	12	1.495	1	Nov-91	Nov-91	6	8.336	7	Mar-89	Sep-89
	1996-2003	5	2.918	2	Oct-99	Nov-99	2	8.579	8	Feb-00	Sep-00
	2004-2011	3	2.421	2	Jan-07	Feb-07	4	2.322	2	Dec-06	Jan-07
	2012-2018	1	1.143	1	Nov-12	Nov-12	2	4.465	4	Dec-16	Mar-17
	1972-2018	**34**	**3.646**	**3**	**Jan-87**	**Mar-87**	**23**	**8.579**	**8**	**Feb-00**	**Sep-00**
AYDIN (17324)	1972-1979	5	3.992	3	Mar-73	May-73	3	9.023	7	May-73	Nov-73
	1980-1987	2	1.417	1	Dec-87	Dec-87	-	-	-	-	-
	1988-1995	13	2.624	2	Nov-95	Dec-95	10	9.367	7	May-89	Nov-89
	1996-2003	3	3.711	3	Dec-99	Feb-00	4	6.364	5	Jun-01	Oct-01
	2004-2011	5	3.449	3	Nov-04	Jan-05	4	1.458	1	Dec-08	Dec-08
	2012-2018	3	1.465	1	May-14	May-14	1	3.836	3	Oct-16	Dec-16
	1972-2018	**31**	**3.992**	**3**	**Mar-73**	**May-73**	**22**	**9.367**	**7**	**May-89**	**Nov-89**
SALİHLİ (17792)	1972-1979	1	3.730	3	Jan-73	Mar-73	2	2.121	2	Dec-73	Jan-74
	1980-1987	7	3.362	3	Jul-87	Sep-87	4	4.918	4	Oct-85	Jan-86
	1988-1995	7	3.703	3	Mar-92	May-92	8	2.544	2	Jan-88	Feb-88
	1996-2003	5	2.284	2	Dec-99	Jan-00	2	2.341	2	Jan-01	Feb-01
	2004-2011	4	1.474	1	Jul-04	Jul-04	6	7.243	6	Mar-07	Aug-07
	2012-2018	7	7.615	6	Nov-17	Apr-18	8	3.763	3	Apr-18	Jun-18
	1972-2018	**31**	**7.615**	**6**	**Nov-17**	**Apr-18**	**30**	**7.243**	**6**	**Mar-07**	**Aug-07**

Table Ap.4 Annual maximum drought durations and severities for moderate drought conditions for Seferihisar, Ödemiş, Sultanhisar, Selçuk and Nazilli Stations (for SPI-6 and SPI-12 month).

		Moderate Drought									
Station	**Period**	**SPI6**					**SPI12**				
		Total Event	**Max Severity**	**Max Duration**	**Beginning Date**	**End Date**	**Total Event**	**Max Severity**	**Max Duration**	**Beginning Date**	**End Date**
SEFERİHİSAR (17820)	1972-1979	7	3.561	3	Feb-73	Apr-73	6	7.393	6	Mar-79	Aug-79
	1980-1987	7	3.726	3	Apr-83	Jun-83	4	6.321	5	May-83	Sep-83
	1988-1995	7	2.566	2	Apr-90	May-90	6	7.165	6	May-90	Oct-90
	1996-2003	3	6.087	5	May-00	Sep-00	3	1.343	1	Oct-00	Oct-00
	2004-2011	6	2.615	2	Apr-08	May-08	4	2.271	2	Oct-07	Nov-07
	2012-2018	3	1.265	1	Dec-16	Dec-16	2	1.175	1	Feb-12	Feb-12
	1972-2018	**33**	**6.087**	**5**	**May-00**	**Sep-00**	**25**	**7.393**	**6**	**Mar-79**	**Aug-79**
ÖDEMİŞ (17822)	1972-1979	5	2.619	2	Dec-72	Jan-73	3	6.468	5	May-73	Sep-73
	1980-1987	7	2.381	2	Aug-87	Sep-87	2	7.247	6	Apr-85	Sep-85
	1988-1995	8	1.329	1	Dec-91	Dec-91	8	5.118	4	Oct-89	Jan-90
	1996-2003	5	1.476	1	Apr-01	Apr-01	3	1.445	1	Sep-01	Sep-01
	2004-2011	1	1.037	1	Feb-05	Feb-05	3	6.968	6	Apr-05	Sep-05
	2012-2018	5	4.186	3	Feb-14	Apr-14	6	8.311	7	Apr-14	Oct-14
	1972-2018	**31**	**4.186**	**3**	**Feb-14**	**Apr-14**	**25**	**8.311**	**7**	**Apr-14**	**Oct-14**
SULTANHİSAR (17850)	1972-1979	6	2.651	2	Apr-73	May-73	4	2.250	2	Dec-73	Jan-74
	1980-1987	6	2.765	2	Nov-87	Dec-87	-	-	-	-	-
	1988-1995	11	2.735	2	Feb-89	Mar-89	10	5.092	4	Oct-89	Jan-90
	1996-2003	5	3.672	3	Oct-00	Dec-00	6	3.225	3	Jun-01	Aug-01
	2004-2011	8	2.915	2	Jun-07	Jul-07	2	1.160	1	Nov-07	Nov-07
	2012-2018	4	2.131	2	Jun-14	Jul-14	4	7.502	6	Mar-14	Aug-14
	1972-2018	**40**	**3.672**	**3**	**Oct-00**	**Dec-00**	**26**	**7.502**	**6**	**Mar-14**	**Aug-14**
SELÇUK (17854)	1972-1979	6	2.473	2	Nov-73	Dec-73	1	5.258	4	Oct-73	Jan-74
	1980-1987	7	2.925	2	Nov-86	Dec-86	2	2.621	2	Jan-87	Feb-87
	1988-1995	9	5.078	4	Feb-89	May-89	8	9.214	7	Apr-90	Oct-90
	1996-2003	3	2.857	2	Jun-02	Jul-02	1	1.078	1	Mar-01	Mar-01
	2004-2011	7	2.432	2	Nov-04	Dec-04	2	3.599	3	Dec-06	Feb-07
	2012-2018	3	1.305	1	Dec-15	Dec-15	3	1.353	1	Feb-14	Feb-14
	1972-2018	**35**	**5.078**	**4**	**Feb-89**	**May-89**	**17**	**9.214**	**7**	**Apr-90**	**Oct-90**
NAZİLLİ (17860)	1972-1979	4	2.631	2	Apr-73	May-73	3	2.567	2	Dec-72	Jan-73
	1980-1987	7	3.908	3	Jul-81	Sep-81	2	1.029	1	Mar-86	Mar-86
	1988-1995	7	2.650	2	Feb-89	Mar-89	7	5.124	4	Oct-89	Jan-90
	1996-2003	4	3.978	3	Sep-99	Nov-99	2	9.161	8	Mar-01	Oct-01
	2004-2011	5	2.349	2	Jan-07	Feb-07	3	1.293	1	Apr-05	Apr-05
	2012-2018	5	2.932	2	Oct-16	Nov-16	4	5.455	4	May-14	Aug-14
	1972-2018	**32**	**3.978**	**3**	**Sep-99**	**Nov-99**	**21**	**9.161**	**8**	**Mar-01**	**Oct-01**

Table Ap.5 Annual maximum drought durations and severities for moderate drought conditions for Manisa, İzmir, Kuşadası, Aydın and Salihli Stations (for SPEI-1 and SPEI-3 month).

		Moderate Drought									
Station	**Period**	**SPEI1**					**SPEI3**				
		Total Event	**Max Severity**	**Max Duration**	**Beginning Date**	**End Date**	**Total Event**	**Max Severity**	**Max Duration**	**Beginning Date**	**End Date**
MANİSA (17186)	1972-1979	6	1.435	1	May-77	May-77	3	1.227	1	Mar-72	Mar-72
	1980-1987	12	1.466	1	Mar-83	Mar-83	6	1.384	1	Jun-85	Jun-85
	1988-1995	7	1.458	4	Jul-93	Oct-93	8	3.871	3	Jul-88	Sep-88
	1996-2003	12	2.377	2	May-00	Jun-00	12	4.886	4	Dec-00	Mar-01
	2004-2011	8	3.442	3	Jan-07	Mar-07	12	2.592	2	Jul-08	Aug-08
	2012-2018	7	2.411	2	Sep-12	Oct-12	5	1.343	1	Apr-17	Apr-17
	1972-2018	**52**	**3.442**	**3**	**Jan-07**	**Mar-07**	**46**	**4.886**	**4**	**Dec-00**	**Mar-01**
İZMİR (17220)	1972-1979	7	1.372	1	Jan-74	Jan-74	5	3.691	3	Mar-77	May-77
	1980-1987	6	1.356	6	May-84	Oct-84	6	2.471	2	Nov-86	Dec-86
	1988-1995	8	1.323	8	Aug-89	Mar-90	7	5.880	5	Jun-88	Oct-88
	1996-2003	12	2.477	2	Apr-99	May-99	11	7.218	6	Jul-99	Dec-99
	2004-2011	11	3.712	3	Jan-07	Mar-07	9	3.921	3	May-07	Jul-07
	2012-2018	9	4.037	9	Jan-17	Sep-17	7	1.347	1	Sep-18	Sep-18
	1972-2018	**53**	**4.037**	**9**	**Jan-17**	**Sep-17**	**45**	**7.218**	**6**	**Jul-99**	**Dec-99**
KUŞADASI (17232)	1972-1979	6	1.324	3	Mar-77	May-77	5	2.293	2	Apr-77	May-77
	1980-1987	10	2.502	2	Mar-86	Apr-86	5	1.438	1	Nov-86	Nov-86
	1988-1995	11	1.470	1	Jun-95	Jun-95	12	3.950	3	Dec-87	Feb-88
	1996-2003	10	3.704	3	May-00	Jul-00	10	3.371	3	Jan-01	Mar-01
	2004-2011	15	3.680	5	Nov-06	Mar-07	7	2.294	2	Apr-04	May-04
	2012-2018	8	1.282	10	Oct-15	Jul-16	7	2.561	2	Oct-12	Nov-12
	1972-2018	**60**	**3.704**	**3**	**May-00**	**Jul-00**	**46**	**3.950**	**3**	**Dec-87**	**Feb-88**
AYDIN (17324)	1972-1979	6	1.397	3	Jan-76	Mar-76	6	3.625	3	Mar-72	May-72
	1980-1987	6	2.501	6	Nov-85	Apr-86	2	1.409	1	Jun-85	Jun-85
	1988-1995	9	1.468	1	Nov-91	Nov-91	11	4.824	4	Oct-87	Jan-88
	1996-2003	12	5.290	4	Jul-01	Oct-01	9	2.817	2	Jan-01	Feb-01
	2004-2011	12	4.786	3	Feb-07	Apr-07	6	3.984	3	Oct-04	Dec-04
	2012-2018	10	2.908	2	Aug-12	Sep-12	12	2.055	2	May-18	Jun-18
	1972-2018	**55**	**5.290**	**4**	**Jul-01**	**Oct-01**	**46**	**4.824**	**4**	**Oct-87**	**Jan-88**
SALİHLİ (17792)	1972-1979	4	1.315	1	Jan-74	Jan-74	2	1.095	1	Jan-74	Jan-74
	1980-1987	7	2.725	2	Apr-85	May-85	3	1.475	1	May-86	May-86
	1988-1995	10	1.482	1	Jun-95	Jun-95	8	2.299	2	May-89	Jun-89
	1996-2003	12	2.160	7	Mar-01	Sep-01	10	3.901	3	Aug-00	Oct-00
	2004-2011	14	2.435	2	Feb-08	Mar-08	7	5.459	4	Mar-07	Jun-07
	2012-2018	10	5.121	8	Aug-13	Mar-14	9	6.282	5	Oct-17	Feb-18
	1972-2018	**57**	**5.121**	**8**	**Aug-13**	**Mar-14**	**39**	**6.282**	**5**	**Oct-17**	**Feb-18**

Table Ap.6 Annual maximum drought durations and severities for moderate drought conditions for Seferihisar, Ödemiş, Sultanhisar, Selçuk and Nazilli Stations (for SPEI-1 and SPEI-3 month).

		Moderate Drought									
Station	**Period**	**SPEI1**					**SPEI3**				
		Total Event	**Max Severity**	**Max Duration**	**Beginning Date**	**End Date**	**Total Event**	**Max Severity**	**Max Duration**	**Beginning Date**	**End Date**
SEFERİHİSAR (17820)	1972-1979	7	2.554	3	Jan-77	Mar-77	7	6.494	5	Jan-77	May-77
	1980-1987	7	1.418	1	Dec-85	Dec-85	6	2.480	2	Nov-86	Dec-86
	1988-1995	2	1.381	8	Jun-88	Jan-89	6	2.464	2	Mar-89	Apr-89
	1996-2003	9	1.432	4	Sep-00	Dec-00	9	1.464	1	Jul-00	Jul-00
	2004-2011	15	2.604	10	Jul-09	Apr-10	8	2.625	2	Apr-04	May-04
	2012-2018	12	3.886	3	Jul-17	Sep-17	10	2.402	2	Jul-16	Aug-16
	1972-2018	**52**	**3.886**	**3**	**Jul-17**	**Sep-17**	**46**	**6.494**	**5**	**Jan-77**	**May-77**
ÖDEMİŞ (17822)	1972-1979	6	1.385	1	Mar-72	Mar-72	6	1.379	1	Mar-76	Mar-76
	1980-1987	11	1.434	7	Jun-84	Dec-84	4	1.467	1	Nov-84	Nov-84
	1988-1995	8	1.468	1	Jan-88	Jan-88	8	2.781	2	Jun-88	Jul-88
	1996-2003	11	2.317	2	Oct-99	Nov-99	8	2.384	2	Aug-01	Sep-01
	2004-2011	13	1.459	3	Jan-04	Mar-04	8	2.436	2	Jul-09	Aug-09
	2012-2018	11	2.689	2	Aug-12	Sep-12	8	3.701	3	Apr-18	Jun-18
	1972-2018	**60**	**2.689**	**2**	**Aug-12**	**Sep-12**	**42**	**3.701**	**3**	**Apr-18**	**Jun-18**
SULTANHİSAR (17850)	1972-1979	5	1.493	3	Mar-77	May-77	4	2.582	2	Dec-73	Jan-74
	1980-1987	9	2.373	7	Oct-85	Apr-86	3	1.320	1	Dec-84	Dec-84
	1988-1995	10	2.757	9	Jun-88	Feb-89	9	5.643	5	Oct-87	Feb-88
	1996-2003	14	3.858	3	Jun-01	Aug-01	11	5.073	4	Jun-00	Sep-00
	2004-2011	12	2.482	7	Aug-07	Feb-08	9	2.619	2	Jun-07	Jul-07
	2012-2018	10	1.487	1	Aug-12	Aug-12	7	2.694	2	Jul-16	Aug-16
	1972-2018	**60**	**3.858**	**3**	**Jun-01**	**Aug-01**	**43**	**5.643**	**5**	**Oct-87**	**Feb-88**
SELÇUK (17854)	1972-1979	5	1.312	1	Nov-72	Nov-72	3	2.327	2	Nov-73	Dec-73
	1980-1987	9	2.368	2	Mar-86	Apr-86	5	2.538	2	Apr-86	May-86
	1988-1995	8	2.949	9	Jun-88	Feb-89	6	4.306	3	Feb-89	Apr-89
	1996-2003	6	2.558	5	Feb-00	Jun-00	9	3.789	3	Jun-02	Aug-02
	2004-2011	14	3.934	9	Oct-05	Jun-06	10	2.791	2	Nov-04	Dec-04
	2012-2018	8	2.259	2	Jul-17	Aug-17	11	3.781	3	Aug-17	Oct-17
	1972-2018	**50**	**3.934**	**9**	**Oct-05**	**Jun-06**	**44**	**4.306**	**3**	**Feb-89**	**Apr-89**
NAZİLLİ (17860)	1972-1979	6	1.244	1	May-73	May-73	7	3.648	3	Nov-73	Jan-74
	1980-1987	7	1.355	6	Nov-84	Apr-85	6	2.742	2	May-85	Jun-85
	1988-1995	10	2.718	9	Jun-88	Feb-89	7	4.964	4	Nov-87	Feb-88
	1996-2003	14	1.395	5	Sep-95	Jan-96	8	3.792	3	Jan-01	Mar-01
	2004-2011	13	2.561	2	Jan-08	Feb-08	13	2.853	2	Jul-09	Aug-09
	2012-2018	8	4.158	3	Aug-12	Oct-12	8	3.531	3	Sep-14	Nov-14
	1972-2018	**58**	**4.158**	**3**	**Aug-12**	**Oct-12**	**49**	**4.964**	**4**	**Nov-87**	**Feb-88**

Table Ap.7 Annual maximum drought durations and severities for moderate drought conditions for Manisa, İzmir, Kuşadası, Aydın and Salihli Stations (for SPI-6 and SPI-12 month).

		Moderate Drought									
Station	**Period**	**SPEI6**					**SPEI12**				
		Total Event	**Max Severity**	**Max Duration**	**Beginning Date**	**End Date**	**Total Event**	**Max Severity**	**Max Duration**	**Beginning Date**	**End Date**
MANİSA (17186)	1972-1979	2	2.248	2	Jun-77	Jul-77	1	2.340	2	Dec-72	Jan-73
	1980-1987	4	3.447	3	Mar-85	May-85	2	5.242	4	Apr-85	Jul-85
	1988-1995	11	3.961	3	Sep-94	Nov-94	8	6.301	5	Dec-90	Apr-91
	1996-2003	9	6.426	5	Apr-01	Aug-01	4	3.791	3	Dec-00	Feb-01
	2004-2011	4	4.795	4	Sep-08	Dec-08	7	2.205	2	Apr-04	May-04
	2012-2018	6	4.555	4	Nov-17	Feb-18	2	4.090	3	Feb-18	Apr-18
	1972-2018	**36**	**6.426**	**5**	**Apr-01**	**Aug-01**	**24**	**6.301**	**5**	**Dec-90**	**Apr-91**
İZMİR (17220)	1972-1979	4	6.131	5	Apr-77	Aug-77	3	2.305	2	Jan-74	Feb-74
	1980-1987	3	3.219	3	Apr-83	Jun-83	2	3.492	3	Jul-85	Sep-85
	1988-1995	10	4.771	4	Mar-89	Jun-89	9	4.527	4	Jan-91	Apr-91
	1996-2003	9	4.041	3	Mar-01	May-01	3	8.329	6	Apr-00	Sep-00
	2004-2011	6	5.161	4	Oct-04	Jan-05	5	8.723	7	Apr-04	Oct-04
	2012-2018	6	5.067	4	Apr-18	Jul-18	5	2.750	2	Mar-18	Apr-18
	1972-2018	**38**	**6.131**	**5**	**Apr-77**	**Aug-77**	**27**	**8.723**	**7**	**Apr-04**	**Oct-04**
KUŞADASI (17232)	1972-1979	5	5.750	5	Jan-73	May-73	1	4.800	4	Oct-73	Jan-74
	1980-1987	4	6.288	5	Nov-86	Mar-87	4	2.655	2	Nov-85	Dec-85
	1988-1995	14	4.653	4	Dec-93	Mar-94	11	9.621	8	Mar-94	Oct-94
	1996-2003	5	3.882	3	Nov-99	Jan-00	4	9.279	8	Feb-00	Sep-00
	2004-2011	6	2.439	2	Jul-04	Aug-04	3	2.515	2	Jan-07	Feb-07
	2012-2018	2	2.835	2	Jul-16	Aug-16	4	10.133	8	Oct-16	May-17
	1972-2018	**36**	**6.288**	**5**	**Nov-86**	**Mar-87**	**27**	**10.133**	**8**	**Oct-16**	**May-17**
AYDIN (17324)	1972-1979	5	3.441	3	Mar-73	May-73	3	2.603	2	Dec-72	Jan-73
	1980-1987	1	1.106	1	Sep-85	Sep-85	-	-	-	-	-
	1988-1995	12	6.431	5	Oct-87	Feb-88	12	7.019	6	May-90	Oct-90
	1996-2003	5	3.949	3	Dec-00	Feb-01	5	4.446	4	Apr-00	Jul-00
	2004-2011	5	5.286	4	Aug-08	Nov-08	3	1.271	1	Nov-08	Nov-08
	2012-2018	5	3.327	3	Feb-14	Apr-14	4	6.458	5	Jan-17	May-17
	1972-2018	**33**	**6.431**	**5**	**Oct-87**	**Feb-88**	**27**	**7.019**	**6**	**May-90**	**Oct-90**
SALİHLİ (17792)	1972-1979	2	1.360	1	May-73	May-73	-	-	-	-	-
	1980-1987	3	2.199	2	Jul-85	Aug-85	1	3.615	3	Jul-85	Sep-85
	1988-1995	7	2.484	2	May-90	Jun-90	4	3.766	3	Apr-89	Jun-89
	1996-2003	8	5.154	4	Oct-99	Jan-00	3	4.580	4	Dec-99	Mar-00
	2004-2011	3	2.979	2	Sep-08	Oct-08	6	4.791	4	Mar-05	Jun-05
	2012-2018	10	3.541	3	Apr-16	Jun-16	8	11.681	9	Feb-14	Oct-14
	1972-2018	**33**	**5.154**	**4**	**Oct-99**	**Jan-00**	**22**	**11.681**	**9**	**Feb-14**	**Oct-14**

Table Ap.8 Annual maximum drought durations and severities for moderate drought conditions for Seferihisar, Ödemiş, Sultanhisar, Selçuk and Nazilli Stations (for SPEI-6 and SPEI-12 month).

		Moderate Drought									
Station	**Period**	**SPEI6**					**SPEI12**				
		Total Event	**Max Severity**	**Max Duration**	**Beginning Date**	**End Date**	**Total Event**	**Max Severity**	**Max Duration**	**Beginning Date**	**End Date**
SEFERİHİSAR (17820)	1972-1979	7	2.515	2	Jan-73	Feb-73	2	3.608	3	Oct-77	Dec-77
	1980-1987	4	3.295	3	Apr-83	Jun-83	1	2.516	2	Jan-87	Feb-87
	1988-1995	5	2.724	2	Apr-92	May-92	5	5.154	4	Sep-92	Dec-92
	1996-2003	3	5.119	4	May-00	Aug-00	4	2.767	2	Jan-01	Feb-01
	2004-2011	7	3.916	3	Oct-04	Dec-04	6	3.720	3	Jun-07	Aug-07
	2012-2018	8	2.265	2	Oct-17	Nov-17	8	3.742	3	Mar-18	May-18
	1972-2018	**34**	**5.119**	**4**	**May-00**	**Aug-00**	**26**	**5.154**	**4**	**Sep-92**	**Dec-92**
ÖDEMİŞ (17822)	1972-1979	2	2.449	2	Apr-73	May-73	2	2.628	2	Oct-73	Nov-73
	1980-1987	3	1.385	1	Nov-86	Nov-86	2	2.289	2	Aug-85	Sep-85
	1988-1995	7	2.651	2	May-92	Jun-92	11	6.609	5	May-89	Sep-89
	1996-2003	7	2.950	2	Nov-00	Dec-00	3	2.462	2	Jan-01	Feb-01
	2004-2011	8	4.210	3	Aug-08	Oct-08	7	7.702	6	Apr-05	Sep-05
	2012-2018	8	5.496	4	Jan-14	Apr-14	6	9.939	9	Apr-18	Dec-18
	1972-2018	**35**	**5.496**	**4**	**Jan-14**	**Apr-14**	**31**	**9.939**	**9**	**Apr-18**	**Dec-18**
SULTANHİSAR (17850)	1972-1979	3	2.223	2	Apr-73	May-73	1	2.113	2	Oct-73	Nov-73
	1980-1987	2	3.703	3	Oct-87	Dec-87	-	-	-	-	-
	1988-1995	10	3.190	3	Jan-94	Mar-94	9	11.482	8	May-92	Dec-92
	1996-2003	9	4.424	3	Sep-00	Nov-00	5	3.418	3	Jul-00	Sep-00
	2004-2011	7	3.864	3	Dec-06	Feb-07	5	3.194	3	Mar-05	May-05
	2012-2018	8	2.515	2	Aug-12	Sep-12	6	9.660	7	Feb-14	Aug-14
	1972-2018	**39**	**4.424**	**3**	**Sep-00**	**Nov-00**	**26**	**11.482**	**8**	**May-92**	**Dec-92**
SELÇUK (17854)	1972-1979	3	1.244	1	Apr-73	Apr-73	1	1.044	1	Oct-73	Oct-73
	1980-1987	-	-	-	-	-	1	1.213	1	Feb-87	Feb-87
	1988-1995	9	7.471	6	Jan-90	Jun-90	10	5.082	4	Mar-89	Jun-89
	1996-2003	6	3.700	3	Mar-01	May-01	3	7.310	6	Apr-01	Sep-01
	2004-2011	13	2.835	2	Nov-10	Dec-10	5	9.057	7	May-08	Nov-08
	2012-2018	9	6.275	5	Mar-18	Jul-18	6	12.993	10	Feb-17	Nov-17
	1972-2018	**40**	**7.471**	**6**	**Jan-90**	**Jun-90**	**26**	**12.993**	**10**	**Feb-17**	**Nov-17**
NAZİLLİ (17860)	1972-1979	2	2.390	2	Apr-73	May-73	2	2.421	2	Oct-73	Nov-73
	1980-1987	4	1.359	1	Dec-84	Dec-84	-	-	-	-	-
	1988-1995	8	2.758	2	May-90	Jun-90	7	4.477	4	Aug-92	Nov-92
	1996-2003	7	8.678	7	Aug-99	Feb-00	4	10.016	7	Mar-01	Sep-01
	2004-2011	9	3.922	3	Oct-04	Dec-04	5	10.987	9	Mar-08	Nov-08
	2012-2018	9	2.292	2	Apr-16	May-16	4	4.317	3	Jun-14	Aug-14
	1972-2018	**39**	**8.678**	**7**	**Aug-99**	**Feb-00**	**22**	**10.987**	**9**	**Mar-08**	**Nov-08**

Table Ap.9 Annual maximum drought durations and severities for severe drought conditions for Manisa, İzmir, Kuşadası, Aydın and Salihli Stations (for SPI-1 and SPI-3 month).

		Severe Drought									
Station	**Period**	**SPI1**					**SPI3**				
		Total Event	**Max Severity**	**Max Duration**	**Beginning Date**	**End Date**	**Total Event**	**Max Severity**	**Max Duration**	**Beginning Date**	**End Date**
MANİSA (17186)	1972-1979	1	1.604	1	Jan-74	Jan-74	1	1.603	1	Jul-77	Jul-77
	1980-1987	4	1.885	1	Nov-86	Nov-86	4	1.948	1	Nov-86	Nov-86
	1988-1995	6	1.958	1	Nov-90	Nov-90	9	3.522	2	Jul-88	Aug-88
	1996-2003	6	3.311	2	May-00	Jun-00	2	1.922	1	Jul-02	Jul-02
	2004-2011	5	1.917	1	Feb-08	Feb-08	5	3.523	2	Feb-08	Mar-08
	2012-2018	5	1.962	1	Nov-14	Nov-14	2	1.955	1	Feb-14	Feb-14
	1972-2018	**27**	**3.311**	**2**	**May-00**	**Jun-00**	**23**	**3.523**	**2**	**Feb-08**	**Mar-08**
İZMİR (17220)	1972-1979	3	1.760	1	Jan-74	Jan-74	4	3.577	2	Dec-72	Jan-73
	1980-1987	5	1.848	1	Dec-85	Dec-85	3	1.942	1	Oct-84	Oct-84
	1988-1995	3	3.878	2	Jan-89	Feb-89	6	1.955	1	Jan-92	Jan-92
	1996-2003	3	1.848	1	Nov-03	Nov-03	2	1.821	1	Jun-99	Jun-99
	2004-2011	2	1.657	1	Mar-10	Mar-10	4	1.898	1	Feb-08	Feb-08
	2012-2018	3	1.856	1	Dec-16	Dec-16	2	1.687	1	Feb-14	Feb-14
	1972-2018	**19**	**3.878**	**2**	**Jan-89**	**Feb-89**	**21**	**3.577**	**2**	**Dec-72**	**Jan-73**
KUŞADASI (17232)	1972-1979	2	1.896	1	Dec-72	Dec-72	3	1.767	1	Sep-79	Sep-79
	1980-1987	1	1.958	1	Apr-85	Apr-85	5	3.817	2	Nov-86	Dec-86
	1988-1995	2	3.276	2	Jan-89	Feb-89	5	3.691	2	Jan-90	Feb-90
	1996-2003	3	1.768	1	Mar-01	Mar-01	4	1.767	1	Sep-79	Sep-79
	2004-2011	3	1.990	1	Dec-06	Dec-06	4	1.767	1	Sep-79	Sep-79
	2012-2018	1	1.966	1	Dec-13	Dec-13	4	1.767	1	Sep-79	Sep-79
	1972-2018	**12**	**3.276**	**2**	**Jan-89**	**Feb-89**	**25**	**3.817**	**2**	**Nov-86**	**Dec-86**
AYDIN (17324)	1972-1979	1	1.970	1	Dec-72	Dec-72	4	1.808	1	Jan-73	Jan-73
	1980-1987	3	1.803	1	Oct-87	Oct-87	4	1.692	1	Nov-87	Nov-87
	1988-1995	4	1.895	1	Nov-90	Nov-90	5	1.890	1	Jan-92	Jan-92
	1996-2003	2	1.978	1	Oct-01	Oct-01	2	1.937	1	Oct-01	Oct-01
	2004-2011	1	1.517	1	Feb-08	Feb-08	6	1.930	1	Jan-07	Jan-07
	2012-2018	2	1.900	1	Dec-13	Dec-13	1	1.688	1	Feb-14	Feb-14
	1972-2018	**13**	**1.978**	**1**	**Oct-01**	**Oct-01**	**22**	**1.937**	**1**	**Oct-01**	**Oct-01**
SALİHLİ (17792)	1972-1979	1	1.746	1	Jan-74	Jan-74	1	1.716	1	Feb-73	Feb-73
	1980-1987	3	1.973	1	Nov-86	Nov-86	3	3.648	2	May-85	Jun-85
	1988-1995	4	1.990	1	Jan-89	Jan-89	6	1.942	1	Mar-90	Mar-90
	1996-2003	3	1.722	1	Jun-00	Jun-00	3	3.551	2	Aug-03	Sep-03
	2004-2011	2	1.742	1	Feb-08	Feb-08	5	7.334	4	Mar-08	Jun-08
	2012-2018	1	1.722	1	Jun-00	Jun-00	2	1.921	1	Mar-14	Mar-14
	1972-2018	**14**	**1.990**	**1**	**Jan-89**	**Jan-89**	**20**	**7.334**	**4**	**Mar-08**	**Jun-08**

Table Ap.10 Annual maximum drought durations and severities for severe drought conditions for Seferihisar, Ödemiş, Sultanhisar, Selçuk and Nazilli Stations (for SPI-1 and SPI-3 month).

		Severe Drought									
Station	**Period**	**SPI1**					**SPI3**				
		Total Event	**Max Severity**	**Max Duration**	**Beginning Date**	**End Date**	**Total Event**	**Max Severity**	**Max Duration**	**Beginning Date**	**End Date**
SEFERİHİSAR (17820)	1972-1979	6	1.749	1	Mar-77	Mar-77	4	3.709	2	Apr-77	May-77
	1980-1987	5	1.695	1	Nov-86	Nov-86	8	3.466	2	May-83	Jun-83
	1988-1995	4	1.952	1	Nov-90	Nov-90	2	3.565	2	Jan-92	Feb-92
	1996-2003	4	1.973	1	Nov-03	Nov-03	3	5.286	3	Nov-99	Jan-00
	2004-2011	5	1.950	1	Dec-06	Dec-06	6	1.884	1	Mar-07	Mar-07
	2012-2018	2	1.934	1	Dec-16	Dec-16	1	1.788	1	Dec-15	Dec-15
	1972-2018	**26**	**1.973**	**1**	**Nov-03**	**Nov-03**	**24**	**5.286**	**3**	**Nov-99**	**Jan-00**
ÖDEMİŞ (17822)	1972-1979	4	1.827	1	May-73	May-73	2	1.640	1	Mar-76	Mar-76
	1980-1987	6	1.947	1	Mar-83	Mar-83	4	1.849	1	May-83	May-83
	1988-1995	3	1.982	1	May-90	May-90	2	1.811	1	Mar-90	Mar-90
	1996-2003	4	1.928	1	Oct-01	Oct-01	2	1.888	1	May-99	May-99
	2004-2011	5	1.939	1	Mar-07	Mar-07	4	5.280	3	Mar-07	May-07
	2012-2018	1	1.754	1	Feb-17	Feb-17	2	1.857	1	Dec-16	Dec-16
	1972-2018	**23**	**1.982**	**1**	**May-90**	**May-90**	**16**	**5.280**	**3**	**Mar-07**	**May-07**
SULTANHİSAR (17850)	1972-1979	2	1.997	1	Mar-76	Mar-76	1	1.685	1	Aug-78	Aug-78
	1980-1987	5	1.722	1	Oct-84	Oct-84	8	1.878	1	May-86	May-86
	1988-1995	3	3.367	2	Jan-89	Feb-89	7	3.913	2	Mar-89	Apr-89
	1996-2003	4	1.902	1	May-78	May-78	5	1.757	1	May-99	May-99
	2004-2011	3	1.982	1	Dec-06	Dec-06	5	3.348	2	Jan-07	Feb-07
	2012-2018	5	1.961	1	Dec-16	Dec-16	1	1.591	1	Aug-12	Aug-12
	1972-2018	**22**	**3.367**	**2**	**Jan-89**	**Feb-89**	**27**	**3.913**	**2**	**Mar-89**	**Apr-89**
SELÇUK (17854)	1972-1979	1	1.970	1	Dec-72	Dec-72	2	1.813	1	Jul-78	Jul-78
	1980-1987	4	1.762	1	Apr-81	Apr-81	7	1.937	1	Oct-87	Oct-87
	1988-1995	3	1.949	1	Feb-89	Feb-89	5	4.795	3	Feb-89	Apr-89
	1996-2003	2	1.748	1	Feb-97	Feb-97	2	1.974	1	Jul-00	Jul-00
	2004-2011	6	1.891	1	May-08	May-08	2	1.998	1	Jan-07	Jan-07
	2012-2018	1	1.831	1	Feb-14	Feb-14	3	1.738	1	Feb-14	Feb-14
	1972-2018	**17**	**1.970**	**1**	**Dec-72**	**Dec-72**	**21**	**4.795**	**3**	**Feb-89**	**Apr-89**
NAZİLLİ (17860)	1972-1979	1	1.720	1	Nov-78	Nov-78	2	3.218	2	Jul-78	Aug-78
	1980-1987	4	1.722	1	Oct-84	Oct-84	6	2.000	1	Jun-85	Jun-85
	1988-1995	2	3.226	2	Jan-89	Feb-89	5	5.484	3	Jun-88	Aug-88
	1996-2003	3	1.704	1	May-99	May-99	2	1.731	1	Jan-96	Jan-96
	2004-2011	3	1.875	1	May-08	May-08	6	7.228	4	Jul-04	Oct-04
	2012-2018	6	1.939	1	Apr-16	Apr-16	2	1.945	1	Jun-16	Jun-16
	1972-2018	**19**	**3.226**	**2**	**Jan-89**	**Feb-89**	**23**	**7.228**	**4**	**Jul-04**	**Oct-04**

Table Ap.11 Annual maximum drought durations and severities for severe drought conditions for Manisa, İzmir, Kuşadası, Aydın and Salihli Stations (for SPI-6 and SPI-12 month).

		Severe Drought									
Station	**Period**	**SPI6**					**SPI12**				
		Total Event	**Max Severity**	**Max Duration**	**Beginning Date**	**End Date**	**Total Event**	**Max Severity**	**Max Duration**	**Beginning Date**	**End Date**
MANİSA (17186)	1972-1979	-	-	-	-	-	1	1.692	1	Dec-72	Dec-72
	1980-1987	3	3.485	2	Oct-84	Nov-84	2	6.728	4	Jun-85	Sep-85
	1988-1995	8	3.651	2	Apr-92	May-92	5	9.709	5	May-89	Sep-89
	1996-2003	-	-	-	-	-	1	3.420	2	Mar-01	Apr-01
	2004-2011	7	3.547	2	Jul-07	Aug-07	3	4.863	3	Dec-07	Feb-08
	2012-2018	-	-	-	-	-	1	1.664	1	Jan-18	Jan-18
	1972-2018	**18**	**3.651**	**2**	**Apr-92**	**May-92**	**13**	**9.709**	**5**	**May-89**	**Sep-89**
İZMİR (17220)	1972-1979	3	3.260	2	Jun-77	Jul-77	2	1.649	1	Jan-73	Jan-73
	1980-1987	4	1.728	1	Aug-83	Aug-83	1	1.608	1	Apr-85	Apr-85
	1988-1995	4	3.716	2	Sep-88	Oct-88	6	5.198	3	Mar-89	May-89
	1996-2003	1	1.896	1	Sep-99	Sep-99	-	-	-	-	-
	2004-2011	3	5.351	3	May-08	Jul-08	2	3.157	2	Nov-08	Dec-08
	2012-2018	1	1.572	1	Dec-16	Dec-16	-	-	-	-	-
	1972-2018	**16**	**5.351**	**3**	**May-08**	**Jul-08**	**11**	**5.198**	**3**	**Mar-89**	**May-89**
KUŞADASI (17232)	1972-1979	-	-	-	-	-	2	1.667	1	Jan-74	Jan-74
	1980-1987	8	3.542	2	Nov-86	Dec-86	2	1.872	1	Feb-87	Feb-87
	1988-1995	8	4.976	3	Jan-90	Mar-90	4	14.813	8	May-92	Dec-92
	1996-2003	1	1.563	1	Jul-02	Jul-02	-	-	-	-	-
	2004-2011	4	3.759	2	Jun-08	Jul-08	3	6.842	4	May-07	Aug-07
	2012-2018	1	1.589	1	Oct-16	Oct-16	-	-	-	-	-
	1972-2018	**22**	**4.976**	**3**	**Jan-90**	**Mar-90**	**11**	**14.813**	**8**	**May-92**	**Dec-92**
AYDIN (17324)	1972-1979	2	1.540	1	Jun-72	Jun-72	1	1.992	1	Dec-72	Dec-72
	1980-1987	2	1.954	1	Nov-87	Nov-87	-	-	-	-	-
	1988-1995	7	3.682	2	May-90	Jun-90	8	5.157	3	Dec-89	Feb-90
	1996-2003	3	3.432	2	Oct-99	Nov-99	2	1.739	1	Feb-00	Feb-00
	2004-2011	4	1.829	1	Aug-07	Aug-07	2	1.841	1	Oct-07	Oct-07
	2012-2018	-	-	-	-	-	-	-	-	-	-
	1972-2018	**18**	**3.682**	**2**	**May-90**	**Jun-90**	**13**	**5.157**	**3**	**Dec-89**	**Feb-90**
SALİHLİ (17792)	1972-1979	2	1.897	1	May-73	May-73	1	3.671	2	Oct-73	Nov-73
	1980-1987	6	5.451	3	Jul-85	Sep-85	2	4.879	3	Apr-85	Jun-85
	1988-1995	5	1.841	1	Sep-89	Sep-89	5	11.013	6	May-92	Oct-92
	1996-2003	-	-	-	-	-	2	6.380	4	Jul-01	Oct-01
	2004-2011	6	5.540	3	Jun-07	Aug-07	4	3.590	2	Oct-07	Nov-07
	2012-2018	2	3.478	2	Mar-14	Apr-14	1	1.702	1	Jan-18	Jan-18
	1972-2018	**21**	**5.540**	**3**	**Jun-07**	**Aug-07**	**15**	**11.013**	**6**	**May-92**	**Oct-92**

Table Ap.12 Annual maximum drought durations and severities for severe drought conditions for Seferihisar, Ödemiş, Sultanhisar, Selçuk and Nazilli Stations (for SPI-6 and SPI-12 month).

		Severe Drought									
Station	**Period**	**SPI6**					**SPI12**				
		Total Event	**Max Severity**	**Max Duration**	**Beginning Date**	**End Date**	**Total Event**	**Max Severity**	**Max Duration**	**Beginning Date**	**End Date**
SEFERİHİSAR (17820)	1972-1979	6	4.985	3	Apr-77	Jun-77	4	3.581	2	Sep-79	Oct-79
	1980-1987	5	3.761	2	Jul-81	Aug-81	1	1.575	1	Oct-83	Oct-83
	1988-1995	2	3.692	2	Apr-92	May-92	2	5.513	3	Oct-92	Dec-92
	1996-2003	2	3.813	2	Nov-99	Dec-99	2	1.698	1	Feb-00	Feb-00
	2004-2011	3	3.737	2	Jul-04	Aug-04	2	3.491	2	Nov-08	Dec-08
	2012-2018	1	1.879	1	Dec-15	Dec-15	-	-	-	-	-
	1972-2018	**19**	**4.985**	**3**	**Apr-77**	**Jun-77**	**11**	**5.513**	**3**	**Oct-92**	**Dec-92**
ÖDEMİŞ (17822)	1972-1979	2	1.585	1	Aug-73	Aug-73	2	3.658	2	Oct-73	Nov-73
	1980-1987	4	1.812	1	Sep-81	Sep-81	-	-	-	-	-
	1988-1995	6	1.933	1	Nov-91	Nov-91	7	5.179	3	Oct-92	Dec-92
	1996-2003	3	3.573	2	Feb-01	Mar-01	3	9.735	6	Mar-01	Aug-01
	2004-2011	6	5.473	3	Nov-04	Jan-05	5	3.321	2	Jul-07	Aug-07
	2012-2018	1	1.865	1	May-14	May-14	2	1.933	1	Nov-14	Nov-14
	1972-2018	**22**	**5.473**	**3**	**Nov-04**	**Jan-05**	**19**	**9.735**	**6**	**Mar-01**	**Aug-01**
SULTANHİSAR (17850)	1972-1979	1	1.666	1	Jan-74	Jan-74	1	3.037	2	Oct-73	Nov-73
	1980-1987	3	1.922	1	Sep-85	Sep-85	-	-	-	-	-
	1988-1995	7	1.987	1	May-90	May-90	6	6.654	4	Mar-89	Jun-89
	1996-2003	3	1.904	1	Jan-96	Jan-96	1	1.871	1	Mar-01	Mar-01
	2004-2011	3	1.733	1	Aug-07	Aug-07	3	14.492	8	Mar-07	Oct-07
	2012-2018	3	3.020	2	Feb-14	Mar-14	2	1.782	1	Nov-14	Nov-14
	1972-2018	**20**	**3.020**	**2**	**Feb-14**	**Mar-14**	**13**	**14.492**	**8**	**Mar-07**	**Oct-07**
SELÇUK (17854)	1972-1979	1	1.739	1	Jan-74	Jan-74	-	-	-	-	-
	1980-1987	3	1.855	1	Sep-85	Sep-85	-	-	-	-	-
	1988-1995	7	3.451	2	Apr-92	May-92	6	6.498	4	Jan-92	Apr-92
	1996-2003	-	-	-	-	-	-	-	-	-	-
	2004-2011	3	3.491	2	Feb-07	Mar-07	3	12.838	7	May-07	Nov-07
	2012-2018	-	-	-	-	-	-	-	-	-	-
	1972-2018	**14**	**3.491**	**2**	**Feb-07**	**Mar-07**	**9**	**12.838**	**7**	**May-07**	**Nov-07**
NAZİLLİ (17860)	1972-1979	1	1.664	1	Jan-74	Jan-74	1	1.501	1	Oct-73	Oct-73
	1980-1987	2	1.758	1	Dec-84	Dec-84	-	-	-	-	-
	1988-1995	4	3.426	2	May-90	Jun-90	7	9.650	5	May-89	Sep-89
	1996-2003	2	1.775	1	Jan-96	Jan-96	1	1.507	1	Jan-96	Jan-96
	2004-2011	6	3.323	2	Jul-11	Aug-11	2	1.912	1	Feb-05	Feb-05
	2012-2018	2	7.153	4	Feb-14	May-14	5	1.957	1	Nov-14	Nov-14
	1972-2018	**17**	**7.153**	**4**	**Feb-14**	**May-14**	**16**	**9.650**	**5**	**May-89**	**Sep-89**

Table Ap.13 Annual maximum drought durations and severities for severe drought conditions for Manisa, İzmir, Kuşadası, Aydın and Salihli Stations (for SPEI-1 and SPEI-3 month).

		Severe Drought									
Station	**Period**	**SPEI1**					**SPEI3**				
		Total Event	**Max Severity**	**Max Duration**	**Beginning Date**	**End Date**	**Total Event**	**Max Severity**	**Max Duration**	**Beginning Date**	**End Date**
MANİSA (17186)	1972-1979	1	1.846	1	Dec-72	Dec-72	-	-	-	-	-
	1980-1987	2	1.644	1	May-84	May-84	1	1.785	1	Nov-84	Nov-84
	1988-1995	7	3.088	2	Jan-89	Feb-89	10	1.898	1	Sep-94	Sep-94
	1996-2003	5	3.264	2	May-03	Jun-03	3	1.692	1	Jul-00	Jul-00
	2004-2011	6	1.664	1	Dec-06	Dec-06	7	4.835	3	Mar-07	May-07
	2012-2018	7	1.934	1	Dec-15	Dec-15	3	5.412	3	Aug-12	Oct-12
	1972-2018	**28**	**3.264**	**2**	**May-03**	**Jun-03**	**24**	**5.412**	**3**	**Aug-12**	**Oct-12**
İZMİR (17220)	1972-1979	2	1.670	1	Dec-72	Dec-72	2	3.227	2	Nov-73	Dec-73
	1980-1987	3	1.581	1	Dec-85	Dec-85	1	1.604	1	Dec-84	Dec-84
	1988-1995	6	3.054	2	Jan-89	Feb-89	6	3.338	2	Jan-92	Feb-92
	1996-2003	3	1.828	1	Mar-01	Mar-01	3	1.871	1	Jun-99	Jun-99
	2004-2011	6	1.997	1	Jun-07	Jun-07	6	3.664	2	Aug-07	Sep-07
	2012-2018	5	1.876	1	Jun-16	Jun-16	6	6.949	4	Aug-12	Nov-12
	1972-2018	**25**	**3.054**	**2**	**Jan-89**	**Feb-89**	**24**	**6.949**	**4**	**Aug-12**	**Nov-12**
KUŞADASI (17232)	1972-1979	1	1.619	1	Dec-72	Dec-72	3	3.386	2	Dec-73	Jan-74
	1980-1987	2	1.931	1	Nov-80	Nov-80	5	3.543	2	Oct-80	Nov-80
	1988-1995	9	1.907	1	Apr-89	Apr-89	4	4.981	3	Jan-90	Mar-90
	1996-2003	1	1.500	1	Jul-01	Jul-01	3	1.913	1	Jul-99	Jul-99
	2004-2011	3	1.765	1	Jun-08	Jun-08	7	3.714	2	Aug-07	Sep-07
	2012-2018	7	3.377	2	Jun-12	Jul-12	5	3.328	2	Jul-16	Aug-16
	1972-2018	**23**	**3.377**	**2**	**Jun-12**	**Jul-12**	**27**	**4.981**	**3**	**Jan-90**	**Mar-90**
AYDIN (17324)	1972-1979	3	1.596	1	May-73	May-73	1	1.544	1	Jan-73	Jan-73
	1980-1987	1	1.576	1	Oct-81	Oct-81	1	1.778	1	May-86	May-86
	1988-1995	7	1.969	1	Apr-89	Apr-89	6	4.666	3	Jan-92	Mar-92
	1996-2003	2	1.793	1	Mar-01	Mar-01	5	5.200	3	May-99	Jul-99
	2004-2011	8	1.890	1	Jul-07	Jul-07	7	5.311	3	Mar-07	May-07
	2012-2018	9	1.969	1	Jul-12	Jul-12	5	5.598	3	Sep-12	Nov-12
	1972-2018	**30**	**1.969**	**1**	**Jul-12**	**Jul-12**	**25**	**5.598**	**3**	**Sep-12**	**Nov-12**
SALİHLİ (17792)	1972-1979	2	1.698	1	Dec-72	Dec-72	1	1.504	1	Feb-73	Feb-73
	1980-1987	1	1.798	1	May-84	May-84	2	3.184	2	May-85	Jun-85
	1988-1995	3	3.135	2	Jan-89	Feb-89	1	1.639	1	Mar-89	Mar-89
	1996-2003	6	1.801	1	Oct-01	Oct-01	5	3.545	2	Nov-00	Dec-00
	2004-2011	5	1.910	1	Aug-07	Aug-07	5	10.213	6	Mar-08	Aug-08
	2012-2018	8	1.943	1	Sep-17	Sep-17	6	3.709	2	Sep-12	Oct-12
	1972-2018	**25**	**3.135**	**2**	**Jan-89**	**Feb-89**	**20**	**10.213**	**6**	**Mar-08**	**Aug-08**

Table Ap.14 Annual maximum drought durations and severities for severe drought conditions for Seferihisar, Ödemiş, Sultanhisar, Selçuk and Nazilli Stations (for SPEI-1 and SPEI-3 month).

		Severe Drought									
Station	**Period**	**SPEI1**					**SPEI3**				
		Total Event	**Max Severity**	**Max Duration**	**Beginning Date**	**End Date**	**Total Event**	**Max Severity**	**Max Duration**	**Beginning Date**	**End Date**
SEFERİHİSAR (17820)	1972-1979	2	1.579	1	Dec-72	Dec-72	3	1.929	1	Jan-73	Jan-73
	1980-1987	-	-	-	-	-	-	-	-	-	-
	1988-1995	7	1.845	1	Apr-89	Apr-89	2	3.032	2	Feb-92	Mar-92
	1996-2003	6	3.027	2	Jul-01	Aug-01	5	5.403	3	Nov-99	Jan-00
	2004-2011	7	3.172	2	Jul-07	Aug-07	9	3.646	2	Mar-07	Apr-07
	2012-2018	7	1.824	1	Sep-18	Sep-18	4	4.689	3	Jul-17	Sep-17
	1972-2018	**29**	**3.172**	**2**	**Jul-07**	**Aug-07**	**23**	**5.403**	**3**	**Nov-99**	**Jan-00**
ÖDEMİŞ (17822)	1972-1979	2	1.703	1	Dec-72	Dec-72	1	1.787	1	Jan-73	Jan-73
	1980-1987	2	1.840	1	Oct-81	Oct-81	3	1.849	1	Dec-84	Dec-84
	1988-1995	5	1.979	1	Jul-88	Jul-88	4	4.815	3	Jan-92	Mar-92
	1996-2003	3	1.887	1	Mar-01	Mar-01	5	5.414	3	May-99	Jul-99
	2004-2011	8	3.470	2	Aug-10	Sep-10	5	8.868	5	Jan-07	May-07
	2012-2018	7	3.802	2	Jun-12	Jul-12	5	3.881	2	Aug-12	Sep-12
	1972-2018	**27**	**3.802**	**2**	**Jun-12**	**Jul-12**	**23**	**8.868**	**5**	**Jan-07**	**May-07**
SULTANHİSAR (17850)	1972-1979	1	1.705	1	Dec-72	Dec-72	1	1.815	1	Jan-73	Jan-73
	1980-1987	2	1.772	1	Oct-81	Oct-81	1	1.642	1	May-86	May-86
	1988-1995	4	1.772	1	Jul-88	Jul-88	5	4.722	3	Jan-92	Mar-92
	1996-2003	2	1.751	8	Oct-98	May-99	5	1.790	1	Oct-01	Oct-01
	2004-2011	8	3.315	2	Jul-07	Aug-07	7	3.489	2	Aug-07	Sep-07
	2012-2018	10	3.468	2	Jun-12	Jul-12	2	1.952	1	Feb-14	Feb-14
	1972-2018	**27**	**3.468**	**2**	**Jun-12**	**Jul-12**	**21**	**4.722**	**3**	**Jan-92**	**Mar-92**
SELÇUK (17854)	1972-1979	2	1.610	1	Dec-72	Dec-72	1	1.535	1	Jan-74	Jan-74
	1980-1987	1	1.655	1	Oct-81	Oct-81	-	-	-	-	-
	1988-1995	4	1.929	1	Nov-90	Nov-90	2	1.686	1	Nov-90	Nov-90
	1996-2003	4	1.804	1	Jul-01	Jul-01	5	1.912	1	Jul-99	Jul-99
	2004-2011	4	1.785	1	Oct-04	Oct-04	6	3.511	2	Mar-07	Apr-07
	2012-2018	9	3.027	2	Jul-12	Aug-12	4	1.870	1	Dec-15	Dec-15
	1972-2018	**24**	**3.027**	**2**	**Jul-12**	**Aug-12**	**18**	**3.511**	**2**	**Mar-07**	**Apr-07**
NAZİLLİ (17860)	1972-1979	4	1.776	1	Dec-72	Dec-72	1	1.785	1	Jan-73	Jan-73
	1980-1987	3	1.828	1	Oct-81	Oct-81	1	1.730	1	Dec-84	Dec-84
	1988-1995	1	3.116	2	Jan-92	Feb-92	3	4.904	3	Jan-92	Mar-92
	1996-2003	1	1.585	10	Aug-98	May-99	2	1.856	1	Jun-99	Jun-99
	2004-2011	6	3.393	2	Jul-07	Aug-07	4	6.979	4	Jun-07	Sep-07
	2012-2018	10	3.621	2	Jun-12	Jul-12	7	5.557	3	Aug-12	Oct-12
	1972-2018	**25**	**3.621**	**2**	**Jun-12**	**Jul-12**	**18**	**6.979**	**4**	**Jun-07**	**Sep-07**

Table Ap.15 Annual maximum drought durations and severities for severe drought conditions for Manisa, İzmir, Kuşadası, Aydın and Salihli Stations (for SPEI-6 and SPEI-12 month).

		Severe Drought									
Station	**Period**	**SPEI6**					**SPEI12**				
		Total Event	**Max Severity**	**Max Duration**	**Beginning Date**	**End Date**	**Total Event**	**Max Severity**	**Max Duration**	**Beginning Date**	**End Date**
MANİSA (17186)	1972-1979	-	-	-	-	-	-	-	-	-	-
	1980-1987	1	1.512	1	Feb-85	Feb-85	1	3.097	2	Aug-85	Sep-85
	1988-1995	6	5.053	3	Jan-92	Mar-92	4	9.953	6	Mar-89	Aug-89
	1996-2003	5	3.054	2	Sep-00	Oct-00	2	10.106	6	Mar-01	Aug-01
	2004-2011	5	7.140	4	Jun-07	Sep-07	5	15.235	9	Dec-07	Aug-08
	2012-2018	1	1.771	1	Dec-12	Dec-12	2	1.700	1	Jan-18	Jan-18
	1972-2018	**18**	**7.140**	**4**	**Jun-07**	**Sep-07**	**14**	**15.235**	**9**	**Dec-07**	**Aug-08**
İZMİR (17220)	1972-1979	1	1.760	1	Jan-74	Jan-74	1	1.733	1	Dec-72	Dec-72
	1980-1987	1	1.526	1	Feb-85	Feb-85	-	-	-	-	-
	1988-1995	4	3.552	2	Mar-92	Apr-92	5	10.116	6	May-92	Oct-92
	1996-2003	2	5.109	3	Sep-99	Nov-99	2	3.297	2	Mar-01	Apr-01
	2004-2011	4	5.118	3	May-08	Jul-08	5	9.751	6	Mar-08	Aug-08
	2012-2018	3	3.276	2	Sep-16	Oct-16	2	7.996	5	May-18	Sep-18
	1972-2018	**15**	**5.118**	**3**	**May-08**	**Jul-08**	**15**	**10.116**	**6**	**May-92**	**Oct-92**
KUŞADASI (17232)	1972-1979	1	1.619	1	Jan-74	Jan-74	-	-	-	-	-
	1980-1987	1	1.686	1	Nov-80	Nov-80	1	1.681	1	Feb-87	Feb-87
	1988-1995	5	9.127	5	Feb-90	Jun-90	5	19.353	11	Dec-89	Oct-90
	1996-2003	1	1.874	1	Oct-99	Oct-99	1	1.529	1	Mar-01	Mar-01
	2004-2011	4	4.995	3	Jun-08	Aug-08	2	10.719	6	Mar-07	Aug-07
	2012-2018	2	1.899	1	Nov-12	Nov-12	-	-	-	-	-
	1972-2018	**14**	**9.127**	**5**	**Feb-90**	**Jun-90**	**9**	**19.353**	**11**	**Dec-89**	**Oct-90**
AYDIN (17324)	1972-1979	-	-	-	-	-	-	-	-	-	-
	1980-1987	-	-	-	-	-	-	-	-	-	-
	1988-1995	4	6.930	4	Jan-92	Apr-92	3	9.615	6	May-92	Oct-92
	1996-2003	3	8.733	5	Aug-99	Dec-99	3	8.406	5	Jun-01	Oct-01
	2004-2011	7	3.391	2	Feb-07	Mar-07	4	3.664	2	Feb-07	Mar-07
	2012-2018	4	5.493	3	Sep-16	Nov-16	3	4.567	3	Jun-16	Aug-16
	1972-2018	**18**	**8.733**	**5**	**Aug-99**	**Dec-99**	**13**	**9.615**	**6**	**May-92**	**Oct-92**
SALİHLİ (17792)	1972-1979	1	1.557	1	Apr-73	Apr-73	-	-	-	-	-
	1980-1987	-	-	-	-	-	-	-	-	-	-
	1988-1995	1	3.296	2	May-89	Jun-89	-	-	-	-	-
	1996-2003	4	1.965	1	Dec-00	Dec-00	2	11.143	6	May-01	Oct-01
	2004-2011	4	8.507	5	Mar-07	Jul-07	4	23.293	14	Jul-07	Aug-08
	2012-2018	8	10.489	6	Nov-17	Apr-18	4	22.002	12	Jan-18	Dec-18
	1972-2018	**18**	**10.489**	**6**	**Nov-17**	**Apr-18**	**10**	**23.293**	**14**	**Jul-07**	**Aug-08**

Table Ap.16 Annual maximum drought durations and severities for severe drought conditions for Seferihisar, Ödemiş, Sultanhisar, Selçuk and Nazilli Stations (for SPEI-6 and SPEI-12 month).

		Severe Drought									
Station	**Period**	**SPEI6**					**SPEI12**				
		Total Event	**Max Severity**	**Max Duration**	**Beginning Date**	**End Date**	**Total Event**	**Max Severity**	**Max Duration**	**Beginning Date**	**End Date**
SEFERİHİSAR (17820)	1972-1979	3	3.286	2	Mar-79	Apr-79	1	3.236	2	Dec-72	Jan-73
	1980-1987	-	-	-	-	-	-	-	-	-	-
	1988-1995	4	1.797	1	Jan-92	Jan-92	2	6.443	4	May-92	Aug-92
	1996-2003	5	3.760	2	Oct-99	Nov-99	2	1.911	1	Mar-01	Mar-01
	2004-2011	5	7.256	4	Jun-07	Sep-07	4	10.311	6	Oct-07	Mar-08
	2012-2018	3	5.179	3	Aug-16	Oct-16	3	4.897	3	Jun-16	Aug-16
	1972-2018	**20**	**7.256**	**4**	**Jun-07**	**Sep-07**	**12**	**10.311**	**6**	**Oct-07**	**Mar-08**
ÖDEMİŞ (17822)	1972-1979	-	-	-	-	-	-	-	-	-	-
	1980-1987	-	-	-	-	-	-	-	-	-	-
	1988-1995	4	3.530	2	Mar-92	Apr-92	3	3.148	2	Jan-92	Feb-92
	1996-2003	3	7.033	4	Jan-01	Apr-01	2	14.140	8	Mar-01	Oct-01
	2004-2011	5	3.490	2	Dec-04	Jan-05	2	5.624	3	Jun-07	Aug-07
	2012-2018	4	1.683	1	May-14	May-14	3	6.320	4	Feb-14	May-14
	1972-2018	**16**	**7.033**	**4**	**Jan-01**	**Apr-01**	**10**	**14.140**	**8**	**Mar-01**	**Oct-01**
SULTANHİSAR (17850)	1972-1979	-	-	-	-	-	-	-	-	-	-
	1980-1987	-	-	-	-	-	-	-	-	-	-
	1988-1995	5	5.413	3	Feb-92	Apr-92	3	4.931	3	Mar-89	May-89
	1996-2003	3	3.308	2	Dec-00	Jan-01	2	14.727	9	Feb-01	Oct-01
	2004-2011	8	5.686	3	May-07	Jul-07	3	7.308	4	Mar-07	Jun-07
	2012-2018	5	5.086	3	Sep-16	Nov-16	4	5.302	3	Oct-16	Dec-16
	1972-2018	**21**	**5.686**	**3**	**May-07**	**Jul-07**	**12**	**14.727**	**9**	**Feb-01**	**Oct-01**
SELÇUK (17854)	1972-1979	1	1.557	1	Jan-74	Jan-74	-	-	-	-	-
	1980-1987	-	-	-	-	-	-	-	-	-	-
	1988-1995	3	3.698	2	Feb-92	Mar-92	3	7.709	5	May-92	Sep-92
	1996-2003	2	5.202	3	Sep-99	Nov-99	2	1.583	1	Oct-01	Oct-01
	2004-2011	8	3.824	2	Jun-08	Jul-08	4	3.916	2	May-07	Jun-07
	2012-2018	4	3.381	2	Aug-18	Sep-18	3	10.195	6	Apr-18	Sep-18
	1972-2018	**18**	**5.202**	**3**	**Sep-99**	**Nov-99**	**12**	**10.195**	**6**	**Apr-18**	**Sep-18**
NAZİLLİ (17860)	1972-1979	1	1.554	1	Jan-74	Jan-74	-	-	-	-	-
	1980-1987	-	-	-	-	-	-	-	-	-	-
	1988-1995	3	5.500	3	Feb-92	Apr-92	1	6.804	4	Mar-89	Jun-89
	1996-2003	1	1.615	1	Mar-01	Mar-01	2	1.539	1	Feb-00	Feb-00
	2004-2011	6	10.362	6	Jun-08	Nov-08	3	5.398	3	Mar-07	May-07
	2012-2018	5	6.648	4	Feb-14	May-14	4	10.746	6	Jun-16	Nov-16
	1972-2018	**16**	**10.362**	**6**	**Jun-08**	**Nov-08**	**10**	**10.746**	**6**	**Jun-16**	**Nov-16**

Table Ap.17 Annual maximum drought durations and severities for extreme drought conditions for Manisa, İzmir, Kuşadası, Aydın and Salihli Stations (for SPI-1 and SPI-3 month).

		Extreme Drought									
Station Name	**Period**	**SPI1**					**SPI3**				
		Total Event	**Max Severity**	**Max Duration**	**Beginning Date**	**End Date**	**Total Event**	**Max Severity**	**Max Duration**	**Beginning Date**	**End Date**
MANİSA (17186)	1972-1979	2	2.118	1	May-77	May-77	1	2.512	1	Jan-73	Jan-73
	1980-1987	2	2.675	1	May-84	May-84	2	4.556	2	Nov-84	Dec-84
	1988-1995	4	3.891	1	Jan-92	Jan-92	6	2.282	1	Jun-88	Jun-88
	1996-2003	1	2.905	1	May-99	May-99	2	2.970	1	Jun-99	Jun-99
	2004-2011	2	2.072	1	May-06	May-06	4	5.495	2	Jan-07	Feb-07
	2012-2018	2	2.428	1	Apr-18	Apr-18	1	2.362	1	Nov-12	Nov-12
	1972-2018	**13**	**3.891**	**1**	**Jan-92**	**Jan-92**	**16**	**5.495**	**2**	**Jan-07**	**Feb-07**
İZMİR (17220)	1972-1979	1	2.025	1	Dec-72	Dec-72	1	2.048	1	Jul-77	Jul-77
	1980-1987	3	2.827	1	May-84	May-84	3	2.110	1	Nov-86	Nov-86
	1988-1995	2	3.034	1	Apr-89	Apr-89	2	4.232	2	Feb-92	Mar-92
	1996-2003	-	-	-	-	-	-	-	-	-	-
	2004-2011	4	2.827	1	May-84	May-84	4	11.107	4	Jan-07	Apr-07
	2012-2018	3	2.471	1	Apr-18	Apr-18	-	-	-	-	-
	1972-2018	**13**	**3.034**	**1**	**Apr-89**	**Apr-89**	**10**	**11.107**	**4**	**Jan-07**	**Apr-07**
KUŞADASI (17232)	1972-1979	-	-	-	-	-	2	2.133	1	Jan-73	Jan-73
	1980-1987	1	2.028	1	Nov-80	Nov-80	5	9.045	2	Oct-80	Nov-80
	1988-1995	3	4.036	1	Apr-89	Apr-89	4	2.138	1	Aug-81	Aug-81
	1996-2003	-	-	-	-	-	3	4.166	2	Jul-99	Aug-99
	2004-2011	2	2.073	1	Feb-08	Feb-08	5	9.693	4	Jan-07	Apr-07
	2012-2018	4	2.538	1	Apr-16	Apr-16	2	2.165	1	Dec-16	Dec-16
	1972-2018	**10**	**4.036**	**1**	**Apr-89**	**Apr-89**	**21**	**9.693**	**4**	**Jan-07**	**Apr-07**
AYDIN (17324)	1972-1979	3	3.231	1	May-77	May-77	1	2.019	1	Jul-78	Jul-78
	1980-1987	1	2.028	1	Oct-84	Oct-84	4	2.295	1	May-86	May-86
	1988-1995	4	4.100	2	Jan-92	Feb-92	5	4.542	2	Feb-90	Mar-90
	1996-2003	-	-	-	-	-	1	4.453	2	Jun-99	Jul-99
	2004-2011	5	5.052	1	Nov-11	Nov-11	4	7.359	3	Feb-07	Apr-07
	2012-2018	4	2.105	1	Apr-18	Apr-18	1	2.461	1	Dec-16	Dec-16
	1972-2018	**17**	**5.052**	**1**	**Nov-11**	**Nov-11**	**16**	**7.359**	**3**	**Feb-07**	**Apr-07**
SALİHLİ (17792)	1972-1979	2	5.388	1	Dec-72	Dec-72	1	3.138	1	Jan-73	Jan-73
	1980-1987	2	2.146	1	May-84	May-84	5	2.419	1	Dec-84	Dec-84
	1988-1995	3	3.022	1	Apr-89	Apr-89	1	4.578	2	Mar-89	Apr-89
	1996-2003	3	3.515	1	Mar-01	Mar-01	3	4.537	2	Dec-00	Jan-01
	2004-2011	3	3.211	1	Dec-06	Dec-06	4	3.128	1	Jul-08	Jul-08
	2012-2018	5	4.542	1	Dec-15	Dec-15	3	2.704	1	Feb-14	Feb-14
	1972-2018	**18**	**5.388**	**1**	**Dec-72**	**Dec-72**	**17**	**4.578**	**2**	**Mar-89**	**Apr-89**

Table Ap.18 Annual maximum drought durations and severities for extreme drought conditions for Seferihisar, Ödemiş, Sultanhisar, Selçuk and Nazilli Stations (for SPI-1 and SPI-3 month).

		Extreme Drought									
Station	**Period**	**SPI1**					**SPI3**				
		Total Event	**Max Severity**	**Max Duration**	**Beginning Date**	**End Date**	**Total Event**	**Max Severity**	**Max Duration**	**Beginning Date**	**End Date**
SEFERİHİSAR (17820)	1972-1979	2	2.052	1	Jan-74	Jan-74	3	2.648	1	Jan-73	Jan-73
	1980-1987	-	-	-	-	-	-	-	-	-	-
	1988-1995	4	4.364	1	Jan-92	Jan-92	4	2.360	1	Nov-90	Nov-90
	1996-2003	1	2.122	1	Mar-01	Mar-01	-	-	-	-	-
	2004-2011	1	2.028	1	Nov-11	Nov-11	2	2.495	1	Feb-07	Feb-07
	2012-2018	3	3.886	1	Apr-18	Apr-18	-	-	-	-	-
	1972-2018	**11**	**4.364**	**1**	**Jan-92**	**Jan-92**	**9**	**2.648**	**1**	**Jan-73**	**Jan-73**
ÖDEMİŞ (17822)	1972-1979	2	3.233	1	Dec-72	Dec-72	1	2.309	1	Jan-73	Jan-73
	1980-1987	1	2.028	1	May-77	May-77	3	3.675	1	Oct-84	Oct-84
	1988-1995	4	4.507	2	Jan-92	Feb-92	4	6.594	3	Jan-92	Mar-92
	1996-2003	-	-	-	-	-	3	5.582	2	Jun-99	Jul-99
	2004-2011	2	3.005	1	Dec-06	Dec-06	1	4.566	2	Jan-07	Feb-07
	2012-2018	6	3.832	1	Dec-15	Dec-15	1	2.310	1	Feb-14	Feb-14
	1972-2018	**15**	**4.507**	**2**	**Jan-92**	**Feb-92**	**13**	**6.594**	**3**	**Jan-92**	**Mar-92**
SULTANHİSAR (17850)	1972-1979	2	2.028	1	May-77	May-77	2	2.983	1	Jul-78	Jul-78
	1980-1987	-	-	-	-	-	1	2.202	1	Oct-84	Oct-84
	1988-1995	3	4.347	2	Jan-92	Feb-92	4	4.515	2	Feb-92	Mar-92
	1996-2003	-	-	-	-	-	1	2.537	1	Jun-99	Jun-99
	2004-2011	2	3.347	1	Mar-04	Mar-04	3	2.777	1	Jul-08	Jul-08
	2012-2018	3	3.175	1	Apr-18	Apr-18	4	2.305	1	Feb-14	Feb-14
	1972-2018	**10**	**4.347**	**2**	**Jan-92**	**Feb-92**	**15**	**4.515**	**2**	**Feb-92**	**Mar-92**
SELÇUK (17854)	1972-1979	1	2.143	1	May-77	May-77	1	2.463	1	Jan-73	Jan-73
	1980-1987	-	-	-	-	-	1	2.028	1	Oct-84	Oct-84
	1988-1995	4	4.256	1	Jan-92	Jan-92	2	2.434	1	Mar-92	Mar-92
	1996-2003	2	2.415	1	Mar-01	Mar-01	1	2.684	1	Jul-99	Jul-99
	2004-2011	4	4.348	1	Nov-11	Nov-11	5	7.283	3	Feb-07	Apr-07
	2012-2018	5	2.098	1	Apr-16	Apr-16	1	2.527	1	Dec-16	Dec-16
	1972-2018	**16**	**4.348**	**1**	**Nov-11**	**Nov-11**	**11**	**7.283**	**3**	**Feb-07**	**Apr-07**
NAZİLLİ (17860)	1972-1979	3	2.316	1	Mar-76	Mar-76	1	2.374	1	Jan-73	Jan-73
	1980-1987	-	-	-	-	-	2	4.066	1	Oct-84	Oct-84
	1988-1995	2	4.544	2	Jan-92	Feb-92	3	7.194	3	Feb-89	Apr-89
	1996-2003	-	-	-	-	-	2	2.307	1	Jun-99	Jun-99
	2004-2011	3	2.822	1	Mar-04	Mar-04	1	2.479	1	May-07	May-07
	2012-2018	2	3.054	1	Apr-18	Apr-18	3	2.766	1	Nov-12	Nov-12
	1972-2018	**10**	**4.544**	**2**	**Jan-92**	**Feb-92**	**12**	**7.194**	**3**	**Feb-89**	**Apr-89**

Table Ap.19 Annual maximum drought durations and severities for extreme drought conditions for Manisa, İzmir, Kuşadası, Aydın and Salihli Stations (for SPI-6 and SPI-12 month).

		Extreme Drought									
Station Name	**Period**	**SPI6**					**SPI12**				
		Total Event	**Max Severity**	**Max Duration**	**Beginning Date**	**End Date**	**Total Event**	**Max Severity**	**Max Duration**	**Beginning Date**	**End Date**
MANİSA (17186)	1972-1979	-	-	-	-	-	-	-	-	-	-
	1980-1987	1	2.173	1	Dec-84	Dec-84	-	-	-	-	-
	1988-1995	5	4.625	2	Feb-92	Mar-92	3	13.327	6	May-92	Oct-92
	1996-2003	1	3.119	1	Sep-99	Sep-99	-	-	-	-	-
	2004-2011	3	11.150	4	Mar-07	Jun-07	3	21.173	9	Mar-07	Nov-07
	2012-2018	1	2.259	1	Nov-12	Nov-12	-	-	-	-	-
	1972-2018	**11**	**11.150**	**4**	**Mar-07**	**Jun-07**	**6**	**21.173**	**9**	**Mar-07**	**Nov-07**
İZMİR (17220)	1972-1979	2	2.166	1	Jan-74	Jan-74	1	2.361	1	Dec-72	Dec-72
	1980-1987	1	2.159	1	Oct-87	Oct-87	-	-	-	-	-
	1988-1995	2	10.508	4	Jan-92	Apr-92	3	16.271	6	May-92	Oct-92
	1996-2003	-	-	-	-	-	-	-	-	-	-
	2004-2011	2	13.559	5	Mar-07	Jul-07	2	6.941	3	Sep-07	Nov-07
	2012-2018	-	-	-	-	-	-	-	-	-	-
	1972-2018	**7**	**13.559**	**5**	**Mar-07**	**Jul-07**	**6**	**16.271**	**6**	**May-92**	**Oct-92**
KUŞADASI (17232)	1972-1979	1	2.018	1	Jan-74	Jan-74	-	-	-	-	-
	1980-1987	2	5.555	1	Nov-80	Nov-80	-	-	-	-	-
	1988-1995	2	6.566	3	Apr-90	Jun-90	3	4.141	2	Dec-89	Jan-90
	1996-2003	-	-	-	-	-	-	-	-	-	-
	2004-2011	2	8.074	3	Apr-07	Jun-07	2	4.137	2	Mar-07	Apr-07
	2012-2018	2	2.219	1	Dec-16	Dec-16	-	-	-	-	-
	1972-2018	**9**	**8.074**	**3**	**Apr-07**	**Jun-07**	**5**	**4.141**	**2**	**Dec-89**	**Jan-90**
AYDIN (17324)	1972-1979	-	-	-	-	-	-	-	-	-	-
	1980-1987	2	3.370	1	Oct-84	Oct-84	-	-	-	-	-
	1988-1995	6	9.548	4	Jan-92	Apr-92	4	14.790	6	May-92	Oct-92
	1996-2003	2	2.297	1	Sep-99	Sep-99	-	-	-	-	-
	2004-2011	4	12.718	5	Mar-07	Jul-07	2	16.698	7	Mar-07	Sep-07
	2012-2018	1	2.209	1	Dec-16	Dec-16	-	-	-	-	-
	1972-2018	**15**	**12.718**	**5**	**Mar-07**	**Jul-07**	**6**	**16.698**	**7**	**Mar-07**	**Sep-07**
SALİHLİ (17792)	1972-1979	1	2.259	1	Apr-73	Apr-73	-	-	-	-	-
	1980-1987	-	-	-	-	-	1	2.049	1	Jul-85	Jul-85
	1988-1995	4	5.380	2	Jun-89	Jul-89	1	2.261	1	Dec-92	Dec-92
	1996-2003	2	15.493	6	Oct-00	Mar-01	2	4.863	2	Mar-01	Apr-01
	2004-2011	3	8.620	3	Jun-08	Aug-08	3	2.636	1	Dec-08	Dec-08
	2012-2018	1	2.479	1	May-14	May-14	1	2.144	1	Nov-14	Nov-14
	1972-2018	**11**	**15.493**	**6**	**Oct-00**	**Mar-01**	**8**	**4.863**	**2**	**Mar-01**	**Apr-01**

Table Ap.20 Annual maximum drought durations and severities for extreme drought conditions for Seferihisar, Ödemiş, Sultanhisar, Selçuk and Nazilli Stations (for SPI-6 and SPI-12 month).

		Extreme Drought									
Station	**Period**	**SPI6**					**SPI12**				
		Total Event	**Max Severity**	**Max Duration**	**Beginning Date**	**End Date**	**Total Event**	**Max Severity**	**Max Duration**	**Beginning Date**	**End Date**
SEFERİHİSAR (17820)	1972-1979	1	2.337	1	Jul-77	Jul-77	1	2.572	1	Dec-72	Dec-72
	1980-1987	1	2.894	1	Oct-84	Oct-84	-	-	-	-	-
	1988-1995	4	6.572	3	Jan-92	Mar-92	2	11.501	5	May-92	Sep-92
	1996-2003	1	6.475	3	Jan-00	Mar-00	1	16.033	7	Mar-00	Sep-00
	2004-2011	1	6.950	3	Mar-07	May-07	-	-	-	-	-
	2012-2018	-	-	-	-	-	-	-	-	-	-
	1972-2018	**8**	**6.950**	**3**	**Mar-07**	**May-07**	**4**	**16.033**	**7**	**Mar-00**	**Sep-00**
ÖDEMİŞ (17822)	1972-1979	-	-	-	-	-	-	-	-	-	-
	1980-1987	3	2.912	1	Oct-84	Oct-84	-	-	-	-	-
	1988-1995	3	9.983	4	Jan-92	Apr-92	2	11.370	5	May-92	Sep-92
	1996-2003	2	11.388	4	Aug-99	Nov-99	-	-	-	-	-
	2004-2011	3	7.715	3	Apr-07	Jun-07	2	4.355	2	Sep-07	Oct-07
	2012-2018	-	-	-	-	-	-	-	-	-	-
	1972-2018	**11**	**11.388**	**4**	**Aug-99**	**Nov-99**	**4**	**11.370**	**5**	**May-92**	**Sep-92**
SULTANHİSAR (17850)	1972-1979	-	-	-	-	-	-	-	-	-	-
	1980-1987	2	2.577	1	Oct-84	Oct-84	-	-	-	-	-
	1988-1995	4	7.234	3	Feb-92	Apr-92	4	13.312	6	May-92	Oct-92
	1996-2003	-	-	-	-	-	-	-	-	-	-
	2004-2011	3	5.842	2	Jul-04	Aug-04	1	2.459	1	Jan-05	Jan-05
	2012-2018	1	2.650	1	Nov-12	Nov-12	-	-	-	-	-
	1972-2018	**10**	**7.234**	**3**	**Feb-92**	**Apr-92**	**5**	**13.312**	**6**	**May-92**	**Oct-92**
SELÇUK (17854)	1972-1979	-	-	-	-	-	-	-	-	-	-
	1980-1987	1	2.512	1	Oct-87	Oct-87	-	-	-	-	-
	1988-1995	4	4.445	2	Sep-88	Oct-88	3	13.578	6	May-92	Oct-92
	1996-2003	1	2.083	1	Sep-99	Sep-99	-	-	-	-	-
	2004-2011	3	7.738	3	Apr-07	Jun-07	1	4.214	2	Mar-07	Apr-07
	2012-2018	1	2.609	1	Dec-16	Dec-16	-	-	-	-	-
	1972-2018	**10**	**7.738**	**3**	**Apr-07**	**Jun-07**	**4**	**13.578**	**6**	**May-92**	**Oct-92**
NAZİLLİ (17860)	1972-1979	-	-	-	-	-	-	-	-	-	-
	1980-1987	2	2.824	1	Oct-84	Oct-84	-	-	-	-	-
	1988-1995	5	7.750	3	Feb-92	Apr-92	5	4.572	2	Aug-92	Sep-92
	1996-2003	-	-	-	-	-	-	-	-	-	-
	2004-2011	5	7.457	3	Apr-07	Jun-07	3	17.979	8	Apr-07	Nov-07
	2012-2018	2	3.402	1	Nov-12	Nov-12	-	-	-	-	-
	1972-2018	**14**	**7.750**	**3**	**Feb-92**	**Apr-92**	**8**	**17.979**	**8**	**Apr-07**	**Nov-07**

Table Ap.21 Annual maximum drought durations and severities for extreme drought conditions for Manisa, İzmir, Kuşadası, Aydın and Salihli Stations (for SPEI-1 and SPEI-3 month).

		Extreme Drought									
Station	**Period**	**SPEI1**					**SPEI3**				
		Total Event	**Max Severity**	**Max Duration**	**Beginning Date**	**End Date**	**Total Event**	**Max Severity**	**Max Duration**	**Beginning Date**	**End Date**
MANİSA (17186)	1972-1979	-	-	-	-	-	1	2.197	1	Jan-73	Jan-73
	1980-1987	-	-	-	-	-	1	2.795	1	Dec-84	Dec-84
	1988-1995	2	5.244	1	Sep-94	Sep-94	-	-	-	-	-
	1996-2003	-	-	-	-	-	1	2.382	1	Jun-99	Jun-99
	2004-2011	1	2.341	1	Aug-10	Aug-10	1	4.309	2	Jan-07	Feb-07
	2012-2018	2	2.221	1	Jul-12	Jul-12	1	2.208	1	Nov-12	Nov-12
	1972-2018	**5**	**5.244**	**1**	**Sep-94**	**Sep-94**	**5**	**4.309**	**2**	**Jan-07**	**Feb-07**
İZMİR (17220)	1972-1979	-	-	-	-	-	-	-	-	-	-
	1980-1987	-	-	-	-	-	-	-	-	-	-
	1988-1995	1	2.185	1	Apr-89	Apr-89	-	-	-	-	-
	1996-2003	-	-	-	-	-	-	-	-	-	-
	2004-2011	2	2.154	1	Aug-10	Aug-10	1	4.653	2	Jan-07	Feb-07
	2012-2018	2	2.134	1	Jul-12	Jul-12	1	4.436	2	May-18	Jun-18
	1972-2018	**5**	**2.185**	**1**	**Apr-89**	**Apr-89**	**2**	**4.653**	**2**	**Jan-07**	**Feb-07**
KUŞADASI (17232)	1972-1979	-	-	-	-	-	-	-	-	-	-
	1980-1987	-	-	-	-	-	-	-	-	-	-
	1988-1995	-	-	-	-	-	-	-	-	-	-
	1996-2003	2	2.788	1	May-99	May-99	-	-	-	-	-
	2004-2011	1	2.060	1	Aug-10	Aug-10	1	2.020	1	Feb-07	Feb-07
	2012-2018	-	-	-	-	-	2	2.174	1	Jun-16	Jun-16
	1972-2018	**3**	**2.788**	**1**	**May-99**	**May-99**	**3**	**2.174**	**1**	**Jun-16**	**Jun-16**
AYDIN (17324)	1972-1979	-	-	-	-	-	-	-	-	-	-
	1980-1987	-	-	-	-	-	-	-	-	-	-
	1988-1995	-	-	-	-	-	-	-	-	-	-
	1996-2003	-	-	-	-	-	1	2.303	1	Oct-01	Oct-01
	2004-2011	-	-	-	-	-	3	2.047	1	Feb-07	Feb-07
	2012-2018	-	-	-	-	-	1	2.243	1	Dec-16	Dec-16
	1972-2018	**-**	**-**	**-**	**-**	**-**	**5**	**2.303**	**1**	**Oct-01**	**Oct-01**
SALİHLİ (17792)	1972-1979	-	-	-	-	-	1	2.116	1	Jan-73	Jan-73
	1980-1987	-	-	-	-	-	-	-	-	-	-
	1988-1995	1	2.028	1	Apr-89	Apr-89	1	2.001	1	Apr-89	Apr-89
	1996-2003	1	2.880	1	Mar-01	Mar-01	1	2.199	1	Jan-01	Jan-01
	2004-2011	1	2.027	1	Jul-07	Jul-07	-	-	-	-	-
	2012-2018	3	2.055	1	Apr-18	Apr-18	3	2.177	1	Feb-14	Feb-14
	1972-2018	**6**	**2.880**	**1**	**Mar-01**	**Mar-01**	**6**	**2.199**	**1**	**Jan-01**	**Jan-01**

Table Ap.22 Annual maximum drought durations and severities for extreme drought conditions for Seferihisar, Ödemiş, Sultanhisar, Selçuk and Nazilli Stations (for SPEI-1 and SPEI-3 month).

		Extreme Drought									
Station	**Period**	**SPEI1**					**SPEI3**				
		Total Event	**Max Severity**	**Max Duration**	**Beginning Date**	**End Date**	**Total Event**	**Max Severity**	**Max Duration**	**Beginning Date**	**End Date**
SEFERİHİSAR (17820)	1972-1979	-	-	-	-	-	-	-	-	-	-
	1980-1987	-	-	-	-	-	-	-	-	-	-
	1988-1995	-	-	-	-	-	1	2.117	1	Nov-90	Nov-90
	1996-2003	1	2.618	1	May-99	May-99	1	2.773	1	Oct-01	Oct-01
	2004-2011	1	2.166	1	Jun-07	Jun-07	1	2.209	1	Feb-07	Feb-07
	2012-2018	1	2.092	1	Apr-18	Apr-18	2	2.668	1	Jun-16	Jun-16
	1972-2018	**3**	**2.618**	**1**	**May-99**	**May-99**	**5**	**2.773**	**1**	**Oct-01**	**Oct-01**
ÖDEMİŞ (17822)	1972-1979	-	-	-	-	-	-	-	-	-	-
	1980-1987	-	-	-	-	-	-	-	-	-	-
	1988-1995	-	-	-	-	-	2	2.597	1	Apr-89	Apr-89
	1996-2003	-	-	-	-	-	-	-	-	-	-
	2004-2011	1	2.083	1	Jul-07	Jul-07	-	-	-	-	-
	2012-2018	1	2.056	1	Jun-16	Jun-16	1	2.015	1	Feb-14	Feb-14
	1972-2018	**2**	**2.083**	**1**	**Jul-07**	**Jul-07**	**3**	**2.597**	**1**	**Apr-89**	**Apr-89**
SULTANHİSAR (17850)	1972-1979	-	-	-	-	-	-	-	-	-	-
	1980-1987	-	-	-	-	-	-	-	-	-	-
	1988-1995	1	2.052	1	Apr-89	Apr-89	1	2.075	1	Apr-89	Apr-89
	1996-2003	-	-	-	-	-	1	2.107	1	Jun-99	Jun-99
	2004-2011	-	-	-	-	-	-	-	-	-	-
	2012-2018	1	2.154	1	Apr-18	Apr-18	3	6.386	3	Sep-12	Nov-12
	1972-2018	**2**	**2.154**	**1**	**Apr-18**	**Apr-18**	**5**	**6.386**	**3**	**Sep-12**	**Nov-12**
SELÇUK (17854)	1972-1979	-	-	-	-	-	1	2.055	1	Jan-73	Jan-73
	1980-1987	-	-	-	-	-	-	-	-	-	-
	1988-1995	-	-	-	-	-	-	-	-	-	-
	1996-2003	3	2.185	1	May-99	May-99	1	2.167	1	Jun-99	Jun-99
	2004-2011	2	4.299	2	Jul-10	Aug-10	4	2.203	1	Feb-07	Feb-07
	2012-2018	-	-	-	-	-	3	2.306	1	Dec-16	Dec-16
	1972-2018	**5**	**4.299**	**2**	**Jul-10**	**Aug-10**	**9**	**2.306**	**1**	**Dec-16**	**Dec-16**
NAZİLLİ (17860)	1972-1979	-	-	-	-	-	-	-	-	-	-
	1980-1987	-	-	-	-	-	-	-	-	-	-
	1988-1995	1	2.107	1	Apr-89	Apr-89	1	2.211	1	Apr-89	Apr-89
	1996-2003	-	-	-	-	-	-	-	-	-	-
	2004-2011	1	2.051	1	Aug-10	Aug-10	1	2.158	1	May-07	May-07
	2012-2018	1	2.170	1	Apr-18	Apr-18	2	2.522	1	Nov-12	Nov-12
	1972-2018	**3**	**2.170**	**1**	**Apr-18**	**Apr-18**	**4**	**2.522**	**1**	**Nov-12**	**Nov-12**

Table Ap.23 Annual maximum drought durations and severities for extreme drought conditions for Manisa, İzmir, Kuşadası, Aydın and Salihli Stations (for SPEI-6 and SPEI-12 month).

		Extreme Drought									
Station	**Period**	**SPEI6**					**SPEI12**				
		Total Event	**Max Severity**	**Max Duration**	**Beginning Date**	**End Date**	**Total Event**	**Max Severity**	**Max Duration**	**Beginning Date**	**End Date**
MANİSA (17186)	1972-1979	-	-	-	-	-	-	-	-	-	-
	1980-1987	-	-	-	-	-	-	-	-	-	-
	1988-1995	-	-	-	-	-	-	-	-	-	-
	1996-2003	1	2.164	1	Sep-99	Sep-99	-	-	-	-	-
	2004-2011	1	6.497	3	Mar-07	May-07	3	6.871	3	Sep-07	Nov-07
	2012-2018	1	2.543	1	Nov-12	Nov-12	-	-	-	-	-
	1972-2018	**3**	**6.497**	**3**	**Mar-07**	**May-07**	**3**	**6.871**	**3**	**Sep-07**	**Nov-07**
İZMİR (17220)	1972-1979	-	-	-	-	-	-	-	-	-	-
	1980-1987	-	-	-	-	-	-	-	-	-	-
	1988-1995	1	2.333	1	Feb-92	Feb-92	-	-	-	-	-
	1996-2003	-	-	-	-	-	-	-	-	-	-
	2004-2011	2	6.554	3	Mar-07	May-07	2	6.539	3	Sep-07	Nov-07
	2012-2018	2	4.265	2	Aug-18	Sep-18	-	-	-	-	-
	1972-2018	**5**	**6.554**	**3**	**Mar-07**	**May-07**	**2**	**6.539**	**3**	**Sep-07**	**Nov-07**
KUŞADASI (17232)	1972-1979	-	-	-	-	-	-	-	-	-	-
	1980-1987	-	-	-	-	-	-	-	-	-	-
	1988-1995	-	-	-	-	-	1	2.347	1	Nov-90	Nov-90
	1996-2003	-	-	-	-	-	-	-	-	-	-
	2004-2011	2	4.334	2	Apr-07	May-07	1	4.144	2	Sep-07	Oct-07
	2012-2018	2	4.507	4	Jul-16	Oct-16	-	-	-	-	-
	1972-2018	**4**	**4.507**	**4**	**Jul-16**	**Oct-16**	**2**	**4.144**	**2**	**Sep-07**	**Oct-07**
AYDIN (17324)	1972-1979	-	-	-	-	-	-	-	-	-	-
	1980-1987	-	-	-	-	-	-	-	-	-	-
	1988-1995	-	-	-	-	-	1	2.040	1	Nov-90	Nov-90
	1996-2003	-	-	-	-	-	-	-	-	-	-
	2004-2011	1	11.042	5	Apr-07	Aug-07	1	15.133	7	Apr-07	Oct-07
	2012-2018	1	2.304	1	Dec-16	Dec-16	1	2.011	1	Nov-16	Nov-16
	1972-2018	**2**	**11.042**	**5**	**Apr-07**	**Aug-07**	**3**	**15.133**	**7**	**Apr-07**	**Oct-07**
SALİHLİ (17792)	1972-1979	-	-	-	-	-	-	-	-	-	-
	1980-1987	-	-	-	-	-	-	-	-	-	-
	1988-1995	-	-	-	-	-	-	-	-	-	-
	1996-2003	2	7.298	3	Jan-01	Mar-01	1	4.431	2	Mar-01	Apr-01
	2004-2011	2	2.070	1	Aug-08	Aug-08	1	2.143	1	Dec-08	Dec-08
	2012-2018	1	2.120	1	Nov-12	Nov-12	-	-	-	-	-
	1972-2018	**5**	**7.298**	**3**	**Jan-01**	**Mar-01**	**2**	**4.431**	**2**	**Mar-01**	**Apr-01**

Table Ap.24 Annual maximum drought durations and severities for extreme drought conditions for Seferihisar, Ödemiş, Sultanhisar, Selçuk and Nazilli Stations (for SPEI-6 and SPEI-12 month).

		Extreme Drought									
Station	**Period**	**SPEI6**					**SPEI12**				
		Total Event	**Max Severity**	**Max Duration**	**Beginning Date**	**End Date**	**Total Event**	**Max Severity**	**Max Duration**	**Beginning Date**	**End Date**
SEFERİHİSAR (17820)	1972-1979	-	-	-	-	-	-	-	-	-	-
	1980-1987	-	-	-	-	-	-	-	-	-	-
	1988-1995	1	2.429	1	Feb-92	Feb-92	-	-	-	-	-
	1996-2003	1	9.283	4	Dec-99	Mar-00	1	19.569	8	Feb-00	Sep-00
	2004-2011	2	2.213	1	Mar-07	Mar-07	2	2.225	1	Sep-07	Sep-07
	2012-2018	2	2.137	1	Sep-17	Sep-17	-	-	-	-	-
	1972-2018	**6**	**9.283**	**4**	**Dec-99**	**Mar-00**	**3**	**19.569**	**8**	**Feb-00**	**Sep-00**
ÖDEMİŞ (17822)	1972-1979	-	-	-	-	-	-	-	-	-	-
	1980-1987	-	-	-	-	-	-	-	-	-	-
	1988-1995	2	2.165	1	Feb-92	Feb-92	-	-	-	-	-
	1996-2003	1	2.149	1	Oct-99	Oct-99	-	-	-	-	-
	2004-2011	1	11.205	5	Apr-07	Aug-07	3	6.545	3	Sep-07	Nov-07
	2012-2018	1	2.180	1	Nov-12	Nov-12	-	-	-	-	-
	1972-2018	**5**	**11.205**	**5**	**Apr-07**	**Aug-07**	**3**	**6.545**	**3**	**Sep-07**	**Nov-07**
SULTANHİSAR (17850)	1972-1979	-	-	-	-	-	-	-	-	-	-
	1980-1987	-	-	-	-	-	-	-	-	-	-
	1988-1995	-	-	-	-	-	-	-	-	-	-
	1996-2003	-	-	-	-	-	-	-	-	-	-
	2004-2011	3	2.100	1	Aug-07	Aug-07	3	8.425	4	Jul-07	Oct-07
	2012-2018	2	2.481	1	Nov-12	Nov-12	-	-	-	-	-
	1972-2018	**5**	**2.481**	**1**	**Nov-12**	**Nov-12**	**3**	**8.425**	**4**	**Jul-07**	**Oct-07**
SELÇUK (17854)	1972-1979	-	-	-	-	-	-	-	-	-	-
	1980-1987	-	-	-	-	-	-	-	-	-	-
	1988-1995	-	-	-	-	-	-	-	-	-	-
	1996-2003	-	-	-	-	-	-	-	-	-	-
	2004-2011	1	4.673	2	Apr-07	May-07	2	10.813	5	Jul-07	Nov-07
	2012-2018	2	2.330	1	Dec-16	Dec-16	-	-	-	-	-
	1972-2018	**3**	**4.673**	**2**	**Apr-07**	**May-07**	**2**	**10.813**	**5**	**Jul-07**	**Nov-07**
NAZİLLİ (17860)	1972-1979	-	-	-	-	-	-	-	-	-	-
	1980-1987	-	-	-	-	-	-	-	-	-	-
	1988-1995	-	-	-	-	-	-	-	-	-	-
	1996-2003	-	-	-	-	-	-	-	-	-	-
	2004-2011	2	4.541	2	Aug-07	Sep-07	3	12.928	6	Jun-07	Nov-07
	2012-2018	3	2.580	1	Nov-12	Nov-12	1	2.118	1	Dec-16	Dec-16
	1972-2018	**5**	**4.541**	**2**	**Aug-07**	**Sep-07**	**4**	**12.928**	**6**	**Jun-07**	**Nov-07**

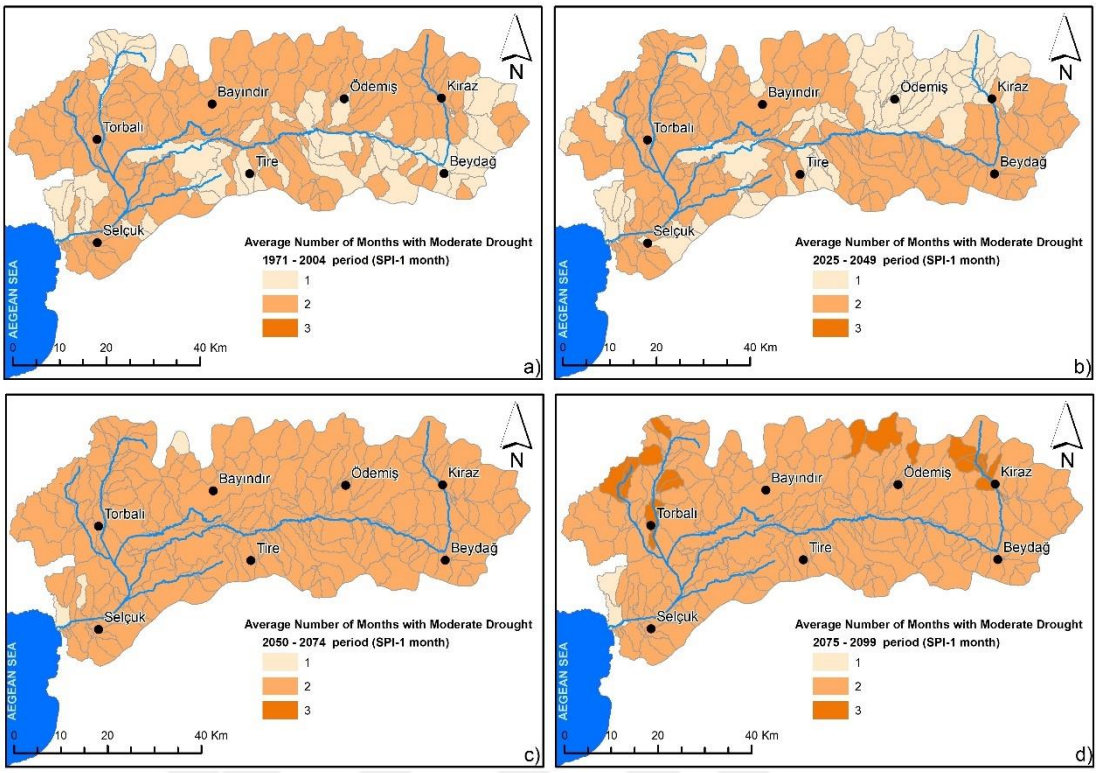


Figure Ap.55 Average number of months with moderate drought of SPI-1 month for the period a)1971-2004, b) 2025-2049, c) 2050-2074, d) 2075-2099.

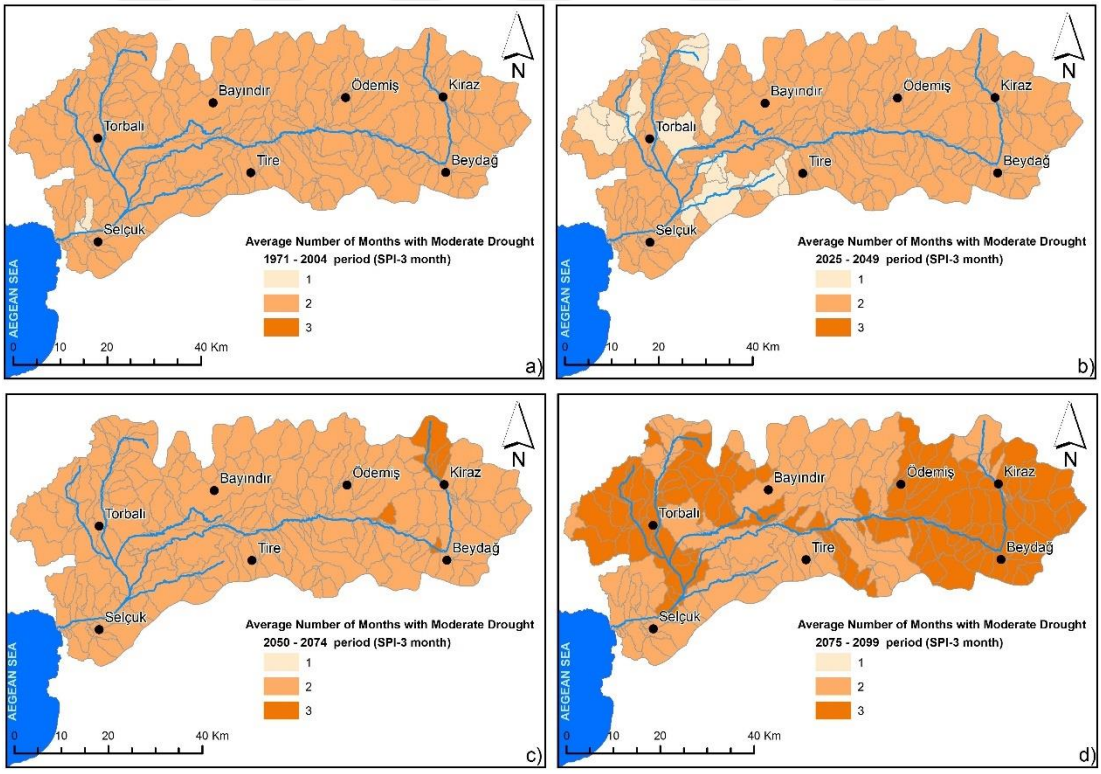


Figure Ap.56 Average number of months with moderate drought of SPI-3 month for the period a)1971-2004, b) 2025-2049, c) 2050-2074, d) 2075-2099.

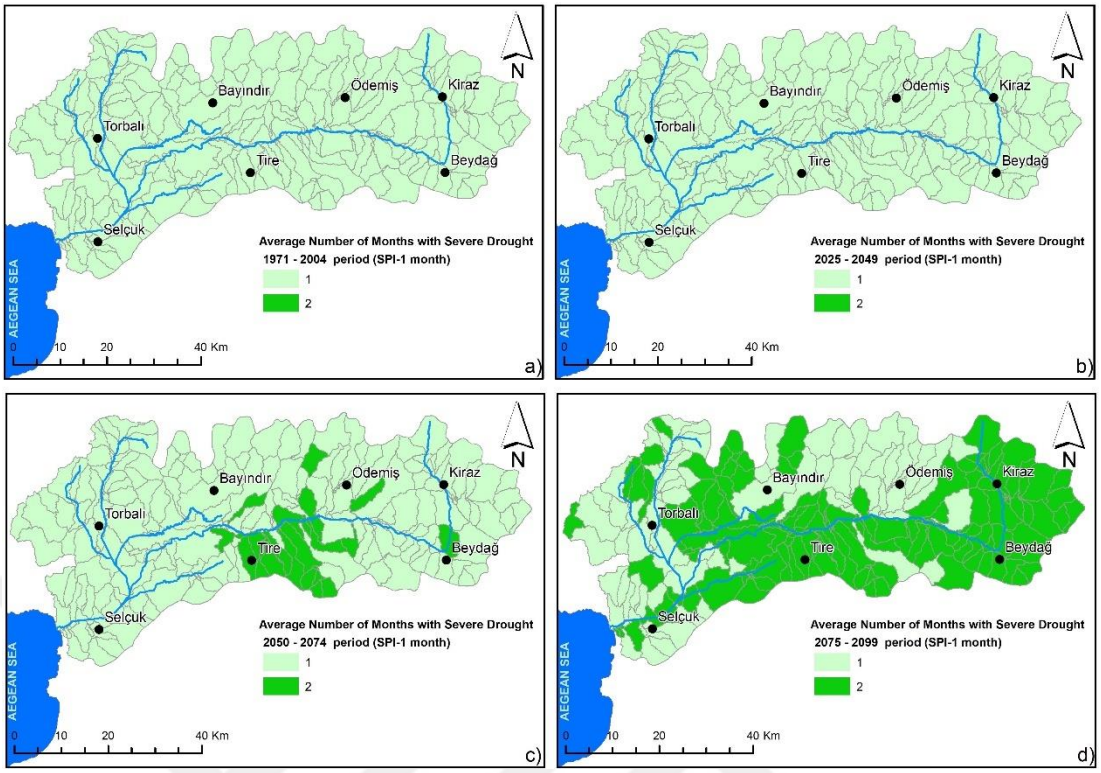


Figure Ap.57 Average number of months with severe drought of SPI-1 month for the period a)1971-2004, b) 2025-2049, c) 2050-2074, d) 2075-2099.

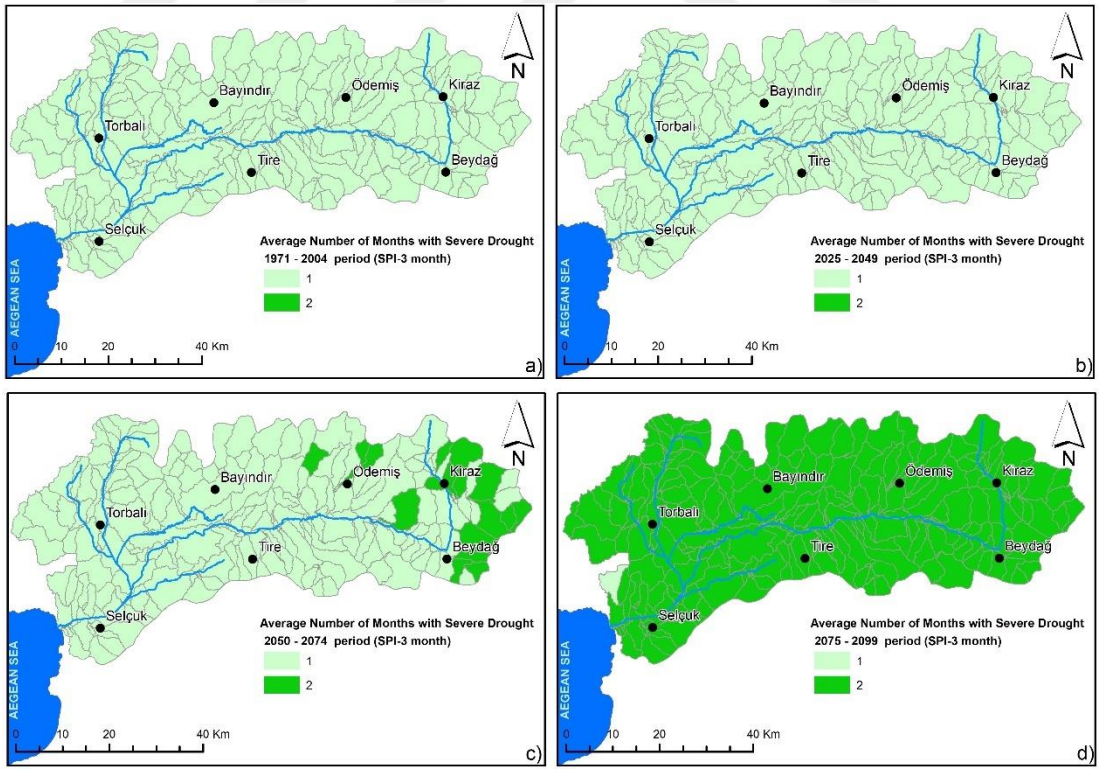


Figure Ap.58 Average number of months with severe drought of SPI-3 month for the period a)1971-2004, b) 2025-2049, c) 2050-2074, d) 2075-2099.

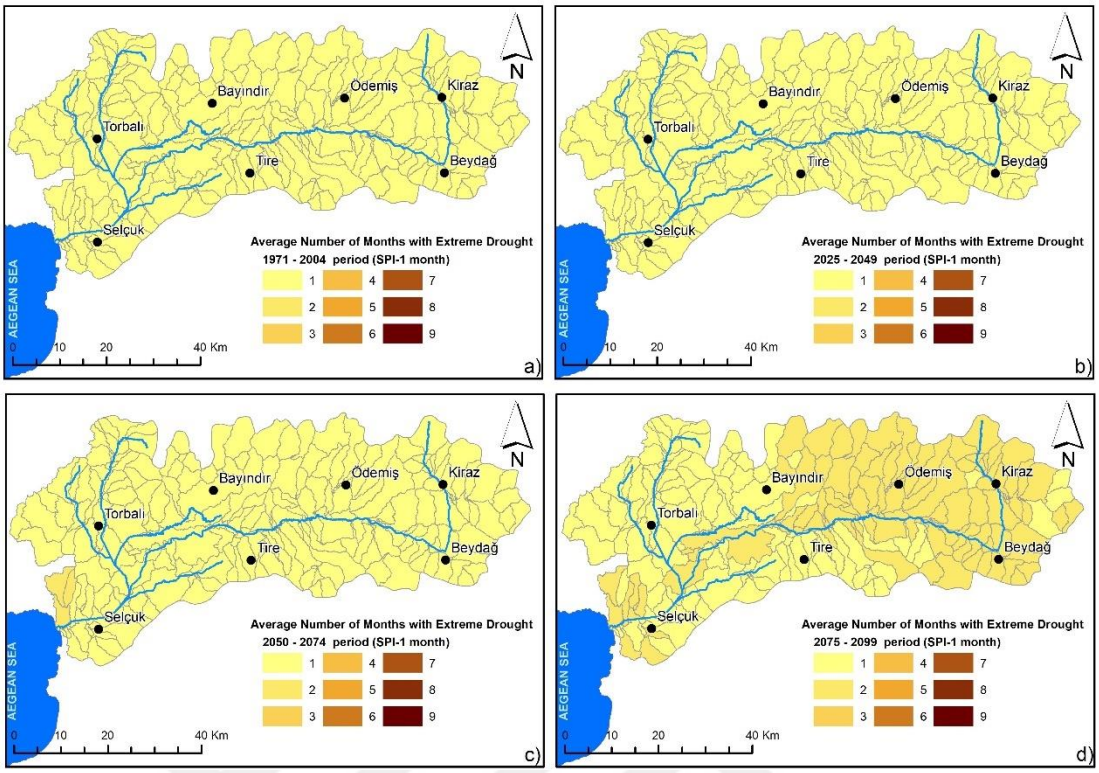


Figure Ap.59 Average number of months with extreme drought of SPI-1 month for the period a)1971-2004, b) 2025-2049, c) 2050-2074, d) 2075-2099.

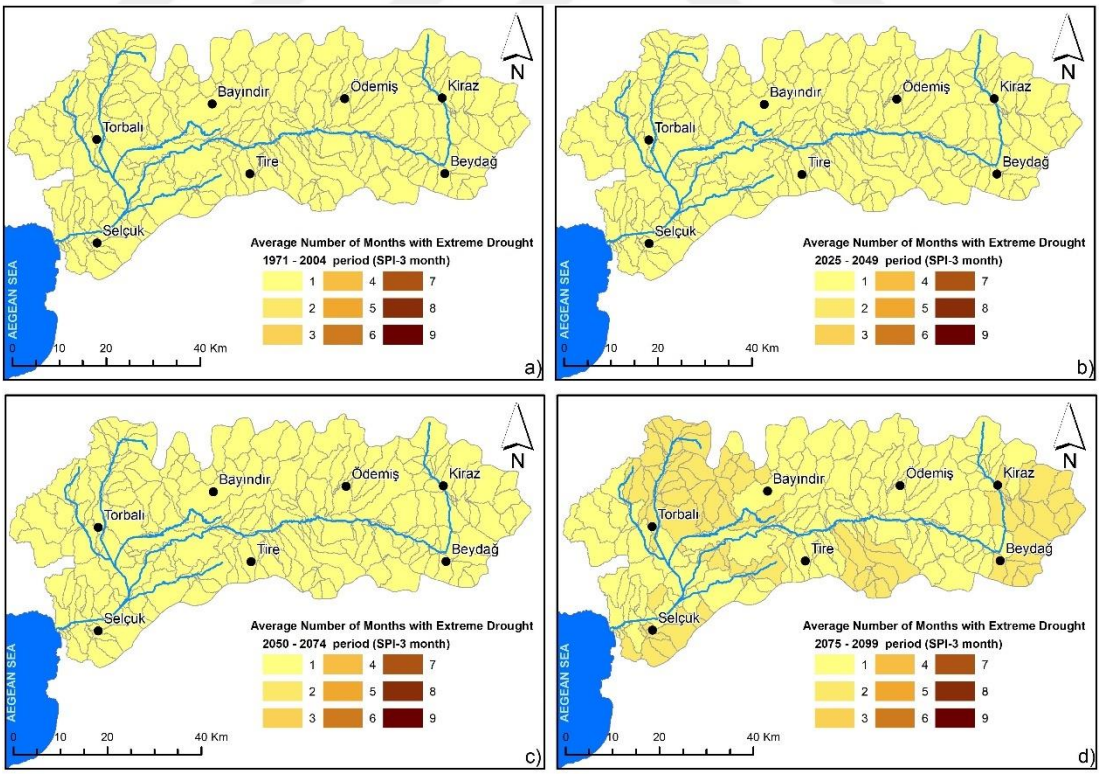


Figure Ap.60 Average number of months with extreme drought of SPI-3 month for the period a)1971-2004, b) 2025-2049, c) 2050-2074, d) 2075-2099.

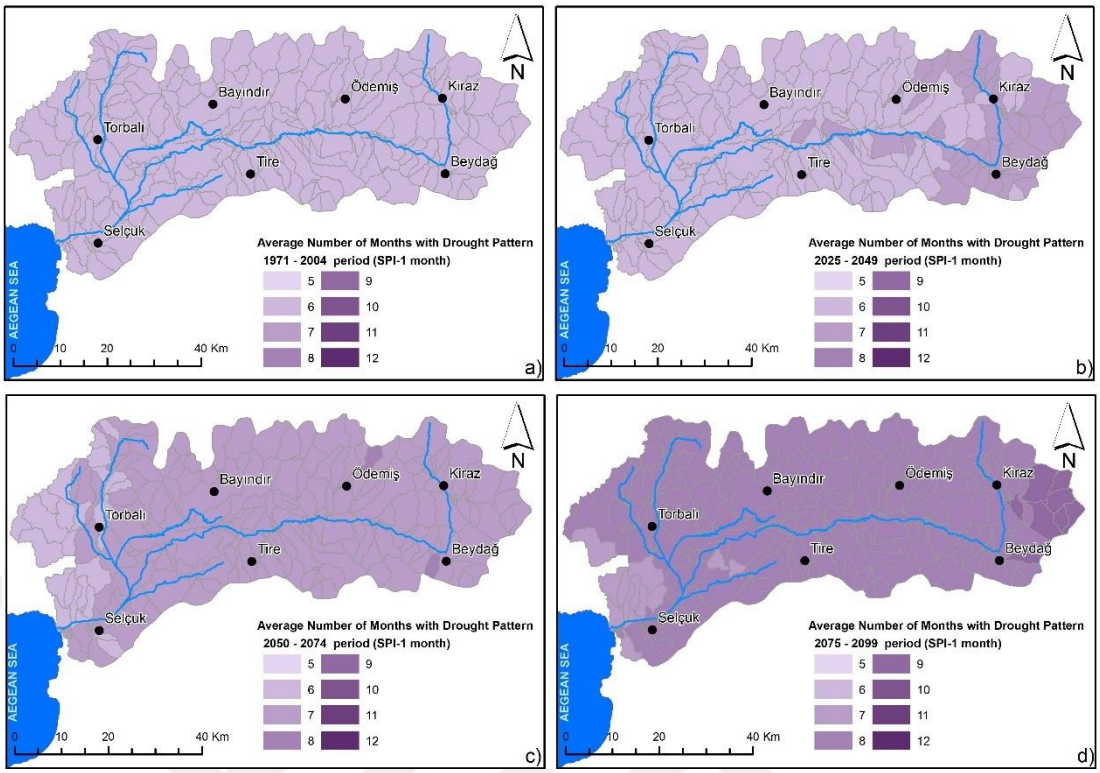


Figure Ap.61 Average number of months with drought pattern of SPI-1 month for the period a)1971-2004, b) 2025-2049, c) 2050-2074, d) 2075-2099.

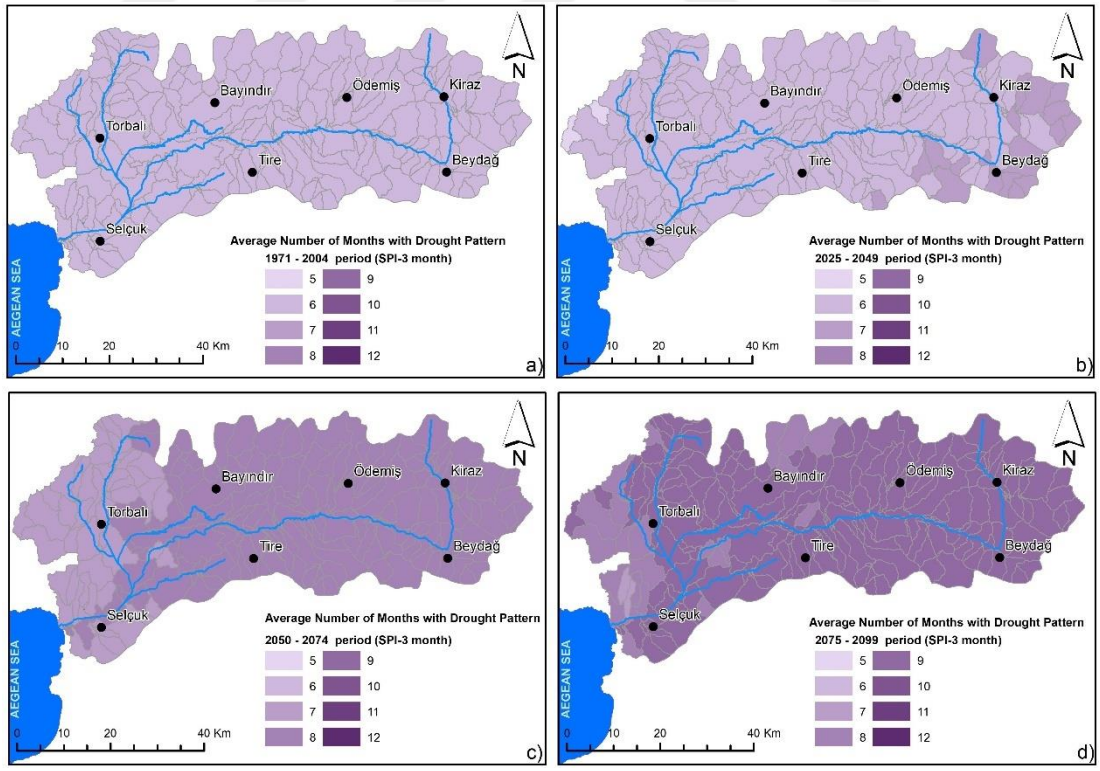


Figure Ap.62 Average number of months with drought pattern of SPI-3 month for the period a)1971-2004, b) 2025-2049, c) 2050-2074, d) 2075-2099.

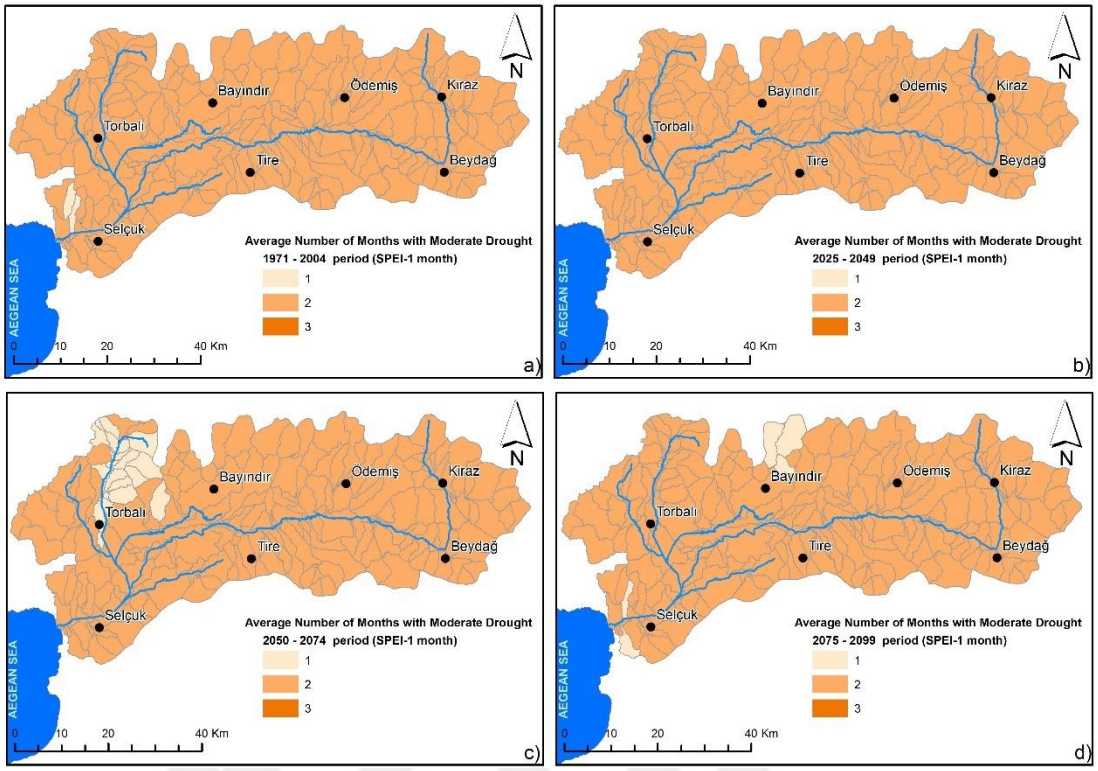


Figure Ap.63 Average number of months with moderate drought of SPEI-1 month for the period a)1971-2004, b) 2025-2049, c) 2050-2074, d) 2075-2099.

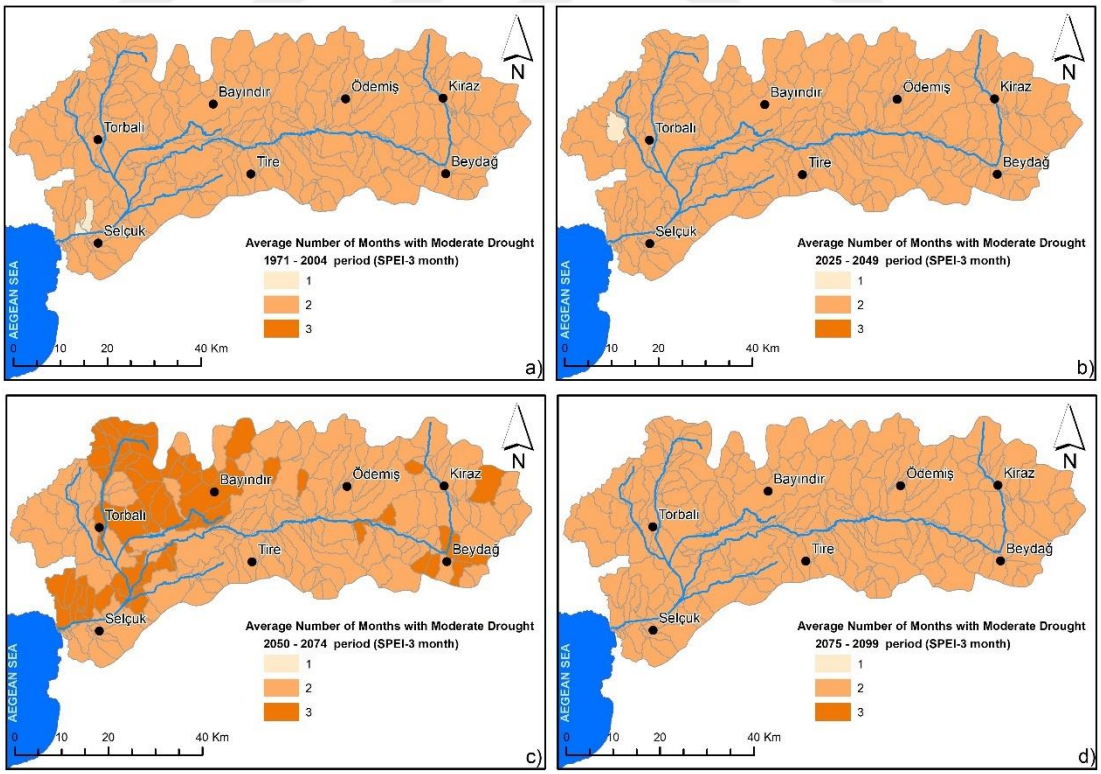


Figure Ap.64 Average number of months with moderate drought of SPEI-3 month for the period a)1971-2004, b) 2025-2049, c) 2050-2074, d) 2075-2099.

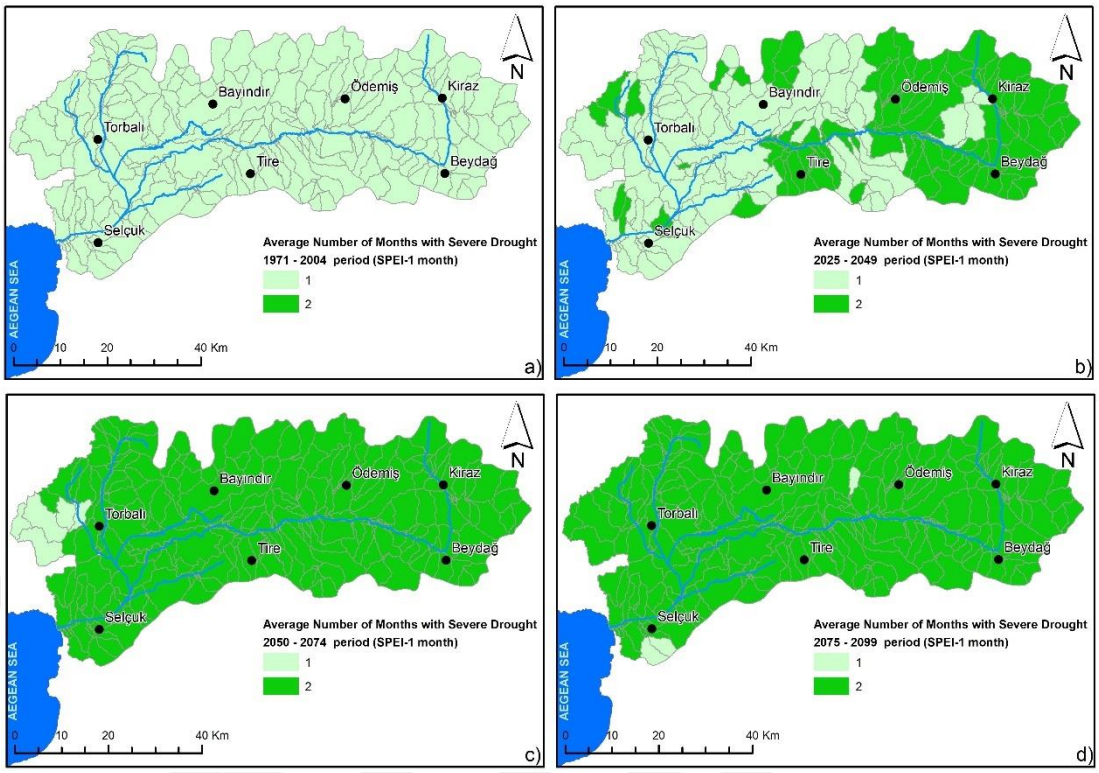


Figure Ap.65 Average number of months with severe drought of SPEI-1 month for the period a)1971-2004, b) 2025-2049, c) 2050-2074, d) 2075-2099.

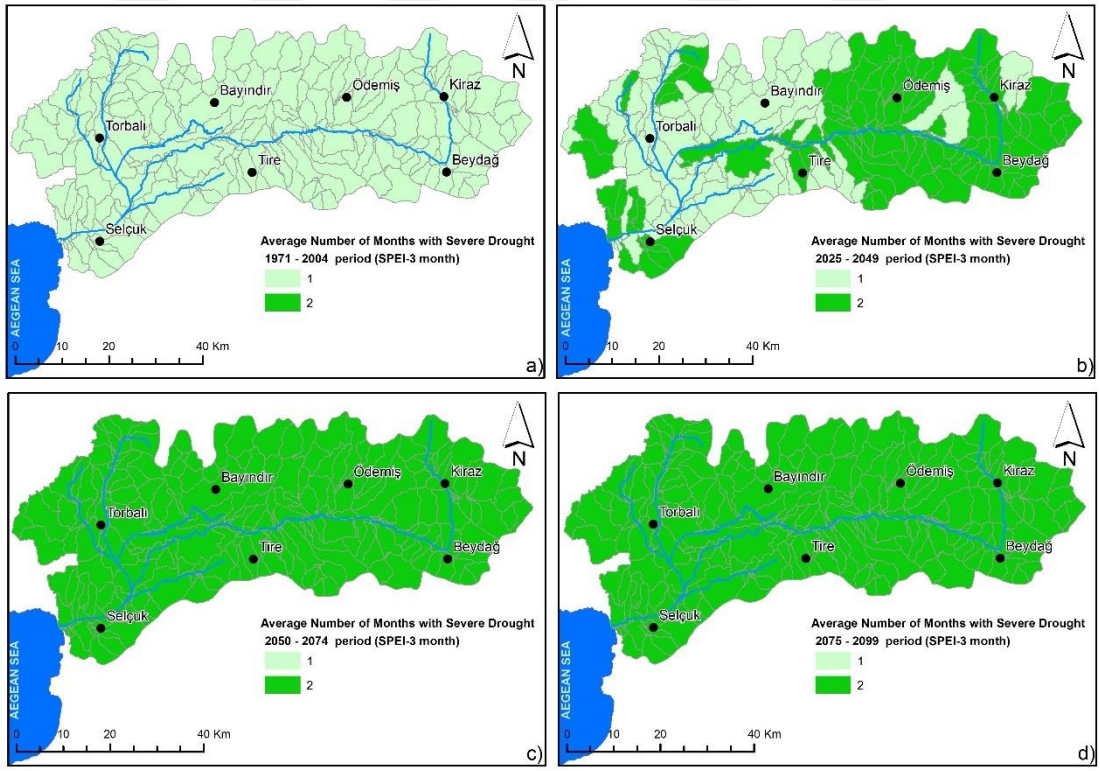


Figure Ap.66 Average number of months with severe drought of SPEI-3 month for the period a)1971-2004, b) 2025-2049, c) 2050-2074, d) 2075-2099.

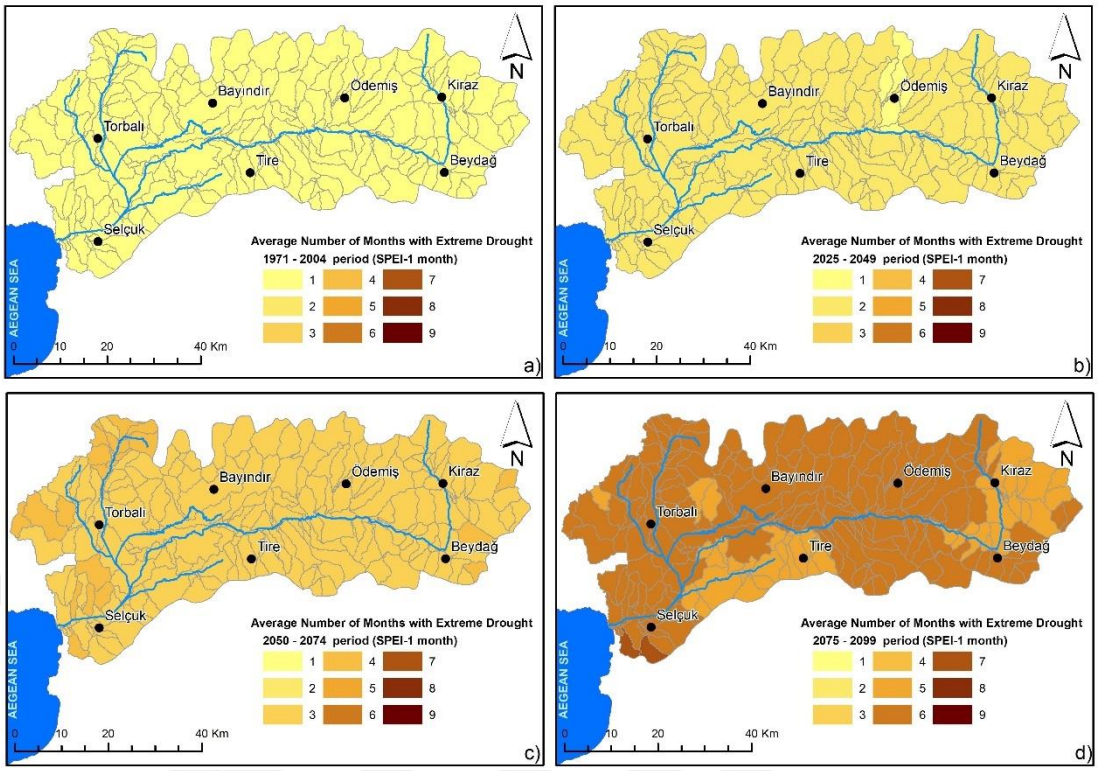


Figure Ap.67 Average number of months with extreme drought of SPEI-1 month for the period a)1971-2004, b) 2025-2049, c) 2050-2074, d) 2075-2099.

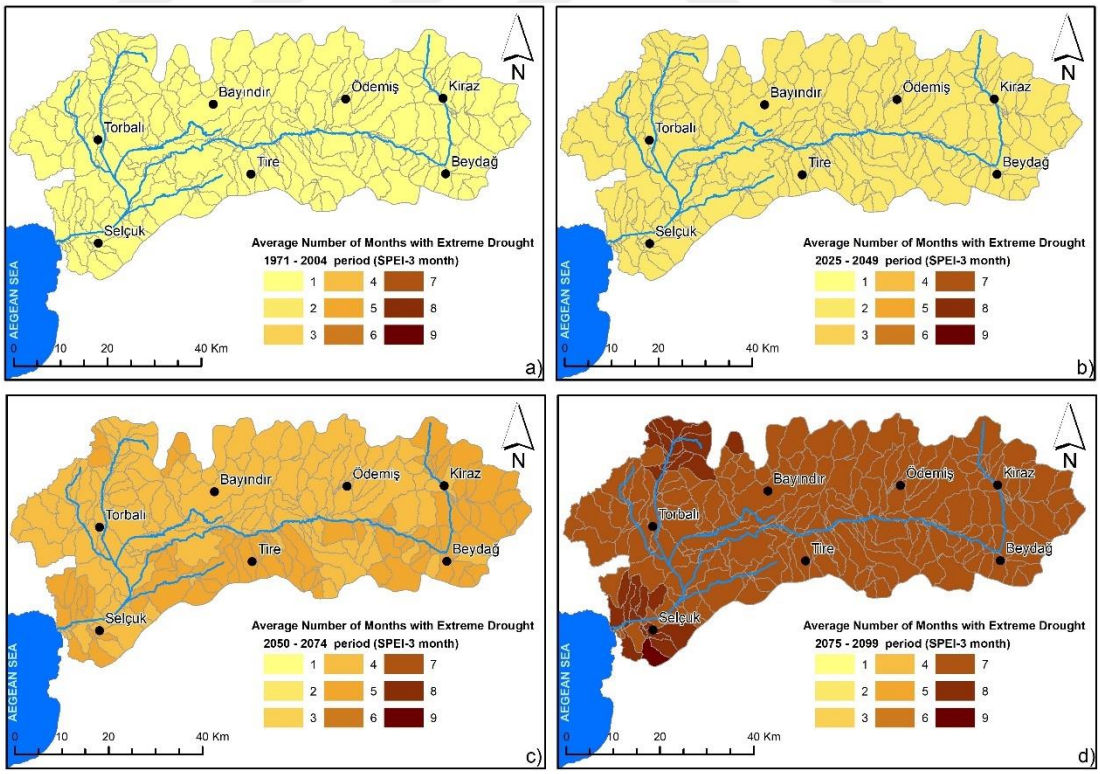


Figure Ap.68 Average number of months with extreme drought of SPEI-3 month for the period a)1971-2004, b) 2025-2049, c) 2050-2074, d) 2075-2099.

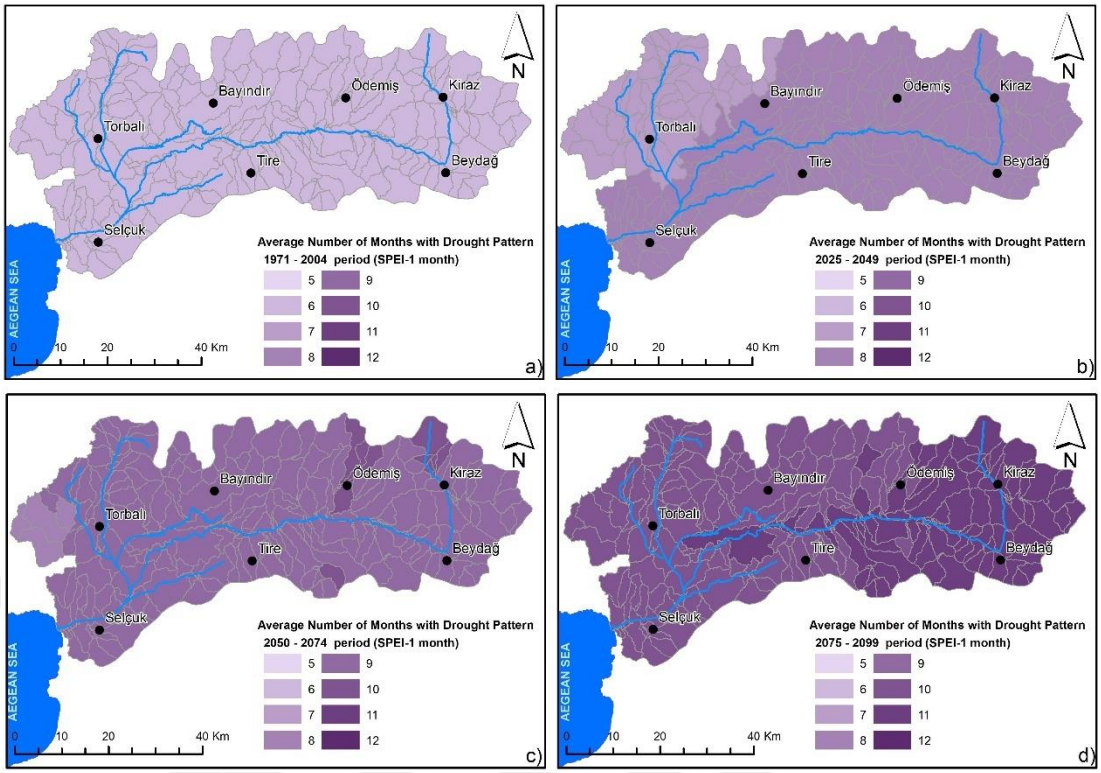


Figure Ap.69 Average number of months with drought pattern of SPEI-1 month for the period a)1971-2004, b) 2025-2049, c) 2050-2074, d) 2075-2099.

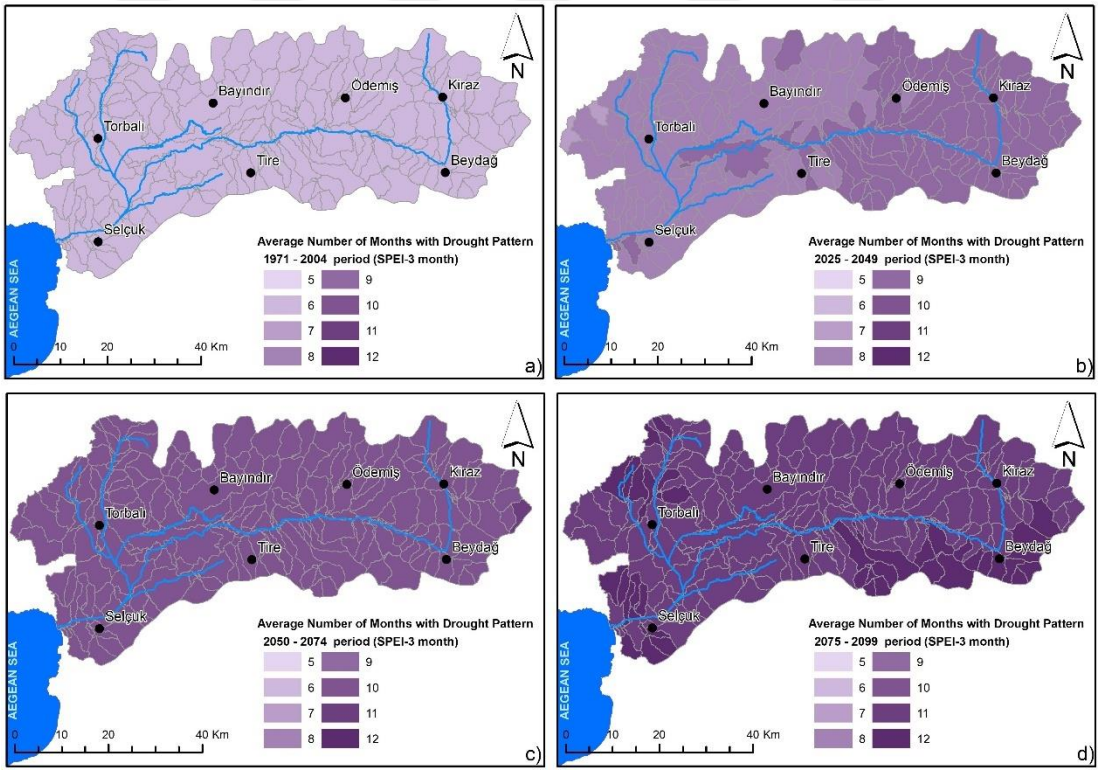


Figure Ap.70 Average number of months with drought pattern of SPEI-3 month for the period a)1971-2004, b) 2025-2049, c) 2050-2074, d) 2075-2099.

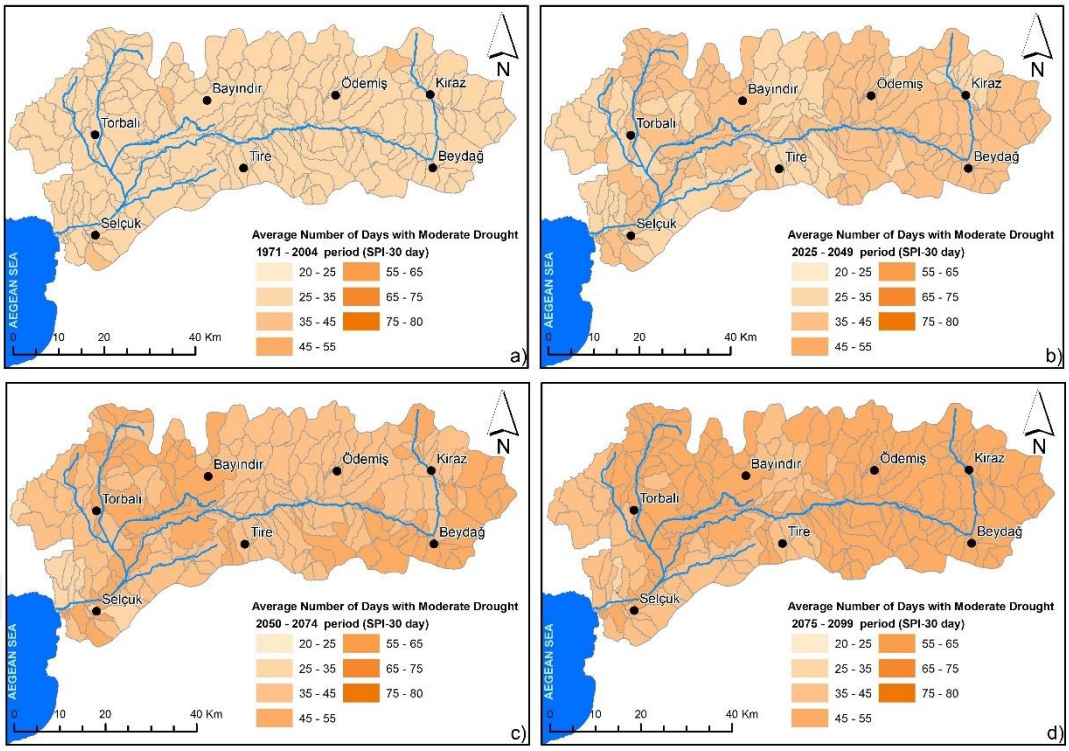


Figure Ap.71 Average number of months with moderate drought of SPI-30 day for the period a)1971-2004, b) 2025-2049, c) 2050-2074, d) 2075-2099.

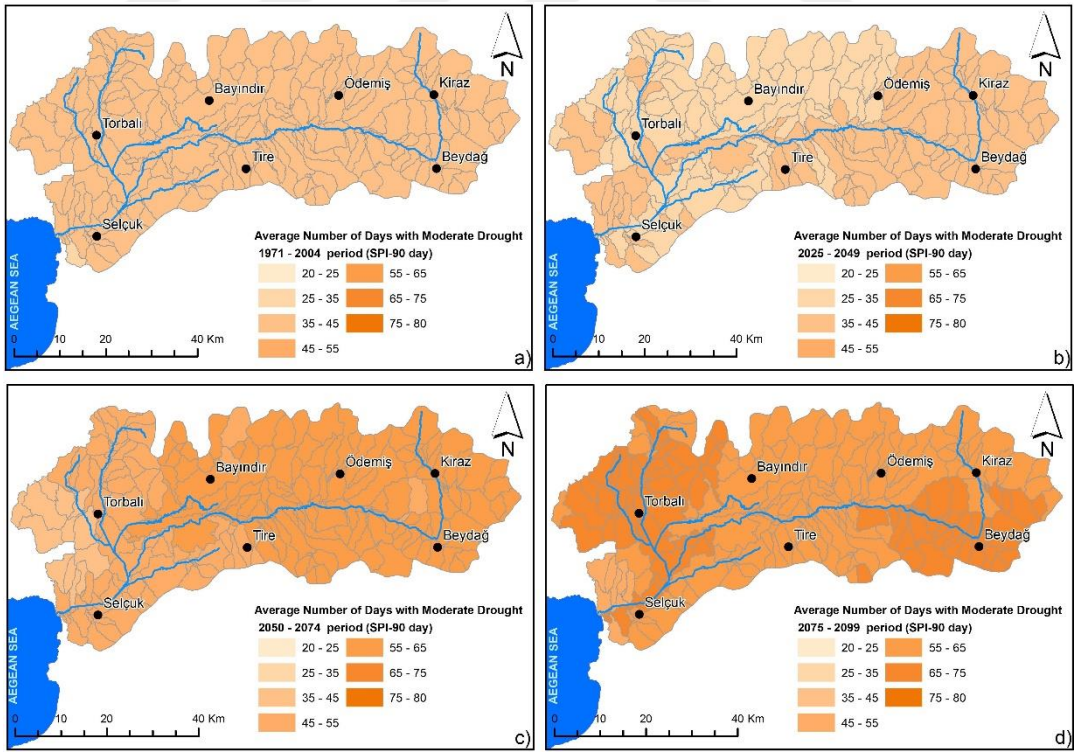


Figure Ap.72 Average number of months with moderate drought of SPI-90 day for the period a)1971-2004, b) 2025-2049, c) 2050-2074, d) 2075-2099.

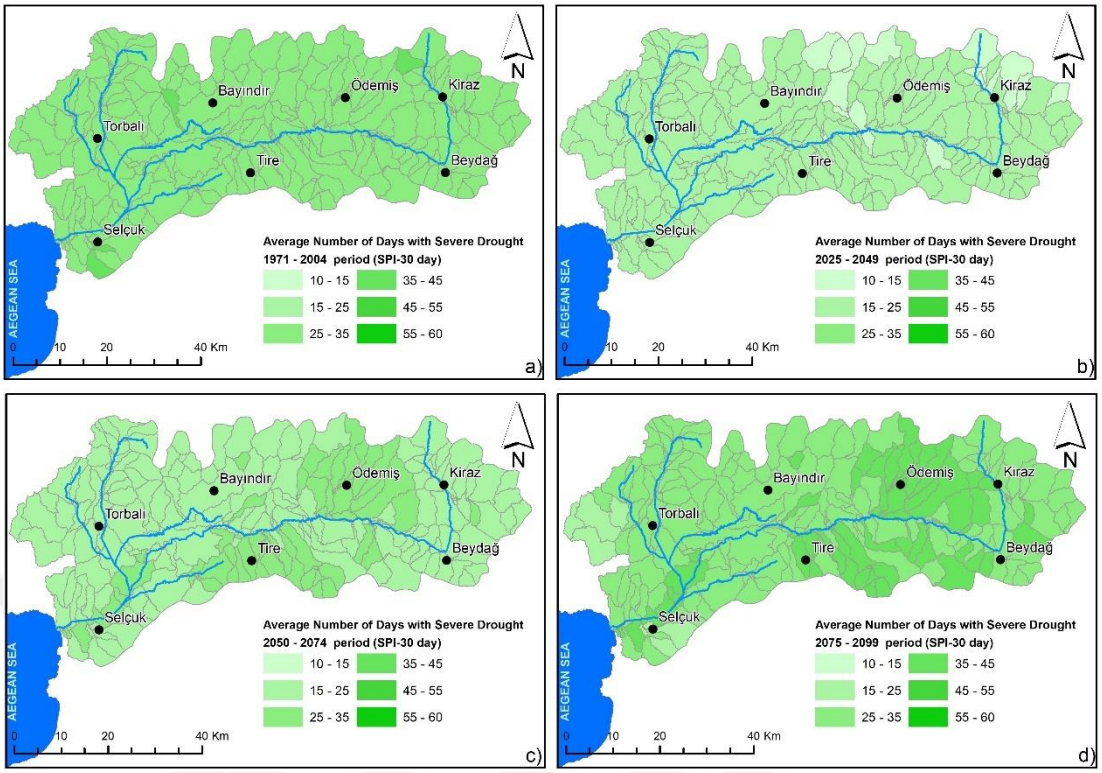


Figure Ap.73 Average number of months with severe drought of SPI-30 day for the period a)1971-2004, b) 2025-2049, c) 2050-2074, d) 2075-2099.

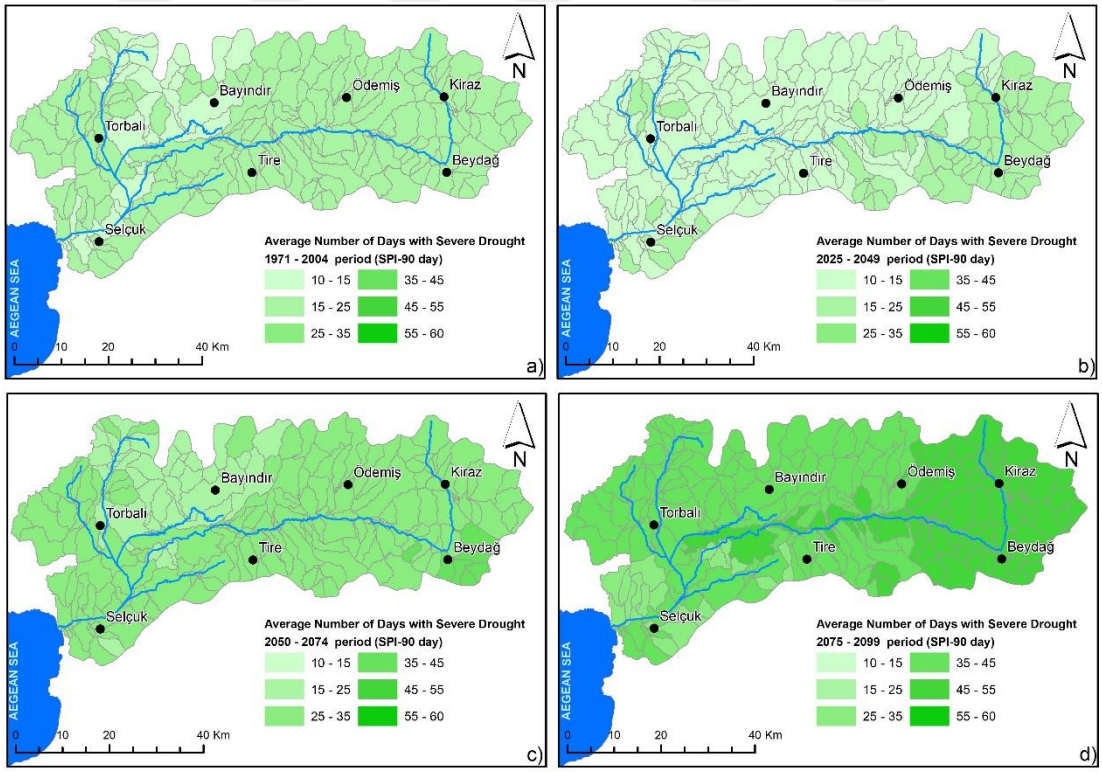


Figure Ap.74 Average number of months with severe drought of SPI-90 day for the period a)1971-2004, b) 2025-2049, c) 2050-2074, d) 2075-2099.

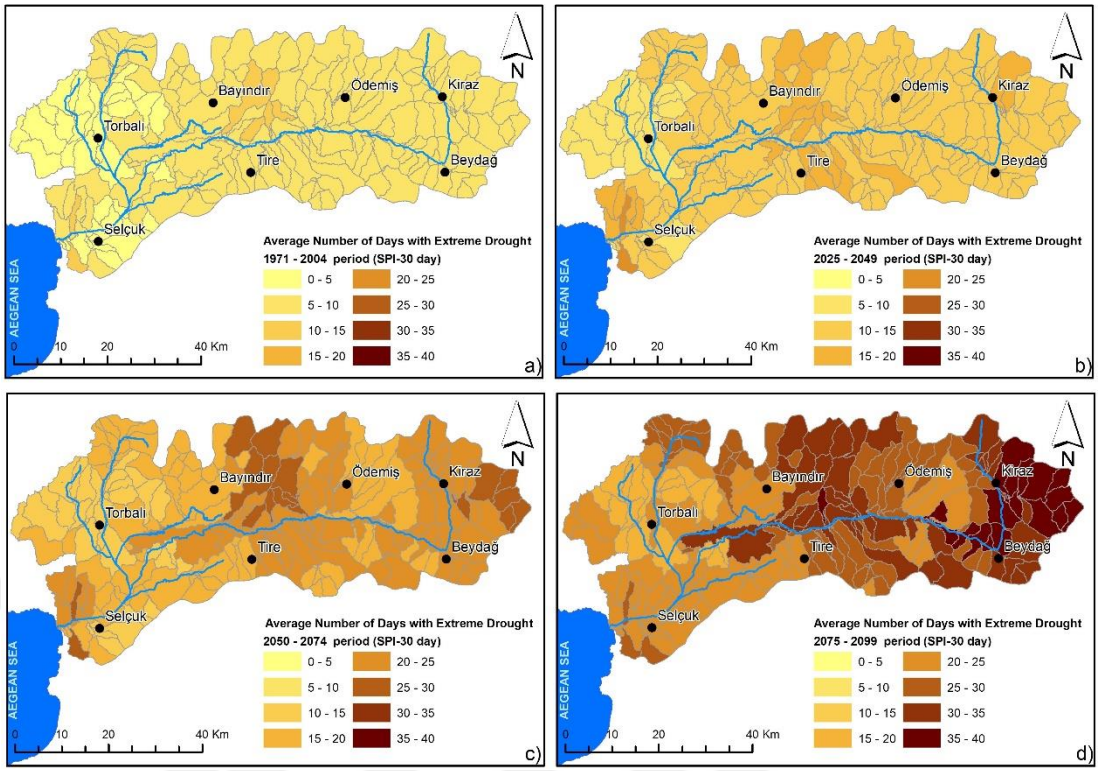


Figure Ap.75 Average number of months with extreme drought of SPI-30 day for the period a)1971-2004, b) 2025-2049, c) 2050-2074, d) 2075-2099.

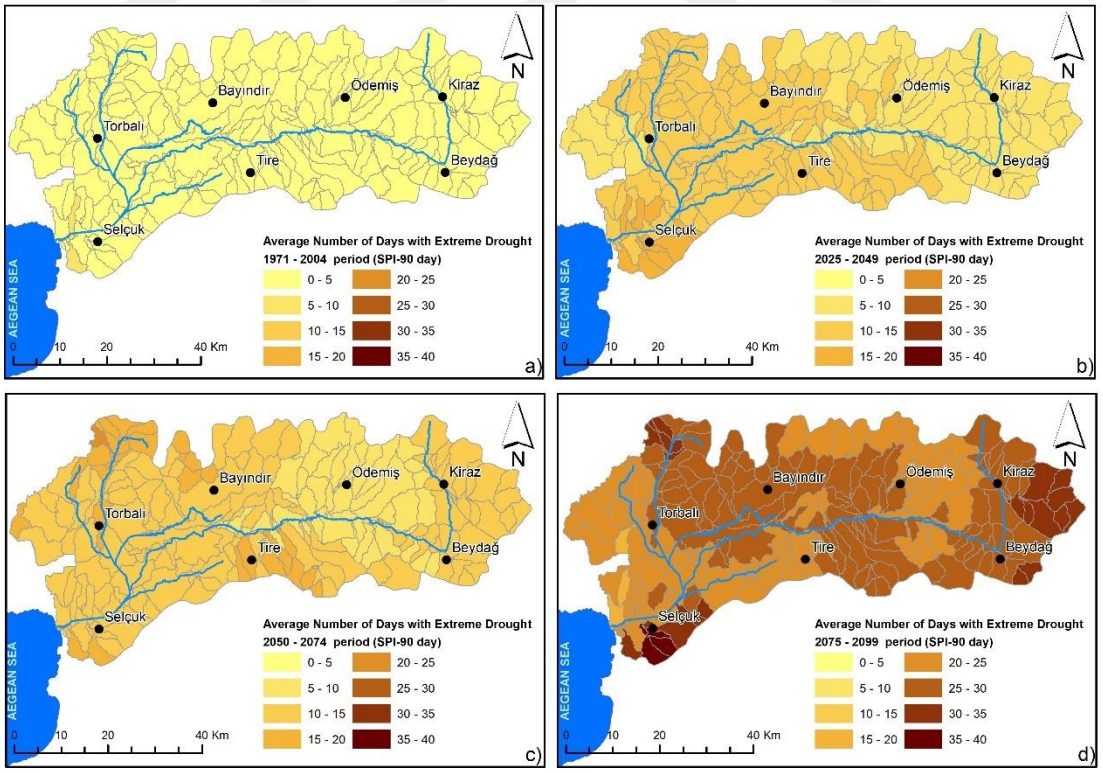


Figure Ap.76 Average number of months with extreme drought of SPI-90 day for the period a)1971-2004, b) 2025-2049, c) 2050-2074, d) 2075-2099.

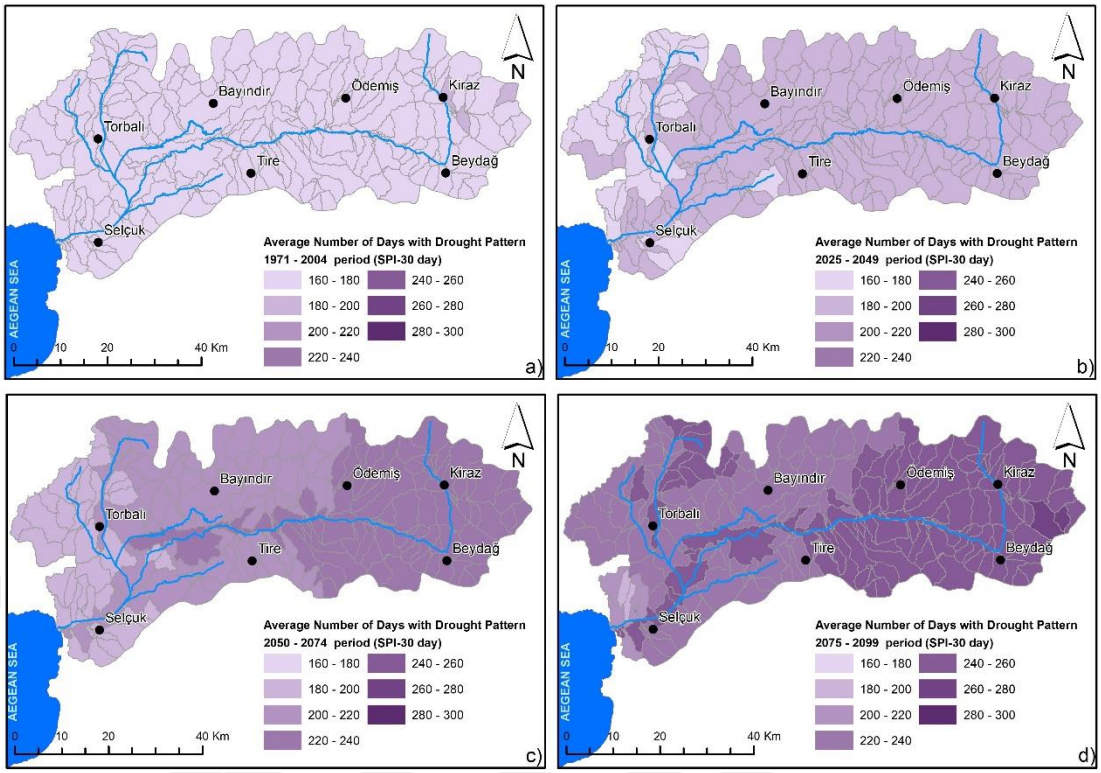


Figure Ap.77 Average number of months with drought pattern of SPI-30 day for the period a)1971-2004, b) 2025-2049, c) 2050-2074, d) 2075-2099.

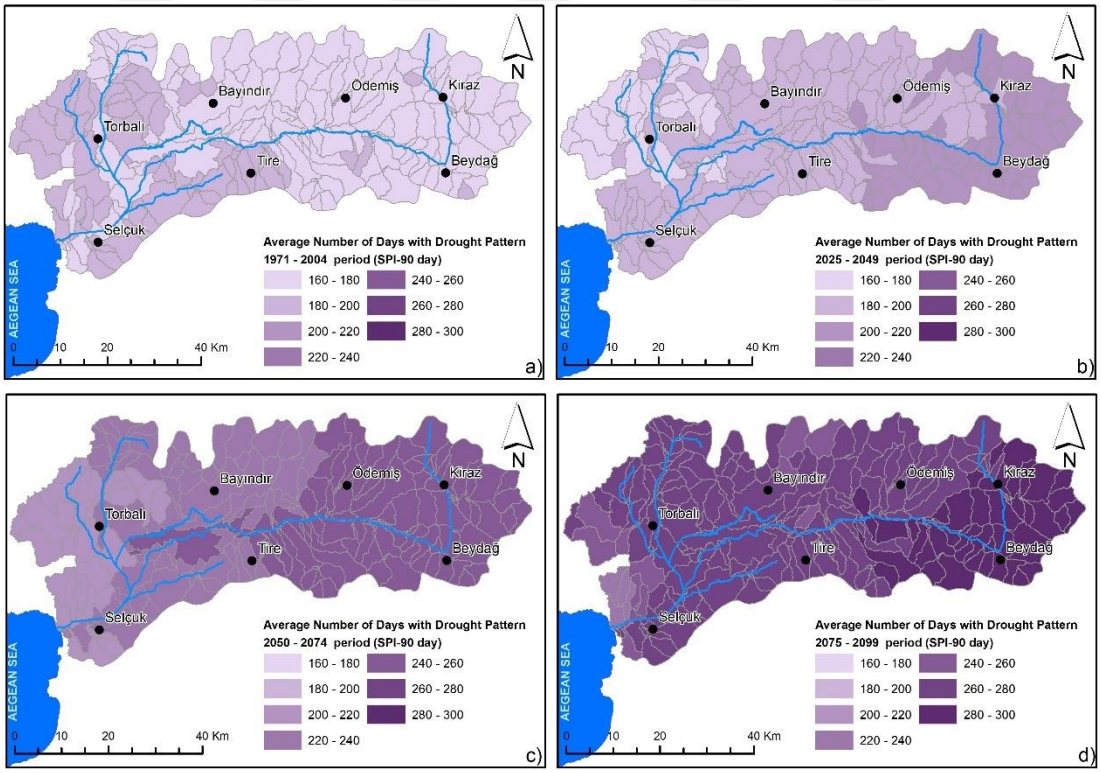


Figure Ap.78 Average number of months with drought pattern of SPI-90 day for the period a)1971-2004, b) 2025-2049, c) 2050-2074, d) 2075-2099.